UNIVERSITY OF Southampton

University of Southampton Research Repository
ePrints Soton

Copyright © and Moral Rights for this thesis are retained by the author and/or other copyright owners. A copy can be downloaded for personal non-commercial research or study, without prior permission or charge. This thesis cannot be reproduced or quoted extensively from without first obtaining permission in writing from the copyright holder/s. The content must not be changed in any way or sold commercially in any format or medium without the formal permission of the copyright holders.

When referring to this work, full bibliographic details including the author, title, awarding institution and date of the thesis must be given e.g.

AUTHOR (year of submission) "Full thesis title", University of Southampton, name of the University School or Department, PhD Thesis, pagination

http://eprints.soton.ac.uk

UNIVERSITY OF SOUTHAMPTON

THE CHEMISTRY OF PHOSPHINE-ANCHORED GROUP VIIIA METAL CLUSTERS ON SILICA

CONTENTS

Section		Page
	CHAPTER ONE	
	THE TETHERING OF TRIOSMIUM CLUSTERS TO PHOSPHINE-MODIFIED SILICAS	
1.1.	Introduction	1
1.1.1.	The Metal Cluster/Surface Analogy	2
1.1.2.	Methods of Heterogenizing Homogeneous Catalysts	5
1.1.3	Support Materials	11
1.2.	Characterisation of Supported Metal Clusters	12
1.2.1	Infrared Spectroscopy	13
1.2.2.	Raman Spectroscopy	13
1.2.3.	Nuclear Magnetic Resonance	14
1.2.4.	Extended X-ray Absorption Fine Structure	14
1.2.5.	Miscellaneous	15
1.2.6.	Characterisation of $[HOs_3(CO)_{10}(OM)]$	16
1.3.	The Anchoring of Metal Clusters to Phosphine-functionalised Silica	19
1.3.1.	The Silica Surface	19
1.3.2.	Surface Modification with Bifunctional Ligands, Preparation of $PPh_2CH_2CH_2SIL$	23
1.3.3.	Possible Routes for Preparing Phosphine-immobilised Metal Clusters	27
1.4.	Preparation and Characterisation of $[M_3(CO)_{12-n}(PPh_2CH_2CH_2SIL)_n]$, (M=Os, n=1; M=Ru, n=1-3)	30
1.4.1.	Ligand Substitution Reactions of $[H_3(CO)_{12}]$	30
1.4.2.	Characterisation of $[Os_3(CO)_{11}(PPh_2Et)]$	40
1.4.3.	Variable Temperature $^{13}C-\{^1H\}$ NMR Study of $[Os_3(CO)_{11}(PPh_2Et)]$	40
1.4.4.	Preparation of $[Os_3(CO)_{11}(PPh_2CH_2CH_2SIL)]$	47
1.4.5.	Preparation of $[Ru_3(CO)_{12-n}(PPh_2CH_2CH_2SIL)_n]$, n=1,2 or 3	52
1.5.	Preparation and Characterisation of $[H_2Os_3(CO)_{10}(PPh_2CH_2CH_2SIL)]$	57
1.5.1.	The Versatile Chemistry of $[H_2Os_3(CO)_{10}]$	57
1.5.2.	Characterisation of $[H_2Os_3(CO)_{10}(PPh_2Et)]$	62
1.5.3.	Variable Temperature $^{13}C-\{^1H\}$ NMR Study on $[H_2Os_3(CO)_{10}(PPh_2Et)]$	63
1.5.4.	Preparation of $[H_2Os_3(CO)_{10}(PPh_2CH_2CH_2SIL)]$	68

1.6.	Preparation and Characterisation of $[H_2Os_3(CO)_9(PPh_2CH_2CH_2SIL)]$	71
1.6.1.	Thermolysis of $[H_2Os_3(CO)_{10}L]$	71
1.6.2.	Characterisation of $[H_2Os_3(CO)_9(PPh_2Et)]$	72
1.6.3.	Variable Temperature ^{13}C NMR Study on $[H_2Os_3(CO)_9L]$; L=CO or PPh_2Et	73
1.6.4.	Preparation of $[H_2Os_3(CO)_9(PPh_2CH_2CH_2SIL)]$	79
1.7.	Elemental Analysis and Conclusions	82
1.8.	Experimental Section	84
1.9.	References	

CHAPTER TWO

A TRIOSMIUM CLUSTER ANCHORED THROUGH A BRIDGING ALKYNYL LINKAGE

2.1.	Other Modes of Attachment on Functionalised Oxides:- Polydentate Ligands	104
2.2.	Reactions of $[M_3(CO)_{12}]$, M=Os or Ru, with Unsaturated Hydrocarbons	107
2.3.	Reaction of Triethoxyvinylsilane with $[Os_3(CO)_{12}]$	115
2.4.	The Chemistry of $[HRu_3(CO)_9(C_2{}^tBu)]$	120
2.5.	Discussion:-Reaction of $[Os_3(CO)_{12}]$ with $R_3SiCHCH_2$, R=Et or Ph	123
2.6.	Preparation of $[HOs_3(CO)_9(C{:}CSIL)]$	130
2.7.	Experimental Section	132
2.8.	References	136

CHAPTER THREE

REACTIONS OF $[H_2Os_3(CO)_9(PR_3)]$, PR_3= PPh_3, PPh_2Et or $P(OMe)_3$, WITH NUCLEOPHILES

3.1.	Reaction of $[H_2Os_3(CO)_{10}]$ with simple Alkenes and Alkynes	141
3.2.	Reaction of $[H_2Os_3(CO)_9(PPh_2Et)]$ with Acetylene	146
3.2.1.	Preparation and Characterisation of $[HOs_3(CO)_9(PPh_2Et)(CHCH_2)]$	146
3.2.2.	Full ^{13}C NMR Study on $[HOs_3(CO)_9(PR_3)(CHCH_2)]$	153
3.2.3.	Summary	158
3.3.	Reaction of $[H_2Os_3(CO)_9(PR_3)]$ with Ethylene	159
3.3.1.	Preparation and Characterisation of $[H_2Os_3(CO)_9(PR_3)(C_2H_4)]$	159
3.3.2.	Preparation and Characterisation of	164

	$[H_2Os_3(CO)_9(PR_3)(CNMe)]$	
3.3.3.	Full ^{13}C NMR Study on $[H_2Os_3(CO)_9(PPh_2Et)(C_2H_4)]$	168
3.3.4.	Discussion	171
3.4.	Pyrolysis of $[HOs_3(CO)_9(PPh_2Et)(CHCH_2)]$	174
3.4.1.	Preparation and Characterisation of $[H_2Os_3(CO)_8(PPh_2Et)(CCH_2)]$	175
3.4.2.	Tentative Assignments for the ^{13}C NMR of $[H_2Os_3(CO)_8(PPh_2Et)(CCH_2)]$	178
3.5.	Hydrogenation of $[H_2Os_3(CO)_8(PPh_2Et)(CCH_2)]$	181
3.6.	Chapter Summary	187
3.7.	Experimental Section	187
3.8.	References	189
	CHAPTER FOUR	
	THE PYROLYSIS OF $[Os_3(CO)_{11}(PPh_2Et)]$: FULL CHARACTERISATION OF $[Os_3(CO)_9(PEt)(C_6H_4)]$	
4.1.	Thermolysis of $[Os_3(CO)_{12}]$ and its Substituted Derivatives	192
4.2.	Pyrolysis of $[Os_3(CO)_{11}(PPh_2R)]$; R=Me, Et or Ph.	204
4.3.	Crystal and Molecular Structure of $[Os_3(CO)_9(PEt)(C_6H_4)]$	209
4.4.	Variable Temperature $^{13}C-\{^1H\}$ NMR Study of $[Os_3(CO)_9(PEt)(C_6H_4)]$	217
4.5.	Discussion	228
4.6.	Experimental Section	233
4.7.	References	235
	CHAPTER FIVE	
	THERMAL STABILITY AND CATALYTIC ACTIVITY OF PHOSPHINE-ANCHORED TRIOSMIUM CLUSTERS	
	SECTION (A): Thermolysis Studies	
5.1.	Supported Rhodium Carbonyl Clusters	239
5.1.1.	Adsorption on Unfunctionalised Oxides	240
5.1.2.	Attachment on Phosphine-modified Silica	244
5.1.3.	Reaction of $[Rh_4(CO)_{12}]$ with 'Aerosil 200' or $PPh_2CH_2CH_2SIL$	248
5.2.	Thermal Degradation of $[HOs_3(CO)_{10}(OSIL)]$	252
5.3.	Pyrolysis of Phosphine-anchored Triosmium Clusters	256
5.3.1.	Experimental Procedure	256
5.3.2.	Thermal Treatment of $[Os_3(CO)_{11}(PPh_2Et)]$ in a KBr	259

	Matrix	
5.3.3.	Pyrolysis of $[Os_3(CO)_{11}(PPh_2CH_2CH_2SIL)]$	262
5.3.4.	Thermal Decomposition of $[H_2Os_3(CO)_{10}(PPh_2CH_2CH_2SIL)]$	264
5.3.5.	Assignment of Degradation Products from Phosphine-tethered Triosmium Clusters	266
	SECTION (B): Olefin Hydrogenation by Phosphine-anchored Triosmium Clusters	
5.4.	Hydrogenation of Ethylene	272
5.5.	Experimental Procedure (Diagram 9)	277
5.6.	Results and Infrared Spectroscopy	279
5.6.1.	Homogeneous Systems	279
5.6.2.	$[Os_3(CO)_{11}(PPh_2CH_2CH_2SIL)]$	282
5.6.3.	$[H_2Os_3(CO)_9(PPh_2CH_2CH_2SIL)]$	284
5.7.	Further Characterisation of the Deactivation Process for Anchored Clusters	289
5.8.	1-Heptene Isomerisation/Hydrogenation	293
5.9.	Discussion	295
5.10.	Other Catalytic Studies	308
5.11.	Appendices	310
5.12.	References	314
	CHAPTER SIX	
	THE REACTIONS OF $[Ru_6C(CO)_{17}]$ WITH PHOSPHINES: FULL CHARACTERISATION OF $[Ru_6C(CO)_{16}(PPh_2R)]$, R=Et or CH_2CH_2SIL	
6.1.	Preparation and Background Chemistry of $[Ru_6C(CO)_{17}]$	319
6.2.	Preparation and Characterisation of $[Ru_6C(CO)_{16}(PPh_2Et)]$	325
6.2.1.	Crystal and Molecular Structure of $[Ru_6C(CO)_{16}(PPh_2Et)]$	328
6.2.2.	^{13}C NMR Solution Studies of $[Ru_6C(CO)_{17-n}(PPh_2Et)_n]$; n=0,1 or 2	343
6.3.	Reaction of $[Ru_6C(CO)_{17}]$ with Trimethylphosphite	346
6.4.	Preparation and Characterisation of $[Ru_6C(CO)_{17-n}(PPh_2CH_2CH_2SIL)_n]$, n=1 or 2.	353
6.5.	Thermal Degradation of $[Ru_6C(CO)_{16}(PPh_2CH_2CH_2SIL)]$	356
6.6.	Experimental Section	360
6.7.	References	363

UNIVERSITY OF SOUTHAMPTON

ABSTRACT

FACULTY OF SCIENCE

CHEMISTRY

Doctor of Philosophy

THE CHEMISTRY OF PHOSPHINE-ANCHORED GROUP VIIIA METAL CLUSTERS ON SILICA

by Simon Charles Brown

The preparation of the silica-heterogenized metal clusters $[Os_3(CO)_{11}(PPh_2CH_2CH_2SIL)]$, $[H_2Os_3(CO)_{10}(PPh_2CH_2CH_2SIL)]$, $[H_2Os_3(CO)_9(PPh_2CH_2CH_2SIL)]$, $[HOs_3(CO)_9(C{:}CSIL)]$ and $[Ru_6C(CO)_{16}(PPh_2CH_2CH_2SIL)]$ is described. Each is identified by comparison with fully characterised homologues.

A cycle for ethylene hydrogenation catalysed by the phosphine-anchored triosmium clusters is developed. Possible causes of loss of activity are explored by carrying out pyrolysis studies on the heterogeneous and homogeneous variants. Thermolysis of $[Os_3(CO)_{11}(PPh_2R)]$ selectively gives $[Os_3(CO)_9(PR)(C_6H_4)]$. Reaction of $[H_2Os_3(CO)_9(PPh_2R)]$ with ethylene, acetylene and hydrogen provides evidence of a cycle intermediate $[H_2Os_3(CO)_9(PPh_2R)(C_2H_4)]$ and the cluster retained deactivation products- $[HOs_3(CO)_9(PPh_2R)(CHCH_2)]$, $[H_2Os_3(CO)_8(PPh_2R)(CCH_2)]$ and $[H_3Os_3(CO)_8(PPh_2R)(CCH_3)]$. Their properties are compared to those of the phosphine unsubstituted counterparts. $[H_3Os_3(CO)_8(PPh_2CH_2CH_2SIL)(CCH_3)]$ is identified as the only cluster species on the spent silicas; along with a mononuclear breakdown product.

The substitution chemistry of $[Ru_6C(CO)_{17}]$ with phosphines and phosphites is investigated. The single crystal, X-ray diffraction determined, structure of $[Ru_6C(CO)_{16}(PPh_2Et)]$ is presented, and the series $[Ru_6C(CO)_{17-n}\ P(OMe)_3\ _n]$, n=1 to 4, is characterised. The corresponding anchored variants $[Ru_6C(CO)_{17-n}(PPh_2CH_2CH_2SIL)_n]$, n=1 or 2, are defined and their subsequent thermal degradation reported.

MEMORANDUM

A dissertation submitted in part fulfilment of the requirements for the degree of Doctor of Philosophy at Southampton. The work described has not been previously submitted for any other degree. Except where specific reference is made to the contrary, the work is original; none of it was done in collaboration.

S.C.Brown

30th. September 1983

ACKNOWLEDGEMENTS

I would like to express my gratitude to the following people for assistance and guidance throughout the duration of this thesis.

Firstly, Dr.L.E.Smart for performing the complete single crystal X-ray diffraction determination on $[Os_3(CO)_9(PEt)(C_6H_4)]$. Dr.M.Webster for leading me through the structural analysis of $[Ru_6C(CO)_{16}(PPh_2Et)]$. Dr.W.Levason for carrying out carbon and hydrogen elemental analyses and, in particular, Mrs.J.M.Street for recording all NMR spectra on the Varian Associates XL-100 spectrometer.

Generally, all the people on the sixth floor, but especially my supervisor Dr.J.Evans. My industrial supervisor Dr.P.Todd and his colleagues at ICI Petrochemicals Division for the use of their laboratory facilities. Also my present associates at BP Chemicals for understanding and encouragement during the preparation of this dissertation.

Finally, my parents, Alison and her parents, for their continued support and affection, and to whom I dedicate this work.

CHAPTER ONE

THE TETHERING OF TRIOSMIUM CLUSTERS TO PHOSPHINE-MODIFIED SILICAS

1.1. Introduction

With the diminishing reserves of crude oil the need for alternative technologies for production of strategic chemicals has become an urgent priority of the industrialised world. One viable route is derived from the hydrogen-deficient materials, coal, lignite, oil shale, tar sands etc., which can be readily converted to syngas, a mixture of hydrogen and carbon monoxide. These inorganic diatomics then constitute the building blocks for new processes in the petrochemical industry(1). For sound economic reasons, conservation of energy and feedstocks, these processes will invariably include a suitable catalyst. Such a material increases the rate at which equilibrium is attained, by substantially lowering the activation energy, without itself being consumed. Where the opportunity of a series of different reaction paths exists, specific reduction in energy for only one can provide high selectivity.

Present day catalysts are essentially of two types, solid-state catalysts e.g. metals and metal oxides, used in heterogeneous catalysis(2) and discrete, soluble metal complexes used in homogeneous catalysis. Most large scale industrial processes, with only a few exceptions, are based on the first class. Usually the metals are dispersed on inorganic oxide supports in order to both increase the effective surface area and dilute the catalyst for better temperature control. They are most commonly prepared by impregnation, in which the refractory support is contacted with a solution containing a salt of the required metal. The solute deposits on the carrier, and the resulting material is thendried and often calcinated before reduction, usually with hydrogen, to form small metal crystallites dispersed on the carrier surface. This reduction step frequently requires high temperatures($400^{o}C$) and aggregation occurs to varying degrees resulting in a wide range of particle sizes, causing loss of selectivity as a catalyst. The state of dispersion affects the sites which predominate on the surface. For a large metal crystal thousands of angstroms in size, the surface atoms are mostly present in the crystal faces. As the crystal size is decreased, the proportion of atoms present in

edges and corners increases. These atoms will have lower coordination numbers, and different surface energy levels, than those present in a crystal face and would be expected to have different affinities for reactant molecules. This makes the class of small metal particles($<20\text{Å}$)(3) very important because they display behaviour different from that of the bulk metal, and may exhibit activity for 'structure sensitive' reactions.

A major drawback in all conventional heterogeneous catalysts is the extreme difficulty in assessing the intimate mechanisms of chemisorption and reaction on the surface, even with the most modern analytical, spectroscopic and diffraction techniques(4). Some advance in understanding chemisorption processes has come from studying the chemistry of idealized, single-crystal metal surfaces(5), but even then identifying adsorption modes can be difficult. In addition, many of the surface physics techniques i.e. LEED, ARUPS, EELS spectroscopy(6), can only be applied at low pressures, an obvious disparity with the normal conditions in heterogeneous reactions.

1.1.1.The Metal Cluster/Surface Analogy

Molecular metal clusters comprise an extremely diverse family in which the formal oxidation state of the metal atoms may vary from +3 to zero, or even have slightly negative values. The normal classification calls for three or more metal atoms or ions mutually bonded to each other, although dinuclear metal complexes with metal-metal bonds are sometimes included(7). These polyhedral arrays, which are usually surrounded and stabilised by ligands, fall into three main binary categories, carbonyls, halides and isocyanides; finally there is the nonligand class(8) of naked metal cluster ions e.g. Bi_9^{5+}, Sn_9^{4-}. By far the largest set are the transition-metal carbonyl clusters, which presently range up to a Pt_{38} core of O_h cubeoctahedral symmetry(9). In these complexes the metal atoms have a formal zero oxidation state, which maximises overlap of the valence-shell orbitals. For this reason clusters of Group VIII metals are favoured with carbonyl ligands, or other groups, capable of drawing electrons out of the antibonding orbitals. In this thesis attention is focused on the Group VIIIa metals,

iron, ruthenium and osmium, which form clusters with three to ten metal atoms, ignoring linked polyhedra.

There is an appealing parallel between these cluster complexes and metal surface chemistry, which has been reviewed at length(6), and developed on two different levels.

The first(10) is as models for chemisorption. The hypothesis starts by proposing that reaction mechanisms as established for homogeneous catalytic reactions may be mimed in a first approximation on an heterogeneous surface. However this approach with discrete mononuclear coordination or organometallic compounds, cannot furnish adequate models for important surface phenomena such as C-H and C-C bond activation. Invariably in homogeneous reactions the reactants all bind initially at the one metal centre. On a surface, for a single metal atom, bound to metal atoms below and minimally to four other at the surface, there remains insufficient space and available orbitals, to form an analogous intermediate. The obvious modification involves adjacent metal atoms so the adsorbed molecules can have several modes of interaction possibly bridging several centres. Also with the reactants at separate sites considerable mobility in the chemisorbed species is invoked in the mechanistic cycles. Both of these concepts are realised on transition metal carbonyl clusters. Obviously while species such as $[Os_3(CO)_{12}]$ bear no relationship to a metal surface the putative model is structured on the periphery of ligand atoms, groups of atoms or molecules and a metal surface with a similar set of ligands chemisorbed at the surface. Perhaps most striking is the propensity of the osmium cluster to coordinate hydrocarbons and cleave C-H and C-C bonds. Thus characterisation of the vibrational frequencies of modes involving the μ_2-methylene ligands in $[H_2Os_3(CO)_{10}(CH_2)]$ and $[Os_3(CO)_{10}(CO)(CH_2)]$(11), the μ_3-η^2-acetylenic ligand in $[Os_3(CO)_9(CO)(C_2H_2)]$(12) and the μ_3-ethylidyne ligands in $[H_3M_3(CO)_9(CMe)]$, M=Ru, Os(13) or Co(14), provide excellent comparisons to EELS data from dissociative adsorption of acetylene on the Ni(111) and W(110) surfaces, associative adsorption on Pt(111) and Pd(111), and associatively adsorbed ethylene on Pt(111) and Ni(111), respectively. Ligand fluxionality, not only over the cluster faces (i.e. carbonyls, organic moieties) but also within the polyhedra (hydrides), is a well-defined feature of

clusters(15). The variable temperature NMR experiment can provide accurate activation parameters, and can often yield unequivocal mechanistic information.

The second analogy treats the whole cluster as a model to small dispersed metal particles, again the analogy has to be relative to a highly chemisorbed surface. In the largest cluster identified to date, $[Pt_{38}(CO)_{44}H]^{-}$, the metal skeleton diameter is 11.6Å(9), which is comparable with the average diameters reported for many highly dispersed supported metal catalysts. Within the Group VIIIa triad both $[Os_{10}C(CO)_{24}]^{2-}$(16) and $[H_4Os_{10}(CO)_{24}]^{2-}$(17) have a metal skeleton which is a fragment of a cubic close packed array, and corresponds to a face-centred cubic unit cell with four tetrahedally related corners removed. This geometry is different to that of osmium bulk metal which has a hexagonal close packed array. The four large planar faces, each consisting of six osmium atoms with six carbonyl ligands approximately perpendicular to each face, probably represents the best analogy so far of a monolayer of carbon monoxide chemisorbed onto a metal surface. With the extended faces the coordination number of the metal atoms increases, whilst the osmium/carbonyl ratio is reduced with increased nuclearity.

Apart from these geometric considerations a true model should also possess electronic characteristics which resemble those of a metal surface. For smaller clusters successful bonding schemes (18) are based on counting skeletal electron pairs, implicitly assuming diamagnetic ground states. The accuracy of this approach is shown by photoelectron spectra of $[Os_3(CO)_{12}]$(19) and $[Os_6(CO)_{18}]$ (20). In contrast the even-electron $[H_2Os_{10}(CO)_{24}]$(21), still possessing the same polyhedral core as the parent dianion, exhibits low temperature Curie-type paramagnetism(22). A shift from Pauli to Curie-type behaviour has been predicted for bulk metals as the particle size decreases, so in terms of magnetic properties the decanuclear cluster behaves as a small metal particle. This was augmented by an EPR study establishing that the trend towards metallic behaviour is well advanced for clusters with ten osmium atoms.

It follows that larger metal clusters, as preformed metal particles at, or near, zero oxidation state, can offer an

attractive method of forming supported small metal crystallites of uniform size, and hence more specific in their activity, because the need for high temperature reductions is avoided.

A third opportunity afforded by clusters is that by their nature they can exhibit catalytic properties intermediate between those of mononuclear complexes and metal surfaces. In particular, they offer the potential of multimetal atom site reactions, with the possiblity of performing unique catalytic reactions impossible to effect at single metal atom centres. The discrete structures, use of bimetallic species and ligand effects, all promise design of highly selective catalysts(23). Accordingly there is a profusion of studies on homogeneous systems in the literature(7).

1.1.2.Methods of Heterogenizing Homogeneous Catalysts

The comparative merits and drawbacks of homogeneous and heterogeneous catalysis are summerised in Table 1.

There exists a third kind of catalyst, a hybrid that attempts to combine the practical advantages of conventional heterogeneous catalysts with the versatility of homogeneous transition metal catalysts. The objective being to obtain a well defined complex that can be highly dispersed throughout the reaction medium while remaining in a separate phase. This heterogenizing of homogeneous catalysts, by immobilising on a high surface area solid support, can be achieved by a variety of methods(24).

1) By causing a metal complex to become physically dispersed within the pore structure of a support, usually achieved by impregnation of the carrier with a solution of the complex followed by solvent evaporation. Zeolites represent an ideal media and several attempts to entrap clusters within the supercage structure have been made, i.e. $[Fe_3(CO)_{12}]$(25), $[Ru_3(CO)_{12}]$(26) and $[Rh_6(CO)_{16}]$(27). The evidence suggests that the cluster integrity is at least first retained, although whether adsorption is in the cavities or on the external surface of the support is questionable.

2) Immobilisation of complexes on the matrix surface.

a) Supported liquid-phase(SLP): This involves dispersing the complex in a similar manner to above, but with the additional presence of a relatively involatile solvent, which

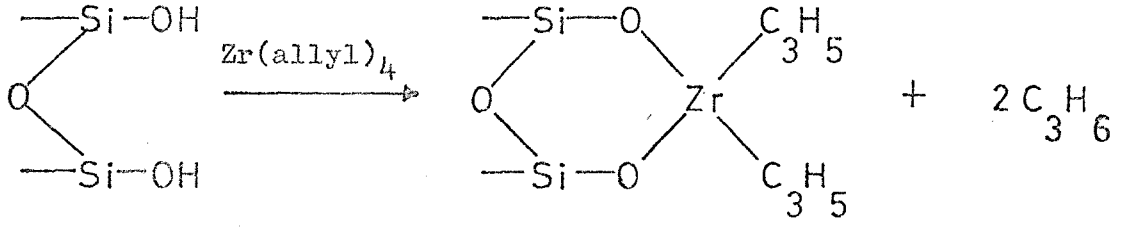
Table 1

Homogeneous verses Heterogeneous Catalysis

PROPERTY	HOMOGENEOUS	HETEROGENEOUS
FORM	Soluble, discrete molecular compounds	Solid-state, metal-oxides or metals (usually supported)
PHASE	Liquid	Gas/solid, liquid/solid
STABILITY	Often sensitive to extreme temperatures, air	Good thermal and mechanical stability
APPLICATION	Reasonable activity under mild conditions Costly separations:- difficult to recover catalyst from products, loss of expensive precious metal Corrosion of reactors	Often energy intensive, high temperatures and pressures Capacity for use in packed and fluidized beds, readily separated from reaction products
ACTIVITY	low	high
SELECTIVITY	High; efficient and reproducible action of metal atoms	Imperfect surface with sites of varying reactivity, antithetical to selectivity
MECHANISM	Well defined on the molecular level	Frequently ill-defined, inaccessible active-sites
COMMENTS	Electronic and steric properties that can be varied and frequently controlled. Logical tailoring of activity	Design and improvements limited through lack of knowledge- a 'black art'

remains in the solid after the evaporation steps and in which the complex is effectively dispersed. The problems of diffusion limited reaction rates, and the possibility of the catalyst being destroyed by immersion in a liquid phase, need to be addressed(28), and have so far limited application of this technique.

b) Grafting: This involves attachment of the metal complex to the carrier through the formation of chemical bonds. The grafting reaction with an inorganic oxide surface involves an interaction with the surface hydroxyl groups, and is analogous to the reaction of a moisture-sensitive organometallic with an alcohol. A good example is the interactions of π-allyl complexes on oxides such as silica(29).



For carbonylmetal clusters the simplest preparative procedure is to interact the species with the oxide, dry the material, and then to heat it in vacuo. This follows through the sequence of initial physisorption, chemisorption, and further carbonyl dissociation. Chemisorption could involve a variety of chemical reactions (Diagram 1):-

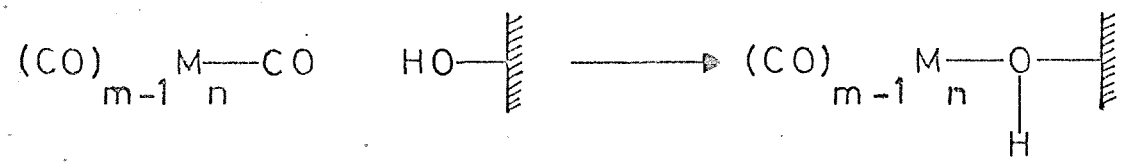
i) substitution of a carbonyl by a surface hydroxyl group. ii) oxidative addition of the hydroxyl group. iii) nucleophilic attack on the carbonyl carbon atom. iv) a Lewis acid interaction with a carbonyl oxygen atom.

There is no compelling evidence for the first process at present. However chemisorption of $[Os_3(CO)_{12}]$ on silica above 150°C involves loss of two carbonyl ligands and oxidative addition of a surface silanol group to afford $[HOs_3(CO)_{10}(OSIL)]$, Ia, (30). Analogous supported osmium clusters were prepared by contact with γ-alumina titania and zirconia in n-octane heated to reflux(31). The interaction with magnesia is more facile taking place at 25°C. However the

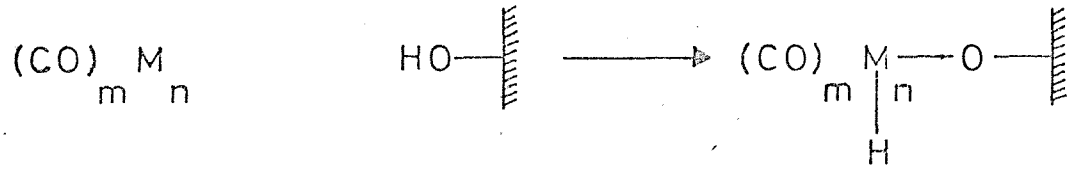
Diagram 1

Possible Chemisorption Processes for a Carbonyl Cluster on an Oxide Surface

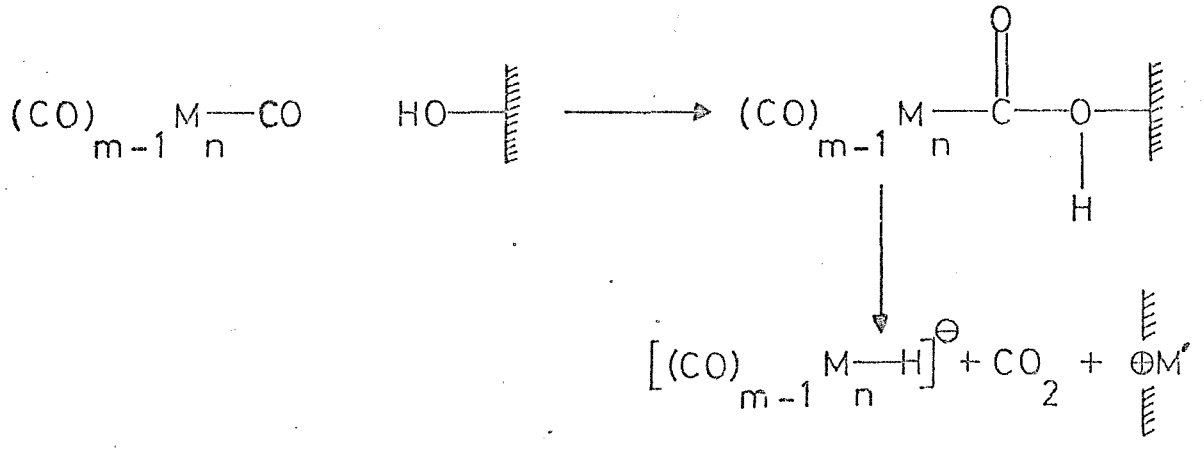
i) Substitution of a carbonyl by a surface hydroxyl group.



ii) Oxidative addition of an hydroxyl group.



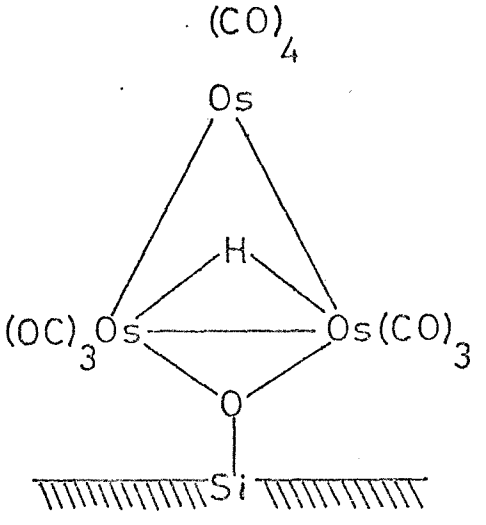
iii) Nucleophilic attack at a carbonyl carbon atom.



iv) Lewis acid interaction with a carbonyl oxygen atom.



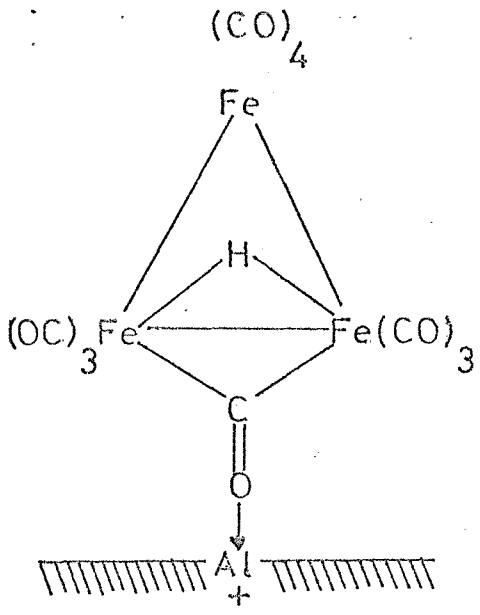
product readily fragments to mononuclear species on exposure to air, which correlates with the increased basicity of this support (32).



Structure of $[HOs_3(CO)_{10}(OSIL)]$

When either $[Fe_3(CO)_{12}]$ or $Fe(CO)_5$ is brought in contact with hydrated magnesia, zirconia or alumina an instantaneous nucleophilic attack of a support hydroxyl group on a carbonyl ligand occurs, with concommitant formation of $[HFe_3(CO)_{11}]^-$, II, ionically bound to the surface(33). The alumina system was studied most. Eliminated carbon dioxide was not detected in the gas phase, but shown by infrared spectroscopy to react with the carrier to form adsorbed carbonates. The outcome was independent of any temperature pretreatment (25-500°C) of the alumina, inferring that hydroxyl groups, rather than molecular water, are resonsible for the formation of II. Again the basicity of the surface groups is critical, and on silica, where they have a very weak Bronsted acidity, $[Fe_3(CO)_{12}]$ is only physisorbed at room temperature and maintained as such without reduction. Significant shifts to lower frequencies for the infrared ν_{CO} bands, and in particular that corresponding to the bridging carbonyl, suggests a tight ion-pair complex in which there is a Lewis acid interaction with the oxygen lone pair(34). There is also evidence(35) of a Lewis acid binding for $[Fe_3(CO)_{12}]$ on a dehydrated HY type of zeolite.

The major drawback in this grafting process is that the



Possible structure of
$Al^{+}[HFe_3(CO)_{11}]^{-}$

very surface reactivity utilized in initially chemisorbing the cluster units can also bring about their destruction to monomeric or raft species upon thermal treatment or exposure to air. Further, the ionically bound species are susceptible to leaching into polar solvents, as illustrated by the addition of HCl causing the reappearance of $[Fe_3(CO)_{12}]$ in solution, or extraction of the anion by metathesis with Et_4NCl.

However, it does present an effective method of preparing small metal particles which have selective Fischer-Tropsch activity(36). Thus a variety of clusters, including $[M_3(CO)_{12}]$, M= Os or Ru, and $[Os_6(CO)_{18}]$ when impregnated on alumina, silica or magnesia and heat treated give a product distribution favouring saturated, low molecular weight, hydrocarbons(37). Thermal decomposition of II, on alumina under syngas, gave small metal particles less than 20Å across, which exhibited a very high selectivity towards propylene. With time aggregation to very large iron particles, up to 500Å, occurs accompanied by a decline in selectivity(38).

c) Anchoring on ligand-functionalised supports:

As evidenced by the ready aggregation above, low oxidation state metal carbonyls have relatively little affinity for oxygen-donating ligands. Functionalisation of the support with a soft donor ligand might help to maintain cluster nuclearity over a wider range of conditions. Phosphines have been most commonly used, and this is

the approach adopted in this thesis. For instance, on silica this is achieved by employing a ligand containing hydrolysable silyl groups, these condense with the surface silanol groups to form strong, covalent siloxane bonds. This class of immobilised catalyst is referred to as inorganic-anchored or tethered. Quaternisation of amine functionalised silica gel or polystyrene allows a variation on the ionic grafting process with isolation of $[SiLCH_2CH_2NH_3][FeCo_3(CO)_{12}]$(39) and $[\textcircled{P}\text{-}CH_2NEt_3][HFe_3(CO)_{11}]$(40).

1.1.3. Support Materials

There are two main types of support, inorganic oxides and organic polymers.

The most widely used polymers are those based on copolymerization of styrene with divinylbenzene(DVB), as a cross-linking agent. Functionalisation then proceeds, for example, by bromination of the phenyl rings followed by reaction with lithium diphenylphosphide. A variation involves copolymerizing a functionalised monomer i.e. p-bromostyrene with styrene and DVB, followed by phosphination. This produces a random distribution of the functional ligand, but because replacement is mass-transfer limited a residual concentration of bromo-groups remain(41), and this can be deterimental to the stability of immobilised species. Another type of support is prepared from styrene, DVB, and the phosphine-functionalised monomer, p-styryldiphenylphosphine. Because of the higher reactivity of the latter monomer, a block polymer is obtained with islands of high ligand concentration. This favours multiphosphine-substituted derivatives of organometallic precursors. The general methods of preparing functionalised polymer membranes, gel-form and macroporous beads has been recently reviewed(42).

From an engineering standpoint inorganic macromolecules have superior physical properties as supports for industrial scale applications. Polymers tend to have non-rigid structures, and this flexibility makes control of intermolecular distances almost impossible facilitating condensation, or polycoordination, of catalyst sites leading to deactivation. They also exhibit pronounced swelling under variable temperature and solution conditions, which can make practical control of diffusional properties difficult,

and their thermal stability is limited, typically 160°C for a macroreticular resin. In contrast, inorganic oxides are mechanically rigid, diffusional characteristics are unaffected by all but the most severe changes in conditions, and thermal stability is primarily a function of the immobilised complex and not the support. However one disadvantage is that, while polymeric hydrocarbons are nearly inert, on inorganic oxides the potential still exists for undesirable side reactions with remaining indigenous active sites even after functionalisation, but this can be largely circumvented by silylation. The lower reactivity of such sites on silica, as witnessed in grafting processes, in combination with the above reasons, made it the macromolecular support of choice in this work.

1.2. Characterisation of Supported Metal Clusters

One of the major difficulties encountered with conventional heterogeneous catalysts is that of characterisation, similar problems arise with heterogenized systems. Since the majority of anchoring procedures are carried out at relatively modest temperatures it is reasonable to assume the physical properties (total specific surface area, pore volume, pore structure) of the support material will remain essentially unaltered. Much less clear, however, is the chemical identity of the supported complex and its mode of attachment to the carrier. The required information frequently falls outside the range of sensitivity of traditional surface science techniques, and beyond that obtainable by the conventional methods of characterising molecular clusters. In particular, the definitive methods of single-crystal X-ray, or neutron, diffraction in determining molecular structures clearly cannot be applied to these non-ordered systems. However advances in technique and sensitivity for vibrational and NMR spectroscopy does permit their application, enabling direct comparison of data for the supported complex and discrete model compounds. No one technique is satisfactory in isolation and until, for example, ultra- high resolution electron microscopy becomes available on a routine basis, reliance on a combination of techniques and/or indirect evidence is necessary. A short review follows of those techniques available which are most relevant to characterisation

of heterogenized metal clusters. The section concludes with a specific example of how this barrage is applied to the most thoroughly defined system to date, $[HOs_3(CO)_{10}(OSIL)]$, I.

1.2.1. Infrared Spectroscopy

Because of its routine accessibility this is the predominant technique used for characterising heterogenized metal clusters. Specifically, the carbonyl stretching vibration frequencies (ν_{CO}) about 2000cm^{-1} are very sensitive (intensities and positions) to changes in structure, including alterations in ligand backbones. It does require a library of spectra for reference model compounds as it is solely applied as a fingerprinting technique. This comparative approach succeeds where the influence of the support is minimal, as with inorganic-tethering through bifunctional ligands where the alkyl chain effectively insulates the two segments. Assignments become more subjective for grafted clusters where electronic effects are transmitted from the support giving rise to large shifts in frequencies. Also simple spectra, as exhibited by mononuclear breakdown complexes, are even less diagnostic, although in cases of relatively high symmetry use of isotopic substitution can provide information about molecular symmetry. The problem of strong background absorptions from the support can be troublesome, but can be minimised by prudent choice of support material and high catalyst loadings. The advent of Fourier transform infrared spectroscopy and microprocessor techniques, allowing spectra subtraction, accumulation and averaging, also permits more detailed identification of vibrations from adsorbed molecules. A final comment is that implicit to characterisation by comparison with solution spectra of model compounds is the assumption that the surface species are isolated with no intermolecular interactions.

1.2.2. Raman Spectroscopy

A distinctive characteristic of a metal cluster is its metal-metal bonds, these are generally highly polarisable and the Raman technique is potentially valuable for determining structures

of supported clusters. Even so the low intensity of the Raman scattering from metal clusters, and the interference of fluorescence by many supports, can make these studies difficult. However the availability of tunable lasers for resonance Raman spectroscopy, and the interfacing of spectrometers with computers, now makes the technique more generally applicable to supported catalysts.

Ultraviolet/visible absorbance and reflectance spectroscopy is also used to determine whether metal-metal bonding is retained, and as a fingerprinting technique.

1.2.3. Nuclear Magnetic Resonance

When applied to solutions, NMR is an extremely powerful tool because the fine details of the spectra (yielding chemical shifts and coupling constants) are very sensitive to molecular structure and conformation. Moreover, selective measurement of spin-lattice relaxation times using Fourier transform techniques allows detailed study of fluxional processes(43). Three obstacles had previously prevented similar high resolution in NMR spectra of solids. These were large dipolar interactions leading to broad resonances, chemical shift anisotropy causing a spread of resonance frequencies for powders, and long spin-lattice relaxation times. However recently a combination of techniques; namely double resonance decoupling, magic-angle spinning(44) and cross-polarization (45) respectively, have been developed overcoming these barriers allowing 'high-resolution' spectra of dilute nuclei to be obtained from solid materials. This should, in principle, furnish both structure determination, and information about mobility, for supported cluster compounds, in a similar fashion to their solution analogues. In anticipation of this exciting prospect, special attention is paid to the ^{13}C NMR features of proposed model compounds in this thesis.

1.2.4. Extended X-ray Absorption Fine Structure

With the availability of synchrotron radiation, and once the methods of data analysis and interpretation are optimised, EXAFS will fulfill its considerable potential for the characterisation

of amorphous heterogeneous systems. Advantages of the technique are that it may be selectively tuned to different elements by appropriate choice of irradiation frequency, no special sample preparation is required, except for low Z elements, and samples can in principle be examined in situ under catalytic reaction conditions. Information on the local enviroment (up to 10Å) of a given element is obtained and this is, of course, particularly relevant to supported metal clusters.

A detailed structure analysis of Wilkinson's catalyst, $[(PPh_3)_3RhCl]$, immobilised on a phosphine-modified polymer has been reported(46). The results revealed that dimerisation takes place on attachment of the free complex, with cleavage of the chlorine bridges occurring upon treatment with hydrogen. Preliminary results also confirmed the structure of $[Ir_4(CO)_{12-x}(PPh_2\text{-}\textcircled{P})_x]$, x=1 or 2(24c).

1.2.5. Miscellaneous

Other spectroscopic techniques with potential include Mossbauer, with obvious application to iron-containing clusters. X-ray photoelectron spectroscopy(XPS) is used to provide valuable information about elecronic states, but the requirement for ultrahigh vacuum and possible sample decomposition in the beam are limiting. Secondary ion-mass spectroscopy(SIMS) is another ultrahigh vacuum technique which should be capable of yielding information on metal cluster/support and metal/support interactions from the observation of metal-support verses metal only mass fragments. The application of magnetic susceptibility measurements and EPR has been mentioned already.

In addition, physical and chemical measurements can supplement this spectroscopic evidence. Elemental analysis of the surface composition is important, but as a bulk technique interpretation of metal/ligand ratios can be misleading, particularly when the support is functionalised prior to contact and mass-transfer limitations can prevent coordination at all the available sites. Temperature-programmed decomposition(TPD) and adsorption experiments can evaluate metal/carbonyl contents, whilst in favourable circumstances the interaction between the complex and

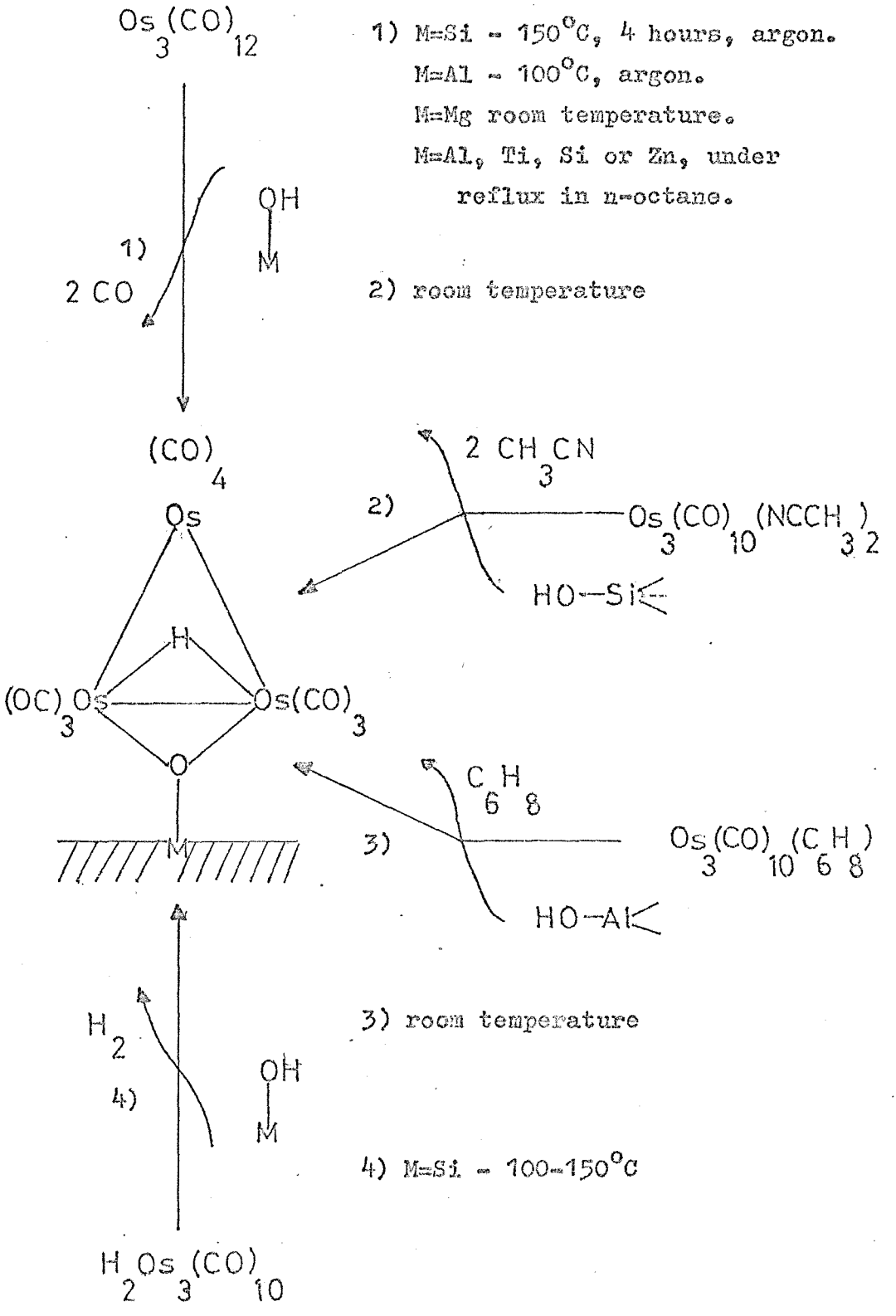
support can be monitored directly by measuring the amount of material displaced (i.e. gas evolution) during the attachment step. The surface nature can the be predicted with some confidence by analogy with known solution chemistry. In some cases the nature of the organometallic species on the surface can be inferred by leaching back into solution, followed by characterisation using 'conventional' methods. This requires the support-to-complex bonding to be weak i.e. ionic, van-der-waal etc., so that negligible perturbation is expected during extraction. This approach has been successfully applied to ionic grafted clusters such as II and $Al^{+}[H_3RuOs_3(CO)_{12}]^{-}$, prepared by heating adsorbed $[H_2RuOs_3(CO)_{13}]$ on alumina under a syngas atmosphere(47), which can be extracted back into solution by metathesis using Et_4NCl and Ph_4AsCl respectively.

1.2.6. Characterisation of $[HOs_3(CO)_{10}(OM)]$

The grafted cluster $[HOs_3(CO)_{10}(OM)]$, M=silica(Ia) or alumina(Ib), effectively illustrates how a variety of these techniques can combine to elucidate a surface structure. In solution $[Os_3(CO)_{12}]$ is known to react with alcohols to form either $[HOs_3(CO)_{10}(OR)]$ or $[Os_3(CO)_{10}(OR)_2]$(48). The surface reaction is probably a similar oxidative addition of silanol groups to an Os-Os bond leading to $[Os_3(CO)_{10}(OSIL)_2]$ or Ia. In agreement with this hypothesis, the correlation between the infrared ν_{CO} spectra of model compounds $[HOs_3(CO)_{10}(OSiR_3)]$, R=Ph or Et, and Ia is quite good(49). Moreover the resolution and sharpness of the bands did not suggest formation of metallic particles covered with carbon monoxide, which only gives two broad bands at 2010 and 1860cm^{-1}(50). However a better correlation apparently existed with the spectra of known dialkoxo-compounds. This uncertainty was overcome by quantitative gas phase analysis during of I by different routes (Diagram 2). When physisorbed $[Os_3(CO)_{12}]$ is thermally decomposed about 2 moles of carbon monoxide per mole of supported cluster is evolved (without any significant traces of H_2, CH_4 or CO_2), but during thermolysis of physisorbed $[H_2Os_3(CO)_{10}]$ only hydrogen was detected by chromatographic analysis. These observations are consistent with the following reactions:-

Diagram 2

Preparation of the Grafted Cluster $[HOs_3(CO)_{10}(OM)]$



1) M=Si - 150°C, 4 hours, argon.
M=Al - 100°C, argon.
M=Mg room temperature.
M=Al, Ti, Si or Zn, under reflux in n-octane.

2) room temperature

3) room temperature

4) M=Si - 100-150°C

$$Os_3(CO)_{12} + H\text{-}O\text{-}Si\equiv \longrightarrow HOs_3(CO)_{10}(O\text{-}Si\equiv) + 2CO$$

$$H_2Os_3(CO)_{10} + H\text{-}O\text{-}Si\equiv \longrightarrow HOs_3(CO)_{10}(O\text{-}Si\equiv) + H_2$$

Further I can be prepared by contacting $[Os_3(CO)_{10}(NCMe)_2]$ with the appropriate support at room temperature. For silica this is accompanied by the evolution of 2 moles of acetonitrile, but on alumina the released acetonitrile is strongly bound to the carrier (as shown by infrared), presumably through interaction with the Lewis acid centres(49). Ib can also be obtained by impregnation of alumina with $[Os_3(CO)_{10}(C_6H_8)]$(51). The known chemistry of these two, lightly stabilised, clusters with HX species under mild conditions strongly pointed to the proposed stoichiometry.

Since Ia is quite stable at room temperature, even in the open air, further characterisation by EXAFS was possible which confirmed that the cluster frame was retained(52). The K^3 Fourier transforms of the EXAFS spectra of Ia and $[Os_3(CO)_{12}]$ were determined; the effect of the phase shift, calculated from the known structure of $[Os_3(CO)_{12}]$(53), was 0.23Å. After correction the average Os-Os nearest neighbour distance is 2.68Å, corresponding to shortening with respect to that of the starting cluster(2.88Å). Although the shape of the EXAFS spectrum did not allow any distinction between the three separate distances, this observation, while small, is consistent with the contraction of the bridged edge in clusters of the type $[HOs_3(CO)_{10}X]$(54). The opposite is true for $[Os_3(CO)_{10}(OMe)_2]$ (55) where an expansion occurs. The Fourier transform did not contain any peak which could be attributed to a second osmium nearest neighbour, in agreement with a lack of aggregation to very small metal particles, and the existence of a molecular species.

A complementary result was obtained from a Raman study on Ib(56). A spectrum was obtained by averaging about 50 scans to provide a suitable signal-to-noise ratio. A strong band was identified at 160cm^{-1}, plus additional features at lower frequencies, which firmly established retention of Os-Os bonding. Comparison with the spectra of $[Os_3(CO)_{12}]$ and $[H_2Os_3(CO)_{10}]$ provided evidence supporting a triosmium cluster as the surface species.

Together these various observations unequivocally characterised the surface species, although this could not be deduced

from each of them separately in isolation.

1.3. The Anchoring of Metal Clusters to Phosphine-functionalised Silica

1.3.1. The Silica Surface

Conventionally silica gel is made by mixing aqueous solutions of sodium silicate and sulphuric acid. Molecules of silicic, disilicic and trisilicic acid are formed which polymerise by condensation of silanol groups ($\geq$Si-OH) to form siloxane ($\geq$Si-O-Si$\leq$) linkages. This stage gives a colloidal solution of spheroidal particles of polysilicic acids, in turn these hydrosol particles aggregate into chains and networks to produce silica gel. The nature of its highly porous structure is much dependent on the method of preparation and dehydration. Direct drying results in collapse of the original, very open, texture, through the mechanical force of retreating water menisci in the pores, until the strength of the agglomerated particles becomes sufficient to resist further shrinkage. This product with a reduced internal surface is known as a xerogel. The contraction can be minimised by either replacing the water with another liquid of lower surface tension before drying, or by removing water vapour at a temperature above its critical point (aerogel).

Such preparations leave the gel relatively pure, but it does contain Na^{+}, Ca^{2+}, Fe^{3+}, Ti^{4+} and Al^{3+} at levels of 0.01 to 0.05% each. In particular, the Al^{3+} impurity can significantly alter the surfaces otherwise catalytically inertness by introducing Lewis sites(57). A much higher purity grade is made by the flame hydrolysis of silicon tetrachloride, to give a non-porous, finely divided silica powder (e.g. 'Cabosil','Aerosil') having a particle size in the region of 40-5nm diameter, with specific surface areas in the range 50-400$m^2.g^{-1}$. This is ideal as a catalyst support because there are no concessions necessary to rates of diffusion in and out of a pore structure. With the vast bulk of the silanol groups on the surface(58) they are readily accessible, and the small particle size/large surface area also impart favourable characteristics to allow infrared studies of adsorbed carbonyl

species. Accordingly the Degussa grade 'Aerosil 200', BET surface area $200m^2.g^{-1}$ and average particle diameter of 12nm, was chosen throughout the bulk of this study.

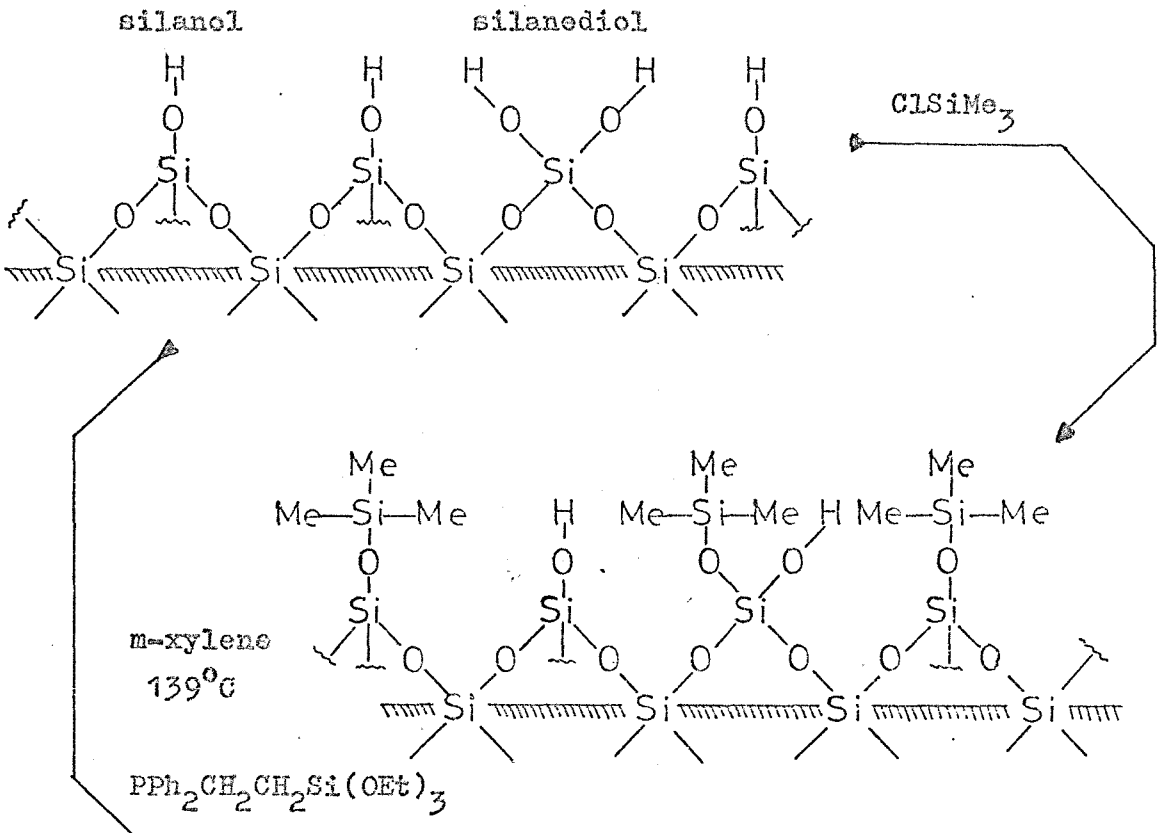
Dehydration of a maximally hydroxylated silica at about 100-150°C, in vacuo, removes only physically adsorbed water, while heating above this temperature results in progressive loss of chemically bound hydroxyl groups. Considering only the surface, infrared spectroscopy identified the presence of at least two types of silanol groups. A broad band around $3400cm^{-1}$ due to surface water disappears at 100°C to leave two features at $3700cm^{-1}$, assigned to 'free' silanol groups, and another at about $3550cm^{-1}$ attributed to perturbed hydroxyl groups, believed to be bound by a mutual hydrogen bond(58). The combination of MAS/CP provides ^{29}Si NMR spectra with a high degree of structural resolution, while the nature of the cross-polarisation experiment, in which ^{29}Si spin polarisation is derived from the proton-spin resevoir, makes it ideal to study surface silicon atoms because it discriminates against silicon nuclei in the interior of a silica particle because of the prohibitively long distances to the available (hydroxyl) protons. Three resonances were observed(59) corresponding to surface silicon atoms with four siloxane attachments (interconnecting lattice sites), three siloxane bonds and one hydroxyl group (silanol sites), and atoms with two siloxane bonds and two hydroxyls (silanediol sites). The last set represent the 'perturbed' groups, but various NMR considerations militated against the alternative interpretation of hydrogen-bonded pairs. Based on this data is the hypothetical surface segment shown in Diagram 3.

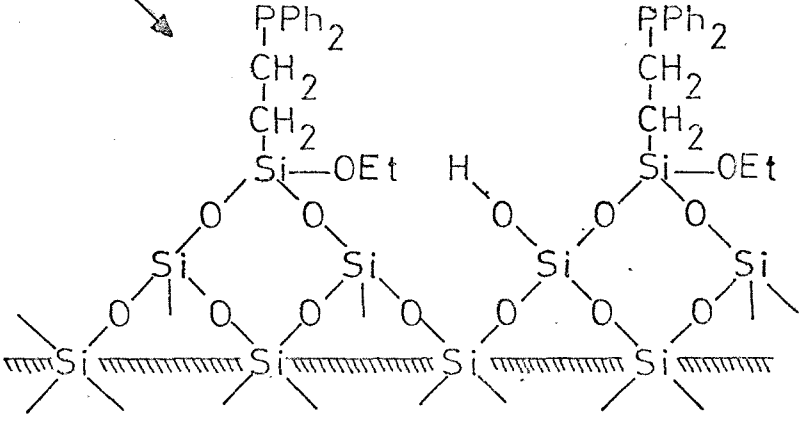
A number of procedures(3) indicated that a well hydrated surface prepared by dehydration at 150-200°C has a concentration of chemically bound hydroxyls of about $5nm^{-2}$. This prompted DeBoer and Vleeskins(60) to propose a model based on the 111 face of crystalline β-cristobalite, where hydroxyl groups are separated by about 5Å and arranged in a hexagonal array that corresponds to a density of $4.55nm^{-2}$. Hockey(61) further developed this model by postulating that higher observed densities on untreated silicas arose from lattice defects giving additional geminal and single hydroxyl sites. Dehydration then proceeds by ready condensation of these close proximity features to give the regular β-cristobalite

Diagram 3

The Silica Surface and attachment of Bifunctional Ligands

Hypothetical segment of a dehydrated Silica surface

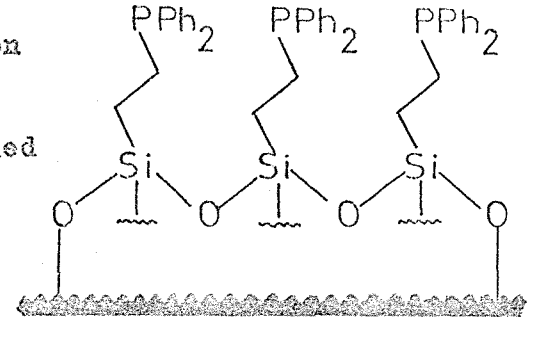




SURFACE STRUCTURE OF $PPh_2CH_2CH_2SIL$

i) Anhydrous preparation

ii) Effect of water contamination forming possible island distributions with cross-linked polysiloxane networks.



surface. Its limitations include no concession to the known presence of spacially adjacent (vicinal) pairs, or a feasible explanation to the much lower densities (ca. 1 OH per nm^{-2}) measured for highly dehydrated surfaces. The alternative model of Peri and Hensley(62) is based on the 100 face having a geminal pair connected to each silicon on the virgin surface (7.9 per nm^2). Whilst inconsistent with the true nature of a fully hydroxylated silica, it does predict that initial dehydration occurs by random condensation of groups along the surface rows to give vicinal pairs, but suffers from no clear mechanism allowing formation of isolated silanols.

Niether model is entirely consistent with spectroscopic detail, CP/MAS(63) and infrared(58), from dehydration/rehydration experiments. These show a preferential decrease of the silanediol population up to 400°C until a plateau is reached, where they are presumably too isolated to allow continued condensation by the mechanism suggested by Peri(62). Above 400°C the isolated silanols progressively disappear, so that typically at 500°C the hydroxyl concentration is 20-30% of the saturated value. At very high temperatures (> 700°C) further elimination of geminal sites occurs. From here rehydration is practically non-existent, probably because the siloxane bonds being hydrophobic(64) offer very improbable sites for the initial specific adsorption of water, which may instead occur at the limited number of remaining uncondensed hydroxyl groups. Thus the surface of silica appears quite heterogeneous containing segments resembling both the 111 and 100 faces of cristobalite i.e. a combination of the two models.

The surface silanol group is weakly acidic with a pK_a in the vicinity of 9 and can act as a weak acid ion exchanger(65). No Lewis acid behaviour is displayed provided the silica is pure. It forms strong hydrogen bonds to water, alcohols, ethers etc. and weak ones even to olefins and benzene; a phenomenon utilized in separations and chromatography. In addition, they undergo a variety of other reactions(66) and can be replaced by the passage of MeOH, CCl_4 or $SOCl_2$ over the silica. The chloro-silica is very reactive, in the same manner as chlorosilanes in general. Indeed a variety of chlorosilanes and related hydrolysable materials, i.e. $ClSiMe_3$, $ClSiMe_2{}^tBu$(67) and $Me_3SiNHSiMe_3$, have long been used as silylating

agents to decrease the polarity of siliceous supports in gas chromatography, producing a lipophilic organic surface. An infrared study with trimethylchlorosilane(58) testified that it is impossible to coat the surface entirely with chemically grafted $-SiMe_3$ groups, and minor defects remain in the modified layer. Practically all the free silanol groups reacted, and it was the silanediols which constituted the remaining groups. With octyldimethylchlorosilane(68), predrying the silica to $> 400^{\circ}C$ minimized their concentration leaving mainly free hydroxyl groups, the reactive ones in the silanizing procedure. This allowed an octyl-silanized silica with only a minor residual hydroxyl content to be prepared. A recent CP/MAS ^{29}Si NMR investigation(69) complimented these results with the appearance of a strong resonance at approximately 100ppm downfield from the silica region, corresponding to the attached $-SiMe_3$ moiety. Differences in the higher shielded area are interpreted as shown in Diagram 3. A geometrical factor preventing both geminal groups from reacting is self evident.

1.3.2. Surface Modification with Bifunctional Ligands, Preparation of $PPh_2CH_2CH_2SIL$

The last reference also contained detail of the interaction with Cl_2SiMe_2 and Cl_3SiMe, where the possibility of multibonding to the surface and siloxane oligomerization exists. These examples conveniently introduce the option of covalently attaching ligand groups to inorganic surfaces. Of the several ways available(70), the most preferred method involves using compounds of the type $RSiX_3$, where R is an organofunctional group and X is a readily hydrolysable group i.e. Cl, OR, OCOR etc. It gives a strong Si-C bond ($\simeq 70 kcal.mol^{-1}$) at the surface which is hydrolytically and thermally stable because of its crosslinking, it is also a one step synthesis that is simple to carryout under mild conditions. In principle any ligand that forms part of an organic molecule can be introduced into the organofunctional group and hence chemically bonded to the silica surface. As tertiary phosphine derivatives of metal clusters tend to be relatively stable, through the π-acidity of the ligand stabilising the zero oxidation state, it was decided to use these as the liganding function. Principally diarylalkyl-

phosphines are employed, preparation of a triarylphosphine ligand-silica is more difficult, but can be accomplished by hydrosilylation of a double bond in a substituted triarylphosphine(70).

Such bifunctional silylalkylphosphine molecules, $PR_2(CH_2)_nSiX_3$, with controlled chain lengths $n>4$, can be prepared by a two step synthesis devised by Oswald, Murrel and Boucher(71). The first step involves silane, X_3SiH, addition to a α,ω-diene in the presence of $K_2[PtCl_6]$ or palladium catalyst. An excess of diene limits formation of α,ω-alkylene bis-silane, similarly low temperatures prevent isomerisation leading to major quantities of the relatively unreactive, internally unsaturated, alkenyl-silane mono-adducts. The second stage to incorporate a secondary phosphine occurs by a free radical mechanism first reported by Niebergall(72). Competing side reactions are suppressed by working under mild conditions, at 15°C with ultraviolet light initiation. Both additions occur in an anti-Markovnikov manner. The shorter chain n=2 or 3 compounds can be prepared directly from commercially available vinyl and allyl-silanes. Alternatively the propyl derivative is prepared by adaption of Issleib's procedure(73), either by reaction of $Cl(CH_2)_3Si(OMe)_3$ with $HPPh_2$ in the presence of sodium hydride(74), or by first anchoring to give a chloropropyl-silica, silylating remaining silanol groups to prevent side reactions, and then contacting with $KPPh_2$ to form the ligand-silica in situ(70). In this study 2-(diphenylphosphino)ethyltriethoxysilane was chosen because the ethoxy groups make handling easier, being less hydrophilic than chlorosilanes, and together with a short chainlength they favour selectivity towards mono-substituted carbonyl adducts. Prepared from triethoxyvinylsilane and $HPPh_2$, it was characterised by spectroscopy and recorded boiling point. A detailed NMR analysis for all elements exists(75), showing that the presence of an ethoxy group in the homologous series $(EtO)_n(Me)_{3-n}Si(CH_2)_2PPh_2$ has a profound effect on the ^{31}P chemical shift, assigned to a direct interaction between phosphorus and oxygen atoms. The product's viscosity at room temperature has also been attributed to (inter-) molecular associations(71).

Covalent anchoring to silica, of all but the trichloro-ligand silanes, is slow at room temperature and is conveniently carried out in a boiling arene solvent, typically m-xylene, using

a Dean and Stark apparatus to allow withdrawal of the condensation products. Normally the silica is dehydrated to remove physisorbed water and reduce the silanediol concentration. The importance of the first action is disputable. With a totally anhydrous material the phosphino-silane could only react with silanol groups leading to individual linking of all molecules to the surface. In the presence of water the Si-X can hydrolyse to Si-OH which can condense either as above or with the silanol of another molecule to give a cross-linked linked polysiloxane network with few chemical bonds to the silica(76). This would give islands of high phosphine density and elemental analysis would not be representative of the micro-enviroment. However Murrell(77) provided evidence that with a sufficient excess of phosphino-silane the same extent of coverage results, corresponding to a monolayer, independent of the degree of dehydration. Polymerisation undoubtedly occurs, but the formed polymers are apparently too sterically constrained to undergo reaction with the surface silanol groups, and are readily removed by Soxhlet extraction. However an alternative method of phosphinating the silica, by hydrolysis of the linking agent in the presence of hydrochloric acid(74), must result in attached polymers. Intermediate structures are probably formed in most cases.

The extent of covalent bonding is difficult to quantify. A recent attempt(78) to gain clarification involved contacting with aminopropyl-silanes. At room temperature subsequent treatment with salicylaldehyde in EtOH gave the salicylaldimine chromophore detected on the surface, and in solution through EtOH solubilising all hydrogen-bonded species. The limited number of covalent bonds initially formed being proportional to the value of n (the number of ethoxy groups originally present). To a degree this progression is lost after oven curing at 80°C when the majority of bonds are of a covalent nature. The still marked increase in stability for n=2 or 3 is indicative of multiple covalent bonds to the surface, but is complicated by postulated oligomerisation from concentrated solutions. Other results(65,77) indicate that for $RSiX_3$ at least one hydrolysable group does not react with the surface, owing to steric limitations, and dianchored ligands predominate. This provides a method of gauging the surface concentration of attached phosphine groups by varying the anchoring functionalities. A study on the

$PPh_2(CH_2)_2SiX_3$ system(77) showed that, after 6 hours at 140°C in xylene, the extent of coverage on a previously dehydrated silica was X=Cl>OMe>OCOMe≥OEt. Further, the amount of covalent anchoring for the ethoxy group was not time or temperature limited. This trend is the inverse of the steric requirements of the silyl groups which control the saturated coverages, and not the more bulky phosphine tail. This represents a second advantage of using ethoxy groups if multisubstitution is to be avoided.

The length of the alkylene chain is also conceptionally important. The catalytic activity of the heterogenized species derived from $[RhCl(COD)(PPh_2(CH_2)_nSiX_3)]$, for hydroformylation of propylene, has been studied as a function of chain length, n=2 or 8(79). For X=OEt only a marginal difference, in favour of the dimethylene derivative, was seen whereas with X=Cl, for n=2 the compound was inactive, yet the octamethylene species had comparable activity to the ethoxy derived derivative. This was equated with poisoning by residual chlorine through the close proximity of the metal centre to the surface, avoided with the longer chain. Chain length can also be used to tailor the stereochemical and electronic enviroments of a metal atom. A long and flexible chain will have a high degree of freedom and react as would the unanchored phosphine to form the most stable metal complex, whereas a short chain, in association with the surface rigidity, can be utilized to isolate thermodynamically unstable species; i.e. monomers which dimerise in solution, or monosustituted adducts which would otherwise undergo further substitution.

In view of the current objectives, both considerations are best met by heterogenisizing $PPh_2CH_2CH_2Si(OEt)_3$. In theory this can be augmented by reducing the coverage to less than a monolayer, increasing the intermolecular separation, but this approach suffers from the inhomogeneity of the surface with groups randomly distributed having no fixed distance between pairs. The required ligand-silica, $PPh_2CH_2CH_2SiL$, was prepared by reacting 'Aerosil 200' , previously dried in vacuo at 145°C, with a large excess of freshly distilled $PPh_2CH_2CH_2Si(OEt)_3$. Optionally the remaining accessible silanol groups were silylated with $ClSiMe_3$. By this technique elemental analysis showed the phosphorus content to be $0.287 mmol.g^{-1}$. Since the surface area of the parent silica is

$200m^2.g^{-1}$, this translates to an average of 0.93 phosphine groups per nm^2, based on the formula- $2.87x10^{-4}/200\{1-(2.87x10^{-4}$xMW of $PPh_2CH_2CH_2SiOEt)\}$(74). This figure is reproducible and similar to the loading achieved by other workers(80). Further characterisation has been sort, weak infrared absorptions attributed to the organofunctional group have been identified(74), and a resonance at δ-8.6 is seen in the solid-state ^{31}P NMR spectrum(81).

1.3.3. Possible Routes for Preparing Phosphine-immobilised Metal Clusters

There are two basic strategies for heterogenizing Group VIII metal clusters to inorganic supports through a phosphine linkage (Diagram 4). The first (SCHEME ONE) involves formation of the heterogeneous complex from the ligand-silica by the same methods used for ligand-polymers, principally ligand exchange or association reactions. One novel variation involves the in situ formation of $[Ir(CO)_{11}-(P)]$ on a dilute phosphinated polystyrene by reduction of [Ir(CO)Cl(p-toluidine)] with zinc(82), in the presence of a good swelling agent(83). It was shown to be active as a catalyst for ethylene(84) and cyclohexene(85) hydrogenation, but suffering decarbonylation and aggregation above 100°C. However, since the reaction with the surface takes place under relatively mild conditions, and does not involve the ligand donor atom, there exists the second option of forming an homogeneous cluster derivative with the bifunctional ligand prior to application to the surface (SCHEME TWO). Both approaches have certain merits and drawbacks, which tend to be complementary.

The main advantages of SCHEME ONE include:-

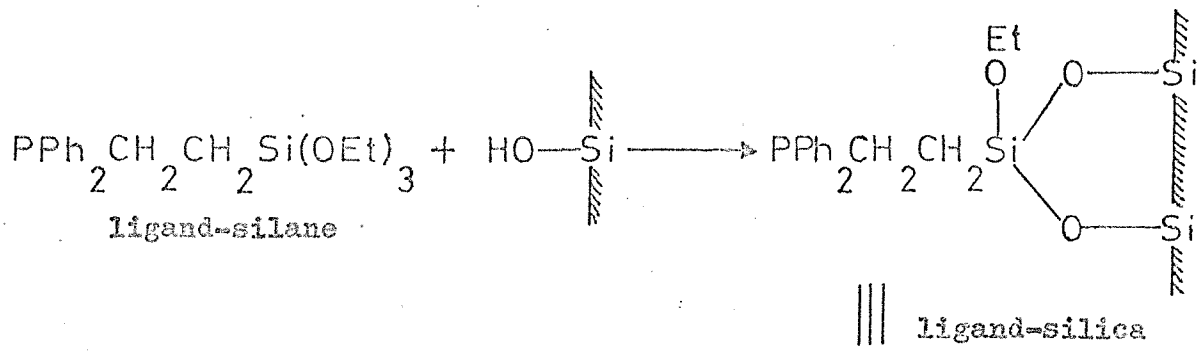
i) As mentioned already, the surface rigidity can allow isolation of species unstable in solution because the opportunity for intermolecular interactions is greatly reduced.

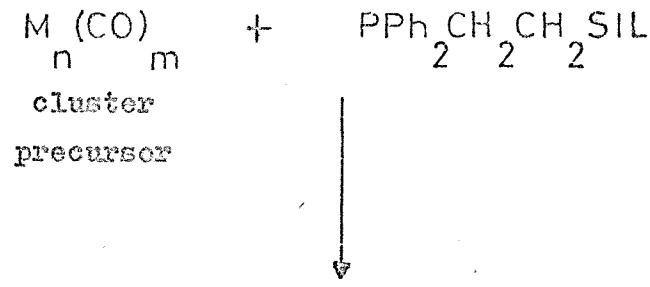
ii) The surface properties of the ligand-silica may be altered prior to reaction with a sensitive metal centre. After attachment of the ligand-silane the remaining, accessible silanol groups can be removed by silylation to produce a lipophilic organic layer. This reduces side reactions with the silica base and makes it possible to control the microenviroment

Diagram 4

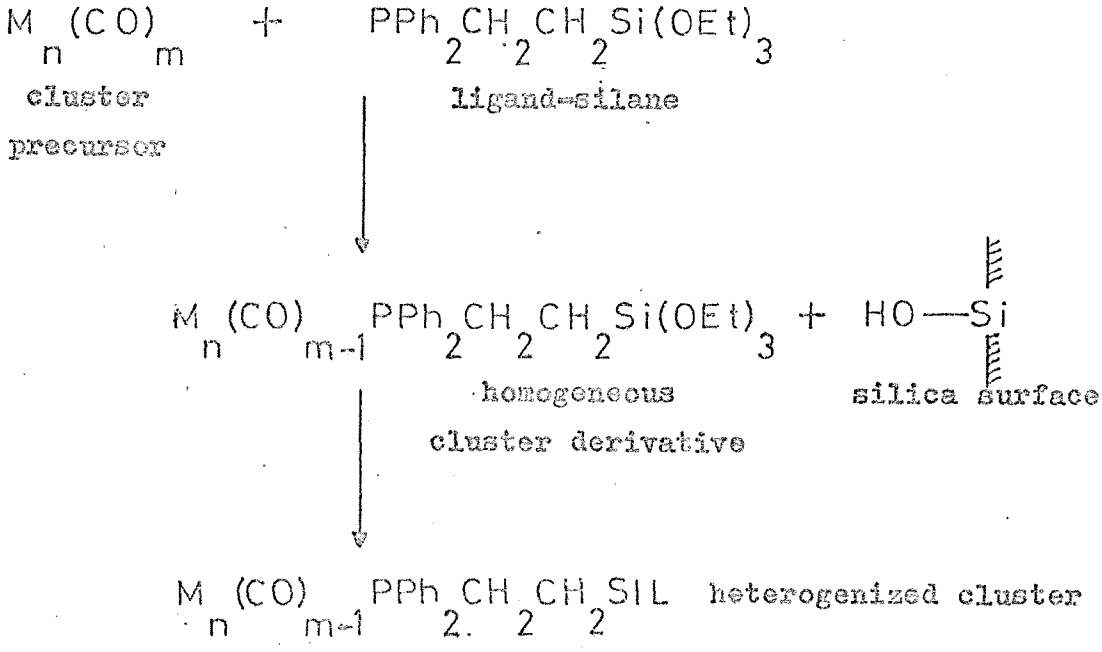
Basic Strategies for tethering Metal Clusters to a Phosphine-functionalised Silica Surface

SCHEME ONE





SCHEME TWO



at the metal centre.

Both these properties are exploited to shift the product distribution from thermal treatment of $[Ru_3(CO)_{12}]$ with phosphines away from the normally, heavily weighted, tris-substituted product.

iii) It is possible to extend the range of liganding groups by standard organic reactions of organofunctional groups attached to the surface, that are not applicable to the $RSiX_3$ species.

Its major disadvantage is that, although rigid, the surface distribution of phosphines is non-ordered. This makes it almost impossible to specifically tailor to the particular requirements of a certain complex, and non-selective reactions in solution are to an extent reproduced on the surface. This can be avoided by modelling syntheses to give selective tethered products, used to a premium in preparing $[H_2Os_3(CO)_{10}(PPh_2CH_2CH_2SIL)]$ and $[Os_3(CO)_{11}(PPh_2CH_2CH_2SIL)]$. However this still leaves certain pitfalls, not least the presence of remaining, sterically inaccessible, ligand-silica groups which only become manifest in subsequent studies (pyrolysis or catalysis).

The main advantages of SCHEME TWO are:-

i) Separation and characterisation, by standard techniques, of a discrete complex is possible, even where direct reaction of the ligand-silica with the complex precursor would give a mixture of products.

ii) The ligand to metal ratio on the surface can be controlled.

Again a series of qualifications exist:-

i) The preparation and separation must be under scrupulously anhydrous conditions owing to the hydrolytic reactivity of the silyl functionality. Thus purification by conventional t.l.c. is limited to only non-hydroxylic phases, although the advent of flash chromatography(86) has relieved this restriction(87). Similarly, greater attention to dehydrating the silica surface prior to attachment is necessary if concentrated complex-containing polymers are to be avoided.

ii) Consideration of the homogeneous complex's stability under the conditions of linking is required.

Caution is expressed regarding attachments at room temperature (87) where adsorption through hydrogen-bonding will predominate, and the number of direct covalent bonds must be limited. Also the complex might be susceptible to reaction with the liberated condensation products.

iii) The increased bulk of the chemisorbed complex makes it more difficult to successfully silylate the remaining silanol groups. Their continued presence can affect the stability of the heterogeneous complex in subsequent reactions, even during tethering precautions, e.g. applied carbon monoxide atmospheres(87), can be necessary to avoid decomposition.

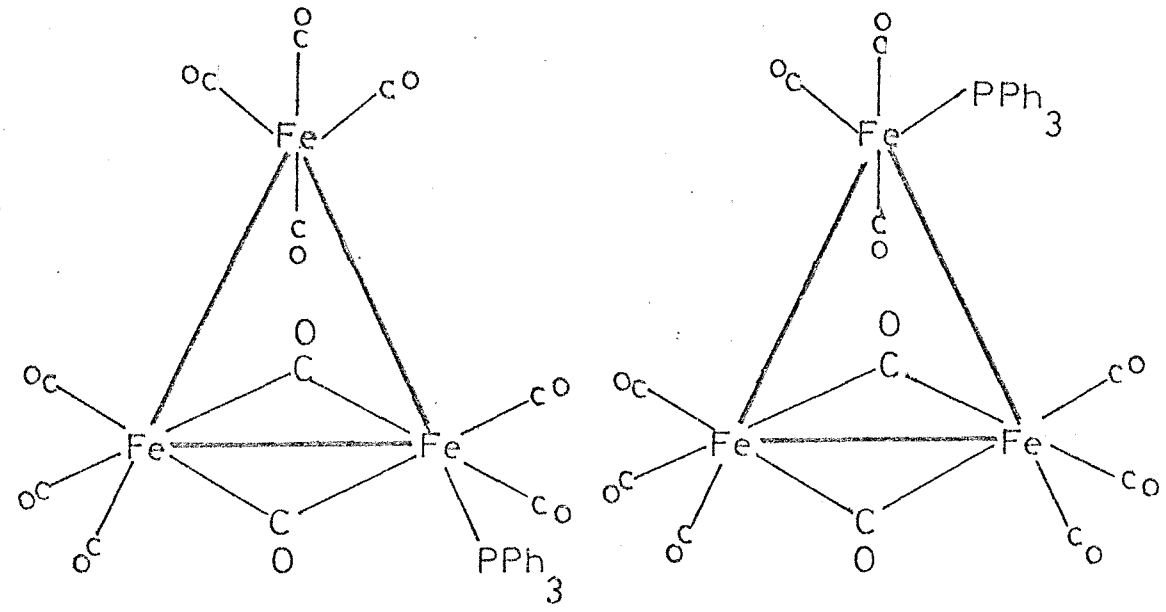
In the following sections, for the chosen targets, SCHEME ONE offered the greater advantages. However, because of its nature, an unadsorbed reference analogue was prepared using PPh_2Et and thoroughly characterised by conventional spectroscopic techniques. Then the integrity of the anchored cluster is confirmed by fingerprinting against this data. Ethyldiphenylphosphine was made by the action of ethylgrignard on diphenylphosphinouschloride(88).

1.4. Preparation and Characterisation of $[M_3(CO)_{12-n}(PPh_2CH_2CH_2SiL)_n]$. (M=Os, n=1; M=Ru, n=1-3)

1.4.1. Ligand Substitution Reactions of $[M_3(CO)_{12}]$

Ligand substitution represents a major branch of cluster chemistry. In these reactions the marked increase in strength of metal-metal bonds upon descending a column in the periodic table is emphasized. With a variety of monodentate nucleophiles $[Ru_3(CO)_{12}]$ and $[Os_3(CO)_{12}]$ both give a series of derivatives $[M_3(CO)_{12-n}L_n]$, n=1-4, with the cluster triangle retained, whilst only in a few cases, using very mild conditions, is this possible with $[Fe_3(CO)_{12}]$. Thus at 70°C in THF it reacts with PPh_3 to produce a mixture of the mononuclear complexes $[Fe(CO)_4(PPh_3)]$ and $[Fe(CO)_3(PPh_3)_2]$(89). However, under milder conditions at 45°C in chloroform, $[Fe_3(CO)_{11}(PPh_3)]$ is isolable, albeit in only a 2% yield and still accompanied by the breakdown products(90). The crystal structure showed that it is structurally similar to the parent cluster, but existing as a mixture of two isomers with the phosphine equatorially

attached to different iron atoms(91). A more comprehensive range



Structural isomers of $[Fe_3(CO)_{11}(PPh_3)]$

of monosubstituted phosphine, and phosphite, derivatives are obtained by dropwise addition of a diluted solution of the appropriate ligand to $[Fe_3(CO)_{12}]$ in benzene at 50°C(92), although yields were still relatively low (3% for PPh_2Et). The observed differences across the solid-state and solution infrared ν_{co} spectra was interpreted as representing a spread of preferred isomeric forms encompassing both those found by crystallography and also non-bridged forms. This reflects the dynamic nature of the molecules, due to a relatively flat potential energy surface over all configurational space between bridged and non-bridged structures. By careful control of conditions disubstituted and trisubstituted products can also be isolated, $[Fe_3(CO)_9(PPhMe_2)_3]$ was recovered as glistening black needles and a structural analysis carried out (93). Each phosphine is bonded to a separate iron atom in the positions found in the two isomers of $[Fe_3(CO)_{11}(PPh_3)]$. Apart from these examples only isocyanides give straightforward substitution products by reaction of two equivalents, in CH_2Cl_2 at room temperature, to give the mixture $[Fe_3(CO)_{12-n}(CNR)_n]$, n=1-3; notably $[Fe_3(CO)_{11}(CNBu^t)]$ was isolated in a 15% yield. Greater isocyanide concentrations gave larger proportions of the more highly

substituted derivatives but, along with higher temperatures, tended to give more mononuclear products(94). Other workers reported similar results but expressed difficulty in preparing the trisubstituted derivatives(95).

The greater metal-metal bond strength for ruthenium clusters makes trinuclear derivatives relatively easy to prepare. This has allowed kinetic investigations to be carried out on several systems which were found to obey the rate law:-

$$\text{Rate} = k_1[\text{cluster}] + k_2[\text{cluster}][\text{ligand}]$$

The two terms are ascribed to a dissociative unimolecular and an associative bimolecular mechanism respectively. The ligand independent step is usually a carbon monoxide dissociative process. Work on Group VIIIb $[M_4(CO)_{12}]$ systems(96) has focused on this being either electronically or sterically induced. The electronic factor could be akin to cis-labilisation in mononuclear complexes (a transition-state phenomenon). This requires carbon monoxide loss from a prior phosphine-substituted metal centre, but steric crowding prevents the incoming ligand occupying the empty coordination site. Instead the unsaturation is transferred by a bridging carbonyl to a second, unsaturated centre which then undergoes substitution. The sterically induced process depends on the whole cluster framework dictating spatial confrontations between ligands, Its only requirement is that the ligand to be dissociated is in close proximity to the previously substituted metal centre, not necessary at the same metal centre as is required by cis-labilisation arguements. An increased lability towards further dissociative-substitution for $[Ru_3(CO)_{12-n}(PPh_3)_n]$, n=1 or 2, over the parent cluster similarly exists(97). A linear free energy relationship has been found(98) for substitution of $[Ru_3(CO)_{12}]$ by PR_3 relating k_2 with the phosphine basicity indicating considerable Ru-P bond formation in the transition-state for the bimolecular path. The transient $[Ru_3(CO)_{12}(PR_3)]$ is predicted to contain only two Ru-Ru bonds. In this system a fine balance exists between substitution and cluster breakdown, and where R=Bu^n Mechanism One (Diagram 5) has been proposed(99) to account for the kinetics and the nature of the products.

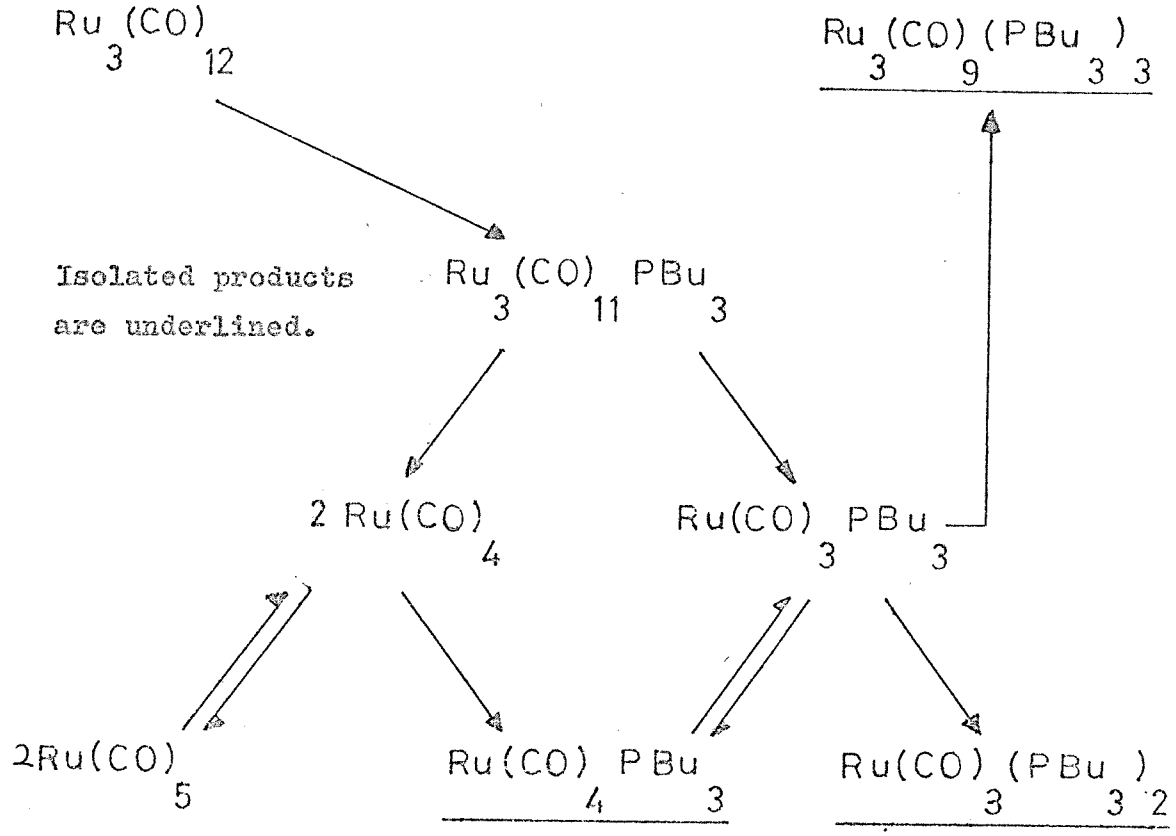
Along with a preliminary investigation(100), these kinetic studies inferred that formation of $[Ru_3(CO)_{11}L]$ is the

Diagram 5

Synthesis of Phosphine-substituted Derivatives of $[Ru_3(CO)_{12}]$

Mechanism One

Cluster fission/recombination route with tributylphosphine.



Mechanism Two

Radical anion pathway to Lewis base substitutions.

$$[Ru_3(CO)_{12}] + Ph_2CO^{\bullet -} \longrightarrow [Ru_3(CO)_{12}]^{\bullet -} + Ph_2CO$$

$$[Ru_3(CO)_{12}]^{\bullet -} + L \longrightarrow [Ru_3(CO)_{11}L]^{\bullet -} + CO$$

$$[Ru_3(CO)_{11}L]^{\bullet -} + [Ru_3(CO)_{12}] \longrightarrow [Ru_3(CO)_{11}L] + [Ru_3(CO)_{12}]^{\bullet -}$$

rate-limiting step, with the reaction proceeding to $[Ru_3(CO)_9L_3]$ without isolation of the mono- and di- substituted derivatives. For $R=Bu^n$ this occurs via degradation to mononuclear species followed by recombination. Contrary to this evidence, others(101) managed to isolate and characterise $[Ru_3(CO)_{12-n}L_n]$, n=1 or 2 (L=tertiary phosphine or arsine), plus a tetrasubstituted complex with L= $PPh(OMe)_2$, by using chromatography instead of the crystallisation previously employed. Thus $[Ru_3(CO)_{11}(PPh_3)]$, IIIa, was obtained in a 16% yield by thermal activation in n-hexane, whilst in smaller quantities by photolysis(102). The second route gave $[Ru(CO)_4(PPh_3)]$ and $[Ru(CO)_3(PPh_3)_2]$ as the major products, their observed stoichiometry supported intermediate formation of IIIa which then undergoes metal-metal bond fission(103). Other undedecacarbonyl derivatives were reported from carbon monoxide induced fragmentation of $[H_2FeRu_3(CO)_{12}(PPhMe_2)]$(104), a side product from reaction with $[Pt(PR_3)_4]$(105), or selectively with the more exotic ligand $[:CNRCH_2CH_2NR]_2$, L_2,(106). In contrast to this preference for multisubstitution with phosphines, reaction with a molar equivalent of t-butylisocyanide gave good yields of $[Ru_3(CO)_{11}(CNBu^t)]$, IV, as the only significant product(94, 107). Greater proportions of ligand yielded the higher substituted derivatives. Both IIIa(102) and IV(107) have been the subjects of detailed single crystal X-ray diffraction studies, the molecular structures are based on that of the parent carbonyl but with the substituents equatorially and axially positioned respectively.

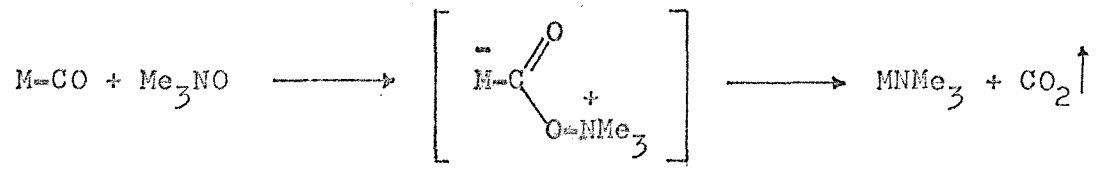
The recent advent(108) of a radical-catalysed pathway now enables selected degrees of substitution to be achieved across the iron triad for M_3 and M_4 clusters. This technique is particularly successful for ruthenium allowing IIIa and IV to be prepared in approximately 80% yields without recourse to chromatography. Typically, a mixture of the cluster carbonyl and the stoichiometrically required amount of ligand are dissolved in THF, and treated dropwise with a solution of sodium diphenylketyl until reaction is complete. The proposed chain mechanism (Mechanism Two, Diagram 5) involves the radical anion $[Ru_3(CO)_{12}]^{\bullet -}$, where the extra electron is in the Ru-Ru antibonding orbital. This causes cleavage of the weakened bond giving a 17e centre which readily undergoes ligand addition with concommitant elimination of carbon

monoxide. Reformation of the Ru-Ru bond gives $[Ru_3(CO)_{11}L]^{\bullet-}$ which rapidly transfers an electron to $[Ru_3(CO)_{12}]$ to continue the catalytic cycle. This has opened up a rich vein of ruthenium cluster chemistry with simple donor ligands, with the possibility of sequential incorporation of different ligands i.e. formation of $[Ru_3(CO)_9(PMe_3)(PPh_3)(P(OMe)_3)]$(109). With bidentate ligands, e.g. $PPh_2CH_2CH_2PPh_2$, variations in catalyst and component concentrations can result in $[Ru_3(CO)_{11}]_n(PPh_2CH_2CH_2PPh_2)_n$, n=1 or 2, with the latter containing two linked monosubstituted cluster triangles(110).

Retention of cluster integrity had never posed a problem for substitution on $[Os_3(CO)_{12}]$. The major difficulty was the actual reluctance to undergo these ligand-exchange reactions, which necessitated either thermal or photochemical ejection of carbon monoxide leading to a non-selective distribution of products, or total conversion to the trisubstituted derivative. Thus reaction with excess PPh_3, in xylene under reflux, gives good yields of $[Os_3(CO)_9(PPh_3)_3]$(111). The corresponding mono- and di-substituted derivatives were first isolated as side-products from reaction with $[(PPh_3)AuCl]$(112). Mixtures of all three derivatives $[Os_3(CO)_{12-n}L_n]$, (n=1-3, L=PPh_2Me, $PPhEt_2$ and PEt_3) were later obtained by direct reaction with phosphine under the slightly less severe conditions of heating to reflux in toluene(113). Variations on this technique provided the monosustituted derivatives, L=PMe_3, PEt_3(114), $PPhMe_2$, $AsPhMe_2$(115), $AsMe_2(CH{=}CH_2)$(116) and $AsMe_2(C_6H_4Me)$(117), used for pyrolysis studies in the absence of a more selective method of preparations. Similar conditions, or even refluxing n-heptane(118), permitted isolation of the isonitrile analogues, $[Os_3(CO)_{12-n}(CNR)_n]$, n=1-4, although in this case the product distribution could be engineered to some extent by varying the ligand excess(119).

The possibility that these complexes could be prepared under milder conditions was highlighted by the room temperature reaction with $[Pt(PPh_2Me)_4]$ to give $[Os_3(CO)_{12-n}(PPh_2Me)_n]$, n=1 or 2, as the only products(105). However, the synthetic breakthrough came with the identification of several lightly stabilised derivatives $[Os_3(CO)_{12-n}S_n]$, n=1 or 2, where S is a good leaving group. These act as potential sources of vacant coordination sites since the weakly bound ligands are easily displaced by a variety of nucleophiles and small molecules (Diagram 6). In particular,

$[Os_3(CO)_{11}(NCMe)]$ has been widely exploited as a useful intermediate in the preparation of undecacarbonyl adducts(120). It is isolated from the action of trimethylamine-oxide on $[Os_3(CO)_{12}]$, in the presence of acetonitrile(121). The carbon monoxide is removed as carbon dioxide, and the mechanism of oxidation is considered to involve the nucleophilic addition of NMe_3O on the coordinated

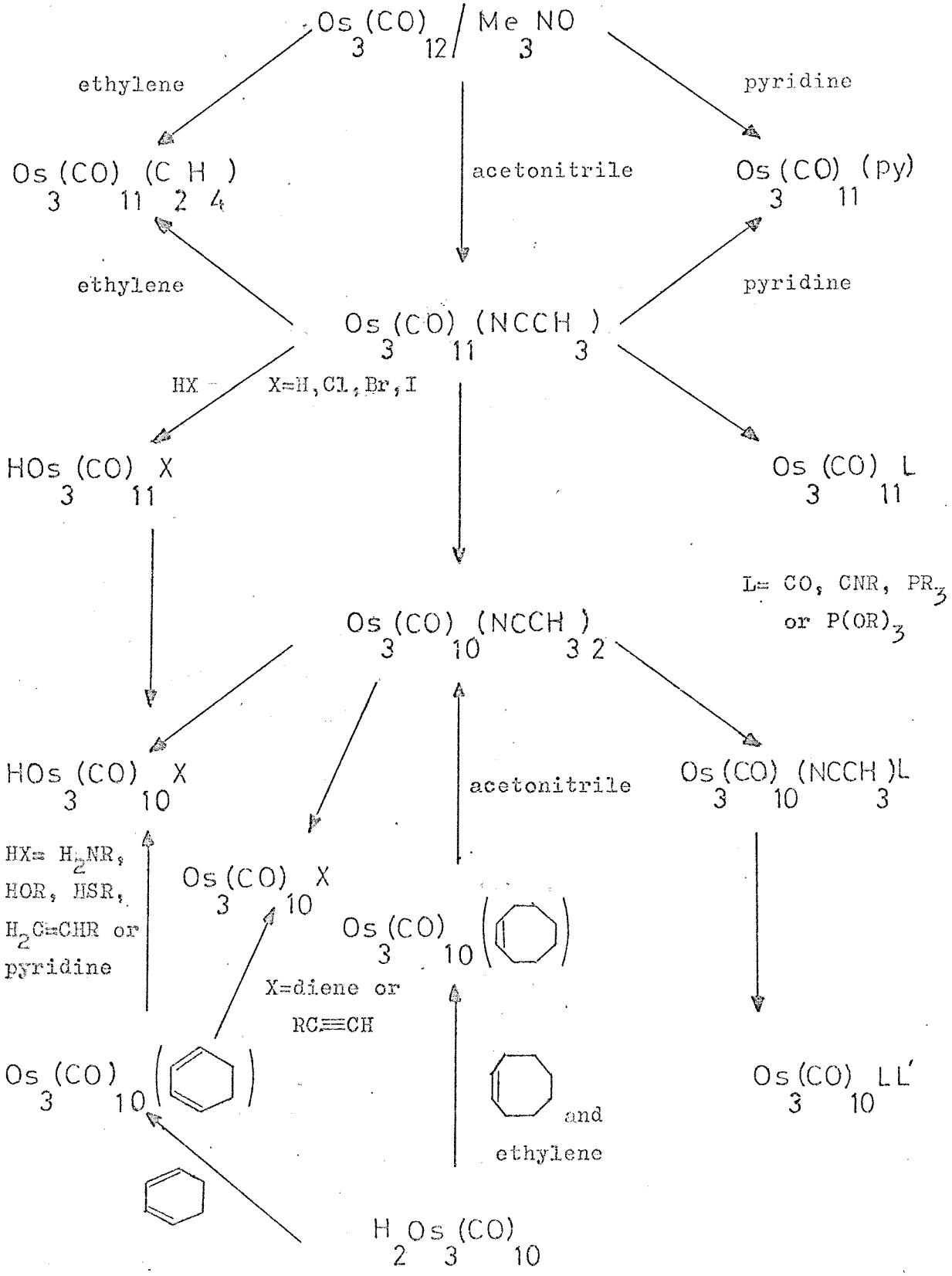


carbonyl ligand. Due to the low coordination ability of the NMe_3 generated, because of its large bulk and high steris restraints, the acetonitrile present in situ successfully competes for the coordination site. In some cases, i.e. ethylene and pyridine, it is unnecessary to proceed via this intermediate acetonitrile species, although this best done, especially if the ligand reacts with the amine-oxide. $[Os_3(CO)_{11}(NCMe)]$ is sufficiently air-stable to be isolated by chromatography as a bright yellow, micro-crystalline, solid and has been fully characterised. Apart from supplying a convenient, mild synthetic route to known adducts, it also allows the preparation of various compounds which are potential intermediates in substitution reactions of the parent carbonyl, but appear unstable at the reaction conditions usually employed i.e. $[Os_3(CO)_{11}(C_2H_4)]$, $[HOs_3(CO)_{11}X]$ etc. The extension of this method to other osmium clusters has proved less successful because significant concentrations of complexes with coordinated tertiary amine are isolated. Thus $[Os_3(CO)_{10}(NO)_2]$ reacts with Me_3NO to give $[Os_3(CO)_9(NO)_2(NMe_3)]$, which has undergone a full structural determination(122).

Under rigorous conditions (exclusion of air, damp and any alternative ligand, and use of pure acetonitrile as solvent), a second carbonyl can be replaced with an acetonitrile, by means of amine-oxide attack, to give $[Os_3(CO)_{10}(NCMe)_2]$ in high yield. This had been previously prepared by ligand-exchange with the bis-cyclooctene species $[Os_3(CO)_{10}(C_8H_{14})]$, in turn derived from passing ethylene through a cyclooctene solution of $[H_2Os_3(CO)_{10}]$, V, (123). This transformation was a matter of convenience, the cyclooctene

Diagram 6

Synthetic Versatility of Lightly Stabilised Triosmium Clusters

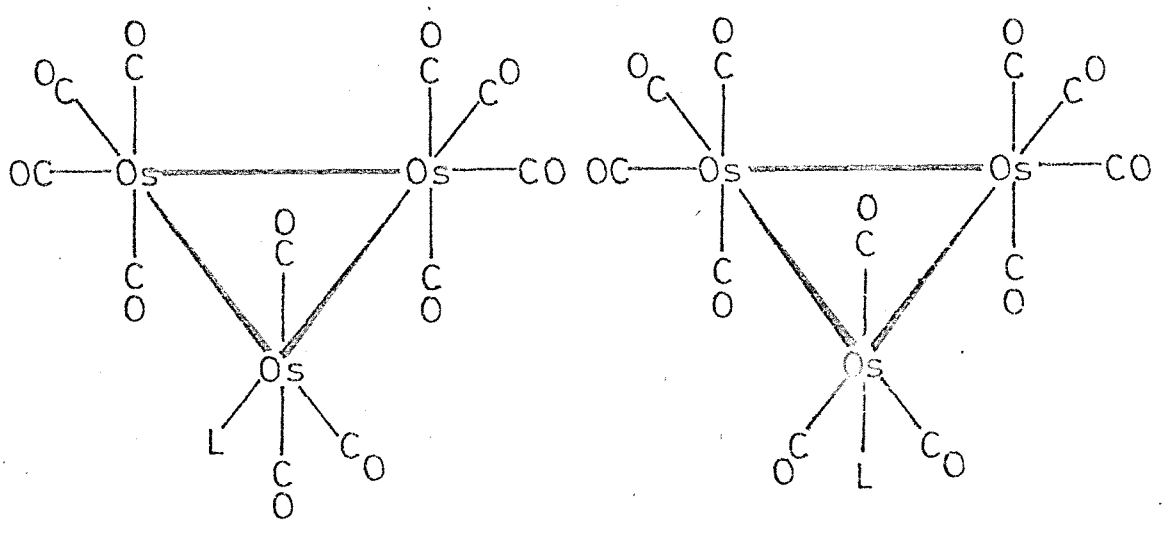


ligands being extremely labile making manipulations difficult, since both are effective sources of the decacarbonyltriosmium moiety in a synthetically useful fashion. Reaction with strong donor ligands provides $[Os_3(CO)_{10}L_2]$, L=phosphine, phosphite, isocyanide etc., with the added bonus of possible sequential addition of different ligands providing a useful entry into mixed decacarbonyl derivatives. They also readily cleave H-X bonds (X is a bridging three-electron donor) to give $[HOs_3(CO)_{10}X]$ adducts, this is a more general route to vinyl compounds from α-olefins, since V does not readily transfer hydrogen to some simple olefins i.e. styrene. A similar function is served by another lightly stabilised complex $[Os_3(CO)_{10}(\eta$-cyclohexa-1,3-diene)](124), prepared from reaction of V with cyclohexadiene in refluxing n-hexane, although slightly more forcing conditions are necessary. Vacant coordination sites can also be generated in systems where adjoining ligands have variable oxidation states. This has been utilised to good effect in $[Os_3(CO)_9(NO)_2]$(125) and $[HOs_3(CO)_9(SR)]$(126).

The molecular structure of $[Os_3(CO)_{11}(P(OMe)_3)]$, as determined by X-ray diffraction(127), is isostructural to that of IIIa with the incoming ligand equatorially positioned. In both, the presence of the bulky ligand has caused an expansion of the ligand packing, compared to the parent carbonyl, and a corresponding increase in metal-metal distances to maintain the optimum overall molecular geometry. This general increase in distances can also, in part, be ascribed to the electronic effect of substituting a good π-acceptor ligand with a lesser one thus promoting a higher electron density in the metal framework which is relieved by expansion. A specific, preferential, increase in the metal-metal bond cis to the substituent is attributed to a steric effect. However, the ligand polyhedra still approximate to a 'twinned cuboctahedron' so it seems that a considerable wider cone angle (PPh_3 145°, $P(OMe)_3$ 107°)(128) is required to expand it sufficiently to permit the alternative icosahedral geometry seen for the iron analogue.

The preference for equatorial substitution can be accounted for on steric grounds, since simple calculations on $[Os_3(CO)_{12}]$ show that equatorial sites in the approximately anticuboctahedral structure are less sterically crowded than axial sites(94). This is illustrated by variable-temperature ^{13}C NMR

study on several of the corresponding monosubstituted isocyanide derivatives(119). Most show only the axial isomer to be present in significant concentrations at low temperatures in solution, with the exception of the most bulky ligand, $CNBu^t$, where an equilibrium mixture of the isomers is obtained at -60°C. At higher temperatures the isomers rapidly interconvert on the NMR time-scale. The fact that less bulky groups favour the axial site suggests that this position is electronically preferred. This is complimented by the ruthenium analogue, IV, where the axial isomer alone resides in the solid-state. Indeed, recent crystal-structure determinations on both acetonitrile derivatives(129) confirmed that the substituents



$L=C_2H_4$, PR_3 or $P(OR)_3$ L=CNR, NCMe or C_5H_5N

Molecular structures of $[Os_3(CO)_{11}L]$ clusters

occupy axial coordination sites; on adjacent osmiums, but on opposite sides of the molecule, for $[Os_3(CO)_{10}(NCMe)_2]$. In these molecules the shortest metal-metal bonds are those associated with the coordinated nitrile ligands. Similar, but less marked trends were observed for IV, but the systematic distortion of the ligand polyhedron caused by the axial ligand in that case was not reproduced in these acetonitrile derivatives.

Clearly phosphine attack on these intermediates may proceed via the kinetically-controlled axial isomer before rearrangement to the observed, thermodynamically favoured, equatorial form occurs. Then the fact that all monosubstituted phosphine derivatives to date exist in the equatorial form may merely reflect

the greater steric bulk of organophosphines over isonitrile ligands. That axial substitution is possible is demonstrated by the preparation of $[Ru_3(CO)_9\ SiMe(PBu_2)_3\ ]$, in which the sterically constrained ligand caps the Ru_3 triangle(130).

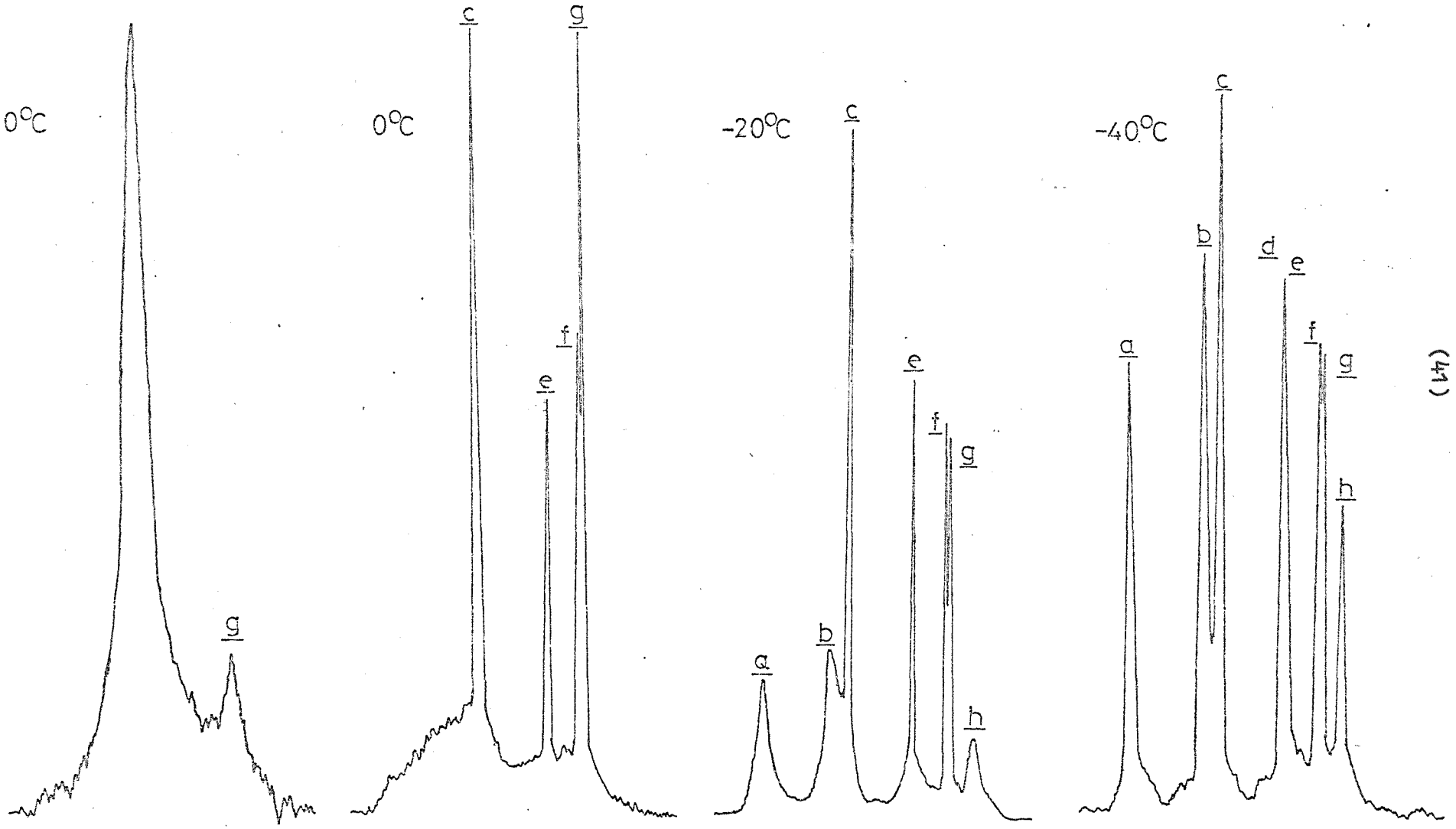
1.4.2. Characterisation of $[Os_3(CO)_{11}(PPh_2Et)]$

Undodecacarbonyl(ethyldiphenylphosphine)triosmium, VIa, to be used as the unadsorbed reference analogue, was prepared in high yield, typically 73%, via the acetonitrile derivative. A pale yellow, crystalline solid its infrared and Raman ν_{CO} spectra show excellent agreement (Table 2) with literature data of related compounds. The ^1H NMR spectrum shows only the expected resonances, all with small downfield shifts relative to the free ligand, as a result of deshielding through coordination of the phosphine. These slight changes in chemical shifts enables discrimination against the presence of any free ligand as impurity. Satisfactory elemental analysis (C and H) was obtained and a parent ion, m/e=1094, as part of an Os_3 isotopic pattern, is seen in the mass spectrum. This molecular ion first loses two carbonyl groups, and then the remaining fragmentation pattern can be assigned to successive carbonyl losses and phosphine degradation. This breakdown pathway is similar to that reported for $[Os_3(CO)_{11}(PPh_3)]$(112).

1.4.3. Variable Temperature $^{13}C-\{^1H\}$ NMR Study of $[Os_3(CO)_{11}(PPh_2Et)]$

A variable-temperature $^{13}C-\{^1H\}$ NMR study was carried out on a sample of VIa prepared from moderately ^{13}CO enriched $[Os_3(CO)_{12}]$. In the absence of exchange, the equatorially substituted isomer found in the solid ground-state would be expected to give rise to eight signals of relative intensity 2:2:2:1:1:1:1:1. The alternative, axially substituted species would be expected to show six resonances of relative intensity 2:2:2:2:2:1. The recorded spectra, over the range -40 to $+40^oC$ ($CDCl_3$), are presented in Diagram 7. The low temperature limiting spectrum shows seven resonances at: a, 192.5; b, 185.0; c, 183.5; d and e, 176.1; f, 172.4; g, 172.0; h, 169.6 δ-with integrated intensities of 2:2:2:2:1:1:1 respectively. This is fully consistent with the

Diagram 7 Variable Temperature $^{13}C-\{^{1}H\}$ NMR Spectra for $[Os_3(CO)_{11}(PPh_2Et)]$



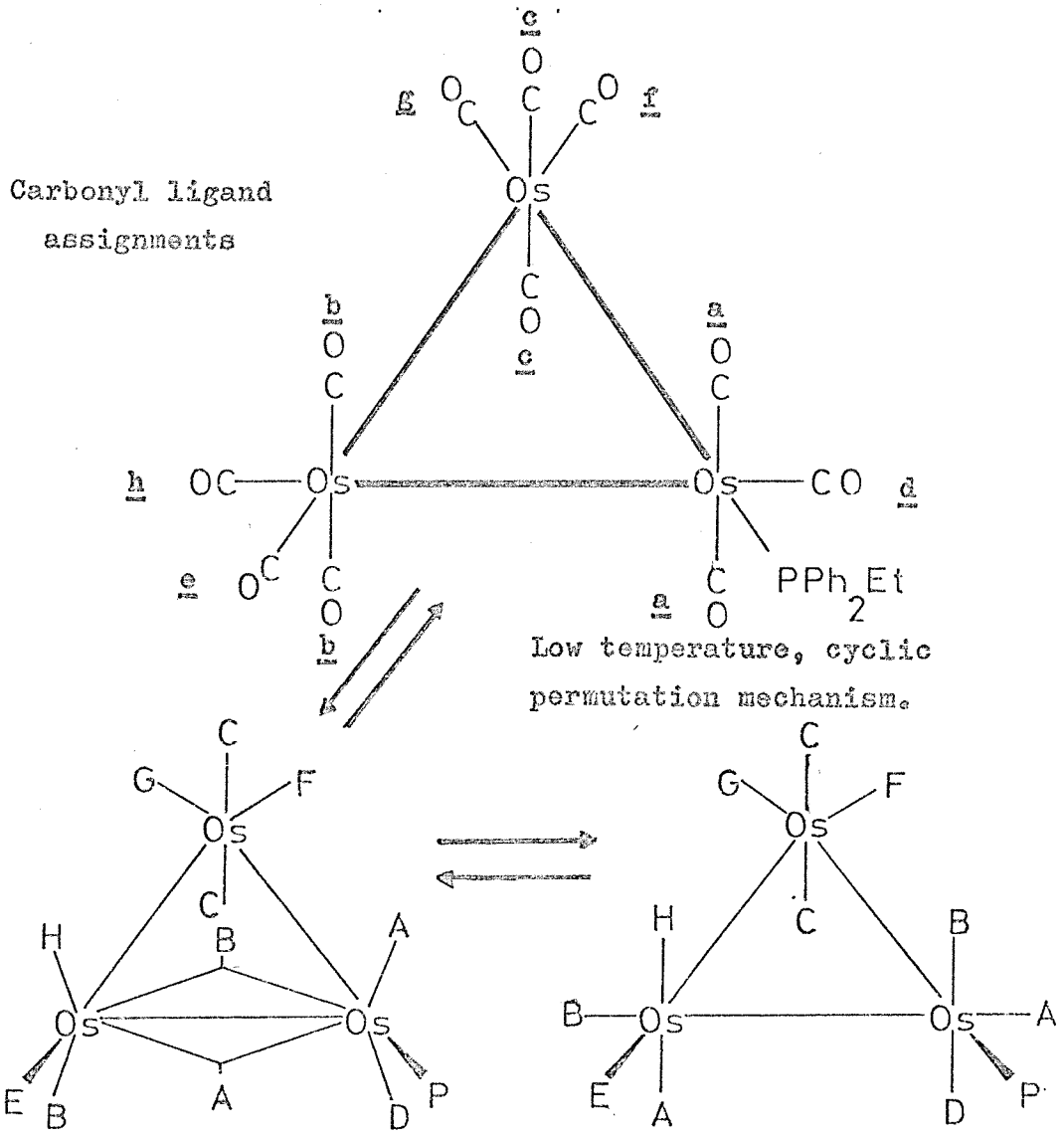
(47)

equatorially substituted structure, with an accidental degeneracy of two resonances, d and e. This anomaly was overcome in the reported spectrum of $[Os_3(CO)_{11}(PEt_3)]$, VIb, where all eight expected resonances are seen(131). The strong correlation between chemical shifts for related resonances in the two sets of data also confirmed that VIa and VIb are isostructural, a small upfield shift for all the resonances of VIa is consistent with a less basic phosphine. The axial carbonyls can be assigned because they have a relative intensity of two, whilst the equatorial carbonyls are of unit intensity. There is a clear definition into two sets with the axial ligands occurring at lower-field than the equatorial ones. Conveniently the two resonances for $[Os_3(CO)_{12}]$, at 182.3 and 170.46(132), fall at the high-field end of each set respectively. Further, this general downfield shift for comparative resonances is most pronounced for groups adjacent to the introduced substrate. Accordingly, the lowest field signal for VIb showed a resolved coupling to the phosphorus, $^2J_{PC}$=6Hz, and was assigned to the axial pair adjacent to the phosphine. Although a similar splitting was not discernible for a in the spectrum of VIa, a comparative loss of intensity supports the presence of an unresolved interaction. The equatorial group on the phosphine-bonded osmium will also be shown to correspond to part of the accidently degenerate signal, which is also the lowest field resonance in the equatorial block.

When the temperature is raised to -20°C the peaks a, b, d and h broaden and coalesce at about 0°C. This process also reveals the accidental degeneracy of d and e, with the latter arbitrarily remaining with unit intensity at -20°C. This fluxional behaviour can be explained provided it is assumed that the phosphine is relatively immobile (as compared to a carbonyl), such that any process involving a change in its position will have a much higher activation energy barrier than one that does not require its transfer. This averaging of six carbonyls can then be explained by pairwise exchange along one edge, via a $D_{3h} \rightleftharpoons C_{2v} \rightleftharpoons D_{3h}$ mechanism as proposed for $[Fe_3(CO)_{12}]$ by Cotton(133), with an intermediate containing two carbonyls bridging an edge as found in one of the isomeric forms of $[Fe_3(CO)_{11}(PPh_3)]$(Diagram 8). It appears that the labilizing influence of a phosphine is necessary for the adjacent carbonyls to form the bridging intermediate at low temperatures

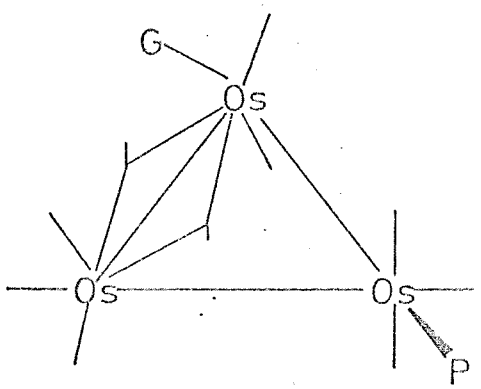
Diagram 8

^{13}CO NMR Assignments and proposed Fluxional Behaviour for $[Os_3(CO)_{11}(PPh_2Et)]$

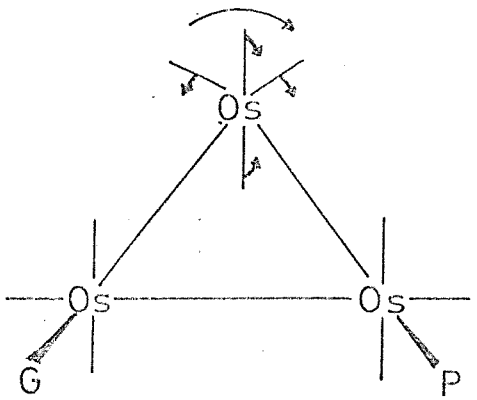


Possible Higher Energy Processes

Extended pair-wise exchange



Polytopal rearrangement



which, combined with the rigid nature of the phosphine, restricts this cyclic permutation to a single edge in a plane not including the phosphine. Independent evidence supports the introduction of tertiary phosphines into polynuclear carbonyl clusters inducing the formation of carbonyl bridges as in the substitution of $[Ir_4(CO)_{12}]$(134). The disubstituted derivatives $[Os_3(CO)_{10}(PEt_3)_2]$ (131), $[Os_3(CO)_{10}(PPh_2CH_2CH_2PPh_2)]$(135) and $[Ru_3(CO)_{10}(PPh_2CH_2PPh_2)]$ (136) also exhibit this mechanism. Identification of this process reinforces the previous assignments of a and d, whilst allocating b and h to the axial pair and equatorial group on the second osmium involved in the motion. The outstanding double-intensity resonance, c, must then correspond to the axial groups on the remaining osmium, leaving just three equatorial groups unassigned. Inspection of line shapes within the spectrum recorded at 0^oC suggests that c, e and f are broadening preferentially in comparison to g. A second fluxional process is apparently operative (Diagram 8). This could be polytopal rearrangement about the third osmium independent of the first motion, but is not fully substantiated because the averaged resonances for each process are not separately observed. An alternative interpretation is the extension of pairwise exchange for carbonyls about the second edge not impaired by the phosphine. This is also expected to be a higher energy process, but has been identified along a non-substituted edge in the related, axially coordinated, isocyanide derivatives(119). Depending on which mechanism is operative, more precise assignments within the equatorial trio, e, f and g, is possible. For a localised axial/equatorial interchange the resonances e and f are allocated to the involved $Os(CO)_4$ group, whilst for the internuclear process one changes its assignment with g on the second $Os(CO)_4$ group. At $+40^oC$ all the signals, apart from a remnant of g, have collapsed into a broad, emerging resonance. Presumably at slightly higher temperatures even this outstanding signal would coalesce indicative of total carbonyl scrambling which appears to involve a breakdown in the rigidity of the phosphine(131). Also present in the $+40^oC$ spectrum were the natural abundance resonances for the coordinated phosphine; at 130.4, 29.4 (J_{PC}=40Hz) and 8.4 δ.

Unfortunately, the above data cannot differentiate between these increased partial scrambling modes. A similar dilemma

between localised and intermetal carbonyl migration also proved difficult to resolve for $[M_3(CO)_{12}]$; M=Fe, Ru or Os. All three give a single resonance at elevated temperatures, and only with $[Os_3(CO)_{12}]$ could this be separated into an arrangement consistent with the solid-state structure. Even so, this might still disguise a 'hidden process', such as localised scrambling of all equatorial groups via a triply-bridged intermediate, provided axial-equatorial interchange is not occurring(137). For $[Fe_3(CO)_{12}]$ the spectrum remains unaltered at $-150^{\circ}C$, indicating that the activation energy for total scrambling is less than $20kJ.mol^{-1}$(138). As an explanation the $D_{3h} \rightleftharpoons C_{2v} \rightleftharpoons D_{3h}$ mechanism(133), with concerted bridge-terminal exchange, appeared attractive as it encompassed the known structures of the homologous series, whilst providing an understanding to the anomalous infrared ν_{CO} spectrum of $[Fe_3(CO)_{12}]$, which varies with solvent polarity(138). This mechanism, operative about all three edges of the Fe_3 core, necessarily involves a 'scissoring' of this triangle since in the ground state it is an isosceles. The present work also supports this approach, although it must be remembered that introduction of a phosphine may give rise to a different mechanism from that occurring in the parent compound.

An attractive alternative, also consistent with the observed data, involves geometrical disposition of the metal core relative to the ligand polytope. For $[Fe_3(CO)_{12}]$, provided the carbonyl groups maintain a flattened icosahedron spatial relationship in solution, a small rotation (about a C_2 axis) of the triangle creates a new form of D_3-symmetry:- not the D_{3h} structure of $[Os_3(CO)_{12}]$. Continued oscillation about the same axis progresses via a third species, containing two triply-bridging groups, before regenerating the C_{2v} structure(139). This pathway causes exchange of all the carbonyls in fewer steps than the Cotton mechanism(133). Apparently the C_{2v} form is favoured in the solid, but in solution, on the basis of the infrared data, the D_3 form predominates.

Such internuclear scrambling is equally applicable to the fluxional behaviour of the more symmetrical $[Os_3(CO)_{12}]$, although stereochemical non-rigidity within independent $Os(CO)_4$ units would also suffice. Several mechanisms for this localised axial-equatorial site exchange have been proposed. An increase in

the OC-Os-CO equatorial angle to 180° and a decrease in the OC-Os-CO axial angle to 120°, followed by rotation of the unit by 90°(132a). A simpler twist mechanism involves a square-based-pyramidal intermediate(140), whilst observation of a two-step process for $[HOs_3(CO)_{10}(COOEt)]$(141), supported a trigonal twist mechanism traversing a trigonal-prismatic intermediate(142). The three line spectrum (relative intensities of 4:4:2) of $[Ru_3(CO)_{10}(NO)_2]$ was often quoted as an unambiguous example for this polytopal rearrangement(132a) but later the axial and equatorial carbonyls on the unique osmium were resolved, in different solvent systems, and remained essentially temperature invariant(140). Then the principle experimental evidence on which this postulate is based is the line broadening observed in the range of molecules $[HOs_3(CO)_{10}X]$, X=three-electron donor. However its occurrence in the absence of internuclear scrambling in clusters with non-labile bridging ligands may be of doubtful relevance to the unbridged $[Os_3(CO)_{12}]$.

Eventually, observation of metal-to-carbon couplings has finally established an internuclear mechanism to be operative for both $[Fe_3(CO)_{12}]$ and $[Os_3(CO)_{12}]$. At room temperature the ^{57}Fe (natural abundance 2.17%) satellite sub-spectrum in the ^{13}C NMR spectrum of $[Fe_3(CO)_{12}]$ appears as a doublet with an inner separation of 8.3Hz(143). In principle two doublets, in the ratio 2:1, are expected because of the two non-equivalent types of iron atoms in the molecule. Therefore, as the spectrum is unaltered at -80°C(144) it was concluded that a fast rearrangement in the iron framework is occurring to make all three atoms equivalent on the NMR timescale, consistent with the mechanisms of both Cotton(133) and Johnson(139). A ^{13}C NMR investigation was carried out on $[Os_3(CO)_{12}]$ prepared from the metal isotope ^{187}Os ($I=\frac{1}{2}$), and enriched by exchange with ^{13}CO(145). The ambient temperature spectrum gave two doublets at 182.3 and 170.4 δ; $^1J_{OsC}$=90 and 115Hz respectively. However at 150°C it has altered to a 1:3:3:1 quadruplet, with $^1J_{OsC}$=33Hz, at 176.4 δ. The value of the average coupling constant and the signal multiplicity proved that, first, the exchange process is intramolecular, and secondly, under conditions of rapid exchange all carbonyls have access to the three osmium atoms. Again this does not identify the specific internuclear process but, interestingly, the same

paper clearly established a two-centre exchange in the mixed cluster $[RuOs_2(CO)_{12}]$. However the stereodynamic behaviour of the complexes $[Fe_3(CO)_{11}L]$, L=phosphine or phosphite, could not be accommodated by either mechanism, and another interpretation was necessary based on a mechanism in which the icosahedral ligand envelope rearranges via a cuboctahedral transition state(146), in identical fashion to the process postulated for $[M_4(CO)_{12}]$(147). In addition, rotation of unsubstituted $Fe(CO)_3$ units appears to occur. This approach is also satisfactorily applied to $[Fe_3(CO)_{12}]$. In view of these results the extended pairwise exchange is preferred as the intermediate process for VIa before total scrambling commences; the assignments in Diagram 8 are based on this assumption.

A final comment, the solid-state ^{13}C NMR spectrum of $[Fe_3(CO)_{12}]$ has been reported(148), and interpreted on the basis of a 60° rotation of the iron triangle through its centre of symmetry, time averaging the two disordered molecules observed crystallographically, on the NMR timescale. The estimated barrier to this rotation ($50kJ.mol^{-1}$) is much larger than that to complete exchange in solution and does not necessarily represent the lowest energy pathway in this second medium. This 'Star-of-David' disorder also exists in several substituted cluster complexes $[M_3(CO)_{12-n}L_n]$, M=Fe or Ru, n=1-3(149). A similar fluxional behaviour might be expected in such systems; where two or more conformations have the same fixed peripheral ligand atom polyhedron, governing the crystal packing interactions, and a random occupation of lattice sites results.

1.4.4. Preparation of $[Os_3(CO)_{11}(PPh_2CH_2CH_2SIL)]$

Several different approaches have been attempted in the preparation of $[Os_3(CO)_{11}(PPh_2CH_2CH_2SIL)]$, VII, (Diagram 9). The first, using the strategy of SCHEME TWO, involved intermediate isolation of $[Os_3(CO)_{11}(PPh_2CH_2CH_2Si(OEt)_3)]$, VIc. Initially, the homogeneous cluster derivative was separated by conventional chromatography from the mixed substitution product by heating $[Os_3(CO)_{12}]$ with an excess of phosphino-silane, in toluene under reflux for 5 hours. Application of the red residue to the

Diagram 9

Different Preparative Routes to $[Os_3(CO)_{11}(PPh_2CH_2CH_2SIL)]$

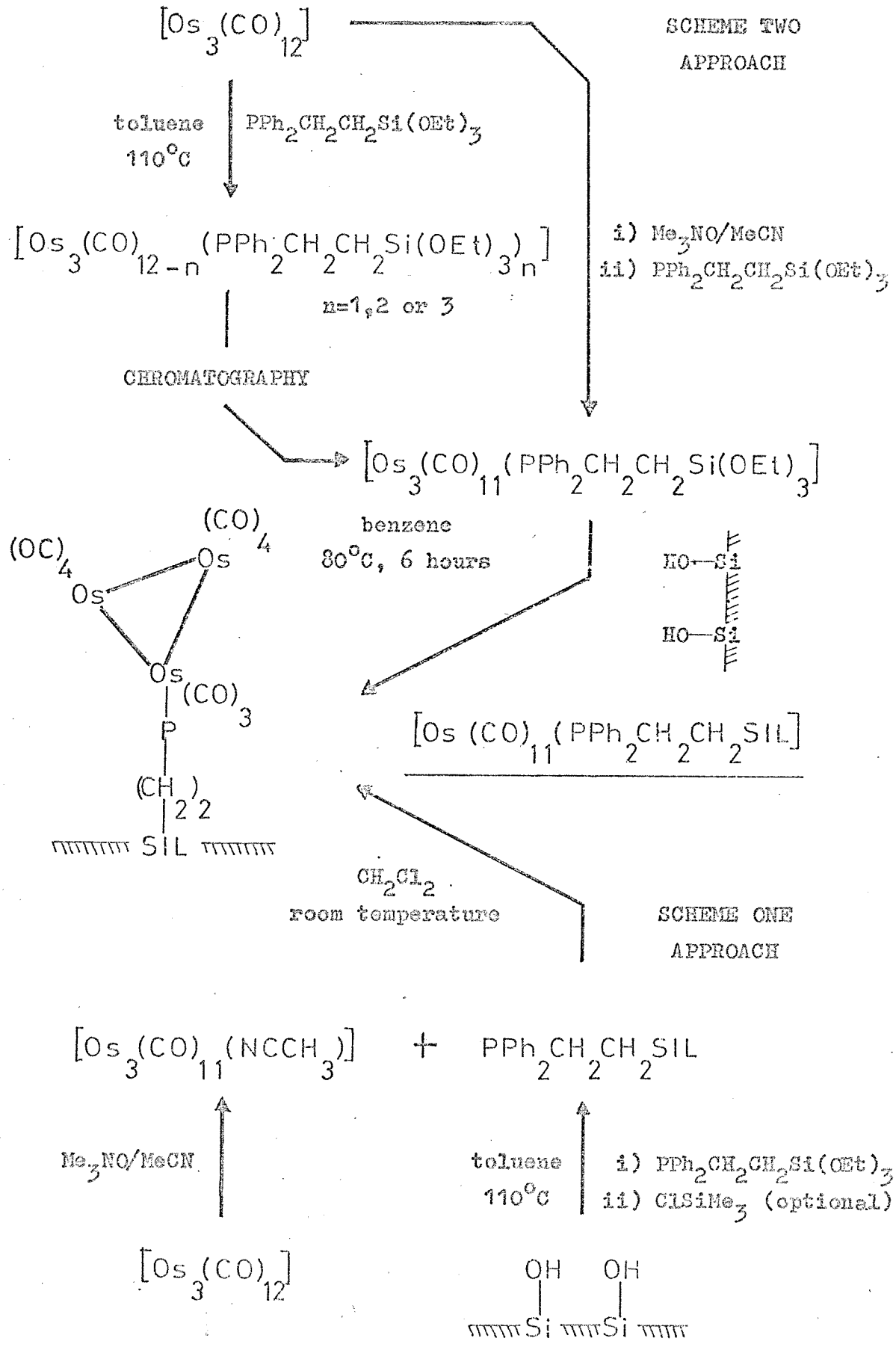


Table 2

Infrared and Raman ν_{CO} Spectroscopic Data for $[Os_3(CO)_{12-n}L_n]$, n=1 or 2, Derivatives

Compound	ν_{CO}/cm^{-1} (cyclohexane unless stated)			
$[Os_3(CO)_{11}(PPh_2Me)]$ (Ref.113)	2107m	2056s	2034s	2021vs
Infrared	2001m	1988m	1970m	1956w
$[Os_3(CO)_{11}(PPh_3)]$ (Ref.112)	2109vs	2054w	2042w	2020w
(solid), Raman	2012w	1999s	1984vs	1967s
	1954w			
$[Os_3(CO)_{11}(PPh_2Et)]$	2107w	2055s	2034m	2020vs
Infrared	2001w	1989m	1980wsh	1974w
	1967.5w	1959vwsh		
(solid), Raman	2104s		2034w	2008s
	1996w	1979m	1974m-w	1968m-w
	1955w			
$[Os_3(CO)_{11}(PPh_2CH_2CH_2Si(OEt)_3)]$	2107m	2054s	2035.5s	2019vs
Infrared	2001.5m	1990m	1977m	1957w
$[Os_3(CO)_{11}(PPh_2CH_2CH_2SiL)]$	2107w	2054s	2034m	2019vs
(nujol mull), Infrared	2000w-m	1989m	1976w-m	1956wsh
$[Os_3(CO)_{10}(PPh_2Me)_2]$ Ref.(113)	2083m	2051w	2024s	2000vs
Infrared	1965m	1954sh		
$[Os_3(CO)_{10}(PPh_2CH_2CH_2Si(OEt)_3)_2]$	2084m	2053w	2028s	2001vs
Infrared	1968m	1950sh		

chromatographic plate, and eluting with n-hexane/toluene (8:6 v/v), resulted in partial separation of three diffuse bands; yellow, orange and red in order of decreasing R_f, corresponding to the mono-, bis- and tris-substituted products. These proved difficult to wash from the silica, and increasingly so with decreasing R_f such that hardly any of the red species could be removed. This highlights the difficulty of chromatographing species containing the hydrolysable Si-OEt group; with the limited number of covalent bonds reflecting the degree of substitution. Oily yellow and orange samples were extracted from the first two bands, although the washed silicas were still highly stained. These were characterised as VIc and $[Os_3(CO)_{10}(PPh_2CH_2CH_2Si(OEt)_3)_2]$ from their infrared ν_{CO} spectra (Table 2) and the anticipated

coordinated ligand resonances in the ^{1}H NMR spectrum of VIc. The fact that some material is retrieved from the plate underlines the limited degree of covalent fixation per phosphino-silane group occurring at room temperature, even when highly concentrated in contact with a silica surface.

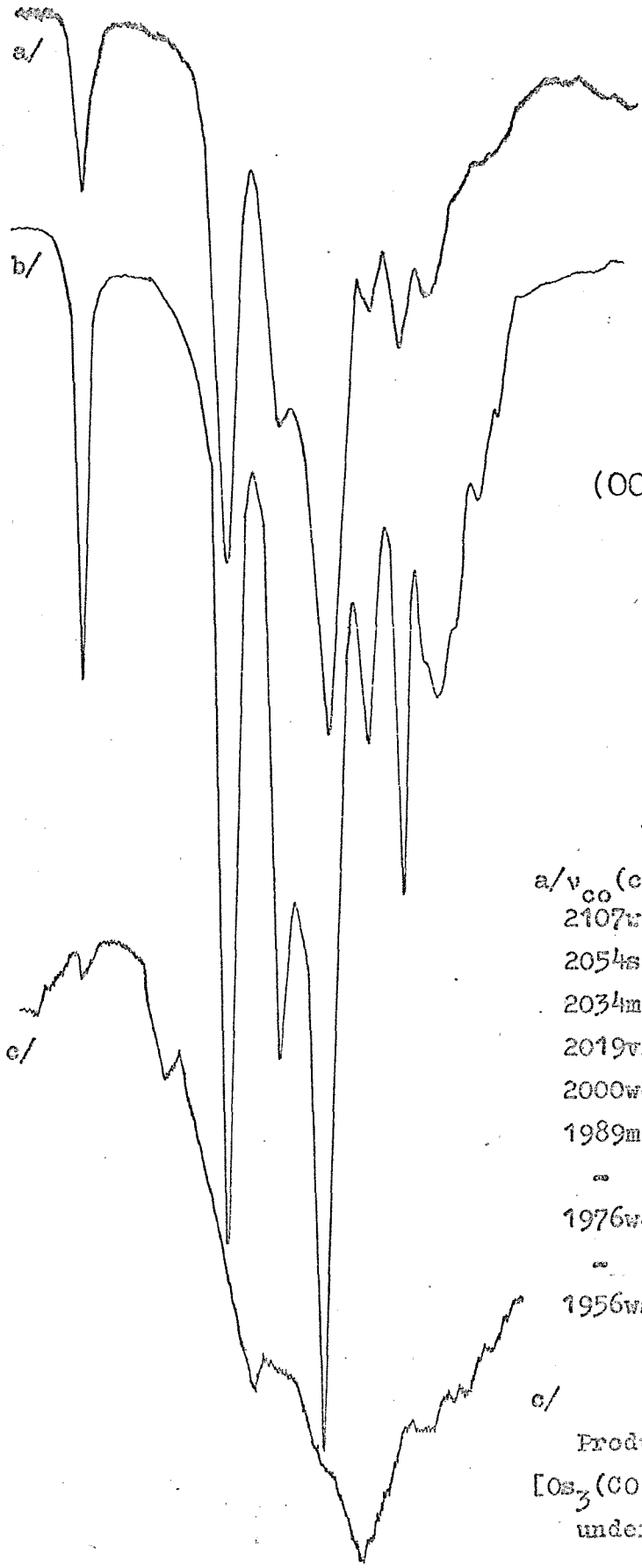
A more successful preparation of VIc utilized the amine-oxide/acetonitrile synthetic route. Provided the intermediate $[Os_3(CO)_{11}(NCMe)]$ is purified (all impurities with the exception of $[Os_3(CO)_{12}]$ can be easily extracted with an aliquot of acetonitrile), then the far superior solubility of the phosphine derivative over that of the intermediate and $[Os_3(CO)_{12}]$ allows its isolation by solvent extraction with n-hexane, circumventing the need for chromatography. Unfortunately, even then it is still a yellow oil and exclusion of any unreacted phosphine is not guaranteed. The final stage for SCHEME TWO was completed by contacting a solution of VIc in benzene with a suspension of activated Aerosil 200 (dehydrated at 150°C in vacuo) and heating under reflux for 6 hours, followed by Soxhlet extraction. When mulled the retrieved, deep yellow, free flowing silica gave an infrared ν_{CO} spectrum exhibiting excellent agreement with those of VIa and VIc confirming specific tethering of the preformed complex by hydrolysis of the silyl group in the phosphino-silane. The formation of strong covalent bonds was inferred by the absence of any leaching during washing with a variety of hot solvents. The stronger resemblance to the solution infrared spectrum of VIa, as opposed to its solid state one, underlines the random nature of the isolated surface complex with no intermolecular interactions. The good correlation in frequency positions also illustrates the absence of transmitted electronic effects from the surface. Another form of VII was derived from the highly stained silica scrapped from the chromatography plate, which was again treated with benzene under reflux to ensure maximum covalent linking. Both these samples had almost indefinite shelf-lifes as witnessed by an unaltered infrared spectrum even after a years storage without any precaution to exclude air.

A more specific synthesis of VII has been devised by adaption of SCHEME ONE. Reaction between silylated $PPh_2CH_2CH_2SIL$ and $[Os_3(CO)_{11}(NCMe)]$ occurs at room temperature in methylene

Diagram 10

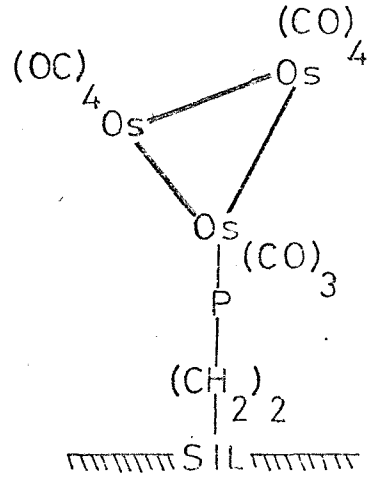
Infrared (ν_{CO}) Spectroscopic Characterisation of

$[Os_3(CO)_{11}(PPh_2CH_2CH_2SIL)]$



a/ $[Os_3(CO)_{11}(PPh_2CH_2CH_2SIL)]$
(Nujol mull)

b/ $[Os_3(CO)_{11}(PPh_2Et)]$
(cyclohexane)



a/ ν_{CO} (cm^{-1})	b/ ν_{CO} (cm^{-1})
2107w	2107w
2054s	2055s
2034m	2034m
2019vs	2020vs
2000w-m	2001w
1989m	1989m
-	1980wsh
1976w-m	1974w
-	1967.5wsh
1956wsh	1959vwsh

c/ Product from contacting $[Os_3(CO)_{12}]$ with $PPh_2CH_2CH_2SIL$ under reflux in toluene.

chloride. The ligand-silica almost immediately begins to acquire the deep yellow coloration indicative of VII. Maximum coverage was ensured by continual addition of the cluster intermediate until its concentration in solution nolonger diminished. The silica was then filtered off, washed, dried and characterised by its infrared ν_{co} spectrum (Diagram 10). An attempt at recording its Raman ν_{co} spectrum was unproductive. Although more indirect, its inherent simplicity makes this the most favourable route for generating the adsorbed osmium cluster. It has the advantage that the covalent bond to the surface is substantiated during the preparation of the ligand-silica and possibly detrimental heat treatment of the immobilised complex is avoided. The mild conditions also militate against interactions with silanol groups, this possibility is further blocked by silylation during the formation of $PPh_2CH_2CH_2SIL$, although the importance of this precaution is only borne out in subsequent studies.

One obvious drawback could be the presence of uncomplexed ligand-silica sites. This inpart may be due to the steric bulk of the complex blocking approach of other molecules to adjacent, free ligand-silicas. An empirical calculation was made, using molecular models, into the minimum separation of $PPh_2CH_2CH_2SIL$ groups required to prevent further than mono-substitution occurring, and by inference eliminating the chance of inaccessible sites. This was based on the bond data from the X-ray crystal structure of $[Os_3(CO)_{11}(P(OMe)_3)]$(127) and the false simplification that the sites are equidistant apart on the surface. The derived value of ca. 16.5Å translates to a phosphine density of one per $2.72nm^2$. In contrast, an actual value of 0.93 per nm^2 for the used $PPh_2CH_2CH_2SIL$ is consistent with the observation that direct reaction with $[Os_3(CO)_{12}]$, under the conditions of reflux in toluene, produces a silica possessing a broad infrared ν_{co} spectrum (Diagram 10) indicative of the mixture $[Os_3(CO)_{12-n}(PPh_2CH_2CH_2SIL)_n]$, n=1,2 or 3, with the bis-substituted derivative predominating.

1.4.5. Preparation of $[Ru_3(CO)_{12-n}(PPh_2CH_2CH_2SIL)_n]$, n=1,2 or 3

In the last section contacting the parent cluster with the ligand-silica, at the conditions known to facilitate thermally-

activated substitution of the core, gave the expected mixed cluster product with the distribution governed by the surface ligand density. The necessary temperature (110°C) was considerably lower than that required to invoke oxidative addition by silanol groups; approximately 150°C as demonstrated by the formation of Ia. However, the situation is reversed with $[Ru_3(CO)_{12}]$, which is more susceptible to attack by the surface hydroxyl groups leading to loss of nuclearity and oxidation, so that direct surface adsorption becomes more competitive than the desired reaction with the attached-phosphine ligands.

The adsorption of $[Ru_3(CO)_{12}]$ on inorganic oxides has been studied quite extensively. Robertson and Webb(150) showed that room temperature impregnation on Aerosil 200 (predried at 500°C), by evaporation of the CH_2Cl_2 solvent, was primarily a physical process. Others substantiated this using vibrational, Raman and infrared, spectroscopy(151). On heating chemisorption occurs and then, as shown by infrared and radiochemical studies, the supported complex undergoes decomposition in a series of well defined stages by loss of carbon monoxide. A TPD experiment was carried out on a ^{14}C-labelled sample. At 80°C an irreversible, rapid transformation takes place from the physisorbed cluster to a pink form with a stoichiometry of $Ru(CO)_{2.7}$ and characterised by infrared ν_{CO} bands at 2070, 2050, 2000 and 1970 cm^{-1}. Further heating to 200°C, or exposure to oxygen, caused a transformation to

$$Ru_3(CO)_{12} \xrightarrow[70^\circ C]{} Ru(CO)_{2.7} \xrightarrow[130^\circ C]{} Ru(CO)_{1.7} \xrightarrow[170^\circ C]{} \text{Ru metal}$$

a white form (2070 and 2000 cm^{-1}). Chemisorption of carbon monoxide on reduced ruthenium dispersed on silica also gives a similar two band spectrum with CO/Ru ratios greater than unity and approaching 2 for low metal loadings(152). Prolonged exposure to air for any of theadsorbed species results in a loss of carbonyl vibrations and aggregation to ruthenium metal. Reduction at elevated temperatures (> 350°C) under hydrogen results in formation of microcrystallites; carbon monoxide adsorption giving sites typical of those on reduced (2039-50) and partially oxidized (2139 and 2062 cm^{-1}) ruthenium atoms(153). These observations being in good agreement with previous investigations into carbon monoxide

adsorption on silica-supported ruthenium. On a fully reduced sample a single band at 2040cm^{-1} characterised the presence of a linearly bonded form. Conversely on a fully oxidized surface a pair of bands develop at 2130 and 2070 cm^{-1}, which are assigned to the symmetric and asymmetric vibrations of a pair of carbonyl ligands adsorbed on a single, oxidized ruthenium centre(154).

Adsorption of $[Ru_3(CO)_{12}]$ on alumina follows a similar pattern, but with decomposition occurring more readily. More detailed structural assignments have been attempted. On untreated surfaces(155), or after dehydroxylation below 400°C(153), physical impregnation in the air is followed by a slow change to a doublet, at 2072 and 2005 cm^{-1}, B, which then gradually disappears leaving a very weak component at 1890cm^{-1}. When contact under inert conditions is followed by heating in vacuo, at 50°C there is evidence for the intermediate formation of the ruthenium analogue of I, with retention of the trimetallic skeleton and which can revert to the initial cluster under carbon monoxide. Then at 150°C a new pair of bands develop at 2054 and 1977 cm^{-1}, C, with shoulders at 2072 and 2005 cm^{-1}. Decarbonylation under hydrogen favours C suggesting that it can be formed from B by reduction above 150°C. If carbon monoxide is present during, or introduced after, pyrolysis an extra feature at 2138cm^{-1}, together with intensity enhancements at lower wavenumbers, appears. After total decarbonylation at 350°C exposure to carbon monoxide gave principally a set of absorptions at 2138 and 2075 cm^{-1}, A.

Thus three well-defined surface carbonylic species were identified. Reflectance spectroscopy inferred that metal-metal bonding is likely to be present in C but absent in A and B. This loss of nuclearity is consistent with an irreverible breakdown of the initial cluster irrespective of whether $[Ru_3(CO)_{12}]$, $[H_4Ru_4(CO)_{12}]$ or $[Ru_6(CO)_{17}C]$ is used. At first Kuznetsov(153) hypothesised a series of species schematically represented by $[Ru(CO)_{4-n}X_2]_m$, n=0-2, where the electrophilic ligands are the surface oxygens. Later(155) this was refuted and the alternative interpretation of all $[Ru(CO)_2X_y]_m$ forms, but with varying oxidation states, namely +3, +2 and 0 in alphabetic order, was proposed. In the absence of oxygen the oxidizing agents are undoubtedly the surface hydroxyls as documented by the evolution of hydrogen and

carbon monoxide. ^{13}CO isotopic substitution(156) identified that all three complexes contained two coupled carbonyl oscillators per ruthenium centre. The approximate angles between the oscillators, calculated from the intensity ratios of the bands, combined with the deduced presence of full coordination spheres from the lack of insertion by simple molecules, suggested tetrahedral and octahedral configurations for A and for B and C, respectively. The latter two were shown to interconvert in reducing and oxidizing enviroments.

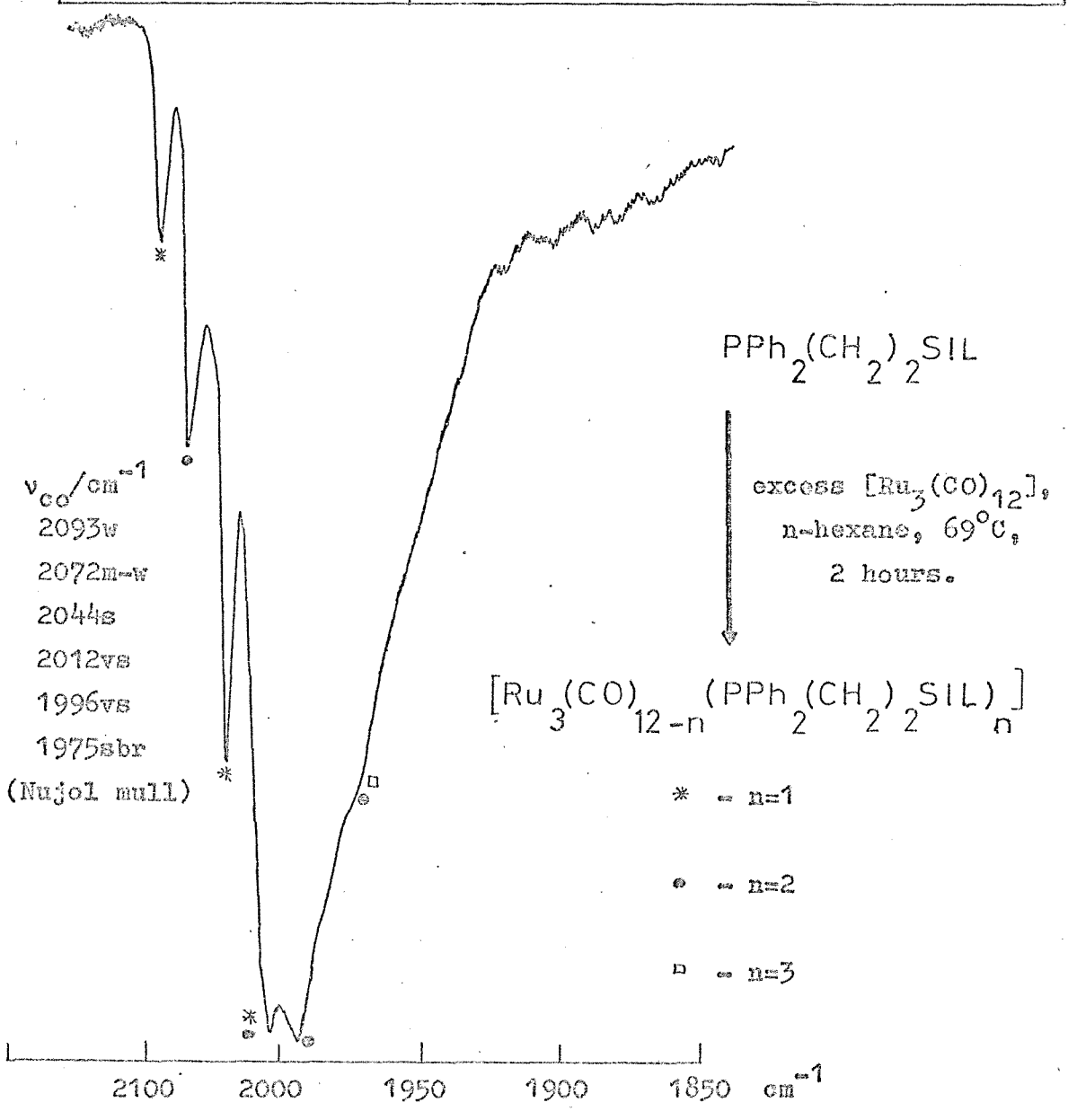
Reaction of excess $[Ru_3(CO)_{12}]$ with an unprotected batch of $PPh_2CH_2CH_2SIL$, by heating to reflux in n-hexane for 2 hours, produced a highly stained, orange-red silica characterised by a broad infrared ν_{co} spectrum containing two bands at 2067 and 1998, with shoulders at 2077 and 2022 cm^{-1}, respectively. In the light of the preceding discussion it is not perhaps surprising that it bears a stronger resemblance to the breakdown products from interaction of the initial cluster directly with an un-modified silica at this temperature, instead of the aimed for mixed-substitution cluster product $[Ru_3(CO)_{12-n}(PPh_2CH_2CH_2SIL)_n]$, n=1,2 or 3, VIII. On leaving in the air this silica gradually decomposes to a gray-green colour with loss of all ν_{co} bands, as previously experienced by Robertson and Webb(150). In contrast, with a silylated sample of $PPh_2CH_2CH_2SIL$, under identical conditions, a crimson-red silica is retrieved which, after successive washes to remove any physisorbed cluster, gives a completely different infrared ν_{co} spectrum (Diagram 11) containing a series of sharp, well-defined absorptions. This time it can be interpreted on the basis of VIII by comparison to that of literature homologues (Table 3). Again the surface rigidity is used to good effect in modifying the product distribution relative to that seen in solution. Indeed, here the move towards the lower mono- and bis-substituted derivatives is even more pronounced; with the latter being favoured. The more demanding spatial requirements for $[Ru_3(CO)_9(PPh_2CH_2CH_2SIL)_3]$ militates against its formation, and it only possibly contributes to the broad shoulder below $2000cm^{-1}$. Presumably at lower phosphine coverages the fraction of $[Ru_3(CO)_{11}(PPh_2CH_2CH_2SIL)]$ would further increase. VIII has a reasonable shelf-life and thermal decomposition, at 100^oC in vacuo, proceeds by a different route to that taken by adsorbed $[Ru_3(CO)_{12}]$ with the formation of

Diagram 11

Infrared (ν_{CO}) Spectroscopic Characterisation of $[Ru_3(CO)_{12-n}(PPh_2CH_2CH_2SIL)_n]$, n=1, 2 or 3.

Table 3

Compound	ν_{CO}/cm^{-1} (cyclohexane unless stated)				
$[Ru_3(CO)_{11}(PMe_2Ph)]$	2096m	2044s	2028s	2016s	2000w
	1987w				
$[Ru_3(CO)_{11}(PPh_3)]$	2097m	2047s	2031sh	2026sh	2017s
(Ref.108b)	2001w	1986w			
$[Ru_3(CO)_{10}(PPh_2Me)_2]$	2070m	2016s	1993sbr	1969sh	
$[Ru_3(CO)_9(PPh_2Me)_3]$	2042w	1966s	1939sh	($CHCl_3$)	
(Ref.101)					



phosphine-containing, pseudo-monomeric, carbonylic entities.

This difference when using unprotected and silylated types of ligand-silica demonstrates the important role of the silanol groups in destabilising the cluster framework, and the efficacy of silylation in overcoming this problem. Others have utilized SCHEME TWO to selectively isolate $[Ru_3(CO)_{11}(PPh_2CH_2CH_2SIL)]$ (87), using the radical anion catalysed substitution reaction with purification by flash chromatography, and $[Ru_3(CO)_9(PPh_2CH_2CH_2SIL)_3]$(157), by contacting the relevant ligand-silane substituted homogeneous derivatives with a silica surface at room temperature: based on the premise that sufficient covalent anchoring of the silyl functionalities will proceed at these conditions where only revesible, physical adsorption of the cluster head is anticipated. Even so, in the first case the preparation was still carried out under carbon monoxide to prevent decomposition, and the remaining silanol groups invariably present must limit the shelf-life of materials formed by this method.

1.3. Preparation and Characterisation of $[H_2Os_3(CO)_{10}(PPh_2CH_2CH_2SIL)]$

1.3.1. The Versatile Chemistry of $[H_2Os_3(CO)_{10}]$

Di-μ-hydro-decacarbonyltriosmium, V, was first reported (158) as one of four products from the reaction of $[Os_3(CO)_{12}]$ with potassium hydroxide in methanol, sodium amalgam or sodium borohydride in THF, followed by acidification with phosphoric acid. Yields obtained by this method varied between 2.8-22%. More recently(159) it has been synthesized in much higher yields, typically up to 73%, by the direct hydrogenation of $[Os_3(CO)_{12}]$ dissolved in refluxing n-octane. The temperature used is only necessary to achieve thermal dissociation of carbon monoxide creating a vacant coordination site. By using the incipient coordinative unsaturation of $[Os_3(CO)_{11}(NCMe)]$ hydrogenation to $[H_2Os_3(CO)_{11}]$, which is known to rapidly convert to V with reduced partial pressures of carbon monoxide, occurs smoothly at room temperature(121). This evidence is consistent with a mechanism first proposed by Shapley(160) where oxidative addition of hydrogen takes place via an activated form of $[H_2Os_3(CO)_{11}]$ with both

$$[Os_3(CO)_{12}] \longrightarrow {}'Os_3(CO)_{11}{}' \longrightarrow [H_2Os_3(CO)_{11}]^{\ddagger} \rightleftarrows [H_2Os_3(CO)_{10}]$$

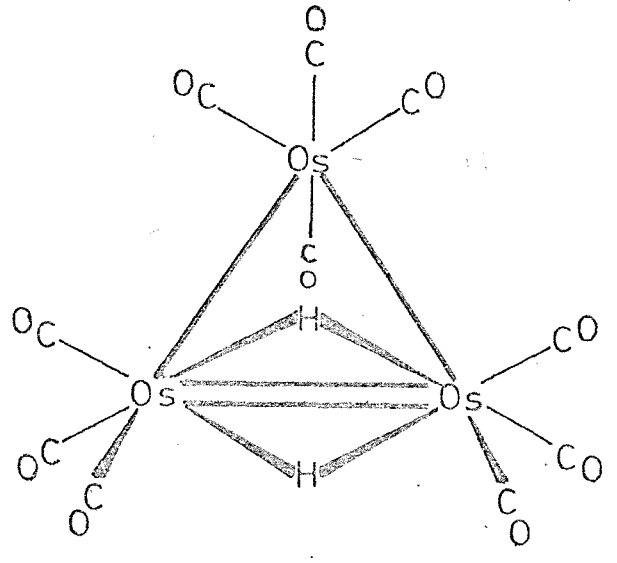
hydrides terminally bonded. Extended treatment at 126°C leads to $[H_4Os_4(CO)_{12}]$ as the only isolated product, albeit in somewhat reduced yields. However it is more successfully prepared from $[Os_3(CO)_{12}]$ in an autoclave, under hydrogen pressure (120atm) at 100°C, where the product almost quantitatively precipitates out of the xylene solution at the end of the reaction(161).

Significantly, when hydrogen was bubbled through $[Ru_3(CO)_{12}]$, under reflux in n-octane, rapid conversion to the tetranuclear $[H_4Ru_4(CO)_{12}]$ occurs without identification of the postulated intermediate $[H_2Ru_3(CO)_{10}]$. Presumably at the conditions employed it lies at a saddle point, and not a minimum of potential energy. Circumstantial evidence for at least the transient existence of this complex is drawn from hydrogenation of $[Ru_3(CO)_{11}(CNBu^t)]$ in refluxing cyclohexane(162). As might be anticipated the tetranuclear hydrido complexes $[H_4Ru_4(CO)_{12-n}(CNBu^t)_n]$, n=0-2, were isolated, but only as minor products. The major species, $[HRu_3(CO)_9(HC{:}NBu^t)]$, has an osmium analogue prepared from the thermolysis of $[H_2Os_3(CO)_{10}(CNR)]$; proceeding via $[H_2Os_3(CO)_9(CNR)]$ which can be isolated if the reaction is halted prematurely(163). This points to the transient formation of $[H_2Ru_3(CO)_9(CNBu^t)]$ but, along with the unsubstituted $[H_2Ru_3(CO)_{10}]$, its propensity to breakdown (to probable dihydro-binuclear units) followed by recombination to tetranuclear products is inhibited by the competitive formation of a stabilising, face-bridging, formimidoyl ligand(164). It has also been shown that $[HRu_3(COH)(CO)_{10}]$, formed by low temperature protonation of $[HRu_3(\mu_2\text{-}CO)(CO)_{10}]^-$, rearranges above -30°C to $[H_2Ru_3(CO)_{11}]$. This inturn decomposes at room temperature, with evolution of gas, to give largely $[Ru_3(CO)_{12}]$ but with small quantities of $[H_4Ru_4(CO)_{12}]$ and $[H_2Ru_4(CO)_{13}]$(165). Then the isolation of V is the fortuitous consequence of a greater potential barrier for the subsequent metal-metal bond breaking than the initial dissociation of carbon monoxide; the reverse applying for the ruthenium system.

The infrared ν_{CO} spectrum of V is reasonably complicated

indicating the compound has low symmetry, and notably no bands due to bridging carbonyl groups are observed. The ^1H NMR shows a single sharp resonance (-11.78, $CDCl_3$) which is close to the typical bridging-hydride region; the signal intensity is equivalent to two hydrogens. The mass spectrum gives a parent ion consistent with the stoichiometry, but the best least-squares fit to a computed isotope pattern was achieved by compensating for overlap due to hydrogen losses(159). The fairly low abundances of these ions, $[HOs_3(CO)_{10}]^+$ and $[Os_3(CO)_{10}]^+$, intuitively ruled out the possibility of terminally bonded hydrogen atoms. The absence of bi- and mono-nuclear fragments in the degradation sequence further suggested a cyclic structure. This spectroscopic evidence, in conjunction with ^{13}C NMR data, indicates that V has a structure comprising of a triangular array of osmium atoms with terminal carbonyl and symmetrically bridging hydride ligands. From a formal electron count there are only 46 electrons associated with the metal valence shells, indicating that four metal-metal bonds are necessary to give each metal atom a share in 18 electrons, suggesting a cyclopropene-type structure with an Os=Os double bond.

X-ray diffraction crystal and molecular structure analyses(55,166) confirmed the predicted shortening of the doubly-



Molecular structure of $[H_2Os_3(CO)_{10}]$

bonded edge of the triangle, consistent with the concept of an increase in bond order, but the hydrogen atoms could not be directly located due to their inherently low X-ray scattering power. This

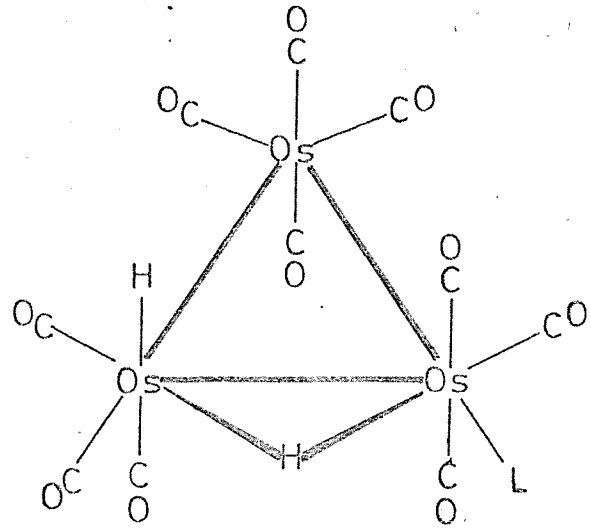
was overcome by two independent, high-precision, neutron diffraction studies(167,168). The osmium atoms define an isosceles triangle with two long (mean 2.814Å) and one short (2.683Å) edge. The two hydride ligands symmetrically bridge the short edge, lying on opposite sides of the Os_3 plane, with the largest amplitude of thermal vibration perpendicular to the metal-metal bond. The four separate Os-H bond lengths are essentially equivalent with a mean value of 1.845Å. The $(\mu\text{-H})Os_2(CO)_4$ fragment is non-planar and is folded along the H...H vector with a dihedral angle of 137.6° between the two $OsH_2(CO)_2$ planes.

This electronic unsaturation instils a large degree of reactivity because the deficiency can be relieved by accepting electrons from incoming ligands without the need to lose those already possessed. Other known electron deficient clusters include the mixed-metal $[HOs_3Au(CO)_{10}(PR_3)]$, prepared from reacting either V with $[AuMe(PPh_3)]$(169) or $[HOs_3(CO)_{11}]^-$ with $[AuCl(PR_3)]$(170), where the unsaturation was found to be localised on the bridged Os-Os bond with the $Au(PPh_3)$ coordinating to the cluster in a similar manner to a hydride in V. Accordingly there are strong parallels in its emerging chemistry(171).

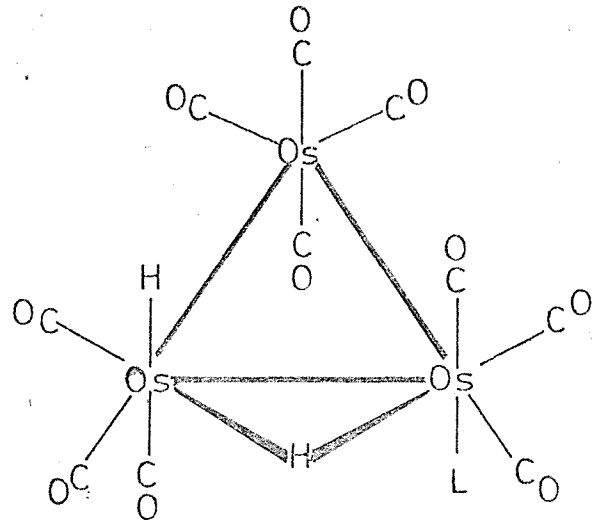
Association of the hydrides with the multiple bond led Broach and Williams(167) to forward a simple LCAO molecular orbital treatment of V where the Os_2H_2 moiety is described in terms of a four centre, four electron bond. This can then be regarded as a protonated double bond like that in the BH_2B bridge of diborane. This model is used to rationalise the observed chemistry which is dominated by nucleophilic addition of two-electron donor ligands. This should depend on the nature of the lowest unoccupied molecular orbital which can be reasonably assumed will be either one of the non-bonding or anti-bonding unoccupied Os_2H_2 four-centre molecular orbitals. Whichever the two electrons enter the M-H-M bridge will be destabilized, probably causing at least one hydrogen to become terminally coordinated. This ability to relieve the saturation, by reaction at room temperature or below with many important molecules, makes it a very good starting material for a good many triosmium clusters. Hence a variety of two-electron donors, such as carbon monoxide(160), phosphines(160,172), phosphites(160), arsines, stibines, amines(173), isocyanides(160,163),

nitriles(172), halides and pseudohalides(173) form 1:1 adducts, $[H_2Os_3(CO)_{10}L]$, by direct addition. In cases where L is an unsaturated molecule the initial addition may be followed by a rapid transfer of hydrogen from the cluster to the ligand. Such processes have been observed for alkenes(174), alkynes(175), isocyanates(176), carbodiimides(177), carbon disulphide(178), organic azides(179) and diazoalkanes(180). In addition, induced hydrogen transfers have been demonstrated for isocyanide ligands(163). The nucleophile may also be metal-centred as in the addition of $[Pt(C_2H_4)(PR_3)]$; two molecules of ethylene are lost to give $[H_2Os_3Pt(CO)_{10}(PR_3)]$(181). This emphasizes another versatile application of V as a precursor to mixed-metal clusters(182) by utilizing its Lewis acid character. Indeed it can even function as an apparent Lewis base to this end as shown by the preparation of $[H_2FeOs_3(CO)_{13}]$(183).

$[H_2Os_3(CO)_{11}]$ was the first of these 1:1 adducts subjected to a X-ray diffraction crystallographic study(53). It was shown to be isomorphous with $[Os_3(CO)_{12}]$, but the analysis was marred by a disorder of the terminal hydride and the axial carbonyl group on the same osmium atom. Also it gave no information on the site taken up by the newly arrived carbonyl ligand. Both these anomalies were avoided in a structural study of $[H_2Os_3(CO)_{10}(PPh_3)]$ (184). Further, both hydrides were directly located by running difference-Fourier syntheses based on different $(\sin\theta)/\lambda$ cut offs of data. The terminal hydride is axially positioned at one end of a metal-metal bond straddled by the second, μ_2-bridging, hydride which lies in the plane of the three osmium atoms. The incoming triphenylphosphine ligand occupies the equatorial site, adjacent to the bridging hydride, at the opposite end of the same metal-metal vector. The corresponding isocyanide adduct has also undergone a full structural determination(185). Here the hydrides were not located, but a seemingly empty coordination site undoubtedly signified the location of the terminal hydride. The only significant difference involves the introduced isocyanide ligand occupying an axial coordination site perpendicular to the Os_3 plane, on the opposite side of the triangle from the terminal hydride. However, in solution it exists as a mixture of isomers, presumably due to different positioning of the isocyanide with the crystal structure



L= CO, PR_3, $P(OR)_3$, AsR_3, or $SbPh_3$



L= CNR, $4\text{-}NC_5H_4X$, N_3^- or CN^-

Molecular structures of $[H_2Os_3(CO)_{10}L]$ clusters

representing the predominant form(163).

This difference can be equated with the axial/equatorial site preferences already outlined for $[Os_3(CO)_{11}L]$ species. The short intermetal distance in V(2.681Å) is lengthened to 2.989(L= CO), 3.000(L=$CNBu^t$) or 3.019(L=PPh_3)Å after the addition. This is consistent with a saturated bond bridged by a hydride atom giving a longer than normal Os-Os distance (2.877Å in $[Os_3(CO)_{12}]$). For all these adducts the hydrides are dynamic in solution undergoing mutual exchange as evidenced by variable-temperature ^1H NMR spectra. The two limiting, low-temperature, hydride signals broaden as the sample temperature is raised, disappear completely into the baseline, before reappearing as a very broad coalesced resonance centred near the mean chemical shift.

1.5.2. Characterisation of $[H_2Os_3(CO)_{10}(PPh_2Et)]$

The required unadsorbed analogue $[H_2Os_3(CO)_{10}(PPh_2Et)]$, IXa, was prepared by addition of a stoichiometric quantity of diphenylethylphosphine to a solution of V in n-hexane. After an immediate colour change, from the characteristic purple of V to yellow, the solution was left overnight to complete precipitation of the product as yellow plates. Its infrared ν_{CO} spectrum (Diagram 15) and the absence of a parent ion in the mass spectrum,

replaced instead by those of the decomposition products $[H_2Os_3(CO)_9(PPh_2Et)]$ and $[Os_3(CO)_{11}(PPh_2Et)]$(186), are consistent with the proposed formulation. Elemental analysis (C and H) also show excellent agreement. In addition to the appropriate ligand ^1H NMR resonances, at -60°C, two equally intense signals are seen at -10.3 and -20.2 δ coupled to each other ($^2J_{HH}$=3.3Hz). The large difference in chemical shifts suggests that only one, the former, corresponds to a terminal enviroment. Consistent with this, only the higher field signal is further split by coupling to the phosphorus ($^2J_{PH}$=11.1Hz), as expected by the anticipated structure. Raising the temperature to ambient results in a loss of resolution in the organic region and a broad coalescence below TMS.

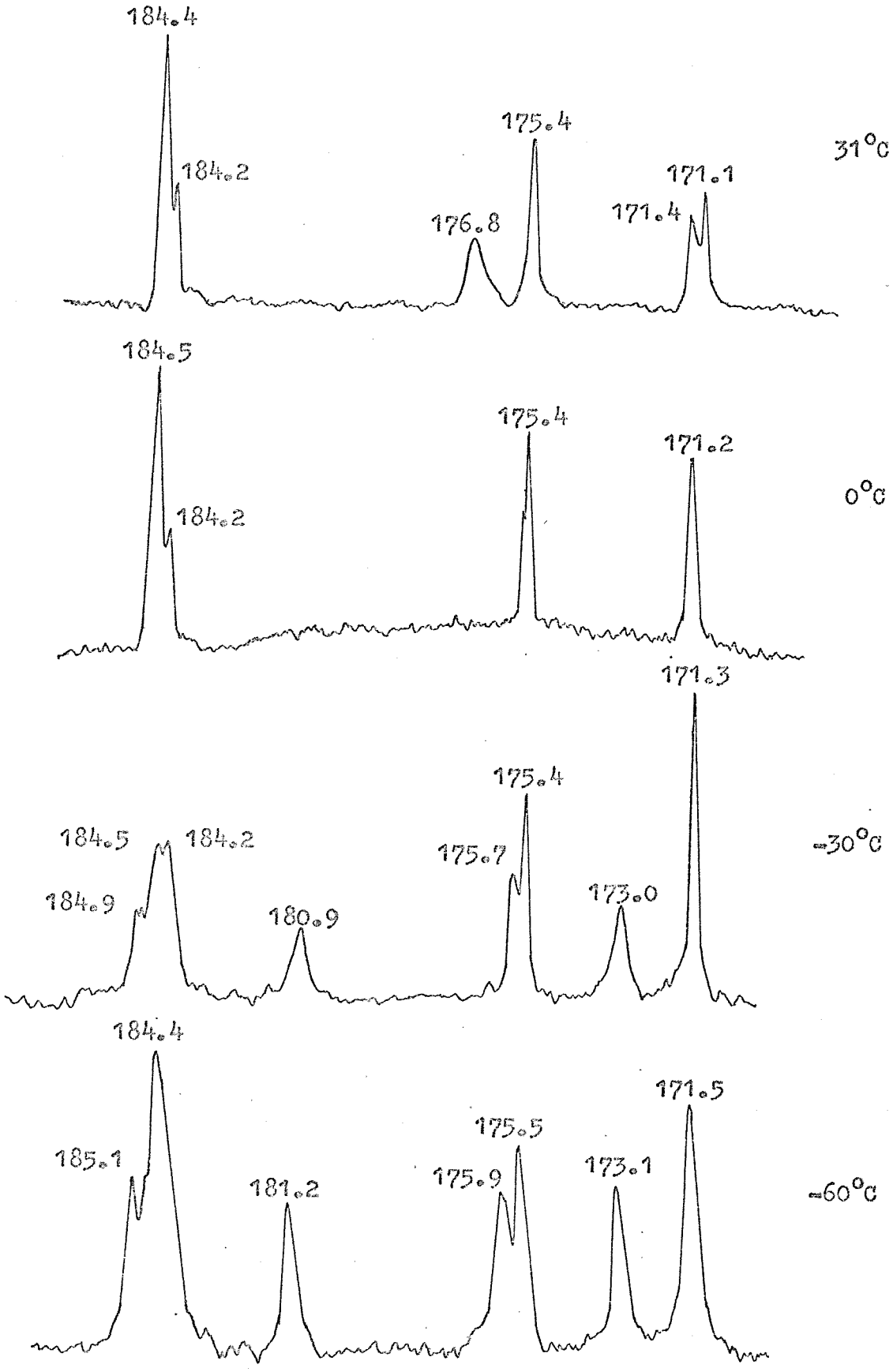
1.5.3. Variable Temperature $^{13}C-\{^1H\}$ NMR Study on $[H_2Os_3(CO)_{10}(PPh_2Et)]$

To ascertain whether the hydride mobility was coupled to a carbonyl migration a variable-temperature ^{13}C NMR study was carried out on a sample prepared from ^{13}CO enriched V. If the solid state structure is retained upon solvation then ten separate carbonyl resonances would be expected in the limiting, low-temperature, ^1H-decoupled spectrum (-60°C, $CDCl_3$), but evidently several are accidently isochronous as only seven are resolved: a, 185.1; b, 184.4; c, 181.2; d, 175.9; e, 175.5; f, 173.1 and g, 171.5 δ-with relative intensities of 1:3:1:1:1:1:2 respectively. There is also definite evidence of a further shoulder on the resonance at 184.46. Subsequent to this work Aime et. al.(187) published similar results for the related PPh_3, IXb, $P(O\text{-}i\text{-}C_3H_7)_3$ and $P(i\text{-}C_3H_7)_3$ adducts, but by varying the phosphine they overcame this unfortunate overlapping gaining better resolution of the signals. As the temperature is increased several resonances broaden and by 31°C they have merged to a single resonance at 176.8 ppm; other minor changes are observed including the highest field signal being resolved into two due to small temperature dependencies (Diagram 12).

On the present evidence alone, with certain relative intensities open to debate, it proved difficult to decide whether the emerging resonance is the result of the coalescence of two, $MEAN_{c+f}$ =177.26, or three, $MEAN_{c+d+f}$= 176.76, signals, although

Diagram 12

Variable Temperature $^{13}C-\{^{1}H\}$ NMR Spectra of $[H_2Os_3(CO)_{10}(PPh_2Et)]$



a small shoulder on e at 0°C would support the former process. Recourse to the data for IXb also supports this preference. This is fundamentally important because it dismisses the possibility of complete polytopal rearrangement about an osmium shared by both hydrides in the intermediate (Mechanism One, Diagram 13). This structure nicely conforms to the 18-electron rule for each osmium, but the fact that it is higher in energy indicates the extra stability associated with bridging hydride ligands. The favoured, more restricted, dynamic process (Mechanism Two) involves a concerted oscillatory motion of only two carbonyl groups with the terminal and bridging hydrides in the octahedral plane defined by these four atoms. Site exchange of the carbonyls occurs bringing the terminal and bridging hydrides to opposite faces of the molecule. The interdependency of these changes is supported by measurements of line broadening in the slow-exchange regions of the ^{1}H and ^{13}C NMR spectra which revealed similar free energies of activation(187). A wider ranging study(173) of $\Delta G^{\ddagger}$ values, as determined from the ^{1}H NMR, established a dependence on the steric and electronic demands of the introduced equatorial ligand, increasing with the cone angle and polarizability (or decreasing basicity) of the donor atom. Both these trends are best accounted for with the postulated, doubly-bridged, transition state. The possibility that CO_C, and not CO_B, is exchanging with CO_A cannot be rigorously excluded but such a process would be of higher energy, it is believed, and also contravene the supporting evidence for the below resonance assignments.

Of the two resonances involved in the dynamic process that at 181.2δ is assigned to CO_A, trans to the terminal hydride, on the basis of the large interaction observed in the ^{1}H-coupled spectrum (Diagram 14). Although with IXb this appears as only a doublet ($^{2}J_{CH}$=24Hz) for IXa, by comparison with the related $[H_2Os_3(CO)_9(PPh_3)(C_2H_4)]$(Chapter Three), it is preferably interpreted as a doublet of doublets ($^{2}J_{CH}$=13.6 and 3.3Hz). The relative chemical shift to the second at 173.1δ, which did not show evidence of ^{1}H-coupling, is also consistent with it representing CO_B approximately trans to the bridging hydride on the same osmium. The only other distinct coupling was to e, as signified by a loss of relative intensity. This must correspond to either CO_C or CO_D,

Diagram 13

Possible Ligand Migration Processes in $[H_2Os_3(CO)_{10}L]$, L=CO or PR_3

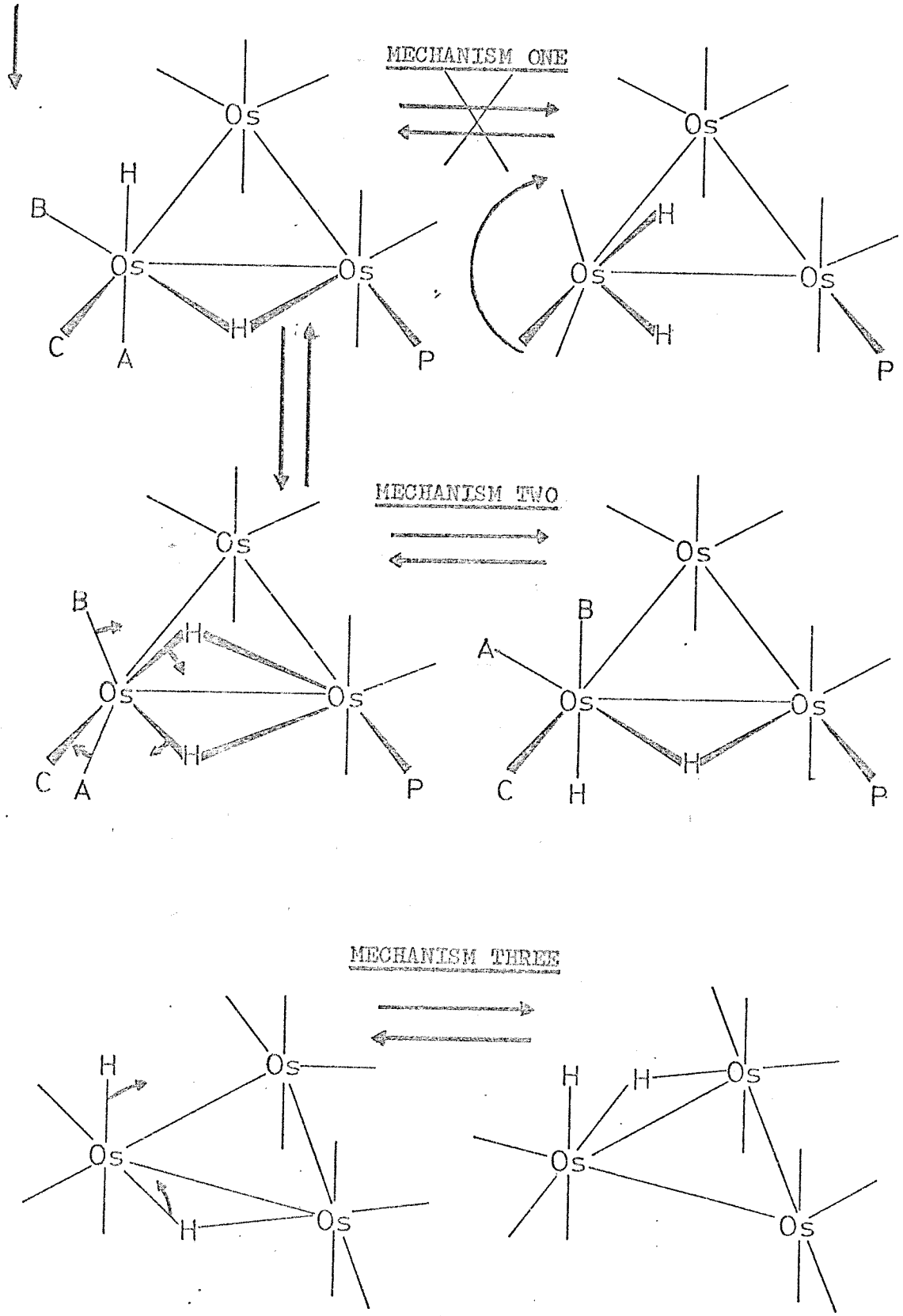
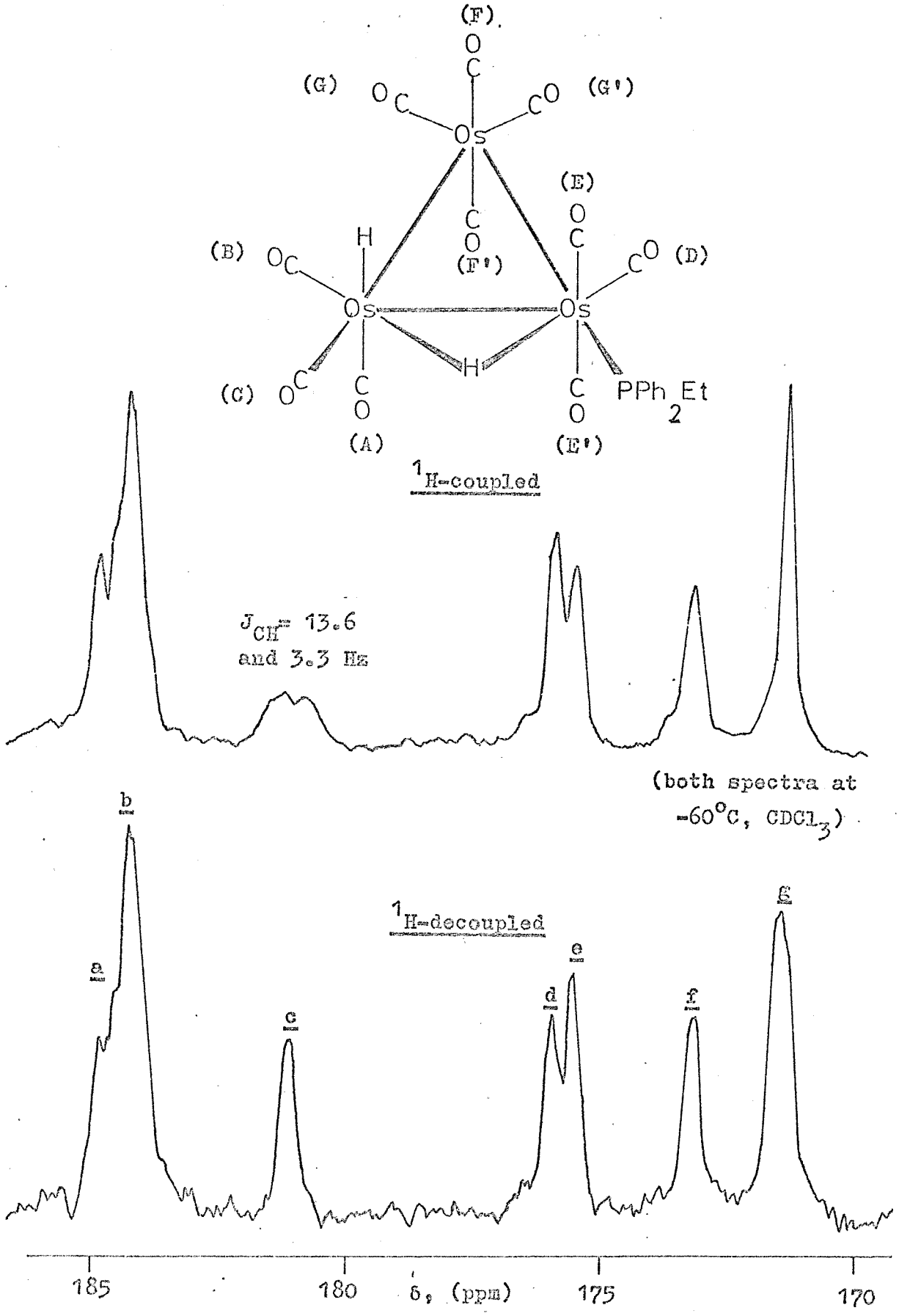


Diagram 14

Low Temperature, Limiting ^{13}C NMR Spectra for $[H_2Os_3(CO)_{10}(PPh_2Et)]$



but is assigned to the first because, whilst the chemical shift of this resonance remains almost invariant to changes in phosphine substituent or temperature, that at 171.18(31°C) shows a large dependence on the nature of the phosphine and was thus assigned to CO_D(187). Its absolute chemical shift conveniently fits into a trend $P(O\text{-}i\text{-}C_3H_7)_3$, 168.86; PPh_3, 170.46; and $P(i\text{-}C_3H_7)_3$, 172.18 of increasing phosphine basicity resulting in a greater downfield shift of the resonance. This leaves the $Os(CO)_4$ and axial groups on the phosphine-bonded osmium unallocated.

The proposed dynamic behaviour will simultaneously cause averaging within the two sets of axial ligands which, combined with the general observation that accompanying resonances are normally found at lower field than those for radial groups, allows them to be collectively assigned to the overlapping signals after 184ppm. At higher temperatures the pattern becomes less complex, as expected on raising the apparent molecular symmetry, and although no attempt is made to rationalise these changes the final arrangement may be deciphered as a singlet, attributed to $CO_F/CO_{F'}$, and a partially obscured doublet, due to a phosphorus-carbon two-bond coupling, as possibly anticipated for $CO_E/CO_{E'}$. The outstanding resonances at 175.9 and 171.4 δ must then correspond to CO_G and $CO_{G'}$. No attempt is made to differentiate these two, but it is interesting to note that these two signals are especially temperature dependent as a similar phenomena is evident for their counterparts in $[H_2Os_3(CO)_9(PPh_3)(C_2H_4)]$.

As yet no complete investigation for $[H_2Os_3(CO)_{11}]$ has been published, but preliminary data(94) is consistent with even greater ligand mobility over a comparable temperature range. Complete polytopal rearrangement about the pivot $Os(CO)_3$ appears to be occurring combined with hydride scrambling along two metal edges as shown in Mechanism Three. The presence of a phosphine appears to restrict hydride migration to a localised process along a single metal-metal bond.

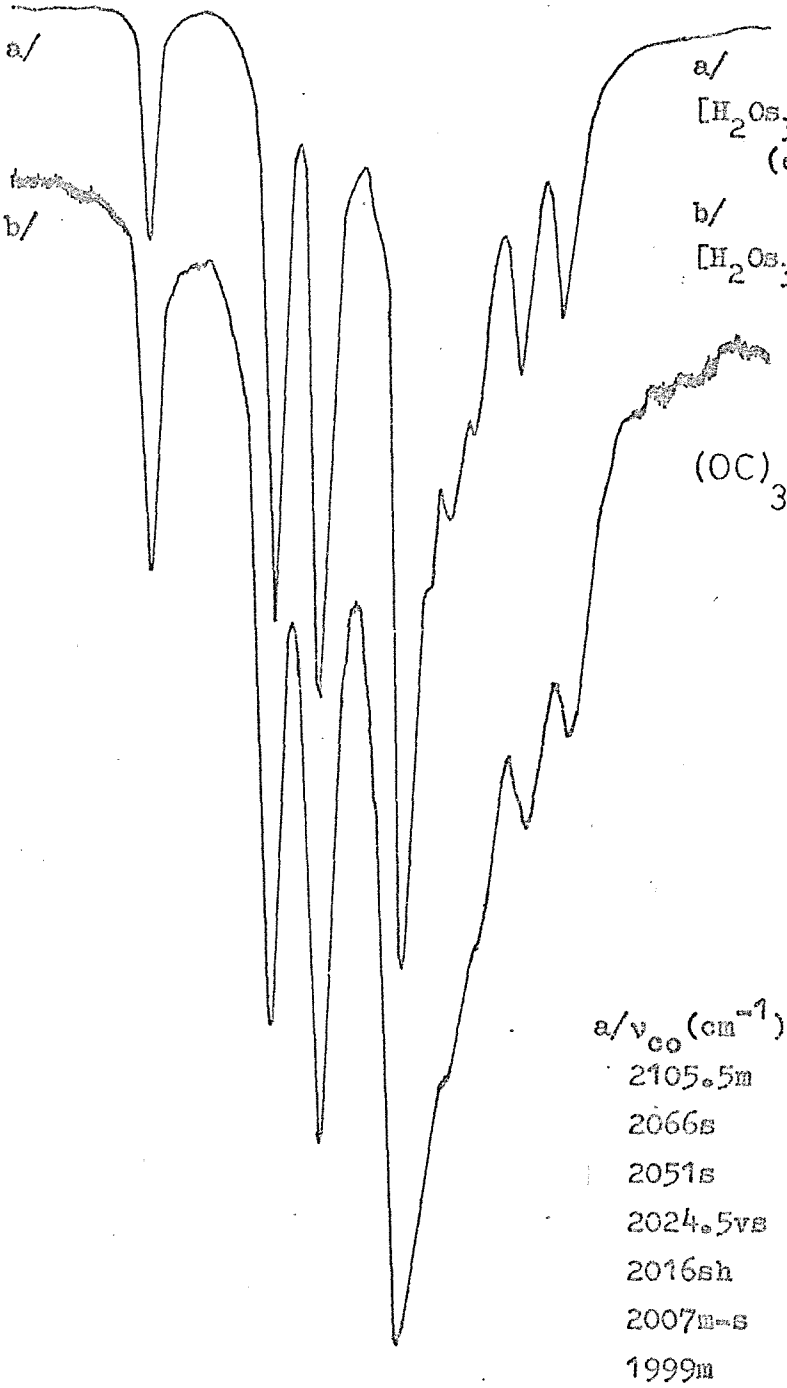
1.5.4. Preparation of $[H_2Os_3(CO)_{10}(PPh_2CH_2CH_2SIL)]$

At first an attempt was made to prepare the 1:1 adduct from reaction with the phosphine-silane, $PPh_2CH_2CH_2Si(OEt)_3$. Again

Diagram 15

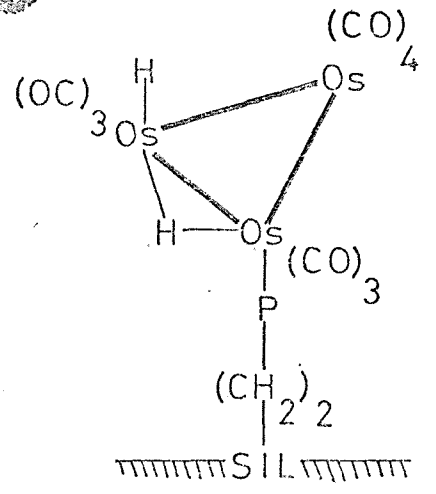
Infrared (ν_{CO}) Spectroscopic Characterisation of

$[H_2Os_3(CO)_{10}(PPh_2CH_2CH_2SIL)]$



a/ $[H_2Os_3(CO)_{10}(PPh_2Et)]$ (cyclohexane)

b/ $[H_2Os_3(CO)_{10}(PPh_2CH_2CH_2SIL)]$ (Nujol mull)



a/ ν_{CO} (cm^{-1})	b/ ν_{CO} (cm^{-1})
2105.5m	2105w
2066s	2065m-s
2051s	2049s
2024.5vs	2024vs
2016sh	-
2007m-s	2006ssh
1999m	1998m
1982.5m	1981m-w
1972m	1970w

on addition an immediate colour change to yellow occurred, but on leaving overnight the solution turned olive-green without hardly any precipitation of the required product. Removal of the solvent and chromatography on silica-gel, with diethyl ether/hexane (5:3 v/v), gave a series of products; those of smaller R_f proving difficult to remove from the plate. None of the resulting infrared ν_{co} spectra resembled that of the expected species. This again demonstrates the difficulty of obtaining adducts with the ligand-silane because of lost selectivity, due to interference from the backbone, and the practical limitation of separations on hydroxylic materials. Even if $[H_2Os_3(CO)_{10}(PPh_2CH_2CH_2Si(OEt)_3)]$ had been selectively prepared, the subsequent conditions necessary to securely anchor it to silica would almost certainly cause loss of species integrity. Therefore a route to the supported complex via SCHEME TWO appeared unappropriate, but the mild conditions required to prepare the 1:1 adducts should favour SCHEME ONE and this has proved the case. As V is known to be reasonably stable on chromatographic plates at ambient temperatures no direct chemical interaction would be anticipated.

A quantity of $PPh_2CH_2CH_2SIL$ was suspended in dry methylene chloride and stirred at room temperature. Successive small (spatula-head) portions of V were added until after two hours from the last addition the supernatent liquor was still purple reminiscent of excess precursor cluster (and indirectly showing maximum complexation on the ligand-silica). In contrast, the silica simultaneously acquired a concentrated light-yellow colour characteristic of the required surface species. Once the reaction had terminated the silica was filtered off, washed several times with fresh solvent, and then dried in the air. It gave a very intense infrared ν_{co} spectrum, shown in Diagram 15, which is in excellent agreement with that of the unadsorbed analogue. Thus, as anticipated, $[H_2Os_3(CO)_{10}(PPh_2CH_2CH_2SIL)]$, X, was successfully prepared, as the exclusive product, via SCHEME ONE. At this stage no difference was apparent whether the ligand-silica was pretreated with a silylating agent or not, since under the mild conditions there is no interaction with the surface silanol groups.

1.6. Preparation and Characterisation of $[H_2Os_3(CO)_9(PPh_2CH_2CH_2SIL)]$

1.6.1. Thermolysis of $[H_2Os_3(CO)_{10}L]$

Whilst the attainment of X is of academic interest it is unlikely to be of any catalytic importance since above room temperature, nominally under reflux in n-hexane, these 1:1 adducts are unstable undergoing smooth conversion back to 46 electron systems. The precise outcome depends on the nature of the pendant ligand. For strongly coordinating species, such as phosphines or isocyanides, carbon monoxide is eliminated to give $[H_2Os_3(CO)_9L]$, which is identical to the parent V except that one of the bridgehead osmium atoms bears the appropriate ligand instead of one of the carbonyls. Thus, overall there is carbon monoxide substitution by an associative pathway with carbon monoxide loss as the slow second step. However, if it is weaker binding than a carbonyl, such as a nitrile, the new ligand is ejected to regenerate V again. Indeed the 1:1 adduct with phenyl cyanide is only stable in solution in the presence of excess ligand, and even isolated crystals will decompose when dried under vacuo. Similarly $[H_2Os_3(CO)_{11}]$ is unstable in solution in the absence of dissolved carbon monoxide. An exception occurs with trifluoroacetonitrile where the presence of an electron-withdrawing substituent sufficiently enhances hydride transfer to the nitrile ligand to facilitate room temperature formation of stabilised edge-bridging moieties(188).

In all examples studied so far the phosphine always adopts an equatorial position both in solution and in the crystal lattice. With isocyanides the situation is more complex and (at least) two different isomers result, with their relative abundancies dependent upon the steric bulk of the nucleophile. The first is analogous to the phosphine derivative, whilst the second has the isocyanide in one of the four pseudo-axial sites. In this latter form the two bridging hydride ligands are inequivalent, and this is seen in the ^1H NMR spectrum where two separate singlets of equal intensities exist. Full X-ray crystallographic analyses on the tert-butyl- and phenyl-isocyanide derivatives have confirmed these preferences, with the bulkier ligand adopting a less hindered equatorial position(185) but the smaller phenylisocyanide occupying

a pseudo-axial position(163).

1.6.2. Characterisation of $[H_2Os_3(CO)_9(PPh_2Et)]$

As expected, pyrolysis of IXa, under reflux in n-hexane, leads to the facile formation of $[H_2Os_3(CO)_9(PPh_2Et)]$, XIa. Direct conversion of V to XIa, without intermediate isolation of IXa, is also possible by addition of an equimolar quantity of phosphine to the solution as it is brought to reflux. After chromatography, XIa is isolated as dark green/black rectangular crystals. Yields were normally high, typically 80%, but on occasions when they were low a broad yellow baseline appeared on the t.l.c. plate. This can be associated with further ligand addition, accompanied by concurrent decomposition, and is discussed further in Chapter Three. The corresponding triphenylphosphine, XIb, and trimethylphosphite, XIc, derivatives were also prepared for use in future studies.

The infrared ν_{CO} spectrum of XIa (Diagram 17) only contains frequencies due to terminal groups and shows excellent agreement with that of known literature analogues. In the mass spectrum a parent ion, m/e=1040, is observed followed by a fragmentation scheme involving predominantly stepwise loss of nine carbonyl groups, but increasingly complicated by phosphine degradation and hydride dissociation. However a naked metal core, $[Os_3]^+$, is clearly seen which possesses an excellent triosmium isotopic pattern. Elemental analysis (C and H) is also consistent with the proposed stoichiometry. In addition to the obvious resonances associated with a coordinated phosphine, the ^1H NMR spectrum (31°C, $CDCl_3$) exhibits a sharp doublet at -10.38 ($^2J_{PH}$= 7.3Hz) which shows no temperature dependence over the range -60 to +90°C studied.

All this data is entirely consistent with XIa being completely isostructural to the previously reported XIc, which has been the subject of a single crystal X-ray diffraction study (189). The molecule is isostructural with V but with the replacement of an equatorial carbonyl group on one of the non-unique osmiums by the phosphine. The presence of the phosphine does not appear to affect the short Os-Os bond, and has little

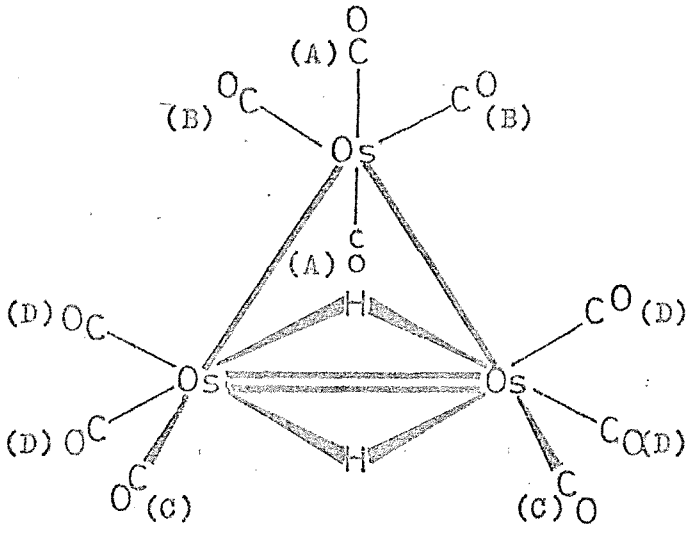
steric influence over the positions of adjacent carbonyl ligands. The hydrides were not located directly, but from their known steric influence(190) the observed Os-Os-C(carbonyl) angles clearly showed that they both bridge the short edge and lie above and below the Os_3 plane.

1.6.3. Variable Temperature ^{13}C NMR Study on $[H_2Os_3(CO)_9L]$; L= CO or PPh_2Et

The ^1H NMR data for XIa implies that both hydrides are equally disposed to the phosphine in solution, consistent with the solid-state structure. However its temperature invariance does not assist identification of any possible fluxional processes present, particularly any involving the carbonyl groups. Accordingly a more detailed confirmation that the crystal structure is retained upon solvation was sort by carrying out a variable temperature ^{13}C NMR study. At this juncture the ^{13}C spectral data for V is first reported since the two sets are shown to be related. After completion of this work some sections have been subsequently published by other workers(191,192).

A sample of ^{13}CO enriched V was prepared from the pretreated $[Os_3(CO)_{12}]$. Four resonances are seen in the room temperature spectrum: a, 182.4; b, 181.4; c, 176.1 and d, 174.9 δ- with relative intensities of 2:2:2:4 respectively. These remain unaltered at -20°C ($CDCl_3$), and below this temperature sample precipitation hindered further study. However this is unimportant because the recorded spectrum is entirely consistent with the solid-state structure and represents the limiting low-temperature case.

From its relative intensity d is immediately assigned to the four equivalent carbonyl groups, CO_D, occupying pseudo-axial positions on the non-unique osmium atoms. Each is trans to an hydride ligand and in the ^1H-coupled spectrum the signal is split into a doublet ($^2J_{CH}$=11.2Hz) enhancing the assignment. It is noticeable that although no discernible cis-couplings were resolved, definite line broadening of a, c and the doublet is indicative of additional interactions. On this basis the signal with the narrowest half-width, b, was tentatively assigned to the



^{13}C Assignments for $[H_2Os_3(CO)_{10}]$

equatorial groups, CO_B, on the unique osmium assuming that through-space coupling with the hydrides will be an order of magnitude smaller than to the corresponding axial pair, CO_A. This is consistent with interatomic distances calculated from the fractional coordinates and cell dimensions obtained in the low temperature (110°K) neutron diffraction study(167). The mean short distance between an hydride and the axial carbonyls on the unique osmium is 2.78Å (the longer, through the plane of the molecule, value is 4.11Å), whilst the average value to the equatorial groups is 4.58Å. Although its actual contribution cannot be quantified here, the importance of such through-space couplings in cluster systems has already been established elsewhere(193).

The same assignments were also reached from studies on an highly (>60%) ^{13}CO-enriched sample of V(194). Both low-field peaks show fine-structure due to $^2J_{CC}$ cis-coupling constants, but a is appreciably broadened by additional coupling to CO_D and can thus be assigned to the pair, CO_A. $^3J_{CC}$ values are expected to be not negligible for carbonyl groups which are three bonds away but trans-related through a metal-metal bond as already found for $[Ir_4(CO)_{11}(CNBu^t)]$(195). The line-broadening for c and d is attributed to more 'conventional' through-bond $^2J_{CH}$ cis-interactions which other reseachers(196) have estimated at approximately 2Hz.

A high-temperature study was carried out to supplement these assignments, using d_8-toluene as solvent. At elevated temperatures signals c and d collapse, coalesce and by 90°C an averaged signal is beginning to emerge. This results from stereochemical non-rigidity of the $Os(CO)_3$ groups, which could occur via axial-equatorial exchange or pair-wise bridge-terminal interchange(43). However, the former process is favoured and evidence from XIa consolidates this view. It is impossible to say whether the hydrides are anyway involved in this motion. These observations confirm that c arises from the equatorial carbonyls, CO_C, common to the bridged edge and a and b belong to the $Os(CO)_4$ unit. The latter signals do not exhibit any appreciable line-broadening at the highest temperature (90°C) studied, and even at the decomposition temperature (ca. 120°C) only a slight broadening is reported(43). Hence there is no evidence to invoke a polytopal rearrangement, via a simple twist mechanism, about this unit.

It is interesting to compare these results with those obtained for the related $[HOs_3(CO)_{10}X]$ and $[Os_3(CO)_{10}X_2]$ systems. For the mono-hydride adducts an extensive study (X=SEt, SPh, NBu^nH, OH, Cl, Br, I, CO_2Me or CO_2CF_3) has shown them to be non-fluxional at room temperature, but in a number of cases above 70°C considerable broadening of the resonances associated with the $Os(CO)_4$ unit occurs, and with X=CO_2Me and CO_2CF_3 coalescence is reached at 90°C(140). This is attributed to carbonyl rotation about the unique osmium, but significantly no evidence for exchange about the $Os(CO)_3$ units was noted. The compounds $[Os_3(CO)_{10}X_2]$, X=Cl, Br, I or OEt, are stereochemically rigid over all the temperatures studied (-90 to 95°C). However, evidence exists for a slow exchange, not on the NMR timescale, within the $Os(CO)_3$ groups. Unenriched samples undergo stereospecific exchange of labelled carbon monoxide at the CO_C sites at room temperature, but a thermal rearrangement (110°C in toluene, less than 5 minutes) occurs to give a statistical distribution amongst the carbonyls on the non-unique osmium atoms(197). The influence of the introduced three-electron donors upon these fluxional processes is clearly important but whether this is primarily a steric or electronic effect is unknown. Certainly from the crystal structure of $[HOs_3(CO)_{10}Cl]$(198) the presence of the chloride has an electronic

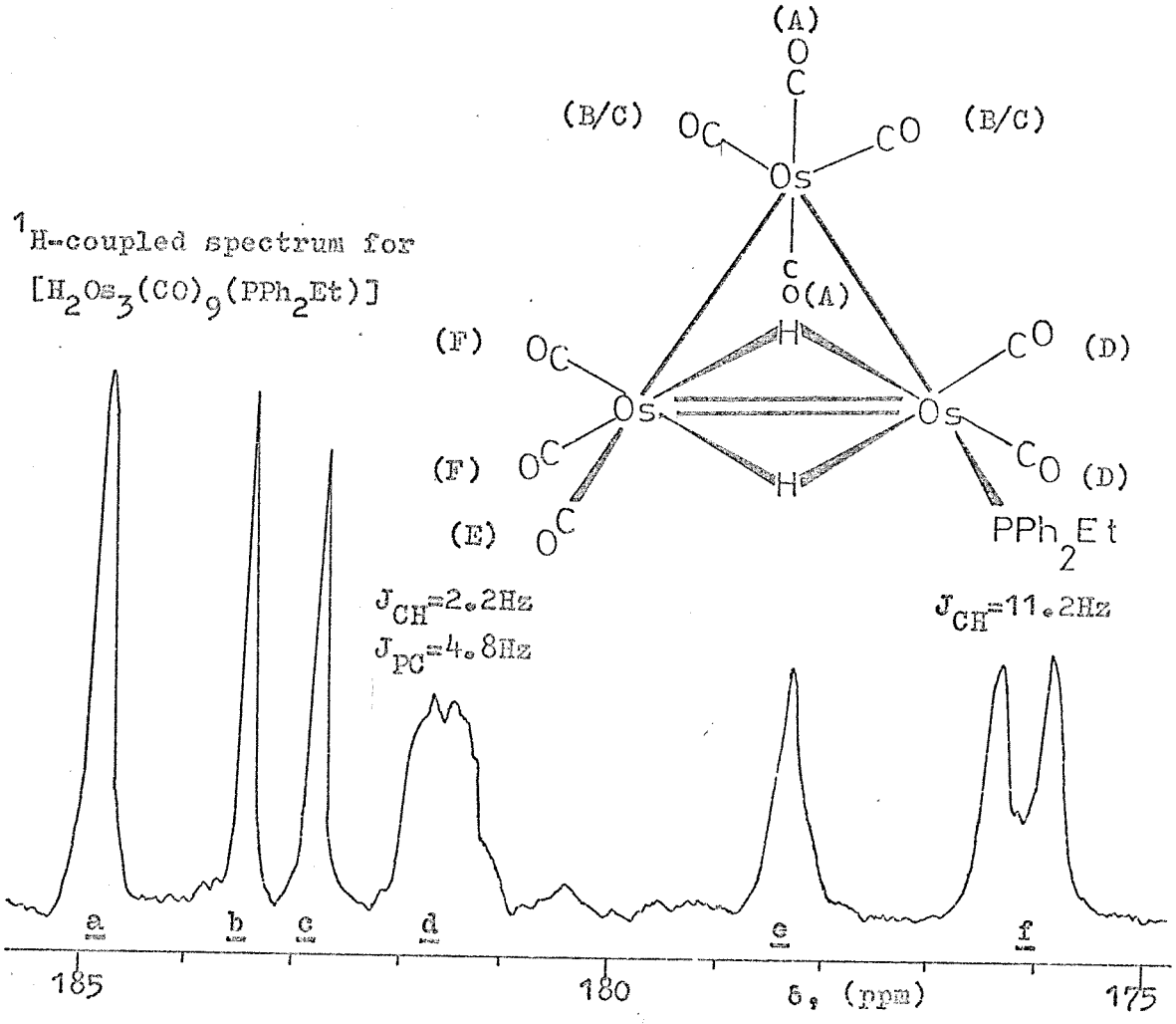
effect significantly shortening the Os-CO distances trans to itself.

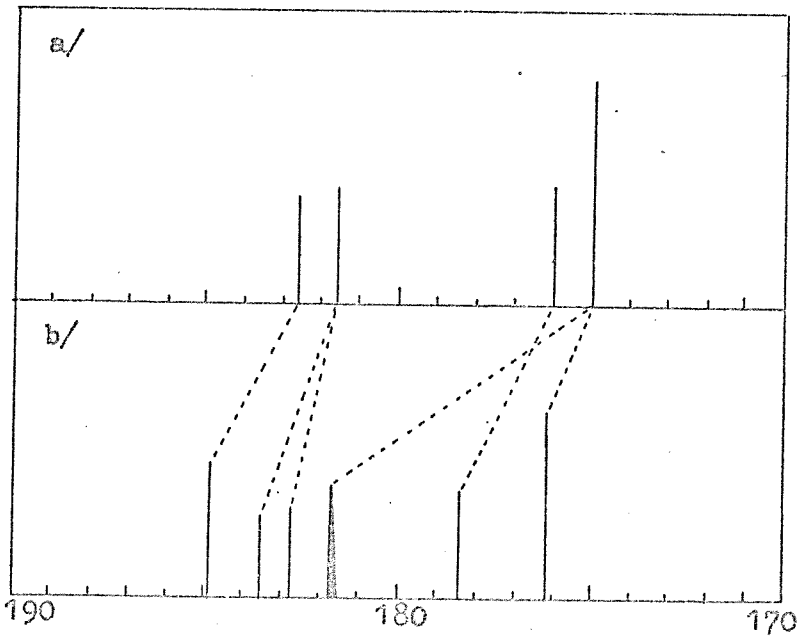
A full, variable temperature, ^{13}C NMR study was carried out a sample of XIa prepared directly from the ^{13}CO enriched V. Introduction of an equatorial phosphine lowers the molecular symmetry from C_{2v} to C_s, with only the plane through the metal triangle retained. Consistent with this geometry six resonances are observed in the room temperature spectrum: a, 184.8; b, 183.4; c, 182.7; d, 181.6; e, 178.3 and f, 176.1 δ- with intensities of 2:1:1:2:1:2. If the phosphine was located in a pseudo-axial site the symmetry is completely destroyed and nine resonances would be expected. However, the observed spectrum remains unchanged at -60°C ($CDCl_3$), the lowest temperature employed, and it is hard to envisage any fluxional process that could account for this provided the phosphine is a rigid entity.

Only d shows coupling to the ^{31}P nucleus ($^2J_{PC}$=4.8Hz) and is consequently assigned to the semi-axial groups, CO_D, sharing the same osmium as the phosphine ligand. Proton-coupling causes all the signals, apart from b and c, to broaden due to interactions with the hydride nuclei (Diagram 16). From their intensities, and by applying the arguements used for V, the two unaffected resonances must correspond to the non-equivalent equatorial groups, CO_B and CO_C, of the $Os(CO)_4$ unit. The remaining resonance of unit intensity, e, is then associated with the equatorial carbonyl, CO_E, of the $Os(CO)_3$ group. Both d and f show resolved couplings, $^2J_{CH}$=2.2 and 11.2 Hz respectively, which confirms the assignment of d, whilst relating f with the pseudo-axial enviroments, CO_F, on the second bridgehead osmium. The almost identical coupling constant to f, and the corresponding sites in V, firmly establishes the similarity in spatial arrangement, as shown by the crystal structure, and electronic enviroments. Conversely, the presence of the phosphine has a considerable effect on the magnitude of the coupling constant. In the absence of a neutron diffraction study it is impossible to postulate any asymmetry it might induce in the bridging hydrides (although the observations with f point against this possibility). However the X-ray diffraction study serves to illustrate that, while the phosphine does not significantly alter the spatial arrangement about the osmium, it does have a noticeable electronic effect

Diagram 16

Low Temperature, Limiting ^{13}C NMR Spectra for $[H_2Os_3(CO)_9L]$; L=CO or PPh_2Et.





Comparison of the limiting spectra for $[H_2Os_3(CO)_{10}]$, a/, and $[H_2Os_3(CO)_9(PPh_2Et)]$, b/.

shortening the Os-CO distances. Since the phosphine is a better σ-donor, but a poorer π-acceptor, than a carbonyl ligand it tends to push electron density onto the osmium which will be taken up by stronger backbonding to the carbonyls; this appears to be reflected in the coupling constant. The outstanding signal, a, is allocated to the axial pair, CO_A, on the $Os(CO)_4$. In view of these assignments it is interesting to note the peak shapes of the signals with unresolved features. With increased resolution e should be a triplet, as a result of cis-coupling to two equivalent hydrides, and has a significantly more pyramidal profile than either a, or the two branches of f, which should be further split into doublets (ignoring the longer range interactions to a); these couplings are estimated at <2Hz.

As the temperature is raised the signals e and f coalesce, and an averaged signal begins to appear above 70^{o}C. This underlines the assignment of these resonances to the $Os(CO)_3$ group, and the persistence of this oscillatory motion upon phosphine substitution highlights its localised nature. Although only a limited number of spectra were recorded, and the quality was poor, it appears the barrier to rotation is unaltered, or marginally lower, in the substituted derivative. The similar rotation at the other osmium is blocked by the rigid phosphine.

A comparison (Diagram 16) of the limiting spectra of V and XIa illustrates a large degree of correlation between the chemical shifts of related carbonyl enviroments. In general, upon substitution the absolute values all undergo a paramagnetic shift of ca. 1-2ppm, with the exception of those affixed to the same osmium as the phosphine whence the shift is more marked (ca. 7ppm). This can be equated with observed crystal structure detail by reference to the increased basicity of a phosphine compared to a carbonyl ligand. The fact that its presence is transmitted throughout the cluster may also be relevant towards a possible lower barrier to polytopal rearrangement within the $Os(CO)_3$, since such a labilizing effect is already known in other cluster systems. These empirical trends are used to good effect in Chapter Three when assigning resonances in phosphine derivatives by comparison to those of the unsubstituted cluster.

PTO

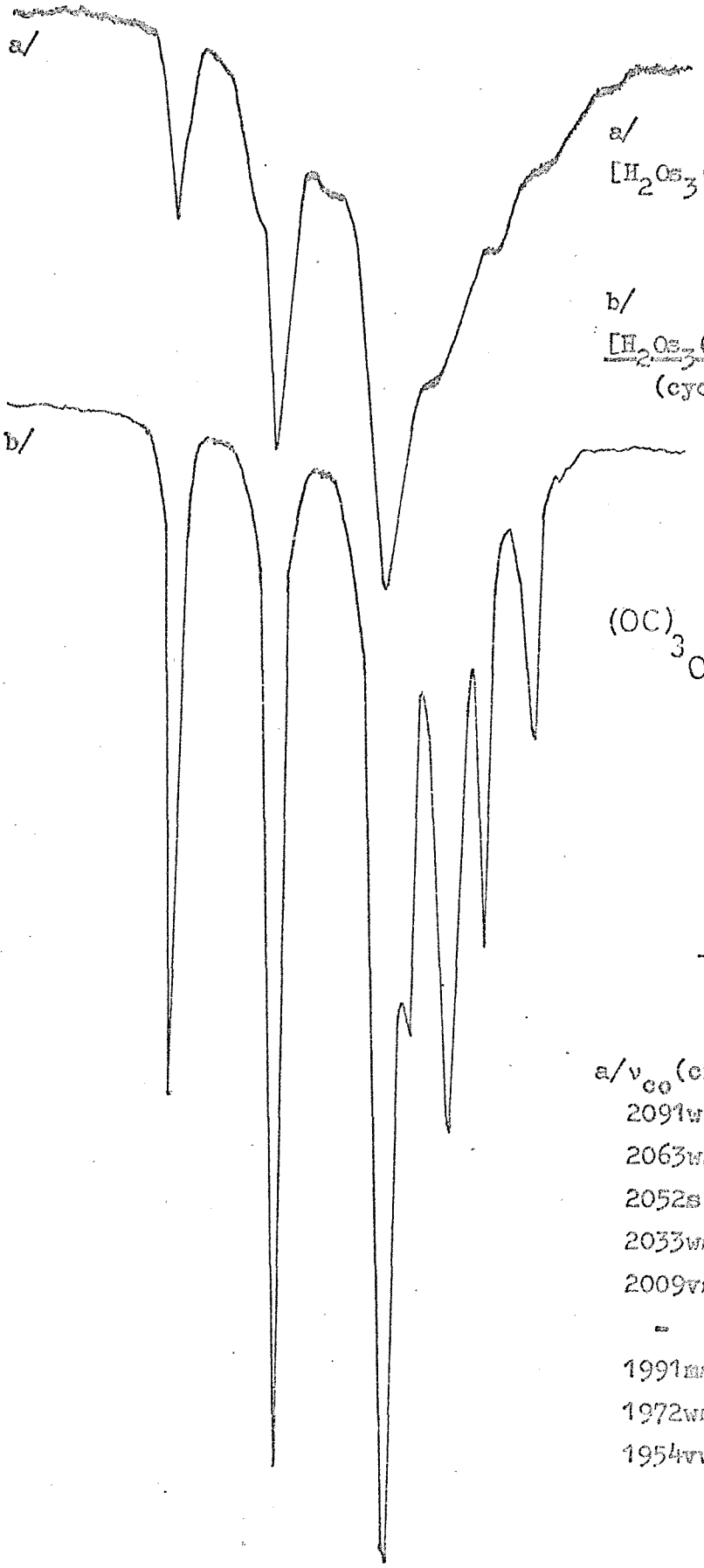
1.6.4. Preparation of $[H_2Os_3(CO)_9(PPh_2CH_2CH_2SIL)]$

It was noticeable that even when recording the infrared ν_{CO} spectrum of X the heat of the beam caused a shoulder to develop at 2095 on the 2105cm^{-1} peak. This indicated that carbonyl loss was quite facile, and conversion to $[H_2Os_3(CO)_9(PPh_2CH_2CH_2SIL)]$, XII, should be easily achieved. Indeed a self-supporting disc of X, mounted in an evacuable cell and held in an infrared beam, rapidly converted to XII within an hour. On a preparative scale a freshly prepared sample of X was heated under vacuo at 40°C overnight. Within a relatively short time the solid began to darken, eventually becoming green in colour. The chosen reaction period was used purely for convenience and to ensure completion; it was not found detrimental to the nature of the product. The recovered silica was still free flowing and its infrared ν_{CO} spectrum (Diagram 17), by comparison with that of XIa, firmly established a successful decarbonylation step to give XII. However, certain discrepancies can be seen and, in particular, the two shoulders at 2063 and 2034cm^{-1} are due to a second surface species believed to result from breakdown of XII by further phosphine substitution and coordination of surface silanol groups. This is discussed in Chapter Five, but demonstrates the major drawback of SCHEME ONE whereby remaining, uncomplexed, phosphines can become important when more vigorous conditions are applied. Secondly, it highlights the disadvantage of incomplete silylation of residual silanol groups left after surface modification with the bulky phosphinosilane. Consistent with this the two shoulders tended to be more pronounced when XII was prepared by the same method as the unadsorbed variant, by heating under reflux in n-hexane for 2 hours, or when no attempt to modify outstanding silanol groups had been taken. When a solvent was employed, niether it nor any subsequent washings had any perceivable coloration, indicating that cluster leaching from the surface had occurred.

Despite the above complication the decarbonylation is the principal reaction and represents one of the first examples where proven solution chemistry is reproduced on an immobilized species. This avenue is receiving greater attention with more sophisticated synthetic chemistry being attempted. Oxidation

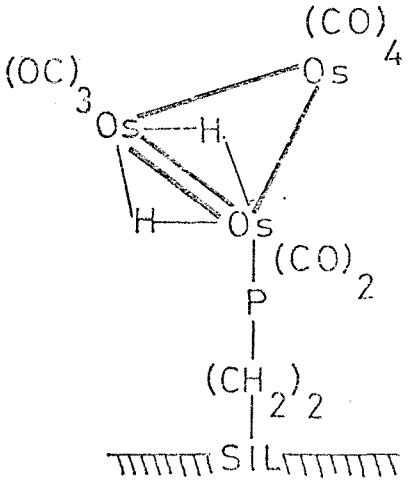
Diagram 17

Infrared (ν_{CO}) Spectroscopic Characterisation of $[H_2Os_3(CO)_9(PPh_2CH_2CH_2SIL)]$



a/ $[H_2Os_3(CO)_9(PPh_2CH_2CH_2SIL)]$
(Nujol mull)

b/ $[H_2Os_3(CO)_9(PPh_2Et)]$
(cyclohexane)



a/ ν_{CO} (cm^{-1})	b/ ν_{CO} (cm^{-1})
2091w	2093m
2063wsh	-
2052s	2054s
2033wsh	-
2009vs	2013vs
-	2005m
1991msh	1990m
1972wsh	1975m-w
1954vwsh	1957w

of one carbonyl group by Me_3NO, in the presence of acetonitrile, has afforded $[HOs_3(CO)_9(NCMe)(S\text{-}OXIDE)]$ on silica and alumina. The introduced acetonitrile ligand represents an incipient vacant site and gives the complex more potential for catalytic activity(13).

The analogue of XII on phosphine functionalised polystyrene, $[H_2Os_3(CO)_9(PPh_2\text{-}$ Ⓟ $)]$, has also been prepared by direct ligand exchange with XIb, avoiding the need for any thermal treatment(199).

The isolation of XII is exciting because it is formally unsaturated with only 46 valence electrons. The resulting inherent reactivity has been already exploited in V to give catalytic hydrogenation and isomerisation of olefins, and the observed parallel chemistry of anchored complexes gives confidence that XII can potentially act as an adsorbed analogue of V. With the phosphine at one side of the unsaturated edge it will presumably induce an asymmetry in electron density which may be manifest in different reactivity. Only a few comparative studies between V and its phosphine-substituted derivative $[H_2Os_3(CO)_9(PPhMe_2)]$, XId, have been published, but they show that the introduced ligand does not drastically affect the chemistry. However, the phosphine does influence the rates of reaction and where competing pathways exist its presence can alter the observed product distribution. Hence reaction with trifluoroacetonitrile(188b) gives a mixture of $[HOs_3(\mu\text{-}\eta^2\text{-}CF_3C{=}NH)(CO)_9L]$ and $[HOs_3(\mu\text{-}\eta^1\text{-}N{=}CHCF_3)(CO)_9L]$ in both cases, but with a higher proportion of the second complex formed from XId in a shorter reaction time. Interestingly, selective formation of the anti-isomer of the latter adduct strongly implies that initial addition is at the phosphine-bonded osmium provided subsequent intramolecular rearrangements are unimportant; this is seen as a general trend for oxidative additions to XI. With carbon disulphide both V and XId give a product where two Os_3 units are linked together by a methanedithiolate group, $(\mu\text{-}S_2CH_2)[HOs_3(CO)_9L]_2$(178). However, while the reaction with V is essentially selective, with XId additional products were isolated from unimolecular pathways which contain dithioformato and thioformaldehyde groups. The reduced tendancy of XI to undergo nucleophilic attack favours the unimolecular route from the postulated pivot intermediate $[H_2Os_3(CO)_9L(CS_2)]$, because a

second molecule will be less susceptible to attack from the uncoordinated sulphur atom. This was supported by concentration studies where the bimolecular process increased in importance with higher levels of XId. These results are encouraging, and in Chapter Three the reactions of XIa with ethylene and acetylene are shown to mirror those of V. These produced a series of model compounds which are used to explain the catalytic activity of XII for ethylene hydrogenation and subsequent deactivation processes.

1.7. Elemental Analysis and Conclusions

The spectroscopic evidence conclusively established selective formation of the phosphine-tethered triosmium clusters VII, X and XII. However, elemental analysis for osmium and phosphorus content on the silicas (Table 4), measured by neutron activation and X-ray fluorescence respectively, shows that complete coverage of the phosphine groups has not been accomplished. In

Table 4

Compound	Os (wt/wt%)	P	Os ($\times 10^4$ mol.g^{-1})	P
$PPh_2CH_2CH_2SIL$		0.89		2.9
$[H_2Os_3(CO)_{10}(PPh_2CH_2CH_2SIL)]$	4.06	0.77	2.1	2.5
$[H_2Os_3(CO)_9(PPh_2CH_2CH_2SIL)]$	5.50	0.94	2.9	3.0
$[Os_3(CO)_{11}(PPh_2CH_2CH_2SIL)]$	3.78	0.80	2.0	2.6

each case there is approximately two free phosphorus groups per anchored cluster. The differences between the data of X and XII must represent experimental error since no leaching was evident during decarbonylation of X, particularly when carried out by the dry technique. The similar coverages achieved with VII and X suggests that mass transfer from solution was not limiting, but instead a function of the surface. If we take VII, the osmium content translates to each cluster molecule effectively occupying 330Å^2, whereas from crystal structure dimensions each might be expected to cover 200Å^2. Even so, this would still

preclude half the phosphines from forming a mono-substituted derivative. Surface irregularities might account for the observed 1 in 3 figure. These uncoordinated ligands can prove problematical at elevated temperatures promoting thermally activated multi-substitution.

Yet another complication with SCHEME ONE has been recently exposed by CP MAS ^{31}P studies on $PPh_2CH_2CH_2SIL(200)$. These identified two chemically distinct phosphorus-containing groups grafted to the surface, with two resonances at -10.5 and 42 ppm. Assignment of the first to supported phosphine was by comparison with the high-resolution solution spectrum of the free ligand, while the deshielded resonance is indicative of a phosphorus(V) species. Careful exclusion of air favoured the supported phosphine, but only by adopting the modified Issleib's procedure, with intermediate capping of remaining silanol groups, was the extent of oxidation drastically reduced. Alternatively the phosphine-oxide could be subsequently removed by reduction with $HSiCl_3$. However, the procedure described did not incorporate insitu silylation of outstanding silanol groups during the preparation, and this will have exaggerated the degree of oxidation. Commercial polystyrene-immobilised tertiary phosphines were also found to contain very large amounts of phosphine-oxide. In contrast, Saito and coworkers(201) did not observe any evidence for phosphine-oxide formation when synthesizing a phosphine-silica using $PPh_2(CH_2)_8SiCl_3$. Experimental conditions, and use of freshly distilled phosphine-silane, are clearly important.

Both these high-resolution ^{31}P NMR studies confirmed the potential of this technique for identifying immobilised organometallic species; cis- and trans-$[PtCl_2(PPh_2R)]$ could be differentiated in the solid-state from the different $^1J_{Pt,P}$ coupling constants. Chemical shift and coupling constant values obtained by solution measurements were shown to be comparable with solid-state values in geometry assignments. However, a substantial dispersion of ^{31}P chemical shifts (ca. 12ppm) was seen in amorphous systems, where a given type of phosphorus atom may be present in a wide variety of enviroments. This broadening due to enviromental effects will not be further reduced by any line-narrowing technique and represents a limitation. Utilisation of

SCHEME TWO gave selective formation of either isomer, whilst adaption of SCHEME ONE using $[PtCl_2(NCPh)_2]$ gave a complex mixture, but with the trans-isomer predominating and all available phosphines coordinated.

These results cast further doubt on the efficacy of SCHEME ONE. Although unproven, the inbalance between immobilised cluster units and available phosphorus atoms is likely to arise from a combination of sterically inaccesible phosphines and a percentage of phosphine-oxides on the surface. The influence of both of these sets at elevated temperatures are then important considerations. Still in its favour is the potential of silylating the surface to remove the bulk of silanol groups, which represent a serious defect of SCHEME TWO. Their detrimental effect at the conditions necessary to ensure covalent anchoring of the homogeneous cluster derivative, and thereafter on its shelflife and thermal stability, has been already demonstrated. For these reasons, for the systems under study, the advantages offered by SCHEME ONE were considered to outweigh these exposed deficiencies. Accordingly, the samples of VII, X and XII, characterised by the given elemental analysis, are used in catalytic investigations reported in Chapter Five.

1.8. Experimental Section

All preparations were carried out under white-spot N_2, unless otherwise stated. Saturated n-alkane solvents were pretreated with conc. H_2SO_4, then distilled from above CaH_2, and stored over 5Å molecular sieves. Sodium dried Et_2O was used in separations. Chromatography was on 20 x 20 x 0.1 cm silica t.l.c. plates.

Mass spectra were recorded on an AEI MS12 spectrometer, using tris(perfluoroheptyl)-sym-triazine as added reference. Quoted parent ions are based on the maximum isotopic abundance, $[Os_3]^+$= 572.

Infrared spectra were either recorded on a Perkin-Elmer 580B with a model 3500 Data Station or a Perkin-Elmer 225 Grating Spectrophotometer, using Spectroscopic Grade solvents (cyclohexane, CCl_4 or KBr) or Na-dried Nujol mull.

Hydrogen-1 and ^{13}C NMR spectra were run on a Varian Associates XL-100 spectrometer; $Cr(acac)_3$ was routinely added as a shiftless relaxation reagent for the latter studies. Spectra of prepared ligands were recorded on a Perkin-Elmer R12.

Metal analyses were determined by Neutron Activation analysis, an ICI Radioisotope Service utilizing the TRIGA nuclear reactor installed at Billingham. Phosphorus contents were by X-ray Fluorescence.

OsO_4

This was generated by oxidation of $K_2[Os(OH)_4O_2]$ in the apparatus shown in Diagram 18, all joints are greaseless.

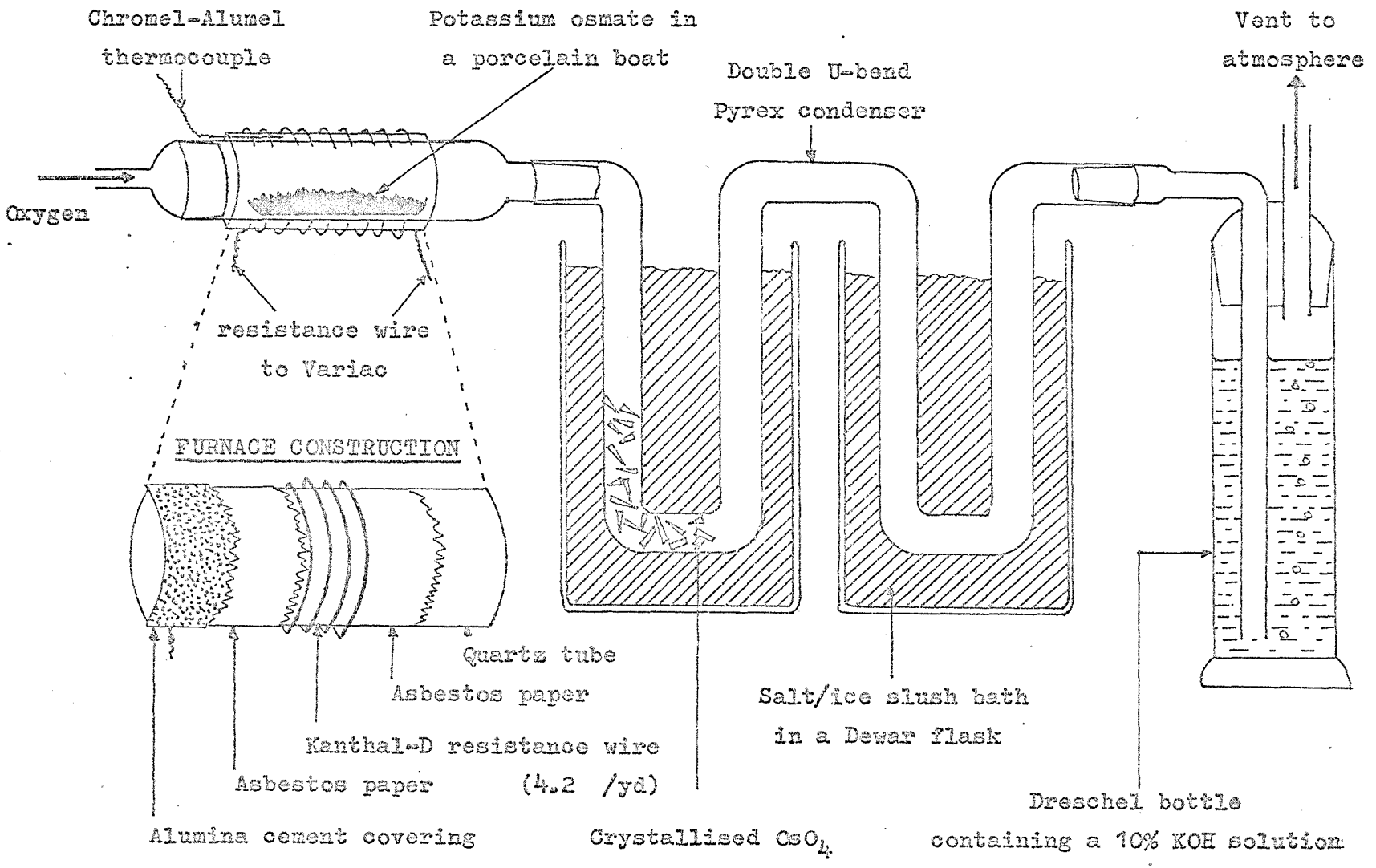
The following procedure leads to its isolation in the absence of water, as desired for the preparation of $[Os_3(CO)_{12}]$. A porcelain boat containing potassium osmate, typically 10g, was placed inside a quartz container with quickfit end connections. This inturn was slid within a tubular, 3 inch long, quartz furnace constructed with Kanthal-D resistance wire as shown. A steady stream of N_2 is then passed over the boat as the temperature was raised to 200°C to remove the water of crystallisation. The off-gas is bubbled directly into a 10% KOH solution as a precaution to trap any entrained OsO_4. Once this had been completed a double U-bend Pyrex condenser was inserted, cooled to ca. -20°C in Dewars containing a salt/ice slush. A flow of O_2 was introduced, and the reaction temperature gradually increased to a maximum of 800°C. Formed OsO_4 was carried into the U-traps where it solidified (m.p.=40.6°C) as white, needle-like, crystals. As the mass builtup application of gentle heat forced the product to the base of the condenser. Once production had ceased, the furnace was cooled down to room temperature and N_2 flushed through. The condenser section was then removed and stoppered, although normally the product was immediately washed out with Analar MeOH and carbonylated to $[Os_3(CO)_{12}]$, without further characterisation.

The spent contents of the boat were shaken in the KOH solution to regenerate fresh $K_2[Os(OH)_4O_2]$, which was precipitated by addition of EtOH and could be used in subsequent preparations.

PTO

Diagram 18

Osmium Tetroxide Generator



$[Os_3(CO)_{12}]$(158)

Osmium tetraoxide(5g) was dissolved in Analar MeOH(40ml) and then poured into an autoclave glass-liner(100ml). Reaction was carried out in a rocking autoclave under CO(75bar) at 125°C overnight. After discharging, the red-yellow methanolic liquor was decanted off leaving insoluble yellow crystals of $[Os_3(CO)_{12}]$ (3.5-4.0g), which were washed out with petroleum ether and recrystallised from hot toluene; yield=60-85%.
IR ν_{co}(cyclohexane): 2068s, 2035s, 2014m, 2002m, cm^{-1}.
Raman ν_{mm}: 162s, 121s, cm^{-1}.
m/e=908.

Enrichment was carried out by treating a sample(0.3g) with ^{13}CO, by heating a m-xylene solution to 140°C for 24 hours, in a closed system.

$[Ru_3(CO)_{12}]$

a)(202): A fast stream of CO was bubbled through a vigorously stirred solution of $RuCl_3.3H_2O$(7.400g) in 2-ethoxy-ethanol(120ml) heated to reflux. After 12-14 hours the solution had turned lemon yellow and was left to cool. Then Analar EtOH(100ml) and 8-30 mesh Zn(9g), previously washed with 10% HCl(250ml), H_2O and dried in an oven overnight, were added and the mixture heated at 85°C with a continued stream of CO for another 7 hours. By this time the mixture had turned red, and orange crystalline $[Ru_3(CO)_{12}]$(3.7647g) could be filtered off and recrystallised from boiling toluene; yield=63%.

b)(203): To prepared(204), crude $[Ru_3O(O_2CCH_3)_6(H_2O)_3]$-$O_2CCH_3$(2.56g) was added 1-propanol(200ml) and NEt_3(4.61g, 6.3ml). Carbon monoxide was passed through the solution, maintained at 75-80°C, which turned from green to orange over a 15 hour period. Cooling in a refrigerator for a day resulted in the precipitation of $[Ru_3(CO)_{12}]$(0.9718g); yield=47%.
IR ν_{co}(cyclohexane): 2061.5vs, 2031.5s, 2012m, cm^{-1}.
m/e=641.

$[H_2Os_3(CO)_{10}]$(159)

A rapid flow of H_2 was bubbled through a solution of $[Os_3(CO)_{12}]$(0.5043g) in n-octane(80ml) at 120°C for 2 hours. The

deep red solution was allowed to cool and decanted from any unreacted starting material. Then it was concentrated on a rotary evaporator, before chromatographing on a 30cm silica column using n-hexane as eluant. One broad fraction moved down the column which on evaporation gave dark purple crystals of $[H_2Os_3(CO)_{10}]$(0.3501g); yield=74%, not accounting for unconsumed $[Os_3(CO)_{12}]$.
IR ν_{CO}(cyclohexane): 2111vw, 2076vs, 2063s, 2026vs, 2011s, 1988m, 1972vw, 1957vw, cm^{-1}.
^1H NMR($CDCl_3$, 31°C): -11.78, s, 2 Os-H-Os.
m/e=854.

PPh_2Et

An ethyl-Grignard was prepared by the gradual addition of EtBr(20g, 0.183mol) to Mg turnings(4.99g, 0.205mol) in Et_2O(200ml), and leaving to stir for ½ hour. To this was slowly added PPh_2Cl(28g, 0.127mol) in Et_2O(100ml), and the resulting solution was gently heated under reflux for a further hour. It was then hydrolysed with dilute NH_4Cl solution, and the Et_2O layer separated and dried over $NaSO_4$. Finally, after removing the solvent, the residue was distilled under vacuum to give PPh_2Et(22.45g) as a clear oil; yield=83%.
b.p.=134-136°C/3 torr, lit.(205) b.p.=138-141°C/1 torr.
methiodide m.p.=181-182°C, lit.(206) m.p.=182-183°C.
^1H NMR($CDCl_3$, 35°C): 7.15δ, m, PPh_2; 1.95δ, dq(J_{HH}=7.2Hz, J_{PH}=2Hz), PCH_2C; 1.08, dt(J_{HH}=7.2Hz, J_{PH}=16.7Hz), $PCCH_3$.

$PPh_2CH_2CH_2Si(OEt)_3$

An n-hexane(100ml) solution of $(EtO)_3SiCHCH_2$(27.09g, 0.142mol) and $HPPh_2$(24.41g, 0.131mol), prepared by the action of Li on PPh_3 followed by hydrolysis, was irradiated with a high intensity ultraviolet lamp for about 100 hours. The solvent was then removed under reduced pressure, and the residual off-white liquor distilled in vacuo to give two fractions. The first (32-34°C, 2.5 torr) being unreacted triethoxyvinylsilane and the major, higher boiling, one the required product, $PPh_2CH_2CH_2Si(OEt)_3$, as a clear viscous liquid which solidified on cooling; yield typically 70%.

b.p.=174-176°C/2.5 torr, lit.(72) b.p.=178-179°C/2 torr.
^{1}H NMR($CDCl_3$ 35°C): 7.36δ, m, PPh_2; 3.78δ, q(J_{HH}=7.1Hz), $SiOCH_2C$; 2.18δ, m, PCH_2C; 1.28δ, t(J_{HH}=7.1Hz), $SiOCCH_3$; 0.76δ, m, $SiCH_2C$.
m/e=376 (27.7%, 70eV; 85.8%, 15eV).

$PPh_2CH_2CH_2SIL$

Aerosil 200(6.9g), previously dried in vacuo at 145°C for 24 hours, was reacted with freshly distilled $PPh_2CH_2CH_2Si(OEt)_3$ (2.2g, vast excess) by heating to reflux in m-xylene(250ml) for 24 hours. Use of a Dean and Stark apparatus allowed some of the boiling solvent to be run off, removing EtOH formed in the reaction. Then a calculated 3-fold excess of $ClSiMe_3$(4.5ml, 0.035 mol), based on an estimated 1.66×10^{-3} mol.g^{-1} of silanol groups, was added and the suspension left refluxing for a further 12 hours. Any remaining silylating reagent was distilled off, and the silica transferred to a Soxhlet finger and extracted with toluene overnight to remove unreacted ligand-silane. Finally the ligand-silica, $PPh_2CH_2CH_2SIL$, was dried in vacuo.
Elemental Analysis 0.89wt/wt%.

$[Os_3(CO)_{11}(PPh_2Et)]$

A quantity of $[Os_3(CO)_{12}]$(0.2000g, 0.22mmol) was dissolved in CH_2Cl_2(60ml) containing MeCN(5ml). Then freshly sublimed Me_3NO(0.0274g, 0.365mmol), in a minimum quantity of Analar MeOH(1ml), was added. The solution almost immediately lightened in appearance, but was usually left stirring for ½ hour before the solvent was removed under vacuum. The lemon yellow residue was scrapped to the bottom of the flask and washed with a small aliquot of MeCN, which extracted any impurities leaving just a mixture of $[Os_3(CO)_{11}(NCMe)]$ and a small fraction of unreacted $[Os_3(CO)_{12}]$. This was not normally further purified, but redissolved in fresh CH_2Cl_2(20ml) and a stoichiometric quantity of PPh_2Et(0.0471g, 0.22mmol) added. This resulted in a colour transformation to a deeper yellow. After ½ hour the volume was reduced on a rotary evaporator and the residue applied to a t.l.c. plate and chromatographed eluting with n-hexane/Et_2O(5:1v/v). One broad band moved up from the baseline, R_f=0.5, which after extraction, washing with n-pentane, and drying gave

$[Os_3(CO)_{11}(PPh_2Et)]$(0.1751g); yield=73%, not accounting for unconsumed $[Os_3(CO)_{12}]$.

IR ν_{CO}(cyclohexane): 2107w, 2055s, 2034m, 2020vs, 2001w, 1989m, 1980wsh, 1974w, 1967.5wsh, 1959vwsh, cm^{-1}.

(KBr): 2106m, 2055m-s, 2029s, 2024s, 2004s, 1995m-s, 1979.5m-s, 1969.5s, 1965s, 1963ssh, 1950m, cm^{-1}.

Raman ν_{CO}(solid) :2104s, 2034w, 2008s, 1996w, 1979m, 1974m-w, 1968m-w, 1955w, cm^{-1}.

^1H NMR($CDCl_3$, 31°C): 7.45δ, m, $P\underline{Ph}_2$; 2.6δ, q(J_{HH}=7.7Hz), $PC\underline{H}_2C$; 0.9δ, dt(J_{HH}=7.7Hz, J_{PH}=18.1Hz), $PCC\underline{H}_3$.

$^{13}C-\{^1H\}$ NMR ($CDCl_3$, 40°C) : 130.4δ, m, $P\underline{Ph}_2$; 29.4δ, d(J_{PC}=40Hz), $P\underline{C}C$; 8.4δ, s, $PC\underline{C}$.

m/e=1094.

Elemental Analysis Cald. C 27.48% H 1.38%

MW=1092.9g.mol^{-1} Obsd. C 26.90% H 1.51%

$[Os_3(CO)_{11}(PPh_2CH_2CH_2Si(OEt)_3)]$

a) This could be prepared in an analogous manner to that described above. The required product was extracted from unreacted $[Os_3(CO)_{12}]$ with n-hexane(5ml), circumventing the need for chromatography, and isolated as an oily yellow solid.

b) $[Os_3(CO)_{12}]$(0.3070g, 0.339mmol) was reacted with an excess of $PPh_2CH_2CH_2Si(OEt)_3$(0.1509g, 0.401mmol) in toluene under reflux for 5 hours. Then the solvent was removed in vacuo, and the red residue chromatographed, with n-hexane/toluene(8:6v/v) as eluant, to give three diffuse bands, of which two could be partially extracted from the plate.

i) R_f=0.35, yellow oil, $[Os_3(CO)_{11}(PPh_2CH_2CH_2Si(OEt)_3]$.

IR ν_{CO}(cyclohexane): 2107m, 2054s, 2035.5s, 2019vs, 2001.5m, 1990m, 1977m, 1957w, cm^{-1}.

ii) R_f=0.15, orange-red oil, $[Os_3(CO)_{10}(PPh_2CH_2CH_2Si(OEt)_3)_2]$.

IR ν_{CO}(cyclohexane): 2084m, 2053w, 2028s, 2001vs, 1968m, 1950sh, cm^{-1}.

$[Os_3(CO)_{11}(PPh_2CH_2CH_2SiL)]$

a) Crude $[Os_3(CO)_{11}(NCMe)]$ was prepared as previously described, containing only $[Os_3(CO)_{12}]$ as an impurity. This was

added in portions to a vigorously stirred suspension of $PPh_2CH_2CH_2SIL$(typically 1.5g) in degassed CH_2Cl_2(100ml). Periodically agitation was halted, allowing the silica to settle out, and if the supernatant liquor was deficient in cluster precursor (infrared ν_{CO}) extra additions were made. Finally, when after a 2 hour interval no further change in discrete cluster concentrations in solution was apparent, the silica was filtered off and successfully washed with several portions of hot n-hexane, followed by cold CH_2Cl_2, until the washings were void of any perceivable coloration. The initial filtrate was shown (infrared ν_{CO}) to still contain excess $[Os_3(CO)_{11}(NCMe)]$ plus $[Os_3(CO)_{12}]$. The silica was then atmospherically dried to yield $[Os_3(CO)_{11}(PPh_2CH_2CH_2SIL)]$ as a rich yellow, free flowing solid.
IR ν_{CO}(Nujol mull): 2107w, 2054s, 2034m, 2019vs, 2000w-m, 1989m, 1976w-m, 1956wsh, cm^{-1}.

Elemental Analysis Osmium 3.78 wt/wt%
Phosphorus 0.80

b) An alternative preparation involved contacting $[Os_3(CO)_{11}(PPh_2CH_2CH_2Si(OEt)_3)]$ with dehydrated Aerosil 200, previously dried in vacuo at 150°C for 24 hours, by heating under reflux in benzene for 6 hours, followed by Soxhlet extraction.

$[H_2Os_3(CO)_{10}(PPh_2Et)]$

A stoichiometric quantity of PPh_2Et(0.0239g, 23.2µl) was added to $[H_2Os_3(CO)_{10}]$(0.0950g) dissolved in n-hexane(25ml). Following an immediate colour change from purple to yellow, the solution was reduced in volume and allowed to stand overnight. The required product $[H_2Os_3(CO)_{10}(PPh_2Et)]$(0.1153g) precipitated as pale yellow platelets; yield=97%.
IR ν_{CO}(cyclohexane): 2105.5m, 2066s, 2051s, 2024.5vs, 2016sh, 2007m-s, 1999m, 1982.5m, 1972m, cm^{-1}.
^1H NMR($CDCl_3$, -60°C): 7.55δ, m, PPh_2; 2.8δ, m, PCH_2C; 1.05δ, dt, $PCCH_3$; -10.32δ, d(J_{HH}=3.3Hz), HOs; -20.22δ, dd(J_{PH}=11.1Hz, J_{HH}=3.3Hz), Os-H-OsP.

Elemental Analysis Cald. C 27.02% H 1.61%
MW=1066.91g.mol^{-1} Obsd. C 26.68% H 1.48%

PTO

$[H_2Os_3(CO)_{10}(PPh_2CH_2CH_2SIL)]$

A sample of $PPh_2CH_2CH_2SIL$(typically 1.5g) was suspended in CH_2Cl_2(100ml), and successive portions(50mg) of $[H_2Os_3(CO)_{10}]$ added until 15 minutes after the final addition the solvent still retained the characteristic purple of the precursor cluster. In contrast, the silica had adopted a concentrated light yellow appearance. This was filtered off and washed several times with CH_2Cl_2, and dried under vacuum at room temperature, to give $[H_2Os_3(CO)_{10}(PPh_2CH_2CH_2SIL)]$.

IR ν_{CO}(Nujol mull): 2105w, 2065m-s, 2049s, 2024vs, 2006ssh, 1998m, 1981m-w, 1970w, cm^{-1}.

Elemental Analysis Osmium 4.06 wt/wt%
Phosphorus 0.77

$[H_2Os_3(CO)_9(PPh_2Et)]$

Addition of an equimolar quantity of PPh_2Et(0.00277g, 27.2μl) to $[H_2Os_3(CO)_{10}]$(0.1135g), dissolved in n-hexane(50ml), caused an immediate colour change from purple to yellow. The solution was then heated to reflux, and within 2 hours the original colour had returned. After allowing to cool, the solvent was removed and the black residue chromatographed using n-hexane/Et_2O(4:1v/v) as eluant. One major band(R_f=0.64) moved up the plate from the yellow baseline, which on workup gave $[H_2Os_3(CO)_9(PPh_2Et)]$ (0.1099g) as a very dark green solid; yield=79.5%.

IR ν_{CO}(cyclohexane): 2093m, 2054s, 2013vs, 2005m, 1990m, 1975m-w, 1957w, cm^{-1}.

(KBr): 2091, 2046, 2006, 1993, 1971br, 1955, 1945, cm^{-1}, all approximately of equal intensities.

^1H NMR($CDCl_3$, 31°C): 7.58δ, m, PPh_2; 2.88δ, m, PCH_2C; 1.14δ, dt(J_{HH}=7.5Hz, J_{PH}=18Hz); -10.60δ, d(J_{PH}=7.3Hz), 2 Os-H-OsP.

m/e=1040.

Elemental Analysis Cald. C 26.57% H 1.64%
Obsd. C 27.10% H 1.55%

The corresponding adducts $[H_2Os_3(CO)_9L]$, L=PPh_3 or $P(OMe)_3$, were also prepared using identical conditions.

$[H_2Os_3(CO)_9(PPh_3)]$ Typical yield=85%(purple crystals).

IR ν_{CO}(cyclohexane): 2091m, 2053s, 2014ssh, 2010vs, 2002m-w, 1992.5m, 1989msh, 1974m, 1961w, cm^{-1}.

(KBr): 2092s, 2059ssh, 2051.5s, 2011vssh, 2002sh, 1986vssh, 1979vs, 1955vs, 1951vssh, 1933wsh, 1921.5w, cm^{-1}.

^1H NMR($CDCl_3$, 31°C): 7.46δ, m, PPh_3; -10.18δ, d(J_{PH}=7Hz), 2 Os-H-OsP.

m/e=1088.

Elemental Analysis Cald. C 29.82% H 1.56%

Obsd. C 29.63% H 1.50%

$[H_2Os_3(CO)_9(P(OMe)_3)]$

IR ν_{CO}(cyclohexane): 2094.5w, 2056s, 2027vw, 2020m, 2011.5s, 2004w, 1999m, 1991msh, 1976w, cm^{-1}.

$[H_2Os_3(CO)_9(PPh_2CH_2CH_2SIL)]$

Freshly prepared $[H_2Os_3(CO)_{10}(PPh_2CH_2CH_2SIL)]$ was transferred to a 50ml round-bottomed flask and dried in vacuo. The flask was then immersed in an oil bath at a constant temperature at 40°C. The silica, stirred to avoid localised heating, under went a smooth conversion to $[H_2Os_3(CO)_9(PPh_2CH_2CH_2SIL)]$ as shown by a darkening in appearance to an eventual green. Normally the temperature was maintained for 12 hours to ensure complete reaction.

IR ν_{CO}(Nujol mull): 2091w, 2063wsh, 2052s, 2033wsh, 2009vs, 1991msh, 1972wsh, 1954vwsh, cm^{-1}.

Elemental Analysis Osmium 5.50 wt/wt%

Phosphorus 0.94

1.9. References

1. E.L.Muetterties and J.Stein, Chem. Rev., 1979, 79, 479.
2. J.H.Sinfelt, Prog. Solid-State Chem., 1975, 10, 55.
3. J.R.Anderson, 'Structure of Metallic Catalysts', Acacdemic Press, London, 1975.
4. E.L.Muetterties, Angew. Chem. Int. Ed. Engl., 1978, 17, 545.
5. a) J.C.Buchholz and G.A.Somorjai, Acc. Chem. Res., 1976, 9, 333.

   b) G.A.Somorjai, Acc. Chem. Res., 1976, 9, 248.
6. E.L.Muetterties, T.N.Rhodin, E.Band, C.F.Brucker and

W.R.Pretzer, Chem. Rev., 1979, 79, 91.

7. E.L.Muetterties and M.J.Krause, Angew. Chem. Int. Ed. Engl., 1983, 22, 135.

8. J.D.Corbett, Prog. Inorg. Chem., 1976, 21, 129.

9. P.Chini, J. Organometallic Chem., 1980, 200, 37.

10. E.L.Muetterties, Bull. Soc. Chim. Belg., 1975, 84, 959.

11. I.A.Oxton, D.B.Powell, N.Sheppard, K.Burgess, B.F.G.Johnson and J.Lewis, J.C.S. Chem. Comm., 1982, 719.

12. C.E.Anson, B.T.Keiller, I.A.Oxton, D.B.Powell and N.Sheppard, J.C.S. Chem. Comm., 1983, 470.

13. J.Evans, Chem. Rev., 1981, 159.

14. M.H.Howard, S.F.A.Kettle, I.A.Oxton, D.B.Powell, N.Sheppard and P.Skinner, J. Chem. Soc. Faraday Trans. II, 1981, 77, 397.

15. R.E.Benfield and B.F.G.Johnson, 'Transition Metal Clusters', B.F.G.Johnson Ed., Wiley, New York, 1980, 471.

16. P.F.Jackson, B.F.G.Johnson, J.Lewis, W.J.H.Nelson and M.McPartlin, J.C.S. Dalton, 1982, 2099.

17. D.Braga, J.Lewis, B.F.G.Johnson, M.McPartlin, W.J.H.Nelson and M.D.Vargas, J.C.S. Chem. Comm., 1983, 241.

18. a) K.Wade, Adv. Inorg. Chem. Radiochem., 1976, 18, 1.
b) K.Wade, 'Transition Metal Clusters', B.F.G.Johnson Ed., Wiley, New York, 1980, 193.

19. B.Delley, M.C.Manning, D.E.Ellis, J.Berkowitz and W.C.Trogler, Inorg. Chem., 1982, 21, 2247.

20. J.C.Green, D.M.P.Mingos and E.A.Seddon, Inorg. Chem., 1981, 20, 2595.

21. P.F.Jackson, B.F.G.Johnson, J.Lewis, W.J.H.Nelson and M.McPartlin, J.C.S. Chem. Comm., 1982, 49.

22. R.E.Benfield, P.P.Edwards and A.M.Stacy, J.C.S. Chem. Comm., 1982, 525.

23. B.C.Gates and J.Lieto, ChemTech, 1980, 195.

24. a) D.C.Bailey and S.H.Langer, Chem. Rev., 1981, 81, 109.
b) Y.I.Yermakov, B.N.Kuznetsov and V.A.Zakharov, Eds., 'Catalysis by Supported Complexes', Elsevier, Oxford, 1981.
c) B.C.Gates and J.Lieto, ChemTech, 1980, 248.
d) M.S.Scurrell, Catalysis, 1977, 1, 215.

25. D.Ballivet-Tkatchenko, G.Coudurier, H.Mozzanega, I.Tkatchenko and A.Kienneman, J. Mol. Catal., 1979, 6, 293.

26. P.Gallezot, G.Coudurier, M.Primet and B.Imelik, Amer. Chem. Soc., Symp. Ser., 1977, 40, 144.

27. P.Gelin, Y.B.Taarit and C.Naccache, J. Catal., 1979, 59, 357.

28. P.R.Rony and J.F.Roth, J. Mol. Catal., 1975/76, 1, 13.

29. Y.I.Ermakov, Catal. Rev., Sci. Eng., 1976, 13, 77.

30. A.K.Smith, B.Besson, J.M.Basset, R.Psaro, A.Fusi and R.Ugo, J. Organometallic Chem., 1980, 192, C31.

31. M.Deeba and B.C.Gates, J. Catal., 1981, 67, 303.

32. M.Deeba, J.P.Scott, R.Barth and B.C.Gates, J. Catal., 1981, 71, 373.

33. F.Hugues, A.K.Smith, Y.Ben Taarit, J.M.Basset, D.Commereuc and Y.Chauvin, J.C.S. Chem. Comm., 1980, 68.

34. F.Hugues, J.M.Basset, Y.Ben Taarit, A.Choplin, M.Primet, D.Rojas and A.K.Smith, J. Amer. Chem. Soc., 1982, 104, 7020.

35. D.Ballivet-Tkatchenko and G.Coudurier, Inorg. Chem., 1979, 18, 558.

36. W.A.Herrmann, Angew. Chem. Int. Ed. Engl., 1982, 21, 117.

37. A.K.Smith, A.Theolier, J.M.Basset, R.Ugo, D.Commereuc and Y.Chauvin, J. Amer. Chem. Soc., 1978, 100, 2590.

38. D.Commereuc, Y.Chauvin, F.Hugues, J.M.Basset and D.Olivier, J.C.S. Chem. Comm., 1980, 154.

39. R.Hemmerich, W.Keim and M.Roper, J.C.S. Chem. Comm., 1983, 428.

40. J-B.N'Guini Effa, B.Djebaïlli, J.Lieto and J-P.Aune, J.C.S. Chem. Comm., 1983, 408.

41. J.Lieto, J.J.Rafalko and B.C.Gates, J. Catal., 1980, 62, 149.

42. J.Lieto, D.Milstein, R.L.Albright, J.V.Minkiewicz and B.C.Gates, ChemTech, 1983, 46.

43. S.Aime and L.Milone, Prog. Nucl. Magn. Reson. Spectroscopy, 1977, 11, 183.

44. E.R.Andrew, Prog. Nucl. Magn. Reson. Spectroscopy, 1971, 8, 1.

45. A.Pines, M.G.Gibby and J.S.Waugh, J. Chem. Phys., 1973, 59, 569.

46. J.Reed, P.Eisenberger, B-K.Teo and B.M.Kincaid, J. Amer. Chem. Soc., 1977, 99, 5217.

47. J.R.Budge, J.P.Scott and B.C.Gates, J.C.S. Chem. Comm., 1983, 342.

48. K.A.Azam, A.J.Deeming, R.E.Kimber and P.R.Shukla, J.C.S. Dalton, 1970, 1853.

49. R.Psaro, R.Ugo, G.M.Zanderighi, B.Besson, A.K.Smith and

J.M.Basset, J. Organometallic Chem., 1981, 213, 215.

50. C.R.Guerra and J.H.Schulman, Surf. Sci., 1967, 7, 229.

51. P.L.Watson and G.L.Schrader, J. Mol. Catal., 1980, 9, 129.

52. B.Besson, B.Moraweck, A.K.Smith, J.M.Basset, R.Psaro, A.Fusi and R.Ugo, J.C.S. Chem. Comm., 1980, 569.

53. M.R.Churchill and B.DeBoer, Inorg. Chem., 1977, 16, 878.

54. M.R.Churchill and R.A.Lashewycz, Inorg. Chem., 1979, 18, 3261.

55. V.F.Allen, R.Mason and P.B.Hitchcock, J. Organometallic Chem., 1977, 140, 297.

56. M.Deeba, B.J.Streusand, G.L.Schrader and B.C.Gates, J. Catal., 1981, 69, 218.

57. P.B.West, G.L.Haller and R.L.Burwell Jr., J. Catal., 1973, 29, 486.

58. V.Y.Davydov, A.V.Kiselev and L.T.Zhuravlev, Trans. Faraday Soc., 1964, 60, 2254.

59. a) G.E.Maciel and D.W.Sindorf, J. Amer. Chem. Soc., 1980, 102, 7606.

b) G.E.Maciel and D.W.Sindorf, J. Chromatogr., 1981, 205, 438.

60. J.H.DeBoer and J.M.Vleeskins, Proc. K. Ned. Akad. Wet., Ser. B: Palaeontol., Geol., Phys., Chem., 1958, B61, 85.

61. J.A.Hockey, Chem. Ind. (London), 1965, 57.

62. J.B.Peri and A.L.Hensley Jr., J. Phys. Chem., 1968, 72, 2926.

63. D.W.Sindorf and G.E.Maciel, J. Amer. Chem. Soc., 1983, 105, 1487.

64. A.V.Volkov, A.V.Kiselev and V.I.Lygin, Zh. Fiz. Khim., 1974, 48, 1214.

65. R.L.Burwell Jr., ChemTech, 1974, 370.

66. H.P.Boehm, Advan. Catal., 1966, 16, 179.

67. J.E.Corey and A.J.Venkateswarlu, J. Amer. Chem. Soc., 1972, 94, 6190.

68. J.L.M.Van de Venne, J.P.M.Rindt and G.J.M.M.Coenen, J. Colloid Interface Sci., 1980, 74, 287.

69. a) D.W.Sindorf and G.E.Maciel, J. Amer. Chem. Soc., 1981, 103, 4263.

b) D.W.Sindorf and G.E.Maciel, J. Amer. Chem. Soc., 1983, 105, 3767.

70. K.G.Allum, R.D.Hancock, I.V.Howell, S.McKenzie, R.C.Pitkethly and P.J.Robinson, J. Organometallic Chem., 1975, 87, 203.

71. A.A.Oswald, L.L.Murrel and L.J.Boucher, Prepr., Div. Petrol.

Chem., Amer. Chem. Soc., 1974, 19, 155.

72. H.Niebergall, Makromol. Chem.; 1962, 52, 218.

73. K.Issleib, Z. Chem., 1962, 2, 163.

74. T.Okano, T.Kobayashi and J.Kiji, Bull. Chem. Soc. Jpn., 1982, 55, 2675.

75. J.Schraml, M.Capka and H.Jancke, Collection Czechoslovak Chem. Comm., 1982, 47, 793.

76. E.P.Plueddemann, J. Paint Technol., 1970, 42, 600.

77. L.L.Murrell, 'Advanced Materials in Catalysis', J.L.Burton and R.L.Garten, Eds., Academic Press, New York, 1977, 235.

78. T.G.Waddell, D.E.Leyden and M.T.DeBello, J. Amer. Chem. Soc., 1981, 103, 5303.

79. L.J.Boucher, A.A.Oswald and L.L.Murrell, Prepr., Div. Petrol. Chem., Amer. Chem. Soc., 1974, 19, 162.

80. H.Knözinger and E.Rumpf, Inorg. Chim. Acta, 1978, 30, 51.

81. L.Bemi, H.C.Clark, J.A.Davies, D.Drexler, C.A.Fyfe and R.Wasylishen, J. Organometallic Chem., 1982, 224, C5.

82. G.F.Stuntz and J.R.Shapley, Inorg. Chem., 1976, 15, 1994.

83. J.J.Rafalko, J.Lieto, B.C.Gates and G.L.Schrader Jr., J.C.S. Chem. Comm., 1978, 540.

84. J.Lieto, J.J.Rafalko, J.V.Minkiewicz, P.W.Rafalko and B.C.Gates, 'Fundamental Research in Homogeneous Catalysis', M.Tsutsui Ed., Plenum Press, New York, 1979, 3, 637.

85. J.Lieto, J.J.Rafalko and B.C.Gates, J. Catal., 1980, 62, 149.

86. W.C.Still, H.Kahn and A.Mitra, J. Org. Chem., 1978, 43, 2923.

87. J.Evans and B.P.Gracey, J.C.S. Chem Comm., 1983, 247.

88. W.Leveson, private communication.

89. A.F.Clifford and A.K.Mukerjee, Inorg. Chem., 1963, 2, 151.

90. R.J.Angelici and E.E.Siefert, Inorg. Chem., 1966, 5, 1457.

91. D.J.Dahm and R.A.Jacobson, J. Amer. Chem. Soc., 1968, 90, 5106.

92. S.M.Grant and A.R.Manning, Inorg. Chim. Acta, 1978, 31, 41.

93. W.S.McDonald, J.R.Moss, G.Raper, B.L.Shaw, R.Greatrex and N.N.Greenwood, J.C.S. Chem. Comm., 1969, 1295.

94. P.D.Gavens, Ph.D. Thesis, Cambridge, 1977.

95. S.Grant, J.Newman and A.R.Manning, J. Organometallic Chem., 1975, 96, C11.

96. a) D.J.Darensbourg and B.J.Baldwin-Zuschke, J. Amer. Chem. Soc., 1982, 104, 3906.

b) D.C.Sonnenberger and J.D.Atwood, Organometallics, 1982, 1, 694.

97. S.K.Malik and A.Poe, Inorg. Chem., 1978, 17, 1484.

98. A.Poe and M.V.Twigg, J.C.S. Dalton, 1974, 1860.

99. A.Poe and M.V.Twigg, Inorg. Chem., 1974, 13, 2982.

100. J.P.Candlin and A.C.Shortland, J. Organometallic Chem., 1969, 16, 289.

101. M.I.Bruce, G.Shaw and F.G.A.Stone, J.C.S. Dalton, 1972, 2094.

102. E.J.Forbes, N.Goodhand, D.L.Jones and T.A.Hamor, J. Organometallic Chem., 1979, 182, 143.

103. B.F.G.Johnson, J.Lewis and M.V.Twigg, J.C.S. Dalton, 1975, 1876.

104. J.R.Fox, W.L.Gladfetter and G.L.Geoffroy, Inorg. Chem., 1980, 19, 2574.

105. M.I.Bruce, G.Shaw and F.G.A.Stone, J.C.S. Dalton, 1972, 1781.

106. M.F.Lappert and P.L.Pye, J.C.S. Dalton, 1977, 2172.

107. M.I.Bruce, D.Schultz, R.C.Wallis and A.D.Redhouse, J. Organometallic Chem., 1979, 169, C15.

108. a) M.I.Bruce, D.C.Kehoe, J.G.Matisons, B.K.Nicholson, P.H.Rieger and M.L.Williams, J.C.S. Chem. Comm., 1982, 442.
b) M.I.Bruce, J.G.Matisons and B.K.Nicholson, J. Organometallic Chem., 1983, 247, 321.

109. M.I.Bruce, J.G.Matisons, B.K.Nicholson and M.L.Williams, J. Organometallic Chem., 1982, 236, C57.

110. M.I.Bruce, T.W.Hambley, B.K.Nicholson and M.R.Snow, J. Organometallic Chem., 1982, 235, 83.

111. C.W.Bradford and R.S.Nyholm, J.C.S. Chem. Comm., 1967, 384.

112. C.W.Bradford, W.van Bronswijk, R.J.H.Clark and R.S.Nyholm, J. Chem. Soc. (A), 1970, 2889.

113. A.J.Deeming, B.F.G.Johnson and J.Lewis, J. Chem. Soc. (A), 1970, 897.

114. A.J.Deeming and M.Underhill, J.C.S. Dalton, 1973, 2727.

115. A.J.Deeming, R.E.Kimber and M.Underhill, J.C.S. Dalton, 1973, 2589.

116. C.J.Cooksey, A.J.Deeming and I.P.Rothwell, J.C.S. Dalton, 1981, 1718.

117. A.J.Arce and A.J.Deeming, J.C.S. Dalton, 1982, 1155.

118. M.J.Mays and P.D.Gavens, J. Organometallic Chem., 1977, 124, C37.

119. M.J.Mays and P.D.Gavens, J.C.S. Dalton, 1980, 911.

120. B.F.G.Johnson, J.Lewis and D.Pippard, J. Organometallic Chem., 1978, 145, C4.

121. B.F.G.Johnson, J.Lewis and D.A.Pippard, J.C.S. Dalton, 1981, 407.

122. B.F.G.Johnson, J.Lewis, P.R.Raithby and C.Zuccaro, J.C.S. Chem. Comm., 1979, 916.

123. M.Tachikawa and J.R.Shapley, J. Organometallic Chem., 1977, 124, C19.

124. E.G.Bryan, B.F.G.Johnson and J.Lewis, J.C.S. Dalton, 1977, 1328.

125. B.F.G.Johnson, J.Lewis and D.Pippard, J. Organometallic Chem., 1978, 160, 263.

126. B.F.G.Johnson, J.Lewis and D.A.Pippard, J. Organometallic Chem., 1981, 213, 249.

127. R.E.Benfield, B.F.G.Johnson, P.R.Raithby and G.M.Sheldrick, Acta Cryst. 1978, B34, 666.

128. C.A.Tolman, Chem. Rev., 1977, 77, 313.

129. P.A.Dawson, B.F.G.Johnson, J.Lewis, J.Puga, P.R.Raithby and and M.J.Rosales, J.C.S. Dalton, 1982, 233.

130. J.J.DeBoer, J.A.van Doorn and C.Masters, J.C.S. Chem. Comm., 1978, 1005.

131. B.F.G.Johnson, J.Lewis, B.E.Reichert and K.T.Schorpp, J.C.S. Dalton, 1976, 1403.

132. a) A.Forster, B.F.G.Johnson, J.Lewis, T.W.Matheson, B.H.Robinson and W.G.Jackson, J.C.S. Chem. Comm., 1974, 1042.
b) S.Aime, O.Gambino, L.Milone, E.Sappa and E.Rosenberg, Inorg. Chim. Acta, 1975, 15, 53.

133. F.A.Cotton and J.M.Troup, J. Amer. Chem. Soc., 1974, 96, 4155.

134. K.J.Kavel and J.R.Norton, J. Amer. Chem. Soc., 1974, 96, 6812.

135. M.Tachikawa, Ph.D. Thesis, University of Illinois, 1977.

136. F.A.Cotton and B.E.Hanson, Inorg. Chem., 1977, 16, 3369.

137. F.A.Cotton and D.Jamerson, J. Amer. Chem. Soc., 1976, 98, 5396.

138. F.A.Cotton and D.L.Hunter, Inorg. Chim. Acta, 1974, 11, L9.

139. a) B.F.G.Johnson, J.C.S. Chem. Comm., 1976, 211.
b) B.F.G.Johnson, J.C.S. Chem. Comm., 1976, 703.

140. E.G.Bryan, A.Forster, B.F.G.Johnson, J.Lewis and T.W.Matheson, J.C.S. Dalton, 1978, 196.

141. P.D.Gavens and M.J.Mays, J. Organometallic Chem., 1978, 162, 389.

142. E.L.Muetterties, Accounts Chem. Res., 1970, 3, 266.
143. F.A.Cotton and B.E.Hanson, Isr. J. Chem., 1977, 15, 165.
144. S.Aime and D.Osella, J. Organometallic Chem., 1981, 214, C27.
145. A.A.Koridze, O.A.Kizas, N.M.Astakhova, P.V.Petrovskii and Y.K.Grishin, J.C.S. Chem. Comm., 1981, 853.
146. R.E.Benfield, P.D.Gavens, B.F.G.Johnson, M.J.Mays, S.Aime, L.Milone and D.Osella, J.C.S. Dalton, 1981, 1535.
147. B.F.G.Johnson and R.E.Benfield, J.C.S. Dalton, 1978, 1554.
148. H.Dom, B.E.Hanson and E.Motell, Inorg. Chim. Acta, 1981, 54, L71.
149. M.I.Bruce, B.K.Nicholson and A.H.White, J. Organometallic Chem., 1982, 240, C33.
150. J.Robertson and G.Webb, Proc. R. Soc. Lond. (A), 1974, 341, 383.
151. A.F.Simpson and R.Whyman, J. Organometallic Chem., 1981, 213, 157.
152. M.Kobayashi and T.Shirasaki, J. Catal., 1973, 28, 289.
153. V.L.Kuznetsov, A.T.Bell and Y.I.Yermakov, J. Catal., 1980, 65, 374.
154. A.A.Davydov and A.T.Bell, J. Catal., 1977, 49, 332.
155. A.Zecchina, E.Guglielminotti, A.Bossi and M.Camia, J. Catal., 1982, 74, 225.
156. E.Guglielminotti, A.Zecchina, A.Bossi and M.Camia, J. Catal., 1982, 74, 240.
157. D.K.Liu and M.S.Wrighton, J. Amer. Chem. Soc., 1982, 104, 898.
158. B.F.G.Johnson, J.Lewis and P.Kilty, J. Chem. Soc. (A), 1968, 2859.
159. S.A.R.Knox, J.W.Koepke, M.A.Andrews and H.D.Kaesz, J. Amer. Chem. Soc., 1975, 97, 3942.
160. J.R.Shapley, J.B.Keister, M.R.Churchill and B.G.DeBoer, J. Amer. Chem. Soc., 1975, 97, 4145.
161. B.F.G.Johnson, J.Lewis, P.R.Raithby, G.M.Sheldrick, K.Wong and M.McPartlin, J.C.S. Dalton, 1978, 673.
162. M.I.Bruce and R.C.Wallis, J. Organometallic Chem., 1979, 164, C6.
163. R.D.Adams and N.M.Golembeski, J. Amer. Chem. Soc., 1979, 101, 2579.
164. M.I.Bruce and R.C.Wallis, Aust. J. Chem., 1982, 35, 709.
165. J.B.Keister, J. Organometallic Chem., 1980, 190, C36.
166. M.R.Churchill, F.J.Hollander and J.P.Hutchinson, Inorg. Chem.,

1977, 16, 2697.

167. R.W.Broach and J.M.Williams, Inorg. Chem., 1979, 18, 314.

168. A.G.Orpen, A.V.Rivera, E.G.Bryan, D.Pippard, G.M.Sheldrick and K.D.Rouse, J.C.S. Chem. Comm., 1978, 723.

169. L.J.Faruggia, J.A.K.Howard, P.Mitrprachachon, J.L.Spencer, F.G.A.Stone and P.Woodward, J.C.S. Chem. Comm., 1978, 260.

170. B.F.G.Johnson, D.A.Kaner, J.Lewis and P.R.Raithby, J. Organometallic Chem., 1981, 215, C33.

171. K.Burgess, B.F.G.Johnson, D.A.Kaner, J.Lewis, P.R.Raithby and S.N.A.B.Syed-Mustaffa, J.C.S. Chem. Comm., 1983, 455.

172. A.J.Deeming and S.Hasso, J. Organometallic Chem., 1976, 114, 313.

173. J.B.Keister and J.R.Shapley, Inorg. Chem., 1982, 21, 3304.

174. J.B.Keister and J.R.Shapley, J. Amer. Chem. Soc., 1976, 98, 1056.

175. a) M.Tachikawa, J.R.Shapley and C.G.Pierpont, J. Amer. Chem. Soc., 1975, 97, 7172.

b) A.J.Deeming, S.Hasso and M.Underhill, J.C.S. Dalton, 1975, 1614.

c) W.G.Jackson, B.F.G.Johnson, J.W.Kelland, J.Lewis and K.T.Schorpp, J. Organometallic Chem., 1975, 87, C27.

176. R.D.Adams, N.M.Golembeski and J.P.Selegue, Inorg. Chem., 1981, 20, 1242.

177. R.D.Adams, D.A.Katahira and J.P.Selegue, J. Organometallic Chem., 1981, 213, 259.

178. R.D.Adams, N.M.Golembeski and J.P.Selegue, J. Amer. Chem. Soc., 1981, 103, 546.

179. K.Burgess, B.F.G.Johnson, J.Lewis and P.R.Raithby, J.C.S. Dalton, 1982, 2085.

180. K.Burgess, B.F.G.Johnson, J.Lewis and P.R.Raithby, J.C.S. Dalton, 1982, 263.

181. L.J.Farrugia, J.A.K.Howard, P.Mitrprachachon, F.G.A.Stone and P.Woodward, J.C.S. Dalton, 1981, 155.

182. a) J.R.Shapley, G.A.Pearson, M.Tachikawa, G.ESchmidt, M.R.Churchill and F.J.Hollander, J. Amer. Chem. Soc., 1977, 99, 8064.

b) M.R.Churchill, F.J.Hollander, J.R.Shapley and D.S.Foose, J.C.S. Chem. Comm., 1978, 534.

c) L.J.Farrugia, J.A.K.Howard, P.Mitrprachachon, J.L.Spencer,

F.G.A.Stone and P.Woodward, J.C.S Chem. Comm., 1978, 260.
d) S.Khaduri, B.F.G.Johnson, J.Lewis, P.R.Raithby and D.J.Watson, J.C.S. Chem. Comm., 1978, 343.

183. J.S.Plotkin, D.G.Alway, C.R.Weisenberger and S.G.Shore, J. Amer. Chem. Soc., 1980, 102, 6156.

184. M.R.Churchill and B.DeBoer, Inorg. Chem., 1977, 16, 2397.

185. R.D.Adams and N.M.Golembeski, Inorg. Chem., 1979, 18, 1909.

186. A.J.Deeming and S.Hasso, J. Organometallic Chem., 1975, 88, C21.

187. S.Aime, D.Osella, L.Milone and F.Rosenberg, J. Organometallic Chem., 1981, 213, 207.

188. a) Z.Dawoodi, M.J.Mays and P.R.Raithby, J. Organometallic Chem., 1981, 219, 103.
b) R.D.Adams, D.A.Kataharia and L.Yang, J. Organometallic Chem., 1981, 219, 85.

189. R.E.Benfield, B.F.G.Johnson, J.Lewis, P.R.Raithby, C.Zuccaro and K.Hendrick, Acta. Cryst., 1979, B35, 2210.

190. a) A.G.Orpen, J. Organometallic Chem., 1978, 152, C1.
b) A.G.Orpen, J.C.S. Dalton, 1980, 2509.

191. G.F.Stuntz and J.R.Shapley, J. Amer. Chem. Soc., 1977, 99, 607.

192. E.G.Bryan, W.G.Jackson, B.F.G.Johnson, J.W.Kelland, J.Lewis and K.T.Schorpp, J. Organometallic Chem., 1976, 108, 385.

193. B.F.G.Johnson, J.Lewis, T.I.Odiaka and P.R.Raithby, J. Organometallic Chem., 1981, 216, C56.

194. S.Aime and D.Osella, J.C.S. Chem. Comm., 1981, 300.

195. J.R.Shapley, G.F.Stuntz, M.R.Churchill and J.P.Hutchinson, J.C.S. Chem. Comm., 1979, 219.

196. E.G.Bryan, private communication to J.Evans.

197. E.G.Bryan, B.F.G.Johnson and J.Lewis, J.C.S. Chem. Comm., 1977, 329.

198. M.R.Churchill and R.A.Lashewycz, Inorg. Chem., 1979, 18, 1926.

199. J-B.N'Guini Effa, J.Lieto and J-P.Aune, J. Mol. Catal., 1982, 15, 367.

200. a) L.Bemi, H.C.Clark, J.A.Davies, C.A.Fyfe and R.E.Wasylishen, J. Amer. Chem. Soc., 1982, 104, 438.
b) H.C.Clark, J.A.Davies, C.A.Fyfe, P.J.Hayes and R.E.Wasylishen, Organometallics, 1983, 2, 177.

201. S.Shinoda, K.Nakamura and Y.Saito, J. Mol. Catal., 1982, 17, 77.

202. A.Mantovani and S.Cenini, Inorg. Syn., 1976, 16, 47.
203. B.R.James, G.L.Rempel and W.K.Teo, Inorg. Syn., 1976, 16, 46.
204. P.Legzdins, R.W.Mitchell, G.L.Rempel, J.D.Ruddick and G.Wilkinson, J. Chem. Soc. (A), 1970, 3322.
205. V.D.Bianco and S.Doronzo, Inorg. Syn., 1976, 16, 158.
206. S.T.D.Gough and S.Trippett, J. Chem. Soc., 1961, 4263.

CHAPTER TWO

A TRIOSMIUM CLUSTER ANCHORED THROUGH A BRIDGING ALKYNYL LINKAGE

2.1. Other Modes of Attachment on Functionalised Oxides:- Polydentate Ligands

The use of tertiary phosphines as the functionalised group by no means offers the only possibility for complexing metal clusters to an inorganic support. Allum et. al.(1) prepared a variety of ligand-silanes containing primary and tertiary amines, nitriles, acetylacetone and thiol donor ligands. They used these to prepare supported mono-nuclear rhodium complexes. Direct extension of this work allows characterisation of the supported cluster $[HOs_3(CO)_{10}\{S(CH_2)_3SIL\}]$. This can be prepared by, either anchoring the thiolate substituted cluster $[HOs_3(CO)_{10}\{S(CH_2)_3Si(OMe)(CH_3)_2\}]$ to methanol treated silica by reflux in benzene, or from reaction of $[Os_3(CO)_{10}(C_6H_8)]$ with thiol modified silica in refluxing cyclohexane(2). At these temperatures contact of $[Os_3(CO)_{12}]$ with the functionalised silica also gives a similar result, but some resolution is consistently lost in the infrared ν_{co} spectrum. A slight improvement occurs if the oxide is first treated with a silylating agent(3). This suggests that although reaction is still selectively at the pendant thiol it is not specific, and some direct binding with surface silanol groups occurs.

The problem of competitive interaction with the oxide itself is even more troublesome with the ruthenium analogues. Reaction between unmodified silica and $[HRu_3(CO)_{10}\{S(CH_2)_3Si(OMe)(CH_3)_2\}]$, under reflux in cyclohexane, does not yield the attached cluster, but gives evidence of decomposition instead. However, the resulting infrared ν_{co} spectra differ from those obtained from interacting $[Ru_3(CO)_{12}]$ directly with the unmodified silica(3), which indicates that the metal carbonyl fragments remain bound to sulphur. The critical importance of the support surface (OH-density) on these degradation reactions was emphasized by the more encouraging results when using Me_3SiCl(3) or methanol(2) treated silicas. Infact contacting $[HRu_3(CO)_{10}\{S(CH_2)_3Si(OMe)_3\}]$ at room temperature did afford a solid which exhibited an infrared ν_{co} spectrum similar to the homogeneous precursor, but the loading was small, and doubt must remain about whether the methoxide groups have been substituted by surface oxygens under such mild conditions(4).

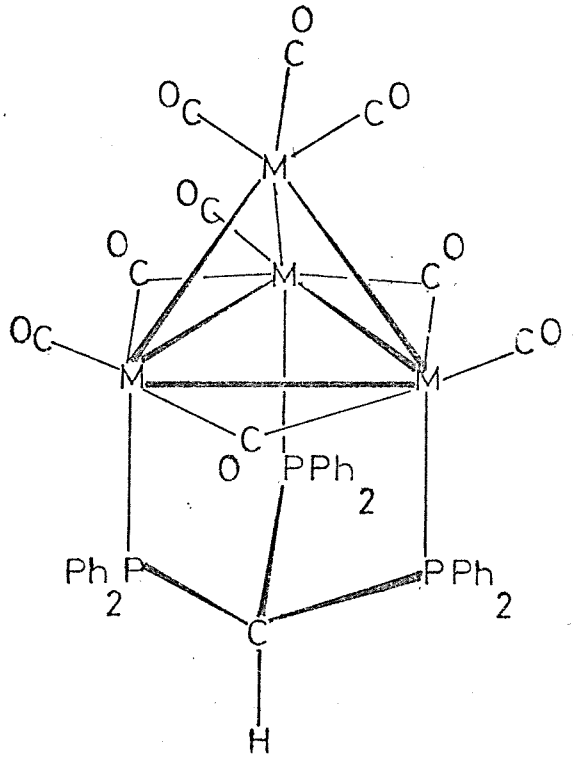
The alternative route, combining $[Ru_3(CO)_{12}]$ with the thiol functionalised silica under reflux in benzene, is far more successful with the reaction being specific towards the attached cluster. Even so, it still has a limited shelf-life, although this can be extended by using 'protected' silicas. Further, the specificity is dependent on the nature of the oxide support, and with other thiol modified oxides (Al_2O_3, TiO_2, SnO_2, ZnO or MgO) an additional broad ν_{co} absorption near $2000cm^{-1}$ was apparent(3).

Attachment through a μ_2-bonding mode is also achieved by the surface accelerated isomerisation of $[H_2Os_3(CO)_{10}\{CN(CH_2)_3Si(OEt)_3\}]$, the simple 1:1 adduct from $[H_2Os_3(CO)_{10}]$ and the isonitrile, to an aminocarbyne complex. This results in the isolation of the oxide supported cluster $[HOs_3(CO)_{10}\{CN(H)(CH_2)_3OXIDE\}]$; oxide=$SiO_2$, Al_2O_3, LiO_2, ZnO or MgO(5). The transformation was previously shown to be catalysed by mild base or strong donor solvents(6). The same authors demonstrated the option of supporting trimetallic clusters via a capping ligand by binding $[Co_3(CO)_9(\mu_3\text{-}CSiCl_3)]$(7) with the appropriate oxide followed by Soxhlet extraction. The recovered purple solids are all air stable and give infrared ν_{co} spectra in good agreement with the homogeneous cluster(3). This approach is receiving increased attention because bridging ligands should stabilise trimetallic cluster compounds against dissociation into mono-metallic species and/or aggregation to metal particles; problems often encountered under catalytic conditions. An obvious possibility would be attachment of $[H_2M_3(CO)_9(PR)]$, known for all three Group VIIIa metals (see Chapter Four), and this has been achieved by contacting isolated $[H_2Ru_3(CO)_9\{\mu_3\text{-}PCH_2CH_2Si(OEt)_3\}]$ with various oxides(8). The μ_3-capping phosphinidene ligand vastly increases the stability of the Ru_3 core relative to $[Ru_3(CO)_{11}(PPh_2CH_2CH_2SIL)]$, and it is even recovered unaltered after several catalysis runs for pentene isomerisations at 80^oC. Use of tridentate ligands capable of simultaneously complexing all three metal centres offers an intreging alternative.

Molecular modelling showed the bite angles of the two tripod ligands $HC(PPh_2)_3$ and $MeSi(PBu_2)_3$ would favour capping a triangular face rather than chelation about a single metal. This was confirmed by isolation of $[M_4(CO)_9\{HC(PPh_2)_3\}]$, M_4=Co_4, Rh_4,

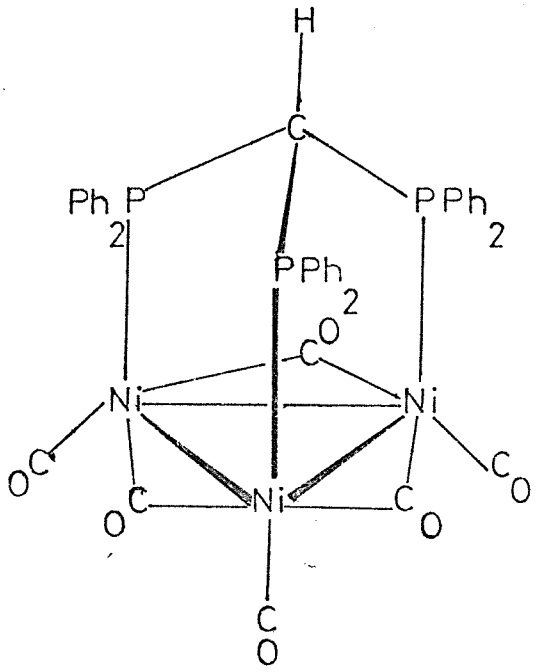
Diagram 1

Examples of Triangular Face-bridging by the Polydentate Ligand, 1,1,1-Tris(diphenylphosphino)methane.

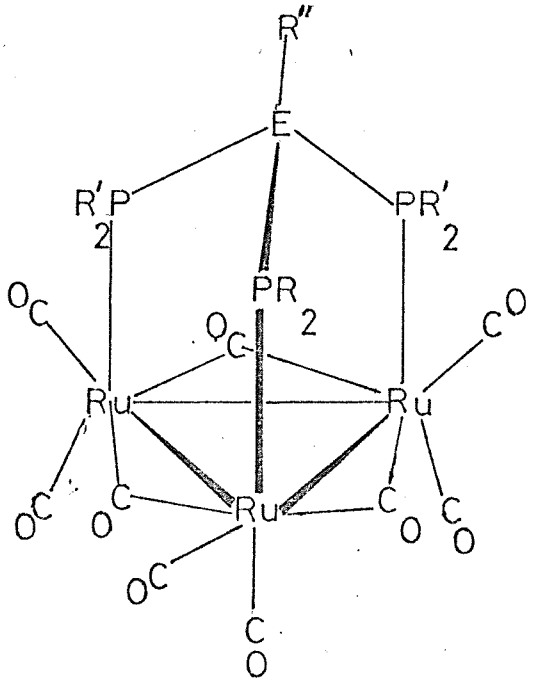


M=Co or Rh

$[M_4(CO)_9\{HC(PPh_2)_3\}]$

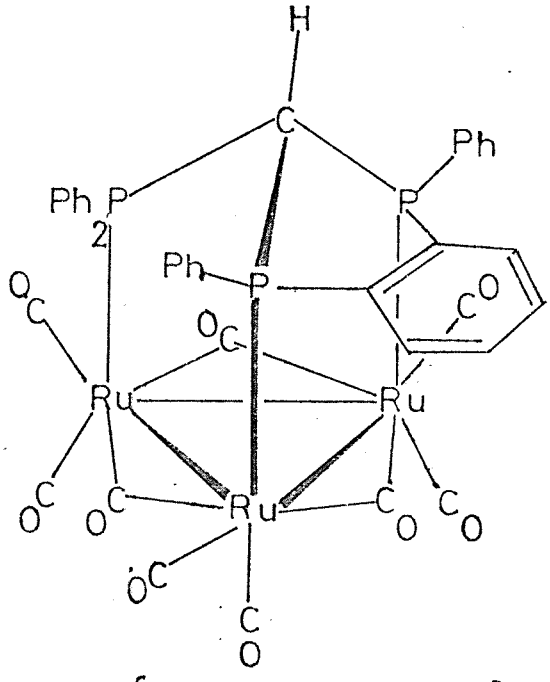


$[Ni_3(CO)_6\{HC(PPh_2)_3\}]$



E=Si, R'=Bu, R''=Me

or E=C, R'=Ph, R''=H



$[Ru_3(CO)_9\{HC(PPh_2)(PhPC_6H_4PPh)\}]$

Ir_4, Co_2Rh_2 or $HFeCo_3$(9); $[M_4(CO)_9\{CH_3Si(PR_2)_3\}]$, M=Co or Rh, R= Et, Pr, Bu; M=Ir, R=Et; $[Rh_6(CO)_{13}\{CH_3Si(PBu_2)_3\}]$(10); and $[Ru_3(CO)_9\{CH_3Si(PR_2)_3\}]$, R=Et, Pr(10) or Bu(11). An investigation into the catalytic activity of the last complex illustrated its greater resistance to dissociation compared to $[Ru_3(CO)_{12}]$ when treated with mixtures of hydrogen and carbon monoxide at high pressures (100bar) and temperature (300°C)(12). Similarly, the tetranuclear clusters, M=Co or Rh, undergo no change in toluene at 100°C under carbon monoxide (30bar), whereas under such conditions the parent carbonyls are unstable(13). Reaction of $HC(PPh_2)_3$ with $[Ru_3(CO)_{12}]$ does give rise to $[Ru_3(CO)_9\{HC(PPh_2)_3\}]$, which is isostructural to the methyltri-(di-n-butylphosphino)silane derivative (Diagram 1), but only in low yields (< 10%) as one of at least eight products(14). This is in part due to the unfavourable position of substitution (axial instead of equatorial), but also because metallation of the phenyl rings occurs i.e. $[Ru_3(CO)_9\{HC(PPh_2)$-$(PhPC_6H_4PPh)\}]$. $HC(PPh_2)_3$ also acts as a template for the stepwise formation of $[Ni_3(CO)_6\{HC(PPh_2)_3\}]$ from $Ni(CO)_4$(15), in a similar fashion $NaIr(CO)_4$ reacts with Cl_3XMe, X=C, Ge or Si, to form $[Ir_3(CO)_9(XMe)]$(16). Simple modification of the alkyl (or H) chain then facilitates binding to a support material(17).

2.2. Reactions of $[M_3(CO)_{12}]$, M=Os or Ru, with Unsaturated Hydrocarbons

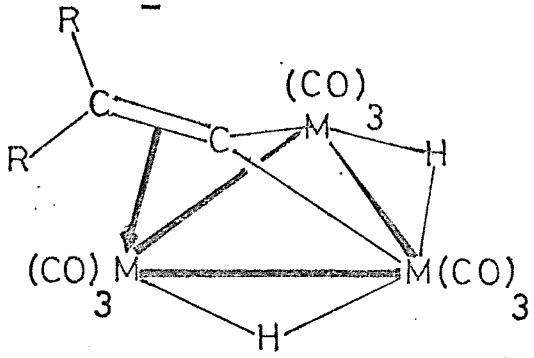
An extensive chemistry is known for $[M_3(CO)_{12}]$ with alkenes and alkynes. In the obtained products the organic substrate normally coordinates in a multiple nature creating a very strong bonding mode. Clearly this offers another opportunity of affixing a cluster to silica through a very stable pendant ligand. The phosphine-silane precursor triethoxyvinylsilane can be regarded as a potential source of a supported alkene. Before considering its reaction with $[Os_3(CO)_{12}]$ an account of the possible products expected is given.

An initial report(18) indicated that $[Ru_3(CO)_{12}]$ reacts with ethylene at atmospheric pressure to give a mixture of the isomeric vinylidene, I, and ethyne, II, complexes, although the precise conditions used were not specified. However, repetition under reflux in n-heptane produced a more complicated result

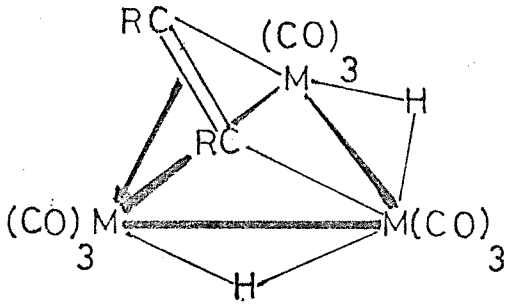
Diagram 2

Common η^2-Bonding Modes of Unsaturated Hydrocarbons.

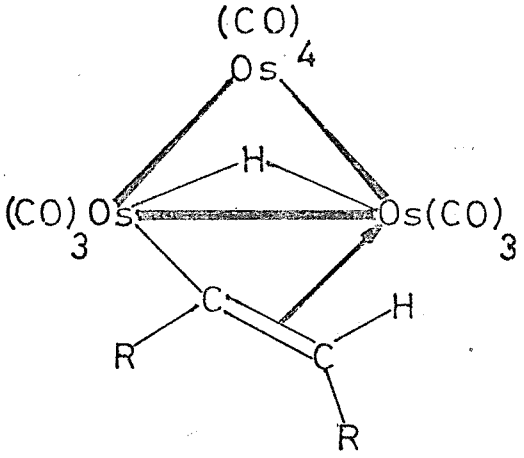
I



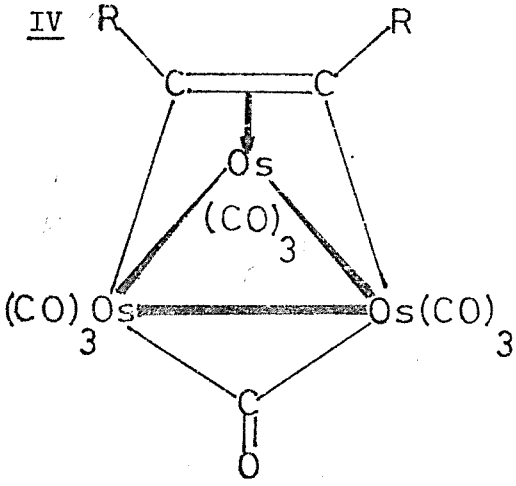
II



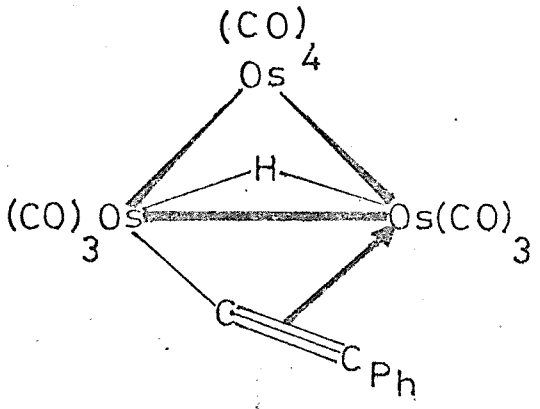
III



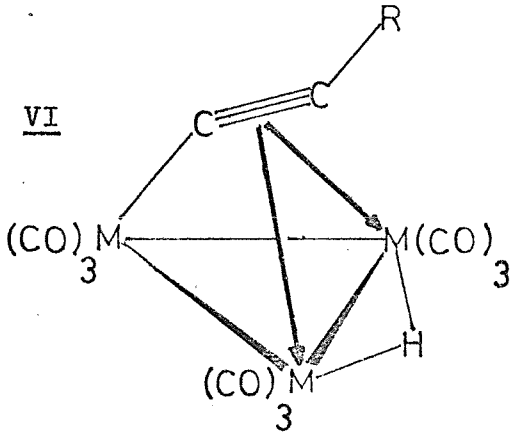
IV



V



VI

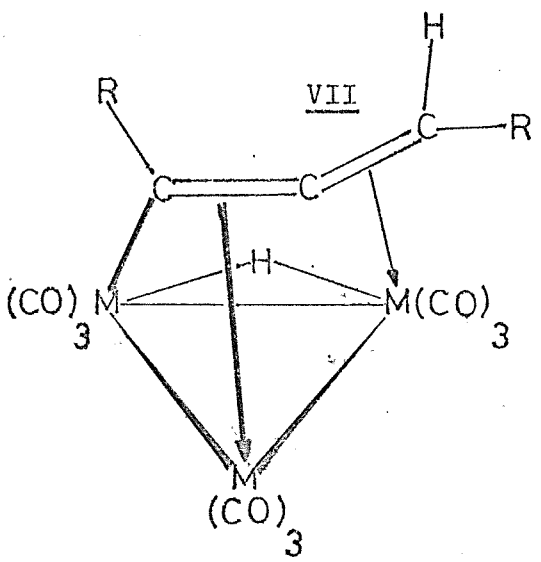


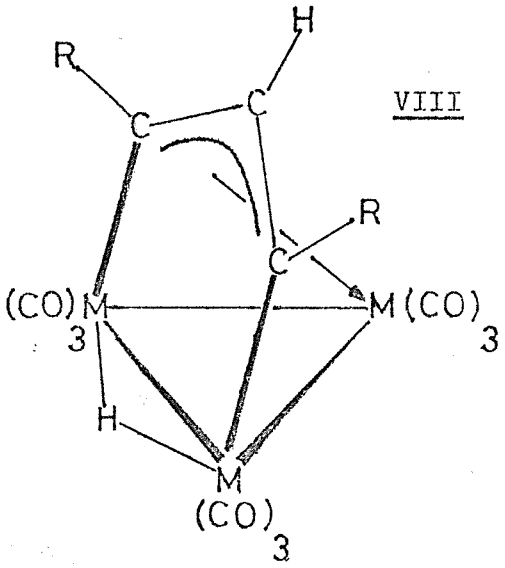
involving almost certain intermediate cluster breakdown to $[Ru(CO)_4(H_2C{:}CH_2)]$(19). Only the vinylidene species was identified in the product distribution, accompanied by several substituted type II and VIII species arising from ethylene oligomerisation. The μ_3-allyl formation appears particularly stable, and is found in products from such unlikely reactions as that of $[Ru_3(CO)_{12}]$ with cyclododeca-1,5,9,-triene(20) or phenyl-lithium(21). Oxidative addition of dienes(22) also gives VIII, but with hexa-2,4-diene an intermediate μ_3-allenyl, VII, group can be isolated which thermally isomerises to the η^3-allyl group with M-C σ-bonds to the terminal carbon atoms(23). The action of hydrogen on $[HRu_3(CO)_9\{Me(H)C{:}C{:}CMe\}]$, but not on $[H_2Ru_3(CO)_9(MeC.CH.CMe)]$, will produce a μ_3-alkyne ligand, II, in $[H_2Ru_3(CO)_9(MeC{:}CEt)]$(24). This emphasizes the stability of the μ_3-allyl system for ruthenium, where possible ligands rearrange to fit this predilection. A further product from the ethylene reaction was the tetranuclear $[Ru_4(CO)_{12}(MeC{:}CMe)]$, previously synthesised at greater pressure and temperature, in conjunction with the even higher nuclearity products $[Ru_6C(CO)_{17}]$ and $[Ru_6C(CO)_{15}(MeCH{:}CH.CH{:}C(H)Me)]$(25).

The chemistry of $[Os_3(CO)_{12}]$ shows similar trends, but the more robust metal ring reduces the tendancy to form higher nuclearity products, whilst alkene-coupling reactions are also retarded. Under an ethylene atmosphere, in refluxing n-octane, selective formation of the 1,1-dimetallated isomer occurs(26). This remains the major species at applied pressures, but accompanied by the tetranuclear 'butterfly' clusters $[Os_4(CO)_{12}(CH{:}CH)]$ and $[Os_4(CO)_{12}(C_4H_6)]$(27). With propene I is still the predominant component in an inseparable oil with small quantities of the 1,2-isomer. Generally 1,1-dimetallation is the preferred route, although large 1-alkenes do occasionally produce some 1,2-isomer (28). Through necessity, in the absence of two geminal hydrogens to transfer, cyclopentene(26) and cyclooctene(29) give 1,2-di-ylidene species. Despite cyclic alkenes and benzene being chemically very different in many respects it still reacts, albeit at greater temperatures (around 195°C), in the same way to give $[H_2Os_3(CO)_9(\mu_3\text{-}C_6H_4)]$(26). Mechanistic studies have shown that the reaction proceeds via the two intermediates, $[Os_3(CO)_{11}(H_2C{:}CH_2)]$ and $[HOs_3(CO)_{10}(CH{:}CH_2)]$, III, which can be isolated by different routes,

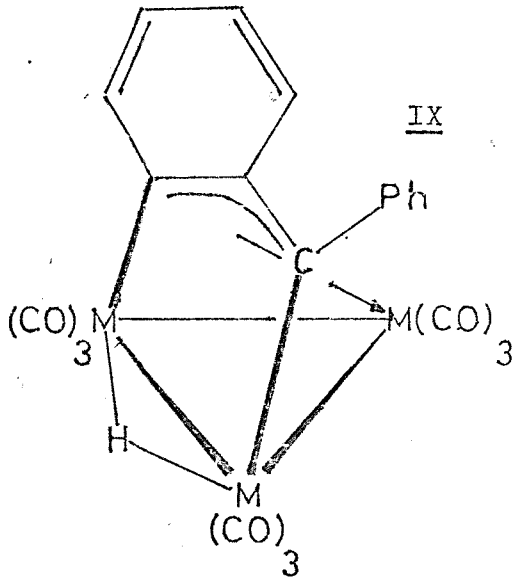
Diagram 3

Extended Bonding Modes of Ligands derived from Unsaturated Hydrocarbons.

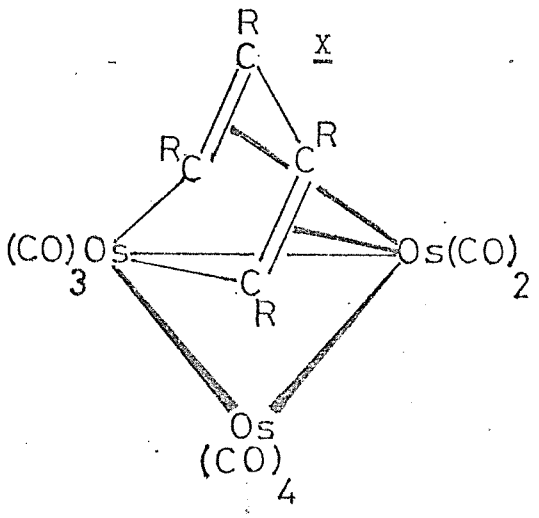


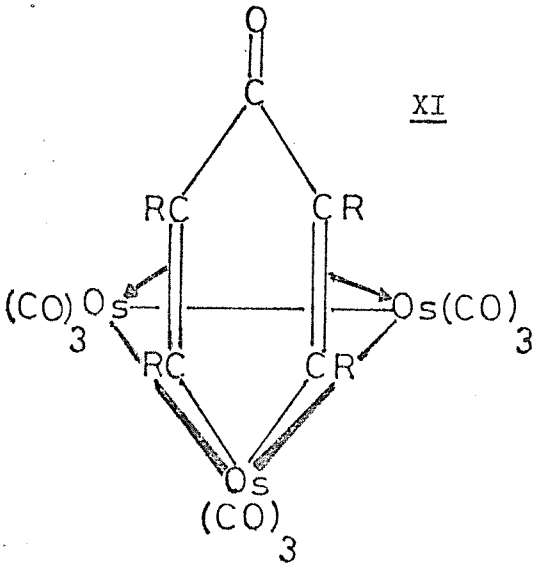


$Ru_3(CO)_{12}$ —(i) PhLi; (ii) H^+→



$H_2Os_3(CO)_{10}$ —(i) $Ph_2C{=}C{=}O$; (ii) HEAT→





but are not observed in the reaction at 125°C, confirming the initial substitution reaction to be rate-determining. A general feature of $[Os_3(CO)_{12}]$ chemistry is at the temperature necessary to displace carbon monoxide the coordinatively unsaturated species generated are very reactive to oxidative addition.

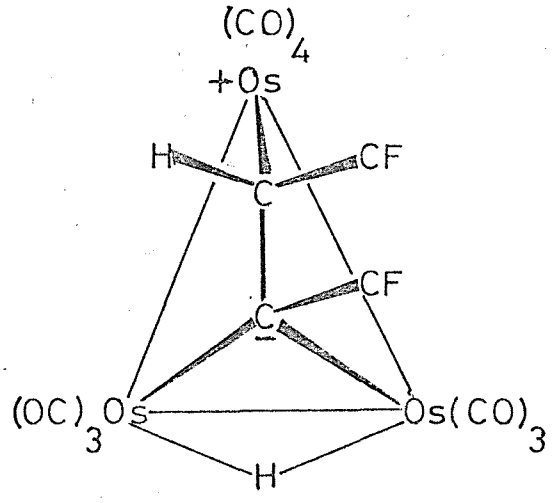
$[HOs_3(CO)_{10}(CH{:}CH_2)]$ can be prepared by reacting either ethylene or acetylene with $[H_2Os_3(CO)_{10}]$ at room temperature. Insertion of an alkyne into an Os-H bond, a cis-addition relative to the alkyne, represents a general route to substituted type III products(30,31), and has allowed a more systematic investigation of their subsequent chemistry. In the presence of excess alkyne dehydrogenation to non-hydridic type IV complexes occurs, with assumed generation of the corresponding alkene(30). The case of this transformation is affected by the nature of the alkyne. For acetylene reflux in n-hexane is necessary, and is complicated by accompanying ogliomerisation reactions(30). Conversely alkyl substitution, as in propyne, leads to a product distribution between III and IV (towards the latter) at room temperature, until with excess 3-hydroxy-3-methylbut-1-yne conversion is almost complete (32). The formation of $[Os_3(CO)_9(\mu_2\text{-}CO)(MeC{:}CMe)]$ with but-2-yne indicates that it is the metal hydride, and the hydrogen on the carbon not formally σ-bonded to the cluster in III, which are lost; assuming the first moiety does not become detached. A dependence on alkyne concentration supports dehydrogenation via interaction with excess alkyne, as opposed to elimination of molecular hydrogen. Diphenylactylene also gives a species of stoichiometry $[Os_3(CO)_{10}(PhC{:}CPh)]$, but a subsequent X-ray crystal structure analysis revealed a subtle difference, with two semi-bridging carbonyls instead of a single μ_2-carbonyl ligand(33).

Extended reaction times, combined with large excesses of alkyne, tend to promote coupling reactions, especially if hydrogen transfer onto the cluster is unfavourable. The metallacyclopentadiene species $[Os_3(CO)_9(C_4H_4)]$, (X, R=H), is one of the co-products with acetylene. With but-2-yne, along with IV, R=Me, $[Os_3(CO)_9(C_4Me_4CO)]$ is isolated which contains a metallatetramethylcyclohexadienone ring, XI (R=Me). The presence of a conjugated ketone was supported by a clear infrared signal at 1616cm^{-1}(30), and for asymmetric acetylenes, i.e. propyne(34), a

SOUTHAMPTON LIBRARY UNIVERSITY

mixture of all three possible isomers is formed. The analogous diphenylacetylene adduct is unstable, and eliminates a carbonyl again, to produce an osmiacyclopentadiene cluster, X (R=Ph). This compound is interesting as it reversibly decarbonylates by feeding two extra electrons into the cluster via metallation of a phenyl ring. Further, with excess diphenylacetylene a third group is incorporated en-route to release of hexaphenylbenzene, and various mono-nuclear osmium species. This completes a cyclotrimerisation reaction induced by $[Os_3(CO)_{12}]$ (Diagram 4); similar results can be achieved with other alkynes(35).

One final acetylenic reaction is that of hexafluorobut-2-yne, $F_3CC{:}CCF_3$, with $[H_2Os_3(CO)_{10}]$(41). This ligand has little likelihood of behaving like but-2-yne because of the widely differing inductive effects of CF_3 and CH_3; having no hydrogens, the wide range of rearrangements on heating (see below) is not also possible. Infact a completely new bonding mode is produced. Although the formula $[HOs_3(CO)_{10}\{F_3CC{:}C(H)CF_3\}]$, is that expected for the vinyl species, III, an X-ray crystal structure shows that the ligand is μ_3-coordinating. There is a formal dipole on the molecule to comply with E.A.N. Rules on each osmium atom, this polarity is in agreement with its poor solubility in hydrocarbon solvents.

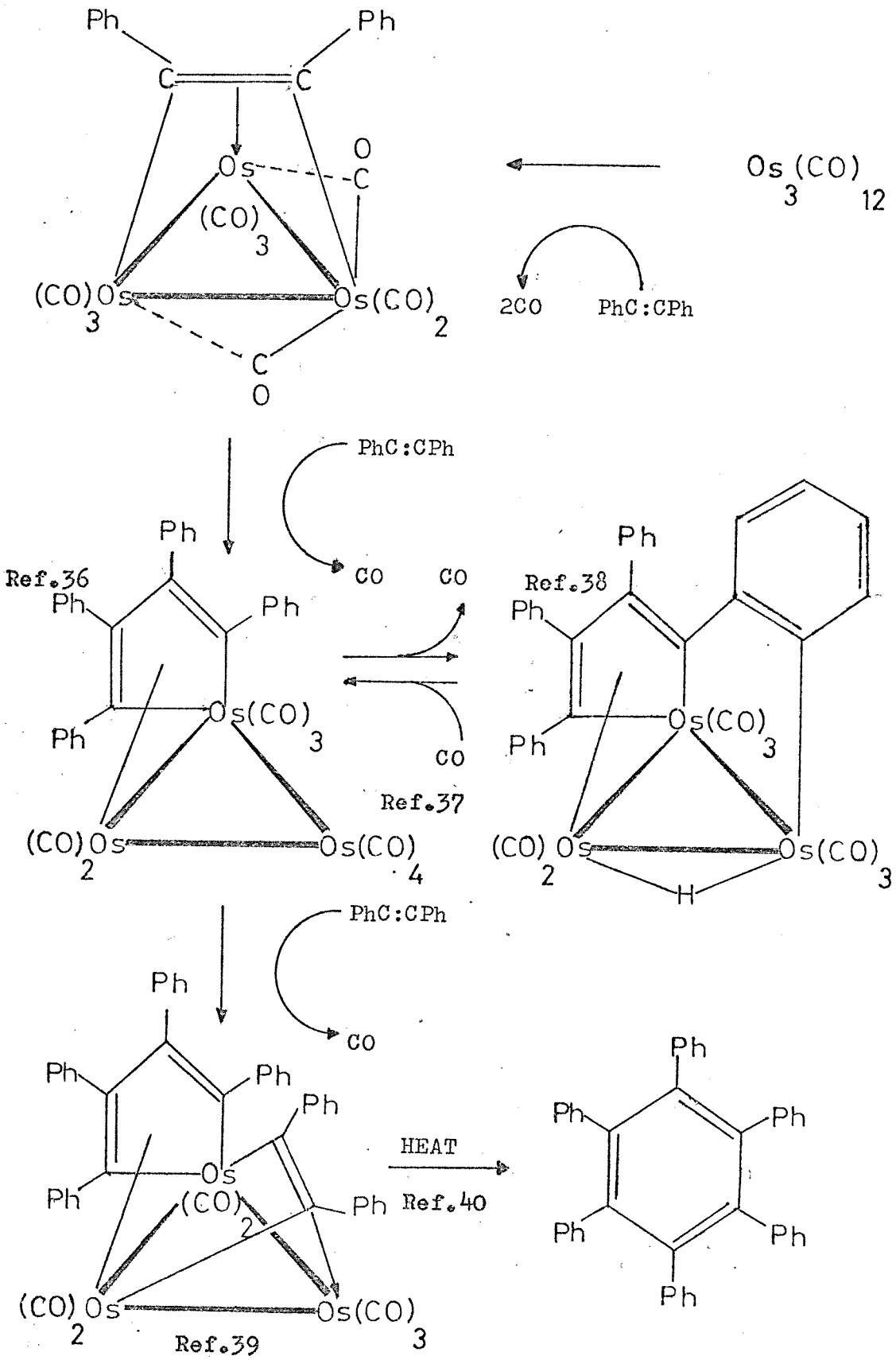


Structure of
$[HOs_3(CO)_{10}\{F_3CC{:}C(H)CF_3\}]$

On refluxing in hydrocarbon solvents these decacarbonyl adducts are converted to nonacarbonyl species. Type IV complexes, derived from terminal acetylenes, undergo thermal displacement of carbon monoxide to give VI by oxidative addition. An intermediate

Diagram 4

[$Os_3(CO)_{12}$] Induced Cyclotrimerisation of Diphenylacetylene.

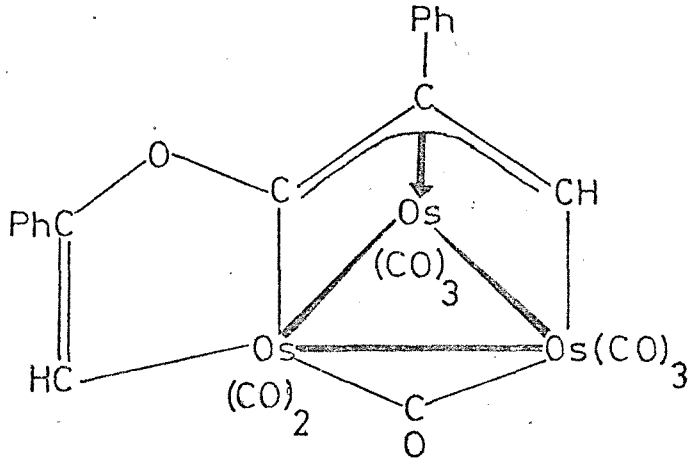


in this transformation is apparently $[Os_3(CO)_9(RC_2R')]$, (R=H, R'=Me), which isomerises in n-octane under reflux(31). This dictates carbon monoxide loss prior to hydrogen transfer from ligand to osmium core. However, this may be a delicate balance as phenylacetylene gives $[HOs_3(CO)_{10}(C{:}CPh)]$, V, instead of IV, at room temperature. The alkynyl ligand is bound in a σ, π manner comparable to the μ_2-vinyl group; and might be considered to represent an alternative pathway to the monohydride, but its thermolysis was not reported(30). Even $[Os_3(CO)_9(\mu_2\text{-}CO)(HC{:}CH)]$ selectively degrades to $[HOs_3(CO)_9(C{:}CH)]$ when heated in n-hexane(42). Type VI complexes can be hydrogenated through to $[H_3Os_3(CO)_9(CH_2R)]$ which almost certainly proceeds via the 1,1-isomer, I. Conversely hydrogenation of IV, accompanied by carbon monoxide loss, leads to the 1,2-isomer, II, and under atmospheric pressure treatment no further hydrogenation takes place(30). From internal alkynes, the absence of an available hydrogen, leads into the ogliomerisation chemistry. However, $[Os_3(CO)_{10}(MeC{:}CMe)]$ in refluxing n-heptane forms $[HOs_3(CO)_9(C_4H_5)]$ which isomerises in a sealed tube at 156°C to a type VIII compound(30). This transformation is almost certainly identical to that for $[HRu_3(CO)_9(C_6H_9)]$, with the first isomer possessing a μ_3-allene configuration. The μ_3-allyl ligand is less abundant in triosmium chemistry, but it is also accessible by insertion of $Ph_2C{=}C{=}O$ into an Os-H bond of $[H_2Os_3(CO)_{10}]$ to give a μ_2-acyl complex which is then pyrolysed(43).

In the presence of an α-hydrogen the nature of the other substituent does not affect the selective degradation of IV. Similarly, pyrolysis of III invariably leads to formation of the dihydridic species I or II. However, a degree of conflict appears with bulky substituents at the vinyl group. With a tertiary-butyl group claims for both selective formation of I(31) and VI(32) exist. With $R=Me_2COH$ mixed formation is reported(32); perhaps the presence of residual alkyne could account for these discrepancies.

Direct reaction of alkynes with $[Os_3(CO)_{12}]$ normally results in complex mixtures due to the temperature required to activate the cluster. Under favourable conditions, species such as $[Os_3(CO)_{10}(CHCR)]$, $[Os_3(CO)_{10}(RCCH)_2]$ and $[HOs_3(CO)_9(C_2R)]$ can be isolated, but usually with excess alkyne the products en-route to cyclotrimerisation, already broached upon, are observed(44).

$[Os_3(CO)_{10}(RC_2R')_2]$ may be a simple acetylene-substitution-for-carbonyl species, but for phenylacetylene it has been found that the structure contains a single ligand moiety incorporating a carbonyl group(45).



Structure of '$[Os_3(CO)_{10}(HC_2Ph)_2]$'

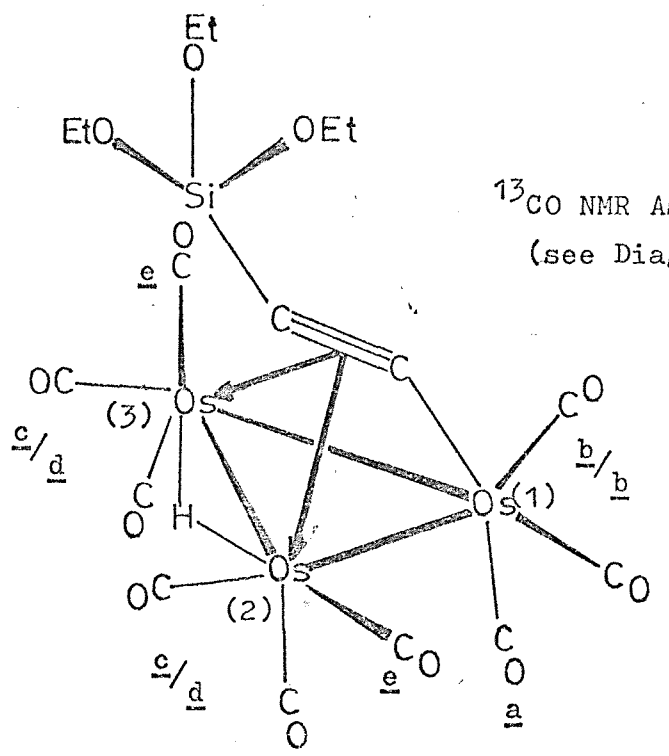
Clearly for osmium the chemistry is complicated, but several trends can be identified depending on the operating conditions. With alkynes, low temperatures and excess ligand favours first IV, and with extended reaction times ogliomerisation. Higher temperatures allow oxidative addition coupled with decarbonylation, again depending on alkyne concentration, to give either I or VI or mixtures thereof: a dependence on the adjoining functionalities is apparent.

2.3. Reaction of Triethoxyvinylsilane with $[Os_3(CO)_{12}]$

Triethoxyvinylsilane was reacted with $[Os_3(CO)_{12}]$ under identical conditions to those employed by Deeming and Underhill(26) with ethylene. After reflux in n-octane overnight the solution had turned orange. Removal of the solvent gave a residue whose infrared ν_{CO} spectrum appeared to be just a mixture of the starting material and a single product. Chromatography on silica-gel, with Et_2O/n-hexane (3:1v/v) as eluant, resulted in only $[Os_3(CO)_{12}]$ moving up the plate. Extraction of the baseline with methylene chloride and methanol gave a considerable quantity of an amorphous orange

Diagram 5

Spectroscopic Data for $[HOs_3(CO)_9(C{:}CR)]$, R=Si(OEt)$_3$ or SIL.



^{13}CO NMR Assignments
(see Diagram 6)

Table 1

Compound	IR ν_{CO}/cm^{-1} (cyclohexane unless stated)			
$[HOs_3(CO)_9\{C{:}CSi(OEt)_3\}]$	2102.5w	2077vs	2054vs	2020vs
	2016.5ssh	1983msh	1981m	
$[HOs_3(CO)_9(C{:}CSIL)]$		2078s	2054s	2022s
(nujol mull)	2014s	1983.5m		
$[HOs_3(CO)_9(C{:}CMe)]$	2101w	2073vs	2053vs	2022vs
(Ref.27)	2012s	1984msh	1982m	
$[H_2Os_3(CO)_9(C{:}CH_2)]$	2109vw	2082vs	2059vs	2052sh
(Ref.23)	2032s	2022s	2019s	2011m
	1993w	1985m		
$[H_2Os_3(CO)_9(HC{:}CMe)]$	2108w	2080vs	2056vs	2031vs
	2025s	2010vs	2001vs	1984m

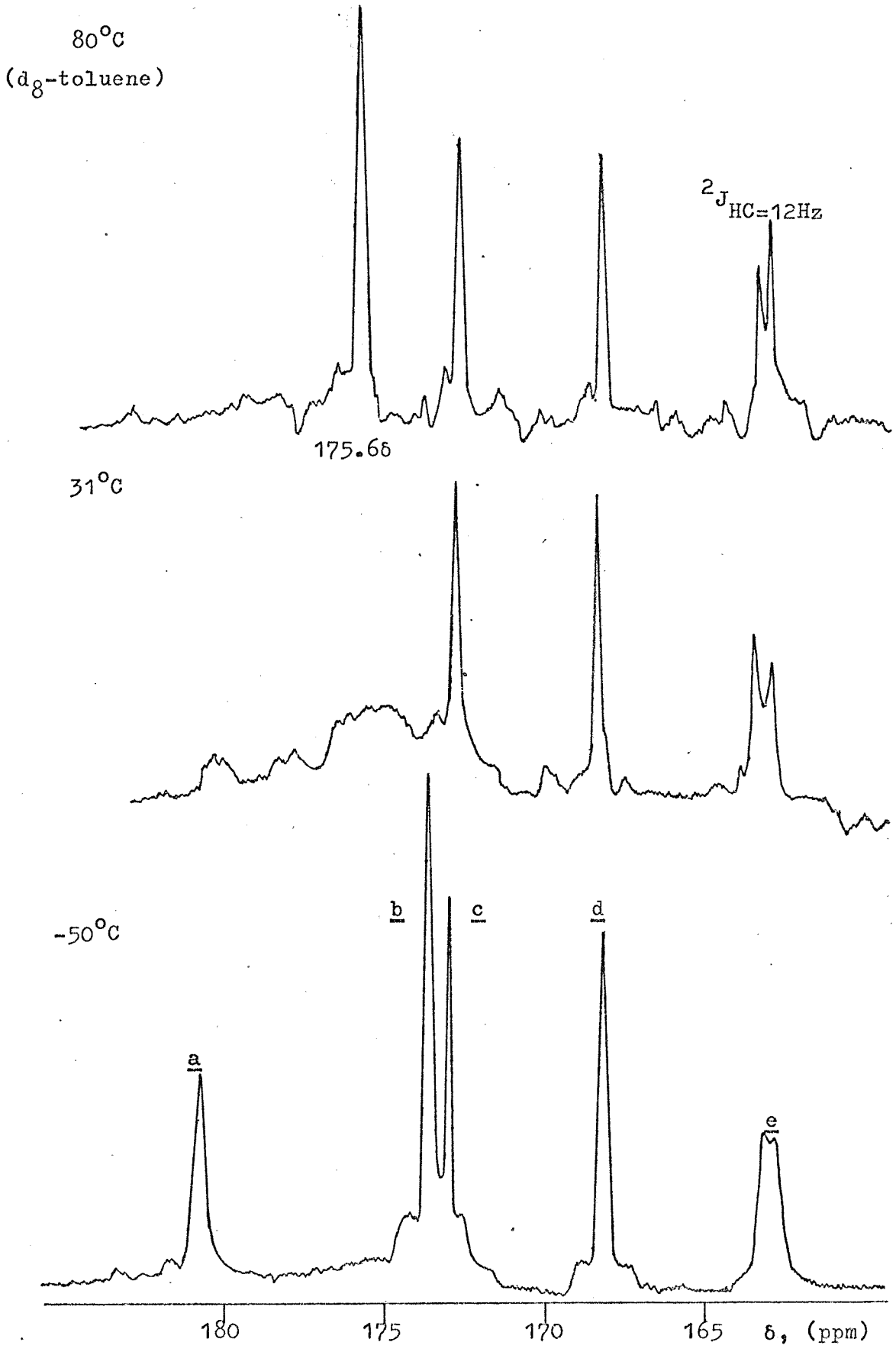
solid. Notably, even when using methanol not all the band was removed which, in conjunction with its immobility, is indicative of retained Si-OEt groups and their strong affinity for the silanol groups.

The infrared ν_{CO} spectrum of this product is very simple (Diagram 10), but surprisingly it does not correspond to that of an expected type I (or II, although the data presented hereafter does not differentiate between these possibilities) product. Instead it closely resembles that of a type VI monohydride complex (Table 1). In support, the mass spectrum has a parent ion maximum at m/e=1012, in a well defined Os_3 isotopic pattern, in accord with a dehydrogenated product. After loss of three carbonyl groups the fragmentation pattern becomes complicated by breakdown of the organic ligand. When operating at 70eV the $[Os_3]^+$ core signal was only faintly visible, and the last significant pattern is consistent with a $[Os_3C_2]^+$ fragment. The ^1H NMR spectrum ($CDCl_3$, 31°C) contains the characteristic hydride singlet for such a compound seen at -23.7δ. At low temperatures (-50°C) no splitting of the signal is observed as would have been anticipated for a dihydrido-species, due to the inequivalence of the hydrides. In addition, apart from the ethoxy-proton resonances, no peaks due to C-H protons on the organic moiety were seen. All this evidence points towards a product of molecular formula $[HOs_3(CO)_9\{C:CSi(OEt)_3\}]$, VIa, and structure as shown in Diagram 5. There is no indication that the retrieved product is polymeric in nature through cross-linking caused by hydrolysis during the work-up procedure. Yields were typically in the region 65-75%, although this is largely limited by the aforementioned extraction problems.

As the product is amorphous in nature a conclusive X-ray crystallographic study would prove difficult. However a ^{13}CO enriched sample was prepared and a variable temperature ^{13}C NMR study carried out. This confirmed the carbonyl distribution to be identical to that of $[HOs_3(CO)_9(C_2{}^tBu)]$(46). In turn this is isostructural with the ruthenium analogue $[HRu_3(CO)_9(C_2{}^tBu)]$, VIb, which has been the subject of a detailed neutron diffraction study. The $\{^1H\}$-^{13}C spectra, recorded over the range -50 to +80 °C, are shown in Diagram 6. The low temperature (-50°C, d_8-toluene) limiting spectrum contains five resonances at: a, 181.0; b, 173.9;

Diagram 6

Variable Temperature $^{13}C-\{^{1}H\}$ NMR Spectra of $[HOs_3(CO)_9\{C:CSi(OEt)_3\}]$.



c, 173.0; d, 168.6; and e, 163.1 δ-with integrated intensities of 1:2:2:2:2 respectively. These chemical shifts and pattern show excellent agreement with those of $[HOs_3(CO)_9(C_2{}^tBu)]$, (-37°C, $CDCl_3$), 183.3, 173.7, 171.8, 169.6 and 162.8 ppm , especially if account of possible, additional, solvent effects is made. The pattern is in accordance with retention of the proposed solid-state structure, possessing a pseudo-mirror plane through Os(1) and bisecting the hydrido-bridged Os(2)-Os(3) bond, upon solvation. This creates five different carbonyl enviroments, and a degree of assignment is possible by observation of several exchange processes. From its intensity a must be assigned to the axial group on Os(1). As the temperature is raised this resonance begins to coalesce with b. At room temperature both have completely collapsed into the baseline, and eventually (+80°C) a sharp, average, resonance at 175.66, of relative intensity three, is seen. Resonances c to e remain unaltered throughout this temperature range. This sequence of events is interpreted to mean that axial-equatorial scrambling is taking place at the unique osmium independent of exchange between metal atoms. Obviously the barrier to a similar process at the two other centres is much higher. This may be related to the differing modes of coordination with the acetylenic ligand, or the presence of the bridging hydride, restricting motion.

Similar dynamics were observed for $[HOs_3(CO)_9(C_2{}^tBu)]$, by Aime and coworkers(46), who favoured the increased electronegativity at the unique osmium, promoted by σ-bonding to the organic group, as the cause for the lower barrier. Further, extension of the upper range identified slight broadening of all resonances at 173°C. As expected, the barrier to this higher exchange process is appreciably lower in the ruthenium analogue where broadening commences just above ambient temperature, with the appearance of an averaged resonance at 153°C. Only a few cases exist, i.e. $[M_3(O{:}CNMe_2)(CO)_{10}]^-$ (47) and $[HM_3(\mu\text{-}CO)(CO)_{10}]^-$(48), where this situation is reversed and the barrier height to a fluxional process is greater for the ruthenium analogue. In the first example the origin is a difference in ground-state structure (bridged verses all-terminal). For VIa, the static nature of the hydride during the dynamic process is emphasized by the observation that it remains coupled to only resonance e, ($^2J_{CH}$=12Hz), throughout the range studied. This allows

e to be assigned to the symmetry related pair approximately trans- to the hydride. Insufficient data is available to discriminate between the other two sets of enviroments on Os(2)/Os(3) represented by resonances c and d.

2.4. The Chemistry of $[HRu_3(CO)_9(C_2{}^tBu)]$

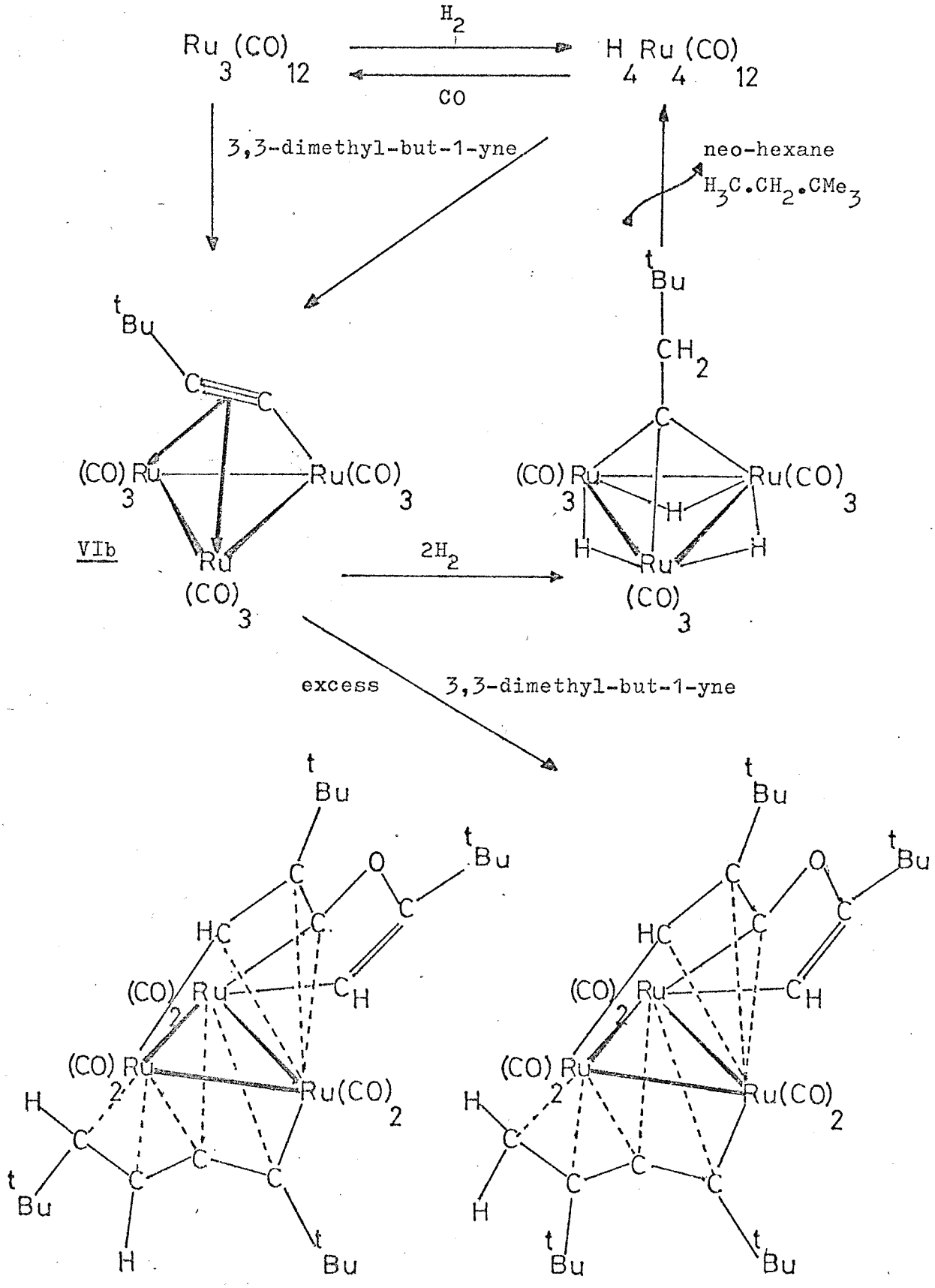
$[HRu_3(CO)_9(C_2{}^tBu)]$, VIb, is formed almost quantitatively from the reaction of $[Ru_3(CO)_{12}]$ with 3,3-dimethyl-but-1-yne under reflux in petroleum ether(40-70)(49). The full molecular structure was determined by a neutron diffraction study(50); it has overall $C_s(m)$ pseudo-symmetry. The Ru_3 cluster has equilateral geometry showing the exact balance between the lengthening effect of the hydride and the shortening effect of the organic ligand on the bridged Ru-Ru bond. Each ruthenium is bonded by two equatorial and one axial terminal carbonyl group. The acetylenic ligand is coordinated to the metallic cluster via a three-centre μ-type bond and a σ-bond with the unique metal. The hydride atom lies on a pseudo-plane of symmetry out of the cluster plane, its position is consistent with the Ru-H-Ru bond being classified as 'open'. The intrinsic stability of this μ_3-η^2 acetylide ligand is demonstrated by its ability to accommodate a wide range of bridging groups, X=H, halogen(51), PR_2(52), HgBr(53) or $AuPPh_3$(54), where the X-ray diffraction determined molecular structures all show it spanning both open and closed trimetallic clusters in $[XRu_3(CO)_9(C_2R)]$, formed by oxidative addition of the appropriate alkyne. Apart from the variation in this bridged vector the $Ru_3(CO)_9(C_2R)$ framework remains practically unchanged indicating a remarkable rigidity.

No doubt due to its accessibility the chemistry of VIb has been extensively studied. In higher boiling hydrocarbon solvents reaction occurs with excess alkyne to give two non-hydridic isomers of stoichiometry $[Ru_3(CO)_6(HC_2CMe_3COHC_2CMe_3)(HC_2CMe_3)_2]$. The organic ligand is formed by two halves, the first originated by the linkage of two molecules of alkyne via a -C-O- bridge, and the second by direct linkage of two further molecules of alkyne. The only difference is in the way the molecules of ligand are joined in the second fragment(55). VIb has been fully established as an intermediate in their formation. Studies with DC_2CMe_3 confirmed hydrogen transfer

Diagram 7

Chemistry of

Nonacarbonylhydrido(t-butylethynyl)-triangulo-triruthenium.



from the ligand to the cluster to form VIb, and from the cluster to the inserted ligand in the next step(56). Further treatment of these clusters with excess ligand reversibly leads to incorporation of another molecule into the first organic segment to give $[Ru_3(CO)_5(C_{19}H_{30}O)(C_{12}H_{20})]$ as determined by X-ray methods(57). VIb also reacts with isopropenylacetylene(58) and diphenylacetylene (59) to give tri- and tetra-alkyne substituted clusters, where again the ligands are combined into larger systems with some delocalisation apparent. However, with hexadienes(60) the two ligands remain separate entities.

Deprotonation of VIb can be affected with hydroxide to give $[Ru_3(CO)_9(C_2{}^tBu)]^-$ which has undergone a complete structural characterisation(61). The only major difference involves a rotation about the Ru-Ru bond of the three carbonyl groups on the non-unique metal centres, relieving the steric hinderance caused by the hydride ligand. Removal of the hydride also results in a lower barrier to rotation as shown by a variable temperature ^{13}C NMR study. IVb also undergoes electrophilic attack by protic acids and molecular hydrogen. Protonation occurs first at the metal core and then directly at the exposed carbon of the acetylenic ligand(62). Similarly $[HRu_3(CO)_9(C_2Ph)]$ shows regiospecific addition of isocyanides at this carbon(63). Phosphine substitution may also occur through the intermediacy of such a 1:1 adduct, as unequivocally demonstrated for the osmium variants(64). A comprehensive study of the electronic structure of VIb, by gas-phase UV photoelectron spectroscopy(65) coupled with quantum mechanical CNDO calculations, provided a theoretical basis for this directionality. The C-C bond is highly polarised with C(1) possessing a positive atomic charge. This novel electrophilicity, combined with a much higher energy for the l.u.m.o. of metal-metal anti-bonding character relative to that in $[Ru_3(CO)_{12}]$, accounts for this alternative pathway for nucleophilic addition.

Hydrogenation was originally believed to give the dihydridic species $[H_2Ru_3(CO)_9(HC_2{}^tBu)]$(56). However a X-ray crystal structure analysis on the product showed this formulation to be incorrect. Infact two molecules of hydrogen are taken up giving $[H_3Ru_3(CO)_9(CCH_2{}^tBu)]$, XII, (66). Under the conditions of reflux in n-heptane $[H_4Ru_4(CO)_{12}]$ is the major by-product, whilst I and

II (R_1=H, R_2=^{t}Bu) are only obtained in low yields. In higher boiling hydrocarbons a further hydrogenation occurs liberating 2,2,-dimethyl-butane (neo-hexane), with $[H_4Ru_4(CO)_{12}]$ the only carbonyl-containing compound identified in solution. Since $[H_4Ru_4(CO)_{12}]$ reacts with 3,3-dimethyl-but-1-yne to regenerate VIb the possibility of a full catalytic cycle is established (Diagram 7). However, one major drawback exists since ejection of neo-hexane is accompanied by considerable formation of ruthenium metal. A partial pressure of carbon monoxide reduces this decomposition, but simultaneously reduces the yields of neo-hexane to zero. Hence, the presence of ruthenium metal may promote the hydrogenation, or at least be the primary product from the decomposition of XII. Whatever, intermediate variations in nuclearity or reduction to metal are not compatible with transferring the cycle to a supported species; especially as the functionalised group is also the substrate to be hydrogenated. Of more possible interest would be the reported phosphine adduct, $[HRu_3(CO)_8(PPh_3)(C_2{}^tBu)]$(67), but related studies have not been published. VIb has been also investigated as a potential catalyst for the water gas shift reaction(68).

2.5. Discussion:-Reaction of $[Os_3(CO)_{12}]$ with $R_3SiCHCH_2$, R=Et or Ph

Here we have the selective formation of $[HOs_3(CO)_9\{C:CSi(OEt)_3\}]$, VIa, in high yields under conditions where other alkenes give type I/II products. Given the proviso that reaction proceeds without intermediate cluster breakdown, then progression through to the vinyl adduct $[HOs_3(CO)_{10}\{CH:C(H)Si(OEt)_3\}]$, IIIa, by the established mechanism is anticipated. This decacarbonyl is unstable at the reaction temperature and will undergo decarbonylation. At least two competing pathways exist as demonstrated with alkynes. One is straightforward hydrogen transfer, whilst the second involves prior dehydrogenation by interaction with excess ligand. The latter only occurs when III is formed under conditions where subsequent decarbonylation is unfavourable. With alkenes this situation is not normally encountered, and it must be here that the silicon-substituent has a fundamental importance.

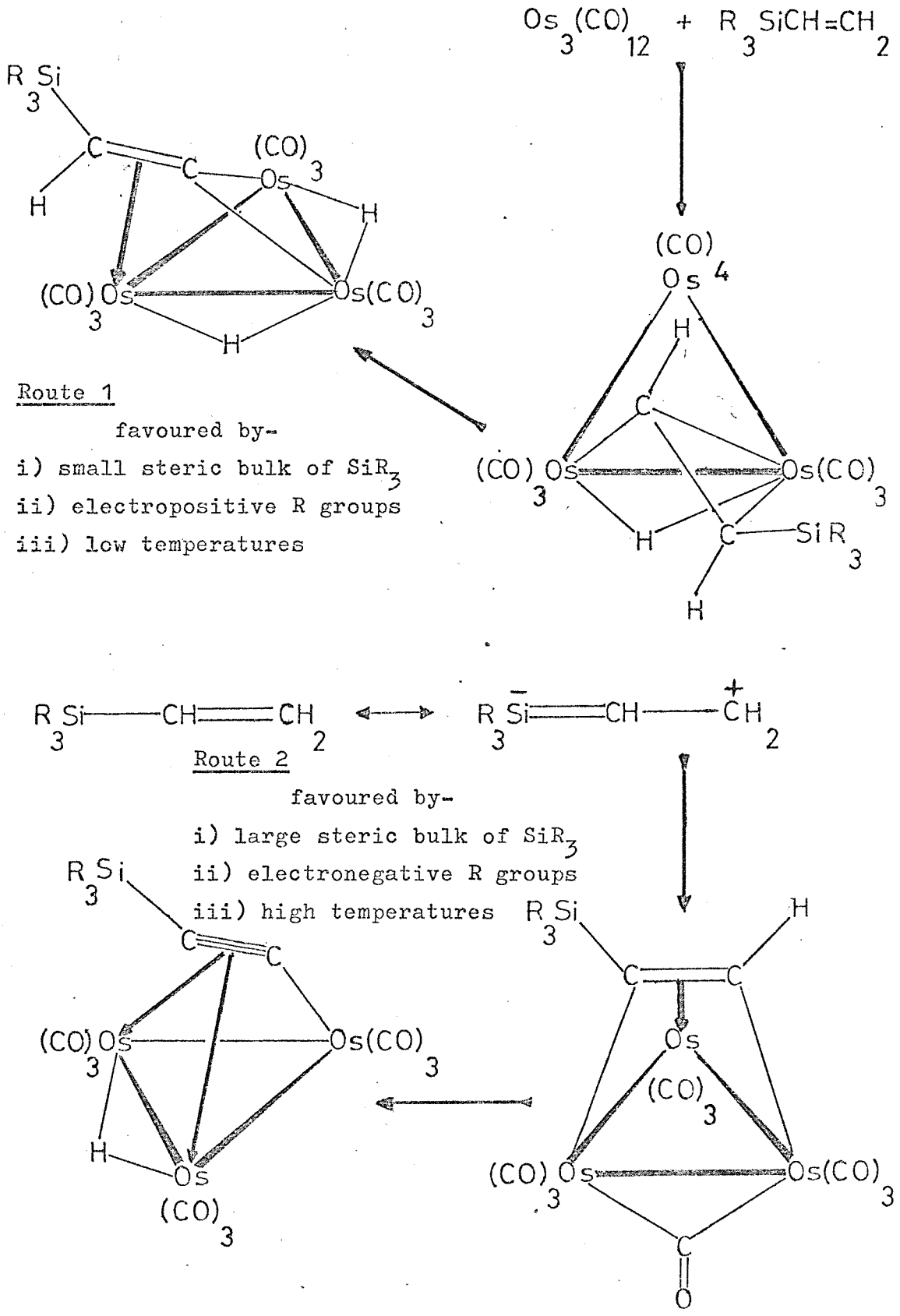
The anomalies in silicon chemistry are reasonably well documented(69). In the absence of any resonance effect the greater

(Pauling) electronegativity of carbon(2.5) versus silicon(1.8) would predict silicon to be an electron-donating centre towards carbon. However, in the present work the ethoxy groups will counteract this +I inductive effect so that it is probably no more pronounced than for a tertiary-butyl group. Hence, any variation in electronic influence will be minimal on the assumed intermediate, III, where no formal unsaturation is present; as shown by the longer than expected C-C bond length for a normal double-bond(70). This leaves the considerable steric bulk to affect the reaction direction. A large group might inhibit any necessary rearrangement to allow formation of the 1,1,-isomer, by decarbonylation and oxidative addition(30), increasing the probability of the competing dehydrogenation route.

If this was the complete answer then the absence of a similar result from other bulky alkenes, i.e. 3,3-dimethyl-but-1-ene, in the literature is surprising. However, if the alternative pathway proceeds via a bimolecular reaction with excess alkene then a possible mechanism for activation of the free alkene towards addition exists. The silicon atom acts to polarise the vinylsilane due to the availability of its d-orbitals to accept the π -electrons. This strong -M mesomeric effect, outweighing the much weaker +I effect, is further enhanced by electron-withdrawing groups on the silicon. Infact the inductive effect of the substituents on the silicon is not a correct measure of its nett electron-attracting power, and a more suitable parameter involves resonance interactions of a d_{π} -p_{π} nature. This occurs when the R-substituent is unsaturated or possesses unshared electron pairs, obviously an ethoxy group falls into this category. One outcome of this effect is the tendancy of trialkylvinylsilanes to undergo anti-Markownikov addition with hydrogen halides(69). Such polarisation within the molecule can be also expected to activate it towards hydrogenation. Previous observations show that it is the metal hydride and the hydrogen geminal to the substituent in III which are lost. These are in reasonably close vicinity on the same side of the cluster. Further, the likely charge distribution at each is in accord with the most favourable approach of the free alkene on both steric and electronic grounds. Then, if an analogy is made to hydrogen adsorption on a catalytic surface, where bond cleavage to give

Diagram 8

Proposed Mechanism for the Reaction of Vinylsilanes with $[Os_3(CO)_{12}]$



activated hydrogen atoms has occurred, cis-hydrogenation of a free vinylsilane can be envisaged; the resulting cluster rearranging to give a type IV complex. Quantitative progression from here to the observed product type has been already firmly established (Diagram 8).

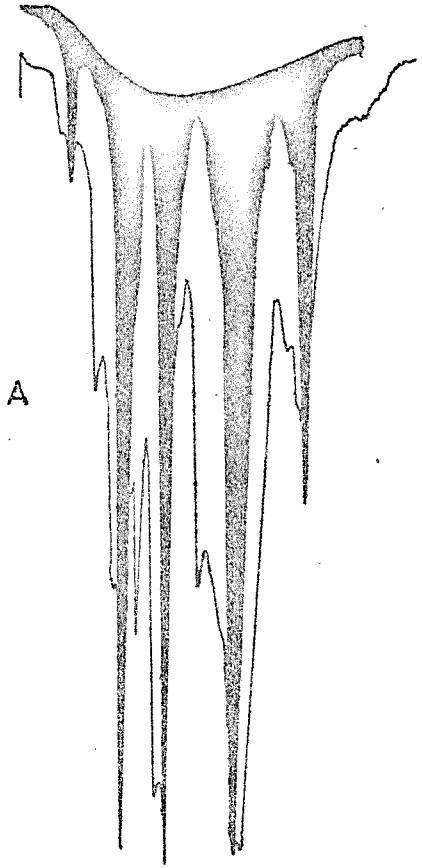
Obviously this represents just one possible mechanism, where even the precise position of decarbonylation is disputable, and many alternatives can be suggested (subsequent dehydrogenation of I is not considered a feasible alternative). However, it does provide an explanation of how the silicon-substituent can govern the direction of reaction; by consideration of its electronic effect, in addition to steric influence, on both the pivot intermediate III and the free alkene. Then subtle variations in reaction conditions, and specifically the R group on the silicon, can be expected to affect the preferred pathway. Indeed, reaction at lower temperatures in refluxing n-heptane for 70 hours gave, after extraction from remaining $[Os_3(CO)_{12}]$, an orange residue. When this was dissolved in cyclohexane the resulting infrared ν_{CO} spectrum contains predominantly VIa, but with additional bands conceivably due to the alternative I/II product. This supports the hypothesis that dehydrogenation is rapid at elevated temperatures, but under milder conditions carbonyl loss and hydrogen transfer to the metal is a competing process. The main problem preventing more detailed mechanistic studies is that, where a mixture of products is formed, the nature of the ethoxy ligands inhibits their separation by conventional chromatography. Two approaches were attempted to overcome this obstacle.

The first involved carrying out the reaction as before, but working up the product by alkylating the Si-OEt bonds insitu before application to a chromatographic plate. As a prequisite the reaction of triethoxyvinylsilane with methyl-lithium was studied. Initially treatment was with a three-fold excess, before quenching with NH_4Cl and extraction of the organic layer. However, distillation did not yield $Me_3SiCH{:}CH_2$, but instead a fraction at 98°C identified as $(EtO)Me_2SiCH{:}CH_2$ from this boiling point(71), a parent ion at m/e=129.72 (2.92%, 70eV), and its ^1H NMR spectrum. Repetition under more forcing conditions, addition at ~20°C followed by reflux in n-pentane for an hour, was marginally more successful with traces of the required product seen. Finally, treatment of the

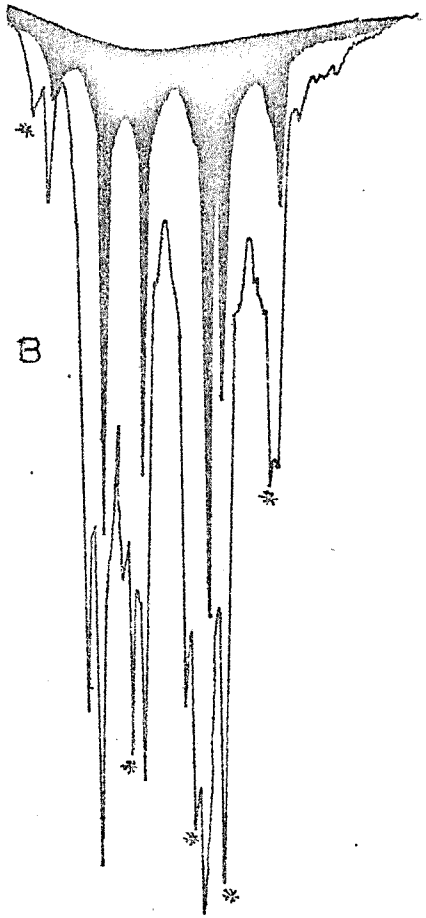
isolated $(EtO)Me_2SiCH{:}CH_2$ with excess methyl-lithium did result in complete methanation as shown by the ^1H NMR spectrum of the crude organic layer. Thus the desired transformation was achieved, but only at reasonably forcing conditions in the presence of a sufficient excess of alkylating agent. The orange solution obtained from reacting $[Os_3(CO)_{12}]$ with three equivalents of $(EtO)_3SiCH{:}CH_2$, under reflux in n-octane overnight, was treated with a five-fold excess of methyl-lithium after first cooling to -20^oC. After quenching, both the organic and aqueous layers were yellow in appearance, whilst a considerable quantity of a brown tar was evident around the reaction vessel. This was partially soluble in methylene chloride but, along with the residue retrieved from the n-octane, gave a broad infrared ν_{CO} spectrum where only bands due to $[Os_3(CO)_{12}]$ were discernible. Possible explanations for this failure include incomplete alkylation leading to subsequent polymerisation on hydrolysis or, more likely with the conditions employed, non-selective attack on the cluster occurs causing loss of integrity. Whatever the precise cause it clearly imposes a severe limitation on this approach.

The second alternative involved replacing the susceptible Si-O linkages by stronger Si-C ($301kJ.mol^{-1}$) bonds. Triphenyl- and triethyl-vinylsilanes were prepared by reacting the appropriate Gringard reagent with trichlorovinylsilane(72). The introduced R groups will both increase the steric bulk of the silicon substituent, but the -M effect will decrease in the order OEt> Ph> Et. Then, variations in reaction should underline the relative importance of each effect. Reaction of $[Os_3(CO)_{12}]$ with either a three-fold excess of $Et_3SiCH{:}CH_2$ or $Ph_3SiCH{:}CH_2$, under reflux in n-octane overnight, gave more complex product distributions than found with $(EtO)_3SiCH{:}CH_2$. Infact the infrared ν_{CO} spectra of the orange residues, after extraction from unreacted starting material and before chromatography, bear a strong resemblance to that obtained with $(EtO)_3SiCH{:}CH_2$ at lower temperatures in n-heptane (Diagram 9). The most intense bands are assigned to a type VI species, whilst the remainder mostly correspond to a type I/II complex (and outstanding $[Os_3(CO)_{12}]$). Direct comparison of the spectra suggests a greater proportion of VI when R=Ph. Chromatography succeeded in separating these products, but the yields were too

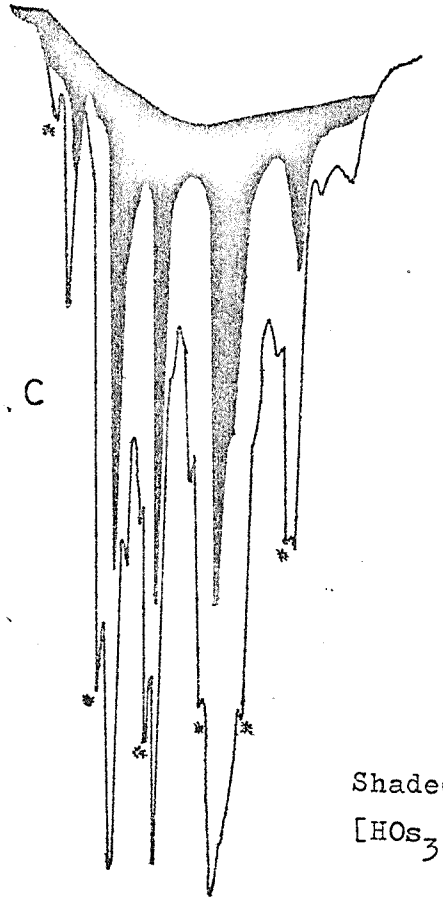
Diagram 9 Infrared (ν_{CO}) Spectra of the Residues from Reaction of $[Os_3(CO)_{12}]$ with Vinylsilanes

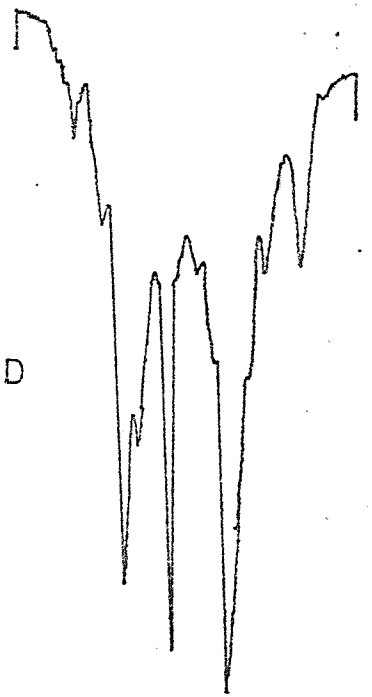


with $(EtO)_3SiCH{:}CH_2$
in n-heptane



with $Et_3SiCH{:}CH_2$
in n-octane





with $Ph_3SiCH{:}CH_2$
C) in n-octane
D) in n-nonane

Shaded inserts-
$[HOs_3(CO)_9(C{:}CSiR_3)]$

*-possible frquencies due to
$[H_2Os_3(CO)_9\{C{:}C(H)SiR_3\}]$

low to provide any meaningful ratios; it also revealed formation of other minor products but these were not fully characterised. When the preparations were repeated at higher temperatures, under reflux in n-nonane, a marked shift towards the mono-hydride is evident, particularly with $Ph_3SiCH{:}CH_2$. When followed by infrared some evidence for intermediate species was seen but it proved impossible to deduce their nature in the absence of isolation. However, the bands due to the observed products emerged together inferring that one was not the precursor of the other. All these trends re-endorse the proposed mechanism with formation of VI favoured by higher temperatures and increased -M effect of the substituent. Steric influence is also important, perhaps in retarding the oxidative addition pathway, but not sufficient alone to control the direction of reaction.

These novel results prompted a short investigation into the reaction of vinylsilanes with $[H_2Os_3(CO)_{10}]$. Initially a sample was stirred with three equivalents of $(EtO)_3SiCH{:}CH_2$, in n-hexane at room temperature for 5 days, but no visible change occurred. Even after heating under reflux for 40 hours the starting material is still the major component. However chromatography did reveal the presence of several products; but the bands tended to be smeared, with most proving difficult to remove, resulting in poor separation. Despite this, one product was partially characterised as $[H_2Os_3(CO)_9\{C{:}C(H)Si(OEt)_3\}]$ from its rough infrared ν_{CO} spectrum and a parent ion, m/e=1014, seen in the mass spectrum. Formation of this dihydride is consistent with the known chemistry of $[H_2Os_3(CO)_{10}]$ with alkenes at this temperature. The infrared spectra of the other products were either broad or very complex which, coupled with the small amounts recovered, prevented more detailed analysis. Some limited mass spectral data was acquired, but this could only be equated with species where (ligand) fragmentation had occurred at some stage.

Another sample heated under reflux in n-octane for 5 hours gave, apart from some $[H_4Os_4(CO)_{12}]$, a considerable quantity of a reasonably mobile compound that was easily removed with methylene chloride from the chromatography plate. This evidence alone suggested that the triethoxysilane moiety was nolonger present. Infrared spectroscopy gave a pattern closely resembling that of

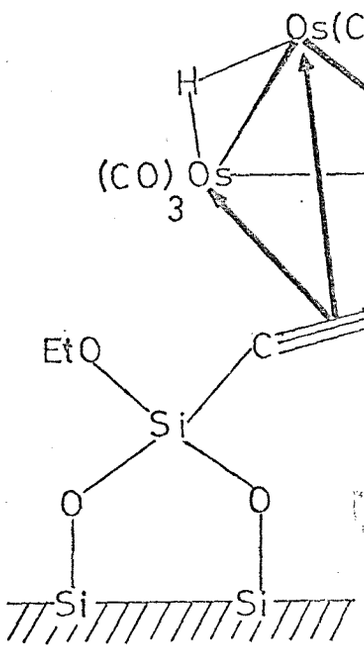
$[H_2Os_3(CO)_9(C:CH_2)]$(26), and this was confirmed by a parent ion, m/e=853, in a very clean mass spectrum. This was a complete surprise and it is difficult to reconcile with the proposed mechanism unless C-Si cleavage occurs prior to generation of the anticipated vinyl complex, IIIa. Selective bond cleavage has been seen for the interaction of alkynes with $[M_3(CO)_{12}]$, but only where no hydrogen is available adjacent to the triple bond. Thus the diols $HOCR_2C{:}CCR_2OH$, R=Me or Ph, react to give $[HM_3(CO)_9(C{:}CCR_2OH)]$(73), whilst $[HRu_3(CO)_9(C{:}CPh)]$ is obtained from $PhC{:}CCO_2H$(49). Experiments with the other two silanes were even less productive as reaction was either too slow or very unselective with considerable decomposition evident.

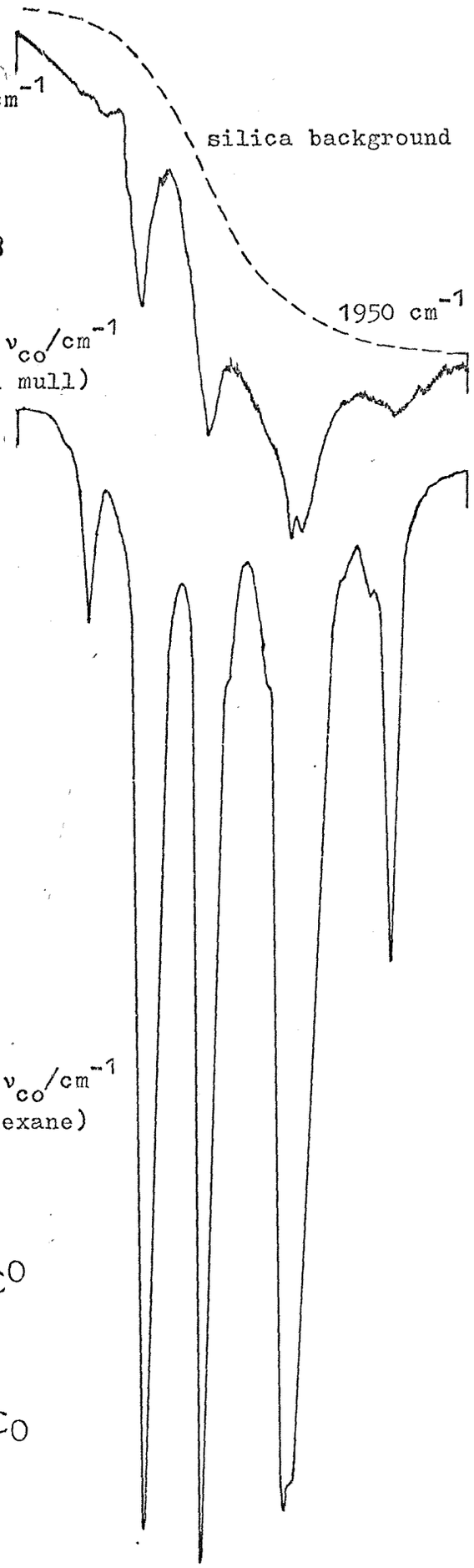
2.6. Preparation of $[HOs_3(CO)_9(C{:}CSIL)]$

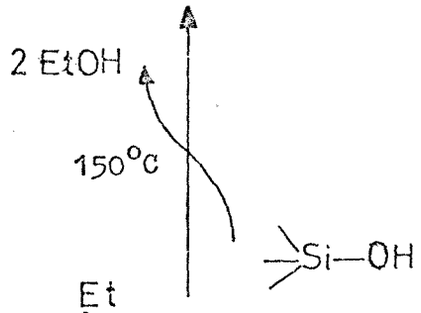
A quantity of VIa was treated with a pre-dried sample of silica in benzene under reflux for 6 hours. The resulting gold-brown solid gave an infrared ν_{CO} spectrum (Nujol mull), shown in Diagram 10, which has a good correlation with that of the unadsorbed species. Notably the weak signal at 2102cm^{-1} was not observed. Also the splitting of the bands at 2022 and 2014 cm^{-1} appears to be much greater in the adsorbed species. This may result from the closer proximity of the cluster to the surface, compared to the phosphine-functionalised silicas, allowing transmission of an oxide electronic effect to the carbonyl ligands. Indeed silica has been already found to exhibit a definite electron-withdrawing effect on $[HOs_3(CO)_{10}(O\text{-}SIL)]$(3). The overall, poor spectral quality is entirely a function of the Sorbisil M60 grade of silica used; throughout the rest of this thesis Aerosil 200 is employed. Their specifications are compared in Table 2. Although the Sorbisil has a superior surface area much of this is involved within the pore structure, and as such the associated silanol groups are inaccessible. Combined with the much larger particle size, the concentration of adsorbed cluster per unit weight will be considerably less than an identically treated sample of Aerosil. This results in reduced transmittance as the particles reflect and scatter the incident radiation, whilst absorbancies due to the background silica (dotted line, Diagram 10) are also significant. The latter results in a

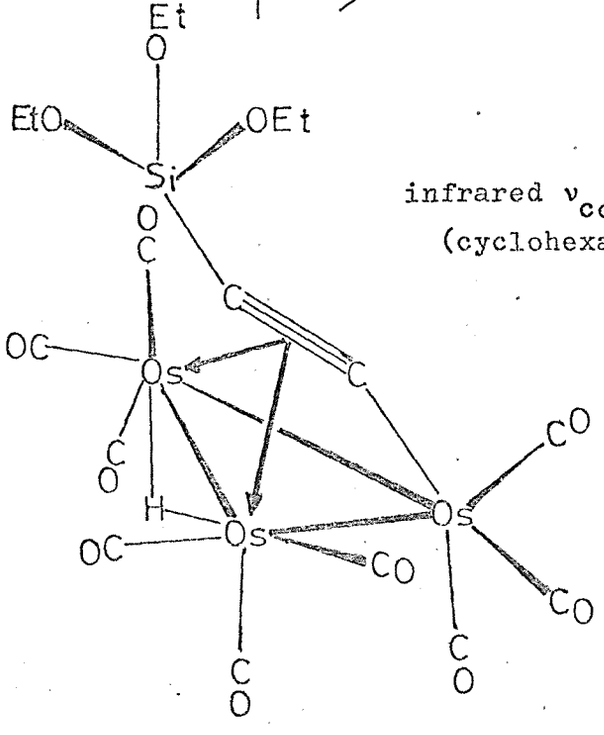
Diagram 10

Preparation of $[HOs_3(CO)_9(C{:}CSIL)]$









infrared ν_{co}/cm^{-1}
(cyclohexane)

Table 2

	Aerosil 200	Sorbisil M60
BET surface area $m^2.g^{-1}$	200	500-650
particle size	ca.12nm	75-100μm
	non-porous	porous

characteristic slope across the carbonyl region. Obviously for a study primarily relying on infrared spectroscopy it is important to achieve the maximum coverage of anchored species to minimize these disadvantages, and this depends on the number of accessible silanol groups, not the total surface area. Fortuitously, this is also the optimum requirement for a catalytic surface so no concessions need be made.

This preparation successfully demonstrates how an adaption of Scheme Two, outlined in Chapter One, can lead to the anchoring of a triosmium cluster through a face-bridging acetylide. It involves characterisation of the preformed cluster derivative before contact with the silica surface, therefore eliminating almost all doubt about the final heterogenised complex, as the mild conditions of attachment are unlikely to alter the cluster integrity. To an extent this compensates for the poor spectral quality. It also ensures the absence of residual free ligand which could affect subsequent activity of the surface.

2.7. Experimental Section

$Et_3SiCHCH_2$

This was prepared according to the method of Eisch and Trainor(72). The Grignard reagent, EtMgBr, was prepared by dropwise addition of EtBr(38.12g, 26.1ml) to a suspension of Mg turnings (9.72g) in Na dried Et_2O(60ml). The solution was refluxed to ensure complete formation of the reagent. Then $Cl_3SiCHCH_2$(15g), dissolved in Et_2O(60ml), was carefully added and the resulting mixture heated under gentle reflux for 72 hours before quenching with aqueous

NH_4Cl solution. The organic layer was separated, reduced in volume, and distilled to give the required product as a clear oil(10g); yield=76%.
b.p.=143-146°C, lit.(72) b.p.=145°C.
m/e=142 (2.9%, 15eV; 1.49%, 60eV).
^{1}H NMR($CDCl_3$, 50°C): 6.28, m, vinyl group; 0.98, complex second order multiplet, $SiEt_3$.

$Ph_3SiCHCH_2$

This was prepared in an analogous manner to the previous compound. The Grignard reagent, from PhBr(34.54g, 23.2ml) and Mg(6.1g), proved slightly more difficult to form and a small crystal of iodine and heat were needed to initiate reaction. THF was used as the solvent, and after addition of $Cl_3SiCHCH_2$(10g) the reaction mixture was heated under reflux for 45 hours, before quenching as above. The extracted organic layer was reduced in volume to give the product as a white waxy solid(15.5g); yield=87%.
m.p.=72°C, lit.(72) m.p.=72°C.
m/e=286 (100%, 15eV; 86.82%, 70eV).
^{1}H NMR($CDCl_3$, 50°C): 7.45, m, $SiPh_3$; 6.28, m, vinyl group.

Reaction of $(EtO)_3SiCHCH_2$ with MeLi

MeLi(17.8ml of a 1.77M Et_2O solution) was added dropwise to a solution of $(EtO)_3SiCHCH_2$(2.22ml) in n-pentane(30ml), cooled to -78°C in an acetone slush bath. This was then allowed to warm to room temperature over 3 hours, before quenching with a saturated NH_4Cl solution. The extracted organic layer was first dried over $MgSO_4$, before carefully distilling off the solvent and transferring the residue to a B10 micro-distillation apparatus. Only one fraction came over and this was identified as $Me_2(EtO)SiCHCH_2$.
b.p.=98°C, lit.(71) b.p.=99°C.
m/e=130 (3.18%, 15eV; 2.92%, 70eV).
^{1}H NMR($CDCl_3$, 50°C): 6.05, m, vinyl group; 3.65, q(J_{HH}=7Hz), $SiOCH_2C$; 1.15, t(J_{HH}=7Hz), $SiOCCH_3$; 0.1, s, $SiCH_3$. A spectrum of the crude product before distillation showed the conversion to be essentially quantitative, there being no evidence for $Me_3SiCHCH_2$.

The recovered $Me_2(EtO)SiCHCH_2$ was reacted with further

MeLi(9ml of 1.77M) at -20°C (CCl_4 slush bath). The solution was heated under reflux for 2 hours prior to quenching. The ^1H NMR($CDCl_3$, 50°C) spectrum of the organic layer showed, in addition to solvent resonances, signals at: 5.9δ, m, 3H; and 0.05δ, s, 9H- consistent with $Me_3SiCHCH_2$.

$[HOs_3(CO)_9\{C:CSi(OEt)_3\}]$

$[Os_3(CO)_{12}]$(0.1957g) was heated under reflux with 2.5 equivalents of $(EtO)_3SiCHCH_2$(0.12ml, 0.1048g) in n-octane(50ml) overnight. After the solvent was removed under reduced pressure, extraction from unreacted $[Os_3(CO)_{12}]$ with cyclohexane(8ml) gave the product as an amorphous orange solid(0.1410g); yield=65% (without accounting for unreacted starting material).
IR ν_{CO}(cyclohexane): 2102.5w, 2077vs, 2054vs, 2020vs, 2016.5ssh, 1983msh, 1981m, cm^{-1}.
^1H NMR($CDCl_3$, 31°C): 3.85δ, q(J_{HH}=7Hz), 3 $SiOC\underline{H}_2C$; 1.28δ, t(J_{HH}=7Hz), 3 $SiOCC\underline{H}_3$; -23.7δ, s, Os-H-Os.
m/e=1012.

The preparation was repeated, but using n-heptane as the solvent, and heating under reflux for 70 hours. The recovered residue was extracted with a small amount of CH_2Cl_2 to leave the bulk of unreacted $[Os_3(CO)_{12}]$ behind. Before an unsuccessful attempt to separate the various species by chromatography the bulk product was taken up in cyclohexane to give an infrared ν_{CO} spectrum: 2107vw, 2100w, 2089w-m, 2080m, 2076vs, 2067m-s, 2057s, 2054vs, 2035m, 2021vs, 2017vs, 1990w-m, 1984m, 1980m, cm^{-1} (plus several shoulders, see Diagram 9).

Reaction of $[Os_3(CO)_{12}]$ with $Ph_3SiCHCH_2$ and $Et_3SiCHCH_2$

The conditions used were similar to those described in the previous preparation. $[Os_3(CO)_{12}]$(0.2g) was heated overnight under reflux in n-octane(50ml) with 3 equivalents of the appropriate vinylsilane, $Ph_3SiCHCH_2$(0.19g) or $Et_3SiCHCH_2$(0.12ml). The solvent was then removed under reduced pressure and the brown residue extracted with CH_2Cl_2(4ml). The crude products gave the following infrared ν_{CO} spectra (cyclohexane):-
a) with $Et_3SiCHCH_2$: 2106w, 2099w, 2084s, 2075vs, 2062.5m-s, 2057s,

2052s, 2031m-s, 2024s, 2020vs, 2011s-vs, 1983m, 1981m, cm^{-1}.
b) with $Ph_3SiCHCH_2$: 2107vw, 2100w, 2081s, 2076vs, 2069m, 2062m, 2057s, 2053vs, 2035w-m, 2028s, 2021vs, 2017vssh, 2009s, 1983m, 1981m, cm^{-1}. (see Diagram 9).

Chromatography was carried out using n-hexane as eluant. Several bands, all of which were easily removed with CH_2Cl_2, appeared but only the following ones were identified.
a) with $Et_3SiCHCH_2$:

i) R_f=0.8, yellow needles, $[HOs_3(CO)_9(C:CSiEt_3)]$.
IR ν_{CO}(cyclohexane): 2099vw, 2073s, 2052s, 2020vs, 2010m-s, 1983vwsh, 1980w, cm^{-1}.
^1H NMR($CDCl_3$, 31°C): -23.58, s, Os-H-Os; SiEt resonances obscured by impurities.
b) with $Ph_3SiCHCH_2$:

i) R_f=0.5, yellow solid, $[H_2Os_3(CO)_9\{C:C(H)SiPh_3\}]$.
IR ν_{CO}(cyclohexane): 2108w, 2081vs, 2067s, 2056vs, 2035s, 2022vs, 2008s, 2000m, 1983m, cm^{-1}.
^1H NMR($CDCl_3$, 31°C): 7.58, m, $SiPh_3$; -18.18, s, and -20.58, s, 2 Os-H-Os; CH probably obscured by phenyl signal.

ii) R_f=0.15, orange solid, $[HOs_3(CO)_9(C:CSiPh_3)]$.
IR ν_{CO}(cyclohexane): 2100.5w, 2076vs, 2053vs, 2021vs, 2017ssh, 1983wsh, 1980w-m, cm^{-1}.
^1H NMR($CDCl_3$, 31°C): 7.68, m, $SiPh_3$; -23.58, s, Os-H-Os.

Both preparations were repeated at the higher temperature of reflux in n-nonane. The crude products from each showed a shift towards the mono-hydride species, that from $Ph_3SiCHCH_2$ gave an infrared ν_{CO} spectrum (cyclohexane): 2100vw, 2081w, 2076vs, 2068m-s, 2053vs, 2034w, 2028m, 2021vs, 2008m, 2000w, 1983wsh, 1980w, cm^{-1}.

Reaction of $[H_2Os_3(CO)_{10}]$ with $(EtO)_3SiCHCH_2$

a) $[H_2Os_3(CO)_{10}]$(0.1g) was heated under reflux with 3 equivalents of $(EtO)_3SiCHCH_2$(0.075ml) in n-hexane for 40 hours. The residue, after removal of the solvent, was chromatographed with n-hexane as eluant to give a series of bands of which the following were identified.

i) R_f=0.64, purple crystals, unreacted $[H_2Os_3(CO)_{10}]$.

ii) R_f=0.3, orange solid, $[H_2Os_3(CO)_9\ C:C(H)Si(OEt)_3]$.
IR ν_{CO}(cyclohexane): 2106m, 2080vs, 2058ssh, 2056vs, 2025vs, 2013vs, 1987m, 1982w-m, 1979w-m, cm^{-1}.
m/e=1014 (probe inserted 215°C).

b) $[H_2Os_3(CO)_{10}]$(0.1g) and $(EtO)_3SiCHCH_2$(0.075ml) were refluxed in n-octane for 5 hours. After the solvent had been removed, the brown residue was chromatographed with n-hexane/Et_2O (4:1 v/v). Just one band moved up the plate which was easily removed with CH_2Cl_2 and identified as $[H_2Os_3(CO)_9(C:CH_2)]$.
IR ν_{CO}(cyclohexane): 2109vw, 2079vs, 2059vs, 2052ssh, 2031s, 2025vs, 2018s, 2010s, 1992m, 1985m-s, cm^{-1}.
m/e=852 (probe not inserted).

$[HOs_3(CO)_9(C:CSIL)]$

A sample of Sorbisil M60 brand of silica(0.23g), predried in vacuo at 127°C for 40 hours, was added to a benzene solution of $[HOs_3(CO)_9\{C:CSi(OEt)_3\}]$(0.14g), which was then stirred vigorously under reflux for 6 hours. The resulting gold-brown silica was filtered off and soxhlet extracted overnight with fresh solvent. The product, after drying under vacuum, gave an infrared ν_{CO} spectrum consistent with formation of the required surface species, $[HOs_3(CO)_9(C:CSIL)]$.
IR ν_{CO}(Nujol mull): 2078s, 2054s, 2022s, 2014s, 1983.5m.

2.8. References

1. K.G.Allum, R.D.Hancock, I.V.Howell, S.McKenzie, R.C.Pitkethly and P.J.Robinson, J. Organometallic Chem., 1975, 87, 203.
2. T.Castrillo, H.Knozinger and M.Wolf, Inorg. Chim. Acta, 1980 45, L235.
3. J.Evans and B.P.Gracey, J.C.S. Dalton, 1982, 1123.
4. J.Evans and B.P.Gracey, J.C.S. Chem. Comm., 1980, 852.
5. J.Evans and B.P.Gracey, J. Organometallic Chem., 1982, 228, C4.
6. R.D.Adams and N.M.Golembeski, J. Amer. Chem. Soc., 1979, 101, 2579.
7. D.Seyferth, C.N.Rudie and M.O.Nestle, J. Organometallic Chem., 1979, 178, 227.
8. S.L.Cook and J.Evans, J.C.S. Chem. Comm., 1983, 713.

9. a) A.A.Arduini, A.A.Bahsoun, J.A.Osborn and C.Voelker, Angew. Chem. Int. Ed. Engl., 1980, 19, 1024.
b) A.A.Bahsoun, J.A.Osborn, C.Voelker, J.J.Bonnet and G.Lavigne, Organometallics, 1982, 1, 1114.
10. D.F.Foster, B.S.Nicholls and A.K.Smith, J. Orgaometallic Chem., 1983, 244, 159.
11. J.J.DeBoer, J.A.van Doorn and C.Masters, J.C.S. Chem. Comm., 1978, 1005.
12. C.Masters and J.A.van Doorn, U.K. pat.no.1,573,422, 1980.
13. R.Whyman, J.C.S. Dalton, 1972, 1375.
14. M.M.Harding, B.S.Nicholls and A.K.Smith, J. Organometallic Chem., 1982, 226, C17.
15. J.A.Osborn and G.G.Stanley, Angew. Chem. Int. Ed. Engl., 1980, 19, 1025.
16. W.Kruppa and G.Schmid, J. Organometallic Chem., 1980, 202, 379.
17. D.F.Foster, J.Harrison, B.S.Nicholls and A.K.Smith, J. Organometallic Chem., 1983, 248, C29.
18. A.J.Deeming, S.Hasso, M.Underhill, A.J.Canty, B.F.G.Johnson, W.G.Jackson, J.Lewis and T.W.Matheson, J.C.S. Chem. Comm., 1974, 807.
19. J.Evans and G.S.McNulty, J.C.S. Dalton, 1981, 2017.
20. a) M.I.Bruce, M.A.Cairns and M.Green, J.C.S. Dalton, 1972, 1293.
b) A.Cox and P.Woodward, J. Chem. Soc. (A), 1971, 3599.
21. A.W.Parkins, E.O.Fischer, G.Huttner and D.Regler, Angew. Chem. Int. Ed. Engl., 1970, 9, 633.
22. G.Gervasio, D.Osella and M.Valle, Inorg. Chem., 1976, 15, 1221.
23. M.Evans, M.Hursthouse, E.W.Randall, E.Rosenberg, L.Milone and M.Valle, J.C.S. Chem. Comm., 1972, 545.
24. M.Castiglione, L.Milone, D.Osella, G.A.Vaglio and M.Valle, Inorg. Chem., 1976, 15, 394.
25. P.F.Jackson, B.F.G.Johnson, J.Lewis, P.R.Raithby, G.J.Will, M.McPartlin and W.J.H.Nelson, J.C.S. Chem. Comm., 1980, 1190.
26. A.J.Deeming and M.Underhill, J.C.S. Dalton, 1974, 1415.
27. R.Jackson, B.F.G.Johnson, J.Lewis, P.R.Raithby and S.W.Sankey, J. Organometallic Chem., 1980, 193, C1.
28. W.G.Jackson, B.F.G.Johnson and J.Lewis, J. Organometallic Chem., 1977, 139, 125.
29. A.J.Canty, A.J.Domingos, B.F.G.Johnson and J.Lewis, J.C.S.

Dalton, 1973, 2056.

30. A.J.Deeming, S.Hasso and M.Underhill, J.C.S. Dalton, 1975, 1614.

31. W.G.Jackson, B.F.G.Johnson, J.W.Kelland, J.Lewis and K.T.Schorpp, J. Organometallic Chem., 1975, 87, C27.

32. S.Aime and A.J.Deeming, J.C.S. Dalton, 1981, 828.

33. C.G.Pierpont, Inorg. Chem., 1977, 16, 636.

34. W.G.Jackson, B.F.G.Johnson, J.W.Kelland, J.Lewis and K.T.Schorpp, J. Organometallic Chem., 1975, 88, C17.

35. O.Gambino, R.P.Ferrari, M.Chinone and G.H.Vaglio, Inorg. Chim. Acta, 1975, 12, 155.

36. G.Ferraris and G.Gervasio, J.C.S. Dalton, 1974, 1813.

37. O.Gambino, G.A.Vaglio, R.P.Ferrari and G.Centini, J. Organometallic Chem., 1971, 30, 381.

38. a) R.PFerrari, G.A.Vaglio, O.Gambino, M.Valle and G.Centini, J.C.S. Dalton, 1972, 1998.

b) G.Ferraris and G.Gervasio, J.C.S. Dalton, 1972, 1057.

39. G.Ferraris and G.Gervasio, J.C.S. Dalton, 1973, 1933.

40. G.A.Vaglio, O.Gambino, R.P.Ferrari and G.Centini, Inorg. Chim. Acta, 1973, 7, 193.

41. M.Laing, P.Sommerville, Z.Dawoodi, M.J.Mays and P.J.Wheatley, J.C.S. Chem. Comm., 1978, 1035.

42. A.J.Deeming, S.Hasso and M.Underhill, Proc. Int. Conf. Coord. Chem. XVth, Dublin, 1974, 4, 35.

43. a) K.A.Azam and A.J.Deeming, J.C.S. Chem. Comm., 1977, 472.

b) K.A.Azam and A.J.Deeming, J. Mol. Cat., 1977, 3, 207.

44. R.P.Ferrari and G.A.Vaglio, Gazz. Chim. Ital., 1975, 105, 939.

45. S.Aime, G.Gervasio, L.Milone, E.Sappa and M.Franchini-Angela, Inorg. Chim. Acta, 1978, 27, 145.

46. S.Aime, O.Gambino, L.Milone, E.Sappa and E.Rosenberg, Inorg. Chim. Acta, 1975, 15, 53.

47. A.Mayr, Y.C.Lin, N.M.Boag and H.D.Kaesz, Inorg. Chem., 1982, 21, 1704.

48. a) C.R.Eady, B.F.G.Johnson, J.Lewis and M.C.Malatesta, J.C.S. Dalton, 1978, 1358.

b) B.F.G.Johnson, J.Lewis, P.R.Raithby and G.Suss, J.C.S. Dalton, 1979, 1356.

49. E.Sappa, O.Gambino, L.Milone and G.Centini, J. Organometallic Chem., 1972, 39, 169.

50. M.Catti, G.Gervasio and S.A.Mason, J.C.S. Dalton, 1977, 2260.
51. S.Aime, D.Osella, A.J.Deeming, A.M.Manotti Lanfredi and A.Tiripicchio, J. Organometallic Chem., 1983, 244, C47.
52. A.J.Carty, S.A.MacLaughlin and N.J.Taylor, J. Organometallic Chem., 1981, 204, C27.
53. R.Fahmy, K.King, E.Rosenberg, A.Tiripicchio and M.Tiripicchio Camellini, J. Amer. Chem. Soc., 1980, 102, 3626.
54. P.Braunstein, G.Predieri, A.Tiripicchio and E.Sappa, Inorg. Chim. Acta, 1982, 63, 113.
55. S.Aime, G.Gervasio, L.Milone, E.Sappa and M.Franchini-Angela, Inorg. Chim. Acta, 1978, 27, 145.
56. S.Aime, G.Gervasio, L.Milone, E.Sappa and M.Franchini-Angela, Inorg. Chim. Acta, 1978, 26, 223.
57. G.Gervasio, E.Sappa, A.M.Manotti Lanfredi and A.Tiripicchio, Inorg. Chim. Acta, 1983, 68, 171.
59. E.Sappa, A.M.Manotti Lanfredi and A.Tiripicchio, Communication to the XIII Convegno Nazionale di Chimica Inorganica, September 23rd 1980, Camerino, Italy.
58. E.Sappa, A.M.Manotti Lanfredi and A.Tiripicchio, Inorg. Chim. Acta, 1979, 36, 197.
60. S.Aime, L.Milone, E.Sappa, A.Tiripicchio and M.Tiripicchio Camellini, Inorg. Chim. Acta, 1979, 32, 163.
61. C.Barner-Thorsen, K.I.Hardcastle, E.Rosenberg, J.Siegel, A.M.Manotti Lanfredi, A.Tiripicchio and M.Tiripicchio Camellini, Inorg. Chem., 1981, 20, 4306.
62. C.Barner-Thorsen, E.Rosenberg, G.Saatjian, S.Aime, L.Milone and D.Osella, Inorg. Chem., 1981, 20, 1592.
63. S.A.MacLaughlin, J.P.Johnson, N.J.Taylor, A.J.Carty and E.Sappa, Organometallics, 1983, 2, 352.
64. K.Henrick, M.McPartlin, A.J.Deeming, S.Hasso and P.Manning, J.C.S. Dalton, 1982, 899.
65. G.Granozzi, E.Tondello, R.Bertoncello, S.Aime and D.Osella, Inorg. Chem., 1983, 22, 744.
66. M.Castiglioni, G.Gervasio and E.Sappa, Inorg. Chim. Acta, 1981, 49, 217.
67. C.Jangala, E.Rosenberg, D.Skinner, S.Aime, L.Milone and E.Sappa, Inorg. Chem., 1980, 19, 1571.
68. R.M.Laine, Annals New York Academy of Sciences, 1980, 333, 124.

69. C.Eaborn, "Organosilicon Compounds", Butterworths Publications Ltd., 1976.

70. A.G.Orpen, A.V.Rivera, E.G.Bryan, D.Pippard, G.M.Sheldrick and K.D.Rouse, J.C.S. Chem. Comm., 1978, 723.

71. M.Cohen and J.R.Ladd, J. Amer. Chem. Soc., 1953, 75, 988.

72. J.J.Eisch and J.T.Trainor, J. Org. Chem., 1963, 28, 487.

73. a) S.Aime, L.Milone and A.J.Deeming, J.C.S. Chem. Comm., 1980, 1168.

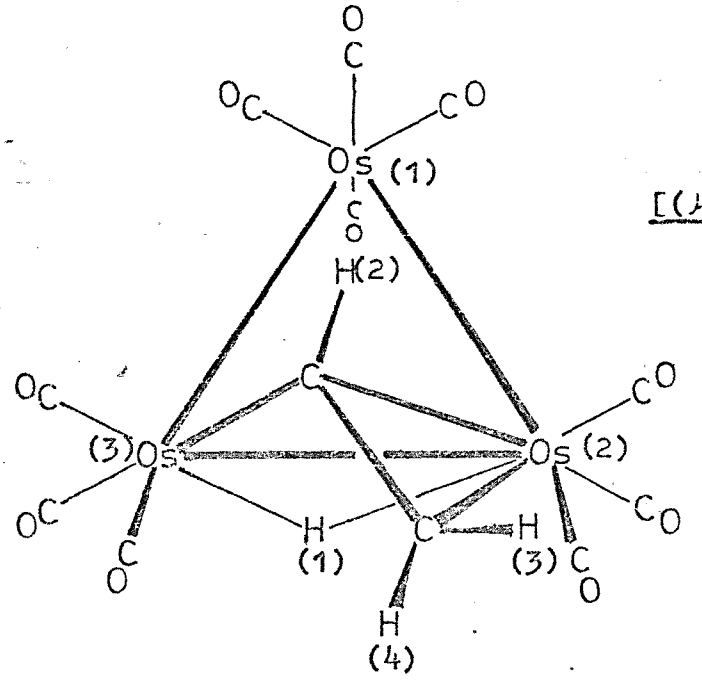
b) S.Aime, A.J.Deeming, M.B.Hursthouse and J.D.J.Backer-Dirks, J.C.S. Dalton, 1982, 1625.

CHAPTER THREE.

REACTIONS OF $[H_2Os_3(CO)_9(PR_3)]$, PR_3= PPh_3, PPh_2Et or $P(OMe)_3$, WITH NUCLEOPHILES

3.1. Reaction of $[H_2Os_3(CO)_{10}]$ with simple Alkenes and Alkynes

When acetylene is passed through a solution of $[H_2Os_3(CO)_{10}]$ at room temperature a smooth conversion to $[(\mu\text{-}H)Os_3(CO)_{10}(\mu\text{-}CHCH_2)]$, I, is observed in quantitative yield (1): a similar result is obtained under a small ethylene pressure(2). This species has been fully characterised, and a combined X-ray and neutron diffraction study(3) elucidated the solid state structure locating all atoms including the hydrogens. The vinyl

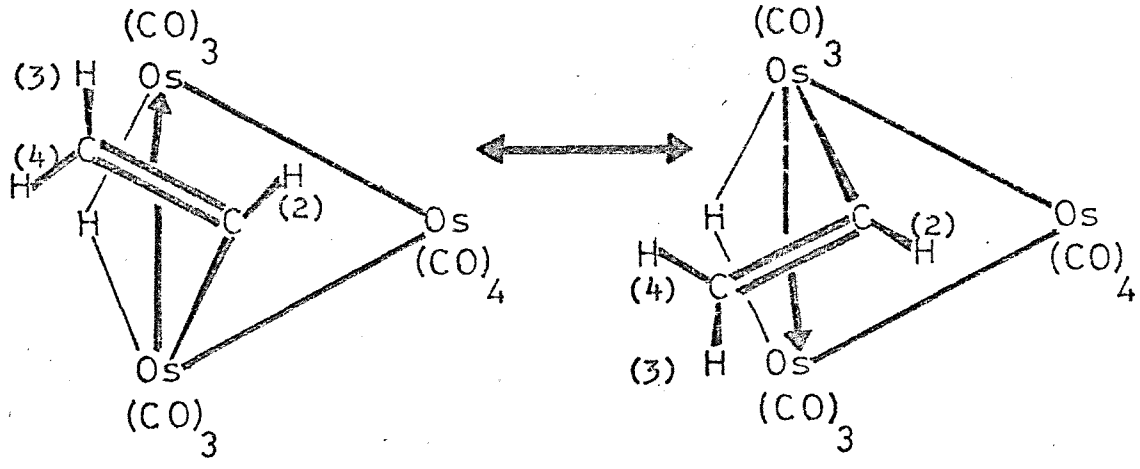


Structure of $[(\mu\text{-}H)Os_3(CO)_{10}(\mu\text{-}CHCH_2)]$

ligand and the hydride bridge the same edge of the Os_3 triangle. Noticeably the Os-H-Os bridge is significantly asymmetrical, a longer bond existing to Os(3) σ-bonded by the vinyl group. This is presumably an electronic effect reflecting the weak π-vinyl interaction to Os(2). The vinyl group and σ-bonded Os(3) are essentially coplanar, the largest deviations being shown by H(2) and H(3) which bend away from Os(2) slightly. Similar structures have been also observed for the 3,3-dimethyl-but-1-enyl(4) and but-1-enyl(5) derivatives, but with the introduced alkyl group substituted for H(3) directed away from the molecule. With substituted 1-alkynes an additional product of stoichiometry

$[Os_3(CO)_{10}(CHCR)]$ is obtained containing a bridging carbonyl but no hydride. This is believed to result from reaction of I with excess alkyne(1). Internal alkynes, RC≡CR', give a whole variety of products, including ones associated with cluster breakdown, whose distribution is very sensitive to the nature of R and R'(6).

In solution I has been shown to have a dynamic structure(7). This results from the σ and π bonds binding the bridging vinylic group rapidly interchanging between the bridged osmium atoms. It creates a pseudo-mirror plane bisecting this Os-Os bond. This process occurs in such a manner that it cannot be identified by ^1H NMR study. However ^{13}C NMR does show equivalence of three pairs of carbonyl groups on these two osmiums,



Fluxional process occurring in $[HOs_3(CO)_{10}(CHCH_2)]$

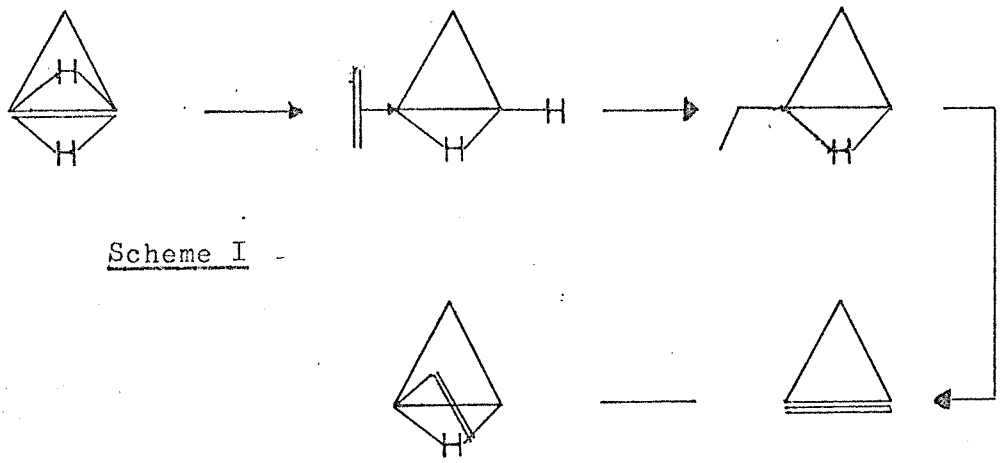
which is only removed on 'freezing out' the dynamic process at -67°C when the true asymmetry of the molecule is revealed.

Reaction with acetylene probably occurs by direct addition facilitated by the inherent unsaturation present in $[H_2Os_3(CO)_{10}]$, addition across the formal Os-Os double bond possibly preceding insertion into the Os-H bond(1). With alkenes the situation is clearly more complicated and several mechanistic schemes have been proposed to accommodate the reaction (Diagram 1). There are several principle steps common to all three depicted mechanisms. In each case the first stage is alkene addition to the double bond followed by insertion into a M-H bond giving a σ-coordinated alkyl species. Then, although the order varies

Diagram 1

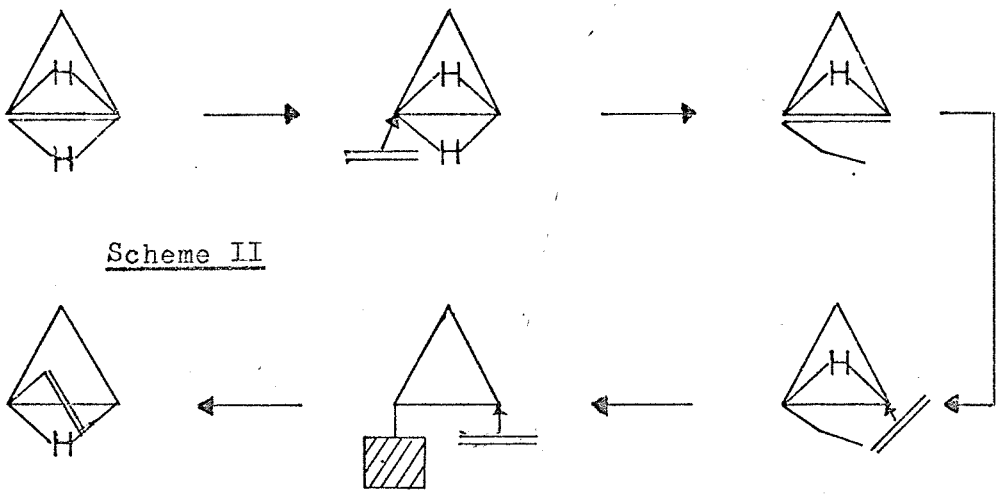
Proposed Mechanisms for the Reaction of Ethylene with $[H_2Os_3(CO)_{10}]$

Shapley et. al.(8)



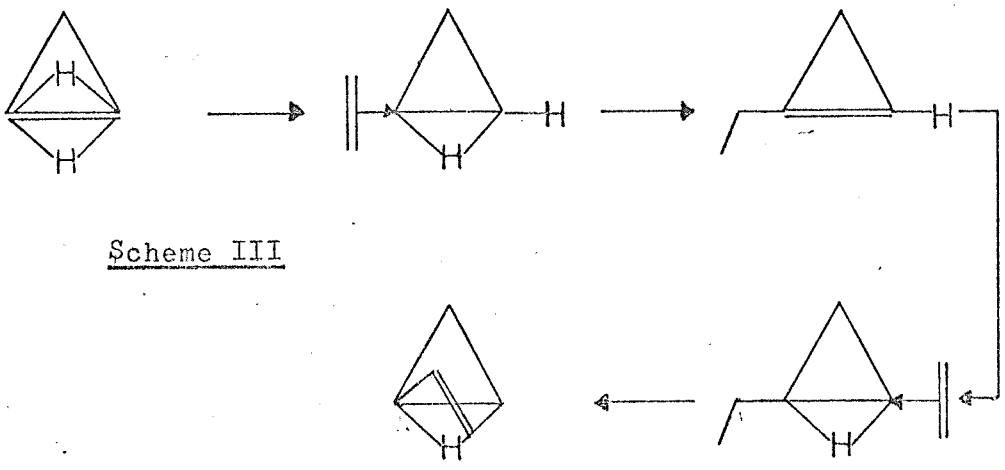
Scheme I

Johnson et. al.(9)



Scheme II

Deeming et. al.(10)

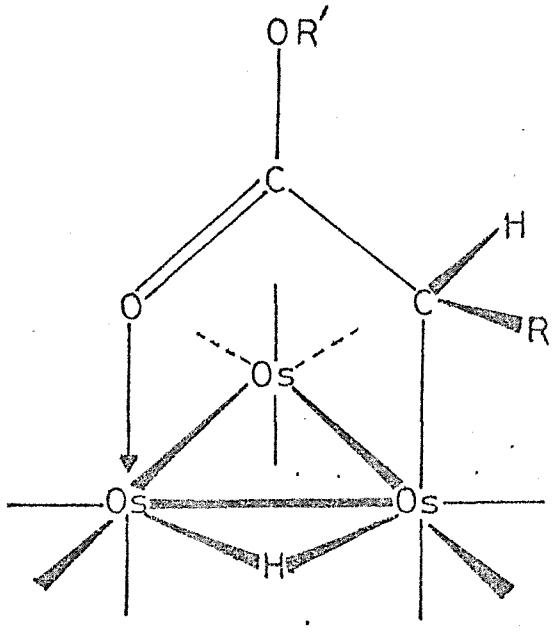


Scheme III

slightly between schemes, activation of the Os-Os bond occurs, by the generation of a degree of 'unsaturation', so that a second ethylene can coordinate. Loss of ethane and metallation of the remaining ethylene then yields I.

Some evidence to support these stages has been compiled. When the reaction was carried out in a sealed vessel ethane was observed in approximately equimolar proportion to the product. This supports the requirement for two molecules of ethylene to take part in the reaction. Use of $[D_2Os_3(CO)_{10}]$ gave I without any incorporation of deuterium. This was taken to signify that the hydrogen originally present in $[H_2Os_3(CO)_{10}]$ is transferred to a molecule of ethylene prior to C-H bond cleavage of the second incoming ethylene(2).

A further investigation into the reactions of substituted terminal alkenes revealed the formation of related products, but the rate being quite sensitive to steric and electronic effects, any effect polarising the alkene positively at the 1-position promoting more rapid reaction. By use of diethyl fumarate it was possible to isolate the hydridoalkyl intermediate $[HOs_3(CO)_{10}(CH(CH_2CO_2Et)CO_2Et)]$, II. Related species were also obtained from maleic anhydride, ethyl acrylate and ethyl diazoacetate(8). Their stability arises from coordination of the organic carbonyl creating a relatively unstrained 5-membered ring.



Proposed structure of
$[HOs_3(CO)_{10}(CH(R)CO_2R')]$

$R=CH_2CO_2Et$, $R'=Et$;
or
$R=CH_2CO=R'$;
or
$R=CH_3$, $R'=Et$.

Addition of terminal alkenes to II provided the corresponding $[HOs_3(CO)_{10}(alkenyl)]$ cluster in high yield, even those inaccessible from the alkene itself; i.e. styrene. Under hydrogen II decomposed to give just $[H_2Os_3(CO)_{10}]$ and diethyl succinate. Solutions alone decomposed to the alkene and uncharacterised osmium containing products. All these observations indicate that II is representative of the σ-coordinated alkyl intermediates formed after alkene insertion into the M-H bond. Their ease of decomposition, even with unfavourable alkenes, suggests the rate limiting step occurs during or prior to their formation.

The observation that decomposition in the presence of hydrogen regenerates $[H_2Os_3(CO)_{10}]$ with effective hydrogenation of the alkene exposed the possibility of the reaction being catalytic. Indeed, a n-octane solution containing a 100:1 mixture of 1-hexene and $[H_2Os_3(CO)_{10}]$, under hydrogen(50psig) at 50°C, resulted in 31 equivalents of n-hexane and 69 equivalents of internal hexenes. Essentially all the catalyst was recovered at the end of the reaction(8). The high degree of isomerisation indicates the reversibility of the alkene coordination and insertion steps, whereas build-up of internal alkenes is consistent with the observed failure of $[H_2Os_3(CO)_{10}]$ to hydrogenate internal alkenes. In the absence of hydrogen catalytic isomerisation of 1-hexene is still seen(10), although slow deactivation of the catalyst was observed by a colour change from purple to yellow. A series of functionalised alkenes similarly underwent isomerisation. Another study(11) using $[1,2\text{-}D_2]$-1-pentene, in toluene solutions at 70.4°C, also showed isomerisation, but accompanied by intramolecular rearrangement of hydrogen and deuterium. In addition, when the reaction was terminated, the catalyst appeared to be partially deuterated. With trans-$[D_2]$-ethylene a similar redistribution of hydrogen isotopes took place. Apart from confirming the presence of a σ-alkyl intermediate this result also illustrates that it is in equilibrium with $[H_2Os_3(CO)_{10}]$, and that the formation of ethane and I is slower than exchange of ethylene. The stoichiometric requirement for two moles of ethylene is thus an over simplification. Deuterium loss from $[D_2Os_3(CO)_{10}]$(2) could be accommodated by statistical redistribution within a vast ethylene excess as a result of the reversible alkene coordination and insertion steps.

Clearly the structural similarities(12,13) between $[H_2Os_3(CO)_{10}]$ and its mono-substituted derivative $[H_2Os_3(CO)_9(PPh_2Et)]$ implies that the latter, at least in theory, should also be capable of catalysing alkene hydrogenation and isomerisation by a related pathway. The silica supported analogue of this species, $[H_2Os_3(CO)_9(PPh_2CH_2CH_2SIL)]$, has also been prepared so an investigation was undertaken into their reactions with alkenes and hydrogen. For convenience ethylene was chosen as the alkene to be used. Prior to studying any possible ethylene hydrogenation by the supported species the reactions of the homogeneous variant with ethylene (and hydrogen) was investigated so that possible catalyst deactivation products could be separated and identified. Then use of infrared subtraction and difference techniques might also facilitate their identification on the surface.

3.2. Reaction of $[H_2Os_3(CO)_9(PPh_2Et)]$ with Acetylene

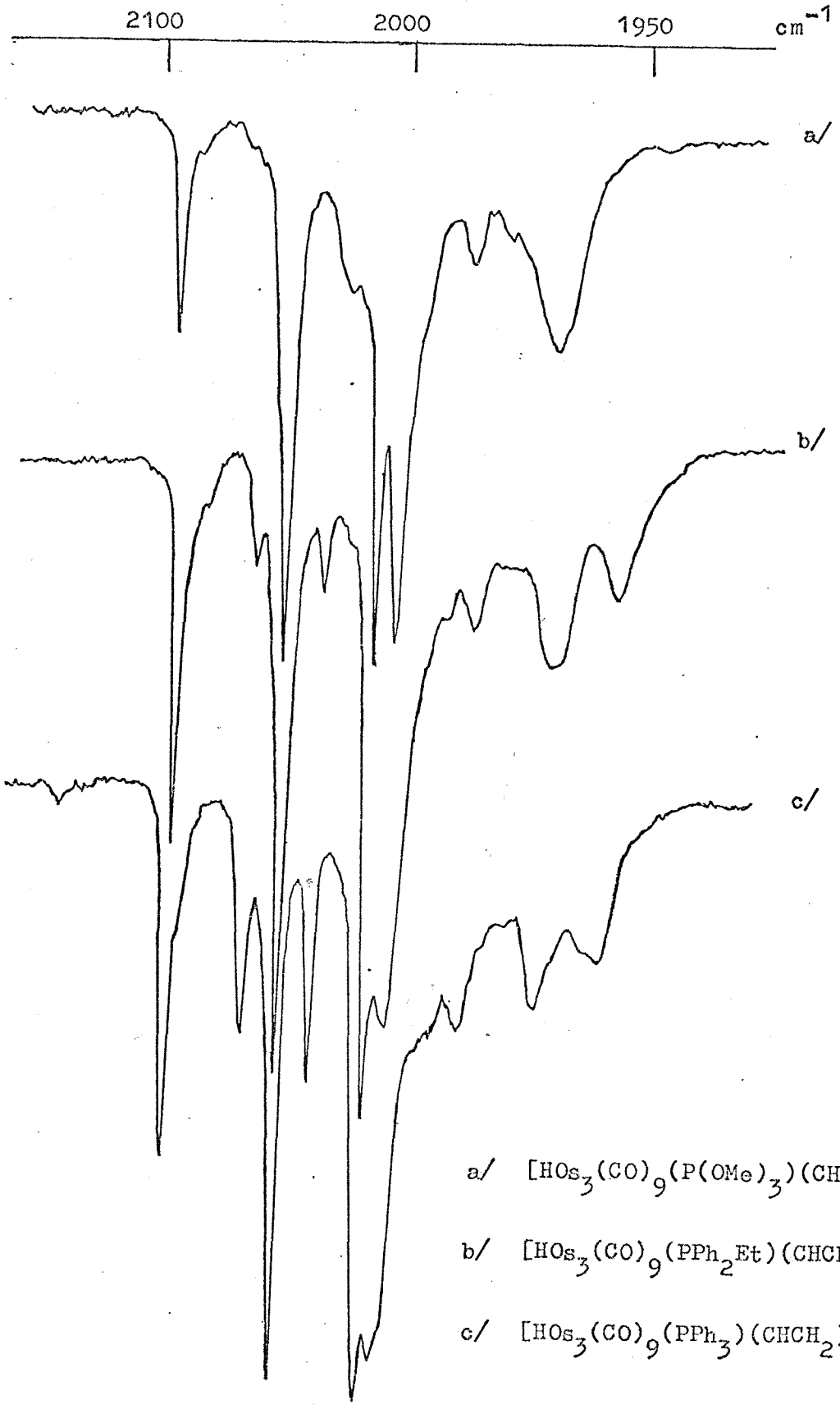
3.2.1. Preparation and Characterisation of $[HOs_3(CO)_9(PPh_2Et)(CHCH_2)]$

On passing acetylene through a n-hexane solution of $[H_2Os_3(CO)_9(PPh_2Et)]$ for several hours it becomes a deep yellow colour. Chromatography of the residue gave just one band, with hardly any baseline, so the reaction is essentially quantitative. From spectroscopy, and its subsequent reactions, this orange compound was identified as $[HOs_3(CO)_9(PPh_2Et)(CHCH_2)]$, IIIa. Its infrared ν_{CO} spectrum contains only bands associated with terminal carbonyl vibrations. Within the mass spectrum a parent ion m/e= 1066, contained in a characteristic Os_3 isotope pattern, is observed. However, operating at 70eV this parent ion is relatively weak and decreases rapidly with increased source temperature. The strongest signal corresponds to the $[M-CO]^+$ ion. Elemental analysis also supports the proposed stoichiometry.

The ^1H NMR spectrum ($CDCl_3$, 31°C) revealed two separate doublets in the hydride region with differing coupling constants to the phosphorus. These occur at -19.20(J_{PH}=6Hz) and -19.42(J_{PH}= 11.5Hz) δ in approximately a 4:1 ratio. Their chemical shifts, which are similar to that for the hydride (-19.376) in I(1,2), imply that both are edge-bridging, whilst the presence of ^{31}P-

Diagram 2

Infrared (ν_{CO}) Spectra for $[HOs_3(CO)_9P(CHCH_2)]$



a/ $[HOs_3(CO)_9(P(OMe)_3)(CHCH_2)]$

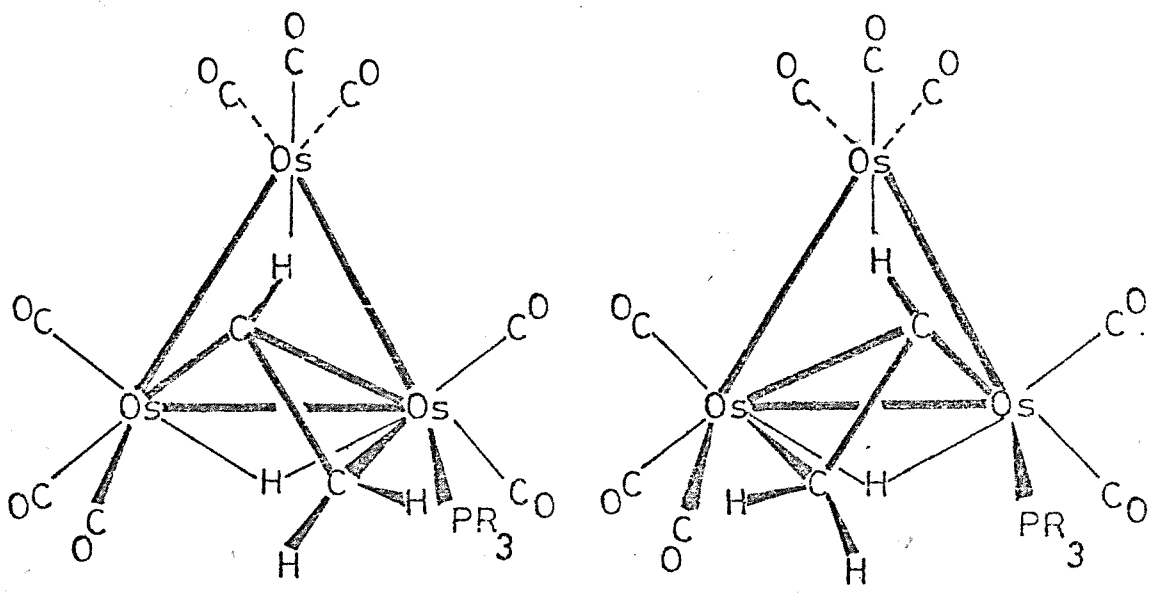
b/ $[HOs_3(CO)_9(PPh_2Et)(CHCH_2)]$

c/ $[HOs_3(CO)_9(PPh_3)(CHCH_2)]$

Table 1 Spectroscopic Data for $[HOs_3(CO)_9L(CHCH_2)]$

Compound	IR ν_{CO}/cm^{-1} cyclohexane	^1H NMR ($CDCl_3$, 31°C) δ/ppm	Assignment	J/Hz	Mass spectrum m/e (Os_3=572)
$L=PPh_2Et$	2091m	7.5 m	P-phenyl		
	2059w	2.74 q	$P-CH_2-C$	J_{HH} 7.5	1066
	2046s	1.01 dt	$P-C-CH_3$	J_{PH} 18	
	2031w	2.44ddd	H_A	J_{AP} ca13	
	2011vs	4.14 d	H_B	J_{BC} 9	
	2003s	7.76 m	H_C	J_{AC} ca13	
	1985w	-19.20 d	H_D	J_{DP} 5.9	
	1969w	obscured	H_a		
	1967w	5.34 d	H_b	J_{bc} 10.5	
	1954w	not resolved	H_c		
		-19.42 d	H_d	J_{dP} 11.7	
$L=P(OMe)_3$	2092.5m	3.74 d	$P-O-CH_3$	J_{PH} 13	976
	2051msh	2.83 dd	H_A	J_{AP} 13	
	2047vs	4.34 d	H_B	J_{BC} 10	
	2023wsh	7.5 m	H_C+H_c?	J_{AC} 13	
	2018wsh	-19.92 d	H_D	J_{DP} 6	
	2011vs	3.10 d	H_a	J_{ac} 15	
	2002s	4.81 d	H_b	J_{bc} 10	
	1987w	-20.03 d	H_d	J_{dP} 10	
	1980w				
	1968.5mbr				
$L=PPh_3$	2091m				1114
	2060w				
	2046vs				
	2032.5mw	see Table 2			
	2011vs				
	2005vs				
	2001ssh	1970w			
	1992wbr	1959vwsh			
	1986w	1956w			

couplings suggests bonding to an edge containing the phosphine-bearing osmium. The preparation was repeated several times and the observed ratio always remained essentially constant. Integration against the resonances due to the phosphine ligand indicated that combined they represent a single hydride, inconsequence they are assigned to different isomers of IIIa. The phosphine destroys the enantiomorphic nature of the two possible spatial arrangements of the vinylic product so that different isomers result; one with the vinyl group π-bonded to the phosphinated osmium, IIIa', the other with it σ-bonded, IIIa".



IIIa' IIIa"

Two possible isomers of $[HOs_3(CO)_9(PPh_2Et)(CHCH_2)]$

Variable temperature studies down to -60°C showed no alteration in the hydride spectrum. Above ambient temperature, using d_8-toluene as solvent, some evidence for line broadening and coalescence was observed. However at 95°C this was not definitive, illustrating that any exchange between the two isomers is slow compared to the NMR time-scale. The presence of the phosphine has substantially raised the activation barrier to interchange of the vinyl bonding mode between the bridged metal atoms. The analogous process in I(7) is not 'frozen out' until -67°C, coalescence occurring at about -50°C. Interestingly at 95°C two emerged doublets centred at -17.46δ and -20.87δ with equal intensities are seen at the expense of the original signals. These were

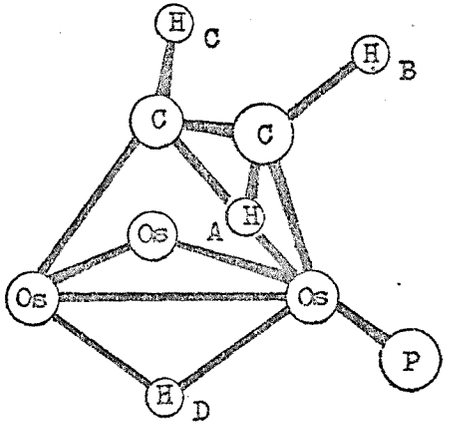
subsequently attributed to the pyrolysis product $[H_2Os_3(CO)_8(PPh_2Et)(CCH_2)]$, IV. Significantly the equilibrium between IIIa' and IIIa" appeared to be maintained during and after this thermolysis.

In the 0-10δ region of the spectrum the expected resonances due to the phosphine ligand are seen. In addition, a series of resonances associated with the coordinated vinyl groups are present. Unfortunately the very existence of the phosphine conceals some of the features. However it is obvious that for each enviroment a pair of signals occur as would be anticipated for two isomers. In particular, a set of doublets centred at 4.14 and 5.34 δ are observed with an intensity ratio parallel to that found for the hydrides. In an attempt to alleviate this masking problem the corresponding $P(OMe)_3$, IIIb, and PPh_3, IIIc, adducts were prepared in an analogous fashion. The rate of formation of the latter, as monitored by infrared sampling, from $[H_2Os_3(CO)_9(PPh_3)]$ and acetylene was appreciably slower taking about 32 hours. Despite this there was still no indication of any intermediate species with significant lifetimes.

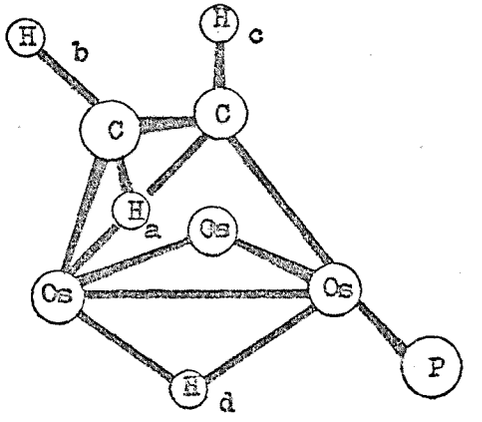
For IIIc it was apparent from the hydride resonances alone that a more even distribution of the two isomers existed. The four expected independent methylene signals were all seen, as were the two methine resonances, although that attributed to the major isomer was partially obscured by the phenyl rings' signal. The distribution of chemical shifts was similar enough to that found in I (Table 2) for them to be adequately assigned in an analogous manner. This was further born out by specific proton-proton double irradiation experiments (Diagram 3) although, unfortunately, the lack of resolution, in part associated with the presence of the phosphine, prevented definite identification of some of the smaller geminal and hydride couplings. However, the larger cis- and trans- splittings were all discernible and, in particular, a large phosphorus-coupling (J_{PH}=13Hz) to H_A but only in the case of the major isomer. For such a methylene hydrogen this implies that the major isomer has the vinylic moiety π-bonded to the phosphine-bearing osmium, akin to IIIa', if the coupling is of the 'conventional' through-bond type (i.e. a $^3J_{PH}$ coupling as opposed to an anticipated smaller $^4J_{PH}$ value). Clearly this is the sterically less favoured isomer and the relative abundance

Table 2 ^{1}H NMR Data for $[HOs_3(CO)_9L(CHCH_2)]$, L=CO or PPh_3

Compound	Resonance δ (ppm)	Assignment	Coupling constants (Hz)
$[HOs_3(CO)_{10}(CHCH_2)]$			
($CDCl_3$, 33°C)	3.43	H_A	J_{AB} 2.8, J_{AC} 14.7, J_{AD} 0.8
	5.00	H_B	J_{AB} 2.8, J_{BC} 9.6, J_{BD} 2.0
	7.59	H_C	J_{AC} 14.7, J_{BC} 9.6, J_{CD} 1.6
	-19.36	H_D	J_{AD} 0.8, J_{BD} 2.0, J_{CD} 1.6
$[HOs_3(CO)_9(PPh_3)(CHCH_2)]$			
($CDCl_3$, 31°C)	7.45	P-phenyl	
Major isomer	2.32	H_A	J_{AB} 2.0, J_{AC} 14.0, J_{AP} 13.0
	4.37	H_B	J_{AB} 2.0, J_{BC} 9.5, J_{BD} 2.0?
	7.89	H_C	J_{AC} 14.0, J_{BC} 9.5, J_{CD} 2.0, J_{CP} 2.0
	-18.87	H_D	J_{BD} 2.0?, J_{CD} 2.0, J_{DP} 7.0
Minor isomer	2.50	H_a	J_{ab} 1.5, J_{ac} 14.5
	5.30	H_b	J_{ab} 1.5, J_{bc} 10.5
	8.95	H_c	J_{ac} 14.5, J_{bc} 10.5, J_{cd} 1.5?
	-19.02	H_d	J_{cd} 1.5?, J_{dP} 12.0



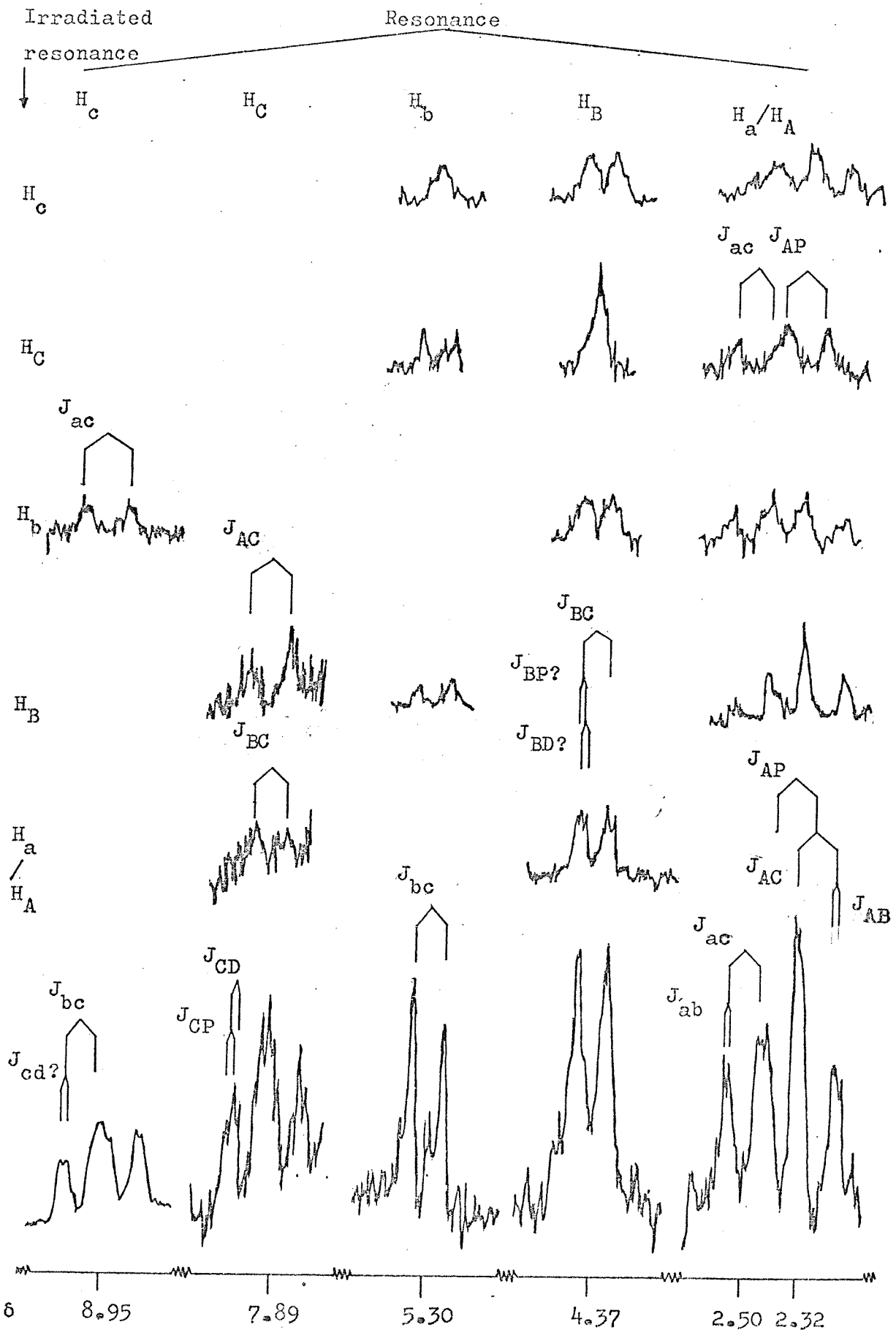
major isomer



minor isomer

Diagram 3

Spin Decoupled Spectra for $[HOs_3(CO)_9(PPh_3)(CHCH_2)]$



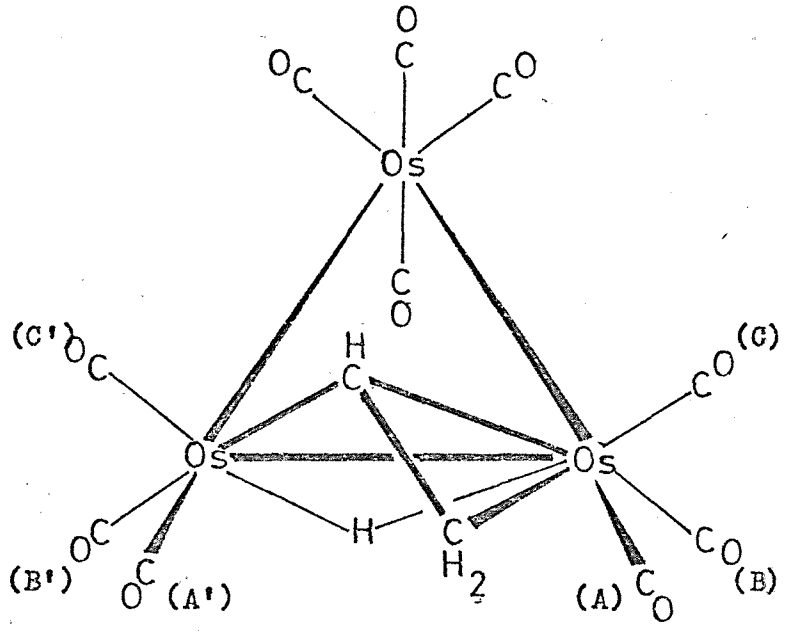
of the other configuration might well be expected to be greatest with the bulkier PPh_3 ligand present. The absence of ^{31}P-couplings to the vinyl protons, the size of $J(H_dP)$, and the unusual chemical shift of the methine, H_c, proton suggests that the phosphine is cis- to both the vinyl and hydride ligands in the minor isomer i.e. IIIa". Comparable spectral features were also seen for IIIb, but with H_c and H_c apparently overlapping, and a larger isomer ratio towards the preferred form, only limited information could be extracted.

3.2.2. Full ^{13}C NMR Study on $[HOs_3(CO)_9(PR_3)(CHCH_2)]$

A $^{13}C-\{^1H\}$ NMR spectrum ($CDCl_3$, 31°C) was recorded for a sample of IIIa prepared from ^{13}CO enriched $[H_2Os_3(CO)_9(PPh_2Et)]$. Because of the known isomer ratio the observed features can be largely attributed to the major form; the minor isomer contributing only a number of weak signals and shoulders. In all nine separate resonances were seen: a, 186.99; b, 185.81; c, 183.66; d, 181.08; e, 175.88; f, 175.27; g, 174.41; h, 173.39 and i, 167.75 δ, assuming that b is coupled to the ^{31}P nucleus ($^2J_{PH}$=6.2Hz). This is consistent with the total lack of molecular symmetry. From 31 down to -70°C all the resonances were entirely temperature independent exemplifying the rigid nature of the two configurations as indicated by the ^1H NMR study. On removing the ^1H-decoupler no resolved splittings were discernible, but loss of relative intensity, accompanied by increased half-widths, for several signals indicated the presence of small couplings ($J_{CH}\leq$2Hz).

Clearly in the absence of any fluxional process, and with only a few possible spin-spin interactions, it is difficult to unequivocally allocate all the resonances. However, by analogy with the effect of phosphine substitution upon the ^{13}C NMR spectrum of $[H_2Os_3(CO)_{10}]$, and using various assumptions previously applied elsewhere(14,15), certain tentative assignments can be made by comparison with the published spectra for I by Shapley and coworkers (7). Unfortunately, for the low temperature limiting spectrum they did not individually apportion the six carbonyls flanking the edge bridged by the hydride and the vinyl group which eventually lead to the three coalesced pairs. In the related molecules

$[HOs_3(CO)_{10}(COR)]$, R=Me or Et, where equivalence results from flipping of the alkyl group, the resonances were assigned according to the magnitude of the difference in chemical shift within the pairs(14). Similar reasoning allows the highest field pair (172.6 and 165.6 δ) for I to be attributed to the carbonyls $CO_C/CO_{C'}$ (see below), this is also in agreement with the observed ^1H-coupling (J_{CH}=12Hz) to the averaged signal consistent with a trans-arrangement to the hydride. The smallest difference (173.9 and 172.2 δ) would be expected for $CO_B/CO_{B'}$ leaving the remaining pair (179.7 and 176.6 δ) assigned to $CO_A/CO_{A'}$. Within each set it can be adequately assumed that the higher field signal corresponds to



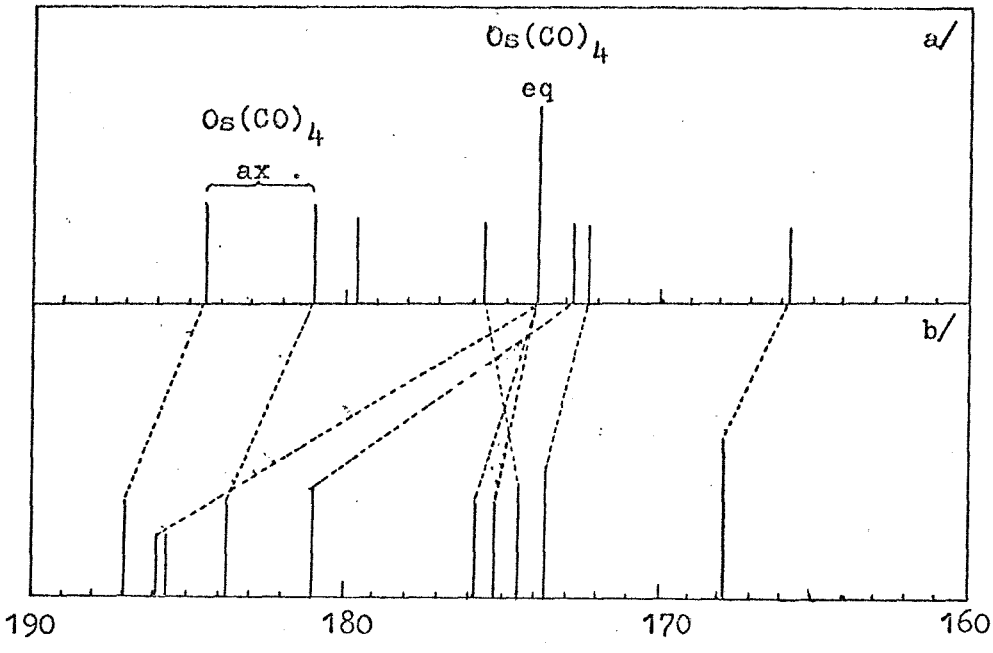
Proposed individual assignments for the bridgehead carbonyls in $[HOs_3(CO)_{10}(CHCH_2)]$

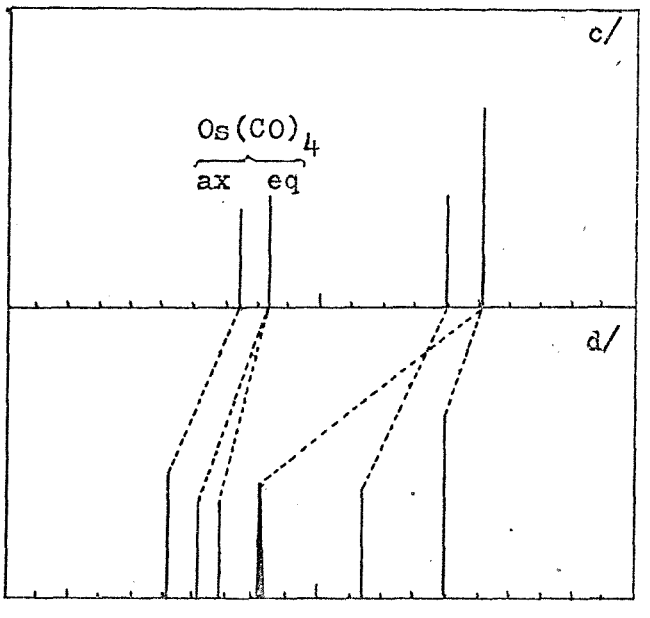
a carbonyl on the more electron deficient osmium. From simple electron-counting this would be anticipated as the metal centre σ-bonded to the vinylic group, and this is re-endorsed by the Os-CO bond lengths in the derived molecular structure of I(3).

Phosphine substitution on $[H_2Os_3(CO)_{10}]$ results in a general downward shift for all the carbonyl enviroments of ca. 1-2ppm with the exception of those sharing the same centre as the introduced ligand where the shift was more marked, approximately 7ppm. Comparison of the spectra of I and IIIa indicates that the same relationships are apparently maintained. This is most obvious for the enviroments on the $Os(CO)_4$ group (Diagram 4). Thus the signals a,c can be assigned to the axial carbonyls of this group, and e,f to the equatorial ones. As would be expected the presence

Diagram 4

$^{13}C-\{^{1}H\}$ NMR Spectrum of $[HOs_3(CO)_9(PPh_2Et)(CHCH_2)]$





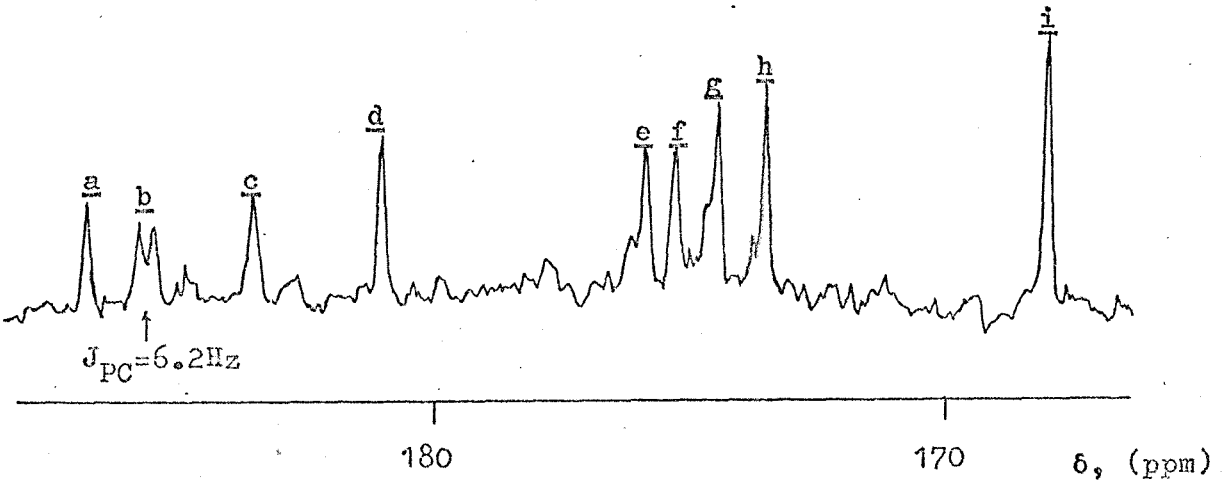
Limiting $^{13}C-\{^{1}H\}$ NMR spectra of:-

a/ $[HOs_3(CO)_{10}(CHCH_2)]$, (6)

b/ $[HOs_3(CO)_9(PPh_2Et)(CHCH_2)]$

c/ $[H_2Os_3(CO)_{10}]$

d/ $[H_2Os_3(CO)_9(PPh_2Et)]$



of the phosphine has lifted the coincidental isochronous nature of the latter pair. The magnitude of this effect being similar to that seen for $[H_2Os_3(CO)_9(PPh_2Et)]$. Further support for these assignments comes from the comparable signal intensities within each set compatible with related enviroments where Overhauser enhancement should be similar. Also symptomatic is the narrow half-widths possessed by all these resonances, and especially the equatorial pair, which were unaltered on removal of the ^{1}H-decoupler.

The remaining resonances must all arise from the ligands coordinated on the two osmiums constituting the bridged edge. Of these, the isolated high field signal i must, by analogy, correspond to CO_C, in I; the trans- carbonyl relative to the hydride on the formally electron deficient osmium. The continued existence of this enviroment further consolidates the proposed arrangement of the major isomer. Although upon ^{1}H-coupling the large interaction seen in I was not reproduced i did show, along with d, the most pronounced signal broadening observed across the spectrum. On this basis, and accompanied by its marked paramagnetic shift (ca. 8.5ppm) relative to CO_C in I, d is attributed to the analogous carbonyl on the phosphine-bonded osmium. This leaves just the pseudo-axial position on this metal unassigned, but this can be conveniently accommodated by resonance b which possesses a resolved ^{31}P coupling (6.2Hz). For an equatorial phosphine such interactions have been already shown to be larger with the axial, as opposed to equatorial, carbonyls in the related $[Os_3(CO)_{11}P]$ system(16). Again its large shift relative to the corresponding signal for I (+11.9ppm) confirms this assignment. From its small downward shift h most likely results from the similar site at the other metal centre. The final undesignated resonance g can, by default, be allocated to the remaining equatorial carbonyl on the osmium σ-bonded to the vinyl group. Its slightly higher field position compared to CO_A, is the only deviation from the anticipated trends upon introducing the phosphine into the system. Of course CO_A for I has no comparison in IIIa' because the phosphine occupies its coordination site. Overall, within the proposed assumptions, the observed ^{13}CO NMR spectrum can be adequately explained in terms of IIIa' being the major isomer; the only discrepancy being that noted above.

A natural abundance $^{13}C-\{^{1}H\}$ NMR spectrum for IIIc revealed two pairs of signals at 29.6, 64.6 and 56.5, 100.0 δ which could be attributed to the vinylic carbon atoms. With IIIa only two resonances at 27.0 and 62.2 δ were apparent (although there was evidence for a third weaker signal at 98.5δ) so the higher field pair in IIIc can be immediately correlated with the major isomer. Apart from these, the expected multiplet centred at ca. 130δ for the phenyl rings and a doublet (J_{PC}=62Hz) at 28.48δ, and a possible singlet below 10δ, are seen consistent with the observed resonances for the phosphine ligand in $[Os_3(CO)_{11}(PPh_2Et)]$ (Chapter One). Independent studies(17) on I identified two resonances at 68.7 and 101.3 δ which were assigned to the methylene and methine carbons respectively on the basis of observed ^{1}H-couplings. There is obviously a strong resemblance between these signal positions and those for the minor isomer of IIIc. However, there is a considerable perturbation to higher field for the major isomer which would be consistent with a shift from sp^2 to sp^3 hybridisation about the carbons, synonymous with a decrease in the olefinic bond-order. This observation can be conveniently rationalised by the Chatt-Dewar MO description of alkene-metal bonding. Coordination to a metal centre of greater electron density, as caused by the presence of a strong σ-donor such as a phosphine, would result in a larger back-donation from filled metal orbitals of suitable symmetry into the lowest-lying π-antibonding orbitals of the vinylic group. This has the synergic effect of increasing overlap of the olefinic π-electron density with a σ-type acceptor orbital on the metal atom. Both of these phenomena result in decreasing the C-C bond-order, lengthening the bond, and hence introducing a greater degree of sp^3 characteristics. Such an interaction is also promoted by electron-withdrawing substituents on the alkene and this could clearly encompass a strong metal-olefin σ-bond to the second, formally electron deficient, osmium. This bonding description is analogous to that invoked for M-CO systems and the effect of phosphine substitution on $[H_2Os_3(CO)_{10}]$ has already been shown, from the X-ray analysis of $[H_2Os_3(CO)_9(PPh_3)]$(13), to decrease the C-O bond-order of the carbonyls bound to the same osmium by increasing back-donation from the metal.

The authenticity of the highest field signal at ca. 28δ in both spectra has been questioned(18). If it is dismissed as an impurity, then the resonances at 64.6 and 100.0 δ are reallocated to the methylene and methine carbons, respectively, for the major isomer of IIIc(19). The companion methine resonance to that at 56.5δ, attributed to the minor isomer, is not observed either because of inherent weakness through various Overhauser and relaxation effects, expected coupling to the phosphorus makes it difficult to spot in the natural abundance spectrum, or it is hidden beneath the solvent peaks between 78-76 δ. Then the similarity in chemical shifts for the resonances for IIIc' and I erases the need for the above arguements based on electronic perturbations.

3.2.3. Summary

Since this work was carried out others(20) have prepared the corresponding PEt_3 adduct, which apparently shows an even greater tendancy towards the major configuration. Further, they have successfully separated the two forms by chromatography and proven them to be isomeric from their identical mass spectra. Notably their reported infrared ν_{CO} spectrum (cyclohexane) for the favoured isomer (2090ms, 2044s, 2008s, 2000s, 1981w, 1974w, 1962ms and 1946 cm^{-1}) bears a strong resemblance to that of IIIb where the same predominance was found. This is consistent with the increased nucleophilicity of an alkyl phosphine, coupled with its smaller cone angle(21), which would result in the greater preference for the vinyl group to be π-bonded to the common centre to facilitate more efficient electron withdrawal.

It can be concluded that phosphine substitution does not drastically alter the reaction of the 'unsaturated' metal-metal bond with acetylene. However, its presence does cause the existence of two isomers which do not readily interconvert on the NMR timescale and can be even separated by chromatography. In general, the major form has the vinyl group π-bonded to the phosphine-bearing osmium, and this can be rationalised on electronic grounds. The proportion of the minor isomer only increases with falling nucleophilicity, and greater steric bulk, of

the phosphine substituent. From subsequent studies with ethylene it was deduced that the absolute ratio of the isomers was dependent on their relative stabilities, and not a result of kinetic control during the reaction.

3.3. Reaction of $[H_2Os_3(CO)_9(PR_3)]$ with Ethylene

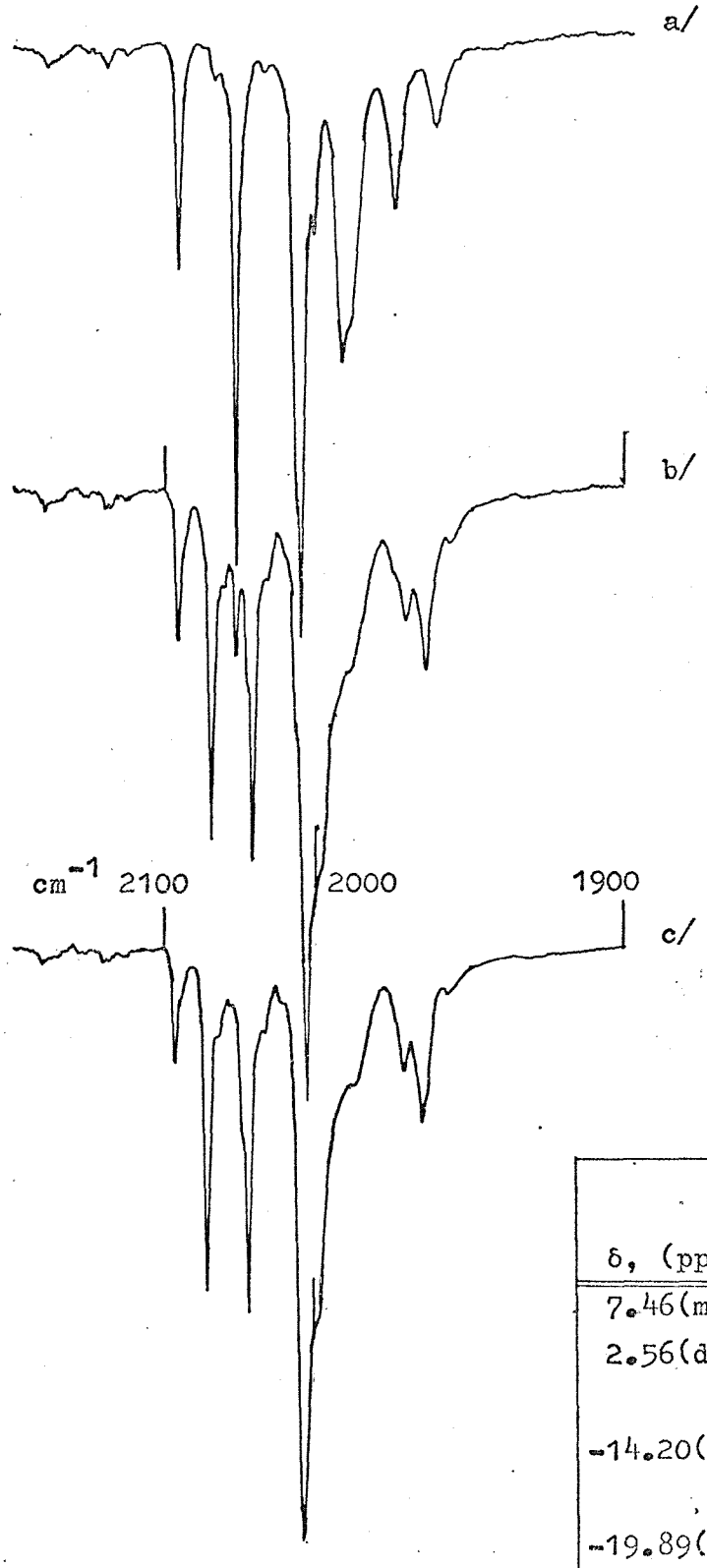
3.3.1. Preparation and Characterisation of $[H_2Os_3(CO)_9(PR_3)(C_2H_4)]$

Intrinsic to the proposed catalytic cycle is the assumption that deactivation results from ethylene producing III, as does acetylene, from $[H_2Os_3(CO)_9(PR_3)]$. Since alkyne insertion occurred under similar conditions to that experienced with $[H_2Os_3(CO)_{10}]$, an n-hexane solution of $[H_2Os_3(CO)_9(PPh_2Et)]$ was stirred at room temperature under a working ethylene pressure of 3 atmospheres overnight in anticipation of forming IIIa. Upon workup the resulting yellow solution gave a broad band on a t.l.c. plate, with essentially no baseline, whose infrared ν_{CO} spectrum indicated it to be a mixture of IIIa, as a minor constituent, and at least one other component; significantly no frequencies related to the starting material were visible. A difference spectrum computed between that of the product and an authentic sample of IIIa, based on the common peak at 2091cm^{-1}, was reasonably simple indicative of a single species. A sample submitted for ^{1}H NMR spectroscopy gave all the expected signals for IIIa, plus a singlet (-14.31δ) and a doublet (-20.33δ, J_{PH}=11.2Hz) in the hydride region. In addition, although it was partially obscured by the phosphine methylene signal, a strong doublet at 2.50δ (J_{PH}=7Hz) is consistent with a coordinated ethylene moiety, from its relative intensity and comparison with literature examples i.e. $[HOs_3(CO)_9(C_2H_4)(SMe)]$, 2.49δ(22). The characteristic doublet for $[H_2Os_3(CO)_9(PPh_2Et)]$ was also observed, and its abundance was found to increase with moderate heating or pumping under vacuum.

In an attempt to avoid the separation problems, the corresponding PPh_3 adduct was prepared under identical conditions. As with acetylene, IIIc formation was sufficiently retarded to enable isolation of the new species as the unique product after recystallisation from a minimal quantity of n-pentane. Apparently

Diagram 5

Spectroscopic Data for $[H_2Os_3(CO)_9(PPh_3)(C_2H_4)]$



Infrared spectra

a/ $[H_2Os_3(CO)_9(PPh_3)]$

b/ Product from the reaction of $[H_2Os_3(CO)_9(PPh_3)]$ with ethylene.

c/ Computer simulated difference spectrum between b/ and a/(based on common absorption at 2053cm^{-1}) -$[H_2Os_3(CO)_9(PPh_3)(C_2H_4)]$

ν_{CO}/cm^{-1} (cyclohexane)
2090w
2069m
2042m
2006vs
1999msh
1989wsh(br)
1970w
1964w

^{1}H NMR data($CDCl_3$, 31°C)			
δ, (ppm)	Intensity	J_{PH}(Hz)	Assignment
7.46(m)	15H		P-Ph
2.56(d)	4H	7.0	coordinated ethylene
-14.20(s)	1H		terminal hydride?
-19.89(d)	1H	12.5	bridging hydride

the formation of these adducts is not adversely affected by a change in phosphine, but the subsequent stage(s) leading to III are. Indeed infrared evidence suggested that the initial alkene addition was complete, in both cases, well within the specified, convenient, time-scale. Both spectroscopic evidence and elemental analysis were consistent with the formulation $[H_2Os_3(CO)_9(PPh_3)(C_2H_4)]$, IVb. The infrared ν_{CO} spectrum was almost identical to that computed for the PPh_2Et analogue, IVa, showing only terminal carbonyl frequencies (Diagram 5). The ^1H NMR spectrum ($CDCl_3$, 31°C) again contained a singlet (-14.26) and a doublet (-19.89δ, J_{PH}= 12.5Hz) in the hydride region, whilst above the TMS signal, apart from the broad phosphine resonance, only a sharp doublet at 2.56δ (J_{PH}=7Hz) was visible once more consistent with a coordinated ethylene molecule coupled to the phosphorus nucleus. The equivalent intensities of the hydride signals only became evident upon cooling to -70°C, whence the singlet in particular sharpened up considerably. Concurrently the alkene signal markedly broadened, although it is not obvious whether this was due to it collapsing or loss of resolution over that region. The former would be anticipated eventually, since it is difficult to envisage a ground state where all four protons are magnetically equivalent. Unfortunately this point was not reached at the lowest temperature (-80°C) studied.

On attempting to obtain a mass spectrum the observed pattern corresponded to the decomposition product $[H_2Os_3(CO)_9(PPh_3)]$ indicating breakdown of the sample within the spectrometer. As with IVa, moderate heating (under N_2 at 40°C for 7 hours) led to complete regeneration of the starting material as traced by infrared monitoring; continued pumping under vacuum also caused a similar liberation of the ethylene. This is synonymous with the ethylene being only weakly bound. Such a reversible addition has already been demonstrated for the equilibrium-

$$[HOs_3(CO)_9(C_2H_4)(SMe)] \rightleftharpoons [HOs_3(CO)_9(SMe)] \qquad (23)$$

-which is facilitated by the variable coordination of the sulphur ligand. The structure of this coordination adduct, as determined by X-ray diffraction,

confirmed the alkene to be coplanar with the metal triangle, but found to be positionally disordered with the equatorial carbonyl group which prevented any detailed assessment of the olefin-metal geometry. Crystal disorder problems similarly prevented full analysis for $[Os_3(CO)_{11}(C_2H_4)]$(24) although again an equatorial position was favoured. Unfortunately IVb also exhibited gross crystallographic disorder(25).

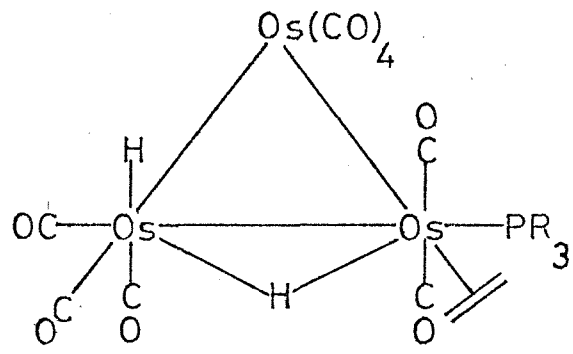
Very few other examples of osmium cluster-alkene species have been reported. The compound $[H_2Os_3(CO)_8(C_2H_4)S]$ is known(23), whilst nucleophilic attack on $[HOs_3(CO)_{10}(CF_3CCHCF_3)]$ gives a series of adducts for which the structures of $[(Ph_3P)_2N][Os_3(CO)_{10}\{CF_3(H)CC(H)CF_3\}Br]$, $[Os_3(CO)_{10}\{CF_3(H)CC(H)CF_3\}(PEt_3)]$(26) and $[Os_3(CO)_{11}\{CF_3(H)CC(H)CF_3\}]$(27) have been fully characterised and the olefin shown in each case to be equatorially disposed. Significantly in the first instance the ^1H NMR spectrum at -60°C demonstrated that the alkene ligand was non-fluxional, and only at +40°C was an averaged signal observed perhaps reflecting the higher barrier to rotation upon substitution.

These chemical and physical properties are reminiscent of those for $[H_2Os_3(CO)_{10}L]$, L=PPh_3, PMe_2Ph etc.(28), except that thermolysis releases ethylene in preference to carbon monoxide. The positions of the hydride resonances, and their couplings, are complementary with an edge-bridging hydride encompassing the phosphine-bonded osmium with the other centre shared with a terminal proton. However, certain discrepancies are obvious and, in particular, the lack of intramolecular scrambling at ambient temperatures. The absence of an hydride-hydride coupling is also adverse, although not unique i.e. $[H_2Os_3(CO)_{10}(PMe_2Ph)]$(28) and, whilst the chemical shift of the bridging hydride shows excellent agreement, that for the terminal entity is to a higher field position (ca. -14.0δ against typically -10.0δ) than expected. In the related compounds $[HOs_3(CO)_{10}X]$, X=Cl, Br or I(10,24) such a position has even been correlated with a bridging enviroment, but this would be inconsistent with the lack of ^{31}P-coupling. With the ethylene bonding the same osmium as the phosphine, from the magnitude of the observed $^2J_{PH}$ splitting, it is not apparent why the terminal hydride should be more perturbed than the bridging one. A plausible explanation may be that it adopts a semi-

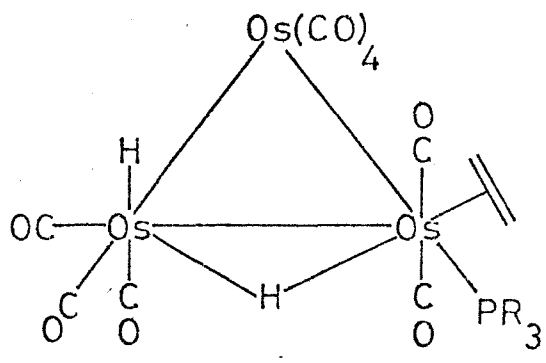
bridging coordination as a result of the weakly bonding alkene not completely 'saturating' the metal-metal bond. However, even smaller configuration changes may also be adequate to cause the observed discrepancy in magnetic properties.

Accepting these reservations only the spatial arrangement of the ethylene remains to be determined. Six plausible configurations are shown below, in which four have the ethylene

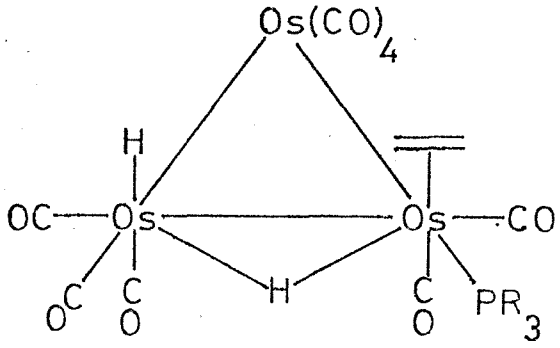
A



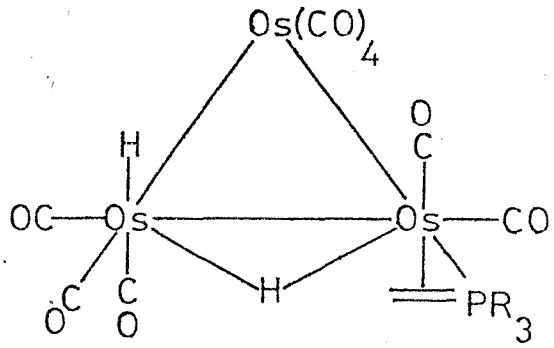
B



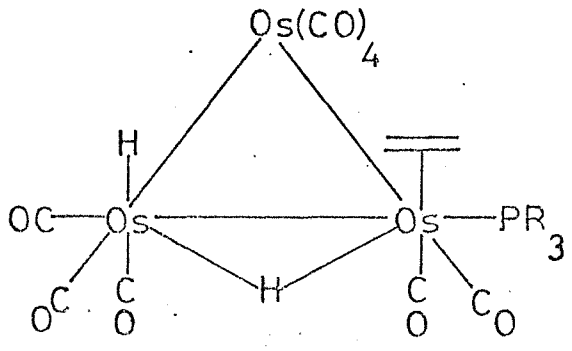
C



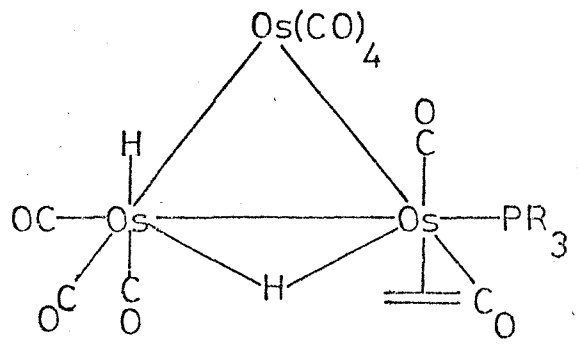
D



E



F



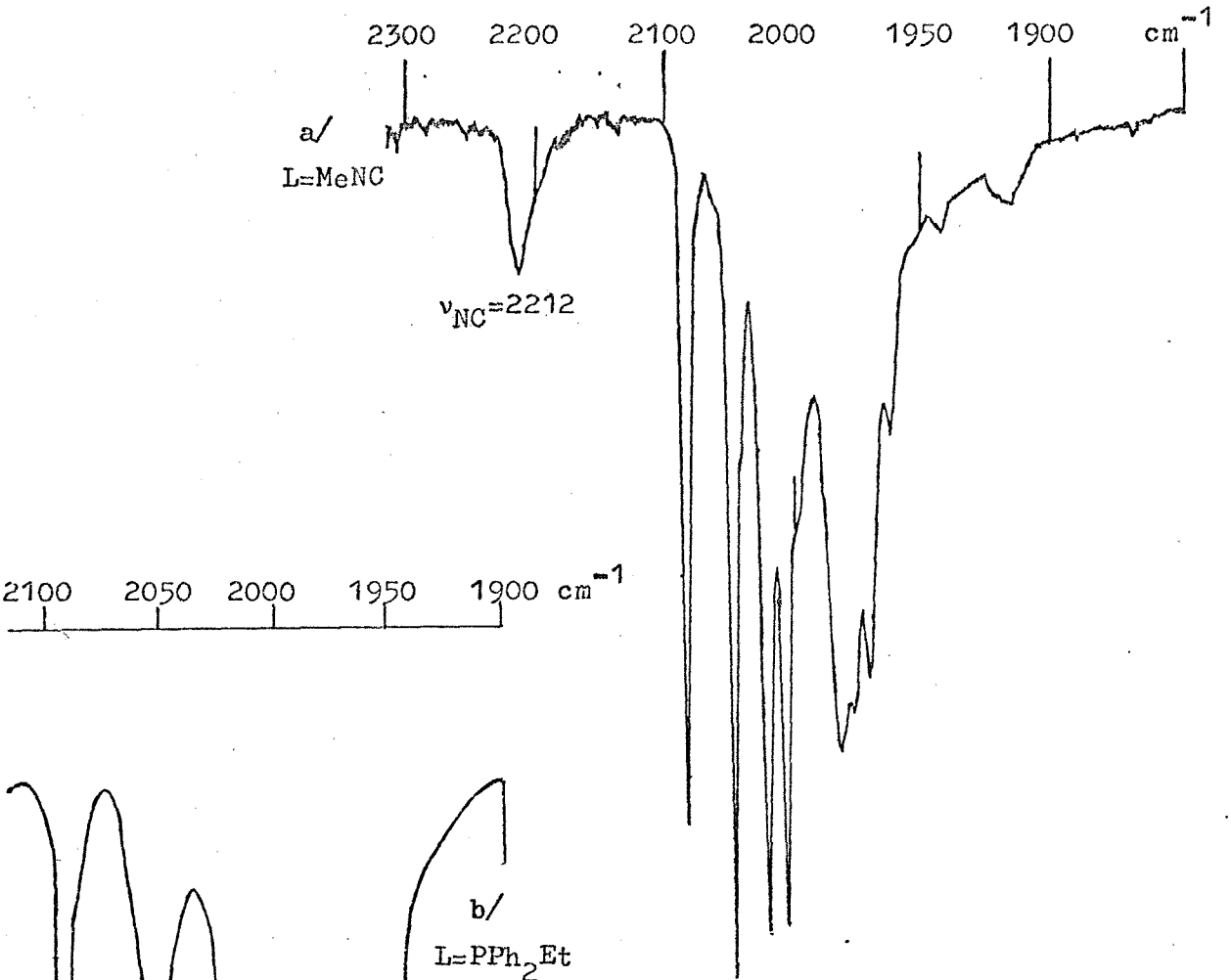
axially disposed, and in the remaining pair it is equatorially positioned. All previous literature examples of ethylene-coordinated triosmium clusters have favoured an equatorial site, and this has been justified on steric grounds(24). Unfortunately, these arguements were in the absence of a bulky phosphine ligand which could clearly complicate the issue. No indication can be drawn from the ^{1}H NMR ethylene resonance, since for either position the total lack of molecular symmetry implies both rapid rotation about the metal-alkene axis, as normally postulated(29), and either a second intramolecular process, e.g. rotation about the C-C axis, causes a second averaging or the chemical shift difference between the end or, more likely, the sides of the ethylene ligand is negligible. The magnitude of the J_{PH} coupling is inconsistent with the phosphine and bridging hydride a trans-arrangement which dismisses structures A, E and F. The validity of C gains some support from the aforementioned perturbation of the terminal hydride resonance.

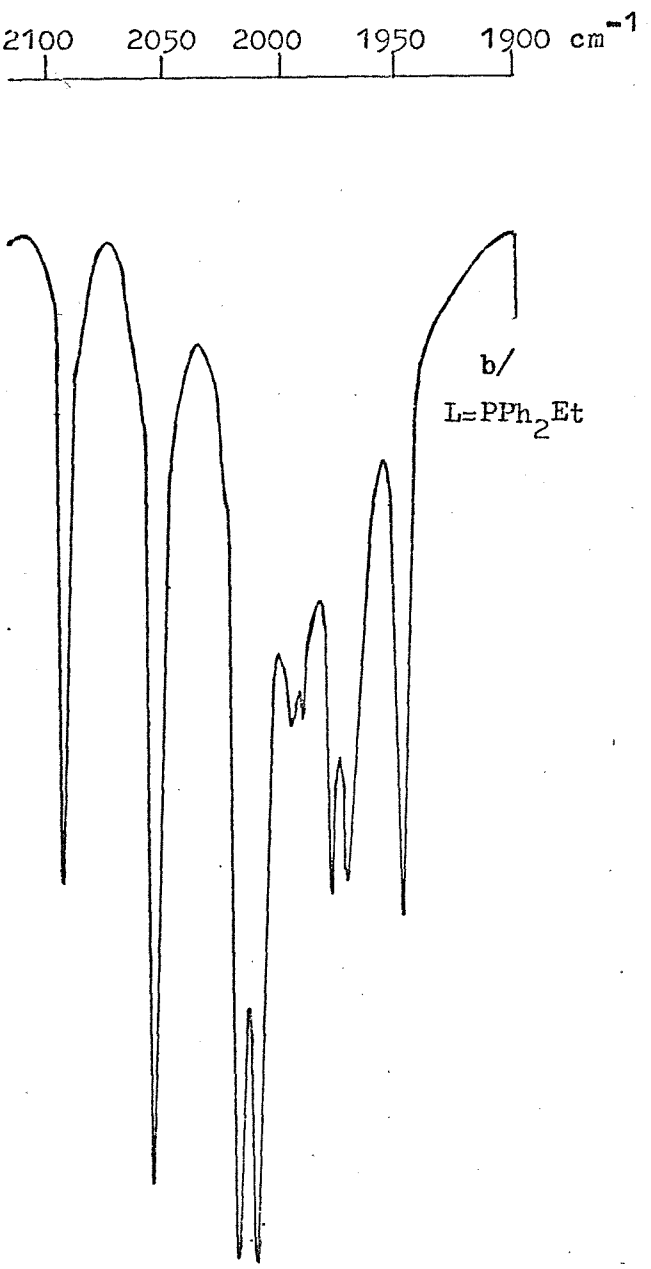
3.3.2. Preparation and Characterisation of $[H_2Os_3(CO)_9(PR_3)(CNMe)]$

To aid resolving this problem the corresponding MeNC adducts of $[H_2Os_3(CO)_9(PR_3)]$ were prepared. Isocyanides, and MeNC in particular, are known to adopt axial sites because of the overriding favourable electronic factors, and its small steric bulk. Addition of an equimolar quantity of isocyanide to a concentrated n-hexane solution caused an immediate transformation in colour. On leaving to stir rapid precipitation of a light yellow solid occurred which was then washed with further solvent and dried in vacuo. These postulated adducts $[H_2Os_3(CO)_9(PR_3)(CNMe)]$, PR_3= PPh_2Et, Va, and PPh_3, Vb, both gave microanalysis (C, H and N) consistent with their formulation. However, their spectroscopic data immediately illuminated a fundamental difference in nature compared to the corresponding IV adduct. There is little resemblance between the infrared ν_{CO} regions of IV and V emphasizing an intrinsic dissimilarity in the carbonyl configurations about the metal core. Such deviations in spectral features has been often used to differentiate between isomeric forms of related species with varying substituents. A prime

Diagram 6

Infrared Spectra for $[H_2Os_3(CO)_9(PPh_2Et)L]$; L=$PPh_2Et$ or MeNC

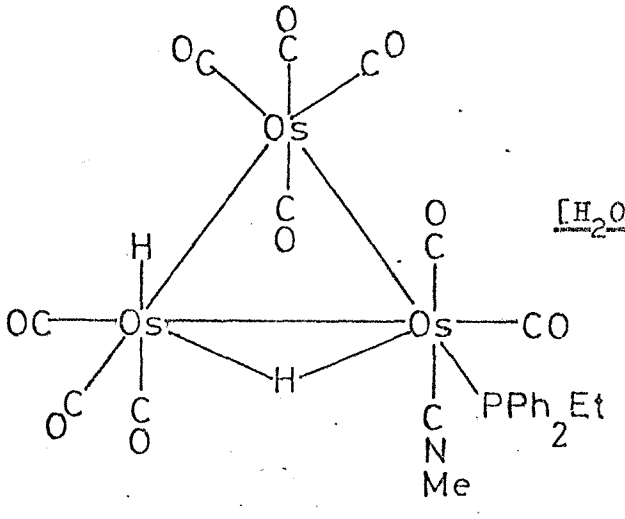




ν_{CO}/cm^{-1} (cyclohexane)	
a/	b/
2081s	2097.5m
2046vs	2054s
2018s	2019vs
2006s	2010vs
1998m-wsh	1994w
1981m	1987.5w
1976msh	1977m
1970m	1970m
1961w	1949m
1943vw	
1917vw	

example is the $[Os_3(CO)_{11}L]$ system where equatorial (phosphines and ethylene) and axial (acetonitrile and isocyanides) substituted isomers are easily discriminated(24). Also present in the infrared spectrum was a weak frequency at 2212cm^{-1} (Va) in total agreement with a terminally bonded isocyanide group(30).

The limiting, low temperature (-60°C, $CDCl_3$), ^{1}H NMR spectrum of Va contains two equally intense signals at -10.11(d) and -20.01(dd) δ; J_{HH}=3.5 and J_{PH}=11.4 Hz. These chemical shifts (Table 3) bear a startling resemblance to those for $[H_2Os_3(CO)_{10}(CNMe)]$(30), apart from the obvious inclusion of the ^{31}P-coupling to the bridging hydride. This latter splitting complies with a cis-arrangement, whilst a doublet at 3.11 (J_{PH}= 2.5Hz) δ is assigned to the isocyanide methyl group; the presence of a nuclei interaction implying that both constituents occupy a common metal centre. ^{1}H NMR spectroscopy indicates that $[H_2Os_3(CO)_{10}(CNMe)]$ exists as a pair of isomers in solution, but the introduction of a phosphine apparently restricts the isocyanide to a single coordination site. If it is assumed that the two forms represent either an axial or equatorial position then the latter would be expected to be blocked by the bulky phosphine. This apart, the former already appears to be the most preferred arrangement provided the X-ray diffraction determined crystal structure(31) reflects the lowest energy configuration. It can then be concluded



Structure of $[H_2Os_3(CO)_9(PPh_2Et)(CNMe)]$

that the structure of Va is a direct combination of those confirmed for the two separate addition adducts, analogous to D, as shown above.

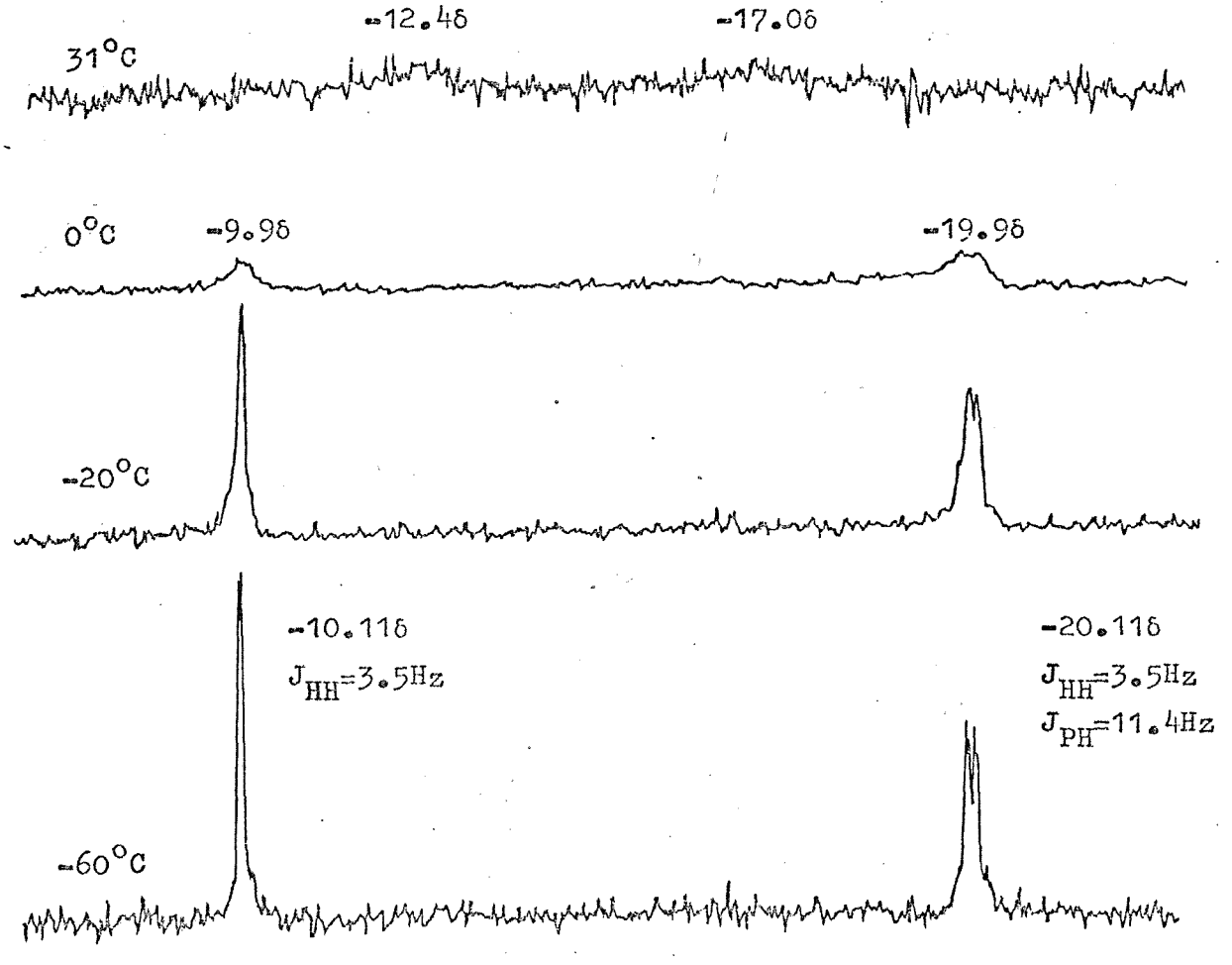
Diagram 7

Variable Temperature ^1H NMR Spectra for $[H_2Os_3(CO)_9(PPh_2Et)(MeNC)]$

Table 3

Limiting spectra($CDCl_3$) for $[H_2Os_3(CO)_9(MeNC)L]$, L=PPh_2Et or CO

$[H_2Os_3(CO)_9(PPh_2Et)(MeNC)]$, -60°C					$[H_2Os_3(CO)_{10}(MeNC)]$, -70°C,(25)		
δ, (ppm)	Intensity	J_{PH} (Hz)	J_{HH}	Assignment	δ, (ppm)	Intensity	J_{HH}(Hz)
3.11(d)	3H	2.5		H_3NC	3.93(s) 3.94(s)	3H	
-10.11(d)	1H		3.5	terminal hydride	-9.88(d) -10.14(d)	1H	3.0 4.3
-20.01(dd)	1H	11.4	3.5	bridging hydride	-19.76(d) -19.84(d)	1H	3.0
7.45(m)	10H			P-Ph			
2.82(q?)	2H		7.0	$P-CH_2-C$			
1.05(dt)	3H	19.0	7.0	$P-C-CH_3$			



On warming to room temperature (31°C) the hydride resonances collapse into the baseline approaching coalescence. This is analogous to all other $[H_2Os_3(CO)_{10}L]$ derivatives where intramolecular hydride exchange is facile (Chapter One). This infers that the mechanism whereby interchange occurs is prohibited in IVa but unimpaired for Va. Since, in either complex, the enviroment about the terminal hydride is essentially identical that of the bridging moiety must be adversely affected. In all the reported mono-substituted species this hydride is trans- to an equatorial carbonyl ligand and this is maintained in Va. If the variation in spectral features is taken to indicate a different position of coordination for the isocyanide and ethylene then it can be assumed that the latter replaces this carbonyl group. This complies with the situation in I(3) where the bridging proton is displaced towards the osmium π-bonded by the vinylic group and in IVa, with the ethylene directly opposite, this ought to be even more pronounced. The nett result is that the potential energy of this hydride is sufficiently altered to effectively raise the barrier to interconversion, on the ^1H NMR timescale, above room temperature. An alternative interpretation may be that, with the second proton possibly adopting a semi-bridging position, an intermediate species with both protons terminal is further destabilised inhibiting the fluxional process. Whatever, the implication is that IVa adopts a structure with both the phosphine and ethylene place equatorial; the latter opposite the bridging hydride, i.e. proposed configuration B.

3.3.3. Full ^{13}C NMR Study on $[H_2Os_3(CO)_9(PPh_2Et)(C_2H_4)]$

For further confirmation a ^{13}CO enriched sample of IVa was prepared (enrichment occurring at $[Os_3(CO)_{12}]$) and ^{13}C NMR spectra recorded from -80 up to 0 °C which are shown in Diagram 8. In addition, the ^1H-coupled spectrum at 0°C was accummulated and is compared to the decoupled spectrum in Diagram 9. The latter contains nine independent resonances: a, 187.26; b, 182.45; c, 181.03; d, 178.83; e, 177.68; f, 174.73; g, 173.23; h, 172.69 and i, 167.72 δ, all with unit intensities. Over the entire temperature range studied no evidence for any fluxionality was revealed. The

Diagram 8 Variable Temperature ^{13}C NMR Spectra for $[H_2Os_3(CO)_9(PPh_3)(C_2H_4)]$

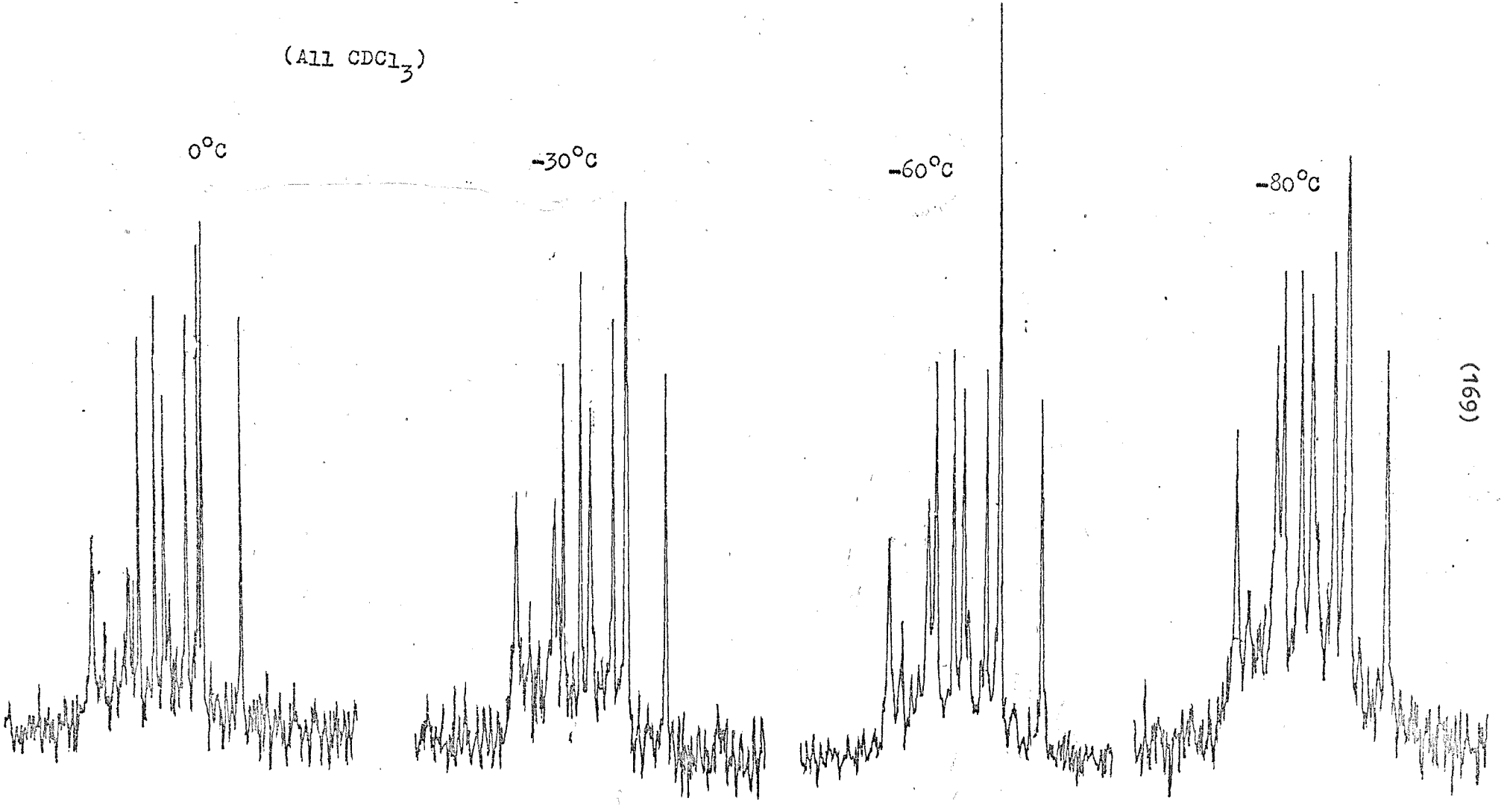
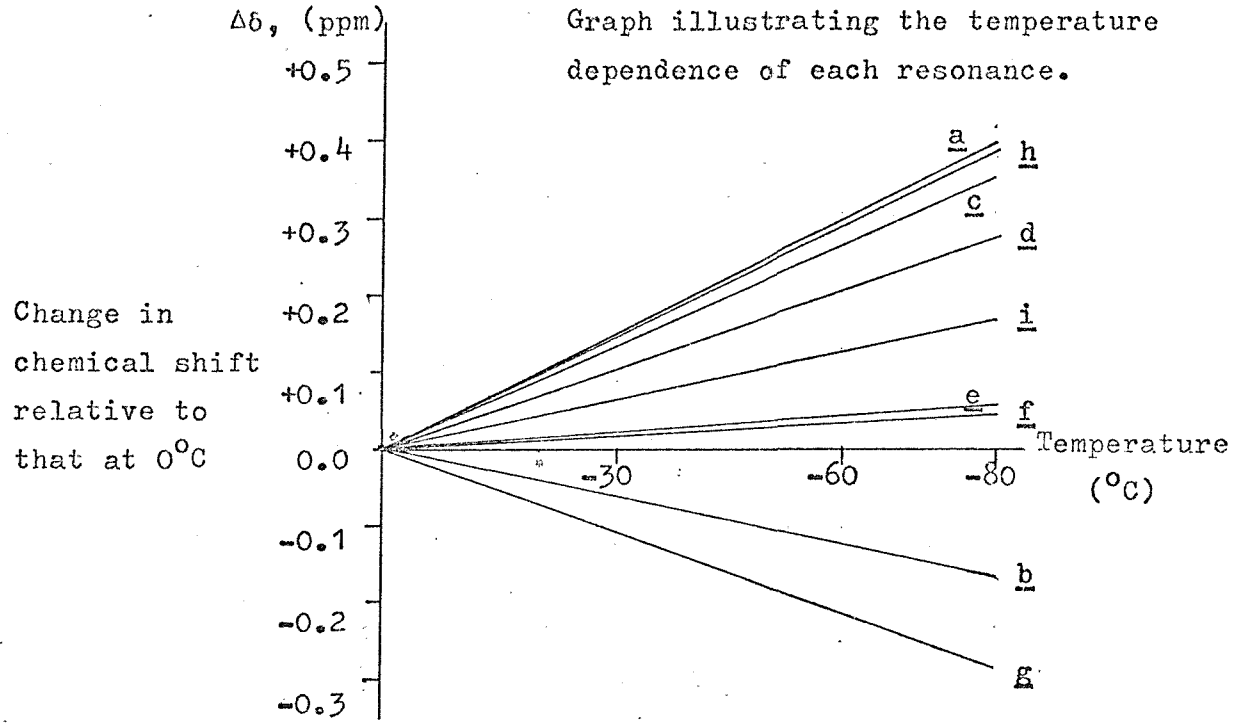


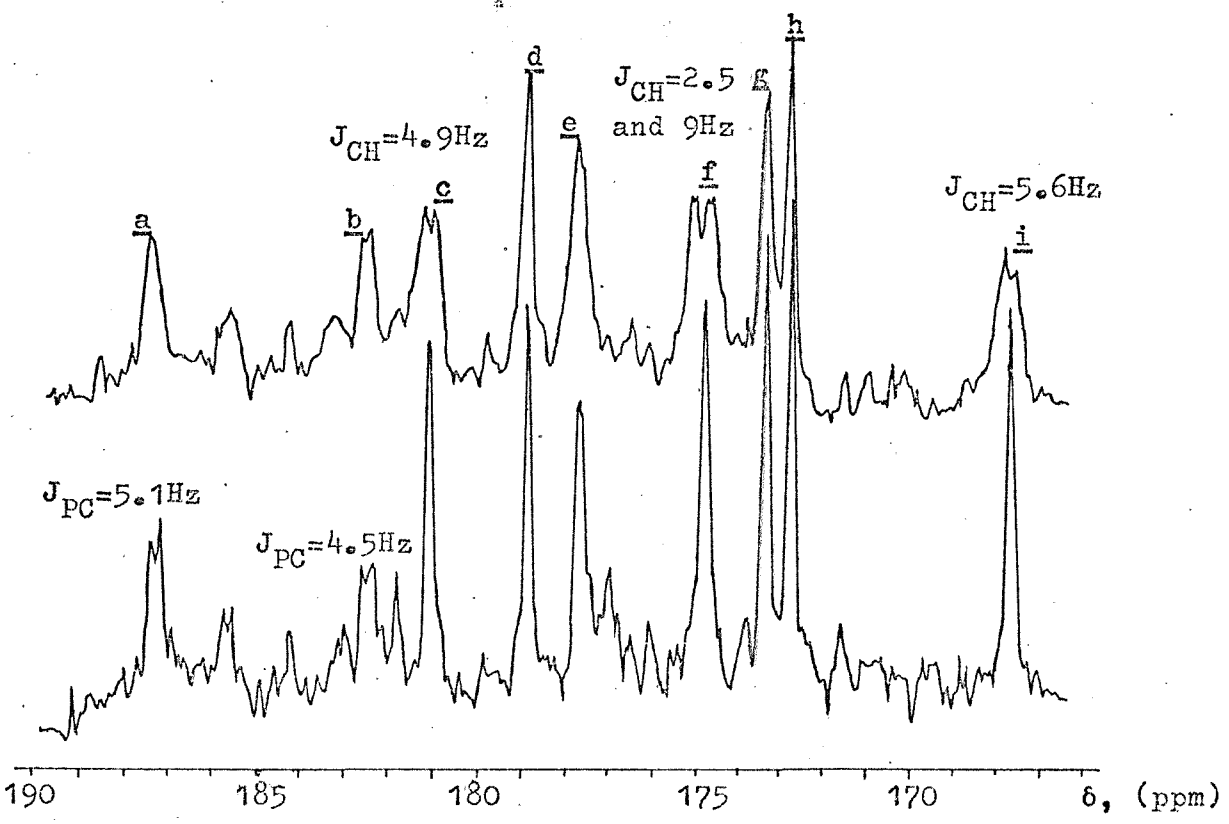
Diagram 9

^{13}C NMR Spectra for $[H_2Os_3(CO)_9(PPh_3)(C_2H_4)]$



Graph illustrating the temperature dependence of each resonance.

^1H-coupled and decoupled spectra, ($CDCl_3$, 0°C)



only complication to a static situation within the spectra was the inverse temperature dependence of the two close signals g and h, which causes them to become accidently isochronous at about -60°C before completely crossing over by -80°C. This is illustrated graphically (Diagram 9), where it is also apparent that b and g have an opposite dependence to the remaining signals, although any significance in this observation is unknown. The presence of nine separate resonances confirms the absence of symmetry within the molecule.

The proposed structure, with the introduced ligands equatorial, conveniently explains the similar J_{PC} values to the lowest field pair of signals, a (5.1Hz) and b (4.5Hz), compared to that observed between phosphorus and adjacent axial carbonyl groups in $[Os_3(CO)_{11}(P(OMe)_3)]$(16). On ^{1}H-coupling no further discernible splitting was seen for either signal, although a slightly broadened, but this may just be a function of spectral quality. However, three other resonances did show resolved ^{1}H-couplings and were thus assigned to the $Os(CO)_3H$ group. In particular, f (J_{CH}=9 and 2.5 Hz) is coupled to both hydrides so by correlation with $[H_2Os_3(CO)_{10}(PPh_2Et)]$ (Chapter One) it must correspond to the trans-carbonyl relative to the terminal hydride. This leaves c (4.9Hz) and i(5.6Hz) assigned to the two equatorial groups and, by comparison with IIIa, the isolated high-field signal i may be individually allocated to the carbonyl approximately opposite the bridging hydride. Then the four resonances left must be associated with the remaining $Os(CO)_4$ group. These fall roughly into two pairs, d,e and g,h, within which line-widths and intensities are similar atypical of related enviroments. By rule of thumb the lower field pair must correspond to the axial ligands, leaving g,h as the remaining equatorial assembly. Notably the last pair have very narrow half-widths, which show little variation upon ^{1}H-coupling, complementing their designation in view of observations made with $[H_2Os_3(CO)_9(PPh_2Et)]$.

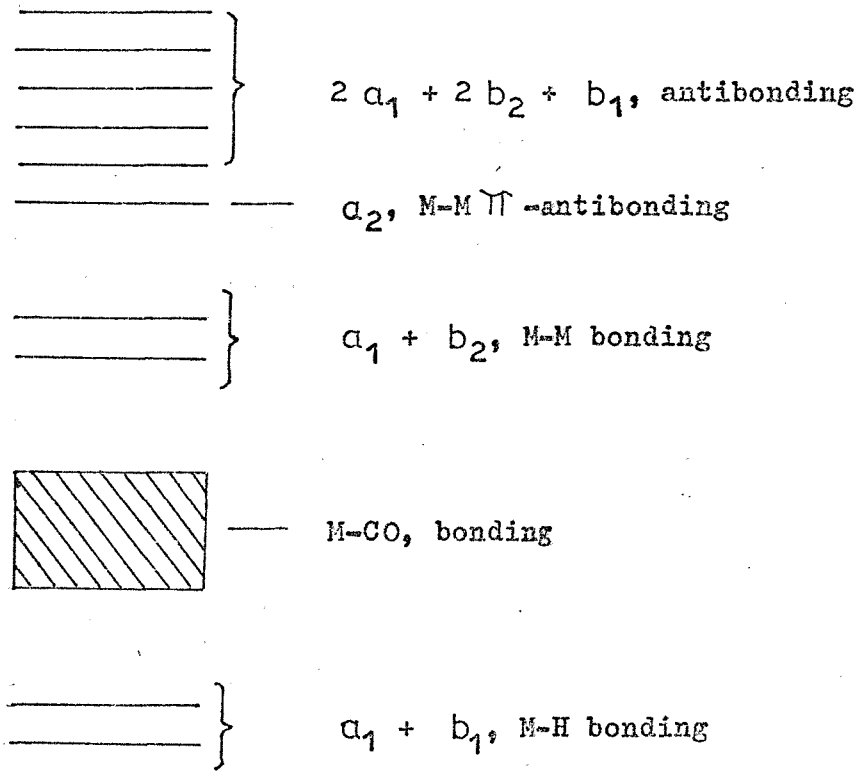
3.3.4. Discussion

In the light of these results it is interesting to recall a previous observation(32) where a n-hexane solution of

$[H_2Os_3(CO)_{10}(PPh_2Et)]$ was inadvertently refluxed in the presence of excess phosphine. When the anticipated darkening in colour, indicative of the formation of $[H_2Os_3(CO)_9(PPh_2Et)]$, did not occur the reaction was continued for 5 hours before the resulting yellow solution was worked up. Chromatography gave several bands but the major product, isolated pure from the t.l.c. plate, gave an infrared ν_{CO} spectrum closely resembling that of Va which, unfortunately, had been previously incorrectly assigned to $[H_2Os_3(CO)_9(PPh_2Et)]$(33). The other identified product from the reaction was $[Os_3(CO)_{11}(PPh_2Et)]$. On reflection, although no further characterisation was carried out, its appearance intuitively suggests a 'saturated' structure so, along with the strong correlation between its ν_{CO} spectrum and that of Va, it should perhaps be more correctly assigned as the disubstituted derivative $[H_2Os_3(CO)_9(PPh_2Et)_2]$. It has also been found that leaving a solution of $[H_2Os_3(CO)_9(PEt_3)]$ to stand for an extended time in the presence of excess phosphine gives a similar result, but accompanied by concurrent decomposition (20). Presumably both phosphines, by analogy with V, bond to the same metal centre with one placed equatorial and the second axial. Clearly on steric grounds alone two PPh_2Et groups are unlikely to occupy adjacent equatorial sites and, whilst axial positions are normally unfavourable, under certain restrained circumstances they are found. For instance, the tripod ligand $MeSi(PBu_2)_3$ reacts with $[Ru_3(CO)_{12}]$ to give $[Ru_3(CO)_9(MeSi(PBu_2)_3)]$(34) where all the phosphine branches coordinate axially on the same face of the molecule, presumably as a result of its restrictive 'bite'.

Reaction of a second nucleophile onto $[H_2Os_3(CO)_9L]$, L=phosphine, appears to be widespread and, indeed, it has been subsequently reported that even acetonitrile can form an identifiable analogue(20). The direction of reaction is interesting since attachment to the phosphine-substituted metal centre is not which might have intuitively expected. Addition to $[H_2Os_3(CO)_{10}]$ by a variety of nucleophiles, both weak and strong, always occurs by attack at one osmium centre of the electron deficient edge accompanied by opening of a hydride from a bridging to terminal axial position onto the second metal. There is little evidence within the structure of $[H_2Os_3(CO)_9(PPh_3)]$ in the crystal for any steric congestion or relief on phosphine substitution(13).

However, the Os-C bond lengths are consistent with the expected increase in electron density on the substituted metal atom, allowing greater metal-to-CO π^* retrodative bonding. So any charge effects would favour the unsubstituted osmium centre at the end of the bridgehead as the site of nucleophilic attack. But orbital control of nucleophilic addition, as expected for 'soft' nucleophiles like MeNC and ethylene, will favour the site of attack being that with the largest-amplitude l.u.m.o. (lowest unoccupied molecular orbital)(35). A qualitative molecular orbital diagram for the metal-metal and metal-hydrogen bonding in $[H_2Os_3(CO)_{10}]$ is given below. The fragment orbitals of the C_{3v} $M(CO)_3$ and C_{2v} $M(CO)_4$ units used(36) and the scheme, before inclusion of the hydrides, is



A qualitative molecular orbital diagram for the metal-metal and metal-hydrogen bonding in $[H_2Os_3(CO)_{10}]$

analogous to the isolobal cyclopropene(37). The probable l.u.m.o. is an Os-Os $\pi_\perp^*$ orbital along the bridged edge (a_2). The increased electron density at the phosphine-substituted metal should raise the energy of its fragment orbital and, accordingly, the l.u.m.o. will have a greater amplitude at that metal atom. Hence, under orbital control, addition to the substituted centre is indeed

favoured.

When a sample of $[H_2Os_3(CO)_9(PPh_3)]$ was left under a pressure of ethylene for an extended period of 5 days the infrared ν_{CO} spectrum of the isolated yellow residue indicated that a considerable quantity of IIIc had been formed, although a large fraction of IVb still remained. Within a similar time essentially complete conversion to IIIa was seen for $[H_2Os_3(CO)_9(PPh_2Et)]$. These observations confirm that IV is an intermediate in the reaction of $[H_2Os_3(CO)_9(PR_3)]$ with ethylene, leading eventually to III by a mechanism parallel to that proposed for $[H_2Os_3(CO)_{10}]$. Their isolation is presumably a result of the anticipated alkene insertion into a metal-hydride bond being sufficiently retarded by the presence of the phosphine to cause it to become rate-limiting. It has been found(24) that the terminal hydride in $[H_2Os_3(CO)_{11}]$ is particularly susceptible to attack (by $CHCl_3$ and CCl_4). Translating this to IV, where the ethylene is directed away from both hydrides, the position of the phosphine might well be expected to restrict formation of a required transient species with both the hydride and ethylene in close proximity. This could be by either directly blocking the necessary site or as a result of its steric bulk, depending on whether insertion is actually into the bridging or terminal moiety. Several alternative mechanisms can be proposed, including the less favoured option of insertion of a second ethylene into the generated terminal hydride but, which ever applies, the inferred transient ethyl group is most likely to reside at the bridgehead osmium away from the phosphine because of the latters unfavourable electron donating properties. The precise mechanism does not evidently determine the final distribution of isomers in III since the ratio for IIIa was unaltered whether it was prepared from the reaction of ethylene or acetylene with $[H_2Os_3(CO)_9(PPh_2Et)]$. This indicates that the absolute value is subject to thermodynamic, as opposed to kinetic, control.

3.4. Pyrolysis of $[HOs_3(CO)_9(PPh_2Et)(CHCH_2)]$

Although formation of IIIa is probably the deactivation stage in catalytic hydrogenation of ethylene by $[H_2Os_3(CO)_9(PPh_2Et)]$

it may still not be present when the reaction is complete. The thermal conditions employed may in turn cause it to react further giving other products, a knowledge of any such transformations is clearly important.

$[HOs_3(CO)_{10}(CHCH_2)]$, I, is known to undergo rapid pyrolysis in refluxing n-octane(1) to give $[H_2Os_3(CO)_9(CCH_2)]$, VI, (70%) and $[Os_3(CO)_{12}]$ (30%). Since I reacts rapidly with carbon monoxide to give $[Os_3(CO)_{12}]$ as the only osmium-containing product, it seems likely that, in the conversion of I into VI the carbon monoxide displaced reacts with unchanged I to account for the preparation of $[Os_3(CO)_{12}]$. VI can also be prepared directly from $[Os_3(CO)_{12}]$ by bubbling ethylene through a n-octane solution under reflux for 24 hours, although the yield is somewhat inferior(38). Under a moderate pressure of ethylene (20bar) at 160°C the yield improves (60%), but the tetranuclear clusters $[Os_4(CO)_{12}(C_2H_2)]$ (10%) and $[Os_4(CO)_{12}(C_4H_6)]$ (30%) were isolated and characterised as by-products(39).

The lack of coupling between the non-equivalent hydrogens on the organic ligand in the ^1H NMR spectrum of VI suggested that the complex contained a coordinated vinylidene (CCH_2) group as opposed to a coordinated acetylene (HCCH)(40). This was confirmed by a single crystal X-ray diffraction study(41) which found that all three Os-Os bonds were different with the C_2 fragment tilted away from the shortest one. The two bridging hydrides give separate signals (J_{HH}=1.4Hz) in the ^1H NMR spectrum which, in association with the asymmetry of the molecule, indicates that they bridge the longer two metal edges. A separate investigation(2) found that the lower field signal was a doublet of triplets ($J(H-CH_2)$=0.7Hz) which allowed it to be tentatively assigned to the hydride positioned equivalently with respect to the two hydrogens on the vinylidene group. Thus I undergoes pyrolysis by carbon monoxide loss and hydrogen transfer from ligand to metal.

3.4.1. Preparation and Characterisation of $[H_2Os_3(CO)_8(PPh_2Et)(CCH_2)]$

A similar reaction for IIIa was expected as circumstantial evidence from a high temperature ^1H NMR study had already been seen. Indeed, under reflux in n-heptane a smooth conversion of IIIa to

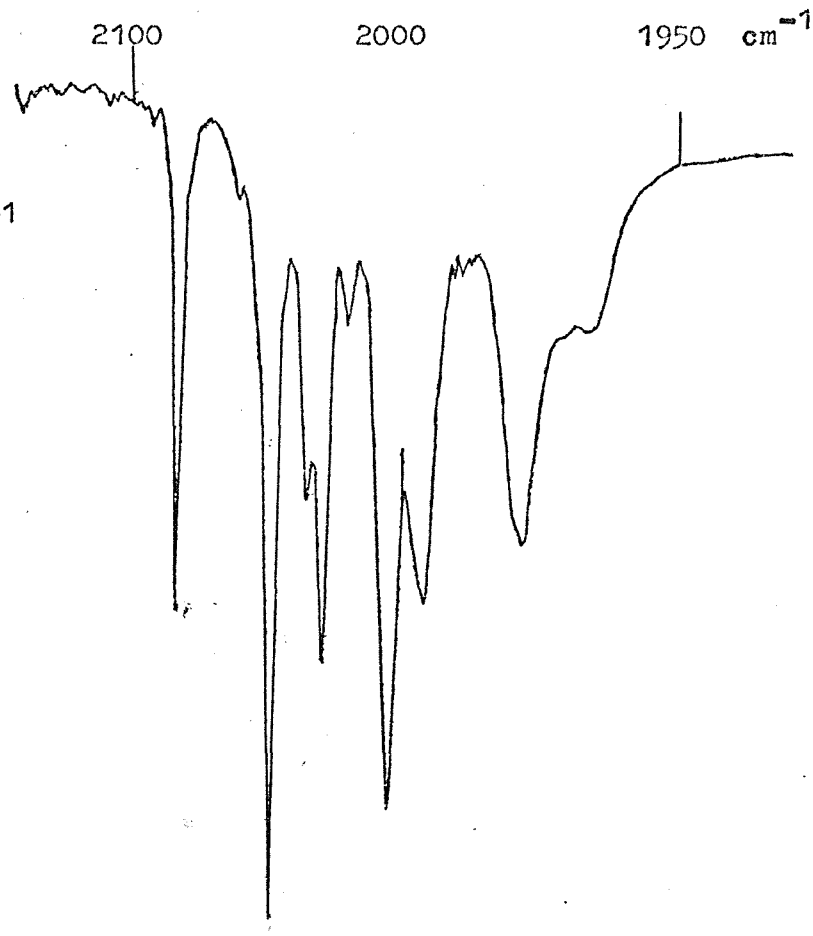
$[H_2Os_3(CO)_8(PPh_2Et)(CCH_2)]$, VII, occurred within 4 hours, with no significant quantities of any other Os_3 products being observed. The reaction of I to VI in n-heptane was considerably slower (20 hours) so the presence of the phosphine clearly facilitates decarbonylation (and subsequent hydrogen transfer) as this was found to be the rate limiting step in the conversion of I(1). The effect of lowering the activation barrier also reduces totally any competing side-reactions. VII crystallises as a pale yellow solid which was fully characterised by spectroscopic and analytical techniques.

The infrared ν_{CO} spectrum (Diagram 10) contains only bands associated with terminal carbonyl groups, whilst the number indicates a structure with little or no symmetry. A prominent parent ion of m/e=1038 was observed in its mass spectrum. Along with the following fragmentation pattern the entire spectrum closely resembles that of IIIa with the exclusion of its parent ion. This reflects the thermal instability of IIIa which undergoes considerable degradation to VII at the source prior to ionization and detection in the mass spectrometer. Elemental analysis (C and H) also gave satisfactory agreement with the calculated values.

The ^1H NMR spectrum ($CDCl_3$, 31°C) is similar to that of VI (Table 4), apart from small paramagnetic shifts, and the appropriate addition of resonances and couplings due to the phosphine ligand. Thus, in the organic region two doublets of equal intensities occur at 6.15 (J_{PH}=9Hz) and 6.63 (J_{PH}=5Hz) δ. Integration against the phosphine indicated that they each represented one hydrogen. In the hydride region two other doublets, each due to a single hydride, are found at -17.46 (J_{PH}=11Hz) and -20.87 (J_{PH}=8.3Hz) δ. The presence of ^{31}P-couplings strongly implies that the hydrides both bridge edges involving the phosphine-substituted osmium, Os(1). Their magnitude and comparable nature suggests that the hydrides both adopt approximately cis-positions relative to a centrally placed phosphine. This would be consistent with the PPh_2Et possessing a trans-configuration to the quaternary carbon beneath the face of the molecule. In the related compound $[H_2Os_3(CO)_8(Ph_2P{\cdot}C_6H_4{\cdot}C_2H)]$(38) the phosphine is constrained in an equatorial site and consequently one of the hydride-couplings is appreciably larger (25.4Hz) due to the enforced trans-arrangement.

Diagram 10

Spectroscopic Data for $[H_2Os_3(CO)_8(PPh_2Et)(CCH_2)]$



infrared ν_{CO}/cm^{-1} (cyclohexane)

2084m
2050vs
2036w
2030m
2021vw
2005s
1997m
1979m
1965wsh

m/e=1038

Table 4

^1H NMR data($CDCl_3$) for $[H_2Os_3(CO)_8(CCH_2)L]$, L=PPh_2Et or CO

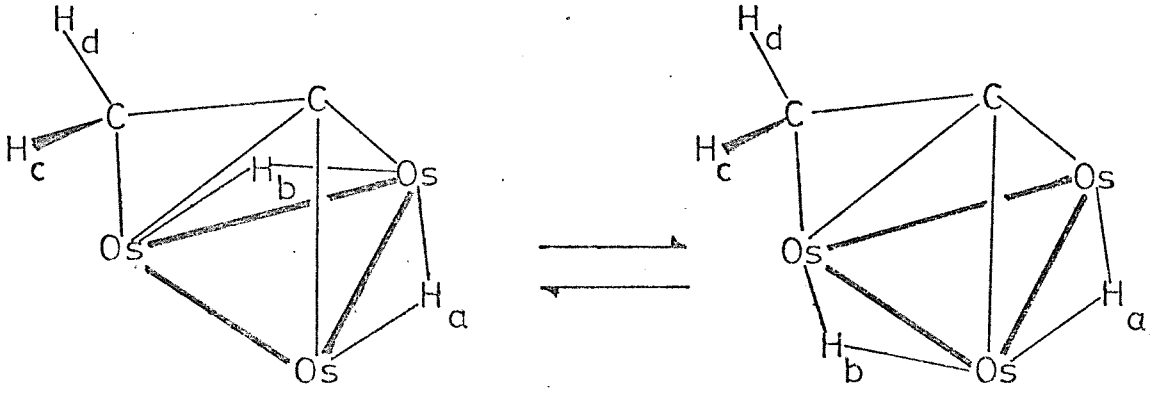
$[H_3Os_3(CO)_8(PPh_2Et)(CCH_2)]$, 31°C					$[H_3Os_3(CO)_9(CCH_2)]$, 27°C,(30)		
δ, (ppm)	Intensity	J_{PH} (Hz)	J_{HH}	Assignment	δ, (ppm)	Intensity	J_{HH}(Hz)
6.63(d)	1H	5.0		vinylidene	6.10(s)	1H	
6.15(d)	1H	9.0		ligand	5.57(s)	1H	
-17.46(d)	1H	11.0		bridging	-18.13(d)	1H	1.4
-20.87(d)	1H	8.3		hydrides	-21.83(d)	1H	
7.47(m)	10H			P-Ph			
2.60(q?)	2H		7.0	P-CH_2-C			
1.00(dt)	3H	19.0	7.0	P-C-CH_3			

All together this data established that VII has the structure shown in Diagram 11, and the following ^{13}C NMR provided further confirmation.

3.4.2. Tentative Assignments for the ^{13}C NMR of $[H_2Os_3(CO)_8(PPh_2Et)(CCH_2)]$

A ^{13}CO enriched sample of VII was prepared from that of IIIa, and the ambient temperature ^1H-coupled and decoupled spectra recorded. The latter contained six resonances: a, 178.37; b, 176.29; c, 175.06; d, 172.32; e, 169.66 and f, 169.06 δ, with an intensity ratio of 1:1:2:1:2. None of these signals showed any evidence of resolved couplings to the phosphine. Clearly, with the anticipated molecular asymmetry, at least two pairs of signals must be accidently isochronous if this represents the slow exchange limiting spectrum as is believed. It is difficult to envisage any mechanism(s) whereby only two separate pairs of the eight independent enviroments equilibrate whilst the remainder are unaffected.

The unsubstituted analogue, VI, has been studied by variable temperature ^1H NMR spectroscopy(38). However, only at elevated temperatures (72°C) was coalescence of the two signals due to the vinylidene ligand seen, whilst even at 115°C, although they had begun to broaden, the two hydrides were still clearly resolved. Two separate fluxional processes were thus identified. The most facile was subscibed to migration of a single hydride to the vacant edge in such a fashion as to cause equivalence of the organic protons without exchange of the hydrides; that being achieved in

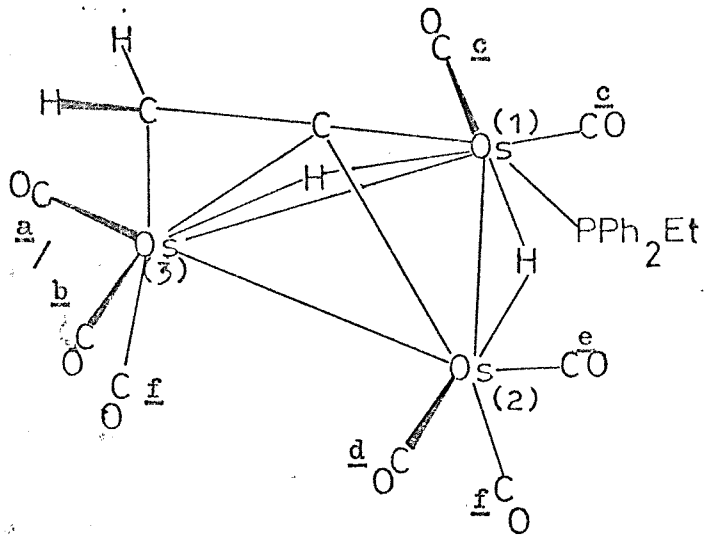


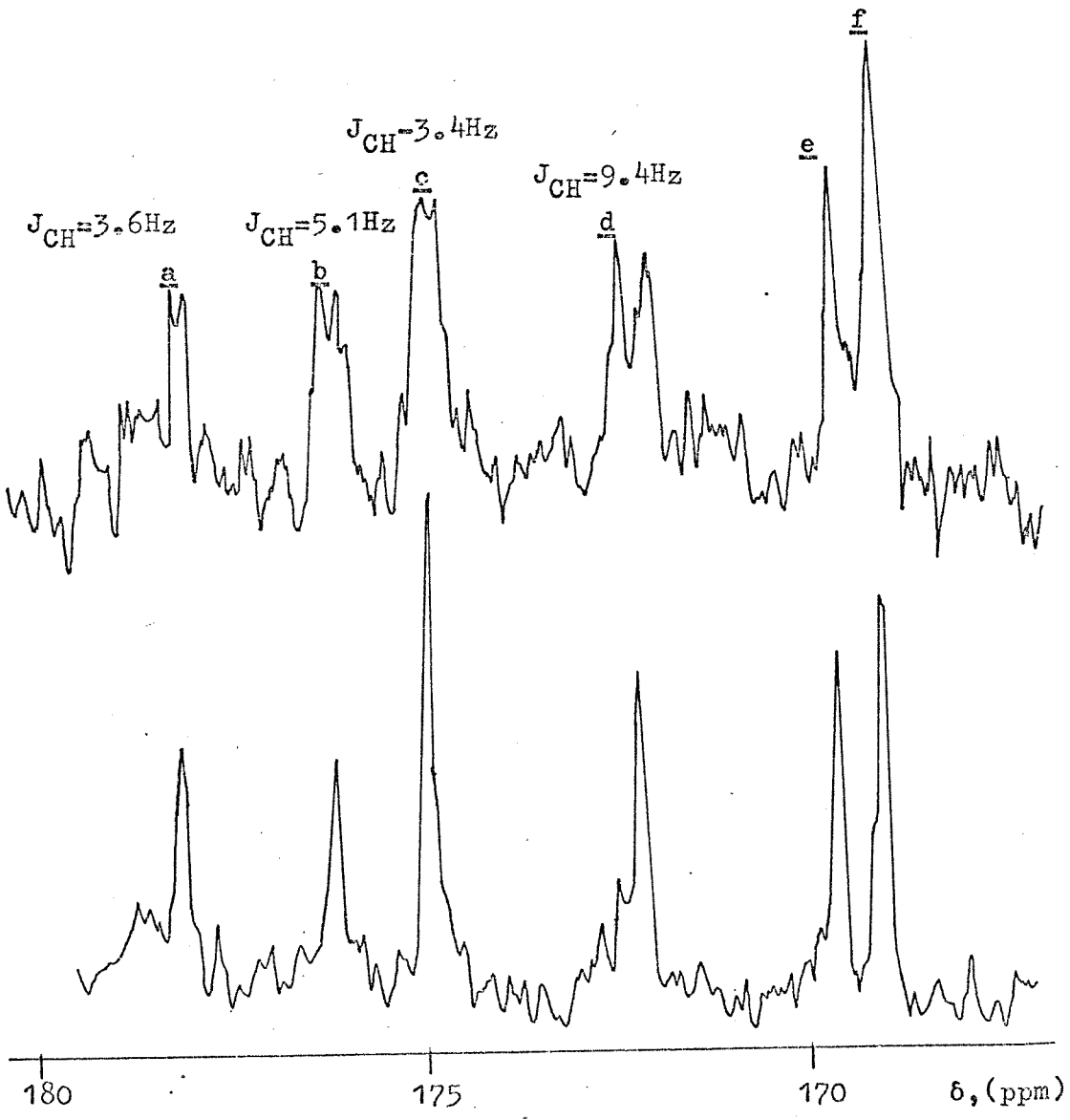
Fast hydride-migration process in $[H_2Os_3(CO)_9(CCH_2)]$

Diagram 11

^{13}C NMR Spectra and Assignments for $[H_2Os_3(CO)_8(PPh_2Et)(CCH_2)]$

δ,(ppm)	Assign-ment
178.37	a
176.29	b
175.06	c
172.32	d
169.66	e
169.06	f





the second motion. An alternative mechanism considered was rotation about the C-C axis, but this was dismissed since it would involve an Os-C bond cleavage. This was later verified by a ^{1}H NMR study on a partially deuterated sample of VI and the diastereomeric analogue $[H_2Os_3(CO)_9(C{=}C(Me)CH_2CHMe)]$(42). An independent ^{13}C NMR investigation(43) also confirmed these deductions since all but one of the nine different carbonyl resonances observed in the slow exchange limit broadened on warming to +100°C consistent with hydride migration. Clearly none of these proposed fluxional processes for VI when transferred to VII could cause the observed ^{13}C spectrum so accidental degeneracy is further endorsed.

Unfortunately no further information, regarding chemical shifts or ^{1}H-couplings, was imparted in this ^{13}C study on VI so it is impossible to assign the features of VII by comparison, as was done for IIIa. Then, on the basis of the observed spectra alone, it is not practical to unambiguously allocate all the resonances. However, the absence of any features above 180δ is in agreement with the lack of $Os(CO)_4$ groups by comparison with the presented spectra of $[H_2Os_3(CO)_9L]$ or $[Os_3(CO)_{12}]$, L=PPh_2Et or CO. The following tentative assignments are suggested, by applying the empirical trends established beforehand, as one possible interpretation for discussion. The absence of any discernible ^{31}P-interactions means that the resonances due to the adjacent carbonyl enviroments are not immediately obvious. This situation is not unusual, and in the hydrogenated derivative $[H_3Os_3(CO)_8(PPh_2Et)(CCH_3)]$, IX, where the related sites were unequivocally assigned, only a marginal broader half-width signified such a coupling. The position of this resonance (175.97δ) is close to that of the double intensity signal, c, and as the configuration about these two osmiums should be essentially identical this could be similarly assigned. The existence of apparent ^{1}H-couplings re-enforces this choice, but the poor standard of spectral resolution prevented detailed analysis of whether it represented an overlapping pair of doublets, as might be envisaged, or just a single splitting ($J_{CH} \simeq 3.4$Hz) indicative of an (accidently) degenerate pair. The resonances a (3.6Hz), b (5.1Hz) and d (9.4Hz) also exhibit couplings to hydrides, presumably due to trans-arrangements to the bridging hydrides.

The lack of any discernible ^{1}H-couplings with e and f suggests that at least two contributions here arise from the two pseudo-axial ligands on Os(2) and Os(3) beneath the molecule. Arbitrarily the highest field, double-intensity, resonance f is assigned through the two enviroments being accidently isochronous. This leaves four single intensity signals to be distributed amongst the quasi-equatorial groups on the same two osmiums. If these are arbitrarily divided into high and low field pairs, then the observed splittings in the former set are completely in agreement with two carbonyls arranged cis- (e) and trans- (d) to an hydride. In the latter pair a degree of perturbation is evident such that intermediate values for the couplings are seen. Such an effect might be anticipated for the carbonyls on Os(3) with the close proximity of the vinylidene moiety, and this is borne out by the published bond angle data of VI(38). Thus, from the magnitude of their ^{1}H-interactions a and b corrspond to the approximately cis- and trans- ligands on Os(3), whilst e and d are similarly allocated on Os(2). These assignments are illustrated in Diagram 11.

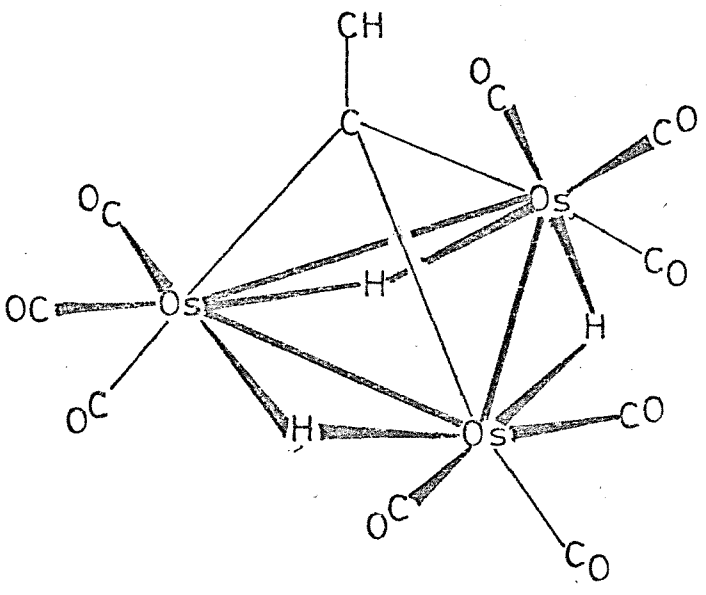
A subsequent private communication(18) of the ^{1}H-decoupled and off-resonance decoupled ^{13}C spectra of VI, containing resonances at: 1, 176.5; 2, 175.0; 3, 173.3; 4, 171.2; 5, 169.7; 6, 169.0; 7, 168.1; 8, 166.7 and 9, 160.4 δ, with 2, 4, 8 and 9 giving hydride couplings, provided support for the assignments of a, b and d. The downward shift from 8 to c of 8.4Hz is also consistent with phosphine-substitution at the osmium. However, the much larger shift from 9, obviously representing a site on the unsubstituted Os(1), to c (14.7Hz) is harder to reconcile. More acceptable would be allocation of half of f to this second carbonyl on the substituted Os(1), leaving e and the other contribution to f ambiguously assigned to the axial groups on Os(2) and Os(3). Then the previous allocation of e is swapped to the second contribution from the accidently isochronous pair c.

3.5. Hydrogenation of $[H_2Os_3(CO)_8(PPh_2Et)(CCH_2)]$

A further parameter to be accommodated when considering possible catalyst deactivation is the presence of hydrogen.

On passing dihydrogen through a n-heptane solution of

VI under reflux for 24 hours a nearly quantitative conversion into the ethylidyne complex $[H_3Os_3(CO)_9(CCH_3)]$, VIII, occurs(41). The same product is obtained from the reaction of $[H_2Os_3(CO)_9(NMe_3)]$ with ethylene in refluxing THF(44). It was characterised by analogy (^{1}H NMR) to $[H_3Ru_3(CO)_9(CCH_3)]$, prepared from reacting ethylene with $[H_4Ru_4(CO)_{12}]$(45), whose structure had been fully elucidated by a combination of ne matic-phase PMR(46) and single-crystal X-ray diffraction(47) studies. Subsequently the structure of VIII was determined by a ne matic-phase PMR/X-ray powder photography investigation(48) and found, as expected, to be similar to that of the ruthenium analogue. Although VIII is formally drawn



Structure of
$[H_3Os_3(CO)_9(CCH_3)]$

with metal-metal bonds the effect of the bridging hydrides in $[H_3Fe_3(CO)_9(CCH_3)]$(49), prepared from $Fe(CO)_5$, B_5H_9 and Vitride (50), and the methylidyne derivative $[H_3Ru_3(CO)_9(CH)]$(51) is shown, by a combination of UV photoelectron spectra and molecular orbital calculations, to provide a description whereby Ru-H bonding is best described as three-centre, two-electron, bonds with no direct metal-metal interactions.

Under similar conditions with VII hardly any reaction was noticeable, as indicated by infrared ν_{CO} monitoring, after 20 hours. However, on changing the solvent to refluxing n-octane total consumption of the starting material was observed within 12 hours. Conversion was essentially quantitative with chromatography yielding a single colourless compound identified as $[H_3Os_3(CO)_8$-

Diagram 12

Spectroscopic Data for $[H_3Os_3(CO)_8(PPh_2Et)(CCH_3)]$

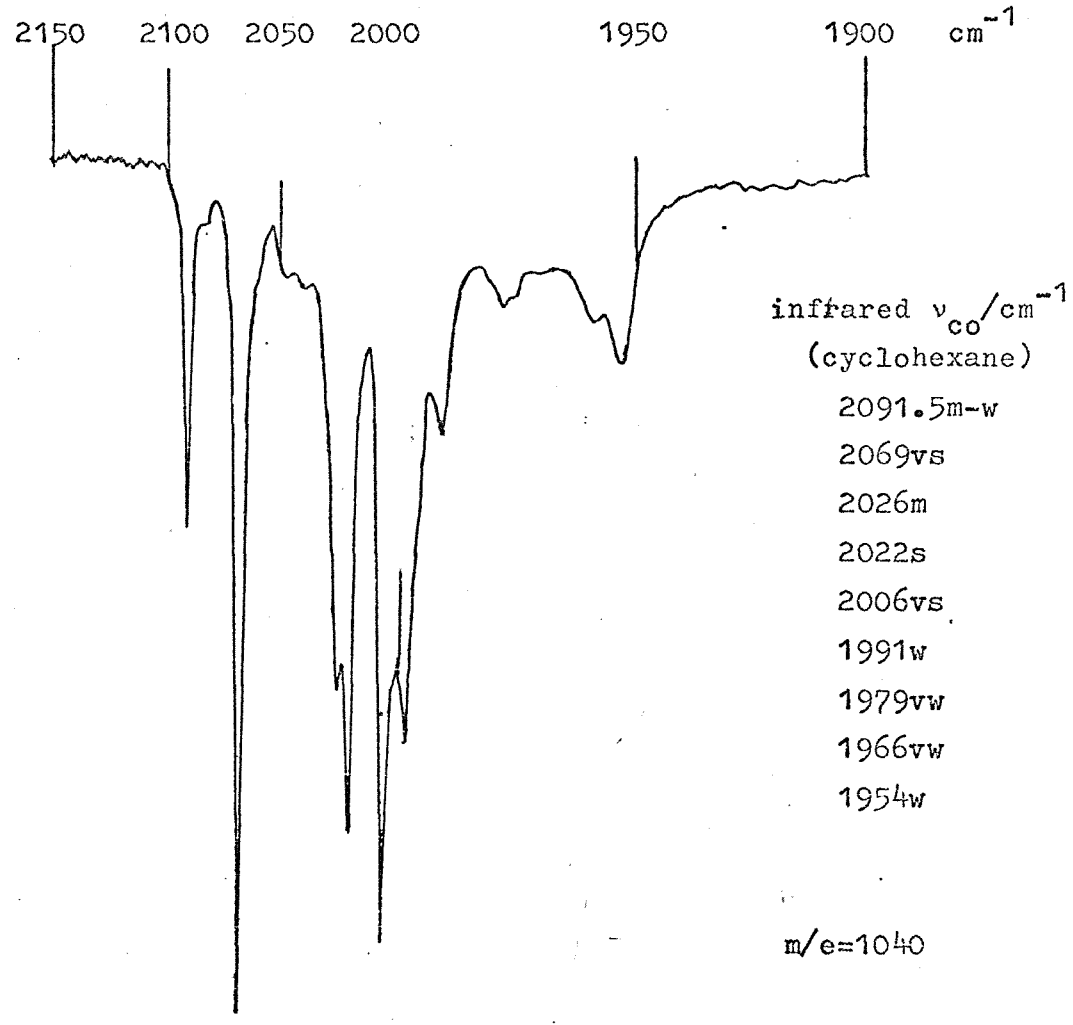


Table 5

^1H NMR data($CDCl_3$) for $[H_3Os_3(CO)_8(CCH_3)L]$, L=PPh_2Et or CO

$[H_3Os_3(CO)_8(PPh_2Et)(CCH_3)]$, 31°C					$[H_3Os_3(CO)_9(CCH_3)]$,(32)	
δ, (ppm)	Intensity	J_{PH} (Hz)	J_{HH}	Assignment	δ, (ppm)	Intensity
4.63(d)	3H	4.0		ethylidyne ligand	4.45(s)	3H
-18.03(d)	2H	11.8		bridging hydrides	-18.58(s)	3H
-18.76(s)	1H					
7.43(m)	10H			P-Ph		
2.60(q?)	2H	19.0	7.0	P-CH_2-C		
0.96(dt)	3H	19.0	7.0	P-C-CH_3		

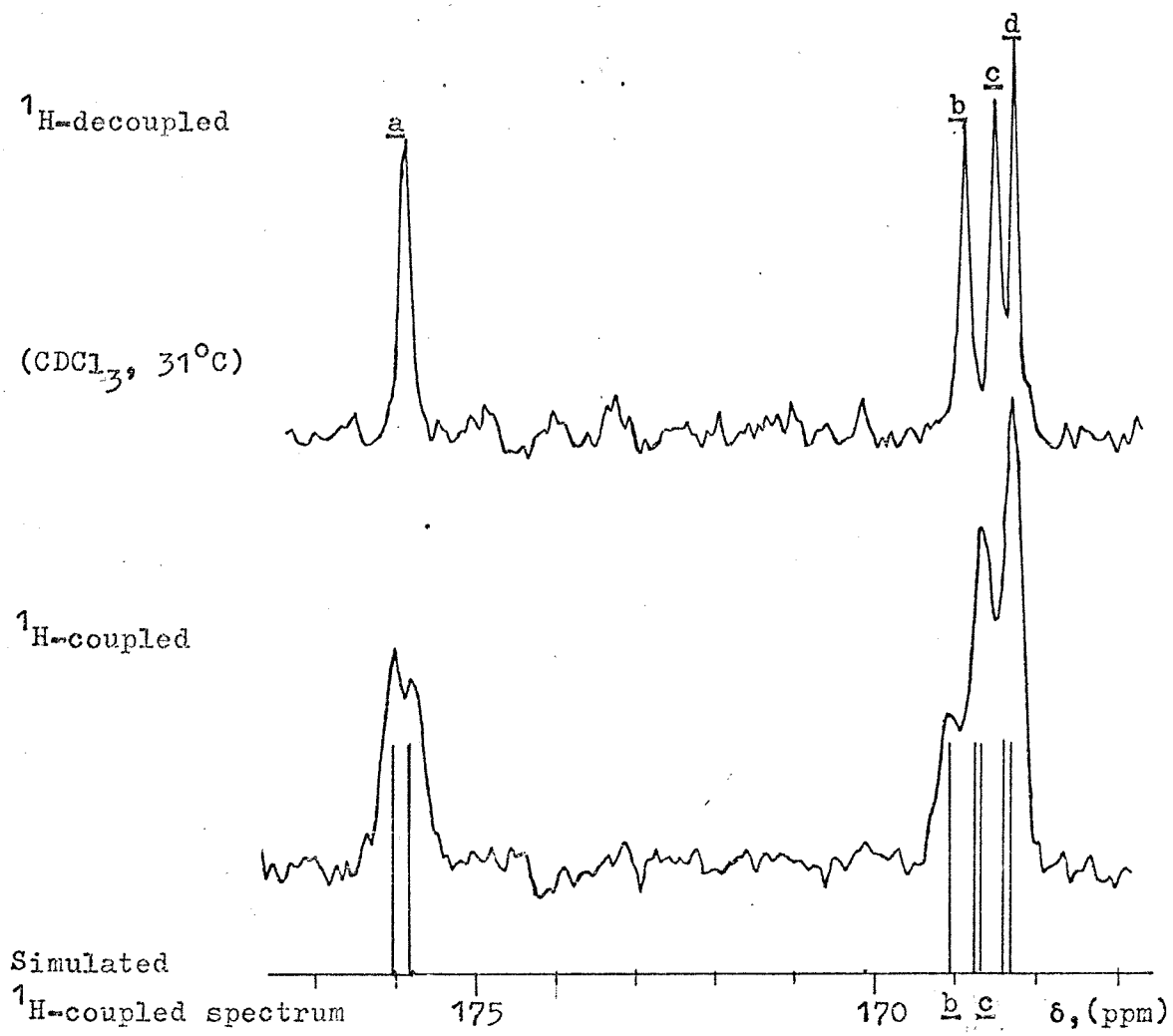
$(PPh_2Et)(CCH_3)]$, IX. A parent ion of m/e=1040 was seen in the mass spectrum followed by successive carbonyl fragmentation, complicated by hydride losses, and phosphine degradation. Elemental analysis also supported the required stoichiometry. The ν_{CO} region of the infrared spectrum contained vibrations representative of only terminal carbonyl groups.

The ^1H NMR spectrum ($CDCl_3$, 31°C) obtained at 100MHz contained all the anticipated phosphine resonances, and in addition a doublet (J_{PH}=4Hz) at 4.63 (3H) δ associated with the ethylidyne ligand. In the hydride region a doublet at -18.03 (J_{PH}=11.8Hz) δ and a singlet at -18.75δ were observed in a 2:1 intensity ratio. The authenticity of the doublet was confirmed by recording the spectrum with an operating radio-frequency of 200MHz which still gave the same frequency separation. The presence of the phosphine has lowered the molecular symmetry, from C_{3v} to C_s, so that the hydrides are no longer all equivalent generating two separate enviroments. With $\delta_{hydride}$(average)=-18.27, and accepting a slight deshielding caused by the phosphine, these characteristic signals are comparable to those of VIII (Table 5).

All this data infers that the phosphine has not altered the nature of reaction, with a direct analogue of VIII being formed with the structure shown in Diagram 13. This is further supported by a ^{13}C NMR study on a ^{13}CO enriched sample of IX. The ^1H-decoupled ($CDCl_3$, 31°C) spectrum shows four resonances at: a, 175.97; b, 169.03; c, 168.65 and d, 168.43 δ, of equal intensities associated with the carbonyl ligands. This is fully consistent with the anticipated limiting spectrum where the molecular symmetry creates separate enviroments each representing two equivalent carbonyls. The resonance a is noticeably broader than the rest and this is attributed to an unresolved ^{31}P-coupling, its large paramagnetic shift relative to the other resonances also implies that it represents the two groups bonded to the phosphine-substituted Os(1). Partial assignment of the remaining three signals is only possible on recording the ^1H-coupled spectrum. Here a shows a trans-coupling of 5Hz but, as in all cases, the anticipated smaller cis-coupling was not observed. The other signals are split into a complex overlapping pattern giving three resolved resonances at 169.16, 168.81 and 168.42 δ with relative intensities of 1.2.3. Analysis

Diagram 13

^{13}C NMR Spectra and Assignments for $[H_3Os_3(CO)_8(PPh_2Et)(CCH_3)]$



δ,(ppm)	Assignment	J_{CH}(Hz)
175.97	a	5.0
169.03	b	7.0
168.65	c	8.0
168.43	d	

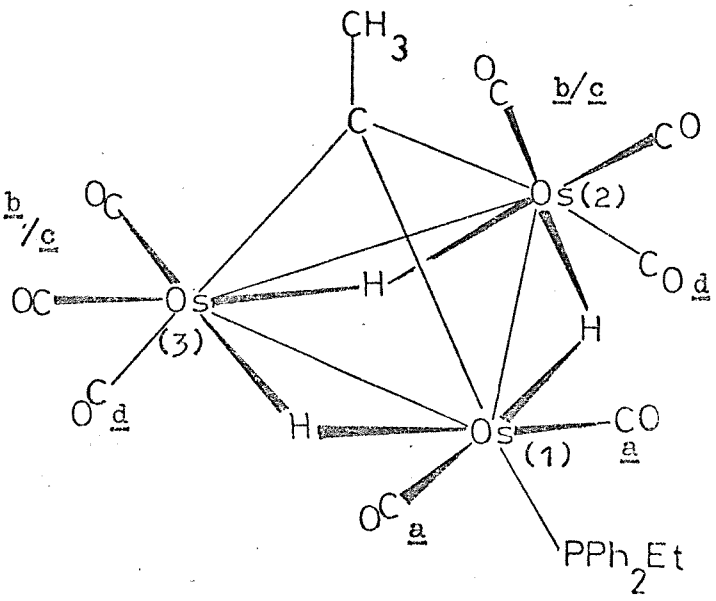
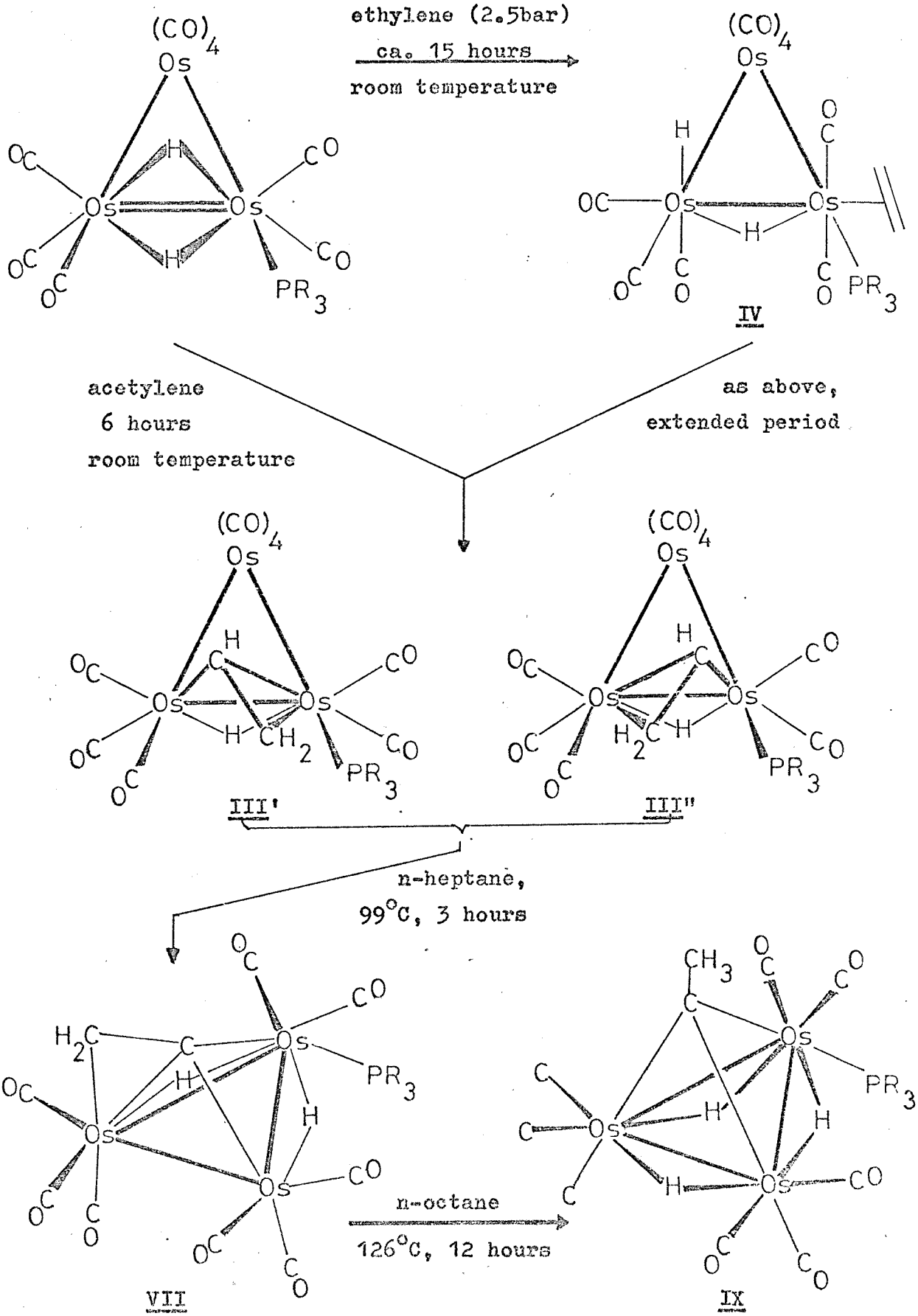


Diagram 14

Summary of established Reactions and isolated Products



of the spectrum reveals ^{1}H-couplings to b (7Hz) and c (8Hz) but not to d. On this basis d is assigned to the two carbonyls on Os(2) and Os(3) in axial sites. Then b and c correspond to the two inequivalent pseudo-equatorial positions on these osmiums where a trans-coupling would be anticipated. Unfortunately on this data alone it is not possible to unequivocally assign them individually.

3.6. Chapter Summary

The sequence depicted in Diagram 14 has been established. Phosphine substitution evidently does not drastically effect the chemistry of $[H_2Os_3(CO)_{10}]$. Thus $[H_2Os_3(CO)_9(PR_3)]$ derivatives react similarly with ethylene, isocyanides and acetylene. Subsequent pyrolysis of $[HOs_3(CO)_9(PPh_2Et)(CHCH_2)]$ and hydrogenation of $[H_2Os_3(CO)_8(PPh_2Et)(CCH_2)]$ also follow the expected pathways, although substitution does accelerate and retard these processes respectively. The major departure is the retarding of the reaction with ethylene to allow observation of the ethylene adducts $[H_2Os_3(CO)_9(PR_3)(C_2H_4)]$.

This catalogue of homogeneous adducts provides an excellent basis from which to assign silica-supported variants produced under ethylene hydrogenation conditions using $[H_2Os_3(CO)_9(PPh_2CH_2CH_2SIL)]$ as catalyst:- see Chapter Five.

3.7. Experimental Section

$[HOs_3(CO)_9(PPh_2Et)(CHCH_2)]$

$[H_2Os_3(CO)_9(PPh_2Et)]$(0.1088g) was dissolved in n-hexane (100ml) and acetylene, previously passed through a concentrated H_2SO_4 trap and a second at -78°C, was bubbled gently through for 6 hours. Over this time the solution slowly became deep yellow in appearance. After the solvent had been removed under reduced pressure the residue was chromatographed with n-hexane to give a single broad band. This yielded $[HOs_3(CO)_9(PPh_2Et)(CHCH_2)]$(0.1104g, 99%) as an orange, crystalline compound after recrystallisation from n-pentane.

Elemental Analysis	Cald. C 28.20% H 1.80%
MW=1064.99g.mol^{-1}	Obsd. C 29.04% H 1.60%

The corresponding $P(OMe)_3$, IIIb, and PPh_3, IIIc, adducts were prepared in an analogous manner but with suitable modification of the reaction time.

For IIIc:-

Elemental Analysis	Cald. C 31.29% H 1.72%
MW=1113.04g.mol^{-1}	Obsd. C 29.72% H 1.80%

$[H_2Os_3(CO)_9(PPh_3)(C_2H_4)]$

$[H_2Os_3(CO)_9(PPh_3)]$(0.0530g) was dissolved in n-hexane (40ml) and charged to a 100ml Roth autoclave, which was then flushed and pressurised to 6bar with ethylene. On commencing agitation this fell to a working pressure of 2.5bar and the solution was left stirring overnight (ca. 15 hours) at room temperature. After discharging, the solvent was removed on a rotary evaporator to leave a yellow residue. Extraction of a small amount of impurity, mainly IIIc, gave $[H_2Os_3(CO)_9(PPh_3)(C_2H_4)]$(0.0524g) as a yellow, crystalline solid; yield=96%.

Elemental Analysis	Cald. C 31.24% H 1.90%
MW=1115.05g.mol^{-1}	Obsd. C 31.82% H 1.56%

MeNC

This was prepared by the method of Casanova et. al.(52). N-methylformamide(15.0g, 0.25mol) was added dropwise, over a 10 minute period, to a stirred solution of toluene-p-sulphonyl chloride(72.5g, 0.38mol) and quinoline(129g, 1.00mol) at ca. 75°C under vacuum of a water pump. The product, methyl isocyanide, distilled rapidly and was collected in a liquid nitrogen trap. It was characterised from a liquid film infrared spectrum, ν_{NC}= 2170cm^{-1} (lit. 2166cm^{-1}) and used without further purification.

$[H_2Os_3(CO)_9(PPh_2Et)(CNMe)]$

A stoichiometric quantity of MeNC(30ul) was added to a solution of $[H_2Os_3(CO)_9(PPh_2Et)]$(0.0466g) in n-hexane(30ml). An immediate colour change occurred and on leaving to stir for 15 minutes a light yellow precipitate formed. This was filtered off, washed with fresh solvent, and dried under vacuo. It was identified as $[H_2Os_3(CO)_9(PPh_2Et)(CNMe)]$(0.0449g) by conventional spectroscopic techniques; yield=93%.

Elemental Analysis	Cald. C 27.80%	H 1.87%	N 1.30%
MW=1080.00g.mol^{-1}	Obsd. C 30.10%	H 1.45%	N 1.30%

[$H_2Os_3(CO)_8(PPh_2Et)(CCH_2)$]

A solution of [$HOs_3(CO)_9(PPh_2Et)(CHCH_2)$] dissolved in n-heptane(60ml) was heated under reflux for 3 hours, during which time the solution lightened in colour to an eventual pale yellow. The solvent was removed under reduced pressure and the residue chromatographed, using n-hexane/Et_2O(5:1v/v) as eluant, to give [$H_2Os_3(CO)_8(PPh_2Et)(CCH_2)$]($R_f$=0.55) as the major product.

Elemental Analysis	Cald. C 27.80%	H 1.85%	
MW=1036.98g.mol^{-1}	Obsd. C 27.63%	H 1.52%	

[$H_3Os_3(CO)_8(PPh_2Et)(CCH_3)$]

A sample of [$H_2Os_3(CO)_8(PPh_2Et)(CCH_2)$] was dissolved in n-octane(50ml) and hydrogen bubbled through the solution, heated at reflux, for 12 hours. Removal of the solvent followed by chromatography, using n-hexane/Et_2O(5:1v/v) as eluant, gave [$H_3Os_3(CO)_8(PPh_2Et)(CCH_3)$]($R_f$=0.64), quantitatively from an infrared trace of the reaction, as a colourless crystalline solid.

Elemental Analysis	Cald. C 27.74%	H 2.04%	
MW=1039.00g.mol^{-1}	Obsd. C 27.93%	H 1.92%	

3.8. References

1. A.J.Deeming, S.Hasso and M.Underhill, J.C.S. Dalton, 1975, 1614.
2. J.B.Keister and J.R.Shapley, J. Organometallic Chem., 1975, 85, C29.
3. A.G.Orpen, D.Pippard, G.M.Sheldrick and K.D.Rouse, Acta Cryst., 1978, B34, 2466.
4. E.Sappa, A.Tiripicchio and A-M.Manotti Lanfredi, J. Organometallic Chem., 1983, 249, 391.
5. J.J.Guy, B.E.Reichert and G.M.Sheldrick, Acta Crystal., 1976, B32, 3319.
6. W.G.Jackson, B.F.G.Johnson, J.W.Kellard, J.Lewis and K.T.Schropp, J. Organometallic Chem., 1975, 87, C27.
7. J.R.Shapley, S.I.Richter, M.Tachikawa and J.B.Keister, J. Organometallic Chem., 1975, 94, C43.

8. J.B.Keister and J.R.Shapley, J. Amer. Chem. Soc., 1976, 98, 1056.
9. B.F.G.Johnson, J.Lewis and D.Pippard, J. Organometallic Chem., 1978, 160, 263.
10. A.J.Deeming and S.Hasso, J. Organometallic Chem., 1976, 114, 313.
11. R.P.Ferrari, G.A.Vaglio and M.Valle, Inorg. Chim. Acta, 1978, 31, 177.
12. A.G.Orpen, A.V.Rivera, E.G.Bryan, D.Pippard, G.M.Sheldrick and K.D.Rouse, J.C.S. Chem. Comm., 1978, 723.
13. R.E.Benfield, B.F.G.Johnson, J.Lewis, P.R.Raithby, C.Zuccaro and K.Henrick, Acta Cryst., 1979, B35, 2210.
14. P.D.Gavens and M.J.Mays, J.Organometallic Chem., 1978, 162, 389.
15. M.J.Mays and P.D.Gavens, J.C.S. Dalton, 1980, 911.
16. B.F.G.Johnson, J.Lewis, B.E.Reichert and K.T.Schorpp, J.C.S. Dalton, 1976, 1403.
17. a) J.R.Shapley, A.C.Sievert, M.R.Churchill and H.J.Wasserman, J. Amer. Chem. Soc., 1981, 103, 6975.
b) G.McNulty, private communication.
18. J.Evans, private communication.
19. S.C.Brown and J.Evans, J.C.S. Dalton, 1982, 1049.
20. J.Banford, First Year Dissertation, Trinity College Cambridge, 1980.
21. C.A.Tolman, Chem. Rev., 1977, 77, 313.
22. B.F.G.Johnson, J.Lewis and D.A.Pippard, J. Organometallic Chem., 1981, 213, 249.
23. B.F.G.Johnson, J.Lewis, D.Pippard and P.R.Raithby, J.C.S. Chem. Comm., 1978, 551.
24. B.F.G.Johnson, J.Lewis and D.A.Pippard, J.C.S. Dalton, 1981, 407.
25. J.Evans, B.P.Gracey and M.Webster, unpublished results.
26. Z.Dawoodi, M.J.Mays, P.R.Raithby and K.Henrick, J.C.S. Chem. Comm., 1980, 641.
27. Z.Dawoodi, K.Henrick and M.J.Mays, J.C.S. Chem. Comm., 1982, 696.
28. A.J.Deeming and S.Hasso, J. Organometallic Chem., 1975, 88, C21.
29. a) R.Cramer, J. Amer. Chem. Soc., 1964, 86, 217.
b) R.Cramer, J.B.Kline and J.D.Roberts, J. Amer. Chem. Soc., 1969, 91, 2519.
30. R.D.Adams and N.M.Golembeski, J. Amer. Chem. Soc., 1979, 101, 2579.
31. R.D.Adams and N.M.Golembeski, Inorg. Chem., 1979, 18, 1909.

32. S.C.Brown, First Year Dissertation, Southampton, 1978.
33. S.C.Brown and J.Evans, J.C.S. Chem. Comm., 1978, 1063.
34. J.J.DeBoer, J.A.Van Doorn and C.Masters, J.C.S. Chem. Comm., 1978, 1005.
35. R.F.Hudson, Angew. Chem., Int. Ed. Engl., 1973, 12, 36.
36. M.Elian and R.Hoffmann, Inorg. Chem., 1975, 14, 1058.
37. J.C.Green, D.M.P.Mingos and E.A.Seddon, Inorg. Chem., 1981, 20, 2595.
38. A.J.Deeming and M.Underhill, J.C.S. Dalton, 1974, 1415.
39. R.Jackson, B.F.G.Johnson, J.Lewis, P.R.Raithby and S.W.Sankey, J. Organometallic Chem., 1980, 193, C1.
40. A.J.Deeming and M.Underhill, J. Organometallic Chem., 1972, 42, C60.
41. A.J.Deeming and M.Underhill, J.C.S. Chem. Comm., 1973, 277.
42. W.G.Jackson, B.F.G.Johnson and J.Lewis, J. Organometallic Chem., 1975, 90, C13.
43. J.Evans, B.F.G.Johnson, J.Lewis and T.W.Matheson, J. Organometallic Chem., 1975, 97, C16.
44. J.Banford, private communication.
45. A.J.Canty, B.F.G.Johnson, J.Lewis and J.R.Norton, J.C.S. Chem. Comm., 1972, 1331.
46. A.D.Buckingham, J.P.Yesinowski, A.J.Canty and A.J.Rest, J. Amer. Chem. Soc., 1973, 95, 2732.
47. G.M.Sheldrick and J.P.Yesinowski, J.C.S. Dalton, 1975, 873.
48. J.P.Yesinowski and D.Bailey, J. Organometallic Chem., 1974, 65, C27.
49. a) K.S.Wong, K.J.Haller, T.K.Dutta, D.M.Chipman and T.P.Fehlner, Inorg. Chem., 1982, 21, 3197.
b) R.L.DeKock, K.S.Wong and T.P.Fehlner, Inorg. Chem., 1982, 21, 3203.
50. K.S.Wong and T.P.Fehlner, J. Amer. Chem. Soc., 1981, 103, 966.
51. D.E.Sherwood,Jnr. and M.B.Hall, Organometallics, 1982, 1, 1519.
52. J.Casanova, R.Schuster and N.D.Werner, J. Chem. Soc., 1963, 4280.

CHAPTER FOUR

THE PYROLYSIS OF $[Os_3(CO)_{11}(PPh_2Et)]$: FULL CHARACTERISATION OF $[Os_3(CO)_9(PEt)(C_6H_4)]$

In any investigation involving possible catalytic properties of (supported) metal clusters an account of any loss of activity (or vice versa) at the elevated temperatures used, arising from modification of the original species, is necessary. Accordingly a study into the pyrolysis of $[Os_3(CO)_{11}(PPh_2Et)]$, Ia, as the homogeneous analogue to the silica supported species $[Os_3(CO)_{11}(PPh_2CH_2CH_2SIL)]$, was undertaken to compliment the results to be reported in Chapter Five. Before describing this work a survey covering the thermolysis of related triosmium complexes, principally $[Os_3(CO)_{12}]$ and its mono-substituted derivatives, will be given. These produced a multitude of novel complexes which at first sight bear little relationship to one another. However, as the depth of published data increased several underlying trends became evident and to a degree it is possible to rationalise the chemistry.

4.1. Thermolysis of $[Os_3(CO)_{12}]$ and its Substituted Derivatives

The formation of higher nuclearity cluster compounnds (HNCC) is favoured at elevated temperatures, probably because of the endothermic nature of most condensation reactions. The positive values of ΔH result from the substitution of stronger metal-to-carbon monoxide bonds by weaker metal-metal bonds. Further, on descending a sub-group the relative increase in the average metal-metal bond energy enhances their stability and therefore an abundance of HNCC are found for osmium. Pyrolysis of $[Os_3(CO)_{12}]$, in a sealed tube at 210°C, gives a dark brown, highly crystalline solid. Extraction into ethyl acetate, followed by chromatographic separation, produced a number of air-stable metal carbonyl complexes. One of these corresponded to a small amount of unchanged $[Os_3(CO)_{12}]$, whilst the remainder were polynuclear carbonyls based on units of five to eight osmium atoms(1). The major product was $[Os_6(CO)_{18}]$(80%) accompanied by $[Os_5(CO)_{16}]$(7%), $[Os_7(CO)_{21}]$(10%) and $[Os_8(CO)_{23}]$(2%). Single crystal X-ray diffraction studies on the first three compounds has shown them to have structures with bicapped tetrahedral(2), trigonal bipyramidal(3) and capped octahedral geometries respectively for the metal atoms with all

carbonyl ligands terminally coordinated. At 250°C the distribution moves towards $[Os_7(CO)_{21}]$(20%) and $[Os_8(CO)_{23}]$(8%), with the disappearance of $[Os_5(CO)_{16}]$. These higher temperatures also allow the necessary disproportionation of carbon monoxide to give the carbides $[Os_5(CO)_{15}C]$(5%) and $[Os_8(CO)_{21}C]$(8%). Good yields (40%) of $[Os_5(CO)_{15}C]$ are also obtained from the direct pyrolysis of $[Os_6(CO)_{18}]$ in an evacuated Carius tube at 255°C(5).

From these results it is apparent that the size of the clusters produced increases with temperature until in the limiting case(260°C) total conversion to osmium metal is observed. Indeed at these greater temperatures traces of the dianion $[Os_{10}(CO)_{24}C]^{2-}$ can be isolated from the insoluble residues, although in vacuo pyrolysis of $[Os_3(CO)_{11}(pyridine)]$ at 250°C gives far superior (ca. 80%) yields(6). Since ionic species are not usually observed in these reactions, it is likely that a neutral carbonyl hydride is originally formed which then dissociates in the polar solvents used for extraction to give the charged cluster. The presence of the pyridine ligand, which can function as a hydrogen source, would then be expected to be more efficient than $[Os_3(CO)_{12}]$, where the hydrogen must come from minute quantities of water present on the glass of the Carius tube itself. This is supported by the characterisation of $[H_nOs_{10}(CO)_{24}C]^{(2-n)-}$, n=1 or 2, from acidification of the dianion with concentrated H_2SO_4(7). The product isolated depends on the basicity of the solvent employed. X-ray analysis of the hydrido-monoanion shows a close-packed carbonyl distribution virtually identical to that of the dianion, the hydride appears to occupy an interstitial tetrahedral site. Significantly, whilst it is stable in non-coordinating solvents, in THF, MeCN, MeOH or H_2O deprotonation readily takes place regenerating the dianion.

This conveniently introduces the possibility of an extra ligand source altering the product distribution by stabilising polyhedra otherwise unfavoured in their absence. Thus, in the presence of small traces of water pyrolysis of $[Os_3(CO)_{12}]$ at 230°C gives a greater range of products. Apart from those already reported, and others previously obtained during the preparation of $[Os_3(CO)_{12}]$ or its reaction with $NaBH_4$(8), a series of HNCC hydrido species $[H_2Os_5(CO)_{16}]$, $[H_2Os_5(CO)_{15}]$, $[H_2Os_6(CO)_{18}]$

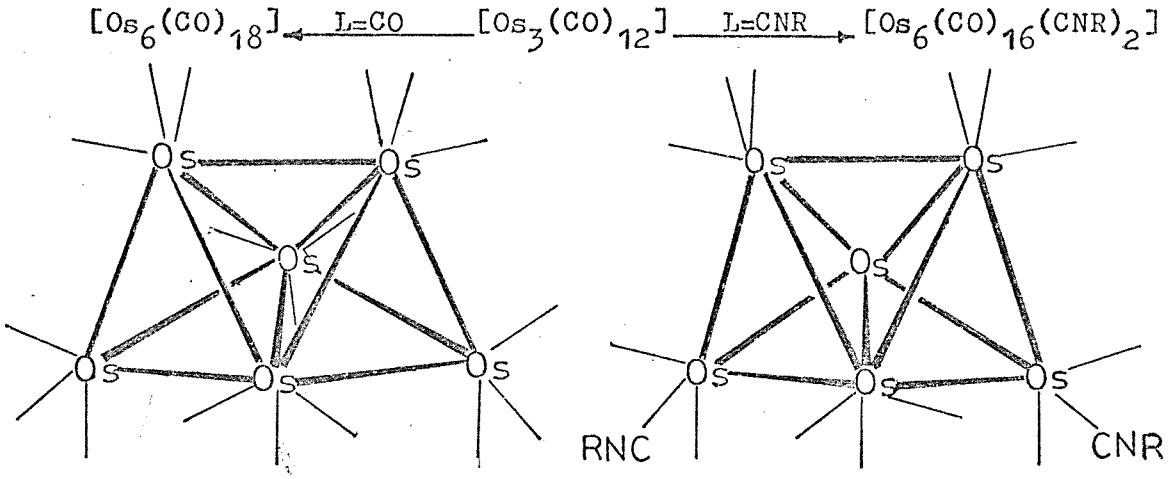
and $[H_2Os_7(CO)_{19}C]$ were also identified(9).

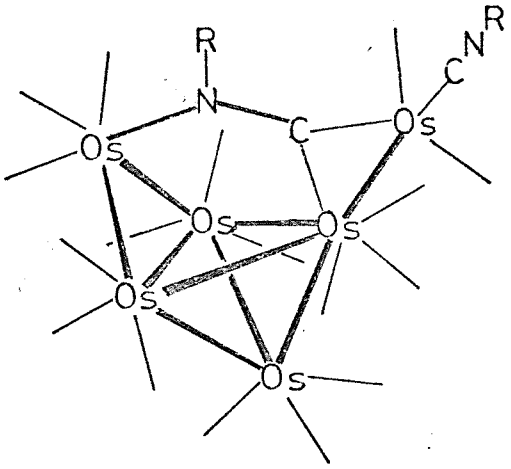
The decanuclear carbide dianion is also isolated (yield=63%) from the stoichiometric combination of $[Os_3(CO)_{12}]$ and sodium in tetraglyme(230-260°C)(10). Infrared spectra of the reaction mixture indicated intermediate formation of $[Os_6(CO)_{18}]^{2-}$, whereas in the other preparation(6) the isolated yield of $[HOs_5(CO)_{15}]^-$ decayed with buildup of $[Os_{10}(CO)_{24}C]^{2-}$. Amongst the products obtained from thermolysis of $[Os_3(CO)_{12}]$ in isobutanol(108°C) is the first non-carbido decaosmium cluster $[H_4Os_{10}(CO)_{24}]^{2-}$(11), which is very similar in structure to the carbido-anion but with the expected contraction of the tetracapped central octahedral Os_6 unit.

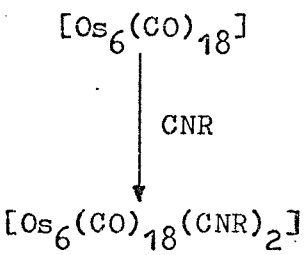
The partial substitution of carbonyl by isocyanide ligands greatly facilitates the condensation reactions. Pyrolysis of $[Os_3(CO)_{11}(CNBu^t)]$, at the significantly lower temperature of 125°C in n-octane, gives $[Os_6(CO)_{18-n}(CNBu^t)_n]$, n=2 or 3, in approximately equal quantities with an overall yield of 60%. Similarly $[Os_3(CO)_{10}(CNBu^t)_2]$ led to the isolation of $[Os_6(CO)_{18-n}(CNBu^t)_n]$, n=3 or 4. In both cases, even after 24 hours, there was no evidence for ligand fragmentation and the hexanuclear complexes, together with some starting material, are the only osmium containing products which are present in solution(12). Direct reaction of $[Os_3(CO)_{12}]$ with a two-fold excess of isocyanide, MeNC or t-BuNC, under these milder conditions gave a broader range $[Os_6(CO)_{18-n}(CNR)_n]$, n=1 to 5. Further increasing the ratio of reactants, or higher temperatures, caused excessive decomposition to osmium metal(13). The crystal structure of $[Os_6(CO)_{16}(CNBu^t)_2]$(14) is derived from that of $[Os_6(CO)_{18}]$ by replacement of one carbonyl group on each of the capping osmiums by a terminal isocyanide ligand. This attachment to the centres of lowest coordination is consistent with steric considerations. The substitution has little effect on the bond-lengths in the central tetrahedron, but causes a slight lengthening of the Os-Os bonds involving the capping metals. Since it is believed that the initial step in these reactions involves fragmentation of the metal triangle, these results would seem to indicate a destabilising effect of the isocyanide on the metal-metal bonds or, alternatively, it may reflect the stability of some

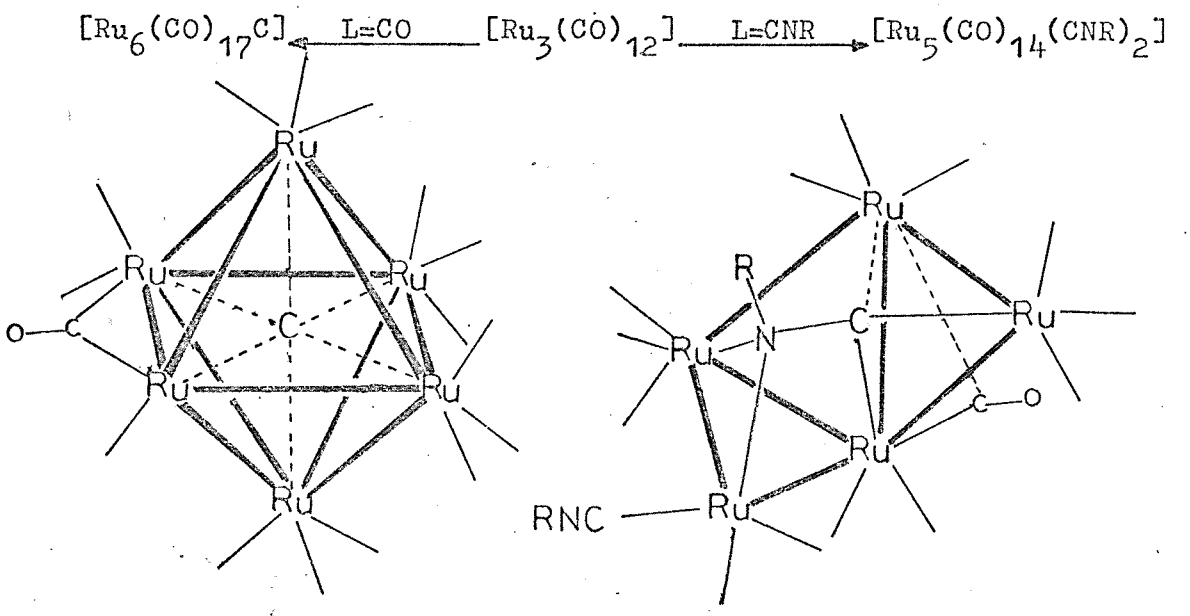
Diagram 1

Effect of Isocyanide Substitution on the Pyrolysis of $[M_3(CO)_{12}]$, M=Os or Ru.









intermediate. Then it is somewhat surprising that no $[Os_6(CO)_{18}]$ was identified which, coupled with the narrow distribution obtained from the substituted trinuclear clusters, implies that total breakdown to mononuclear units does not occur. The pathway is also not via isocyanide dissociation, followed by substitution of preformed $[Os_6(CO)_{18}]$, since an independent study isolated $[Os_6(CO)_{18}(CNPh)_2]$ from the direct reaction of isocyanide with $[Os_6(CO)_{18}]$ (Diagram 1). An X-ray structural analysis(15) confirmed the presence of an unusually bonded isocyanide where the nitrogen bridges across two osmiums while the carbon bonds to a third. The ligand is thus acting as a four electron donor, so in total six more electrons are available relative to $[Os_6(CO)_{18}]$, or $[Os_6(CO)_{16}(CNBu^t)_2]$, and this is compensated by there being three fewer metal-metal bonds. The central tetrahedron is retained but one previously capping atom now bridges one edge of the tetrahedron while the other, coordinated by the conventional isocyanide ligand, is terminally bound to another vertex. The novelly bonded isocyanide spans these two osmiums.

Pyrolysis of the corresponding aryl-isocyanide (p-$MeOC_6H_4NC$ and PhNC) derivatives gave more complex mixtures and preliminary data(13) indicated a range of nuclearity products coupled with increased ligand interaction with the metal skeleton. This introduces a second pathway for thermolysis reactions whereby further involvement of the substituent ligands with the core, via fragmentation or metallation, can affect the degree of increased nuclearity or even preclude it. This is aptly demonstrated by the analogous ruthenium systems. The only HNCC obtained from heating $[Ru_3(CO)_{12}]$ under reflux in anhydrous di-n-butylether(140°C) is $[Ru_6(CO)_{17}C]$(16), although coproduction of $[H_4Ru_4(CO)_{12}]$ and $[H_2Ru_4(CO)_{13}]$ normally results from traces of water present(9). For a second row element the presence of a central carbide atom, lending a significant contribution to the bonding energy of the cluster, appears necessary to prevent total decomposition to ruthenium metal. Other non-carbido containing hexaruthenium clusters can be prepared, but by the different method of base reduction of $[Ru_3(CO)_{12}]$ followed by acidification (17). In comparison, moderate heating of $[Ru_3(CO)_{11}(CNBu^t)]$ at 120°C, 16 hours, affords reasonable yields of $[Ru_5(CO)_{14}(CNBu^t)_2]$

(18). The five metal atoms form a swallow-shaped cluster. Although one isocyanide is terminally coordinated, the second spans the molecule donating six electrons being formally bonded to four ruthenium and semi-bridging through the carbon to the fifth.

This progression is continued with phosphites but, instead of increased metallation at the expense of ligand multiple bonds, P-O and C-O bonds are cleaved to produce several interesting ligand moieties. A red-brown solid results from the pyrolysis of $[Os_3(CO)_{11}(P(OMe)_3)]$ at 210°C, in vacuo, in a sealed vessel. Extensive chromatography produced a series of penta-osmium, phosphorus containing, clusters. Four of these have been fully characterised by X-ray analysis as $[Os_5(CO)_{15}(POMe)]$, II, (19); $[Os_5C(CO)_{14}H(OP(OMe)_2)]$, III, (20); $[Os_5C(CO)_{13}H(OP(OMe).OP(OMe)_2)]$, V, (21); and $[Os_5C(CO)_{13}H(OP(OMe)_2)(P(OMe)_3)]$, IV, (22) (Diagram 2). They can be separated into two sets representing different degradation pathways under the harsh reaction conditions.

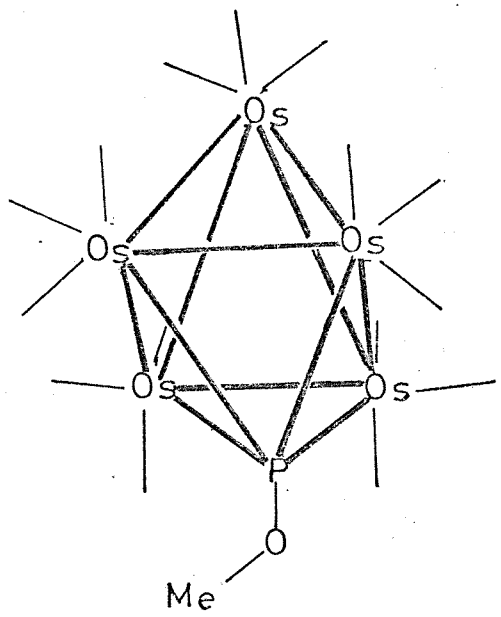
The series of complexes III, IV and V, which are all 76 electron clusters, define a stepwise substitution of a carbonyl group on a cluster by a phosphite ligand followed by ligand rearrangement to give the observed ligand linking three metal atoms via two phosphorus and one oxygen atom. In III the metal atoms form a distorted trigonal bipyramid and the carbide lies in the equatorial plane coordinating to all five osmiums. Two edges are sufficiently extended to preclude any metal-metal interaction. The phosphonate ligand, which acts as a three electron donor, coordinates to two osmium atoms forming an Os-P-O-Os chain. In IV the incoming phosphite substitutes a carbonyl group on the metal coordinated to the phosphonate oxygen atom. This adjacent position to the phosphorus-bonded osmium participating in the Os-P-O-Os bridge may be important when rearrangement to form the second P-O bond in V occurs to give the complex Os-P-O-P(Os)-O-Os arrangement. The metal skeleton remains unaltered throughout these transformations. Unfortunately the low yields and harsh conditions prohibited the establishment of whether pyrolysis of IV gives V. If this progression was substantiated it would infer intermediate phosphite dissociation from an osmium before recombination with the higher nuclearity III.

The complex II is formally a 74 electron cluster and

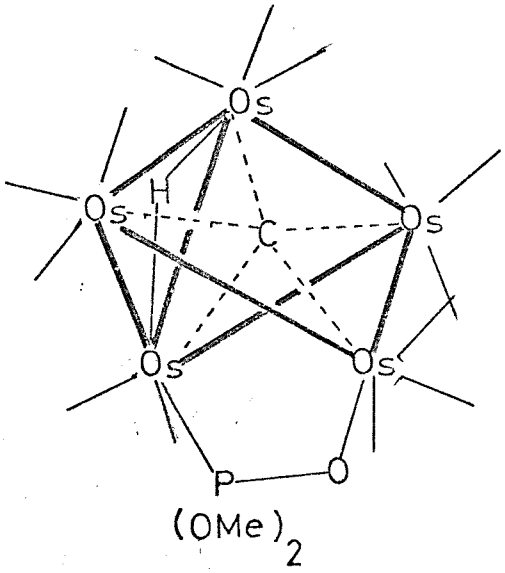
Diagram 2

Crystal Structures for the Products from Pyrolysis of $[Os_3(CO)_{11}(P(OMe)_3)]$

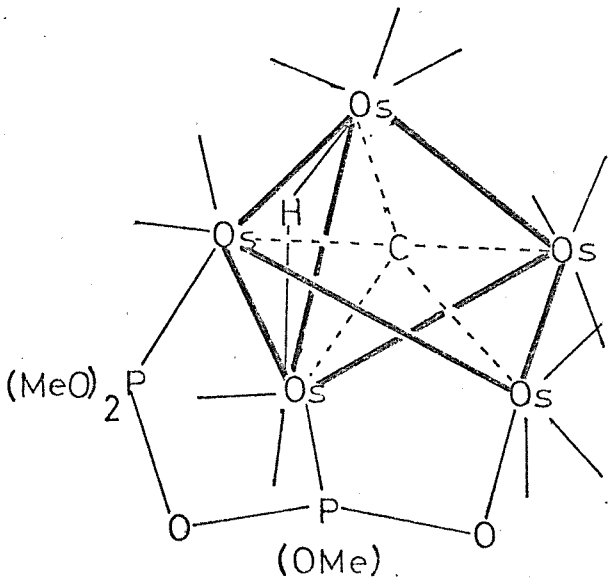
$[Os_5(CO)_{15}(POMe)]$, II



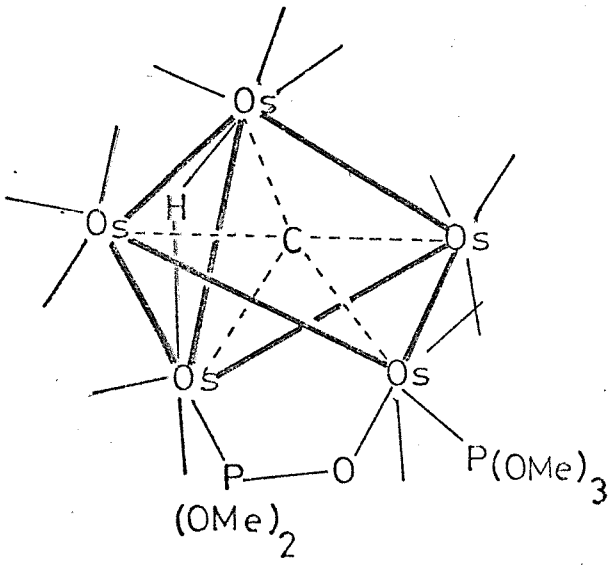
$[Os_5C(CO)_{14}H(OP(OMe)_2)]$, III



$[Os_5C(CO)_{13}H(OP(OMe).OP(OMe)_2)]$, V



$[Os_5C(CO)_{13}H(OP(OMe)_2).(P(OMe)_3)]$, IV



(The hydrides were not located directly)

bears less resemblance to the other three compounds, but illustrates another degradation product of the phosphite ligand at the high temperatures employed. The metal atoms adopt a square-pyramidal geometry. The phosphinato group, which acts as a 4 electron donor, lies below the basal Os_4 plane and bonds (fairly) symmetrically to all four metals. Each osmium is also bonded to three terminal carbonyl groups so that all five metals are seven coordinate. The ruthenium analogue $[Ru_5(CO)_{15}(PR)]$, R=Ph, Me, Et or CH_2Ph, has also been prepared but by a different route. Prolonged reaction (48 hours) of $[(C_6H_5)(CO)_2Mn(PRCl_2)]$ with $[Ru_3(CO)_{12}]$, in refluxing toluene, results in its isolation as a green crystalline compound, as the only recovered pure complex apart from the starting materials(23). The manganese species clearly acts as a source of the phosphide as the related $[(CO)_5Cr(PRCl_2)]$, and even $PRCl_2$ itself, serve the same function although the yields are inferior.

All four structures are consistent with Wade theory(24) which predicts a square-pyramidal geometry for a 74 electron system with seven skeletal electron pairs. Then the geometry of the Os_5C core in III, IV and V is a consequence of breaking one metal-metal bond upon inclusion of two more electrons to give the distorted capped 'butterfly' metal framework. This is stabilised by the presence of the carbide, whereas the μ_4-phosphite performs a similar function in II. The observed distribution must reflect the relative ease of formation for the two groups since a ready source of the phosphinato-ligand, as with the ruthenium system, greatly affects the direction of reaction promoting non-carbide containing adducts. Indicative of the complex nature of reaction was the identification of the leading eluted band as a mixture of $[Os_3(CO)_{12}]$ and $[H_4Os_4(CO)_{12}]$. This suggests that breakdown followed by reclusterfication is the major route, with the degree of nuclearity governed by the stabilising influence of generated ligands. Clearly phosphites do not promote HNCC formation to the same extent as isocyanides but similarly activation of the ligand, principally through cleavage of P-O and C-O bonds, requires comparable temperatures as reflected in the observed products.

Activation of C-H and P-C bonds in tertiary phosphines is considerably more facile, and at lower temperatures, typically

150°C, a variety of adducts arise solely from oxidative addition of the addendum molecule. Presumably condensation is not competitive under these conditions, or the formed ligands have a synergic stabilising effect with the Os_3 unit preventing cluster reformation. Historically pyrolysis of $[Os_3(CO)_{10}(PPh_3)_2]$ was studied first, but in the guise of reacting $[Os_3(CO)_{12}]$ with a two-fold excess of PPh_3 in refluxing xylene(25). In addition to the anticipated mono-, di-, and tri-substituted derivatives, a series of six compounds were obtained resulting from metallation and/or fragmentation of the affixed phosphine ligands. All these retain two phosphorus moieties. Solution spectroscopy was not diagnostic and only one compound(IX) gave a parent ion in its mass spectrum. However recourse to X-ray diffraction methods(26,27) provided clear characterisation of $[HOs_3(CO)_9(PPh_3)(PPh_2C_6H_4)]$,VI; $[HOs_3(CO)_8(PPh_3)(PPh_2C_6H_4)]$,VII; $[Os_3(CO)_8(PPh_2)(Ph)(PPhC_6H_4)]$,VIII; $[Os_3(CO)_7(PPh_2)_2(C_6H_4)]$,IX; and $[HOs_3(CO)_7(PPh_2)(PPh_3)(C_6H_4)]$,X, (Diagram 3). Suitable crystals of the sixth compound were not obtained and consequently its true formula is not known but postulated as $[Os_3(CO)_8'(PPh_3)(PPh_2)']$,XI. Since these reactions are believed to be intramolecular in nature the products must result from pyrolysis of $[Os_3(CO)_{10}(PPh_3)_2]$ in preference to further substitution. This is borne out by the separate thermolysis of an isolated sample of $[Os_3(CO)_{10}(PPh_3)_2]$ where the same six compounds are formed with the addition of a seventh, $[HOs_3(CO)_7(PPh_2)(PPh_2C_6H_4C_6H_3)]$,XII, also fully characterised by a X-ray crystallographic study(27). This route must be concentration controlled as the combination of $[Os_3(CO)_{12}]$ with a large excess of PPh_3, under reflux in xylene, produced only $[Os_3(CO)_9(PPh_3)_3]$(28).

Mechanistic studies indicated that reaction occurs via the pathway outlined below. The yields of VI and VII decrease with

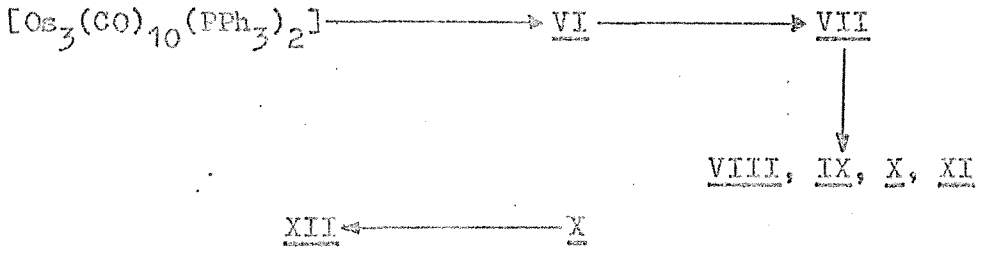
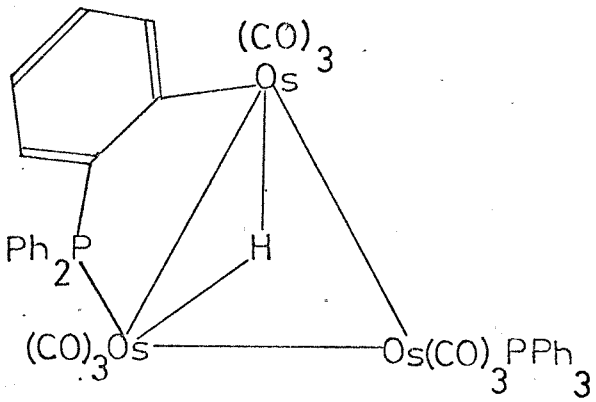
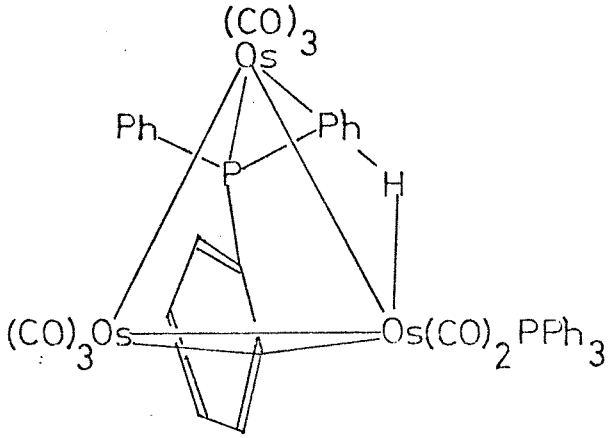


Diagram 3

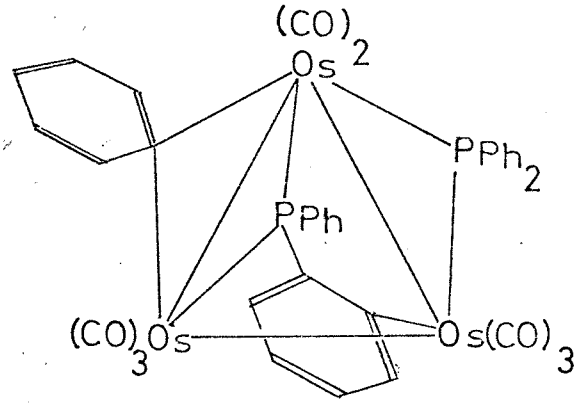
Crystal Structures for the Products from Pyrolysis of $[Os_3(CO)_{10}(PPh_3)_2]$



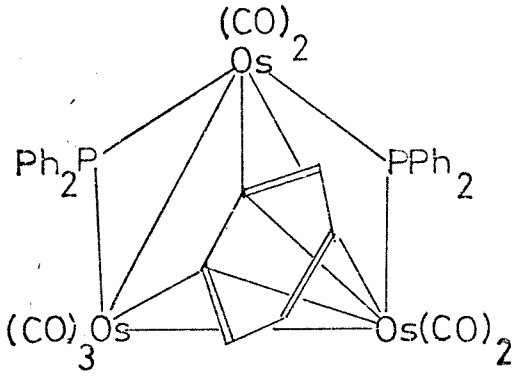
$[HOs_3(CO)_9(PPh_3)(PPh_2C_6H_4)]$, VI



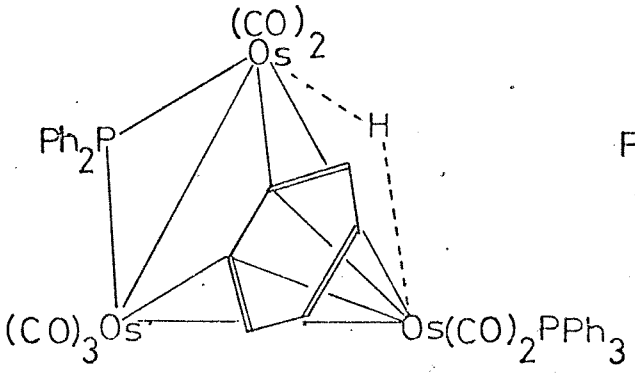
$[HOs_3(CO)_8(PPh_3)(PPh_2C_6H_4)]$, VII



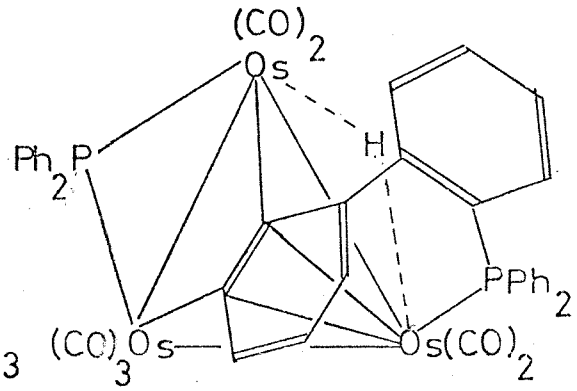
$[Os_3(CO)_8(PPh_2)(Ph)(PPhC_6H_4)]$, VIII



$[Os_3(CO)_7(PPh_2)_2(C_6H_4)]$, IX



$[HOs_3(CO)_7(PPh_2)(PPh_3)(C_6H_4)]$, X



$[HOs_3(CO)_7(PPh_2)(PPh_2C_6H_4C_6H_3)]$, XII

(The hydrides were not located directly)

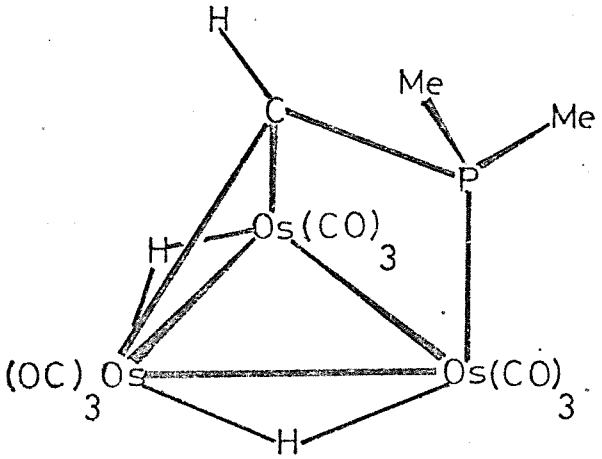
reaction time suggesting that the decomposition proceeds via these hydrides. This was confirmed by heating VII under similar conditions whence IX, XI and XII were identified in the reaction mixture. It appears that VI is first formed by ortho-metallation of a C-H bond of one PPh_3 ligand with a second osmium atom to form an Os-C bond and a five-membered chelate ring. Then loss of carbon monoxide forms VII, which in turns decomposes to VIII, IX, X and XI. Compound XII is probably derived from X by elimination of hydrogen from the benzyne ligand, and an ortho-C-H bond of the terminal phosphine ligand, with the formation of a C-C bond. The crystal structures (Diagram 3) display several interesting features including benzyne(ortho-phenylene) groups bridging three osmium atoms in IX, X and XII, a phenyl group bridging two osmium atoms in VIII, and the formation of a C-C bond, as described above, in XII.

The NMR spectra for these PPh_3 derivatives in the aromatic region were too complicated to be readily interpreted. However by reduction of the number of phenyl groups, both the number of products is reduced and simpler spectra provided more useful structural information. On heating $[Os_3(CO)_{11}(PPhMe_2)]$ under reflux in n-nonane the only product obtained is $[HOs_3(CO)_9(PMe_2)(C_6H_4)]$(29). The corresponding arsino-adduct can be similarly prepared and has been the subject of a X-ray study(30). The presence of a benzyne ligand had been established by ^1H NMR, but retention of the triangulo-(3Os-Os) framework required it to act as only a two electron donor to satisfy electron-counting rules. However the crystal structure showed an identical geometry to that found in the PPh_3-derivatives at the expense of a metal-metal bond. A similar pathway exists for reaction of alkyl-phenylsulphides with $[Os_3(CO)_{12}]$ where cleavage of the phenyl group from the sulphur atom occurs to give $[HOs_3(CO)_9(SR)(C_6H_4)]$ isolated in small yields(2.4%). A full X-ray diffaction study(31) established a methanethiolato group bridging the 'open' edge of the cluster and a triply-bridging benzyne inclined at an angle of 71.5° from the Os_3 plane.

The dimeric $[HOs_2(CO)_6(AsMe_2)(C_6H_4)]$ was also isolated from the thermolysis of $[Os_3(CO)_{11}(AsPhMe_2)]$. The same two products were obtained, in conjunction with $[Os_3(CO)_7(AsMe_2)_2C_6H_4)]$,

from the pyrolysis of $[Os_3(CO)_{10}(AsPhMe_2)_2]$. In contrast, $[Os_3(CO)_{10}(PPhMe_2)_2]$ gives only trimetallic products retaining both original phosphorus atoms. Thus in refluxing n-nonane $[Os_3(CO)_7(PMe_2)_2(C_6H_4)]$, isostructural to IX, and $[HOs_3(CO)_8(Me_2PC_6H_4C_6H_3)(PMe_2)]$ are isolated, whilst at lower temperatures in n-octane $[HOs_3(CO)_8(PPhMe_2)(PMe_2)(C_6H_4)]$ is the only product. The first stage in these reactions is believed to be ligand dissociation from the coordinatively saturated starting material before activation of an ortho-aryl C-H bond can occur. The difference in products can then be rationalised since an arsine will be more weakly bound than a phosphine and can dissociate in competition with carbon monoxide.

Clearly activation of an α-alkyl C-H bond is less facile but, in the absence of an available phenyl group, does occur so that degradation of $[Os_3(CO)_{11}(PMe_3)]$, under reflux in n-nonane, gives high yields (ca. 60%) of $[H_2Os_3(CO)_9(Me_2CHP)]$(32). The structure shown is favoured without support of an X-ray study.



Structure of
$[H_2Os_3(CO)_9(Me_2CHP)]$

The basic interaction between the Me_2PCH group and the metal atoms is almost certainly through σ-Os-C bonds to two osmiums with a donor interaction between the phosphorus atom and the third. With the corresponding PEt_3 analogue the possibility of activating the hydrogens on the β-carbon exists, but the spectroscopic evidence unambiguously shows dehydrogenation at the α-methylene group to give the Et_2PCMe ligand. With complexes containing one metal atom five-membered ring formation is favoured(33), and as in either

case the β-methyl lies much closer to the metal than the α-methylene, so here electronic rather than steric reasons appear the controlling factor. From $[Os_3(CO)_{10}(PR_3)_2]$, R=Me or Et, related products are obtained with only one phosphine dehydrogenated; with the PMe_3 adduct two isomers were identified and assigned to the unchanged ligand occupying different coordination sites on the same metal atom. The extra phosphine is positioned on the osmium bonded to both hydrogens on the basis of ^1H NMR coupling patterns.

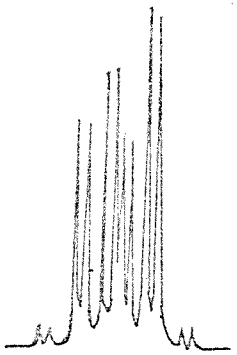
4.2. Pyrolysis of $[Os_3(CO)_{11}(PPh_2R)]$; R=Me, Et or Ph.

The principle aim of this study was to investigate the behaviour of $[Os_3(CO)_{11}(PPh_2Et)]$, Ia, as the homogeneous analogue of $[Os_3(CO)_{11}(PPh_2CH_2CH_2SIL)]$, at raised temperatures. However, because of their relevance in establishing the universal nature of the following reaction, the corresponding PPh_2Me, Ib, and PPh_3, Ic, derivatives were also examined. These were prepared in an analogous manner to that already described for Ia (Chapter One) and characterised by their infrared ν_{co} spectra and elemental analysis. Their ^1H NMR spectra displayed only the expected resonances for coordinated phosphine ligands. Further, a parent ion was seen in the mass spectrum of Ib followed by successive loss of eleven carbonyl groups; operating at an electron energy of 15eV the $[M-2CO]^+$ ion is the strongest with $[M-CO]^+$ absent, whilst at 70eV further ligand fragmentation occurs leading to an observed $[Os_3]^+$ core.

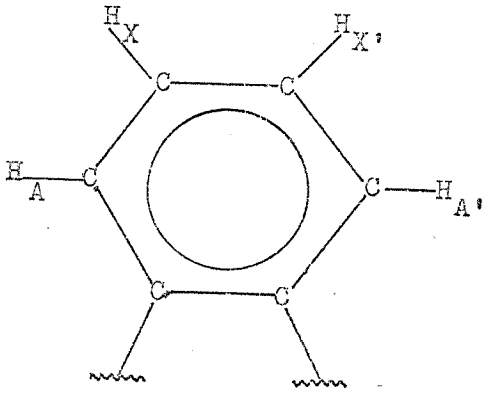
A n-nonane solution of Ia was heated under reflux for an hour. No apparent colour change was observed but infrared ν_{co} monitoring indicated total consumption of the starting material by the disappearance of its characteristic 2107cm^{-1} vibration. The simplicity of the emerged spectrum also suggested formation of only a single product and this was substantiated by chromatography. With n-hexane as eluant only one broad band moved up the t.l.c. plate and noticeably no residual baseline, which often accompanies pyrolytic experiments, was left; hence conversion is essentially quantitative with reported yields only reflecting the workup procedure. It has been fully characterised as $[Os_3(CO)_9(PEt)(C_6H_4)]$, XIIIa. Similar results were obtained from Ib and Ic with the corresponding $[Os_3(CO)_9(PR)(C_6H_4)]$, R=Me(XIIIb) or Ph(XIIIc)

Diagram 4

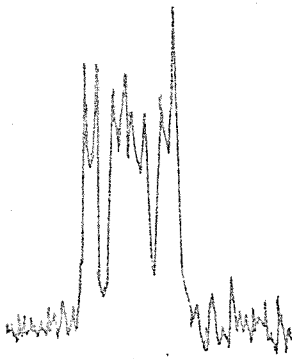
Computed Coupling Constants for the Benzyne-Phosphorus System

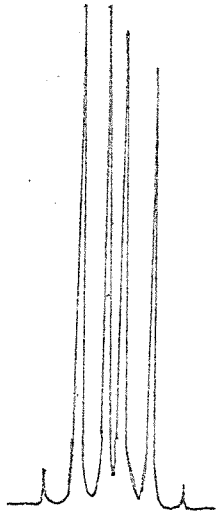


Coupling Constant (Hz)	R=Et; $[Os_3(CO)_9(PR)(C_6H_4)]$; R=Me	
$J_{A'X''}$, J_{AX}	7.64(±0.13)	7.59(±0.07)
$J_{A'X}$ $J_{AX'}$	1.14	1.44
$J_{A'A}$	0.00	0.00
$J_{A'P}$, J_{AP}	1.12	1.30
$J_{XX'}$	8.59,	7.76



P





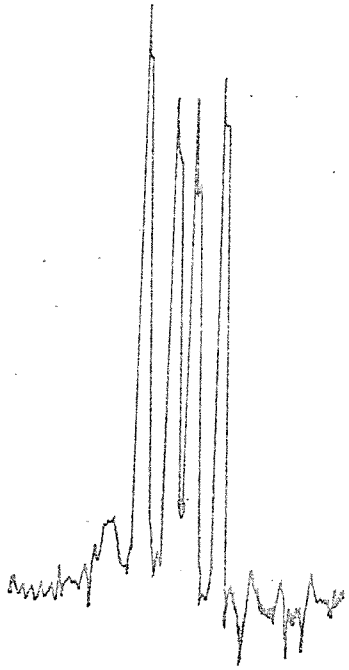
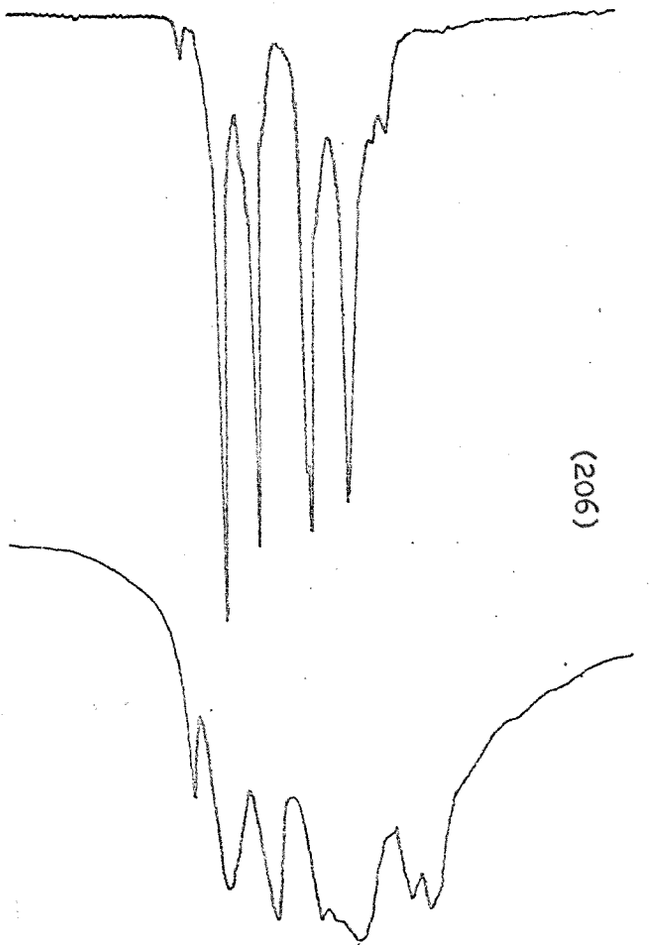


Diagram 5

Spectroscopic Data for $[Os_3(CO)_9(PR)(C_6H_4)]$, R=Me or Et

	$[Os_3(CO)_9(PMe)(C_6H_4)]$	$[Os_3(CO)_9(PEt)(C_6H_4)]$
infrared ν_{CO}/cm^{-1} (cyclohexane)	2086vw 2064vs 2049vsh 2042s 2010m-s 2006s 1992s 1989msh 1982m 1976w	2086vw 2064vs 2050wsh 2041s 2010s 2007s 1991s 1989msh 1982w 1976w (opposite)
infrared ν_{CO}/cm^{-1} (KBr disc)		2084m-w 2059s 2029s 2002s 1989vs 1978m 1971.5s 1964s (below)
^1H NMR, ($CDCl_3$) 31°C δ,(ppm)	7.37(AA'XX'P) 4H benzyne 3.04(d) 3H P-C$\underline{H}_3$ J_{PH}=10.3Hz	7.35(AA'XX'P) 4H benzyne 3.10(q?) 2H P-C$\underline{H}_2$-C J_{HH}=8Hz 1.45(dt) 3H P-C-C$\underline{H}_3$ J_{HH}=8Hz J_{PH}=22.5Hz
mass spectrum m/e (Os_3=572)	942	960



(206)

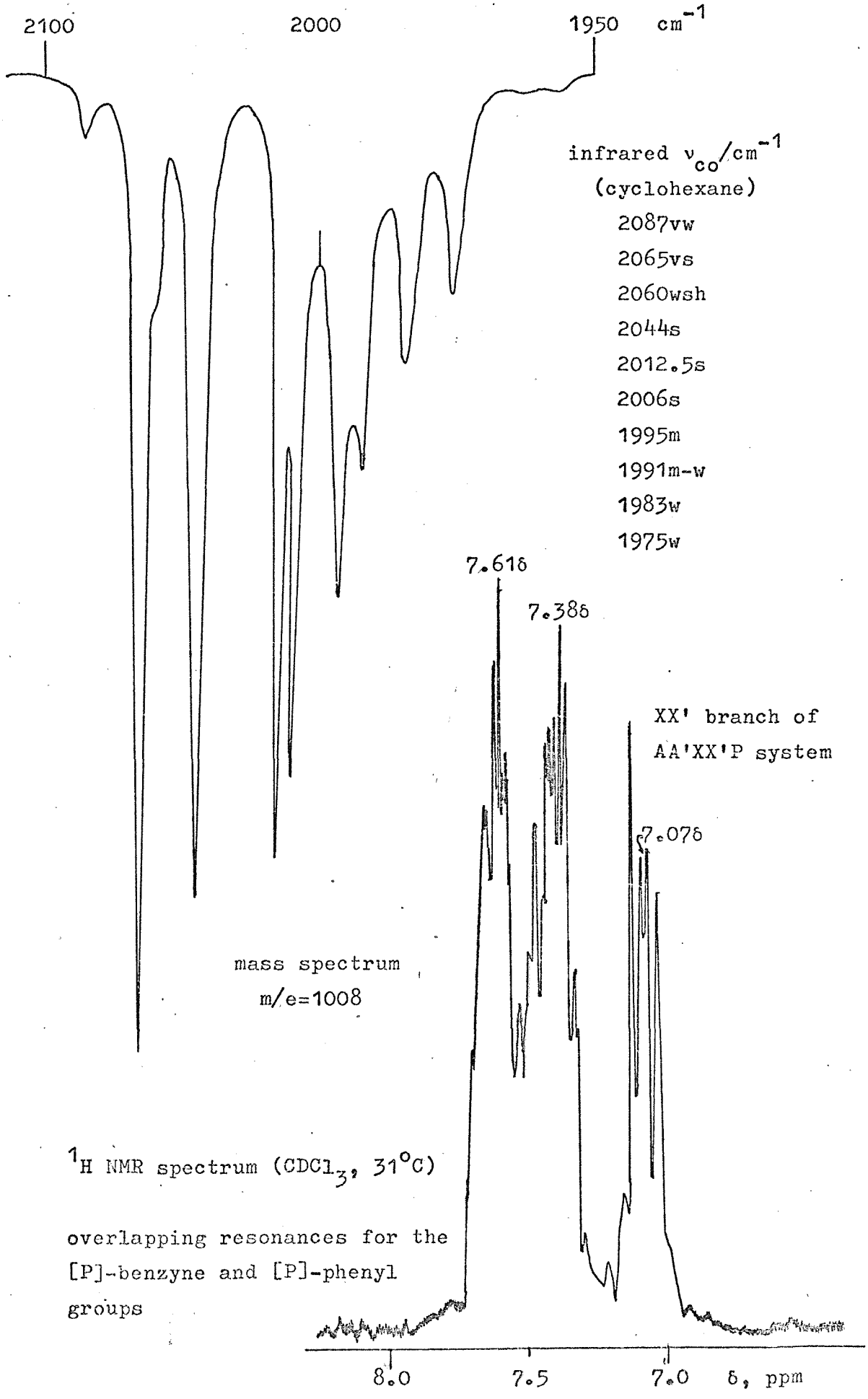
adducts being isolated.

The mass spectrum of XIIIa contains essentially ten successive Os_3 isotope patterns due to sequential loss of nine carbonyl groups, the highest atttibuted to the parent ion, m/e=960. The majority show excellent agreement with that for a theoretical Os_3 distribution, this empirically implies the absence of any metal-hydrides whose presence usually results in distortion caused by overlapping fragments. Additional fragmentation of the remaining organic ligands is also seen but, significantly when operating at 70eV, no $[Os_3]^+$ ion was observed. The spectra of XIIIb and XIIIc are similar with parent ions, but again no naked metal fragment, seen. For the phenylphosphido-adduct the lowest pattern, possessing an excellent Os_3 isotopic arrangement, can be attributed to an $[Os_3(H_2)P]^+$ fragment. In all three cases elemental analysis (C and H) is in full agreement with the proposed stoichiometry.

At 31°C the ^1H NMR ($CDCl_3$) spectrum of XIIIa contains resonances due to a ^{31}P-coordinated ethyl group and two complex branches, at 7.01 and 7.63 δ, of an AA'XX'P system attributed to a benzyne (ortho-phenylene) group coupled to the phosphorus nucleus. Analysis of this pattern, by using the PANIC computer programme associated with the Brucker CXP NMR spectrometer, enabled the various coupling constants to be determined by iteration of a theoretically computed spectrum, calculated on the basis of the observed spectral parameters, with the real one (Diagram 4). These reveal the symmetrical nature of the benzyne with an apparent mirror-plane bisecting it perpendicular to the plane of the ligand. Only the J_{PH}-coupling to the X-branch was not found through lack of resolution but can be estimated at slightly less than 0.5Hz. The asymmetry in the two branches only arises because of different coupling constants to the phosphorus for the separate hydrogen enviroments. Studies down to -70°C showed all the signals to be temperature invarient over this range, which is consistent with a symmetrical ortho-disubstituted benzene. Extensive scanning over the metal-hydride region gave no signals. The spectrum for XIIIb is almost identical, apart from the obvious change in the alkyl region with a methyl doublet (J_{PH}=10.3Hz) present. Again the various coupling constants in the

Diagram 6

Spectroscopic Data for $[Os_3(CO)_9(PPh)(C_6H_4)]$



AA'XX'P system were estimated by computer simulation. For the phenyl derivative the situation is more complicated (Diagram 6) because the signals for the two aromatic groups overlap, but the higher-field branch of an AA'XX'P system is still easily discernible.

The agreement between the solution ν_{CO} infrared spectra of XIIIa-c confirmed the adducts to be isostructural, whilst the lack of vibrations below 1950cm^{-1} showed that all the carbonyl groups are terminally bonded. To satisfy the molecular symmetry inferred by ^{1}H NMR these are allocated to three $Os(CO)_3$ units of which at least two are identical. The PR group is formally a four electron donor and is most favourably accommodated by it acting as a μ_3-ligand capping the metal core. The benzyne has the ability to act as either a two or four electron donor. In accordance with the 18 electron rule, and assuming retention of the Os_3 triangle, it would be assigned as a two electron donor bridging a single Os-Os bond. This would be analogous to the situation found in the dimeric complexes $[H_nOs_2(CO)_6(AsMe_2)_{2-n}(C_6H_4)]$, n=0 or 1,(29) which also showed temperature-independent AA'XX' NMR spectra. Alternatively, cleaving an Os-Os bond would allow it to act as a four electron donor forming an additional π-bond to the third osmium atom in a manner retaining the molecular symmetry. Possible evidence for the required cleavage may be drawn from the absence of the $[Os_3]^+$ ion in the mass spectra. As the solution studies could not differentiate between these possibilities a single crystal X-ray diffraction study was carried out on XIIIa to ascertain the solid-state structure.

4.3. Crystal and Molecular Structure of $[Os_3(CO)_9(PEt)(C_6H_4)]$

Crystal Data for $[Os_3(CO)_9(PEt)(C_6H_4)]$

$C_{17}H_9O_9POs_3$ MW=958.6g.mol^{-1}

Triclinic Space group $P\bar{1}$

Cell dimensions a=8.385(2) b=9.391(4) c=14.900(9) Å

α=94.57(4) β=94.05(4) γ=68.60(3) °

Z=2

U=1087.9(9) $Å^3$ F(000)=852 $\mu(Mo\text{-}K_\alpha)=169.0cm^{-1}$

R=0.0793 R_W=0.0793 R_G=0.0968 R_M=0.0969

Yellow needle-like crystals were grown from a n-hexane/dichloromethane solution. A suitable crystal was used to collect data on a Syntex P3 four-circle diffractometer using Mo-K_α radiation (λ=0.71069Å). The structure was solved by heavy atom methods for 2783 independent reflections ($Io > 2.5\sigma(I)$, and $2.9 < 2\theta < 50^\circ$) with the restriction that all atoms isotropic other than the osmiums and phosphorus. At present refinement gives R=0.079(141 parameters refined). The unit cell contains two crystallographically equivalent molecules and the atomic coordinates for one are given in Table 1, with all significant inter-atomic distances and angles summarized in Table 2.

Each molecule (Diagram 7) consists of a bent chain of three osmium atoms, each coordinated by three carbonyl groups. The plane of the three osmium atoms is coordinated on one side by a face-bridging PEt ligand and on the opposite side by a benzyne ligand. The Os-Os distances of 2.789(2), 2.929(2) and 4.008(2) Å, coupled with the wide Os(3)-Os(2)-Os(1) bond angle of 89.0°, clearly indicates that Os(3)-Os(2) and Os(2)-Os(1) are the only formal metal-metal bonds. A similar situation exists in the related benzyne containing cluster $[HOs_3(CO)_9(AsMe_2)(C_6H_4)]$, XIV, (30), where although the relevant parameters ($\angle$=85.5°, d=3.929(5)Å) are slightly less exaggerated they still represent a significant deviation from a triangulo-framework as typified by $[Os_3(CO)_{12}]$ ($\angle$=60°, d=2.8771(27)Å)(34).

The PEt ligand effectively occupies a central position above the metal core being appropriately displaced towards the non-bonded vector. With Os(1)-P, 2.335(8); Os(2)-P, 2.415(9); and Os(3)-P, 2.306(9) Å; the average distance of 2.352A is comparable to that observed in $[H_2Os_3(CO)_9(PPh)]$, d=2.329Å(35). This (distorted) tetrahedral arrangement with an apical heteroatom is increasing being recognized as a very stable configuration. For osmium clusters this mode of coordination has also been found with

Table 1

Fractional Atomic Coordinates(10^4) and Isotropic Thermal Parameters($Å^2 \times 10^4$) for $[Os_3(CO)_9(PEt)(C_6H_4)]$

Atom	x/a	y/b	z/c	U11
Os(1)	-2284(2)	-424(1)	-2148(1)	427(9)
Os(2)	-360(2)	1466(2)	-2020(1)	326(9)
Os(3)	-3214(2)	3797(2)	-2937(1)	502(9)
P	-3412(12)	2230(9)	-1869(7)	393(48)
C(10)	4372(48)	-3076(43)	771(26)	490(91)
C(11)	6372(65)	-3622(57)	905(34)	764(135)
C(1)	2986(48)	653(43)	1011(26)	475(89)
O(1)	3288(39)	812(34)	319(22)	688(81)
C(2)	319(114)	2628(106)	2211(60)	1454(300)
O(2)	-409(57)	3769(54)	2086(30)	1102(134)
C(3)	3956(52)	958(45)	2774(28)	525(96)
O(3)	5083(45)	1232(39)	3158(24)	820(96)
C(4)	302(50)	-2536(45)	885(27)	509(93)
O(4)	298(44)	-3208(39)	203(24)	831(97)
C(5)	-992(54)	-2233(48)	2636(29)	576(103)
O(5)	-1768(46)	-2694(40)	3070(24)	849(100)
C(6)	-1649(88)	271(80)	1513(46)	1285(198)
O(6)	-2626(60)	1439(55)	1423(31)	1180(144)
C(7)	2103(55)	-4546(48)	3730(30)	595(107)
O(7)	1298(49)	-4991(43)	4191(26)	945(112)
C(8)	3683(54)	-5413(48)	2002(29)	577(104)
O(8)	3682(44)	-6343(39)	1419(24)	827(97)
C(9)	5428(60)	-4654(52)	3547(31)	646(115)
O(9)	6780(51)	-5174(44)	3866(27)	966(114)
C(12)	256 (47)	-1718(41)	3750(25)	454(86)
C(13)	3162(57)	-1335(50)	4567(30)	626(111)
C(14)	2453(67)	115(60)	4999(36)	798(142)
C(15)	1048(56)	1266(49)	4587(30)	602(107)
C(16)	451(54)	932(48)	3752(29)	583(105)
C(17)	1151(55)	-463(49)	3252(30)	608(109)

Table 2

Important Interatomic Distances and Bond Angles (with estimated standard deviations in parentheses) for $[Os_3(CO)_9(PEt)(C_6H_4)]$

a) Distances(Å)

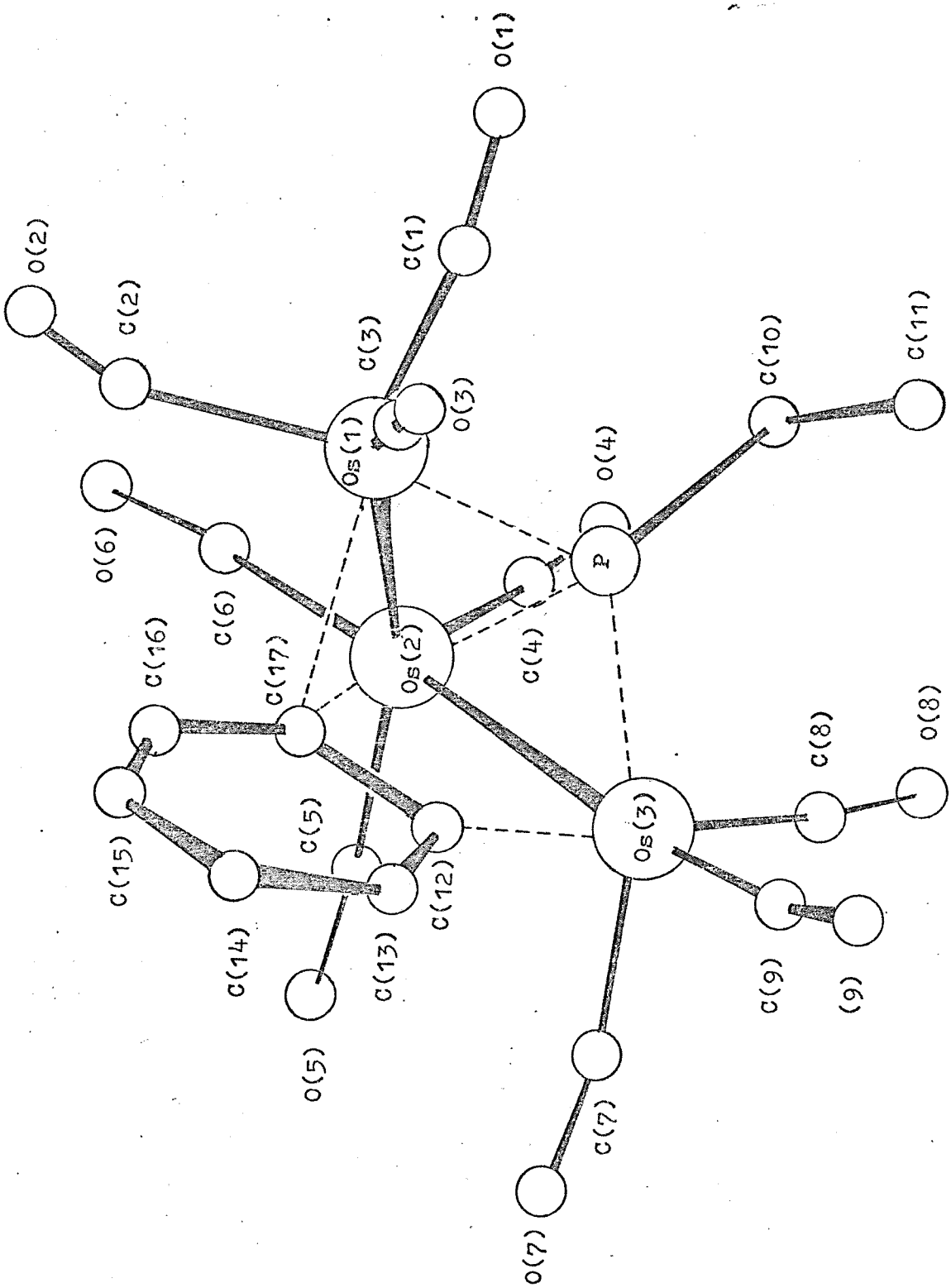
Os(1) - Os(2)	2.789(2)		
Os(2) - Os(3)	2.929(2)		
Os(1)...Os(3)	4.008(2)		
Os(1) - P	2.335(8)	P - C(10)	1.86(4)
Os(2) - P	2.415(9)	C(10) - C(11)	1.57(6)
Os(3) - P	2.306(9)		
Os(1)...C(12)	3.18(3)	C(12) - C(13)	1.36(6)
Os(2)...C(12)	3.04(3)	C(13) - C(14)	1.40(6)
Os(3) - C(12)	2.13(3)	C(14) - C(15)	1.42(6)
Os(1) - C(17)	2.31(3)	C(15) - C(16)	1.37(6)
Os(2) - C(17)	2.17(3)	C(16) - C(17)	1.40(6)
Os(3)...C(17)	2.99(3)	C(17) - C(12)	1.53(5)
Os(1) - C(1)	1.89(3)	C(1) - O(1)	1.11(5)
Os(1) - C(2)	2.12(3)	C(2) - O(2)	1.05(5)
Os(1) - C(3)	1.83(3)	C(3) - O(3)	1.17(5)
Os(2) - C(4)	1.90(3)	C(4) - O(4)	1.15(5)
Os(2) - C(5)	1.87(3)	C(5) - O(5)	1.16(5)
Os(2) - C(6)	2.02(3)	C(6) - O(6)	1.12(5)
Os(3) - C(7)	1.88(3)	C(7) - O(7)	1.19(5)
Os(3) - C(8)	1.92(3)	C(8) - O(8)	1.18(5)
Os(3) - C(9)	1.93(3)	C(9) - O(9)	1.14(5)

b) Angles(deg)

Os(1)-Os(2)-Os(3)	89.0(.1)	P-Os(1)-Os(2)	55.4(.2)
		P-Os(2)-Os(1)	52.7(.2)
Benzyne - Os_3		P-Os(2)-Os(3)	50.0(.2)
interplanar angle	58.9	P-Os(3)-Os(2)	53.3(.2)
C(12)-C(13)-C(14)	122.7(4.3)	C(15)-C(16)-C(17)	124.9(4.1)
C(13)-C(14)-C(15)	120.3(4.7)	C(16)-C(17)-C(12)	115.1(3.8)
C(14)-C(15)-C(16)	118.4(4.2)	C(17)-C(12)-C(13)	118.2(3.6)

Diagram 7

Molecular Structure of $[Os_3(CO)_9(PEt)(C_6H_4)]$



the chalconide elements(36), nitrogen(37) and carbon(38). Related μ_3-phosphido capped clusters had been previously reported for other group VIII metals, i.e. $[Co_3(CO)_9(PPH)]$(39), $[Fe_3(CO)_9(PPh)_2]$ (40) and $[MnFe_2(CO)_{9,8}(C_5H_5)(PPh)]$(41), but this represented the first published example(42) incorporating an osmium core. Subsequently Iwasaki et.al.(43) and Huttner and workers(35) have independently reported data for the related $[H_2M_3(CO)_9(PPh)]$, M= Ru or Os, complexes and the latter group have even isolated the iron analogue by the reaction of $[Fe_3(CO)_{12}]$ with the relevant primary phosphine(44). Others(45) also identified the co-production of $[Fe_3(CO)_9(PPh)_2]$ after extended reaction times under reflux in toluene. The retention of the iron core highlights the stability imparted by the facile formation of a μ_3-phosphido group since, even under milder conditions(46), reaction with a tertiary phosphine to give simple substituted products is accompanied by considerable degradation to mononuclear species. Obviously $[Fe_3(CO)_{11}(PPhH_2)]$ is only transient enroute to the stabilised capped derivative. The complete reaction pathway was established for the osmium(35) and ruthenium(43) systems where, after initial substitution, successive oxidative additions occur with the intermediate $[HM_3(CO)_9(PPhH)]$ fully characterised. With the ruthenium system the use of slightly more forcing conditions, in toluene under reflux, leads to the formation of condensation products containing μ_4- phosphido capping groups(47), with the identification of the previously discussed $[Ru_5(CO)_{15}(PR)]$ and $[Ru_4(CO)_{10}(\mu_2\text{-}CO)(\mu_4\text{-}PPh)_2]$. For $[H_2Ru_3(CO)_9(PPh)]$ the inherent stability is again demonstrated by its reaction with Me_3NO/ nucleophiles where substituted adducts were isolated, whereas $[Ru_3(CO)_{12}]$ suffers complete breakdown under identical conditions.

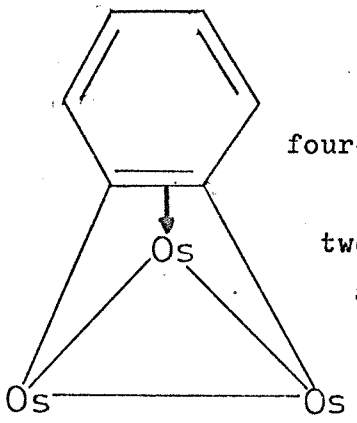
The heterometallic cluster $[MnFe_2(CO)_8(C_5H_5)(PPh)]$ is particularly interesting since it can add substrates, CO or PPh_3, reversibly with opening of a Mn-Fe(48). Such addition of a substrate molecule with rupture of a metal-metal bond, and elimination of the modified substrate with regeneration of the metal-metal bond could form the basis of a catalytic cycle involving cluster participation. The formally coordinatively unsaturated $[Ru_4(CO)_{10}(\mu_2\text{-}CO)(\mu_4\text{-}PPh)_2]$ can also reversibly add carbon monoxide to give $[Ru_4(CO)_{13}(\mu_3\text{-}PPh)_2]$, but with rearrangement

of the cluster framework so that the product can be considered as a derivative of $[Ru_3(CO)_9(PPh)_2]$ in which an $Ru(CO)_4$ unit has been inserted into one of the Ru-P bonds(49). In contrast, $[Fe_4(CO)_{10}(\mu_2\text{-}CO)(\mu_4\text{-}PPh)_2]$ adds a single carbon monoxide to yield $[Fe_4(CO)_{12}(\mu_4\text{-}PPh)_2]$(50) where the four iron atoms are perfectly square-planar and the carbonyls are all terminal. The ruthenium analogue is presumably an intermediate to the observed product.

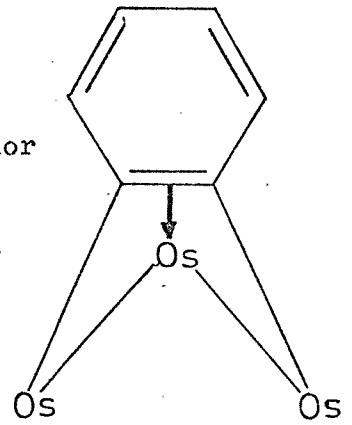
The benzyne ligand is bound asymmetrically to the osmium chain with one carbon linked to Os(3) only, and the adjacent carbon atom bonded to both Os(1) and Os(2). The relevant distances are: Os(3)-C(12), 2.13(3); Os...C(12), 3.04(3); Os(2)-C(17), 2.17(3); and Os(1)-C(17), 2.31(3) Å. No restrictions were imposed on the internal interatomic parameters during refinement and, significantly, the C(12)-C(17) distance (1.53(5)Å) is lengthened to a value consistent with a single C-C bond (1.54Å), while the remaining values (average 1.39Å) are closer to that found in an aromatic ring (1.397Å). The dihedral angle between the metal plane and that of the aryne is 58.9°. This contrasts with the situation found in other reported triosmium benzyne clusters. Three such compounds were obtained from $[Os_3(CO)_{10}(PPh_3)_2]$(25), including one where an additional intramolecular oxidative addition to a β C-H bond of a terminal phosphine has occurred. Even so, their geometries are still identical with no significant deviation from a mean C-C bond length of 1.42Å, at the stage of refinement reported, and in each case the interplanar angle was $69\pm3°$. This conformation reflects the approximately coplanar nature of the ligand with two osmium atoms, and the mode of attachment is best described as the ring forming σ-bonds to these two metal atoms (Os-C, 2.16Å) and donating through the π-system to the third (Os-C, 2.39Å). This attachment to the cluster is essentially symmetrical via a five-centre, four-electron bond. With this bonding description an increase in the aforementioned dihedral angle to approximately 90° would be expected to vastly reduce, or even eliminate, the π-interaction leaving the aryne as only a two-electron donor. This is exemplified by the crystal structure of $[H_3Os_3(CO)_8(HC{=}NC_6H_5)(C_6H_4)]$, isolated in small amounts from the pyrolysis of $[H_2Os_3(CO)_{10}(CNC_6H_5)]$(51), where the benzyne is nearly

Diagram 8

Possible Bonding Modes for a Benzyne Ligand



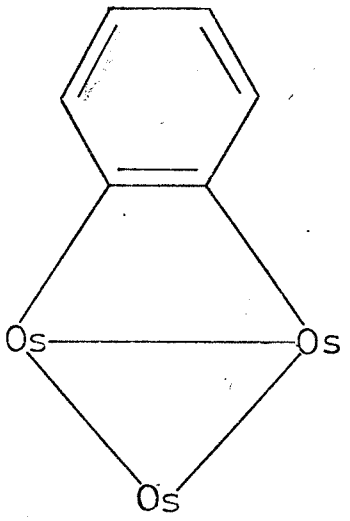
five-centre
four-electron donor
through
two σ-bonds and
a π-donation



$[Os_3(CO)_7(PPh_2)_2(C_6H_4)]$

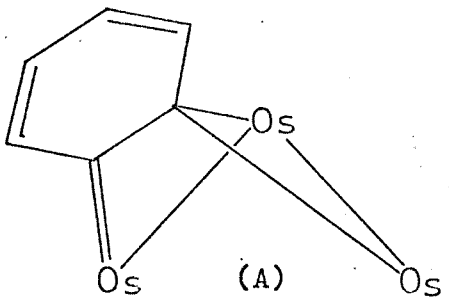
$[HOs_3(CO)_7(AsMe_2)(C_6H_4)]$

four-centre
two-electron donor

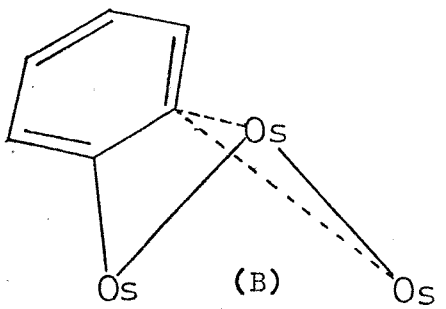


additional ligands
omitted for clarity

$[H_3Os_3(CO)_8(HC{=}NC_6H_5)(C_6H_4)]$



five-centre four-electron donor
through a multiple bond and
a carbene interaction



five-centre two-electron donor

perpendicular to the metal plane with the angle expanded to 79.0°. The ligand bridges one edge of the cluster with the two coordinated carbons each σ-bonded to a single, different, osmium. Within the benzyne the C-C distances show no deviation from a mean value of 1.37Å at the precision of definition.

Obviously XIIIa does not comply with this progression and an alternative bonding description is necessary. With the aromaticity of the ring lifted two arrangements appear plausible (Diagram 8). One where the benzyne ligand acts as a four electron donor with a C(12)-Os(3) multiple bond and C(17) adopting a Bridging carbene arrangement. However the mean Os-C(17) distance of 2.24Å is approximately 0.1Å longer than in typical carbene clusters such as $[H_2Os_3(CO)_9(CH_2)]$(52) and $[H_2Os_4(CO)_{12}(CHCH_2Ph)]$ (53). Indeed the various C-Os distances suggest that the ligand is acting as a terminal, C(12), and a bridging, C(17), aryl group, i.e. a two electron donor, but which renders the cleavage of the Os(1)-Os(3) bond problematical. To avoid this predicament the overall situation for the ring is best described as an ortho-phenylene ligand with some carbenoid character i.e. contributions from both descriptions.

4.4. Variable Temperature $^{13}C-\{^1H\}$ NMR Study of $[Os_3(CO)_9(PEt)(C_6H_4)]$

Whilst the preceding discussion attempts to rationalise the observed crystal features, perhaps some attention should be focused on them possibly being the consequence of packing restrictions. All attempts to compliment the solid-state structure with other spectroscopic techniques has so far proved inconclusive. The solution and KBr disc infrared ν_{CO} spectra are not sufficiently dissimilar (Diagram 5), especially when taking into account the further interactions possible in the latter, to warrent proposing different molecular structures. Yet the appearance of the solution spectrum closely resembles that of other triosmium clusters with C_{2V} symmetry, a feature employed elsewhere(54) to infer related geometries in different molecules, which would necessitate a more symmetrical configuration. The recorded NMR (^{13}C and ^1H) data is also inconsistent with the crystal structure.

Such a dilemma is epitomized by $[Fe_3(CO)_{12}]$ where a

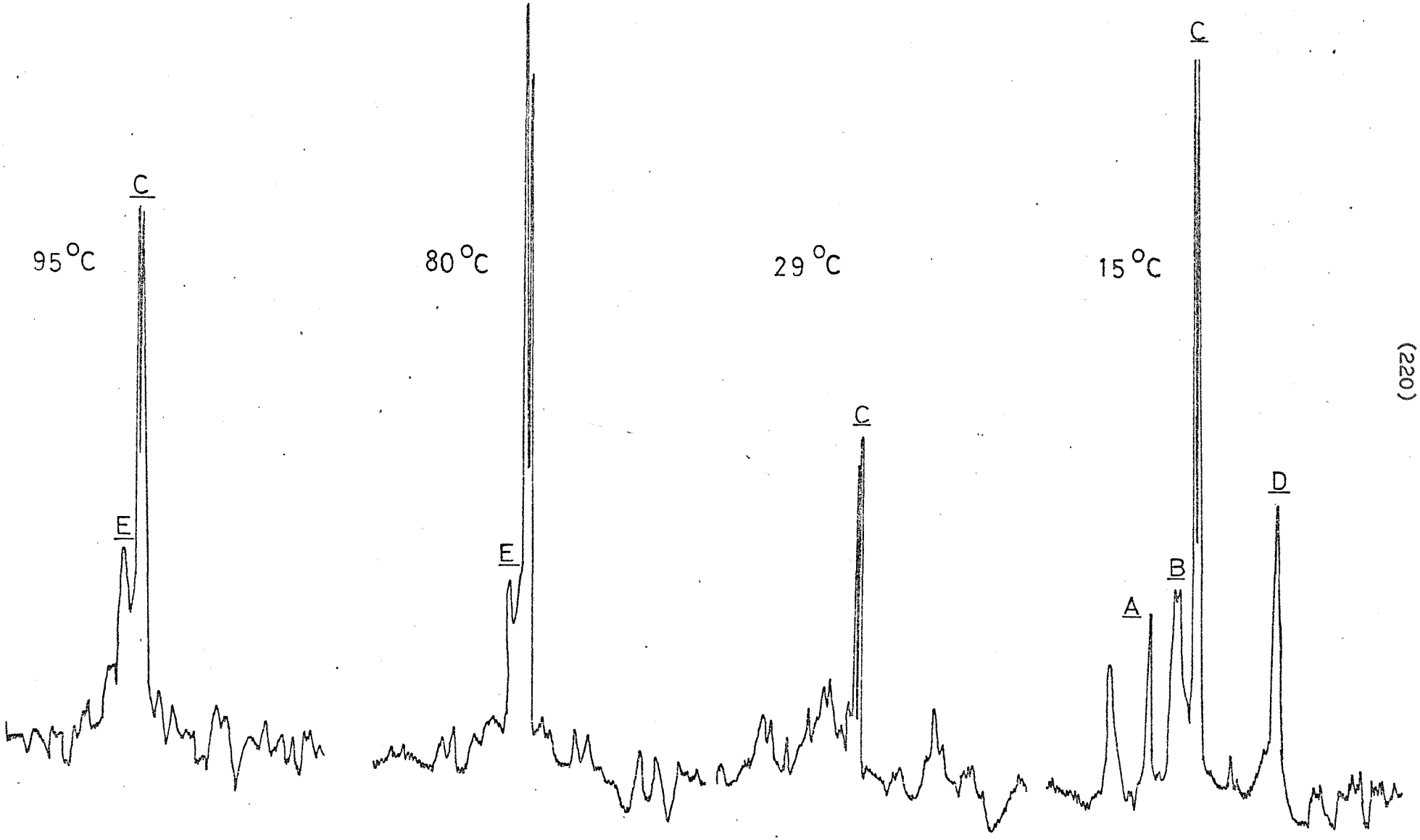
different structure clearly predominates in solution(55) to that found by X-ray crystallography(56), due to the nearly equi-energic character of a whole range of possible configurations. The solid-state conformation just representing a shallow energy minimum stabilised by crystal packing forces. As a consequence dynamic interconversion should be rapid(57), and this prediction was confirmed by a ^{13}CO NMR study where the single resonance remains unchanged even at -150°C indicating an activation energy $\leq$ 6kcal. mol^{-1}(58). Two mechanisms have been forwarded to account for this scrambling involving either pairwise opening of the carbonyl bridges, to give an intermediate with D_{3h} symmetry(57), or simple rotation of the carbonyl icosahedron about the Fe_3 triangle, or vice versa(59). An extension of the last process, involving polytopal rearrangement via a cube-octahedral transition-state, is proposed to explain the observed ^{13}CO fluxional behaviour of the mono-substituted phosphine/phosphite derivatives(60). A direct parallel clearly exists for XIIIa where rapid migration of the benzyne ligand above the metal plane apparently occurs, and is unresolved at the lowest temperature studied. Again the identified crystal structure represents one of a series of configurations enveloped by the motion, the narrow energy profile encompassing them allows different ones to be favoured under the varying restraints imposed in solution and solid-states.

To further expand this treatise a variable temperature ^{13}C NMR study was undertaken. Enrichment with ^{13}CO occurred at $[Os_3(CO)_{12}]$, and then a sample of XIIIa was prepared in the manner already outlined. Spectra were recorded over the range -132 to +95 °C using d_8-toluene or $CD_2Cl_2/CHCl_2F$ mixtures as solvent for the higher and lower temperatures, respectively. The results are collated in Table 3 and Diagram 9. From the crystal structure nine separate resonances would be expected in the low temperature, limiting spectrum but this was not attained at the lowest temperature achieved. At -132°C five resonances were observed at: a, 183.4; b, 180.1; c', 179.9; c", 179.4; d, 173.9 δ- with integrated intensities of 2:2:2:1:2 respectively. On raising the temperature c' and c" quickly coalesce, and an averaged signal, c($^2J_{PC}$=7.6Hz), emerges and remains unaltered throughout the upper region. The remaining three signals collectively collapse just above ambient

Table 3 Carbonyl ligand ^{13}C NMR Data for $[Os_3(CO)_9(PEt)(C_6H_4)]$

Assignment Temperature	A	B	C	D	E	C'	C''
(d_8-toluene)							
+80			177.6(287) 7.4Hz		178.6(40)		
+28			177.8 7.7Hz				
+15	182.6(56) 65Hz	179.3(75) 6.2Hz	177.8(287) 7.5Hz	172.2(57)			
0	182.6(87) 66.1Hz	179.2(99) 8.6Hz	177.9(238) 7.8Hz	172.2(94)	Figures in parentheses are signal intensities.		
-20	182.6(168) 66.1Hz	179.2(155) 8.8Hz	178.0(308) 7.6Hz	172.3(164)	Chemical shifts as p.p.m.		
-60	182.6(80)	179.1(111)	178.2(169)	172.3(89)			
$CD_2Cl_2/CFHCl_2$	66.2Hz	7.1Hz	7.1Hz		Temperatures as °C.		
-80	183.4(300) 66.2Hz	179.6(371) 9.2Hz	179.2(510) 7.6Hz	173.4(269)			
-100	183.5(176) 66.4Hz	179.7(240) 7.6Hz	179.4(220) 7.6Hz	173.6(213)			
-120	183.5(177) 66.8Hz	179.8(281) 8.3Hz		173.8(203)			
-132	183.4(125) 41.2Hz	180.1(223) 4.2Hz		173.9(102)		179.9(118)	179.4(54)

Diagram 9a Variable Temperature ^{13}CO NMR Spectra for $[Os_3(CO)_9(PEt)(C_6H_4)]$



Variable Temperature ^{13}CO NMR Spectra for $[Os_3(CO)_9(PEt)(C_6H_4)]$

Diagram 9b

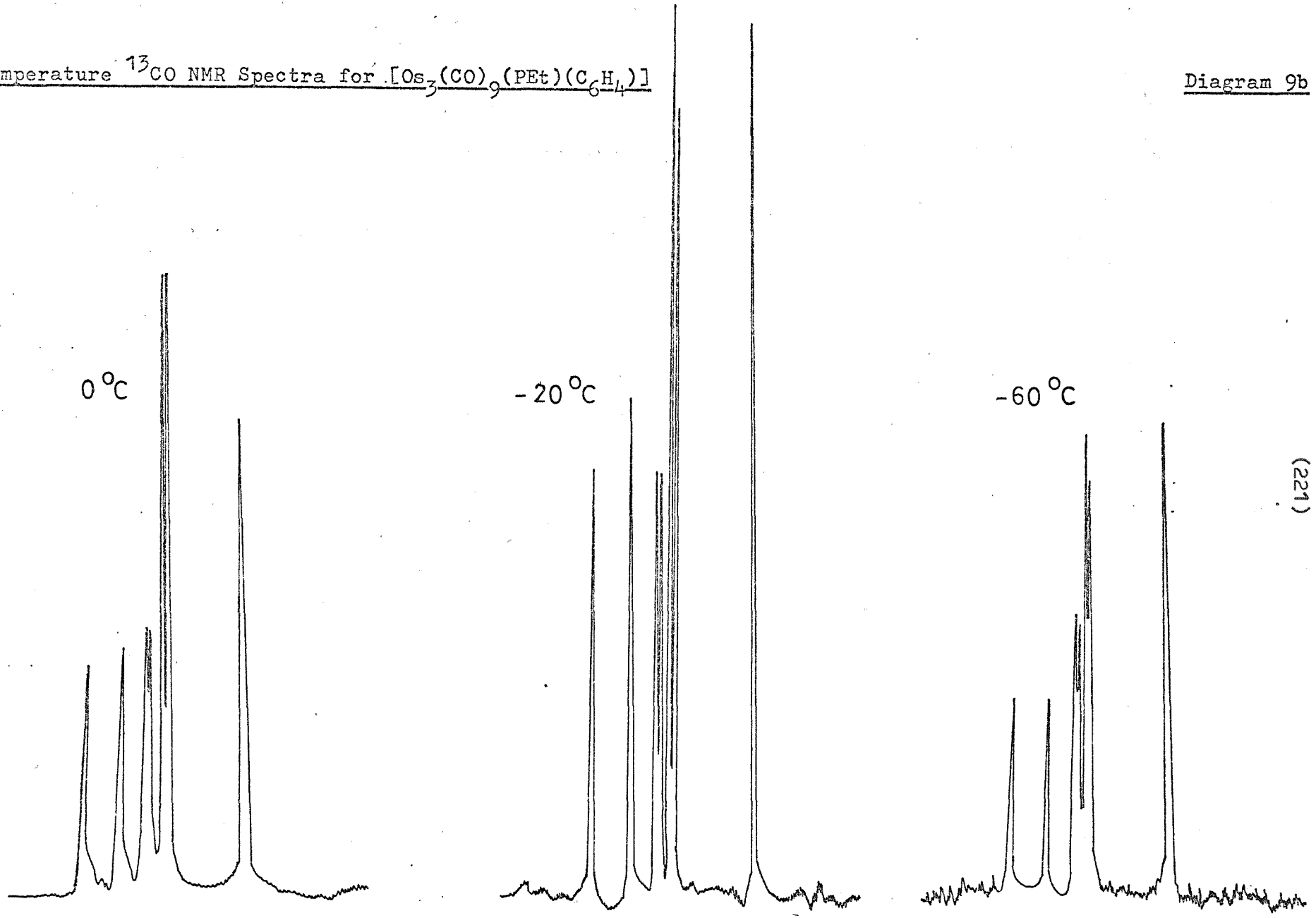
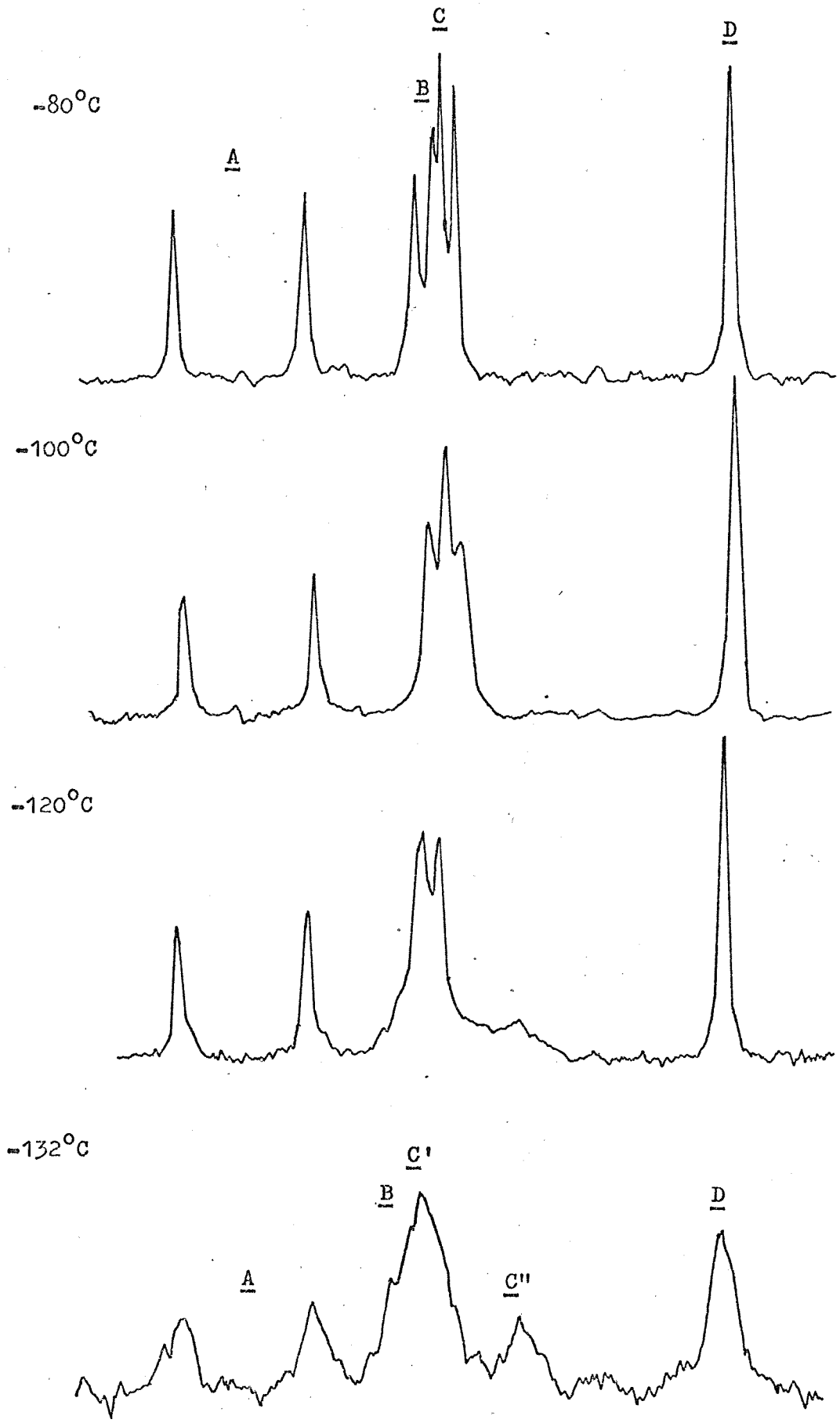


Diagram 9c

Variable Temperature ^{13}CO NMR Spectra for $[Os_3(CO)_9(PEt)(C_6H_4)]$



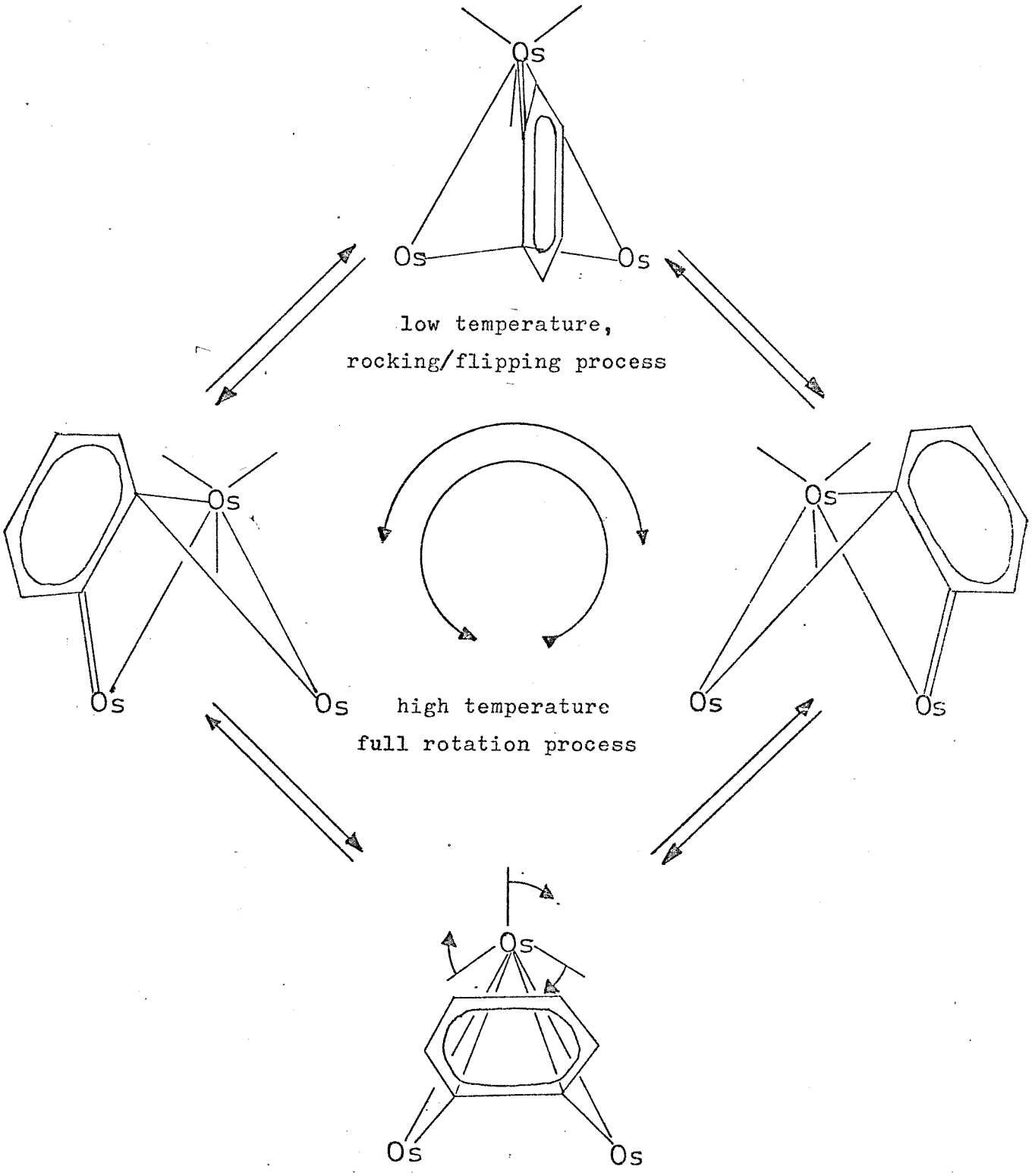
temperature into a single resonance at 178.66(+80°C), although even at +95°C it has still not reached its true intensity. The signals a and b also display $^2J_{PC}$ couplings of 66.1 and 9 Hz, respectively.

These features can be interpreted in terms of the combined rotation of all the carbonyls about their independent osmiums in association with two benzyne motions, first rocking/flipping and then full rotation, above the metal plane. Even at -132°C a fast exchange process is still evident which imparts a time-averaged plane of symmetry through Os(2) and the plane of the aryne. This is assigned to benzyne rocking, as shown in Diagram 10, which itself does not cause symmetrisation within the ligand. Hence the ^1H NMR spectrum at this temperature should be an ABXYP system but this was not recorded due to practical limitations; at the lowest temperature attained (-90°C) the AA'XX'P pattern still persisted. At about -100°C the emergence of c, with its intensity and position, must indicate that it is associated with localised carbonyl rotation about Os(2). Coincidently, the observed perpendicular mirror-plane through the benzyne infers that it is rotating above the metal core. Although this evidence is not conclusive enough to conclude that these two processes are interdependent, a precedent does exist in XIV(30) where the onset of aryne rotation is similarly accompanied by axial-equatorial carbonyl exchange about the centre osmium. A related migratory process is also found in $[H_2Os_3(CO)_{11}]$, where the bridge-terminal hydride interchange is tied with an oscillatory motion of two carbonyl groups(61). The absence of any identified couplings to the phosphido group, and their relative intensities, is consistent with a spatial arrangement of the sets c' and c'' as exemplified by the crystal structure i.e. the symmetry related pair(c') adjacent to the benzyne ligand. An inverse configuration, with the unique ligand trans- to the phosphorus atom, would demand a significant $^2J_{PC}$ value which is not observed. The coupling constant seen for c(7.1Hz) must represent a time-averaged value across the rotation.

The outstanding resonances correspond to the six carbonyl groups on Os(1) and Os(3) in three symmetry related pairs. From its large $^2J_{PC}$ value (66Hz) a is immediately assigned to the pair, C(7) and C(2), adopting a trans-configuration with the phosphido

Diagram 10

Fluxional Behaviour of the Benzyne Ligand in $[Os_3(CO)_9(PEt)(C_6H_4)]$

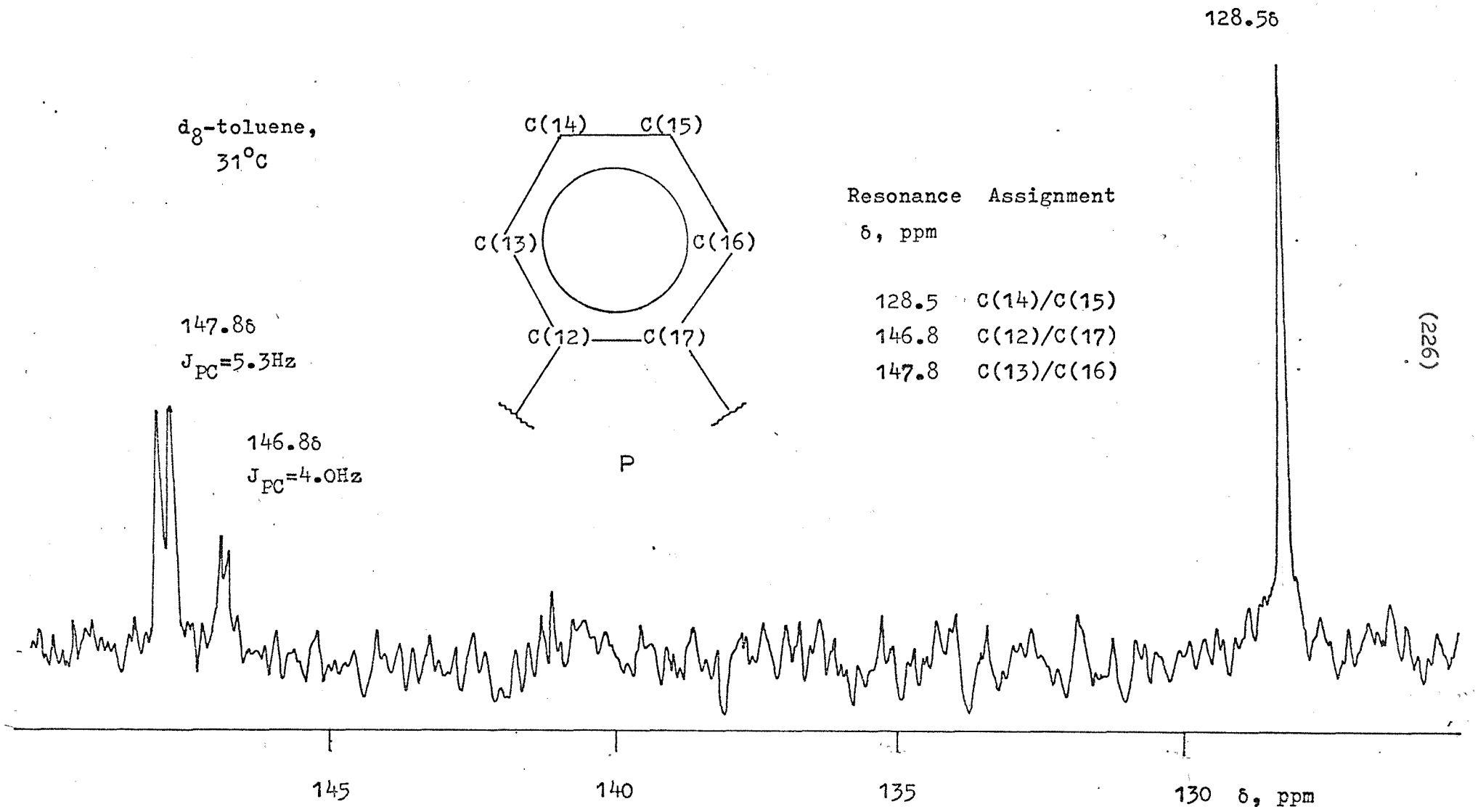


ligand. The much smaller coupling to b and d, 8 and 0 Hz respectively, are consistent with the remaining two pairs but, unfortunately, the data is insufficient to unequivocally differentiate between them. On approaching room temperature these signals coalesce and an averaged signal, e, eventually emerges. This can be attributed to the onset of these carbonyls rotating about the osmium atoms. The absence of an Os(1)-Os(3) bond reduces the possibility of this occurring by a two-centre mechanism, and further there is no evidence to suggest that it is accompanied by an increase in aryne mobility. In the related molecule $[Os_3(CO)_7(AsMe_2)_2(C_6H_4)]$, XV, a different situation prevails whereby carbonyl exchange by an internuclear route is associated with a rotation/flipping of the aryne.

Study of the ^{13}C natural abundance resonances observed for the ligand itself also supports the existence of a rotational motion above -132°C. At ambient temperature three resonances consistent with the benzyne are seen at 147.8(d, J_{PC}=5.3Hz); 146.8(d, J_{PC}=4.0Hz); and 128.5 δ. The assigned couplings were not further substantiated by ^{31}P-decoupling or operation at a different frequency. However the corresponding groups in both XV, and the more asymmetrical XIV, similarly show three signals, across the same chemical shift range, whilst a symmetrical AA'XX' pattern persists in the corresponding ^1H NMR spectrum(30). This re-enforces the existence of ^{31}P-couplings for XIIIa whence, of the three symmetry related pairs, the singlet at 146.8δ must correspond to C(14) and C(15). Although the differences between the two other resonances are not sufficient to confirm assignments, the greater Overhauser/relaxation effects for that at 146.8δ favours it corresponding to the pair, C(12) and C(17). For XIV and XV cooling towards -50°C causes a transformation to an ABXY ^1H spectrum, which is accompanied by loss of the time-averaged plane through the C_6 ring, resulting in six separate ^{13}C signals (two with accidental coincidence for XV). Study of the $(C_6H_3Pr^i)$ analogue of XIV clearly substantiated that this resulted from the $Os_3(C_6H_4)$ framework being dynamic; an hydride migration not being sufficient. Concommitant with this aryne motion commencing is the simultaneous broadening and collapse of the nine separate carbonyl resonances and the emergence of four signals (at 100°C), with

Diagram 11

$^{13}C-\{^{1}H\}$ NMR Spectrum for the Benzyne Ligand



relative intensities of 2:3:2:2, invoking a concerted local carbonyl exchange on the central osmium. This is identical to the proposed benzyne full rotation in XIII. For XIIIa even at -120°C the three benzyne resonances still remain unaltered, but at -132°C they have apparently collapsed. Unfortunately, the viscous nature of the solution, and the absence of specific enrichment, precludes precise identification of whether this is a true coalescence or just due to loss of resolution.

Thus, whilst the higher energy motion is fully verified for XIIIa, the flipping/rocking process is only inferred by the discrepancy between the refined crystal structure and the lowest temperature NMR spectra recorded. This is embodied in the persistance of symmetry related pairs of carbonyl groups below the coalescence temperature of the full rotation. Ofcourse, if the static solution structure was different, and more symmetrical, such deductions regarding any unresolved motion would be invalid. However such a flipping mechanism has been established for XV, by introduction of an isopropyl group on the benzyne ligand. Then, even when the faster process was frozen out (-60°C), coalesced signals still remained for the potentially diastereotopic methyl groups on the $CHMe_2$ substituent in a static molecule (the possibility of accidental coincidence being dismissed). This also highlights the flipping feature of the motion whereby opposite faces of the organic ring interchange. From the initially tilted position it passes through a vertical orientation before finally readopting a tilted configuration with the opposite face towards the metal core. Unfortunately such an investigation on XIII would still not differentiate between the possibility of different zero-energy structures existing in the solution and crystal states; the only definitive result would be observing the nine separate carbonyl signals demanded by the crystal structure (the chirality of an isopropyl group would also become evident simultaneously).

On first inspection XIII and XIV are both structurally similar, possessing a common $(C_6H_4)Os_3(CO)_9$ framework with an open metal-metal vector, yet a large difference in the barrier to full rotation of the benzyne exists, with coalescence temperatures of ca. -120 and > -40°C, respectively. Whilst it is dangerous to make comparisons without considering the full effects (steric and

electronic) of all addendum ligands, the respective carbonyl spatial arrangements are illuminating. For XIII, with the phosphido-group central beneath the molecule, they generally adopt positions away from the benzyne reducing steric hindrance to any motion. The situation in XIV is different, with the μ_2-arsine impinging on both sides of the molecule which causes the aromatic ring to tilt towards the third osmium. This mode of coordination, and the carbonyl arrangement at this osmium, corresponds directly to the proposed activated intermediate of XIII for the onset of full rotation. If this is the ground state of XIV it emphasizes the increased potential energies of the remaining configurations favoured for XIII, no doubt due to the steric influence of the arsine. If, as proposed, this benzyne rotation is interdependent with the carbonyl exchange then it can be surmised that carbonyl rotation is the limiting factor in the process for XIII, whilst the aryne motion for XIV.

Two resonances were also observed in the ambient temperature spectrum at 31.51(J_{PC}=90Hz) and 14.91 δ which can be assigned to the α and β carbons of the PEt group respectively.

4.5. Discussion

The isolation of XIII, as the only product from thermal decomposition of I, can be rationalised as part of a progression replacing alkyl groups on the tertiary phosphine ligand by aromatic ones. To demonstrate this a mechanism is proposed (Diagram 12) for the conversion which utilises features characteristic of other products identified in the series. Unfortunately heating I under milder conditions, in toluene(111°C) or n-octane(126°C), did not produce any degradation so, in the absence of observed intermediates, the mechanism cannot be verified and must be accordingly viewed as only one possibility based on intuitive grounds alone.

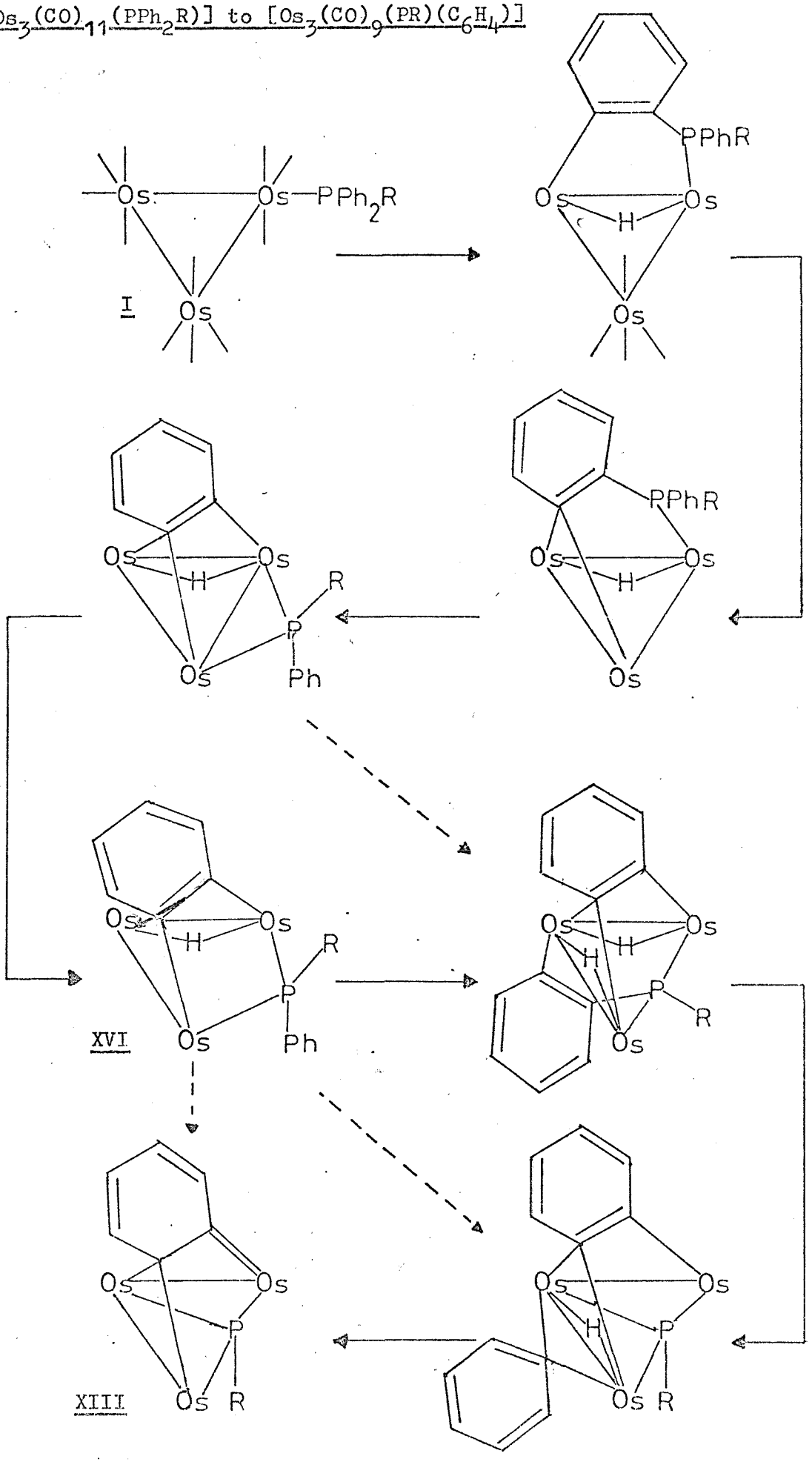
The temperature(151°C) employed is believed necessary to thermally dissociate a carbon monoxide ligand from the coordinatively saturated starting material before activation of a C-H bond takes place. This could either occur at an ortho-position on a phenyl ring, or the α-carbon of the alkyl group, but the

isolation of $[HOs_3(CO)_9(PR)(C_6H_4)]$, XVI, from $[Os_3(CO)_{11}(PPhR_2)]$, R=Me or Et(29), clearly established the former process to be more facile. Then reaction almost certainly proceeds via intermediates similar to VI and VII shown to be transient in the formation of X, amongst other products, from $[Os_3(CO)_{10}(PPh_3)_2]$(25). These three complexes did not suffer from interaction of the second phosphine complicating the issue, and the route was supported by experimental observation. Hence, orthometallation of a phenyl group is followed by a further carbon monoxide loss with a simultaneous increase in ring coordination through the β-carbon bridging two osmium atoms. From here transformation to XVI is easily visualised which, in the absence of thermal decarbonylation, requires breaking an Os-Os bond to maintain 54 valence electrons. This contains several steps and an intermediate with the formed benzyne acting as a two-electron donor, coordinating through adjacent terminal and bridging carbons, can be envisaged.

Another fragmentation pathway to XVI, involving P-C cleavage before hydrogen abstraction onto the cluster, also has to be considered. This has been substantiated as a possible route in the corresponding arsine system. Although no intermediates were isolated from the thermal conversion of $[Os_3(CO)_{11}(AsPhMe_2)]$ several were found with the related dimethylvinylarsine derivative. Careful selection of solvents allowed both a complex resulting from As-C cleavage, containing independent η_2-vinyl and μ-arsino groups, and a vinylidene adduct, from further decarbonylation and hydrogen transfer, to be identified chiefly on the basis of ^{1}H NMR evidence(62). The latter compound isomerises at higher temperatures to give a product isostructural with XVI, as shown by the similarity in ν_{CO} spectra. For aromatic groups this would necessitate an intermediate possessing a μ_2-bridging phenyl moiety. Then it is significant that using (2- or 4-methoxylphenyl)dimethylarsine gives the substituted benzyne derivative of XIV, but with the same positional isomerisation in both cases, with the methoxy-group adjacent to the metallated carbons. Conversely, thermolysis of $[Os_3(CO)_{11}\ AsMe_2(C_6H_4Me\text{-}2)]$ gave only the 4-substituted form of XIV, so that the direction appears electronically, rather than sterically, controlled. The forwarded explanation(63) involved a reversible reaction transforming the hydrido-μ_3-benzyne into a

Diagram 12

Proposed Mechanism for the Thermal Degradation of $[Os_3(CO)_{11}(PPh_2R)]$ to $[Os_3(CO)_9(PR)(C_6H_4)]$



short-lived phenyl compound, allowing the benzyne ligand to interchange the metal-bound carbon atoms to adopt the most stable configuration. Whilst this pathway may be applicable throughout the arsine range, the greater P-C bond strength is believed to exclude this option with phosphines.

As mentioned previously, thermal decarbonylation to a complex related to X would represent an alternative route and the influence of a second phosphine obviously promotes this pathway. This demonstrates the sensitive way electronic and steric effects are relayed from one part of a cluster to another, so that the cluster as a whole must be considered. In this instance electronic factors appear governing since the spatial geometries of X and XVI are not sufficiently dissimilar to warrent steric reasons.

For dialkylphenylphosphine derivatives XVI signifies the end-point under the conditions used in this study. However, for tertiary diphenylphosphines a further interaction with the metal core is possible with stoichiometric elimination of benzene yielding XIII. This could simply result from P-C(aryl) cleavage and hydride transfer, without any interaction of the phenyl ring with the metal skeleton. However activation is believed to proceed by orthometallation as with the first ring. Then a combined P-C(aryl) cleavage and transfer back of hydrogen gives a transient μ_2-bridging phenyl (one electron donor) accompanied by formation of the μ_3-phosphido group. For electron counting purposes such a pathway requires the benzyne to revert to a two-electron donor. A similar ligand-metal redox system, creating a vacant coordination site, has previously been reported with $[HOs_3(CO)_9(SR)]$ where the thiol has multi-donor properties. The proven fluxional nature of the aryne is also consistent with it being capable of interchanging between coordination modes. Alternatively, if the XVI analogue is by-passed, metallation of the second phenyl results from/in loss of the metal-metal bond and the benzyne does not become a four-electron donor until after ejection of benzene. Whichever route is operative, activation of the remaining phenyl ring on the phosphine can be accommodated by an established mechanism. Once the bridging phenyl and hydride are formed in close vicinity elimination of benzene is easily forseen to give XIII as the isolated product. Perhaps it is pertinent to observe

that the only bridging phenyl complex, VIII, identified from the conversion of $[Os_3(CO)_{10}(PPh_3)_2]$ is a non-hydrido species which presumably stabilises it relative to reductive elimination of benzene.

Activation of the second phenyl group is unlikely to occur before formation of the μ_2-phosphide because until then it will be projected away from the cluster. Even at that stage a possibility of two isomers exists, and only one has the correct configuration to promote the conversion to XIII. However, from the known structure of XVI, the steric influence of the benzyne might be expected to favour this form with the phenyl group directed towards the other side of the cluster. Ofcourse such considerations are superfluous with the PPh_3 derivative. A similar situation exists in the degradation of $[Os_3(CO)_{11}(PPhH_2)]$, where the intermediate $[HOs_3(CO)_{10}(PPhH)]$ can adopt either syn- or anti-configurations but X-ray crystallography clearly identified only the latter form to be present. This has the phosphorus-bound hydrogen atom lying over the metal triangle with the phenyl group directed away. This provides a ready explanation for the facile formation of the capped species $[H_2Os_3(CO)_9(PPh)]$ by oxidative addition of P-H with concommitant loss of a carbonyl group. The opposite orientation would promote orthometallation as found for the conversion of $[HOs_3(CO)_{10}(NHPh)]$ under similar conditions(64). This kinetic control is supported by the fact that $[H_2Os_3(CO)_9(NHC_6H_4)]$ isomerises slowly to the capped species $[H_2Os_3(CO)_9(NPh)]$ on extended heating(65).

XIII is the observed final product because its molecular geometry effectively excludes any further intramolecular reaction between the remaining organic group on the phosphorus, even for XIIIc, and the osmium core. With more severe conditions the possibility could exist of an intermolecular route or cluster breakdown leading to higher nuclearity products. The influence of trace quantities of water could also cause further complications.

In the above mechanism the precise cause for loss of a metal-metal bond was left debatable. The decomposition of $[Os_3(CO)_{11}(PRH_2)]$ shows that the formation of the μ_3-phosphide does not necessitate the cleavage, but similarly nor does a four-electron donor benzyne as illustrated by the products from

$[Os_3(CO)_{10}(PPh_3)_{10}]$. Neither is it believed that the combined spatial restraints of both ligands require the opening to accommodate them. Instead the driving force to attain these two stable moieties causes the sacrifice of the metal-metal bond to maintain the 18-electron rule. As inferred previously the preferential loss of the bond, instead of further decarbonylation, is almost certainly an electronic effect. Intuitively with the variable coordinating properties of the benzyne its tendancy towards a four-electron donor might be assigned the most likely origin if a choice was made.

The isolation of just a single product from the pyrolysis of Ic contrasts with the nine compounds obtained from the reaction of $[Os_3(CO)_{12}]$ with a two fold excess of PPh_3 in xylene under reflux. However a preliminary experiment with Ic, evidently contaminated with unreacted phosphine, did give a more complex mixture. Two bands were retrieved from initial chromatography and the major red constituent identified by its infrared ν_{co} spectrum as IX. Presumably more extensive separation would have yielded more of the compounds originally prepared by Bradford and Nyhlom. This consolidates additional substitution to be more facile than pyrolysis of I, so that in the presence of uncoordinated phosphine isolation of $[Os_3(CO)_{10}(PPh_3)_2]$ degradation products would be expected in preference to any from XIII followed by additional substitution. This is further supported by an infrared ν_{co} trace of the reaction where a transient vibration at $2087cm^{-1}$, which had disappeared at the end of the ninety minute reaction period, can be conceivably associated with either the disubstituted derivative or even VII.

4.6. Experimental Section

$[Os_3(CO)_{11}(PPh_2R)]$, R=Me or Ph.

These were both prepared in an analogous manner to that already described for the ethyldipenylphosphine derivative (Chapter One).

For $[Os_3(CO)_{11}(PPh_3)]$ preparative t.l.c. using n-hexane/Et_2O(5:1v/v) as eluant, was hampered by concurrent crystallisation with unreacted phosphine. However removal from the plate and

extraction with ethanol(5ml) left pure $[Os_3(CO)_{11}(PPh_3)]$.

$[Os_3(CO)_{11}(PPh_3)]$ Typical yield=65%
IR ν_{CO}(cyclohexane): 2107w, 2054m-s, 2035w-m, 2019vs, 2000w, 1990w, 1978.5w, 1958vw, cm^{-1}.
^1H NMR($CDCl_3$, 31°C): 7.456, m, $P\underline{Ph}_3$.
Elemental Analysis Cald. C 30.53% H 1.33%
MW=1140.95g.mol^{-1} Obsd. C 31.1% H 1.25%

$[Os_3(CO)_{11}(PPh_2Me)]$ Typical yield=48%
IR ν_{CO}(cyclohexane): 2107w, 2053s, 2032m, 2018vs, 2000w, 1989w-m, 1971w, 1958vw, cm^{-1}.
^1H NMR($CDCl_3$, 31°C): 7.56, m, $P\underline{Ph}_2$; 2.28, d(J_{PH}=10Hz), $PC\underline{H}_3$.
m/e=1080.
Elemental Analysis Cald. C 26.72% H 1.21%
MW=1078.88g.mol^{-1} Obsd. C 26.1% H 0.9%

$\underline{[Os_3(CO)_9(PEt)(C_6H_4)]}$

$[Os_3(CO)_{11}(PPh_2Et)]$(0.1404g) was dissolved in n-nonane (40ml) and the solution heated under reflux for an hour. Then after allowing to cool, the solvent was removed in vacuo and the residue chromatographed, with n-hexane as eluant, to give a single broad band. Extraction of the recovered product with n-pentane(1ml) left $[Os_3(CO)_9(PEt)(C_6H_4)]$(0.0993g, 81%) as a bright yellow, air stable, crystalline solid.
Elemental Analysis Cald. C 21.23% H 0.95%
MW=958.78g.mol^{-1} Obsd. C 21.54% H 1.01%

The corresponding adducts from $[Os_3(CO)_{11}(PPh_2R)]$, R=Me or Ph, were prepared using identical conditions.

$[Os_3(CO)_9(PMe)(C_6H_4)]$ Typical yield=64%
Elemental Analysis Cald. C 20.34% H 0.75%
MW=944.75g.mol^{-1} Obsd. C 21.0% H 0.7%

$[Os_3(CO)_9(PPh)(C_6H_4)]$ Typical yield=75%
Elemental Analysis Cald. C 25.05% H 0.90%
MW=1006.82g.mol^{-1} Obsd. C 25.98% H 1.1%

4.7. References

1. C.R.Eady, B.F.G.Johnson and J.Lewis, J.C.S. Dalton, 1975, 2606.
2. R.Mason, K.M.Thomas and D.M.P.Mingos, J. Amer. Chem. Soc., 1973, 95, 3802.
3. C.R.Eady, B.F.G.Johnson, J.Lewis, B.E.Reichert and G.M.Sheldrick, J.C.S. Chem. Comm., 1976, 271.
4. C.R.Eady, B.F.G.Johnson, J.Lewis, R.Mason, P.B.Hitchcock and K.M.Thomas, J.C.S. Chem. Comm., 1977, 385.
5. C.R.Eady, B.F.G.Johnson, J.Lewis and T.Matheson, J. Organometallic Chem., 1973, 57, C82.
6. a) P.F.Jackson, B.F.G.Johnson, J.Lewis, M.McPartlin and W.J.H.Nelson, J.C.S. Chem. Comm., 1980, 224.
   b) P.F.Jackson, B.F.G.Johnson, J.Lewis, W.J.H.Nelson and M.McPartlin, J.C.S. Dalton, 1982, 2099.
7. P.F.Jackson, B.F.G.Johnson, J.Lewis, M.McPartlin and W.J.H.Nelson, J.C.S. Chem. Comm., 1982, 49.
8. B.F.G.Johnson, J.Lewis and P.A.Kilty, J. Chem. Soc. (A), 1968, 2859.
9. C.R.Eady, B.F.G.Johnson and J.Lewis, J. Organometallic Chem., 1973, 57, C84.
10. C-M.T.Hayward and J.R.Shapley, Inorg. Chem., 1982, 21, 3816.
11. D.Braga, J.Lewis, B.F.G.Johnson, M.McPartlin, W.J.H.Nelson and M.D.Vargas, J.C.S. Chem. Comm., 1983, 241.
12. M.J.Mays and P.D.Gavens, J. Organometallic Chem., 1977, 124, C37.
13. P.D.Gavens, Ph.D. Thesis, Cambridge, 1977.
14. A.G.Orpen and G.M.Sheldrick, Acta Cryst. 1978, B34, 1989.
15. A.V.Rivera, G.M.Sheldrick and M.B.Hursthouse, Acta Cryst., 1978, B34, 1985.
16. B.F.G.Johnson, J.Lewis and I.G.Williams, J. Chem. Soc. (A), 1970, 901.
17. C.R.Eady, P.F.Jackson, B.F.G.Johnson, J.Lewis, M.C.Malatesta, M.McPartlin and W.J.H.Nelson, J.C.S. Dalton, 1980, 383.
18. M.I.Bruce, J.G.Matisons, J.R.Rodgers and R.C.Wallis, J.C.S. Chem. Comm., 1981, 1070.
19. a) J.M.Fernandez, B.F.G.Johnson, J.Lewis and P.R.Raithby, J.C.S. Chem. Comm., 1978, 1015.

b) J.M.Fernandez, B.F.G.Johnson, J.Lewis and P.R.Raithby, Acta Cryst., 1979, B35, 1711.

20. J.M.Fernandez, B.F.G.Johnson, J.Lewis, P.R.Raithby and G.M.Sheldrick, Acta Cryst., 1978, B34, 1994.

21. A.G.Orpen and G.M.Sheldrick, Acta Cryst., 1978, B34, 1992.

22. J.M.Fernandez, B.F.G.Johnson, J.Lewis and P.R.Raithby, J.C.S. Dalton, 1981, 2250.

23. K.Natarajan, L.Zsolnai and G.Huttner, J. Organometallic Chem., 1981, 209, 85.

24. K.Wade, Chem. Br., 1975, 11, 177.

25. C.W.Bradford and R.S.Nyholm, J.C.S. Dalton, 1973, 529.

26. C.W.Bradford, R.S.Nyholm, G.J.Gainsford, J.M.Guss, P.R.Ireland and R.Mason, J.C.S. Chem. Comm., 1972, 87.

27. C.W.Bradford, R.S.Nyholm, G.J.Gainsford, J.M.Guss, P.R.Ireland, and R.Mason, J. Organometallic Chem., 1972, 40, C70.

28. C.W.Bradford and R.S.Nyholm, J.C.S. Chem. Comm., 1967, 384.

29. A.J.Deeming, R.E.Kimber and M.Underhill, J.C.S. Dalton, 1973, 2589.

30. A.J.Deeming, I.P.Rothwell, M.B.Hursthouse and J.D.J.Backer-Dirks, J.C.S. Dalton, 1981, 1879.

31. R.D.Adams, D.A.Katahira and L-W.Yang, Organometallics, 1982, 1, 235.

32. A.J.Deeming and M.Underhill, J.C.S. Dalton, 1973, 2727.

33. C.Masters, J.C.S. Chem. Comm., 1973, 191.

34. M.R.Churchill and B.G.DeBoer, Inorg. Chem., 1977, 16, 878.

35. K.Natarajan, L.Zsolnai and G.Huttner, J. Organometallic Chem., 1981, 220, 365.

36. B.F.G.Johnson, J.Lewis, P.G.Lodge, P.R.Raithby, K.Hendrick and M.McPartlin, J.C.S. Chem. Comm., 1979, 719.

37. K.A.Azam, A.J.Deeming, R.E.Kimber and P.R.Shukla, J.C.S. D Dalton, 1976, 1853.

38. a) R.B.Calvert and J.R.Shapley, J. Amer. Chem. Soc., 1977, 99, 5225.

b) A.J.Deeming and M.Underhill, J.C.S. Chem. Comm., 1973, 277.

39. L.Markó and B.Markó, Inorg. Chim. Acta, 1975, 14, L39.

40. P.M.Treichel, W.K.Dean and W.M.Douglas, Inorg. Chem., 1972, 11, 1609.

41. a) G.Huttner, A.Frank and G.Mohr, Z. Naturforsch, 1976, B31,

1161.

b) G.Huttner, A.Frank and G.Mohr, Angew. Chem. Int. Ed. Engl., 1976, 15, 687.

42. S.C.Brown, J.Evans and L.E.Smart, J.C.S. Chem. Comm., 1980, 1021.

43. F.Iwasaki, M.J.Mays, P.R.Raithby, P.L.Taylor and P.J.Wheatley, J. Organometallic Chem., 1981, 213, 185.

44. G.Huttner, J.Schneider, G.Mohr and J.von Seyerl, J. Organometallic Chem., 1980, 191, 161.

45. S.L.Cook, J.Evans, L.R.Gray and M.Webster, J. Organometallic Chem., 1982, 236, 367.

46. a) R.J.Angelici and E.E.Siefert, Inorg. Chem., 1966, 5, 1457.
b) S.M.Grant and A.R.Manning, Inorg. Chim. Acta, 1978, 31, 41.

47. J.S.Field, R.J.Haines and D.N.Smit, J. Organometallic Chem., 1982, 224, C49.

48. G.Huttner, J.Schneider, H.D.Muller, G.Mohr, J.von Seyerl and L.Wohlfahrt, Angew. Chem. Int. Ed. Engl., 1979, 18, 76.

49. J.S.Field, R.J.Haines, D.N.Smit, K.Natarajan, O.Scheidsteger and G.Huttner, J. Organometallic Chem., 1982, 240, C23.

50. H.Vahrenkamp and D.Walters, Organometallics, 1982, 1, 874.

51. R.D.Adams and N.M.Golembeski, J. Organometallic Chem., 1979, 172, 239.

52. A.J.Shultz, J.M.Williams, R.B.Calvert, J.R.Shapley and G.D.Stucky, Inorg. Chem., 1979, 18, 319.

53. B.F.G.Johnson, J.Lewis, A.L.Mann and P.R.Raithby, J.C.S. Chem. Comm., 1980, 547.

54. M.Poliakoff and J.J.Turner, J.C.S. Chem. Comm., 1970, 1008.

55. J.Knight and M.J.Mays, J.C.S. Chem. Comm., 1970, 1006.

56. C.H.Wei and L.F.Dahl, J. Amer. Chem. Soc., 1969, 91, 1351.

57. F.A.Cotton and J.M.Troup, J. Amer. Chem. Soc., 1974, 96, 4155.

58. F.A.Cotton and D.L.Hunter, Inorg. Chim. Acta, 1974, 11, L9.

59. B.F.G.Johnson, J.C.S. Chem. Comm., 1976, 703.

60 R.E.Benfield, P.D.Gavens, B.F.G.Johnson, M.J.Mays, S.Aime, L.Milone and D.Osella, J.C.S. Dalton, 1981, 1535.

61. S.Aime, D.Osella, L.Milone and E.Rosenberg, J. Organometallic Chem., 1981, 213, 207.

62. C.J.Cooksey, A.J.Deeming and I.P.Rothwell, J.C.S. Dalton, 1981, 1718.

63. A.J.Arce and A.J.Deeming, J.C.S. Dalton, 1982, 1155.
64. C.C.Yin and A.J.Deeming, J.C.S. Dalton, 1974, 1013.
65. E.Sappa and L.Milone, J. Organometallic Chem., 1973, 61, 383.

CHAPTER FIVE

THERMAL STABILITY AND CATALYTIC ACTIVITY OF PHOSPHINE-ANCHORED TRIOSMIUM CLUSTERS

SECTION (A): Thermolysis Studies

In this chapter the potential of $[Os_3(CO)_{11}(PPh_2CH_2CH_2SIL)]$,I, and $[H_2Os_3(CO)_9(PPh_2CH_2CH_2SIL)]$,II, as catalysts for alkene hydrogenation/isomerisation is explored. However, before these results are presented consideration of their thermal stability is necessary, for two reasons:-

1) Almost certainly elevated temperatures will be necessary to promote rates approaching industrial interest. At these conditions catalyst deactivation may occur by the pathways already discussed (Chapter Three and Four). Alternatively breakdown may result from interaction with remaining surface ligands, either pendent phosphines or groups indigenous to silica. A knowledge of such a process would obviously assist analysis of spent catalysts.

2) For a saturated cluster, activation will result from either metal-metal bond cleavage or, more likely, dissociation of carbon monoxide creating a vacant site. The stability of such partially decarbonylated species is therefore important(1). A wider aspect involves the potential of heterogenized metal clusters as precursors to forming small metal dispersions(2). This route could provide increased control of the particle structure, the binding ligands restricting aggregation, giving small, uniform metal groupings of the order of magnitude often postulated of great activity in catalytic reactions i.e. Fischer-Tropsch.

5.1. Supported Rhodium Carbonyl Clusters

In pursuit of the second objective considerable effort has been focused on the stability of rhodium carbonyl clusters on a variety of inorganic oxide supports. The results illustrate several important trends; highlighting the importance of the support nature, introduced pendent ligands, surface water and aerial oxidation, have on determining the observed surface species. It is only when the latter two factors are fully considered that apparently conflicting claims for the adsorption of $[Rh_6(CO)_{16}]$ on alumina and silica can be rationalised.

5.1.1. Adsorption on Unfunctionalised Oxides

When $[Rh_6(CO)_{16}]$ is contacted with alumina, in the air, the support acquires a golden hue. The product rapidly decarbonylates with evolution of carbon dioxide until it exhibits no infrared ν_{CO} spectrum. This process is retarded if an attempt to remove physically adsorbed water is made. However, when an atmosphere of carbon monoxide is introduced and maintained, and provided a partial pressure of water exists, the material changes to a deep violet and $[Rh_6(CO)_{16}]$ can be extracted back into $CHCl_3$(3). When impregnation is carried out in the absence of air the stability of the initial cluster increases if the alumina has been previously outgassed at elevated temperatures (500°C)(4). Variations in the positions of the ν_{CO} absorptions for the adsorbed molecule were equated with the extent of hydrogen bonding of the complex to the support, which altered with the degree of hydration of the support.

Carbonylation occurs in two stages, with an intermediate ,III, characterised by two bands at 2090 and 2020 cm^{-1}. The second stage leading to the formation of adsorbed $[Rh_6(CO)_{16}]$ (bands at 2060 and 1815cm^{-1}), which is accompanied by carbon dioxide production, is slow unless water is introduced whence the second stage bands predominate soon after initiating the experiment. Decarbonylation with dioxygen alone only proceeds very slowly (150 hours) to stage one, but again water vapour (10 torr) completely removes all ν_{CO} bands within 4 hours. However water alone did not initiate the process. These results are interpreted differently by the research groups of Basset and Watters because of conflicting additional evidence from gas volumetric studies.

Isotopic $^{18,18}O_2$ studies by the first group(5) suggested that dioxygen is non-dissociatively adsorbed in the partially (III) and totally decarbonylated forms, but is incorporated in the released carbon dioxide on carbonylation, a process in which water does not directly participate but may assist in weakening support interactions. They concluded that both forms are oxoclusters, containing bridging dioxygen ligands, and proposed MECHANISM ONE, consistent in stoichiometry with the volumetric studies. This excludes the need for strong bonding to the support, although it was conceded that its nature effects the chemistry.

Conversely, Basset(4) claimed a combined release of hydrogen and carbon dioxide during decarbonylation. At higher temperatures ($>60^{o}C$) some hydrogen is incorporated as hydrocarbons, while if the alumina had undergone exchange with deuterated water this was reflected in the off-gases(6). The direct involvement of physisorbed water in the second stage was also favoured. This led

MECHANISM ONE (Watters)

Decarbonylation

$$[Rh_6(CO)_{16}] + 8O_2 \longrightarrow [Rh_6(CO)_{12}(O_2)_6] + 4CO_2$$

$$[Rh_6(CO)_{12}(O_2)_6] + 6O_2 \longrightarrow [Rh_6(O_2)_6] + 12CO_2$$

Carbonylation

$$[Rh_6(O_2)_6] + 12CO \longrightarrow [Rh_6(CO)_{12}(O_2)_6]$$

$$[Rh_6(CO)_{12}(O_2)_6] + 16CO \longrightarrow [Rh_6(CO)_{16}] + 12CO_2$$

MECHANISM TWO (Basset)

Decarbonylation

$$[Rh_6(CO)_{16}] + H\text{-}O\text{-}Al \longrightarrow (OC)_2RhO\text{-}Al + 4CO + 3H_2$$

Carbonylation

$$(OC)_2RhO\text{-}Al + 7CO + 3H_2O \longrightarrow [Rh_6(CO)_{16}] + 6H\text{-}O\text{-}Al + 3CO_2$$

to the infrared ν_{CO} doublet for III being assigned to the symmetric and asymmetric stretching modes of two geminal carbonyl ligands coordinated to an oxidized rhodium atom. In position and intensities these frequencies show good agreement with those of Rh(I) complexes such as $[Rh(CO)_2Cl]_2$, whose chemisorption also supported the hypothesis. These cis-$Rh(I)(CO)_2$ fragments are chemically bound to the support through surface oxygen linkages. Then carbonylation of III in MECHANISM TWO is a direct analogy to the conventional

synthesis(7) whereby $[Rh_4(CO)_{12}]$, and then $[Rh_6(CO)_{16}]$, are formed by room temperature carbonylation of $[Rh(CO)_2Cl]_2$ under basic conditions in the presence of water. Retention of the hexarhodium core through the entire cycle is therefore not paramount, although under the mild conditions the moieties probably remain in close vicinity on the surface. Hence, even $RhCl_3$ deposited to a 4% loading can enter the cycle. Under carbon monoxide the infrared ν_{CO} spectrum exhibits a band at 2135cm^{-1}, attributed to a surface Rh(III) species(8), but at 60°C two sharp bands synonymous with a a $Rh(I)(CO)_2$ species develops at its expense. A greater resistance to hydrogen reduction is indicative of initially retained halide bridges.

Whatever the pretreatment, III is reduced at moderate temperatures (>60°C) with hydrogen, or water alone, to a species characterised by broader bands at 2020 and 1850cm^{-1}. These features are typical of linear and bridged forms of carbon monoxide adsorbed on dispersed metallic Rh(0) crystallites(9). They are easily removed with oxygen and carbonylation reforms III. Evacuation alone at very high temperatures (500°C) could not facilitate this reduction, although XPS measurements did confirm the presence of highly dispersed metal particles. This XPS investigation(10) could not resolve the true nature of III as the recorded binding energy was more consistent with fragmentation into mononuclear Rh^{3+} species, contrary to the other evidence. An EPR study was equally uninformative.

On silica similar trends are found, but the more severe conditions necessary reflect the different nature of the surface hydroxyl groups. Thus deposition of both $[Rh_4(CO)_{12}]$ and $[Rh_6(CO)_{16}]$ onto an unspecified grade of silica at 25°C, even without precautions to exclude air, led to only physical adsorption(3). Under more controlled conditions(11) contacting $[Rh_6(CO)_{16}]$ with Aerosil 200, pretreated at 300°C under vacuum, caused a partial decarbonylation signified by evolution of carbon dioxide, and a modification in the relative intensities of the ν_{CO} bands. Breakdown of the cluster cage does not apparently occur as the original cluster is regenerated by carbonylation at 200°C, and thereafter remains indefinitively stable under argon. However, under vacuum (150°C) decomposition takes place giving two ν_{CO} bands, at 2048 7(sharp)

and 1893±10(broad)cm^{-1} representative of terminal and bridging carbonyl groups adsorbed on small metallic(0) particles. Their positions vary with their intensities in accord with different degrees of coverage on the rhodium surface. The particle size is governed by the water content, suggesting it assists migration of carbonylated zerovalent rhodium species. If decomposition at 100°C is in the presence of carbon monoxide and oxygen the pellet reverts to a dark brown and two intense bands at 2093 and 2038cm^{-1} form, corresponding to the oxidized surface species, III. Again it undergoes reversible decarbonylation, and is easily reduced to the metallic species with hydrogen.

When a low loading of $[Rh_4(CO)_{12}]$ is impregnated a complete transformation to physisorbed $[Rh_6(CO)_{16}]$ occurs, but can be blocked by introduction of carbon monoxide(12). When larger amounts are adsorbed a mixture of both clusters is obtained(13), indicating that, although the silica was dehydroxylated at 500°C, some oxidized groups remain which are quickly consumed. These also cause the partial decarbonylation of $[Rh_6(CO)_{16}]$, and once removed from the coordination sphere the cluster remains intact. Of course the subsequent formation of the metallic and oxidized surface species is possible, additionally with carbon monoxide in the presence of sufficient water, the regeneration of $[Rh_6(CO)_{16}]$ with intermediate identification of $[Rh_4(CO)_{12}]$ was demonstrated.

Here the credibility of surface $Rh(I)(CO)_2$ fragments is supported by the properties of the isolable model compound $[Rh(CO)_2(OSiPh_3)]_2$(14), the corresponding methyl derivative was less stable(12). Both were easily reduced by traces of water to a decarbonylated black material, presumably rhodium metal. Handled under wet carbon monoxide the silanolates were transformed into $[Rh_4(CO)_{12}]$; carbon dioxide and free silanol being formed and identified in this reaction. Related alcoholates also behave similarly(15). Thus a good parallism in chemical behaviour exists between the homogeneous and heterogeneous variants. The absence of any strong Raman signals assignable to metal-metal vibrations for III is also consistent with the fragments only being connected by rather weak interactions(16).

Overall the mechanisms of Basset and Watters both have merit. Certainly the much more facile chemisorption on alumina is

the consequence of the much greater ionicity of the surface oxygens, hydroxyl(OH_s^-) or oxides(O_s^{2-}), favours an oxidative decarbonylation process. On silica, containing hydroxyl groups with only a very weak Brönsted acidity, the importance of strong support-fragment interactions may be less and oxoclusters predominate initially, to be gradually replaced on (thermal) ageing. This also accounts for the greater propensity to form the metallic(0) state, instead of III, on silica by evacuation. Silica-alumina, which has a strong Brönsted acidity of hydroxyl groups, is even less reactive and $[Rh_6(CO)_{16}]$ is stable for several days, even under vacuum(4). Ichikawa made similar observations on other acidic oxides such as ZnO, La_2O_3 and ZrO_2(17). Conversely on highly basic magnesia, even when pretreated at 500°C, the decomposition is quite instantaneous to the metallic, but predominantly oxidized, species (4).

These systems, and the small metal aggregates derived thereof from, act as catalysts for Fischer-Tropsch synthesis(18), being more active and selective for methanol and ethanol production (19) than those obtained by conventional salt impregnation. Ichikawa (20) also demonstrated their effectiveness, particularly on ZnO, for olefin hydroformylation. Under much milder conditions hydrogenation of 1,3-trans-pentadiene by III on alumina has been established(21).

5.1.2. Attachment on Phosphine-modified Silica

Introduction of a pendent ligand strongly coordinating a metal centre is expected to further prevent agglomeration to metal crystallites. Attachment of $[Rh_6(CO)_{16}]$ at 60°C, from a saturated $CHCl_3$ solution, by ligand exchange with $PPh_2CH_2CH_2SIL$ (Aerosil 380) yielded a product, IV, characterised by two strong bands at 2070 and 1995cm^{-1} in its infrared ν_{CO} spectrum(22); if maintained under carbon monoxide. The positions of these bands closely resembled those of phosphine substituted clusters such as $[Rh_6(CO)_{13}(PPh_3)_3]$(23) supporting the hypothesis that the cluster had undergone a similar degree of substitution but retained its integrity after tethering. The expected bridging vibrations were believed to be obscured by absorptions arising from the support

lattice. From elemental analysis the high ratio between the number of available phosphine groups and attached clusters (typically 100:1) was also in agreement with a relatively high degree of substitution, whilst the failure to observe metal crystallites by TEM(22) was consistent with the presence of very small metal particles. Once formed, the increased stability of IV stands it apart from those species obtained on unmodified silica. It is reasonably stable under oxygen at room temperature, and remains unaltered under carbon monoxide. On evacuation at 150°C the bands only lose ca. 65-80% of their original intensities, but are quickly re-established on exposure to carbon monoxide. A preferential decrease of the band at 2070cm^{-1}, and coordination experiments with ethylene, suggested the presence of a partially decarbonylated form.

Subsequently, Knözinger et. al.(24) published a more detailed assignment of the infrared ν_{CO} spectrum, assisted by ^{13}CO substitution experiments, which showed their original interpretation to be incorrect. The support contained $Rh(CO)_2$ groups when fully carbonylated, with the formation of a monocarbonyl species upon decarbonylation. The presence of a mononuclear geminal dicarbonyl complex, IV, was unambiguously confirmed by the four isotopically shifted bands observed. An XPS study indicated that the rhodium is in the +1 oxidation state(25). The broadness of the low frequency band arises from its composite nature, representing contributions from the antisymmetrical stretch of the $L_nRh^+(CO)_2$ moiety and the ν_{CO} band of the $L_nRh^+(CO)$ species. The model compounds, $[Rh(CO)(PR'_3)(OSiR''_3)]$, R'=Ph or Bu, R''=Ph or Me, have been prepared and exhibit a ν_{CO} band at about 1960cm^{-1}(26).

Exposure to hydrogen above 80°C causes a complete change in the spectrum leaving only a single band at 1975cm^{-1}. Recarbonylation reproduces the original features plus a new band at 2020cm^{-1}, which could be removed during a brief evacuation at cell temperature. More severe conditions cause the 2020 band to dominate. This coincided with an observed change from a pale brown of the original sample to dark gray after the final treatment. This was assigned to carbon monoxide adsorbed on rhodium crystallites, formed at the expense of the mononuclear species. Electron microscopy produced further confirmation showing no metal particles greater than 5Å

across initially, whereas a large number of rhodium crystallites (12-15Å) are present after treatment with hydrogen at 140°C. This agglomeration process was slower on an amine-modified surface(27).

These results are complimented by those of Howell et. al.(28) who contacted $[Rh(CO)_2Cl]_2$ with $PPh_2CH_2CH_2SIL$. Two reactions were anticipated, substitution of a carbonyl ligand or splitting of the halide bridge(29), but the infrared evidence pointed to only the latter giving $[RhCl(CO)_2(PPh_2CH_2CH_2SIL)]$ as a yellow silica, (2090 and 2018cm^{-1}). Alternatively, they were able to isolate and characterise $[RhCl(CO)(PPh_2CH_2CH_2Si(OEt)_3)_2]$, (1966cm^{-1}), by reaction with excess phosphino-silane, and subsequently attach it to silica to yield the heterogenized form. Together these represent, provided the halide groups are replaced by oxygen linkages to the surface, the two components seen when contacting $[Rh_6(CO)_{16}]$ with the modified silica. These, and related phosphine-silica immobilised rhodium carbonyl species, were studied as hydroformylation catalysts. Rigorous exclusion of oxygen was necessary to avoid rhodium elution caused by (rhodium catalysed) oxidation of the tertiary phosphine to phosphine oxide, which no longer coordinates to the rhodium centre. Significantly, the anchored $[RhH(CO)(PPh_2CH_2CH_2Si(OEt)_3)_3]$ had markedly better resistance to leaching(30).

Smith and coworkers(31,32) have also studied the $[Rh_6(CO)_{16}]/PPh_2CH_2CH_2SIL$ system. However some of their results are more consistent with direct reaction with the surface, rather than with the anchored phosphine groups. Further the outcome is dependent on the adsorption conditions. Treatment at ambient temperature under argon gives a blue-gray powder which, on introduction of carbon monoxide, gives ν_{CO} bands at 2084, 2052, 2004 and 1860cm^{-1}. The behaviour of the two intense bands at 2084 and 2002cm^{-1} to various treatments is entirely consistent with IV. The second set (2052 and 1860cm^{-1}) show identical properties to the 'metallic' state observed when physisorbed $[Rh_6(CO)_{16}]$ on silica is heated to 150°C under vacuum(31). The second preparation involved refluxing in benzene for 3 hours. Introduction of carbon monoxide gave infrared absorptions at 2090, 2031 and 1870cm^{-1}, corresponding to two different species which are very similar to the metallic and oxidized, (III), forms seen on unmodified silica.

However (significant) differences in the frequencies, particularly for the metallic state, were taken to infer that some coordination through phosphine ligands still existed. This would appear to represent an intermediate case, where the number of pendent phosphines available is limited, such that interaction with the silanol groups is the principle consideration. When preformed $[Rh_4(CO)_{10}(PPh_2CH_2CH_2Si(OEt)_3)_2]$ is deposited on silica, the associated infrared spectrum can be interpreted as a combination of the two oxidized species, III and IV(32). Thus even on modified silicas the influence of remaining surface groups cannot be overlooked, and will determine both the nature, and distribution, of the products if not removed. Significantly the pendent phosphines do stabilise the oxidized mononuclear species against decarbonylation and agglomeration.

Interestingly, a parallel development occurred for $[Rh_6(CO)_{16}]$ on phosphine-functionalised polystyrene membranes, with a similar misconseption of retained hexarhodium core by comparison of the relatively simple ν_{co} spectrum with that of $[Rh_6(CO)_{13}(PPh_3)_3]$. At 25°C the initial complex undergoes aerial oxidation, and the golden brown transparent membrane exhibits no carbonyl absorptions prior to exposure to carbon monoxide(33). Afterwards, ν_{co} bands develop at 2078 and 2010-1985, typically 2008, cm^{-1}; the actual position depending on the extent of carbonylation. TEM showed no evidence of metal particles greater than 15Å across. When brought in contact at 50°C the resulting membrane is gray or black, and TEM showed that metal aggregates, having an average diameter of 25-40Å, were present(34). Carbonylation produced ν_{co} bands at 2046 and 1900cm^{-1}. These observations show a compelling resemblance to those seen on inorganic oxides. The light coloured catalysts are almost certainly analogous to III, and the dark material denotes carbon monoxide adsorbed on rhodium crystallites. The high concentration of bromo-groups invariably left on the polymer by the method of functionalisation are the chemical equivalent to the hydroxyl groups on oxide supports. The agglomeration process is accelerated by oxygen, leading to oxidation of the chelating phosphine ligands as evidenced by the emergence of bands at 1120 and 1170cm^{-1} matching the most intense ones for triphenylphosphine-oxide. Accordingly, during studies into alkene hydrogenation, a

longer catalyst lifetime was experienced with membranes having a high ratio of phosphines to rhodium atoms(34), but lower activity. The active catalyst was shown to be the decarbonylated form of III (35). Similarly in a flow-reactor, with related polymer bound rhodium monomers, oxygen contamination caused loss of activity by rhodium elution from the system in the product stream(30).

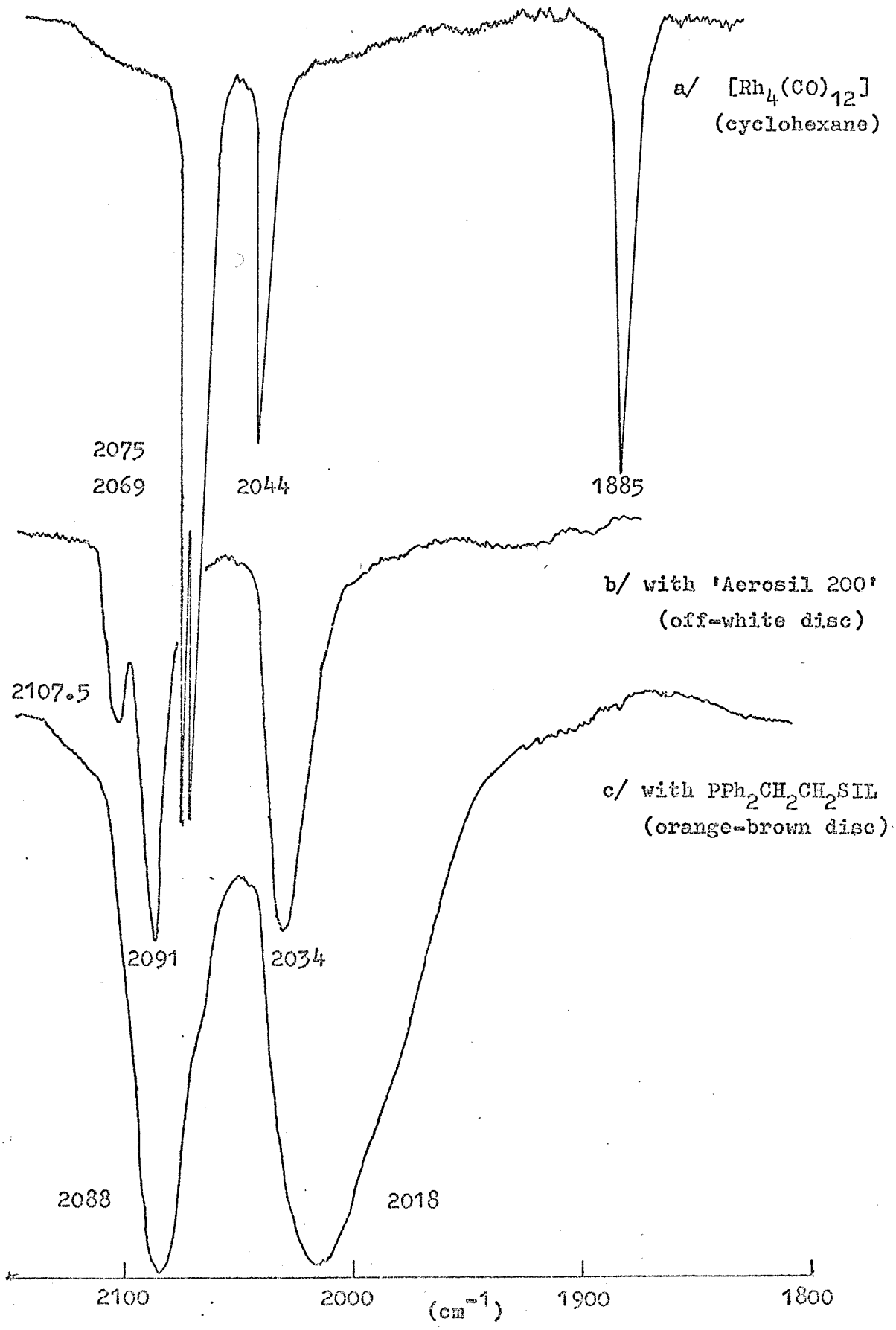
5.1.3. Reaction of $[Rh_4(CO)_{12}]$ with 'Aerosil 200' or $PPh_2CH_2CH_2SIL$

A large excess of $[Rh_4(CO)_{12}]$ was added to a n-hexane suspension of untreated (thermally or chemically) 'Aerosil 200', and left stirring under dry nitrogen overnight. Then the silica was filtered off and washed with consecutive portions of CH_2Cl_2 until they nolonger had any perceivable coloration. The original filtrate was shown to contain only unreacted $[Rh_4(CO)_{12}]$. After drying in the air the obtained silica had a light orange appearance. Elemental analysis established a rhodium content of 0.055wt/wt%, an average of 1.5 rhodium atoms per $100nm^2$. This demonstrates the only limited interaction with the virgin surface, the preparative method removing all physisorbed material leaving only grafted species. A pressed, self-supporting, disc gave an infrared ν_{CO} spectrum with bands at 2107.5m, 2091s and 2034s, cm^{-1} (Diagram 1). This is inconsistent with adsorbed cluster, but is almost identical to that observed for Rh(I) dicarbonyl sites, III, previously derived from $[Rh_6(CO)_{16}]$. In the preceding discussions the highest wavenumber vibration was always treated separately, invariably as a Rh(III) site(36). However, this three band arrangement is strongly reminiscent of that for $[Rh(CO)_2Cl]_2$, and based on this analogy III would have a dimeric structure (with chloride ions being replaced by surface oxide ions). This third vibration is a consequence of the bent structure, and the ratio of intensities of these bands can be used to calculate the dihedral angle(37). Under more forcing conditions, or on other supports, this more ordered structure may disintegrate to isolated $Rh(I)(CO)_2$ fragments with simultaneous loss of the highest absorption.

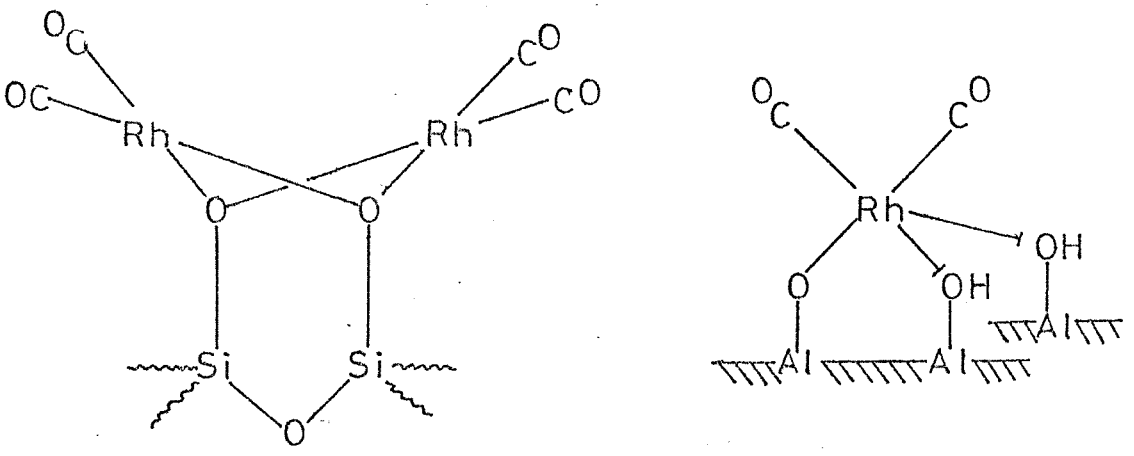
To further test this supposition $[Rh(CO)_2Cl]_2$ was similarly contacted with virgin 'Aerosil 200'. Over the same duration the retrieved silica had only acquired a faint coloration, but a

Diagram 1

Infrared (ν_{CO}) Spectra of Products from contacting $[Rh_4(CO)_{12}]$ with Silica Surfaces



self-supporting disc gave ν_{co} bands at 2109m, 2092.5s and 2036.5s, cm^{-1}. This is almost identical to the spectrum of the free species, but because it persisted after successive washes it is attributed to a chemically attached derivative on silica, with ligand substitution of one or both halide bridges. Although not quantified,



Possible structures of III

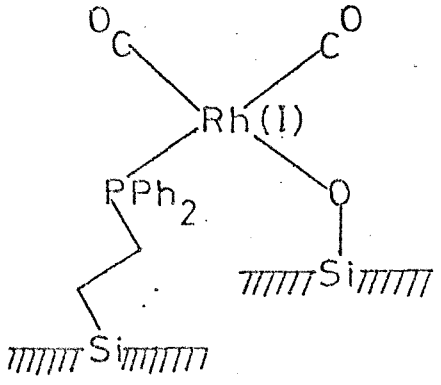
the obviously reduced loading compared to that achieved with $[Rh_4(CO)_{12}]$, must reflect the greater difficulty of this displacement compared to oxidative addition across a Rh-Rh bond.

Under identical conditions the uptake of rhodium by the functionalised silica, $PPh_2CH_2CH_2SIL$, was much greater (2.55wt/wt%). The final orange-brown silica, IV, was pelletised to produce a strong doublet, at 2088 and 2018cm^{-1}, in its infrared ν_{co} spectrum (Diagram 1). This shows good agreement (Table 1) to that reported from reaction of $[Rh(CO)_2Cl]_2$ with the ligand-silica(28); substantial differences with that of similar units derived from $[Rh_6(CO)_{16}]$ suggests that the nature of the remaining ligands in the coordination shell is highly dependent upon the preparative conditions. The rhodium content translates to an approximate density of 0.75 molecules per nm^2, which is close to the average phosphine coverage ($0.93nm^{-2}$). Unless fortuitous, this is good circumstantial evidence for cis-$Rh(I)(CO)_2$ moieties now each bound to a phosphine. Secondly, almost complete coordination of all available ligands suggests that only a limited phosphine-oxide concentration exists on the surface. This much higher loading on the modified surface indicates that

Table 1

Compound	IR ν_{CO}/cm^{-1}(solvent)	Reference
III, (this work)	2107.5m 2091s 2034s (solid disc)	
$[Rh(CO)_2Cl]_2$	2105m 2089s 2035 (hexane)	(38)
IV, (this work)	2088 2018(solid disc)	
$[RhCl(CO)_2(PPh_2CH_2CH_2SIL)]$	2090 2018(nujol mull)	(28)
cis-$[RhCl(CO)_2(PPh_3)]$	2088 2002(hexadecane)	(39)
IV, (Knözinger)	2070 1995(solid disc)	(24)
IV, (Smith)	2084 2002(solid disc)	(31)
trans-$[RhCl(CO)(PPh_3)_2]$	1961(nujol mull)	(40)
cis-$[RhCl(CO)(PPh_3)_2]$	1978(nujol mull)	(41)
$[Rh(CO)(PR'_3)(OSiR''_3)]$	1967-1956 (nujol mull or hexane)	(26)

initial contact is through the phosphine groups, and that involvement of other appendages is secondary. Thus multi-substitution of the cluster framework probably precedes breakdown, tethering holding the unit in closer proximity to the other indigenous species promoting degradation. Potential involvement with silanol groups is feasible, since the ligand-silica employed had not been protected by silylation, although the influence of surface water and oxygen cannot be dismissed. These prepared samples of III and IV where used in cyclohexene hydrogenation experiments, as comparisons against I and II, to demonstrate the increased activity of second row transition elements.



Proposed structure of IV

5.2. Thermal Degradation of $[HOs_3(CO)_{10}(OSIL)]$

For the Group VIIIa metal carbonyl clusters, with $[Fe_3(CO)_{12}]$ on the more reactive oxides the hydroxyl groups behave as nucleophiles toward coordinated carbon monoxide, with concomitant formation of $[HFe_3(CO)_{11}]^-$; reversible physisorption only occurring on silica(42). Thermal decomposition of such supported clusters generates very small metal particles showing Fischer-Tropsch catalytic activity. The fate of ruthenium clusters in contact with oxides, at elevated temperatures, is discussed in Chapter Six.

On a variety of oxides the originally physisorbed triosmium clusters thermally undergo oxidative addition by a surface hydroxyl group forming the grafted cluster $[HOs_3(CO)_{10}(OM)]$, M=Si(Va), Al(Vb), Ti(Vc), Mg(Vd) or Zn(Ve)(43,44). In turn, this species irreversibly breaksdown to pseudo-monomeric oxidised complexes, at varying temperatures reflecting the reactivity of the surface hydroxyl groups. Again the involvement of molecular oxygen and water is emphasized. For instance on alumina thermal decomposition, at 150-200°C in vacuo, causes the disappearance of the original infrared ν_{CO} bands, to be simultaneously replaced by a new set at 2125, 2031 and 1970cm^{-1}. The high frequency band at 2130 was clearly reduced during decarbonylation, while that of the broad feature at 1970 increased. An observed linear correlation between the integrated intensities of these bands inferred an interconversion of two carbonyl species. This was endorsed by treatment with carbon monoxide (typically 6.5 x10^{3}N.m^{-2}), between 200-250°C, resulting in the disappearance of the band at lower wavelength and a parallel increase in intensity of the 2130 band, while that at 2050 shifted to 2037cm^{-1}. In the presence of a partial pressure of water these final two absorptions are sharper. Heating in vacuo regenerated the initial spectrum, until at 300°C only a remnant at 2128 exists, and the final spectrum is characterised by two strong absorptions at 2040 and 1970cm^{-1}.

A similar transformation occurs on silica but slightly more drastic conditions (> 200°C) are necessary, and the corresponding bands are shifted to higher wavenumbers consistent with the more acidic nature of the support. Again evidence of an

equilibrium between two surface species existed, which are interconverted by a reversible carbonylation(45). Conversely, when Vd is exposed to air at ambient conditions, within 12 hours a doublet centred at 2013 and 1920cm^{-1} appeared, consistent with the more decarbonylated form(44). Infact the onset of cluster degradation, as evident by additional bands near 2130, 2050-30 and 1970-40cm^{-1}, even occurred on alumina at 25°C when exposed to the air, particularly if the support was not dehydroxylated(46).

The general pattern of these infrared spectra are comparable, both in position and in relative intensity of the absorption bands, with those of the known Os(II) derivatives $[Os(CO)_3X_2]$, X=Cl, Br or I, and polymeric $[Os(CO)_2I_2]_n$(47)(Table 2). As pointed out elsewhere(48) their structures offer very improbable sites for surface oxygens, with the planar halo-bridges creating impossible crowding for the axial ligands close to the surface. However, it can be considered that these very constraints on the surface stabilise alternative isomeric forms(49) not otherwise favoured. Therefore they should be only regarded as representative of typical enviroments and on the surface, where the concept of overall molecular symmetry is lost, only the localised system need be considered. A series of other observations, and spectroscopic data, provided further evidence that the surface species are oxidised divalent osmium units bound to the support through O-M linkages, so that on silica $[Os(CO)_3(OSIL)_2]$, VI, and $[Os(CO)_2(OSIL)_2]_n$, VII, are present.

XPS measurements(51) on the alumina forms gave evidence for the osmium being in the +2 oxidation state. Its Raman spectrum showed no bands in the low frequency region (below 200cm^{-1}) consistent with the absence of any ordered Os-Os(52). The EXAFS K^3 Fourier transform of the silica species did not contain any peak attributable to a second osmium nearest neighbour(45), in agreement with the lack of aggregation to very small metal particles and the existence of highly dispersed mononuclear complexes. Assignment of the higher doublet to a tricarbonyl compound with local C_{3v} symmetry (A_1 and doubly degenerate $E(B_1)$ modes) permitted a more detailed analysis of the infrared spectrum(46). This furnished an estimate of the C-Os-C bond angle(97°), and the orientation of the carbonyl groups to the plane of the support(30°). Development of a tentative

model on steric grounds for the closest approach of a neighbouring group led to a shortest possible Os-Os distance of about 5.9Å. This is jointly responsible with the known propensity of osmium to form extremely strong Os-O bonds(53) for the atomic dispersion of osmium species. The model compound $[Os(CO)_3(OSiPh_3)_2]_n$ was prepared and shown to have comparable spectroscopic features(45). The doublet of the dicarbonyl species is assigned to symmetric and antisymmetric stretching modes for a cis-(C_{2v} symmetry) arrangement. The same species can be obtained by thermal treatment of physisorbed $[Os_6(CO)_{18}]$, or by slow incorporation of $Os(CO)_3$ units when $[Os(CO)_3Cl_2]_2$ is contacted with silica at 200°C under vacuum, or impregnation with $OsCl_3$ and treatment at 150°C with a partial pressure of carbon monoxide to give first the three band, and finally the two band pattern(45). This lack of dependence on initial nuclearity again suggested a complete rupture of the cluster cage.

Additional evidence for the formation of divalent osmium species is derived from gas phase analysis above η-alumina, which shows the evolution of three moles of hydrogen per mole of grafted cluster, consistent with the mass balance given in Diagram 2. The important role of surface hydroxyl groups in the degradation is illustrated by the greater stability of Vb on a fluorinated alumina surface, from which the most basic groups are eliminated, so the remaining ones have properties comparable to those of silica. Similarly more dehydroxylated surfaces enhance the stability of V.

These oxidised Os(II) surface species are thermally, and chemically, more stable than the corresponding Rh(I) complexes. Only on approaching 400°C, under vacuum, does the sample turn brown and complete decarbonylation occur, but carbon monoxide at room temperature again regenerates VI. However, in the presence of hydrogen at 400°C, a similar complete disappearance takes place, but the sample turns gray and when carbon monoxide is reintroduced it remains so, and only a broad absorption centred at 2030cm^{-1} develops(45). This corresponds to carbon monoxide chemisorbed on metallic osmium; the dispersed nature of the metal still permits regeneration of VI by sequential treatment with oxygen and carbon monoxide. Selective catalytic hydrogenation of carbon monoxide to methane has been reported over silica, alumina(45) or magnesia(44) at conditions where the oxidised osmium carbonyl species should

Diagram 2

Thermal Degradation of the Grafted Cluster $[HOs_3(CO)_{10}(OM)]$; M=Si or Al

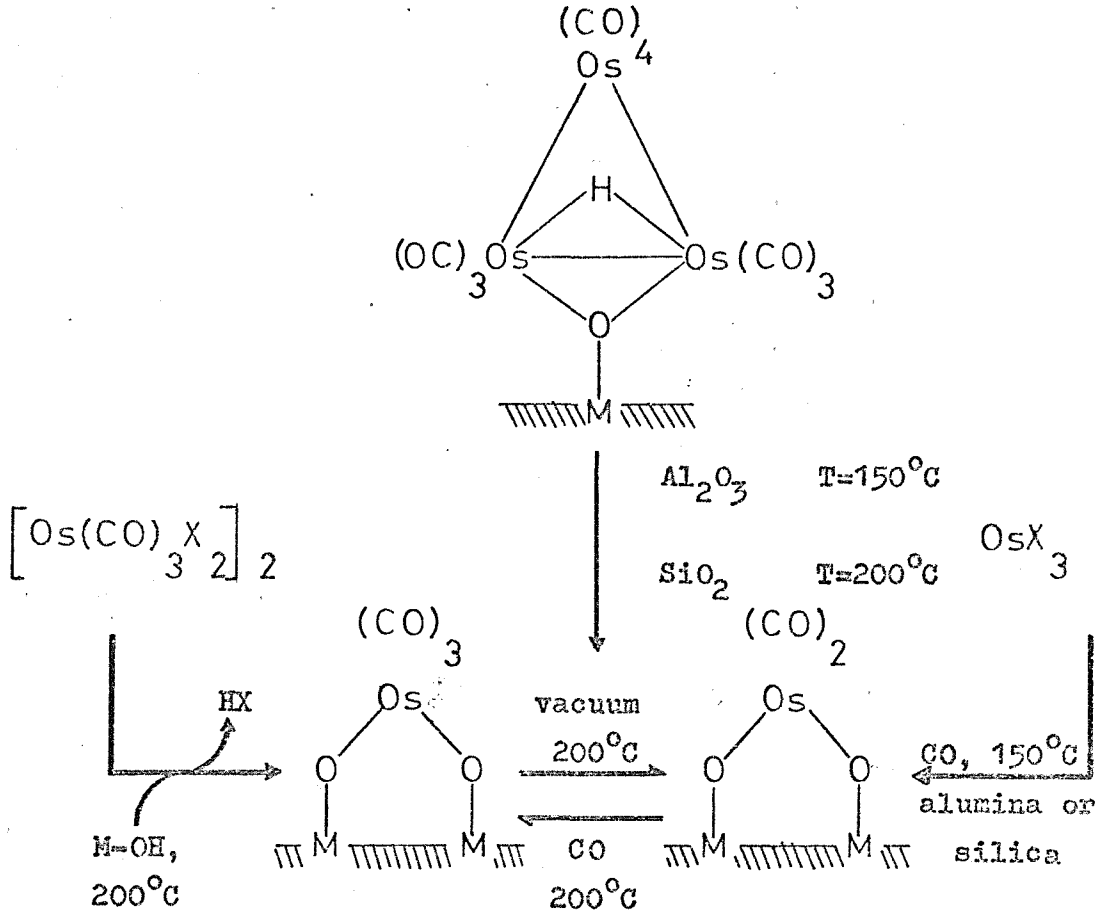


Table 2

Compound	IR ν_{CO}/cm^{-1} (solvent)			Reference
$[Os(CO)_2(OAl)_2]_n$	(solid disc) 2045		1970	(46)
$[Os(CO)_2(OSi)_2]_n$	2135-30m	2055-45vsbr	1960-75m	(45, 50)
$[Os(CO)_2I_2]$	(2119) (Nujol mull)	2045	1988	(47)
$[Os(CO)_3(OAl)_2]_m$	2128s	2037sbr	(solid disc)	(46)
$[Os(CO)_3(OSi)_2]_m$	2135-30m	2052-45sbr	(solid disc)	(45, 50)
$[Os(CO)_3(OSiPh_3)_2]_m$	2109m	2023s	(Nujol mull)	(45)
$[Os(CO)_3Cl_2]_2$				
α-isomer	2137s	2064s	($CHCl_3$)	(49)
β-isomer	2129s	2048s	2035s	(49)
$[Os(CO)_3I_2]_n$	2119s	2051s	(CCl_4)	(47)
$[Os(CO)_3Cl_2]_n$	2136s	2061s	(CCl_4)	(47)

persist. Small but detectable amounts of C_2-C_4 hydrocarbons were seen at lower temperatures. However the influence of extremely divided metal particles could not be rigorously excluded.

In opposition to all this evidence, a communication(54) has appeared which gives the three band spectrum an entirely different interpretation, proposing an increased cluster nuclearity with between Os_{12}-Os_{18} units on the surface. This arguement was largely based on transitions observed in the ultraviolet/visible reflectance spectra attributed to metal-metal bonding. Also, the relative infrared ν_{CO} band intensities were apparently independent of the osmium/carbonyl ligand ratios as determined from TPD studies. The three vibrations are taken to indicate the presence of carbonyl ligands bonded to osmium atoms in formal zero, partial negative, and partial positive oxidation states. Notably this 'self-spread' state was achieved without carbon monoxide loss at room temperature when impregnated $[Os_6(CO)_{18}]$ was left to stand in the dark for some weeks. Thia apparent divergence, enhancing increased nuclearity on heating, is possibly the consequence of more extensive dehydroxylation (500°C) reducing the support reactivity. However this approach is rather less convincing, and somewhat retrograde, when viewed in the context of the rhodium systems and the following results using the phosphinated-silica.

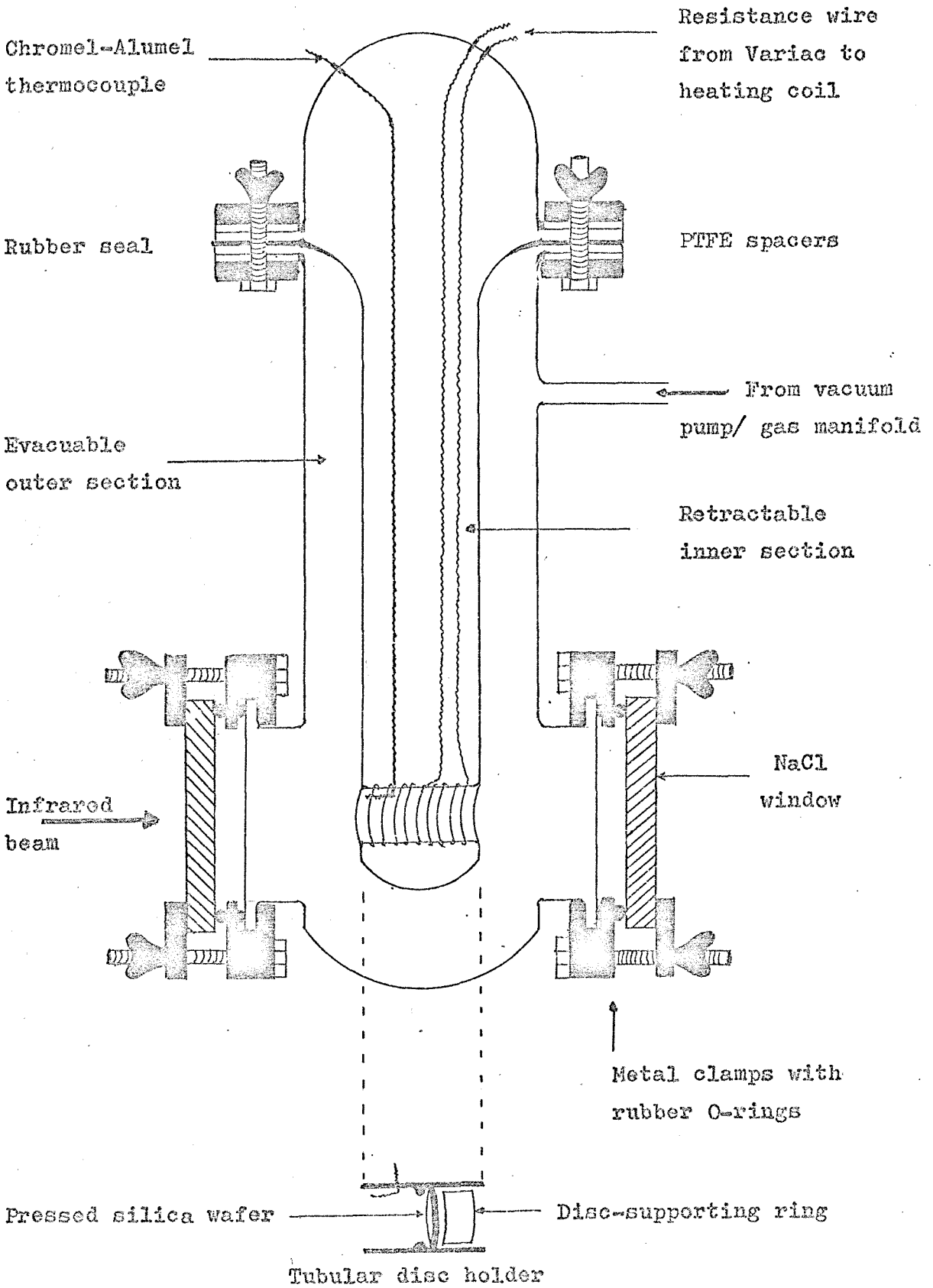
5.3. Pyrolysis of Phosphine-anchored Triosmium Clusters

5.3.1. Experimental Procedure

The evacuable infrared cell depicted in Diagram 3 was used to carryout insitu thermolytic studies in association with the Perkin-Elmer 580B spectrometer. Fabricated from pyrex, it consists of two halves. The outer body incorporates two sodium chloride windows, fastened between rubber seals by metal clamps. The retractable top section contains a tubular holder allowing a self-supporting wafer of the material under study to be held perpendicular to the incident infrared beam. A resistance wire coil around the outside of the holder provided a furnace, with power supplied from a Variac, to allow study at an elevated constant temperature. This was monitored by a Chromel-Alumel thermocouple,

Diagram 3

Evacuable Infrared Cell used in Pyrolysis Studies



connected to a digital readout, positioned inside the holder adjacent to the pellet. Once assembled the cell could operate under vacuum or any controlled atmosphere, being connected via a gas manifold to a conventional mercury diffusion/rotary pump arrangement. For the current work, experiments were carried out in vacuo at reduced pressures of typically 10^{-2}torr($1.33 N.m^{-2}$). After outgassing for ½hour the temperature was gradually raised to the required setting; experience showed the degree of decomposition to be largely independent on the rate of heating.

Two approaches were adopted. To form a reasonably transparent pellet (10mm diameter) a pressure of ca. $2x10^{8} N.m^{-2}$ was applied to an evacuable die, although as it did not influence the pellet quality evacuation was normally deleted. This pressure is considerably higher than used elsewhere (ref.22, $6x10^{6} N.m^{-2}$), but probably arises from functionalisation increasing particle size, and the attempt to silylate the remaining surface. The formed lipophilic layer imparts nonpolar characteristics to the silica particles so that they tend to repel each other. Even so, the considerable scattering of the incident radiation by, and strong absorptions particularly below $2000cm^{-1}$ of, the background silica, coupled with alignment problems with the cell, resulted in very weak and poorly resolved spectra. At such a sample compression there is concern about alterations in the surface structure; scanning electron microscopy has shown(55) that for pure silica (10 μm particle size) pressures of $7.5x10^{5} N.m^{-2}$ cause loss of observable particle boundaries. This will restrict desorption (CO, H_2O etc.) processes, but also bring many groups into closer contact on a modified surface, and thus possibly altering decomposition pathways.

A compromise which improved spectral quality, and reduced the problem of close contact, involved diluting in a potassium bromide matrix. With this method it was not normally necessary to hold an optically equivalent, compensating silica disc in the reference beam. However a reference beam attenuator was still used to adjust the baseline. This allowed the surface species to be studied insitu throughout an experiment but did introduce a further parameter. For this reason each run was carried out in duplicate, being repeated using the cell solely as a furnace and treating an opaque silica disc, formed under the minimum compression, at identical

conditions, cooling and then mulling to characterise the surface species. No difference was taken to indicate the inertness of the potassium bromide matrix. The cell was used solely for convenience, a more exact mull technique would involve treatment of the free-flowing silica in a sealed evacuated tube, and then preparing the mull in a purged glove-box(55). The alternative method of cluster impregnation onto a preformed disc was considered inappropriate only further aggrevating the infrared transmission problems.

5.3.2. Thermal Treatment of $[Os_3(CO)_{11}(PPh_2Et)]$ in a KBr Matrix

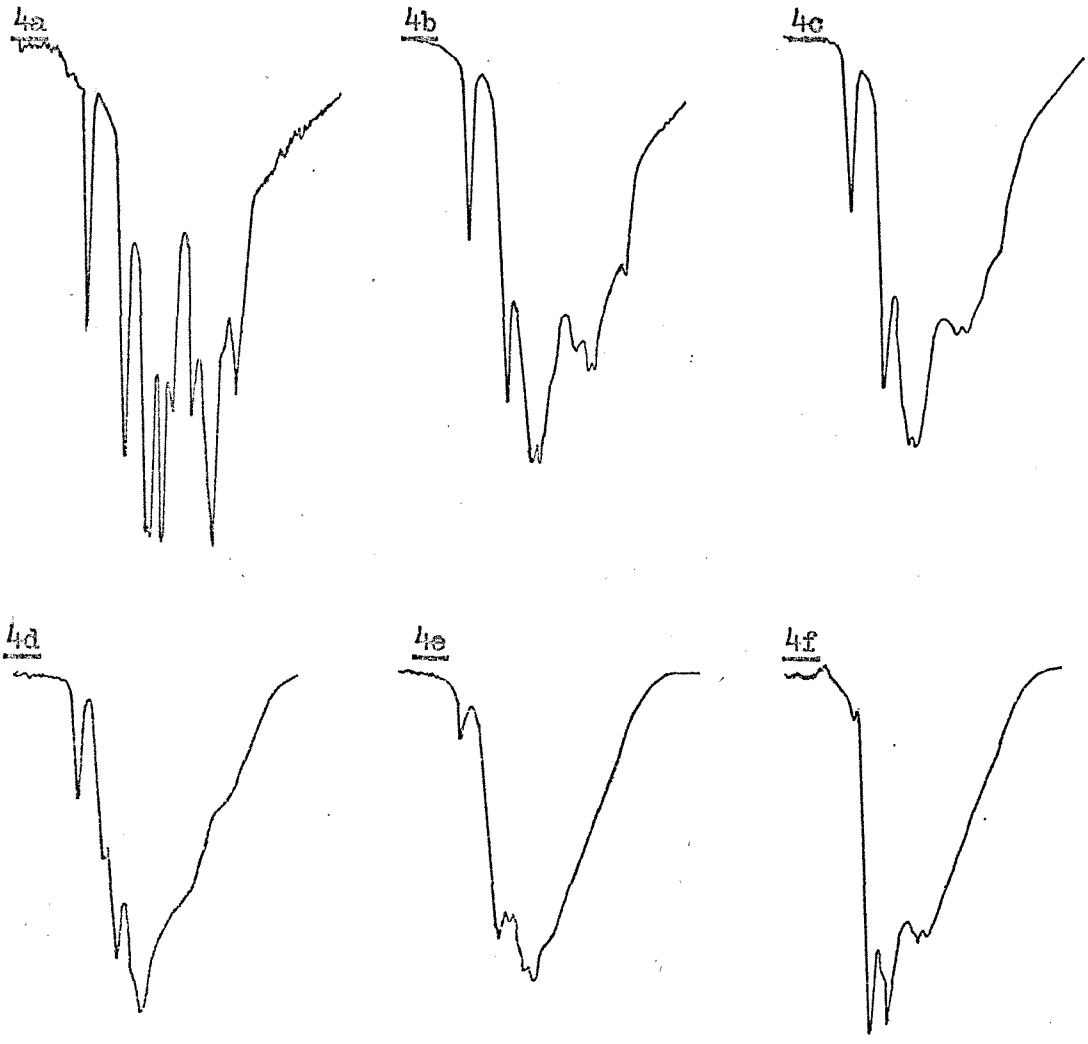
As a reference, the pyrolysis of $[Os_3(CO)_{11}(PPh_2Et)]$, VIII, dispersed in a KBr matrix is reported. Spectroscopic Grade KBr, predried in an oven at 110°C, was used. A small, spatula-head quantity of VIII was ground with sufficient KBr to produce a disc giving reasonable ν_{CO} absorptions when mounted in the evacuable cell. It was transparent with only a faint yellow appearance. The cell was pumped down to a working pressure of 2×10^{-1} torr and the infrared ν_{CO} spectrum recorded at 26°C (Diagram 4). This, 4a, is more complex than that observed in solution, being consistent with a polycrystalline sample. As such, the frequencies show a better correlation to those in the Raman ν_{CO} spectrum reported elsewhere (56), and confirmed in this thesis.

The temperature was gradually raised through the first hour to 75°C. Spectra were recorded at 15 minute intervals, over the region 2200-1800cm^{-1}, with a scan time of 3 minutes (mode 4A). On approaching the operating temperature a rapid transformation occurred(4b) with the emerged spectrum more closely resembling that found in solution. This change is irreversible since after a 3½ hour period the sample was cooled down to 20°C but the spectrum did not revert to its original state. No further modification occurred on reheating to 74°C and leaving for 16 hours. A similar phenomenon was observed for $[H_2Os_3(CO)_9(PPh_2Et)]$, IX, held in a KBr disc at about the same temperature. The likely explanation involves breakdown of the microcrystalline particles with the molecules intimately mixing in the KBr so becoming truely matrix isolated.

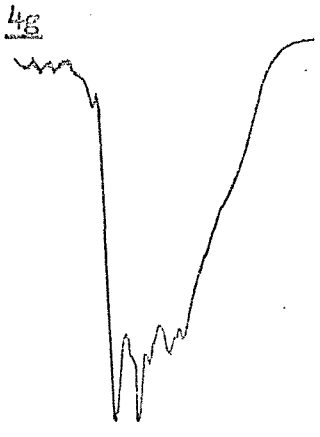
A fresh disc was prepared, and after evacuation, the

Diagram 4

Infrared Traces from Pyrolysis of $[Os_3(CO)_{11}(PPh_2Et)]$ dispersed in a Potassium Bromide Matrix



Infrared (ν_{CO}) Spectra (2200-1800 cm^{-1})



4a - $[Os_3(CO)_{11}(PPh_2Et)]$ in KBr, room temperature

4b - After 15 minutes at 77°C in vacuo

4c - " 3.5 hours at 75°C " "

4d - " 75 minutes at 113°C " "

4e - " 3.5 hours at 127°C " "

4f - " 2 hours at 150°C " "

4g - After 18 hours at 127°C and then cooling to room temperature:-
2099vw, 2062vs, 2030vs,
2016m, 1996m, 1985m, cm^{-1}

temperature quickly raised to 113°C within ½ hour to give the same result. This temperature was maintained for 2 hours before increasing to 127°C, and holding for another 18 hours. Over the initial 8 hour period spectra were recorded every 15 minutes, with a scan time of 0.7 minutes (mode 4). During this stage (4d and 4e) the emergence of several new bands, particularly one at ca. 2065cm^{-1}, was evident. At the end almost all the frequencies due to VIII had disappeared, to be replaced by ones at 2099vw (possibly still a remnant), 2062vs, 2030vs, 2016m, 1996m and 1985m, cm^{-1}. These remained essentially unaltered on cooling (4g) and then reheating to 150°C for 2 hours (4f).

The general complexity of this spectrum suggests the product has retained the cluster framework. If the KBr matrix is completely inert, then by analogy with the known solution chemistry $[Os_3(CO)_9(PCH_2CH_2SIL)(C_6H_4)]$ might be expected. Indeed, there is a vague resemblance in ν_{CO} pattern, but unfortunately an attempted extraction with CH_2Cl_2 did not yield sufficient material for further characterisation. The reduced degrees of freedom imposed by the KBr could also stabilise an otherwise reactive intermediate in the degradation pathway.

Alternatively an interaction with the KBr is possible. The reaction of $[Ru_3(CO)_{12}]$ with KBr, in the presence of Me_3NO followed by acidification, to give $[HRu_3(CO)_{10}Br]$ has been reported (57). The assumed intermediate $K[Ru_3(CO)_{10}Br]$ is conceivably isolable in a solid-state reaction. However the present spectrum seems more consistent with a neutral, rather than ionic, cluster. Trace amounts of water could also be important. $[HOs_3(CO)_{10}(OH)]$ is isolated as one of the products from the high temperature preparation of $[Os_3(CO)_{12}]$(58). Potassium hydroxide also reacts with the parent carbonyls by nucleophilic attack at a ligand to yield $K[M_3(CO)_{11}]$, M=Ru(59) or Os(60), protonation leading to $[HOs_3(CO)_{10}(OH)]$ through reaction of the intermediate $[H_2Os_3(CO)_{11}]$ with water. Direct reaction with KH also gives $K[HRu_3(CO)_{11}]$(61). However, an attempt to react $[H_2Os_3(CO)_{10}(PPh_2Et)]$ with water(4ml) in CH_2Cl_2 was unsuccessful, eventually heating to reflux only gave decarbonylation to IX which remained unaltered even at 100°C overnight. However, the infrared of the matrix product does show some similarity to that reported for $[Os_3(CO)_9(PPh_3)HX]$ (Table 4). Whatever, this

uncertainty does underline the importance of repeating runs in duplicate to dismiss any effect due to the KBr matrix.

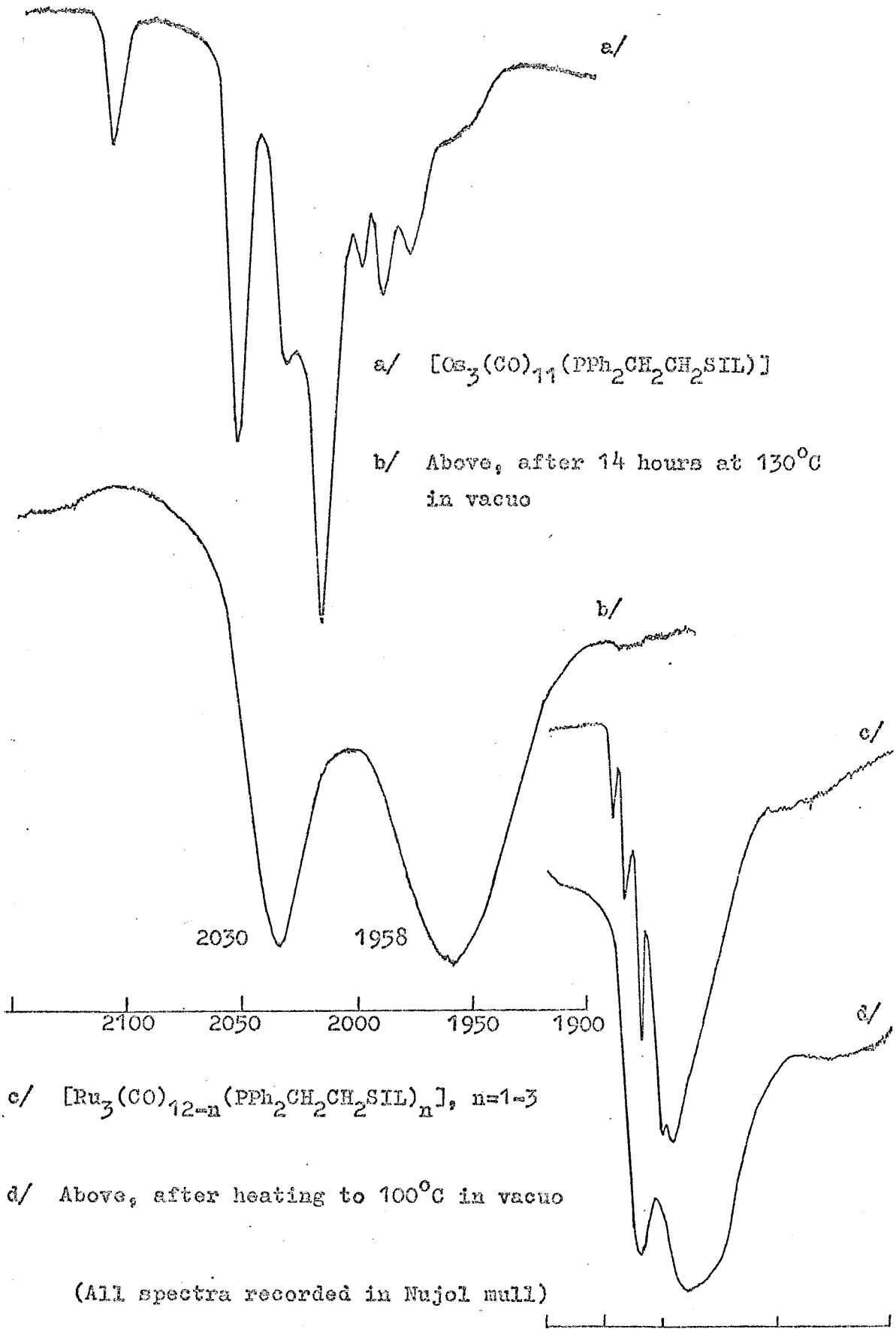
The above observations are interesting when compared to an infrared investigation carried out on the thermal decomposition of a series of parent neutral carbonyl clusters supported in KBr(62). In all cases it exerted a matrix effect which increased the temperature of decomposition, and of transformation of the clusters to metallic particles. For $[M_3(CO)_{12}]$, M=Os or Ru, kept in the matrix competitive sublimation of the cluster, or a decomposition intermediate, is prevented; a problem encountered in a companion thermogravimetric study in the same paper. It was concluded that an inert matrix imposes mass transfer limitations hindering the process of diffusion to the surface.

5.3.3. Pyrolysis of $[Os_3(CO)_{11}(PPh_2CH_2CH_2SIL)]$

An $[Os_3(CO)_{11}(PPh_2CH_2CH_2SIL)]$, I/KBr disc was mounted in the cell which was then pumped down to 10^{-2} torr. The infrared ν_{CO} spectrum confirmed retention of the original cluster species after compression and evacuation. The temperature was raised to 130°C over an hour, and then held for another 14 hours, spectra being recorded on an hourly basis between 2200-1800cm^{-1}. A remaining background absorption from the silica still masked the lower region, reducing the spectrum quality. However, within the first hour the almost total decay of I was evident, with a broad absorption centred about 2000cm^{-1} seen. With time this gradually separated into two strong bands, a weak shoulder at ca. 2120cm^{-1} present after an hour also slowly disappeared. At the end, the cell was cooled to room temperature before the tan-coloured wafer was removed and mulled to give two bands of equal intensities at 2030 and 1958cm^{-1} (Diagram 5). No attempt to protect the final disc from air was made, but this did not effect the integrity of the final species, X. In contrast, a preliminary experiment involving heating I under reflux in n-nonane for 5 hours gave a silica paler in appearance than the starting material. This gave a broad infrared ν_{CO} spectrum (2094vw, 2075m, 2061m-ssh, 2043s, 2018-2015vs and 2000-1950brsh, cm^{-1})(63), without any indication of X. Although not further investigated, these conditions appear more conducive to retention of the cluster frame-

Diagram 5

Infrared Spectra of recovered Silicas from Pyrolysis of $[M_3(CO)_{12-n}(PPh_2CH_2CH_2SIL)_n]$; M=Os or Ru, n=1-3.



a/ $[Os_3(CO)_{11}(PPh_2CH_2CH_2SIL)]$

b/ Above, after 14 hours at 130°C in vacuo

c/ $[Ru_3(CO)_{12-n}(PPh_2CH_2CH_2SIL)_n]$, n=1-3

d/ Above, after heating to 100°C in vacuo

(All spectra recorded in Nujol mull)

work, and the product may be a combination of the thermolysis species from $[Os_3(CO)_{12-n}(PPh_2CH_2CH_2SIL)_n]$, n=1-3.

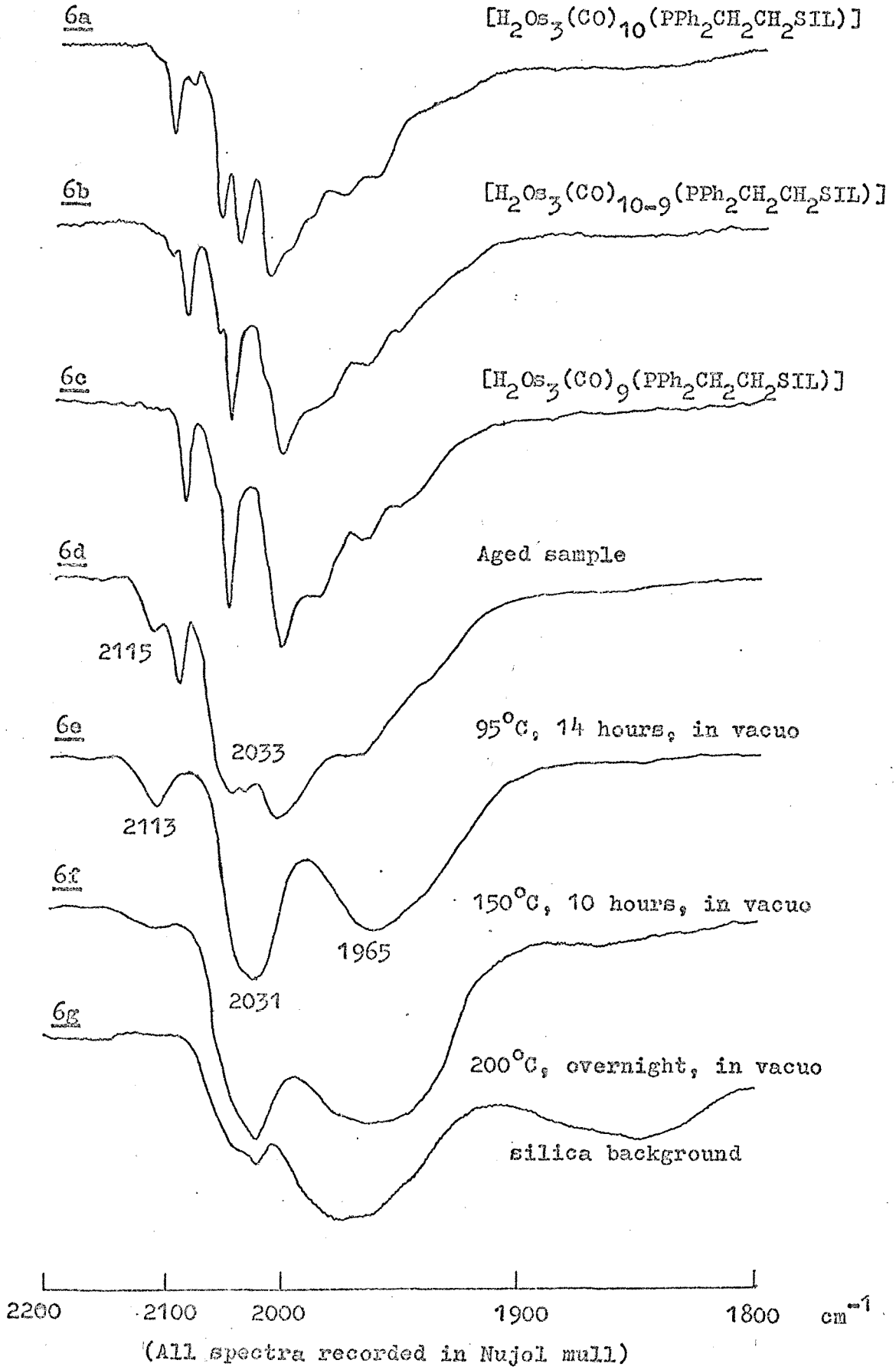
As a comparison the behaviour of physisorbed $[Os_3(CO)_{12}]$ on unfunctionalised 'Aerosil 200' was studied briefly. The silica (0.0502g), previously washed and dried in vacuo at 130°C for 24 hours, was suspended in CH_2Cl_2 and a solution of $[Os_3(CO)_{12}]$(0.0147g) added. Nitrogen was purged through to remove the solvent leaving a light yellow silica (calculated 14.3wt/wt% osmium). A formed KBr disc gave the expected 16 band spectrum(54) consistent with the presence of cluster crystallites at such a high loading. After evacuation, the temperature was raised rapidly to 130°C and the transformation to the grafted cluster, Va, occurred within 2 hours. The general broadness, and slight shifts to lower wavenumbers, was consistent with a highly hydroxylated surface. Thereafter spectra recorded at ½ hourly intervals for 10 hours revealed only slight changes attributed to the onset of breakdown to VI(ca. 2120 and 2035cm^{-1}). This divergence in result compared to that on PPh_2CH_2SIL confirms an active participation of the pendent ligands in the accelerated degradation of I.

Finally the decomposition of $[Ru_3(CO)_{12-n}(PPh_2CH_2CH_2SIL)_n]$, n=1-3, is mentioned here, but discussed further in Chapter Six. Pyrolysis of a self-supporting disc in the evacuated cell at 100°C caused a rapid change to give a doublet at 2052 and 1981cm^{-1} (Diagram 5). A similar result was obtained from $[Ru_6(CO)_{17}C]$ showing the pyrolysed material to be independent of the originally supported cluster. The frequencies are sufficiently different from those reported for pyrolysis of $[Ru_3(CO)_{12}]$ adsorbed on unfunctionalised silica-gel to indicate that probably the ruthenium atoms are still bonded to phosphorus under these conditions. Infact a large P:Ru ratio of ca. 15:1 allowed a tentative assignment to an oxidised ruthenium(II) species by comparison with the ν_{CO} spectrum of cis-$[Ru(CO)_2Cl_2(PPh_2Me)_2]$(2059 and 1996$cm^{-1}$)(48). As thermal contact of $[Os_3(CO)_{12}]$ with $PPh_2CH_2CH_2SIL$, under reflux in toluene, also gives the mixed product $[Os_3(CO)_{12-n}(PPh_2CH_2CH_2SIL)_n]$, n=1-3, thermolysis of I might be expected to proceed similarly by phosphine-substitution at each metal centre prior to breakdown.

5.3.4. Thermal Decomposition of $[H_2Os_3(CO)_{10}(PPh_2CH_2CH_2SIL)]$

Diagram 6

Infrared Spectra of recovered Silicas from Pyrolysis of $[H_2Os_3(CO)_{10}(PPh_2CH_2CH_2SIL)]$



(All spectra recorded in Nujol mull)

This was studied in greater detail. For completeness the investigation began from $[H_2Os_3(CO)_{10}(PPh_2CH_2CH_2SIL)]$, XI. As described in Chapter One, when held in the infrared beam a rapid decarbonylation occurs in less than an hour, with the disappearance of the characteristic bands of XI (6a) and simultaneous emergence of those for II (6c). The trace 6b clearly illustrates this transition with the bands at 2105 and 2065 now only shoulders on new ones at 2091 and 2052cm^{-1}, a shift to lower wavenumber for the strongest absorption is also obvious. Through this transformation the disc darkened from yellow to a deep green.

In most preparations of II two shoulders also appear at 2063 and 2033cm^{-1} which are due to a second species. When a sample was stored for an extended period, without particular precaution to exclude air or light, its infrared ν_{CO} spectrum (6d) shows a further increase in these features, combined as a broad band centred at 2033 cm^{-1}, and the growth of a second band at 2115cm^{-1}. Below 2000cm^{-1} a loss of definition is indicative of other changes; these modifications were augmented by the silica becoming yellower in appearance. This ageing process is taken to completion if II is heated to 95°C in vacuo overnight. The final disc (6e) is a straw colour and exhibits three absorptions in the ν_{CO} region at 2113w, 2033vs and 1968m-s, cm^{-1}. If in turn this material is heated at 150±2°C, in the evacuated cell for 10 hours, the highest wavenumber band slowly disappears, while that at 2033 loses intensity relative to that at 1968cm^{-1} until both are of approximately equal strength. The eventual positions, at 2031 and 1965cm^{-1}, are similar to those seen, (X), from pyrolysis of I at 130°C, and the disc was brown (6f). Finally, heating overnight at 200°C caused the sample to turn black and the prominence of the background silica absorption below 1900cm^{-1} shows that it is almost totally decarbonylated (6g). Presumably formation of metallic osmium has occurred, but no attempt to qualify the extent of aggregation was made.

5.3.5. Assignment of Degradation Products from Phosphine-tethered Triosmium Clusters

On first inspection, the product from thermal decomposition of II at 95°C (6e) has an infrared ν_{CO} spectrum similar to that

obtained by thermal oxidation of $[Os_3(CO)_{12}]$ on silica above 150°C (45), but with all absorptions moved to lower wavenumber positions by approximately 15cm^{-1}. Perhaps the arguement proposed by Smith(31) for adsorption of $[Rh_6(CO)_{16}]$ on a surface with a limited number of available phosphine groups is applicable accounting for this shift. However, in the current work contacting $[Os_3(CO)_{12}]$ directly with virgin 'Aerosil 200' also resulted in comparable shifts, and may thus just represent a variation in the surface nature of the unmodified silica. The same experiment also provided the strongest evidence for a direct involvement of the pendent phosphines in the accelerated degradation of I.

The analytical data for the anchored clusters is reproduced below. An osmium/phosphorus ratio of about unity for each silica

Table 3

Compound	Os (wt/wt%)	P	Os (x10^{4}mol.g^{-1})	P
$PPh_2CH_2CH_2SIL$		0.89		2.9
$[H_2Os_3(CO)_{10}(PPh_2CH_2CH_2SIL)]$	4.06	0.77	2.1	2.5
$[H_2Os_3(CO)_9(PPh_2CH_2CH_2SIL)]$	5.50	0.94	2.9	3.0
$[Os_3(CO)_{11}(PPh_2CH_2CH_2SIL)]$	3.78	0.80	2.0	2.6

indicates that there are approximately two free phosphines per anchored cluster (neglecting the possibility of a fraction being present as phosphine-oxide). The phosphorus content (ca. 0.85wt/wt%), corresponding to an average of 0.9 groups per nm^2, falls well within the necessary requirement (0.37 molecules/nm^2) to allow potential multisubstitution of a triosmium core. Ofcourse, this figure is based on a perfectly even coverage whereas in reality concentrated islands are likely to exist further enhancing this possibility. Even so, whilst it is relatively easy to envisage disustitution, it is very unlikely that three groups will be oriented correctly to match the more demanding surface geometry required to stabilise a trisubstituted derivative, without previously being attached to some kind of template. This is aptly demonstrated by contacting $[Ru_3(CO)_9\{PP_2CH_2CH_2Si(OEt)_3\}_3]$ with silica at room temperature which

does yield the fully tethered form, as witnessed by nearly quantitative photochemical disassembly-reassembly to $[Ru(CO)_4(PPh_2CH_2CH_2SIL)]$. Attachment by SCHEME TWO dictates the distribution of fragments. Conversely, photolysis of the anchored derivative from $[Ru(CO)_4\{PPh_2CH_2CH_2Si(OEt)_3\}]$ did not produce the cluster because the random distribution (complicated by a lower coverage) was incompatible with the spatial requirements(64).

Thus, if formed through thermal activation, the strain present in $[Os_3(CO)_9(PPh_2CH_2CH_2SIL)_3]$ could be sufficient to rupture the framework to give unsaturated d^8 '$Os(CO)_3(PPh_2CH_2CH_2SIL)$' fragments. The Effective Atomic Number rule could be satisfactorily met by coordination of a second phosphine to give $[Os(CO)_3(PPh_2CH_2CH_2SIL)_2]$, with the osmium still in the zero oxidation state. However, this is inconsistent with the limited number of phosphines available on the surface, and the reported single absorption at $1890cm^{-1}$ in the infrared ν_{co} spectrum of $[Os_3(CO)_3(PPh_3)_2]$(65). Both d^8 complexes are susceptible to oxidative addition to form stable adducts of d^6 configuration; thus $[Os(CO)_2(PR_3)_2X_2]$ is obtained with HX or X_2, X=halogen, the latter via a 1:1 adduct(65). Just as known halide complexes were used(45) as suitable models for the surface adsorbed species on the various inorganic oxides, then known phosphine derivatives may represent the most likely candidate structures now.

$[Os_3(CO)_{12}]$ reacts with HCl, at 170°C in a sealed tube, to give the dimeric $[Os(CO)_3Cl_2]_2$(49). The action of Cl_2 on $[Os_3(CO)_{10}Cl_2]$ at room temperature gives the same product plus cis-$[Os(CO)_4Cl_2]$(66). At the more forcing conditions (extended reflux in benzene) necessary to form the original halocarbonyl cluster the latter species would also decarbonylate to the dimeric species(47). In comparison, $[Os_3(CO)_9L_3]$, L=PEt_3, $PPhEt_2$ or PPh_2Me, reacts immediately (15 seconds) with excess Cl_2 at room temperature to give selectively $[Os(CO)_3(PR_3)Cl_2]$(66). In turn, at higher temperatures, this will dimerise to the known $[Os(CO)_2(PR_3)Cl_2]_2$, also obtained from halogenation of $[Os_3(CO)_{10}L_2]$(66). With excess phosphine both monomers react to yield $[Os(CO)_2(PR_3)_2Cl_2]$. Comparison with the infrared ν_{co} data of these model compounds immediately dismisses $[Os(CO)_3(PPh_2CH_2CH_2SIL)(OSIL)_2]$, XII, being the observed surface species.

Just as $[Os_3(CO)_{12}]$ on silica undergoes thermal degradation

Table 4

Compound	IR ν_{CO}/cm^{-1} (solvent)			Reference
X, breakdown product from I, 130°C, in vacuo	(nujol mull)	2030vs	2058vs	This work
II/XI decompostion product, i) 95°C, in vacuo	2113w (nujol mull)	2033vs	1968m-s	This work
ii) 150°C, in vacuo	(nujol mull)	2031vs	1965vs	
$[H_2Os_3(CO)_9(PPh_2-$ (P) $)]$ breakdown product	2122w (membrane)	2030br	1962m	(67)
$[Os_3(CO)_{12}]$/silica, 150°C	2128m (solid disc)	2045vs	1973m	(45)
$[Os(CO)_3(OSIL)_2]_n$	2120s (nujol mull)	2035s		This work
$[Os(O_2)(CO)_2(PPh_3)_2]$		2005vs	1945vs	(68)
trans-$[Os(CO)_3(PPh_3)_2]$	(KBr)		1890vs	(65)
trans-$[Os(CO)_2(PPh_3)_3]$			1895vs	(68)
$[Os(CO)_2(PPh_3)_2X_2]$ X=Cl	(CH_2Cl_2)	2043vs	1971vs	(56)
Br		2043vs	1974vs	or
I		2041vs	1975vs	(69)
$[Os(CO)_3(PPh_3)Cl_2]$	2123w (nujol mull)	2048s	2017w 1978s	(70)
$[Os(CO)_3(PEt_3)Cl_2]$	2144w (cyclohexane)	2070vs	2023s	(66)
$[Os(CO)_2(PPh_3)Cl_2]_2$	$(CHCl_3)$	2051s	1981s	(66)
$[Os(CO)_2(PPh_2Et)Cl_2]_2$	(CH_2Cl_2)	2043s	1971s	(71)

initially to the tricarbonyl adduct, VI, so by analogy on a phosphinated silica the substituted $[Os(CO)_2(PPh_2CH_2CH_2SIL)(OSIL)_2]_n$, X, is formed. This is consistent with the observed surface stoichiometry, whereas a species analogous to the more frequently met $[Os(CO)_2(PR_3)_2X_2]$, which show a better correlation in positions of infrared ν_{CO} absorptions (Table 4), is not. However the sample at 130°C has darkened considerably suggesting that some decomposition

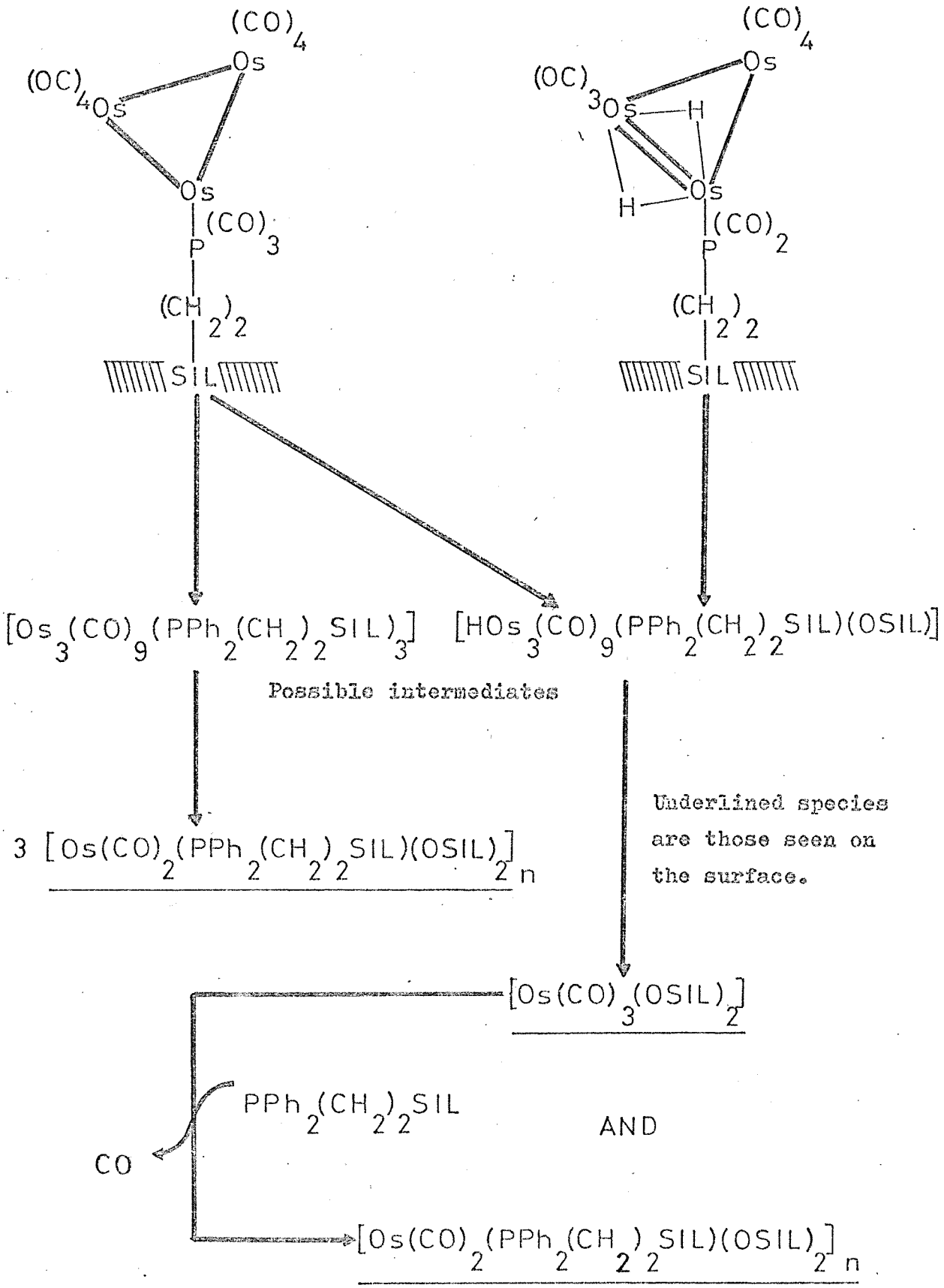
to metallic osmium had occurred, particularly as the homogeneous analogues tend to be colourless in the absence of a strong chromophore. Then the elemental analysis may no longer be diagnostic, or the carbonyl containing species be the only osmium ones on the surface. Although X and XII are formally designated as containing two surface oxide linkages this is probably an over simplification. For both I and II the ligand-silica employed had been silylated during preparation, so the silanol concentration will be limited. Then the influence of surface water and oxygen (or phosphine-oxides) has to be considered. Interestingly the dioxygen complex $[Os(O_2)(CO)_2(PPh_3)_2]$ (68) can be isolated by dissociation of a phosphine ligand.

Again the constraints imposed by the surface can stabilise a species otherwise unfavourable in solution. Whereas $[Os(CO)_{4-3}X_2]$, X=halogen, react with phosphine to give $[Os(CO)_2L_2X_2]$, without reported isolation of $[Os(CO)_3(PR_3)X_2]$, it has been shown that certain circumstances do allow its formation, namely halogenation of $[Os(CO)_9L_3]$ in the absence of free donor ligand. Then formation of $[Os_3(CO)_9(PPh_2CH_2CH_2SIL)_3]$, followed by cleavage of the metal-metal bonds to give XII (and decarbonylation to give the observed X), is supported by the recorded P:Os ratio and the known tendancy of $[Os_3(CO)_{12}]$ to undergo progressive substitution at the three metal centres. Substantial amounts of bis-phosphine complex would only be anticipated in the presence of carbonyl-only adducts, or considerable breakdown to osmium metal.

The observed sequence with II is more complicated, although the eventual doublet at 150°C can be treated as above. At 95°C a third band at 2113cm^{-1} is present representing another species, whose formation is a function of the originally supported cluster. A divergence in behaviour with excess phosphine has already been established for the solution chemistry of VIII and IX, but then $[Os(CO)_2(PPh_2CH_2CH_2SIL)_2(OSIL)_2]$, XIII, would be projected and this is not consistent with the infrared data. There is an overall resemblance to the spectrum of $[Os(CO)_3(PPh_3)Cl_2]$, however the continued persistence of a residual feature even at 150°C militates against this. In preference, the co-formation of $[Os(CO)_3(OSIL)_2]_2$, VI, is proposed, which accounts for the increased intensity of the middle absorption through overlap with the accompanying vibration at 2035cm^{-1} (this work). Then at higher temperatures it reacts with

Diagram 7

Proposed Thermal Decomposition Pathways for Phosphine-anchored Triosmium Clusters



remaining uncoordinated phosphines to give X, or decarbonylates to a metallic form; at intermediate temperatures the former will be favoured. The susceptibility of the double bond in $[H_2Os_3(CO)_{10}]$ to addition, at low temperatures under vacuum, leading to the grafted cluster Va is well established(45). By analogy, $[HOs_3(CO)_9(PPh_2CH_2CH_2SIL)(OSIL)]$, XIV, would be expected, but the lack of any interim, complex spectrum suggests, that if formed at the conditions employed, the strain caused by the two linkages in close proximity must be sufficient to rupture the cluster framework, causing genesis of both phosphine containing, and absent, metal carbonyl fragments (Diagram 7). Interestingly, a three band spectrum (Table 4) is also produced from thermal breakdown of the anchored variant of II on modified-polystyrenes(67). This was rapid on random copolymers containing residual bromo-groups, but still occurred, at 120°C under vacuum, on block polymers where no such groups exist (representing a parallel with unprotected and silylated silica surfaces).

SECTION (B): Olefin Hydrogenation by Phosphine-anchored Triosmium Clusters

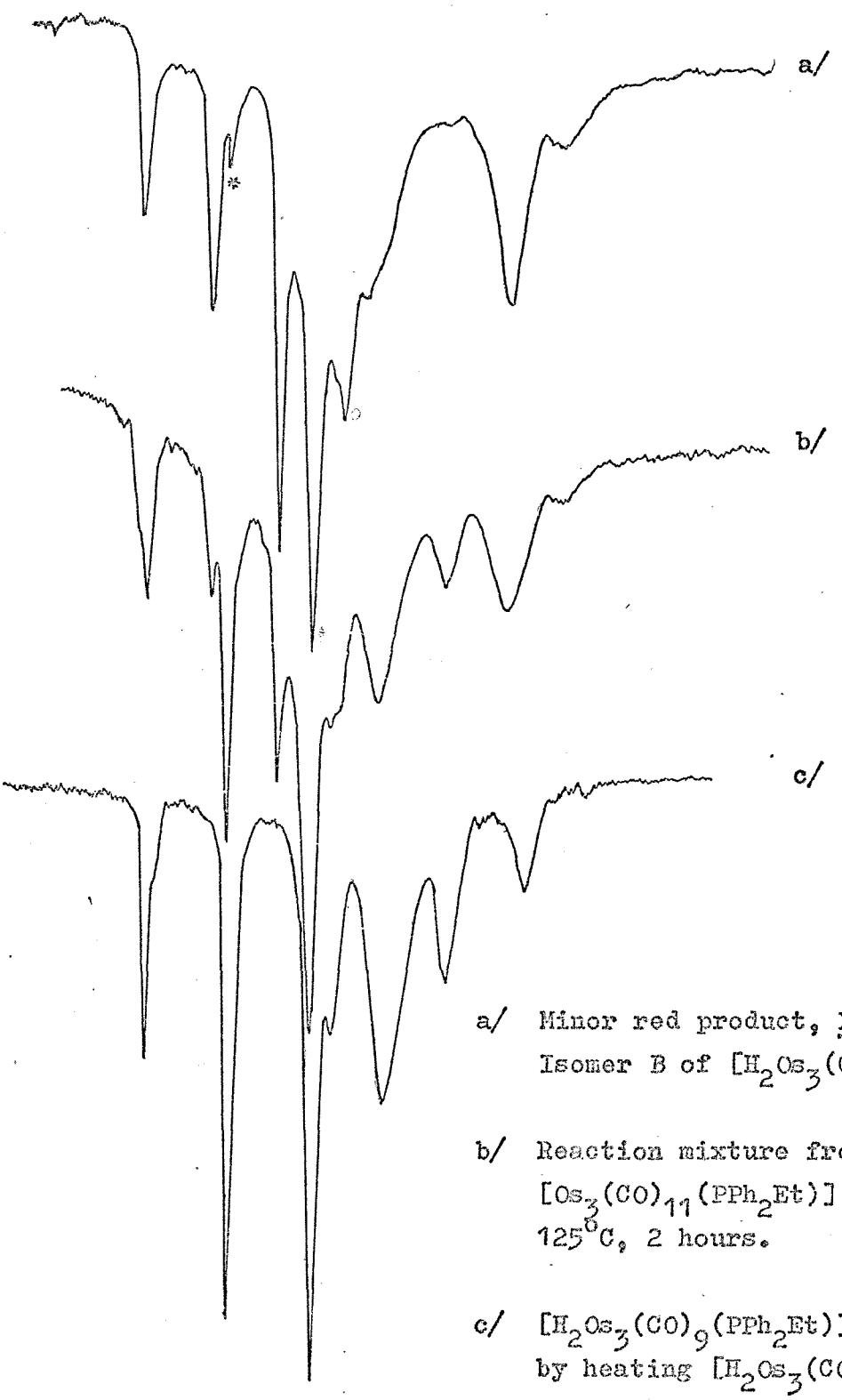
5.4. Hydrogenation of Ethylene

There are scarcely any well established catalytic cycles involving metal clusters, but a notable exception is olefin isomerisation and hydrogenation by $[H_2Os_3(CO)_{10}]$. Several intermediates were identified, and a catalytic cycle established, As described (72), its phosphine substituted derivative, IX, has a similar chemistry with olefins, namely ethylene, and hydrogen. Further, the effect of the phosphine has also allowed isolation of another proposed intermediate in the mechanistic cycle. As a close analogue to II, this extensive solution chemistry provides a firm basis from which to study the potential catalytic activity of the anchored cluster. More specifically, ethylene hydrogenation was chosen as a model system for the following reasons:-

i) To avoid the complication of competing 1-alkene isomerisation ii) The greater simplicity of the anticipated

Diagram 8

Infrared (ν_{CO}) Spectra of the Products from Hydrogenation of $[Os_3(CO)_{11}(PPh_2Et)]$



a/ Minor red product, XV, possible Isomer B of $[H_2Os_3(CO)_9(PPh_2Et)]$

b/ Reaction mixture from hydrogenation $[Os_3(CO)_{11}(PPh_2Et)]$ in n-octane, 125°C, 2 hours.

c/ $[H_2Os_3(CO)_9(PPh_2Et)]$ prepared by heating $[H_2Os_3(CO)_{10}(PPh_2Et)]$

(a/ and c/ recorded in cyclohexane)

organometallic derivatives will aid infrared spectroscopic identification.

iii) To minimise, or prevent, rates of diffusion on the support becoming limiting.

This is extended to include I as a catalyst precursor. Catalytic activity will be initiated by a coordinatively unsaturated site, which is inherent in II and IX, but must be generated by dissociation of a carbonyl ligand from I and VIII at the operating conditions. Thermal activation of $[Os_3(CO)_{12}]$ to coordinate hydrogen (73) or ethylene(74) only occurs upon heating under reflux in n-octane. Hydrogen coordination to give $[H_2Os_3(CO)_{10}]$ is the more facile reaction so, by analogy, I would be expected to transform into II, and thus enter the same catalytic cycle.

Evidence for this necessary conversion has appeared(75), but without any experimental detail or quantification. A qualitative verification was sort by attempting atmospheric hydrogenation of VIII(0.051g) in different boiling range hydrocarbon solvents. Under reflux in n-heptane(b.p.=98.5°C) no change in the infrared ν_{CO} spectrum was seen after 3 hours. However, in n-octane(b.p.=125°C) nearly all the frequencies due to the starting material had disappeared within 2 hours. The emerged spectrum broadly resembles that of I. After a further ½ hour the solution was cooled down, and the residue chromatographed using n-hexane/Et_2O (4:1 v/v) as eluant. A small leading, lime-yellow, band was identified as a remaining trace of VIII. The following, purple-green, band was I as the major product; the desired conversion being successfully achieved. Beneath this was one other prominent red band, XV, which gave the infrared ν_{CO} spectrum shown in Diagram 8. This is clearly the only other component providing a significant contribution to the observed spectrum after 2 hours. Further characterisation was not undertaken, but several observations are pertinent.

i) Its spectrum does not resemble that of any of the crude products seen from a preliminary pyrolysis of IX at the higher temperature of reflux in n-nonane. Niether is there any correlation with the adducts isolated from thermolysis of $[Os_3(CO)_{11}(PR_3)]$.

ii) Extended reaction times, in the presence of dihydrogen, might be expected to yield the tetra-osmium species

Table 5

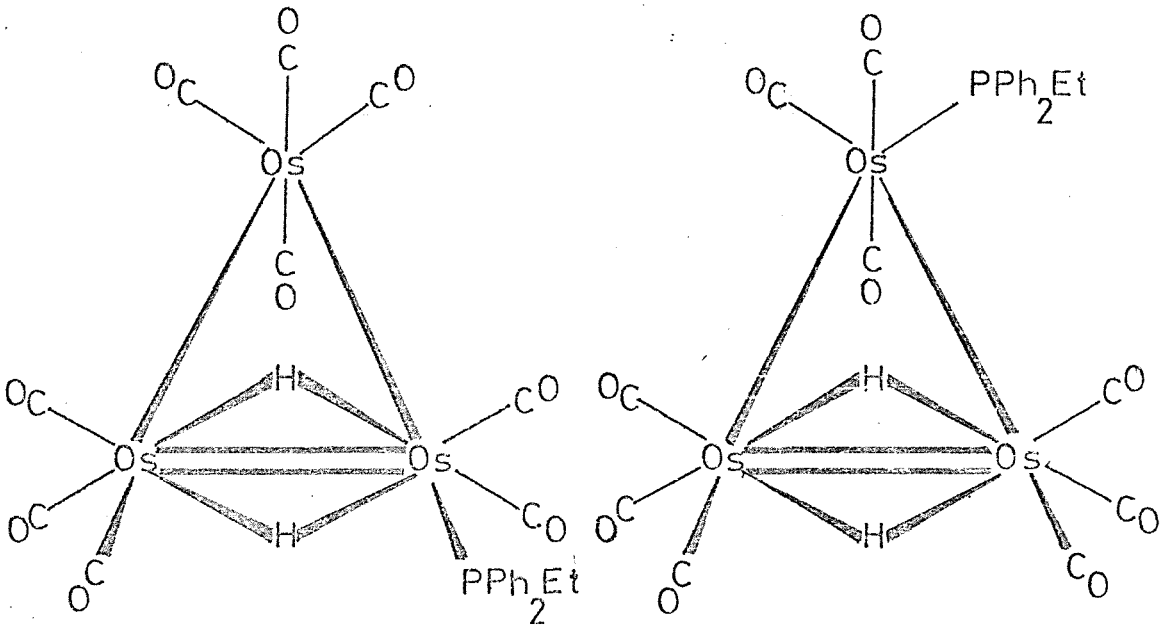
Compound	IR ν_{CO}/cm^{-1} (cyclohexane unless stated)			
$[H_2Os_3(CO)_9(PPh_2Et)]$	2093m	2054s	2013vs	2005m
Isomer (A)	1990m	1975m	1957w	
Isomer (B)	2096w-m	2063s	2055w	2030s
	2014vs	2000m-s	1960.5m	1947.5w
$[Os_3(CO)_9(PPh_3)HI]$	2095vw	2090w	2063s	2058sh
(Ref.80) Isomer (A)	2035s	2007s	1997m	1970w
	1964vw	1957vw		
$[H_4Os_4(CO)_{11}(P(OMe)_3)]$	2095w	2070vs	2060vs	2020s
(Ref.76)	2000s	1990w	(n-pentane)	
$[H_4Ru_4(CO)_{11}(P(OMe)_3)]$	2097m	2068vs	2060sbr	2032vs
(Ref.77)	2030vs	2017s	2008s	1974w
$[H_4Ru_4(CO)_{10}\ P(OMe)_3\ _2]$	2080m	2059s	2039w	2023vsbr
	2001s	1967w		

$[H_4Os_4(CO)_{12-n}(PPh_2Et)_n]$, n=0-2. However, the reported data for $[H_4Os_4(CO)_{11}(P(OMe)_3)]$(76), and the related ruthenium adducts(77,78), is incompatible with this proposition.

iii) More likely is the existence of an alternative isomer of VIII.

The isocyanide analogues are known to exist as an equilibrium mixture of isomers in solution, with the ligand either occupying an equatorial or pseudo-axial position on the bridge-head osmium(79). The tertiary-butyl- and phenyl-derivatives selectively crystallised in the equatorial and axial forms respectively, and were structurally characterised. As a sterically controlled distribution this type of isomerisation is not a suitable explanation. Instead, an isomeric form with the phosphine located on the osmium away from the unsaturated edge is preferred. This is supported by a reasonable correlation to the infrared ν_{CO} spectra of $[Os_3(CO)_9(PPh_3)HX]$, X=Cl or I, for which such a structure has been established. The method of preparation can effect the final configuration of a cluster as epitomised by $[Os_3(CO)_9(PPh_3)(\mu_2\text{-SR})(\mu_2\text{-H})]$. Room temperature treatment of $[Os_3(CO)_9(\mu_2\text{-H})(\mu_3\text{-SR})]$

with PPh_3 gives the equivalent of XV(81); whilst thermal treatment (80°C) of $[Os_3(CO)_{10}(\mu_2\text{-}H)(\mu_3\text{-}SPh)]$ gives a mono-substituted product with a structure analogous to IX, but in association with di- and, most likely, tri-substituted derivatives(82). Then the orbital control that gives selective formation of Isomer (A), from the conventional route to IX, may not be operative during thermally activated hydrogenation of VIII and a more statistical distribution of isomers results. If correct, the presence of XV will not distract



Isomer (A) Isomer (B)

Possible Isomeric Forms of $[H_2Os_3(CO)_9(PPh_2Et)]$

from the potential catalytic activity of VIII, indeed it might be expected to resemble more closely that of $[H_2Os_3(CO)_{10}]$.

As a consequence, a temperature of 110°C was chosen for catalytic studies involving I and VIII. A lower temperature of 75°C was used for II and IX, to allow closer comparison to literature data for $[H_2Os_3(CO)_{10}]$ and recent work published dealing with alkene isomerisation by II. A total pressure (NPT) of 300psig was used, with ethylene and hydrogen partial pressures of 75psi and 240psi respectively. This ratio of gases was somewhat arbitary, but an excess of hydrogen served two functions.

i) To compensate for its lower solubility.

ii) For the proposed catalytic cycle (Diagram 19) a greater hydrogen concentration is expected to reduce the rate of

deactivation, by ∝-hydrogen abstraction from a second coordinated ethylene after evolution of ethane. Even for 1-alkene isomerisation the presence of hydrogen is reported to extend the catalysts lifetime(83).

5.5. Experimental Procedure (Diagram 9)

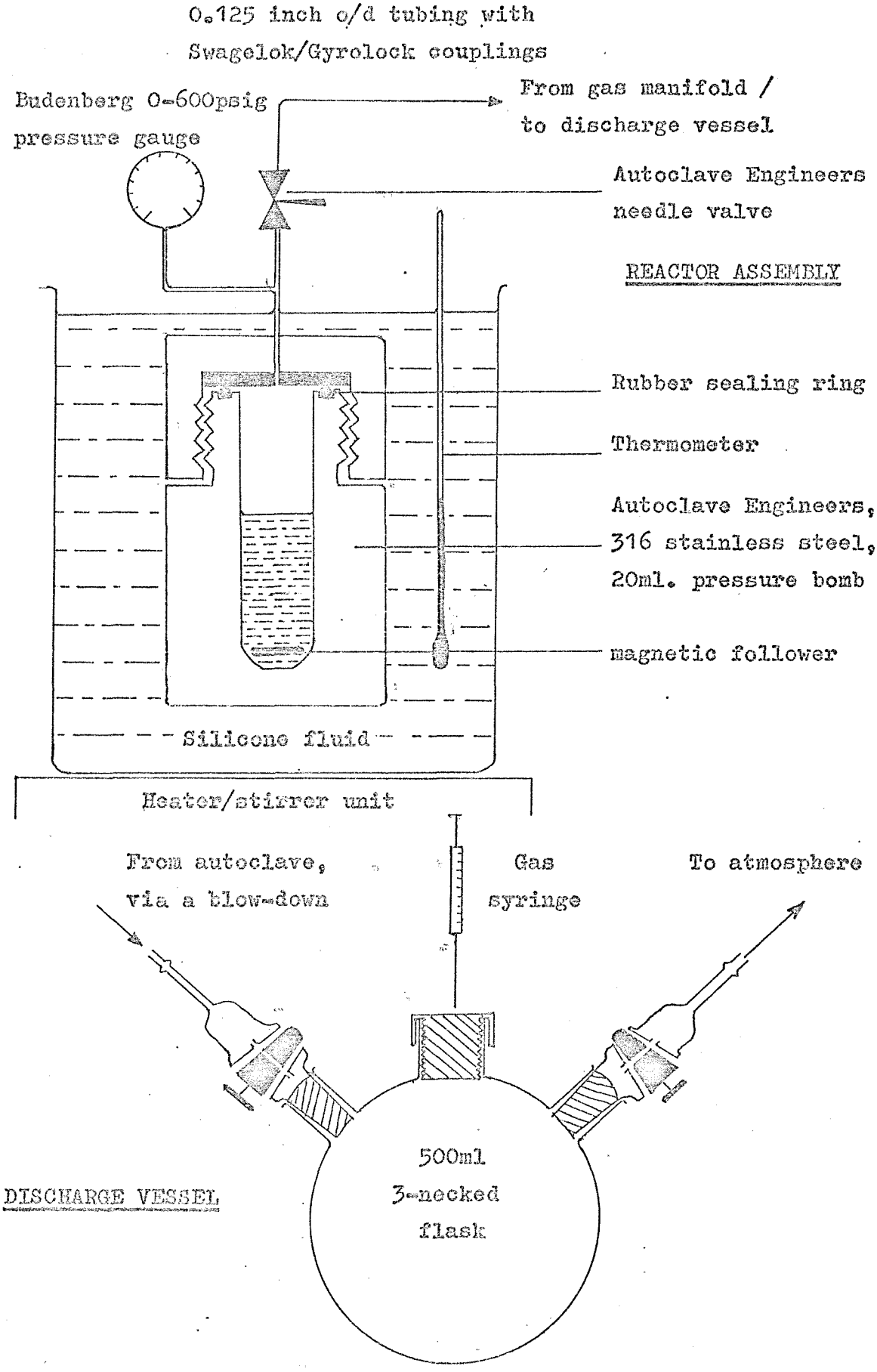
The catalysts used were those prepared and characterised in Chapter One, they were not pretreated in any manner before use.

Ethylene hydrogenation reactions were carried out in a batch system. This incorporated an Autoclave Engineers bench top autoclave, fabricated in 316 stainless steel, connected to a 0-600psig Budenberg pressure gauge, a needle valve, and a gas manifold, by 0.125 inch o/d tubing with Gyrolock/Swagelok compression fittings. The bomb had a nominal volume of 20ml. This was loaded with the appropriate catalyst (typically the equivalent to $2x10^{-5}$ mole of Os_3) suspended, or dissolved, in 10ml of a non-polar, de-gassed, solvent. For $[H_2Os_3(CO)_9(PPh_2R)]$ this was n-heptane, and iso-octane for $[Os_3(CO)_{11}(PPh_2R)]$. The system was then flushed twice by pressurising to 50psig with ethylene, and quickly venting to atmosphere without agitating the solution. A charge of ethylene (75psi) and hydrogen (240psi), both CP Grade reagents, was introduced. The assembly was suspended in a silicone-oil bath, preheated to the desired constant temperature, and agitation with a magnetic follower commenced.

After the designated time interval, the bomb was withdrawn from the bath and cooled to room temperature by immersion in water. It was then carefully vented through a 500ml, 3-necked, flask; fitted with gas inlet and outlet tap assemblies and a suba-seal cap to facilitate sampling by syringe. This had previously been thoroughly purged with white-spot nitrogen. Once the venting was complete, the discharge vessel was closed off and a gas sample taken and the ratio of ethylene to ethane determined by gas chromatography. Analysis was performed on a 2m x 0.24m, 2% Porapak Q (80-100 mesh) column at 50°C with nitrogen carrier gas (16psig). A relative response factor of 1.47, in favour of ethylene, was found by flushing the discharge vessel with the appropriate gas (CP Grade ethane), injecting 50 µl aliquots and measuring the average peak

Diagram 9

Apparatus used for Ethylene Hydrogenation Reactions



height. The absolute amount of hydrogenation was then calculated on the basis of the known pressure of ethylene used and the dead volume (10ml) above the solution, no agitation being incorporated during charging and the highest steady pressure recorded before absorption became appreciable.

5.6. Results and Infrared Spectroscopy

The results from the ethylene hydrogenation reactions are summarized in Table 6. A more detailed listing of the precise conditions for each run, and the product analysis, is given in Appendix 1.

5.6.1. Homogeneous Systems

The ethane yields (moles of ethane per mole of triosmium cluster present) for IX and VIII are approximately 95 and 101, after 20 and 24 hours, respectively. In both cases the recovered hydrocarbon solutions were yellow in appearance and gave the infrared ν_{CO} spectra in Diagram 11. Clearly cessation of catalytic activity had occurred well within the designated run time and no rate data can be derived, except that turnover numbers are well in excess of 4 hr^{-1}. One run using IX, where a leak from the bomb developed, afforded a lower ethane yield of 75 after 20 hours, although the composition of the recovered solution was virtually identical. Combined with the observation that the percentage of ethylene converted with both catalysts is very similar (ca. 85%), this implies a dependence on ethylene, and/or possibly hydrogen, partial pressures.

The infrared ν_{CO} spectra of the spent catalyst solutions cannot be interpreted in terms of the various species characterised in Chapter Three. However, the product distributions represented by the two spectra appear related, with that obtained from VIII being a further progression on from that with IX due to the higher temperature. Unfortunately, insufficient material was available for detailed analysis, but the extended reaction times, in conjunction with super pressures of hydrogen and ethylene at elevated temperatures, will conceivably promote alkene coupling reactions, or formation of higher nuclearity products, as already seen with

Diagram 10

Kinetic Measurements for Ethylene Hydrogenations catalysed by Triosmium Clusters

Table 6

Temperature (°C)	Duration (hours)	Moles of Os_3 used	Moles of ethane formed	Ethane Yield moles/mole Os_3
$[H_2Os_3(CO)_9(PPh_2CH_2CH_2SIL)]$				
	4	1.7×10^{-5}	4.44×10^{-5}	2.61
All at	20	3.37×10^{-5}	3.40×10^{-4}	10.09
75°C	20	1.7×10^{-5}	1.43×10^{-4}	8.42
	44	3.38×10^{-5}	4.42×10^{-4}	13.08
$[H_2Os_3(CO)_9(PPh_2Et)]$				
75	20	1.94×10^{-5}	1.84×10^{-3}	94.90
75	20	1.94×10^{-5}	1.50×10^{-3}	76.33
$[Os_3(CO)_{11}(PPh_2CH_2CH_2SIL)]$				
110	24	1.41×10^{-5}	9.87×10^{-4}	70.00
$[Os_3(CO)_{11}(PPh_2Et)]$				
110	24	1.82×10^{-5}	1.83×10^{-3}	100.66

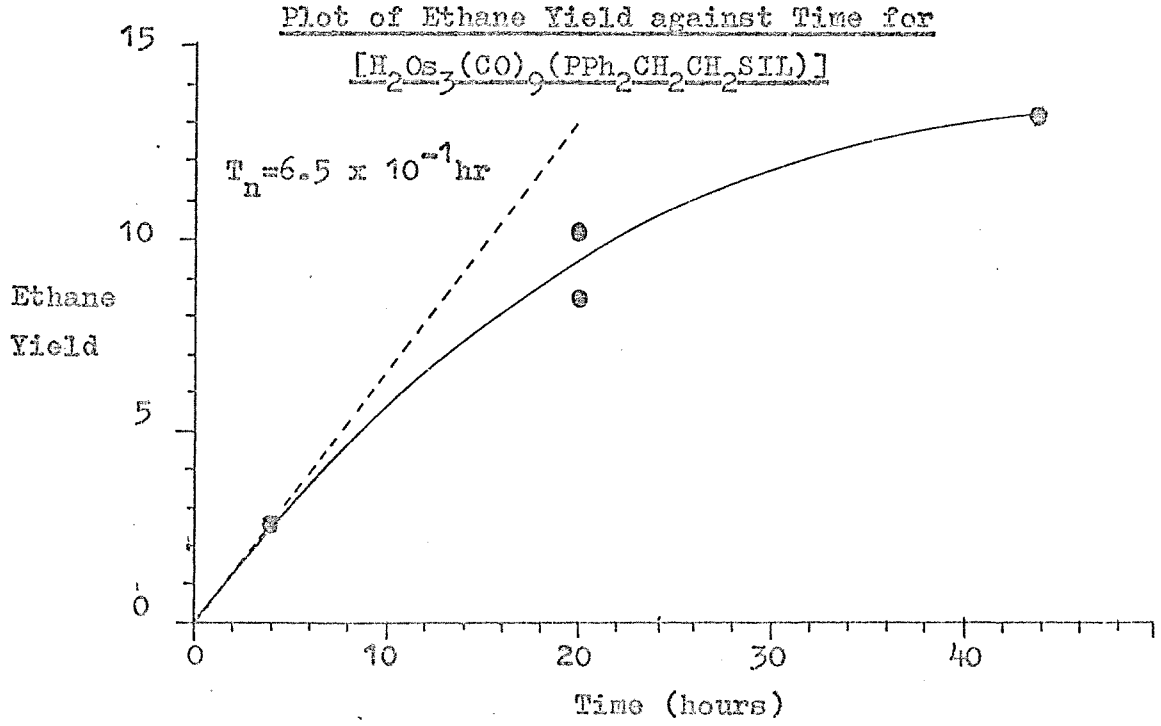
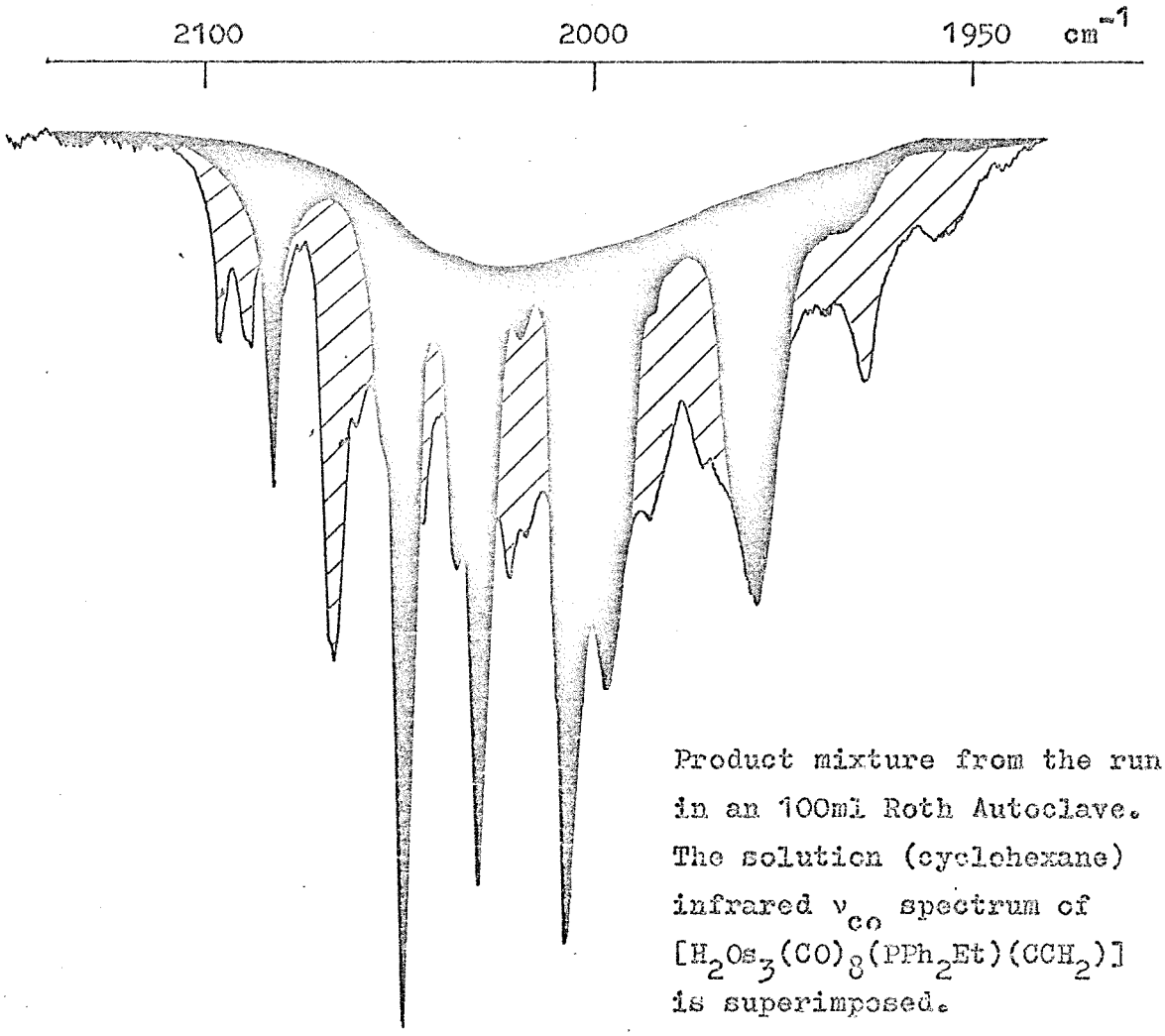


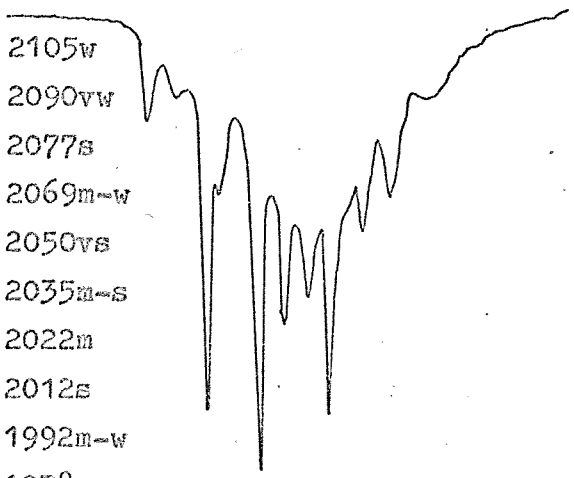
Diagram 11

Infrared (ν_{CO}) Spectra of Spent Catalyst Solutions from Ethylene Hydrogenations with Homogeneous Triosmium Clusters



Product mixture from the run in an 100ml Roth Autoclave. The solution (cyclohexane) infrared ν_{CO} spectrum of $[H_2Os_3(CO)_8(PPh_2Et)(CCH_2)]$ is superimposed.

i) Recovered solution from $[Os_3(CO)_{11}(PPh_2Et)]$ run.



ii) Retrieved solution from $[H_2Os_3(CO)_9(PPh_2Et)]$ run.



$[Os_3(CO)_{12}]$. Both these processes will be less favoured for an anchored variant.

For further clarification, the reaction with IX(0.0608g) was repeated in an 100ml Roth autoclave but terminated after 4 hours. Similar conditions (110°C) were used with the same ratios of gases, but with a higher total pressure (46atm) and n-hexane(35ml) as solvent. Chromatography of the orange-yellow residue isolated $[H_2Os_3(CO)_8(PPh_2Et)(CCH_2)]$, XVI, confirmed as the major constituent by superimposing a spectrum of an authenticated sample over that of the crude mixture (Diagram 11). This supports initial catalyst deactivation by formation of the saturated vinyl adduct $[HOs_3(CO)_9(PPh_2Et)(CHCH_2)]$, XVII, which rapidly decarbonylates at the operating temperature. Although caution is necessary when comparing results obtained under different conditions, particularly in different autoclaves, this result indicates that at least for the homogeneous systems subsequent hydrogenation to the stable ethylidyne complex $[H_3Os_3(CO)_8(PPh_2Et)(CCH_3)]$, XVIII, does not compete with the alternative pathways when the reaction time is extended.

In conclusion, these virtually identical results with VIII and IX strongly implies that catalysis is by a unified mechanism; the hydrogenation of VIII to IX/XV occurring rapidly insitu. Secondly they demonstrate that phosphine substitution does not inhibit the reactivity of $[H_2Os_3(CO)_{10}]$.

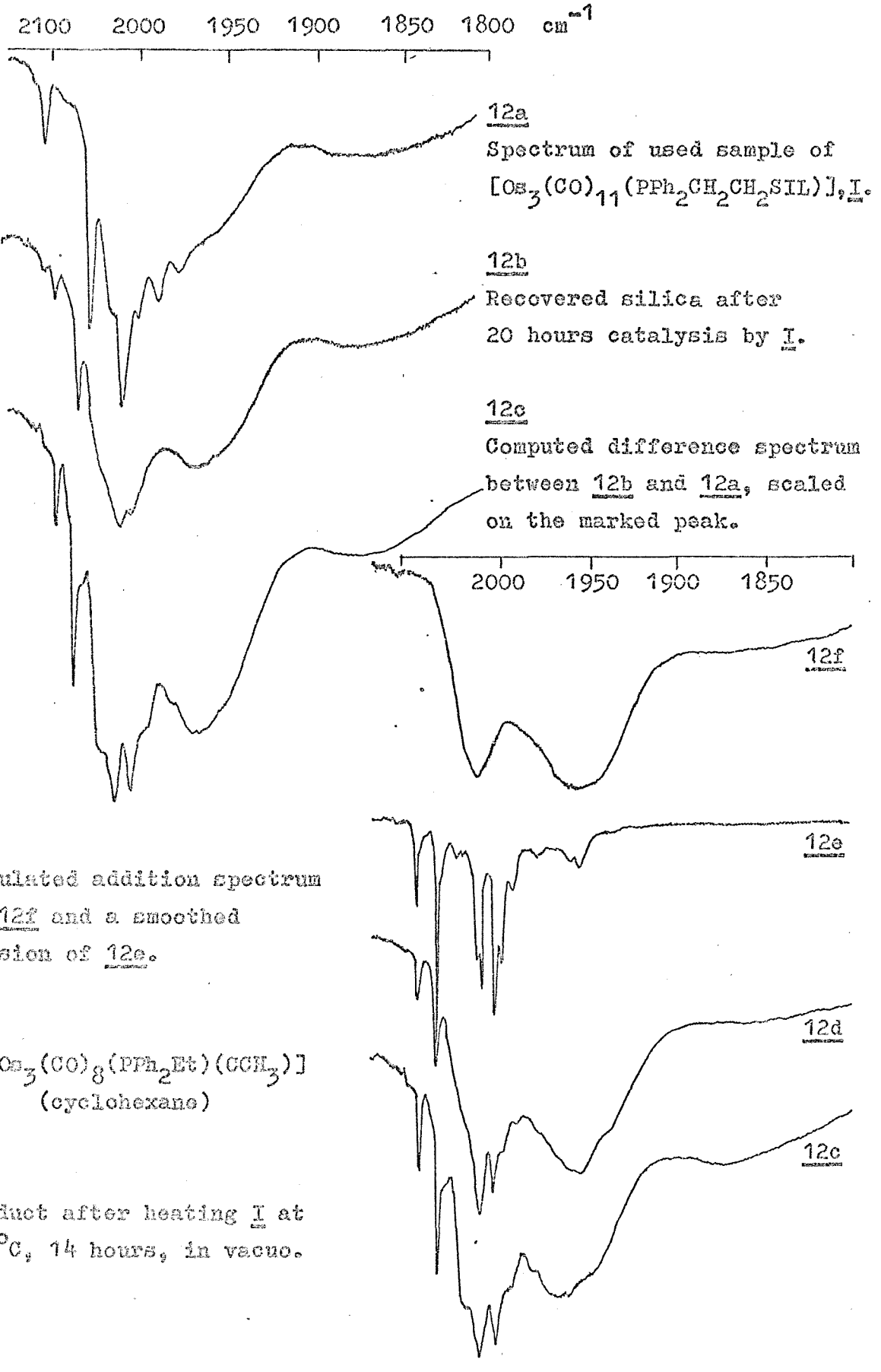
5.6.2. $[Os_3(CO)_{11}(PPh_2CH_2CH_2SIL)]$

At 110°C, under the same gas mixture, I gave an ethane yield of 70 molecules per cluster after 24 hours. This represents only a slight reduction in efficiency upon cluster immobilisation to the phosphine-modified silica, compared to the figure of 101 obtained for VIII in the same period. Thus, anchoring apparently imparts no physical limitation to the clusters ability to perform catalysis.

The recovered, light yellow, silica was mulled and the infrared ν_{CO} spectrum recorded. This is shown as 12b in Diagram 12. The presence of a weak absorption at 2107cm^{-1} indicates that some I remained at the end of the run. Its contribution can be removed

Diagram 12

Computer Interpretation of the Surface Species on spent Silicas from Catalysis by $[Os_3(CO)_{11}(PPh_2CH_2CH_2SIL)]$



12a
Spectrum of used sample of $[Os_3(CO)_{11}(PPh_2CH_2CH_2SIL)]$, I.

12b
Recovered silica after 20 hours catalysis by I.

12c
Computed difference spectrum between 12b and 12a, scaled on the marked peak.

12d
Simulated addition spectrum of 12f and a smoothed version of 12e.

12e
$[H_3Os_3(CO)_8(PPh_2Et)(CCH_3)]$ (cyclohexane)

12f
Product after heating I at 130°C, 14 hours, in vacuo.

by using the Model 3500 Data Station. This gives 12c, the difference between 12b and 12a, the recorded spectrum for the batch of I used in the catalytic study, scaled on the marked peak in the window 2110-2098cm^{-1}. Most of its features can be reproduced by the addition of the spectrum of X (12f), the product from thermal breakdown of the anchored cluster by interaction with the support appendages, to that of an artificially broadened version (repeated smoothing operations to reduce resolution) of that for XVIII (12e). This yields a simulated spectrum, 12d, which is almost identical to 12c. No evidence for the catalytically active species, II, is seen. Loss of activity evidently proceeds by two routes. One is the anticipated deactivation process, via formation of $[HOs_3(CO)_9(PPh_2CH_2CH_2SIL)(CHCH_2)]$, XX, which leads to the isolation of $[H_3Os_3(CO)_8(PPh_2CH_2CH_2SIL)(CCH_3)]$, XXI, at the end of the run. The second is cluster decomposition to monomeric units by further interaction with the support surface, as discussed previously. This most probably occurs with II, but any intermediate with a transient vacant coordination site will also be susceptible: direct breakdown of I is less likely.

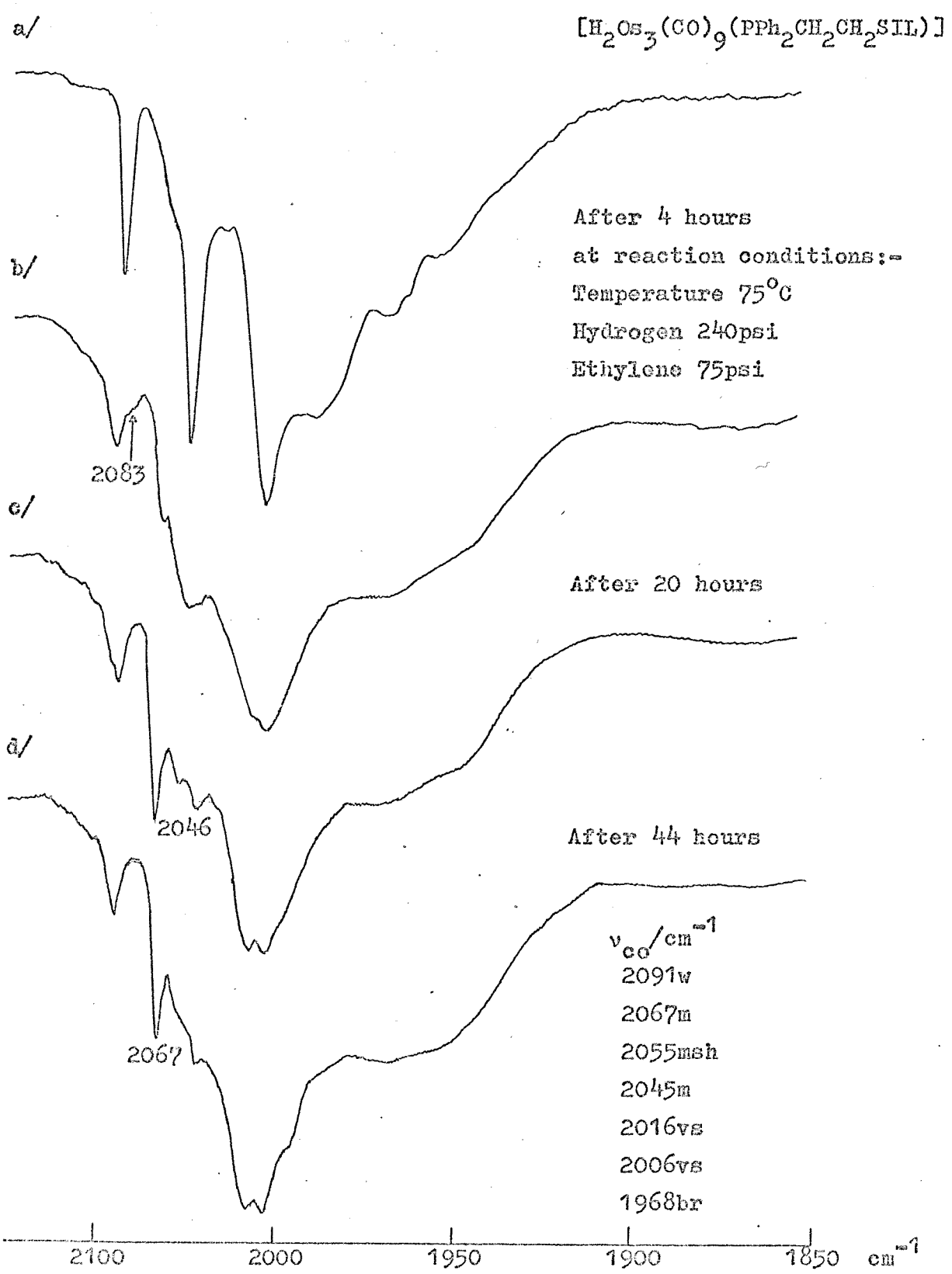
5.6.3. $[H_2Os_3(CO)_9(PPh_2CH_2CH_2SIL)]$

This was studied in more detail. Runs with suspensions of II, in n-heptane at 75°C, gave ethane yields of 2.6, 10.1 and 13.1 molecules per cluster, after 4, 20 and 44 hours reaction time, respectively. The 20 hour run was repeated with a half-weight of catalyst, and the obtained turnover of 8.5 shows that the rate of reaction is (first order) proportional to the metal concentration. When this data is plotted (Diagram 10) a deterioration in activity with time is evident, with cessation of reaction occurring well within 44 hours. A tangent to the initial period gives an estimated turnover number of 6.5×10^{-1} hour. At the end, still only 20% of the ethylene is converted, so even if a first order dependence on its concentration exists, as only a fraction of the half-life the loss of rate must be a function of catalyst deactivation.

Comparison with the result for I (95 turnovers in 20 hours) indicates that anchoring reduces the rate of reaction by almost an order of magnitude. In every case the final supernatent solution had no perceivable coloration, which is good evidence for

Diagram 13

Infrared (ν_{CO}) Spectra of recovered Silicas from Ethylene Hydrogenations with $[H_2Os_3(CO)_9(PPh_2CH_2CH_2SIL)]$



the absence of leaching. This is supported by an osmium analysis of 4.3wt/wt% on the recovered silica from the 44 hour run.

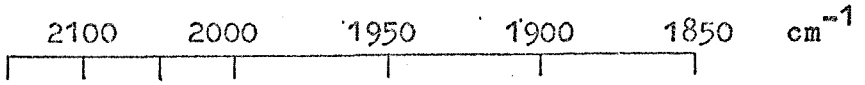
The decline in catalytic acitivity can be correlated with an accompanying change in the infrared ν_{CO} spectra of the recovered silicas (Diagram 13). These were all noticeably pale yellow/off-white in appearance, compared to the green-purple of the starting material. In addition to bands due to II, after 4 hours there is a weak band at 2083cm^{-1}, coincident with an absorption of XVI, which is later lost. An emerging absorption at 2067cm^{-1} is evidence of a third species which increases in concentration after 20 hours at the expense of II, as seen by a small shift for the highest band and the gradual disappearance of the 2052cm^{-1} feature. There is little subsequent change after 44 hours, except that the absorption at 2046cm^{-1}, seen at 20 hours, is less prominent and almost all indication (2055cm^{-1} shoulder) of II has gone. Below 2000cm^{-1} a broad band, centred at 1970cm^{-1}, quickly develops over the initial stages and remains at the end. This final spectrum closely resembles that for the spent catalyst from I. Again two carbonyl containing species are present after cessation of catalysis, the ethylidyne complex, XXI, and a cluster decomposition product, X. This can be verified by several different treatments of the spectra using the Model 3500 Data Station.

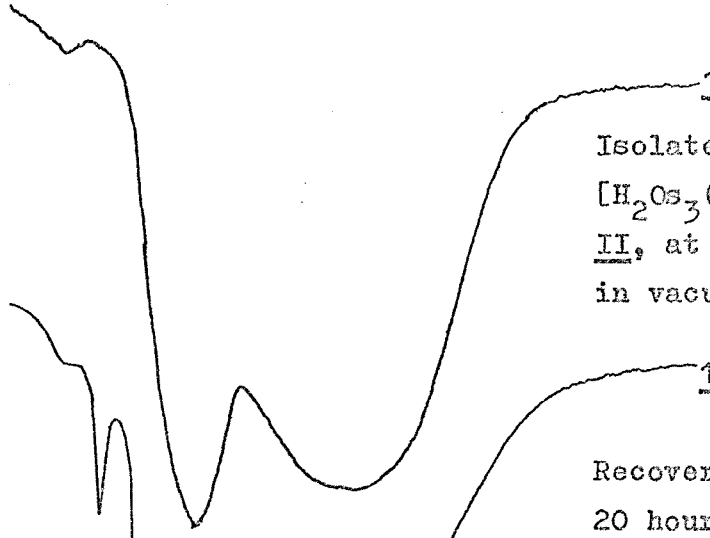
The difference spectrum, 14d, (no specified region) between that of the product from heating II to 150°C in vacuo for 16 hours, 14a, and that of the 20 hour silica, 14b, correlates well with the spectrum of XVIII in cyclohexane solution, 14c. The band at 2046cm^{-1} could be an artifact, however in a similar treatment of the 44 hour silica it is less pronounced, and as it coincides with the strongest absorption for XVI, it may be evidence for $[H_2Os_3(CO)_8(PPh_2CH_2CH_2SIL)(CCH_2)]$, XIX, which is hydrogenated over the longer period.

Alternatively, the spectrum of the 4 hour silica, 15a, can be subtracted from that of the 20 hour silica, 15b, and in turn the decomposition product spectrum, 15d, subtracted to give 15f. This result is more aesthetically pleasing as the relative intensities are closer to those of XVIII. An absorption at 2046cm^{-1} is again present. A difference spectrum between 15a and 15b, based on the 1960-1901cm^{-1} region, directly gives a spectrum with strong

Diagram 14

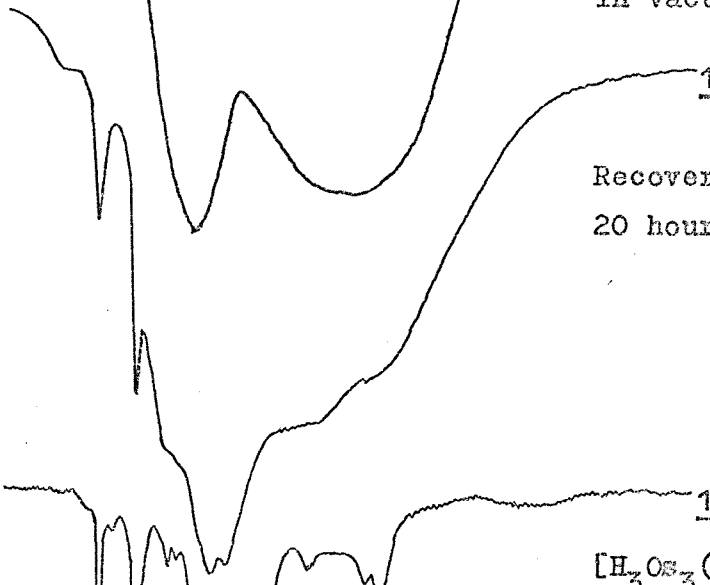
Computer Interpretation of the retrieved Silica after Ethylene Hydrogenation catalysed by $[H_2Os_3(CO)_9(PPh_2CH_2CH_2SIL)]$





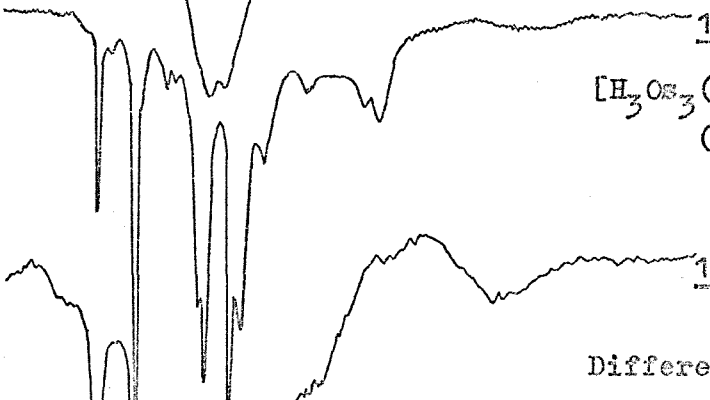
14a

Isolated product after heating $[H_2Os_3(CO)_9(PPh_2CH_2CH_2SIL)]$, II, at 150°C for 16 hours in vacuo.



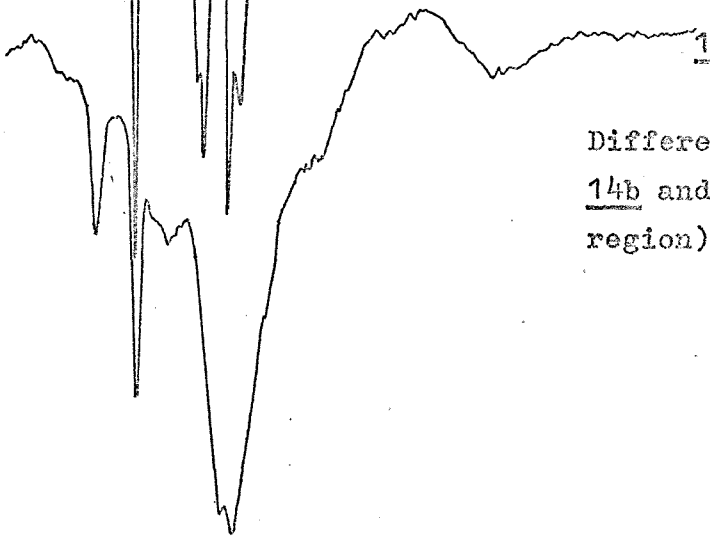
14b

Recovered silica after 20 hours catalysis by II.



14c

$[H_3Os_3(CO)_8(PPh_2Et)(CCH_3)]$ (cyclohexane)



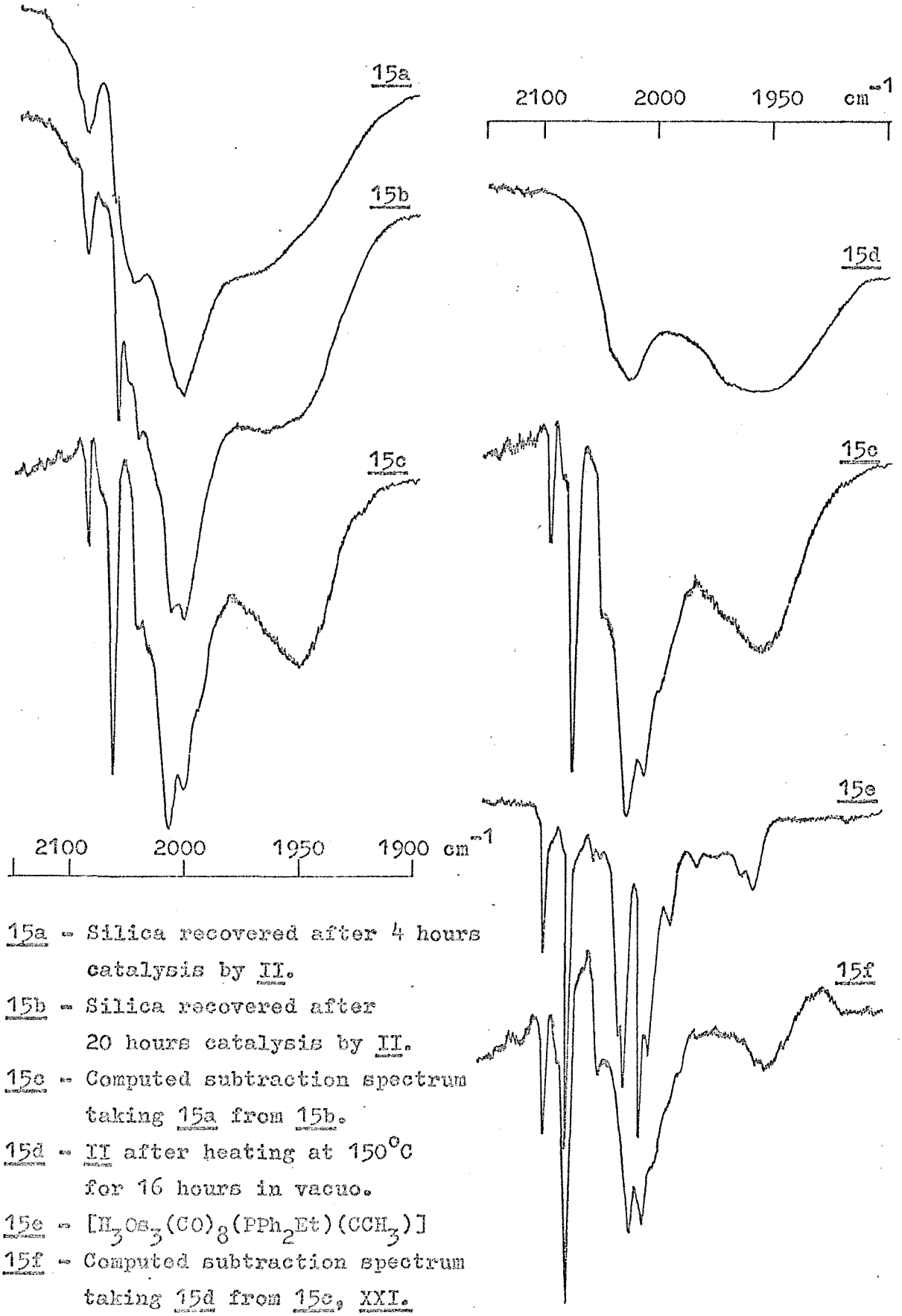
14d

Difference spectrum between 14b and 14a (no specified region), XXI.

(All silica spectra recorded in Nujol mull)

Diagram 15

An Alternative Method of Infrared Characterisation for $[H_3Os_3(CO)_8(PPh_2CH_2CH_2SIL)(CCH_3)]$



15a - Silica recovered after 4 hours catalysis by II.

15b - Silica recovered after 20 hours catalysis by II.

15c - Computed subtraction spectrum taking 15a from 15b.

15d - II after heating at 150°C for 16 hours in vacuo.

15e - $[H_3Os_3(CO)_8(PPh_2Et)(CCH_3)]$

15f - Computed subtraction spectrum taking 15d from 15c, XXI.

similarities to that of XVIII(84), but suffers from negative absorptions through no account being taken of remaining II. Three important conclusions can be drawn from these results.

i) The loss of conversion with the emergence of X and XXI indicates that neither they, nor the silica support itself, are the active species. The catalytic activity deteriorates as the concentration of II present on the silica falls.

ii) The same product distribution is seen on the spent silicas from both I and II, establishing the presence of a common catalytic cycle/deactivation process.

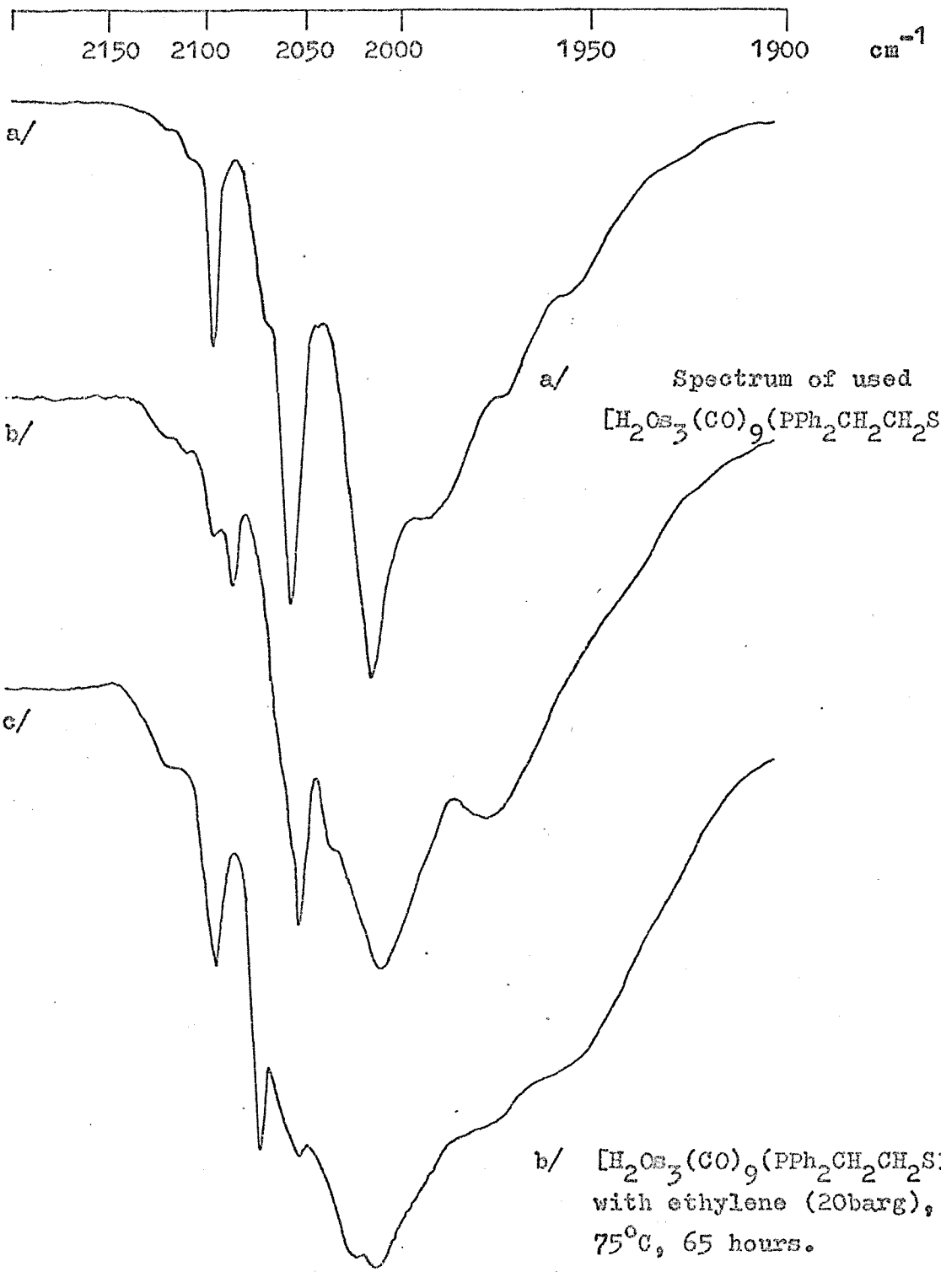
iii) The recovered products from deactivation are different for the homogeneous and heterogeneous systems.

5.7. Further Characterisation of the Deactivation Process for Anchored Clusters

All the above studies were carried out using the high-pressure facilities at ICI's Billingham or Wilton laboratories. From the results there was strong circumstantial evidence for the intermediate formation of XIX. At Southampton further clarification of the deactivation process was undertaken. The catalytic reaction was repeated in the 100ml Roth autoclave, at the same temperature ($75^{o}C$) but with a slightly higher total pressure (28barg). The infrared ν_{co} spectrum of the recovered silica (Diagram 16) compares well with that obtained at Wilton. However, if a fresh sample of II was similarly treated, but under an ethylene pressure (20barg) alone, the retrieved solid possessed a different spectrum. Reaction had obviously occurred as the characteristic peaks at 2091 and 2052 cm^{-1} for II have diminished in intensity, and are now only shoulders on emerged absorptions at 2081 and 2046 cm^{-1} respectively. Other changes involve a shoulder at 2027 plus bands at 2004vs and 1974m-s, cm^{-1}. All these features are highlighted in a difference spectrum obtained with that of II, based on the common band between 2100-2085cm^{-1}. They show (Table 7) good agreement with the ν_{co} pattern of XVI, thereby establishing the formation of $[H_2Os_3(CO)_8(PPh_2CH_2CH_2SIL)(CCH_2)]$, XIX, as a surface species. This compliments the frequently observed band at 2046cm^{-1}, and transient at 2083cm^{-1}, seen in the full catalytic study.

Diagram 16

Infrared (ν_{CO}) Spectra from reactions of $[H_2Os_3(CO)_9(PPh_2CH_2CH_2SIL)]$ with Ethylene and Hydrogen



a/ Spectrum of used $[H_2Os_3(CO)_9(PPh_2CH_2CH_2SIL)]$

b/ $[H_2Os_3(CO)_9(PPh_2CH_2CH_2SIL)]$ with ethylene (20barg), 75°C, 65 hours.

c/ $[H_2Os_3(CO)_9(PPh_2CH_2CH_2SIL)]$ with hydrogen/ethylene(3:1), 28barg, 75°C, 65 hours.

(All spectra recorded in Nujol mull)

Table 7

A	B	C	D	E
2115vw			2112wsh	
2103vw	2105vw			
2091m	2090wsh		2090m	2091.5mw
	2081w	2084m	2067s	2069vs
2063msh			2045ssh	2026m
2052s	2052mssh		2015vs	2022s
	2046s	2050vs	2006vs	2006vs
		2036w		1991w
	2027mssh	2030m	1974ssh	1979vw
2009vs		2021vw	1955msh	1966vw
	2004vsbr	2005s		
1991ssh		1997m		
1972msh	1974ms	1979m		
1954wsh		1965wsh		

A: - $[H_2Os_3(CO)_9(PPh_2CH_2CH_2SIL)]$, II, (nujol mull)

B: - II with ethylene (20barg), 75°C, 65 hours, (nujol mull)

C: - $[H_2Os_3(CO)_8(PPh_2Et)(CCH_2)]$, XVI, (cyclohexane)

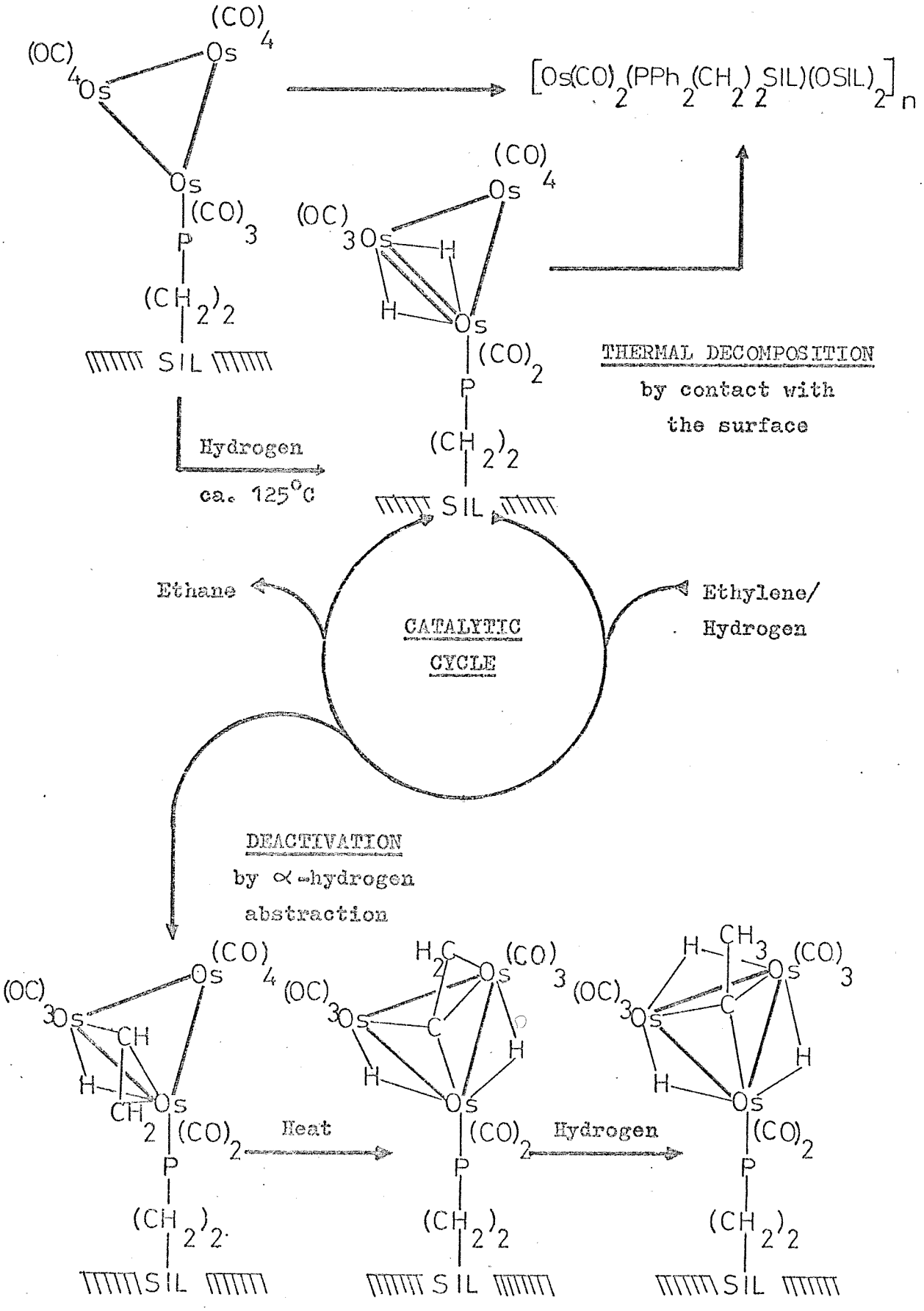
D: - II with hydrogen/ethylene(3:1), 28barg, 75°C, 65 hours, (nujol mull)

E: - $[H_3Os_3(CO)_8(PPh_2Et)(CCH_3)]$, XVIII, (cyclohexane)

The one remaining omission from the proposed deactivation process is isolation of the supported vinyl adduct, XX. Infact a quantity of II was treated with ethylene at room temperature. It was suspended in n-heptane(10ml) and the 20ml bench-top autoclave pressurised to 60psig. On starting agitation the pressure dropped to 25psig, and more gas was introduced until the operating level was 45psig. It was then left stirring over a weekend (65 hours) before discharging the bomb. During this time the solid changed in colour from green to yellow but its infrared ν_{CO} spectrum (2092w, 2072wsh, 2056m, 2046msh, 2036s, 2030s, 2006vs,

Diagram 17

Possible Catalyst Degradation Routes during Ethylene Hydrogenation by Phosphine-anchored Triosmium Clusters



1975ssh, cm^{-1}, nujol mull) was not very diagnostic. Considerable modification has occurred, and the complexity indicates a probable mixture of cluster species spanning from II through to the required vinyl adduct, and including the intermediate containing a coordinated ethylene. This is perhaps not unexpected when compared to the reaction of IX with ethylene under similar conditions (Chapter Three). Infact Freeman et.al.(85) have reported the infrared data(2090m, 2041s and 2008vs, cm^{-1}, KBr pellet) for a yellow product from reacting II with acetylene at ambient temperature and pressure for 4 hours. This method should be more selective towards the supported vinyl adduct, and this appears the case based on the limited information presented. They also prepared the stabilised alkyl-intermediate $[HOs_3(CO)_9(MeO_2CCHCH_2CO_2Me)(PPh_2\text{-SUPPORT})]$, from II and dimethyl fumarate, and isolated small amounts of dimethyl succinate from subsequent hydrogenation reactions(86). These results are summarized in Diagram 17. Loss of catalytic activity occurs by two pathways.

i) Deactivation by α-hydrogen abstraction to generate the saturated vinyl adduct, XX. Under the conditions employed subsequent carbon monoxide loss and reaction with hydrogen gives the isolated XXI.

ii) Decomposition by further interaction with the silica appendages causing cluster breakdown to X.

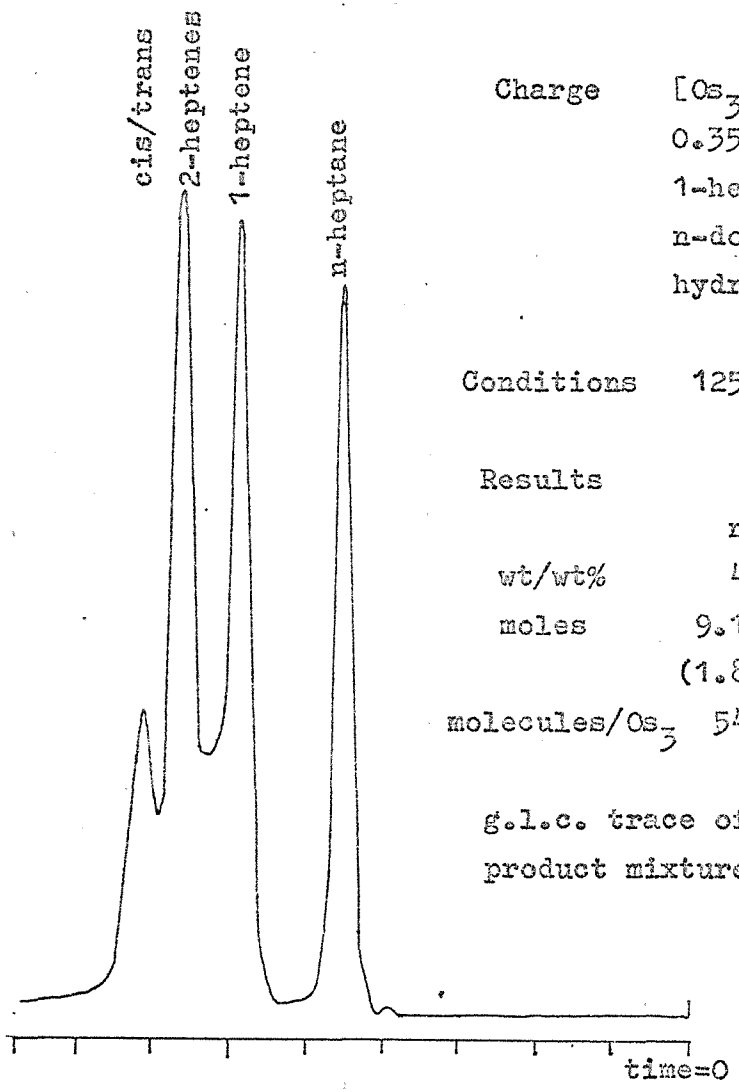
5.8. 1-Heptene Isomerisation/Hydrogenation

This experiment was carried out to determine the influence of a long alkyl chain on the reaction. It would also provide comparative data to the reported 1-hexene isomerisation/hydrogenations reported for $[H_2Os_3(CO)_{10}]$, II(85) and the related material on phosphine-functionalised polystyrenes(67,85). However, because of the greater success with I it was chosen as the catalyst precursor.

The batch reaction was performed in a stainless steel, 100ml autoclave, with agitation by a 'flip-flop' device. A charge of I(0.2523g) and 1-heptene(3ml), in n-dodecane(45ml) as solvent, was loaded into the bomb, flushed with hydrogen, and brought up to pressure (170barg) and held at 125°C for 4 hours. Then the electrical induction heating was removed and the bomb rapidly cooled with

Diagram 18

Catalytic Hydrogenation/Isomerisation of 1-Heptene by $[Os_3(CO)_{11}(PPh_2CH_2CH_2SIL)]$



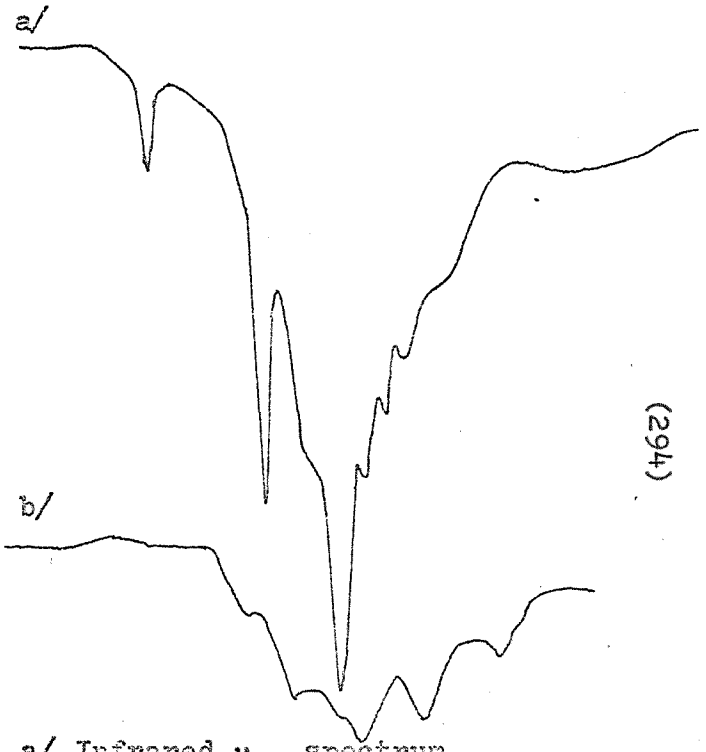
Charge	$[Os_3(CO)_{11}(PPh_2CH_2CH_2SIL)]$,	
	0.3523grams (1.67×10^{-5} moles$_{Os_3}$)	
	1-heptene	2.091grams(3ml)
	n-dodecane	45ml (solvent)
	hydrogen	170barg

Conditions 125°C, 4 hours

Results

	n-heptane	2-heptenes
wt/wt%	4.39(9.06)	74.22(53.37)
moles	9.159×10^{-4}	1.582×10^{-2}
	(1.894×10^{-3})	(1.139×10^{-2})
molecules/Os_3	54.8(113.4)	947.3(682.0)

g.l.c. trace of product mixture



a/ Infrared ν_{CO} spectrum of the fresh catalyst.

b/ Infrared ν_{CO} spectrum of the spent catalyst solution.

(Both recorded as Nujol mulls)

compressed air jets. The recovered solution was analysed on a 4m x 0.24cm, 20% Reoplex in 60/80 AW-W, column, using relative response factors for the identified components. The results were normalised and equated to the initial weight of 1-heptene to give the absolute number of moles formed (Appendix 2). Because some doubt surrounds the calibration technique, using an unknown 2-heptene mixture of predominantly the cis-isomer to obtain an averaged response factor, when the trans-isomer is prevalent in the product, the data was also reworked using unit reponse factors: the figures so obtained are quoted in parentheses.

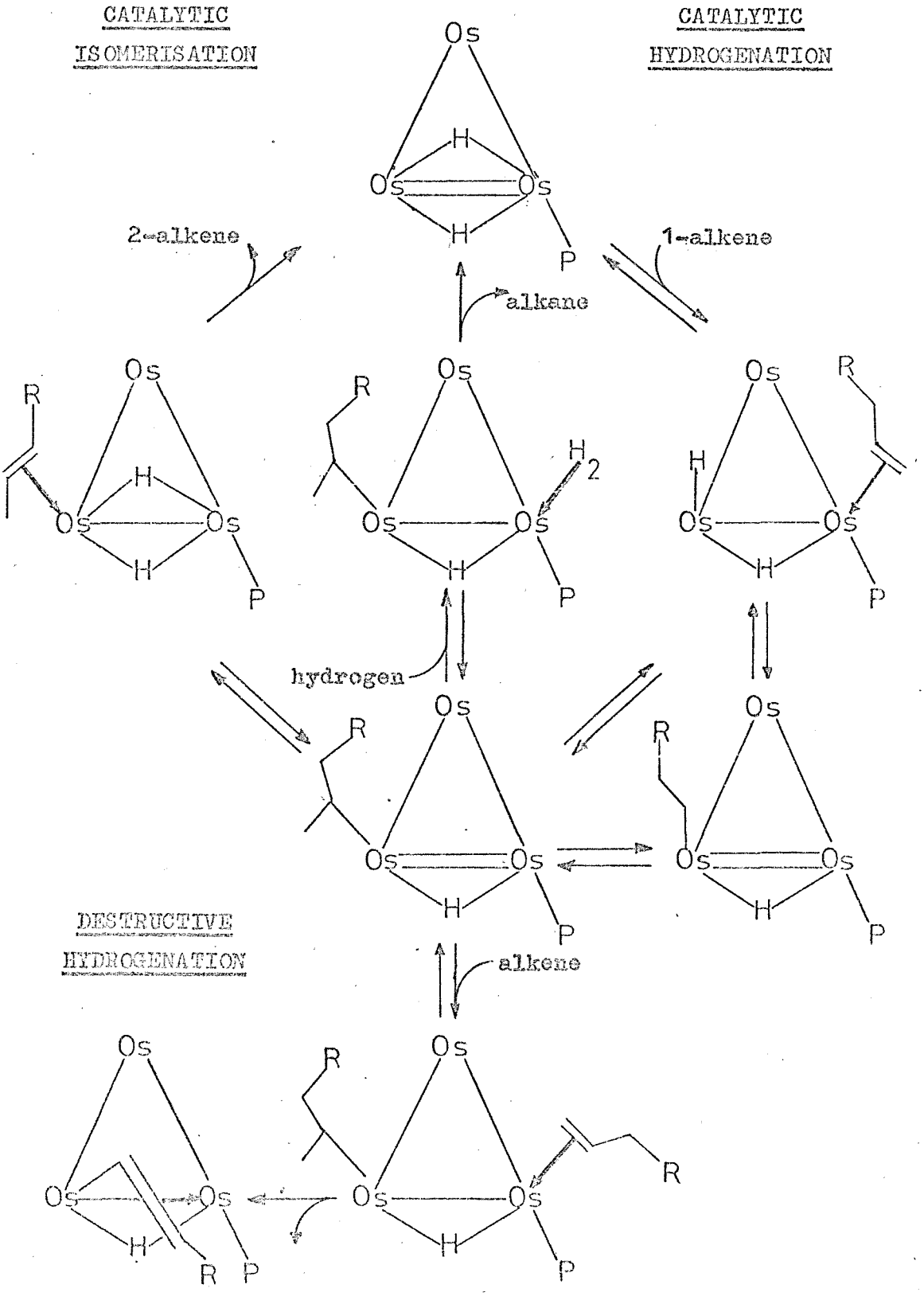
The discharge from the bomb was colloidal, indicating a good dispersion of the catalyst in solution during reaction. The infrared ν_{CO} spectrum (Diagram 18) of the separated solid is reasonably broad. Significantly the pattern is different to that obtained from the corresponding ethylene study. Its complexity is indicative of retained cluster compounds, whilst there is noticeably less contribution due to the decomposition product, X. The recovered C_7 mixture contained 74.2(53.4)wt/wt% of 2-heptenes and 4.4(9.1) wt/wt% n-heptane, with 21.4(37.6)wt/wt% of unconverted 1-heptene remaining at the end. These amounts represent conversions of 55(113) and 947(682) molecules of 1-heptene per cluster for hydrogenation and isomerisation, respectively, after 4 hours. No evidence for 3-heptenes was seen on the gas chromatography trace. A blank run with the unfunctionalised silica gave no reaction.

5.9. Discussion

A unified mechanism for catalytic isomerisation and hydrogenation of 1-alkenes by $[H_2Os_3(CO)_9L]$, L=CO, tertiary phosphine or phosphine-functionalised support, is presented in Diagram 19. The driving force is the interplay between electron-precise and electron-poor metal cluster systems. Thus each step in the sequence is governed by the interconversion between 46$\rightleftharpoons$48 electron species, and also the ability of the cluster to expand its coordination sphere from 12 to 13. The loss and uptake of ligands is allowed by varying the metal-metal bond order so that no carbonyl groups need be displaced, and all intermediates conform with the E.A.N. rule. Thus a small carbon monoxide partial pressure does not appreciably

Diagram 19

Catalytic Cycle for 1-Alkene Isomerisation / Hydrogenation by $[H_2Os_3(CO)_9(PPh_2R)]$; R=Et or CH_2CH_2SiL



affect the rate of 1-pentene(46mM) isomerisation by $[H_2Os_3(CO)_{10}]$ at 70.4°C in toluene(87). Higher pressures might be expected to block reaction by formation of $[H_2Os_3(CO)_{11}]$. In support, a preliminary 1-heptene hydrogenation using $[H_2Os_3(CO)_{10}(PPh_2CH_2CH_2SIL)]$, XI, under identical conditions to those employed with I, but at 75°C for 4 hours, resulted in negligible reaction and the removed silica had only partially decarbonylated to the active II over the period.

Shapley(88) showed that the isolable hydridoalkyl species $[HOs_3(CO)_{10}(CH(CH_2CO_2Et)CO_2Et)]$, XXII, from reaction of $[H_2Os_3(CO)_{10}]$ with diethyl fumarate, decomposes under hydrogen, in the absence of excess alkene, to regenerate the initial cluster and release diethyl succinate. This dismisses the need for hydrogenation to proceed via an intermediate containing both σ-alkyl and π-bonded alkene moieties, as proposed elsewhere(89). Indeed formation of such a species leads rapidly to the saturated vinyl adduct, as evidenced by the reaction of XXII with alkenes not normally reactive towards $[H_2Os_3(CO)_{10}]$ i.e. styrene. Then the key intermediate in the cycle is $[HOs_3(CO)_9L(alkyl)]$, XXIII. As a 46-electron system, like $[H_2Os_3(CO)_{10}]$, it requires a double Os-Os bond and is expected to undergo similar addition reactions. It can suffer one of three fates:-

1) Hydrogen atom transfer back from a β-carbon of the alkyl group. For a secondary alkyl-metal intermediate this can result in CATALYTIC ALKENE ISOMERISATION.

2) Addition of hydrogen, followed by alkane elimination and regeneration of $[H_2Os_3(CO)_9L]$, CATALYTIC HYDROGENATION. 3) Coordination of a second alkene with release of alkane, but deactivation by α-hydrogen abstraction to generate the saturated bridging vinyl complex, DESTRUCTIVE HYDROGENATION.

A forth possibility for the supported variant involves interaction with the surface groups.

For 1) and 2), the structure of XXIII favours addition of a second substrate prior to loss of alkane, rather than by a unimolecular process with a highly unsaturated 44-electron species, $[Os_3(CO)_{10}]$(88). The structure of XXII shows this to be a two metal centre process. The relative rates of these three parallel reactions will determine the predominant path of the overall reaction. Provided

1) and 2) are faster than 3) a catalytic cycle will be established. At room temperature $[H_2Os_3(CO)_{10}]$ can transform 510 equivalents of 1-hexene to internal alkenes, after which the solution has turned from purple to yellow and no further conversion is observed(85). This figure must reflect the relative rates of 1) and 3) at these conditions. When the quantity of 1-alkene is restricted to 100 equivalents, at 50°C in the presence of hydrogen(50psig), conversion to 31 equivalents of n-hexane and 69 equivalents of 2-hexenes occurs, with essentially all the catalyst recovered at the end(88). Thus for 1-hexene catalytic isomerisation > catalytic hydrogenation > destructive hydrogenation.

The kinetics for the isomerisation reaction with $[H_2Os_3(CO)_{10}]$ has been most widely studied. The redistribution of hydrogen isotopes in trans-$C_2H_2D_2$(22.1mM) takes place to a large extent when treated with $[H_2Os_3(CO)_{10}]$(1.87mM) at 70.4°C in toluene solution(87). This confirmed that the initial addition and insertion steps are reversible and, even for ethylene, faster than destructive hydrogenation. Thus, although ethylene exchange is a hidden process in the absence of isotopic substitution, it will be occurring as a competing pathway during the hydrogenation studies. With [1,2-D_2]-pentene an accumulation of deuterium on C-1 must be due to σ-alkyl intermediates originating from both Markownikov and anti-Markownikov additions (secondary and primary alkyls respectively). A buildup on C-3 was ascribed to the exchange, in the σ-alkyl intermediate, of a hydrogen on C-3 of the deuterated 1-pentene with a deuterium linked to the metal cluster(87), and not to a slower isomerisation of 2-alkene back to the terminal form. At 32.5°C, in $CDCl_3$, Deeming(83) established overall second-order rate kinetics, given by:-

$$-\frac{d\,[\text{alkene}]}{dt} = k_2[H_2Os_3(CO)_{10}][\text{alkene}]$$

-so that the observed first order rate coefficient is given by:-

$$k_1 = k_2[H_2Os_3(CO)_{10}]$$

Similar values of k_2 for a series of compounds of the type $CH_2{=}CHCH_2R$ (R=C_3H_7, Ph, OPh or OH) showed little dependence on R, implying that initial coordination and/or insertion are rate determining and not hydrogen atom transfer back to osmium. Allylic

alcohols were also isomerised to aldehydes and ketones (displaced enol rapidly converting to organic carbonyl) and the effect of methyl substitution at the allyl group studied. No change of rate



was observed whether R^3=H or Me confirming hydrogen abstraction to be rapid from either a secondary or tertiary carbon. However, substitution at the vinylic positions (R^1 or R^2=Me) produced a marked rate reduction, and, in particular, at R^2 a complete lack of isomerisation, is consistent with the difficulty of forming tertiary-alkyl intermediates. This does not preclude reversible insertion to give primary alkyl species in this and other cases, but this does not lead to isomerisation. For R^1=Me reaction does proceed, via a secondary alkyl intermediate, to butanal but slower by a factor of 66 compared to the unsubstituted molecule. Thus the reaction is quite sensitive to steric and electronic effects, and others(88) found that ethyl acrylate and vinyl acetate react faster than ethylene, whereas propene and isobutylene react slower, with no reaction observed for cyclooctene or norbornene. Clearly the ease of σ-alkyl formation is primary > secondary > tertiary. One hypothesis would involve selective formation of a primary σ-alkyl with 1-alkenes and the equilibrium with the secondary form only occurring after insertion.

For the homologous series of straight chain 1-alkenes, from 1-butene onwards, isomerisation to 2-alkenes will accompany hydrogenation, and their observed buildup is consistent with the aforementioned limitations to secondary alkyl formation. For the same reason the presence of 3-alkenes etc. has not been reported. Detailed kinetics for the hydrogenation and deactivation reactions are not known. However, as $[H_2Os_3(CO)_{10}]$ scrambles deuterium with $C_2H_2D_2$ and [1,2-D_2]-pentene, the rate determining step is probably after formation of XXIII. Based on the assumption that this is the bimolecular reaction with the second substrate molecule. Then:-

$$[H_2Os_3(CO)_{10}] \; + \; \text{alkene} \underset{k_{-1}}{\overset{k_1}{\rightleftharpoons}} [HOs_3(CO)_{10}(\text{alkyl})] \xrightarrow{\text{fast}}$$

A B C

For isomerisation the unimolecular reaction of C, to give 2-alkene, is fast and the first step is rate-determining, so the concentration of C will approach zero. In these circumstances, the rate law is:-

$$\text{Isomerisation}_{\text{RATE}} = k_1[A][B] \text{ (as proven experimently)}$$

The two other parallel reactions are:-

$$[HOs_3(CO)_{10}(\text{alkyl})] + H_2 \underset{k_{-2}}{\overset{k_2}{\rightleftharpoons}} \underset{D}{[HOs_3(CO)_{10}(\text{alkyl})(H_2)]} \xrightarrow{\text{fast}}$$

and

$$[HOs_3(CO)_{10}(\text{alkyl})] + \text{alkene} \underset{k_{-3}}{\overset{k_3}{\rightleftharpoons}} [HOs_3(CO)_{10}(\text{alkyl})(\text{alkene})] \downarrow \text{fast}$$

substituting $[C] = k_1/k_{-1}[A][B]$ gives:-

$$\text{Hydrogenation}_{\text{RATE}} = k_2 \cdot k_1/k_{-1}[A][B][D]$$

$$\text{Deactivation}_{\text{RATE}} = k_3 \cdot k_1/k_{-1}[A][B]^2$$

So that the relative rates of reaction are:-

Isomerisation	:	Hydrogenation	:	Deactivation
1	:	$k_2/k_{-1}[H_2]$	:	$k_3/k_{-1}[\text{alkene}]$

From this simplified treatment the following deductions are possible:-

i) k_{-1} will be large, so that the rate of isomerisation will exceed that for the two competing pathways.

ii) The value of k_2 will be largely independent of steric considerations for the alkyl group, so that hydrogenation

is favoured by higher partial pressures of hydrogen and small values of k_{-1}. This is fulfilled by less reactive, higher substituted or branched 1-alkenes. Notably with reactive ethyl acrylate the number of cycles was limited by destructive side reactions(88).

iii) Destructive hydrogenation is promoted by high alkene concentrations; the higher reactivity of XXIII implies that $k_3 > k_1$ and deactivation will be less discriminating on the nature of the second incoming alkene.

Ethylene hydrogenation by other immobilised clusters i.e. $[Ir_4(CO)_{12-n}(PPh_2\text{-}\textcircled{P})_n]$(90), or $[Ir_4(CO)_9(PPh_3)_n(PPh_2\text{-}\textcircled{P})_n]$ (91), n=1 or 2, show a best fit to a similar rate equation to that proposed above, whilst others, for example $[H_4Ru_4(CO)_{12-n}(PPh_2\text{-}\textcircled{P})_n]$, n=1-4(92), show saturation kinetics and, in the case of the monosubstituted cluster, inhibition of reaction by ethylene at higher partial pressures. The bimetallic clusters, $[Fe_2Pt(CO)_8(PPh_2\text{-}\textcircled{P})_2]$ and $[RuPt_2(CO)_5(PPh_2\text{-}\textcircled{P})_3]$(93) also exhibit this behaviour. Translated to the current study this

$$\text{RATE} = kK.P^1_{C_2H_4}.P^m_{H_2} \;/\; [1+K.P_{C_2H_4}]^n$$

inverse factor on alkene concentration is consistent with the proposed destructive hydrogenation kinetics.

Introduction of a phosphine destroys the symmetry across the catalyst, such that both ends of the bridgehead are now distinct. The evidence from solution chemistry shows that orbital control directs addition to the phosphine-bonded osmium. Isolation of $[H_2Os_3(CO)_9(PPh_3)(C_2H_4)]$, XXIV, demonstrated that insertion into a hydride bond is retarded by the phosphine, so that it is definitely the rate-limiting step. This may be an electronic, stronger alkene-to-metal bonding, or steric effect. The greater retardation by PPh_3 pointed to the latter and, from the proposed structure of XXIV, rearrangement to an activated form is necessary to facilitate the insertion and a bulky, immobile phosphine may restrict this process. Similarly, phosphine substitution retards acetylene insertion, and more so on changing from PPh_2Et to PPh_3. The rates of insertion for sustituted alkynes into $[H_2Os_3(CO)_{10}]$ also show a tentative dependence on the steric nature of the hydrocarbon(94). Indeed the competitive formation of $[Os_3(CO)_{10}(R'C{:}CR'')]$ may occur by insertion

of a second alkyne molecule into an activated metal-hydride bond in $[H_2Os_3(CO)_{10}(R'C{:}CR'')]$, and release of the corresponding alkene, with the remaining cluster rearranging to the observed product, without invoking $[HOs_3(CO)_{10}(R'C{:}CR''H)]$ as an intermediate. The favoured structure of XXIII is that with the σ-alkyl bonded to the osmium away from the phosphine, based on the considerations in Chapter Three. Then the phosphine can be expected to have a less significant effect on degradation of XXIII by isomerisation (or hydrogenation), compared to a slowing down of deactivation by α-abstraction from a second coordinated alkene. Again this barrier will be more pronounced for higher 1-alkenes. Then higher conversions, but slower rates, might be forecast for the phosphine derivatives.

Two attempts to directly compare the catalytic activity of $[H_2Os_3(CO)_9(PPh_3)]$, IXb, with that of $[H_2Os_3(CO)_{10}]$ have appeared, but the results are conflicting. At ambient temperature and pressure Gates et.al.(85) found that the parent carbonyl produced 510 moles of internal hexenes before conversion ceased, but they were unable to obtain any quantitative data with IXb because cluster decomposition rapidly occurred. In contrast, Lieto(67) found a comparable transformation of 100 equivalents of 1-hexene, to 70 equivalents of 2-hexenes and 30 equivalents of n-hexane, with nearly complete catalyst recovery, at the conditions previously employed by Shapley(88). The first group had much greater success with anchored catalyst II. On both silica and polymer-supports, at 75°C approximately 1000 molecules of isomers were formed before the cessation of catalysis. This roughly twofold greater yield, compared to the soluble $[H_2Os_3(CO)_{10}]$, re-enforces the importance of the phosphine in hindering coordination of a second alkene, enhancing the competing, catalytic reactions. This is further exaggerated on the tethered variant where the support can act essentially as a large ligand. Then the poor results with IXb must reflect the possible coupling reactions in solution which are avoided on the support. However, contrary to the present predictions quantitative kinetic data for 1-pentene isomerisation showed similar dependences but a threefold larger rate constant relative to $[H_2Os_3(CO)_{10}]$. This does not match the observed solution chemistry, and the slight reductions in rate seen upon anchoring, in this thesis. Gates also studied 1-hexene hydrogenation (60psig,

75°C) with II and, again with a limited excess of alkene (109:1 alkene/cluster), observed conversion of 19% to hexane and 79% to internal hexenes over 45 hours, with no catalyst decomposition observed by infrared spectroscopy.

Immediately, the catalyst lifetime for the current 1-heptene study, giving approximately 1000(800) transformations before termination, is comparable to these results with 1-hexene, albeit at different conditions. The absence of any detected 3-heptenes is in agreement with the cluster catalysed mechanism. The much greater degree of isomerisation, even under much higher hydrogen partial pressures, may be the consequence of the unknown temperature dependence of the two pathways, with isomerisation being favoured at higher temperatures. However, the higher pressures appear to stabilise the cluster against degradation, by contact with surface groups, to monomeric units.

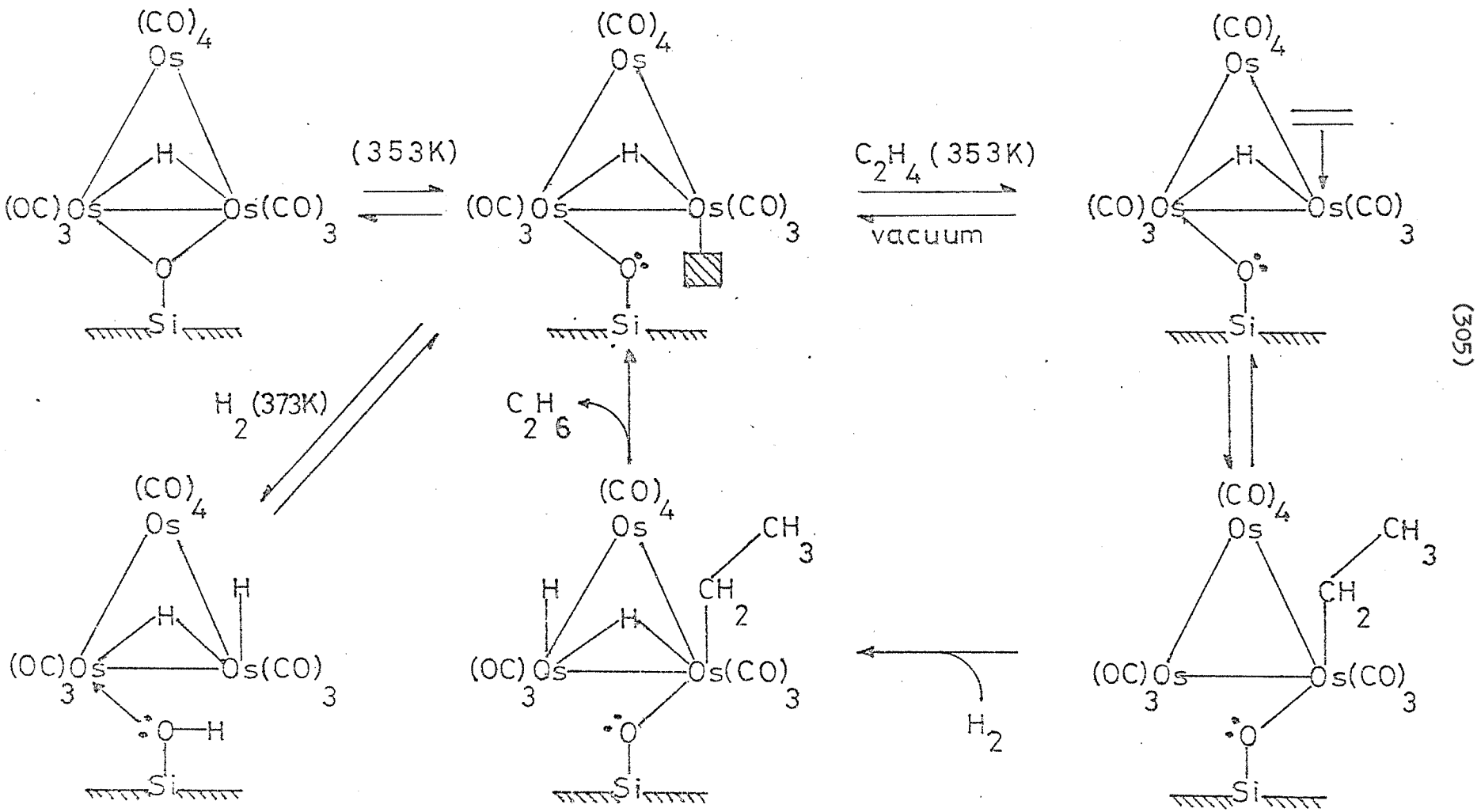
Interestingly, in a flow system 1-hexene hydrogenation (P_{hexene}=8 x 10^3N/m^2 and $P_{hydrogen}$=4.7 x 10^4N/m^2 diluted in helium) at atmospheric pressure and 90°C, using $[H_2Os_3(CO)_9(PPh_2$- (P))], IIb, gave more than 10,000 transformations per cluster before catalyst decomposition became appreciable. A steady state conversion of 1.7% gave 76% 2-alkenes (4:1 trans/cis) and 24% n-hexane. Then the final, deactivated membrane exhibited infrared ν_{CO} absorptions, at 2022w, 2030br and 1962m, cm^{-1}, consistent with the thermal decomposition product, X, and not the alkylidyne cluster adduct, XXI. This fits the prediction that low alkene/cluster ratios will reduce destructive hydrogenation to insignificant levels. At the same conditions, the same workers(67) were unable to detect ethylene hydrogenation ($P_{ethylene}$=4 x 10^3N/m^2 and $P_{hydrogen}$=6.5 x 10^4N/m^2) within the precision of their analytical equipment. Similarly others(93) could not detect any measureable activity of $[H_2Os_3(CO)_9(PPh_2CH_2CH_2CH_2SIL)]$, IIc, for propylene hydrogenation at 100°C and atmospheric pressure in a flow system, although it did have unspecified activity for 1-butene isomerisation at 110°C. This reiterates the large values of k_{-1}, and the need for super-pressures to make hydrogenation competitive as achieved in this treatise.

Thus, as a catalytic reaction, ethylene hydrogenation has only limited appeal. However, it does serve as an excellent

model system, providing detailed characterisation of a possible intermediate and various deactivation processes. Formation and maintenance of XXI, with its face-bridging carbyne ligand, illustrates the stabilising influence of a capping group retarding total cluster decomposition. A major consideration for the anchored species is also the presence of the various surface appendages. Two considerations are important. One is that they provide another mechanism for loss of catalyst activity, by breakdown to pseudo-monomeric species. Comparison with the results of Gates(85) and Lieto(67) shows the importance of incomplete coordination of phosphine during preparation of the catalysts, and the presence of remaining silanols, and bromo-groups on functionalised polystyrenes. The apparently greater stability of II in the investigations of Gates may derive from the more complete coverage of all the pendent phosphines, as shown by elemental analysis (P=1.0wt/wt%, 0.0323moles; Os=14wt/wt%, 0.0245moles of Os_3).

An explanation for the increased activity with I as the catalyst precursor, over direct use of II, is necessary. Since the experiments were carried out at different temperatures a direct comparison is difficult, without a fuller knowledge of the kinetics for the competing reactions. However the greater parity in catalytic activity between VIII and its anchored variant indicates that the reduction in rate accompanying tethering is not a physical effect (caused by mass transfer limitations). Both I and II were prepared from the same batch of ligand-silica, achieving similar degrees of coverage, stored under identical conditions, and with no variations in pretreatment before the catalytic runs. Two factors may explain this discrepancy in activity. The broad shoulder in the infrared ν_{CO} spectrum of II used in the study suggests that a degree of decomposition had occurred during storage. Then the calculated turn-over numbers may be an under-estimate of the cluster activity, since X is known to be inactive. Further, as the operating temperature is approached, enhanced decomposition may be operative with II before the rate of hydrogenation becomes appreciable. With I, where insitu formation of the active II only occurs at about the reaction temperature, this problem does not occur. A more subtle consideration is the position of the formed Os-Os 'double-bond' as discussed for the homogeneous analogue. A greater proportion of the alternative isomer, with the unsaturation away from the phosphine, may be favoured by the steric

Diagram 20 Proposed Scheme for Catalytic Hydrogenation of Ethylene with $[HOs_3(CO)_{10}(OSiL)]$



(305)

influence of the support. Directed away from the silica surface this will be less susceptible to breakdown.

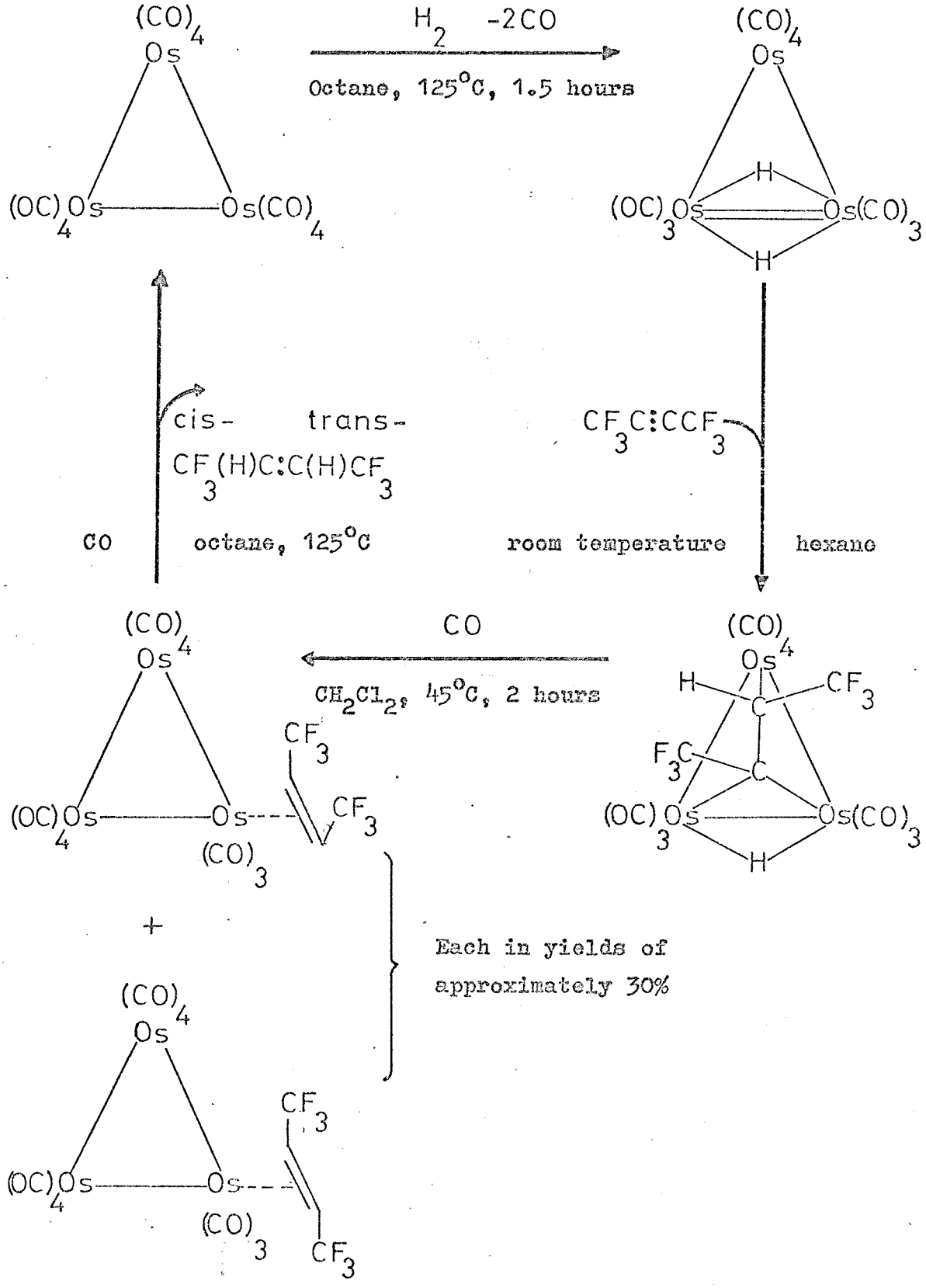
An alternative view of support interactions provides evidence of a secondary mechanism enhancing activity on silica. The ability of the grafted cluster $[HOs_3(CO)_{10}(OSIL)]$, Va, to catalyse ethylene hydrogenation in a flow reactor has been established(36,95). Under a mixture of hydrogen ($5.05 \times 10^4 N/m^2$) ethylene ($7.2 \times 10^3 N/m^2$) diluted in helium ($4.2 \times 10^4 N/m^2$) at 90°C a steady-state activity was observed, without any induction period, with a turnover of $144hr^{-1}$ (4×10^{-2} mol.(mol of cluster)$^{-1}$.s^{-1}) (differential conditions). Mechanistic studies showed that Va undergoes reversible coordination of ethylene, quantitatively as determined by volumetric measurements, at 80°C; whilst above 100°C it can coordinate hydrogen as identified by infrared spectroscopy. By analogy to the addition of ethylene to $[HOs_3(CO)_9(SMe)]$ to give $[HOs_3(CO)_9(SMe)(C_2H_4)]$(96), a mechanism was proposed (Diagram 20) involving the opening of the Os-O-Os bridge to create a vacant coordination site on one metal. An alternative route could involve reversible Os-Os bond cleavage. None of the transient species appear susceptible to further attack by silanol groups, or other oxidants, and Va is itself stable, under argon, below 200°C. The catalyst is recovered unchanged after several runs.

If formation of $[HOs_3(CO)_9(PPh_2CH_2CH_2SIL)(OSIL)]$, XIV, represented the major secondary interaction with the support it might also be expected to show activity. Then, either it is destabilised by the imposed strain as previously postulated, or coordination of a second phosphine, followed by breakdown, is the preferred route. Significantly for Va, orders of zero and one with respect to ethylene and hydrogen, indicates that the step involving oxidative addition of hydrogen is rate limiting. The postulated σ-alkyl species involved bears some resemblence to XXIII where a dependence on hydrogen partial pressure is also predicted.

One further model catalytic cycle, for hydrogenation of $CF_3C{:}CCF_3$, involving a triosmium cluster has been forwarded (Diagram 21)(97). Overall there is no loss or gain of carbon monoxide, and the cycle is supported by experimental evidence in that each step takes place in good yield and is defined by the isolation and full characterisation of each of the intermediates.

Diagram 21

Model Cycle for Hydrogenation of 1,2-Bis(trifluoromethyl)ethyne with $[Os_3(CO)_{12}]$ as Catalyst



Extrapolation to ethylene hydrogenation would invoke the intermediacy of the vinyl species, normally regarded as the deactivation product, and a possible dependence on carbon monoxide. Infact bubbling carbon monoxide through a refluxing solution of $[HOs_3(CO)(CH{:}CH_2)]$, in n-hexane for 4½hours, does give essentially selective formation of $[Os_3(CO)_{12}]$ and presumed evolution of ethylene(94). Similar treatment with hydrogen led directly to $[H_2Os_3(CO)_{10}]$, but with undetermined release of ethylene or ethane. Whilst this infers that formation of XX is not necessarily an irreversible process, provided that CO/H_2 attack is quicker than carbon monoxide elimination, it is still viewed as an unfavoured, high energy route.

5.10. Other Catalytic Studies

A series of other preliminary catalytic studies were attempted, which afforded an opportunity to demonstrate the higher activity of second row transition metals (ruthenium and rhodium).

Cyclohexene hydrogenations were performed in the same autoclave as that used for the 1-heptene work. A typical charge consisted of 0.33g of catalyst, 8.1g(10ml) of cyclohexene and dried methanol(40ml) as solvent. The autoclave was purged and then pressurised with hydrogen (100atm), and the reaction carried out at 75°C, unless stated (Table 8a), for 4 hours. The liquid product was analysed for both cyclohexene and cyclohexane by gas chromatography, using n-octane as an added internal standard. The results were then modified, to account for material lost during let-down of the pressure, by extrapolation back to the original cyclohexene charge. The retrieved silicas were analysed for metal content by neutron activation (Table 8b). Within analytical error only with IV is there any suggestion of leaching.

Both I and II were inactive as catalysts at 75°C, but exhibited slight activity at 125° and 150°C, respectively. This onset of activity with increasing operating temperature also coincided with loss of the carbonyl frequencies on the spent silicas which were both metallic in appearance. This is consistent with metal aggregates being the active catalyst, and the inability of the cluster framework to isomerise/hydrogenate internal alkenes. In comparison, III and IV, and $[Ru_6(CO)_{16}C(PPh_2CH_2CH_2SIL)]$

Table 8a Hydrogenation of Cyclohexene

Catalyst	Metal content (moles)	Cyclohexane yield (grams)	(moles)	Conversions /metal atom
Blank, 75°C		0.048		
III	1.75×10^{-6}	1.060	0.0120	6.83×10^{3}
IV	8.2×10^{-5}	8.3	0.0986	1.2×10^{3}
XXIV	6.8×10^{-6}	1.144	0.0130	1.9×10^{3}
I	4.22×10^{-5}	0.026		inactive
II	1.32×10^{-4}	0.043		inactive
I, 125°C	3.43×10^{-5}	0.091	0.00014	4.1
II, 150°C	1.32×10^{-4}	0.134	0.00065	4.9
Blank, 150°C		0.079		

Table 8b Metal Content on Initial and Spent Silicas

Catalyst	Metal content (wt/wt%) initial	final	Comments
III (rhodium)	0.055	0.033	
IV (rhodium)	2.55	1.23	Gray-black, no ν_{CO} absorptions
I (osmium) 75°C	2.52	2.00	unchanged starting material
I (osmium) 125°C	2.52	2.51	off-white, no ν_{CO} absorptions
II (osmium) 75°C	7.87	6.61	unchanged starting material

(0.2wt/wt% ruthenium), XXIV, gave far superior yields of cyclohexane (100, 12.5 and 13.5% respectively). These represent conversions per metal atom of 1200, 6,860 and 1900 (11,400 per hexaruthenium cluster) respectively. However, in all three cases, the spent catalysts were again dark, indicative of supported metal aggregates.

Finally, a screening test for Fischer-Tropsch activity

produced, in all cases, no positive results as seen by analysis of the discharge gases. However, one significant observation was made with IV. After treatment under 800atm (50:50 syngas mixture), at 200°C for 4 hours, the supernatent toluene(40.3g) liqueur was yellow and contained 72ppm of rhodium, but less than 5ppm of phosphorus. Its infrared ν_{CO} spectrum exhibited a multitude of sharp absorptions encompassing both terminal and bridging carbonyl groups; indicative of cluster compounds. The spent silica, which gave no ν_{CO} bands, was also analysed and shown to contain 0.8wt/wt% rhodium, as opposed to 2.55wt/wt% on the starting material. Together this accounts for 69.2% of the rhodium charged, the remainder possibly adhering to the reactor walls. This represents the only example in this thesis where considerable leaching of the anchored species from the support has been identified. The conditions are clearly very severe, whilst trace contaminants causing phosphine oxidation may also play an important role.

5.11. Appendices

Throughout these calculations the following data is used.

Compound	Osmium content wt/wt%
$[H_2Os_3(CO)_9(PPh_2CH_2CH_2SIL)]$	5.50
$[H_2Os_3(CO)_9(PPh_2Et)]$ (MW=1038.9g.mol^{-1})	54.92
$[Os_3(CO)_{11}(PPh_2CH_2CH_2SIL)]$	3.78
$[Os_3(CO)_{11}(PPh_2Et)]$ (MW=1092.9g.mol^{-1})	52.21

1atm = 14.7psi = $1.013 \times 10^5 N.m^{-2}$

1 mole of ideal gas occupies 24,461cm^3 at 25°C

5.11.1 Appendix 1: Data and Calculations for Ethylene Hydrogenations by Triosmium Clusters

Table 9a Run Conditions

PTO

Run Number	Weight (grams)	Moles of Os_3	Duration (hours)	Ethylene psig/psi	Hydrogen psi
	$[H_2Os_3(CO)_9(PPh_2CH_2CH_2SIL)]$				
1	0.1771	1.7×10^{-5}	4	60/74.7	230
2	0.3497	3.37×10^{-5}	20	55/69.7	235
3	0.1772	1.7×10^{-5}	20	65/79.7	240
4	0.3508	3.38×10^{-5}	44	60/74.7	235
	$[H_2Os_3(CO)_9(PPh_2Et)]$				
5	0.0202	1.94×10^{-5}	20	60/74.7	235
6	0.0204	1.96×10^{-5}	20	as 5, leak during run	
	$[Os_3(CO)_{11}(PPh_2CH_2CH_2SIL)]$				
7	0.2122	1.41×10^{-5}	24	60/74.7	240
	$[Os_3(CO)_{11}(PPh_2Et)]$				
8	0.0200	1.82×10^{-5}	24	65/79.7	240

Product Analysis

Assume ideality for all three component gases i.e. compressibility factors remain unity at applied pressures (gross approximation for ethylene).

10ml of headspace contains $10/24,461 = 4.088 \times 10^{-4}$ moles

Then 55psig corresponds to 1.938×10^{-3} moles of ethylene
60psig " " 2.078×10^{-3} " "
65psig " " 2.217×10^{-3} " "

Table 9b G.C. Calibrations
(Average from 5, 50μl, sample injections)

Component	Ethylene	Ethane
Retention time (min)	13	18
Peak Height (mm)	99.6	67.7
Relative Response Factor	1	1.47

Table 9c Moles of Ethane Produced

All injections 75μl, except runs 1 and 2 (50μl)

Figures in parentheses are Peak Height x Response Factor (1.47)

Run Number	Peak Height		% mole conversion	moles of ethane formed
	Ethylene	Ethane		
1	$69.5 \times 8 \times 10^2$	$41.3 \times 2 \times 10$ ($60.7 \times 2 \times 10$)	2.14	4.440×10^{-5}
2	$131 \times 4 \times 10^2$	$19 \times 4 \times 10^2$ ($27.9 \times 4 \times 10^2$)	17.56	3.403×10^{-4}
3	$121 \times 8 \times 10^2$	$113.6 \times 4 \times 10$ ($167 \times 4 \times 10$)	6.46	1.431×10^{-4}
4	$97.4 \times 8 \times 10^2$	$71.6 \times 2 \times 10^2$ ($105.3 \times 2 \times 10^2$)	21.28	4.421×10^{-4}
5	110×10^2	$145.5 \times 4 \times 10^2$ ($213.9 \times 4 \times 10^2$)	88.61	1.841×10^{-3}
6	$92 \times 4 \times 10^2$	$161 \times 4 \times 10^2$ ($236.7 \times 4 \times 10^2$)	72.01	1.496×10^{-3}
7	$106.3 \times 4 \times 10^2$	$130.8 \times 2 \times 10^2$ ($192.3 \times 2 \times 10^2$)	47.49	9.869×10^{-4}
8	102.8×10^2	$83.1 \times 4 \times 10^2$ ($122.2 \times 4 \times 10^2$)	82.62	1.832×10^{-3}

5.11.2. Appendix 2: Calculations for 1-Heptene Hydrogenation/ Isomerisation by $[Os_3(CO)_{11}(PPh_2CH_2CH_2SIL)]$

Weight of catalyst used = 0.2523g (1.67×10^{-5} moles of Os_3)

Weight of 1-heptene used = 2.091g (2.13×10^{-2} moles)

Table 10a G.C. Calibrations

(Average from 5, 1μl, sample injections)

Component	n-heptane	1-heptene	2-heptenes
Peak Height (64×10^3)	128	107	43.3
$Density_{20}$	0.684	0.697	0.705
R.R.F.	0.852	1.000	2.443

Table 10b Product Analysis with Relative Response Factors

Component	n-heptane	1-heptene	2-heptenes
Peak Height (4×10^2)	109	452	642
wt/wt %	4.39	21.39	74.22
mole %	4.30	21.41	74.29
moles	9.159×10^{-4}	4.560×10^{-3}	1.582×10^{-2}
$molecules/Os_3$	54.8	———	947.3
Ratio	1	:	17.3

Table 10c Product Analysis with Unit Response Factors

Component	n-heptane	1-heptene	2-heptenes
wt/wt %	9.06	37.57	53.37
mole %	8.89	37.57	53.47
moles	1.894×10^{-3}	8.017×10^{-3}	1.139×10^{-2}
$molecules/Os_3$	113.4	———	682.0
Ratio	1	:	6.01

5.12. References

1. J.R.Anderson, P.S.Elmes, R.F.Howe and D.E.Mainwaring, J. Catal., 1977, 50, 508.
2. J.R.Anderson, 'Structure of Metallic Catalysts', Academic Press, London, 1975.
3. G.C.Smith, T.P.Chojnacki, S.R.Dasgupta, K.Iwatate and K.L.Watters, Inorg. Chem., 1975, 14, 1419.
4. A.K.Smith, F.Hugues, A.Theolier, J.M.Basset, R.Ugo, G.M.Zanderighi, J.L.Bilhou, V.Bilhou-Bougnol and W.F.Graydon, Inorg. Chem., 1979, 18, 3104.
5. K.L.Watters, R.F.Howe, T.P.Chojnacki, C-M.Fu, R.L.Schnieder and N-B.Wong, J. Catal., 1980, 66, 424.
6. A.K.Smith, A.Theolier, J.M.Basset, R.Ugo, D.Commereuc and Y.Chauvin, J. Amer. Chem. Soc., 1978, 100, 2590.
7. a) P.Chini and S.Martinengo, Inorg. Chim. Acta, 1969, 3, 315.
   b) P.E.Cattermole and A.G.Osborne, J. Organometallic Chem., 1972, 37, C17.
8. A.Sacco, R.Ugo and A.Moles, J. Chem. Soc. (A), 1966, 1670.
9. P.R.Ford, Adv. Catal. Rel. Subj., 1970, 21, 51.
10. S.L.T.Andersson, K.L.Watters and R.F.Howe, J. Catal., 1981, 69, 212.
11. J.L.Bilhou, V.Bilhou-Bougnol, W.F.Graydon, J.M.Basset, A.K.Smith, G.M.Zanderighi and R.Ugo, J. Organometallic Chem., 1978, 153, 73.
12. A.Theolier, A.K.Smith, M.Leconte, J.M.Basset, G.M.Zanderighi, R.Psaro and R.Ugo, J. Organometallic Chem., 1980, 191, 415.
13. R.Ugo, R.Psaro, G.M.Zanderighi, J.M.Basset, A.Theolier and A.K.Smith, 'Fundamental Research in Homogeneous Catalysis', M.Tsutsui Ed., Plenum Press, New York, 1979, 3, 579.
14. A.Vizi-Orosz and L.Marko, Transition Met. Chem., 1982, 7, 216.
15. A.Vizi-Orosz, G.Palyi and L.Marko, J. Organometallic Chem., 1973, 57, 379.
16. R.Whyman, 'Transition Metal Clusters', B.F.G.Johnson Ed., Wiley, New York, 1980, 583.
17. M.Ichikawa, ChemTech, 1982, 674.
18. D.Commereuc, Y.Chauvin, F.Hugues, J.M.Basset and D.Oliver, J.C.S. Chem. Comm., 1980, 154.

19. K.Shikakura, M.Kawai, M.Ichikawa and K.Sekigawa, J. Mol. Catal., 1981, 11, 169.
20. M.Ichikawa, J. Catal., 1979, 55, 127; ibid, 1979, 59, 67.
21. P.Michelin Lausarot, G.A.Vaglio and M.Valle, J. Organometallic Chem., 1982, 240, 441.
22. H.Knözinger and E.Rumpf, Inorg. Chim. Acta, 1978, 30, 51.
23. K.Iwatate, S.R.Dasgupta, R.L.Schnieder, G.C.Smith and K.L.Watters, Inorg. Chim. Acta, 1975, 15, 191.
24. H.Knözinger, E.D.Thornton and M.Wolf, J. Chem. Soc. Faraday I, 1979, 75, 1888.
25. a) H.Conrad, G.Ertl, H.Knözinger, J.Kuppers and E.E.Latta, Chem. Phys. Letters, 1976, 42, 115.
b) H.Knözinger, Inorg. Chim. Acta, 1979, 37, L537.
26. A.Vizi-Orosz and L.Marko, Transition Met. Chem., 1982, 7, 216.
27. E.D.Thornton, H.Knözinger, B.Tesche, J.J.Rafalko and B.C.Gates, J. Catal., 1980, 62, 117.
28. K.G.Allum, R.D.Hancock, I.V.Howell, S.McKenzie, R.C.Pitkethly and P.J.Robinson, J. Organometallic Chem., 1975, 87, 203.
29. Yu.S.Varshavsky, T.G.Cherkasova and N.A.Buzina, J. Organometallic Chem., 1973, 56, 375.
30. K.G.Allum, R.D.Hancock, I.V.Howell, R.C.Pitkethly and P.J.Robinson, J. Catal., 1976, 43, 322.
31. J.L.Bilhou, V.Bilhou-Bougnol, W.F.Graydon, J.M.Basset and A.K.Smith, J. Mol. Catal., 1980, 8, 411.
32. A.K.Smith, W.Abboud, J.M.Basset, W.Reumann, G.L.Rempel, J.L.Bilhou, V.Bilhou-Bougnol, W.F.Graydon, J.Dunogues, N.Ardoin and N.Duffaut, 'Fundamental Research in Homogeneous Catalysis', M.Tsutsui Ed., Plenum Press, New York, 1979, 3, 621.
33. J.P.Collman, L.S.Hegedus, M.P.Cooke, J.R.Norton, G.Dolcetti and D.N.Marquardt, J. Amer. Chem. Soc., 1972, 94, 1789.
34. M.S.Jarrell, B.C.Gates and E.D.Nicholson, J. Amer. Chem. Soc., 1978, 100, 5727.
35. M.S.Jarrell and B.C.Gates, J. Catal., 1978, 54, 81.
36. J.M.Basset, B.Besson, A.Choplin and A.Theolier, Phil. Trans. R. Soc. Lond. A, 1982, 308, 115.
37. J.G.Bullitt and F.A.Cotton, Inorg. Chim. Acta, 1971, 5, 637.
38. J.A.McCleverty and G.Wilkinson, Inorg. Syn., 1966, 8, 211.
39. R.Poublanc and J.Gallay, J. Organometallic Chem., 1971, 27, C53.

40. J.Chatt and B.L.Shaw, J. Chem. Soc. (A), 1966, 1437.
41. J.Blum, E.Oppenheimer and E.D.Bergmann, J. Amer. Chem. Soc., 1967, 89, 2338.
42. F.Hugues, J.M.Basset, Y.Ben Taarit, A.Choplin, M.Primet, D.Rojas and A.K.Smith, J. Amer. Chem. Soc., 1982, 104, 7020.
43. M.Deeba and B.C.Gates, J. Catal., 1981, 67, 303.
44. M.Deeba, J.P.Scott, R.Barth and B.C.Gates, J. Catal., 1981, 71, 373.
45. R.Psaro, R.Ugo, G.M.Zanderighi, B.Besson, A.K.Smith and J.M.Basset, J. Organometallic Chem., 1981, 213, 215.
46. H.Knözinger and Y.Zhao, J. Catal., 1981, 71, 337.
47. L.A.W.Hales and R.J.Irving, J. Chem. Soc. (A), 1967, 1932.
48. S.C.Brown and J.Evans, J.C.S. Dalton, 1981, 2263.
49. M.I.Bruce, M.Cooke, M.Green and D.J.Westlake, J. Chem. Soc. (A), 1969, 987.
50. A.K.Smith, B.Besson, J.M.Basset, R.Psaro, A.Fusi and R.Ugo, J. Organometallic Chem., 1980, 192, C31.
51. H.Knözinger, Y.Zhao, B.Tesche, R.Barth, R.Epstein, B.C.Gates and J.P.Scott, Faraday Discuss. Chem. Soc., 1981, 72, 53.
52. M.Deeba, B.J.Streusand, G.L.Schrader and B.C.Gates, J. Catal., 1981, 69, 218.
53. L.Brewer and G.M.Rosenblatt, Advan. High Temp. Sci., 1969, 2, 1.
54. G.Collier, D.J.Hunt, S.D.Jackson, R.B.Moyes, I.A.Pickering, P.B.Wells, A.F.Simpson and R.Whyman, J. Catal., 1983, 80, 154.
55. J.L.M.Van De Venne, J.P.M.Rindt and G.J.M.M.Coenen, J. Colloid. Interface Sci., 1980, 74, 287.
56. C.W.Bradford, W.van Bronswijk, R.J.H.Clark and R.S.Nyholm, J. Chem. Soc. (A), 1970, 2889.
57. N.M.Boag, C.E.Kampe, Y.C.Lin and H.D.Kaesz, inorg. Chem., 1982, 21, 1706.
58. B.F.G.Johnson, J.Lewis and P.A.Kilty, J. Chem. Soc. (A), 1968, 2859.
59. C.Ungermann, V.Landis, S.A.Moya, H.Cohen, H.Walker, R.G.Pearson, R.G.Rinkler and P.C.Ford, J. Amer. Chem. Soc., 1979, 101, 5922.
60. C.R.Eady, B.F.G.Johnson, J.Lewis and M.C.Malatesta, J.C.S. Dalton, 1978, 1358.
61. J.C.Bricker, C.C.Nagel and S.G.Shore, J. Amer. Chem. Soc., 1982, 104, 1444.

62. R.Psaro, A.Fusi, R.Ugo, J.M.Basset, A.K.Smith and F.Hugues, J. Mol. Catal., 1980, 7, 511.
63. S.C.Brown and J.Evans, J.C.S. Chem. Comm., 1978, 1063.
64. D.K.Liu and M.S.Wrighton, J. Amer. Chem. Soc., 1982, 104, 898.
65. J.P.Collman and W.R.Roper, J. Amer. Chem. Soc., 1966, 88, 3504.
66. A.J.Deeming, B.F.G.Johnson and J.Lewis, J. Chem. Soc. (A), 1970, 897.
67. J-B.N'Guini Effa, J.Lieto and J-P.Aune, J. Mol. Catal., 1982, 15, 367.
68. B.E.Cavit, K.R.Grundy and W.R.Roper, J.C.S. Chem. Comm., 1972, 60.
69. L.A.W.Hales and R.J.Irving, Spectrochim. Acta, 1967, 23, 2981.
70. C.W.Bradford, Plat. Met. Rev., 1967, 11, 104.
71. S.C.Tripathi, S.C. Srivastava, R.R.Mani and A.K.Shrimal, Inorg. Chim. Acta, 1975, 15, 249.
72. S.C.Brown and J.Evans, J.C.S. Dalton, 1982, 1049.
73. S.A.R.Knox, J.W.Koepke, M.A.Andrews and H.D.Kaesz, J. Amer. Chem. Soc., 1975, 97, 3942.
74. A.J.Deeming and M.Underhill, J.C.S. Dalton, 1974, 1415.
75. E.G.Bryan, W.G.Jackson, B.F.G.Johnson, J.W.Kelland, J.Lewis and K.T.Schorpp, J. Organometallic Chem., 1976, 108, 385.
76. C-Y.Wei, L.Garlaschelli, R.Bau and T.F.Koetzle, J. Organometallic Chem., 1981, 213, 63.
77. S.A.R.Knox and H.D.Kaesz, J. Amer. Chem. Soc., 1971, 93, 4594.
78. M.I.Bruce, D.C.Kehoe, J.G.Matisons, B.K.Nicholson, P.H.Rieger and M.L.Williams, J.C.S. Chem. Comm., 1982, 442.
79. R.D.Adams and N.M.Golembeski, J. Amer. Chem. Soc., 1979, 101, 2579.
80. B.F.G.Johnson, J.Lewis and D.A.Pippard, J.C.S. Dalton, 1981, 407.
81. B.F.G.Johnson, J.Lewis and D.A.Pippard, J. Organometallic Chem., 1981, 213, 249.
82. A.J.Deeming, B.F.G.Johnson and J.Lewis, J. Chem. Soc. (A), 1970, 2517.
83. A.J.Deeming and S.Hasso, J. Organometallic Chem., 1976, 114, 313.
84. S.C.Brown and J.Evans, J. Organometallic Chem., 1980, 194, C53.

85. M.B.Freeman, M.A.Patrick and B.C.Gates, J. Catal., 1982, 73, 82.

86. K.J.McQuade, R.Pierantozzi, M.B.Freeman and B.C.Gates, Amer. Chem. Soc. Div. Petrol. Chem. Prec., 1980, 25, 751.

87. R.P.Ferrari, G.A.Vaglio and M.Valle, Inorg. Chim. Acta, 1978, 31, 177.

88. J.B.Keister and J.R.Shapley, J. Amer. Chem. Soc., 1976, 98, 1056.

89. S.C.Brown and J.Evans, J. Mol. Catal., 1981, 11, 143.

90. J.Lieto, J.J.Rafalko and B.C.Gates, J. Catal., 1980, 62, 149.

91. J.Lieto, J.J.Rafalko, J.V.Minkiewicz, P.W.Rafalko and B.C.Gates, 'Fundamental Research in Homogeneous Catalysis', M.Tsutsui Ed., Plenum Press, New York, 1979, 3, 637.

92. Z.Otero-Schipper, J.Lieto and B.C.Gates, J. Catal., 1980, 63, 175.

93. R.Pierantozzi, K.J.McQuade, B.C.Gates, M.Wolf, H.Knözinger and W.Ruhman, J. Amer. Chem. Soc., 1979, 101, 5436.

94. A.J.Deeming, S.Hasso and M.Underhill, J.C.S. Dalton, 1975, 1614.

95. B.Besson, A.Choplin, L.D'Ornelas and J.M.Basset, J.C.S. Chem. Comm., 1982, 843

96. B.F.G.Johnson, J.Lewis, D.Pippard and P.R.Raithby, J.C.S. Chem. Comm., 1978, 551.

97. Z.Dawoodi, K.Henrick and M.J.Mays, J.C.S. Chem. Comm., 1982, 696.

CHAPTER SIX

THE REACTIONS OF $[Ru_6C(CO)_{17}]$ WITH PHOSPHINES: FULL CHARACTERISATION OF $[Ru_6C(CO)_{16}(PPh_2R)]$, R=Et or CH_2CH_2SiL

6.1. Preparation and Background Chemistry of $[Ru_6C(CO)_{17}]$

μ_6-Carbido-μ-carbonyl-hexadecacarbonyl-octahedro-hexaruthenium was first prepared by Piacenti et. al.(1) from the pyrolysis of $[Ru_3(CO)_{12}]$ in benzene and cyclohexane at 150°C. On the basis of an osmometric measurement it was wrongly assigned as $[Ru_6(CO)_{18}]$. The relatively low intensity band at 1850cm^{-1} being assigned as a non-fundamental, instead of a bridging, carbonyl vibration band. An observed parent ion in its mass spectrum(2) and a subsequent X-ray diffraction structure determination(3) corrected this situation with the compound being identified as $[Ru_6C(CO)_{17}]$, I.

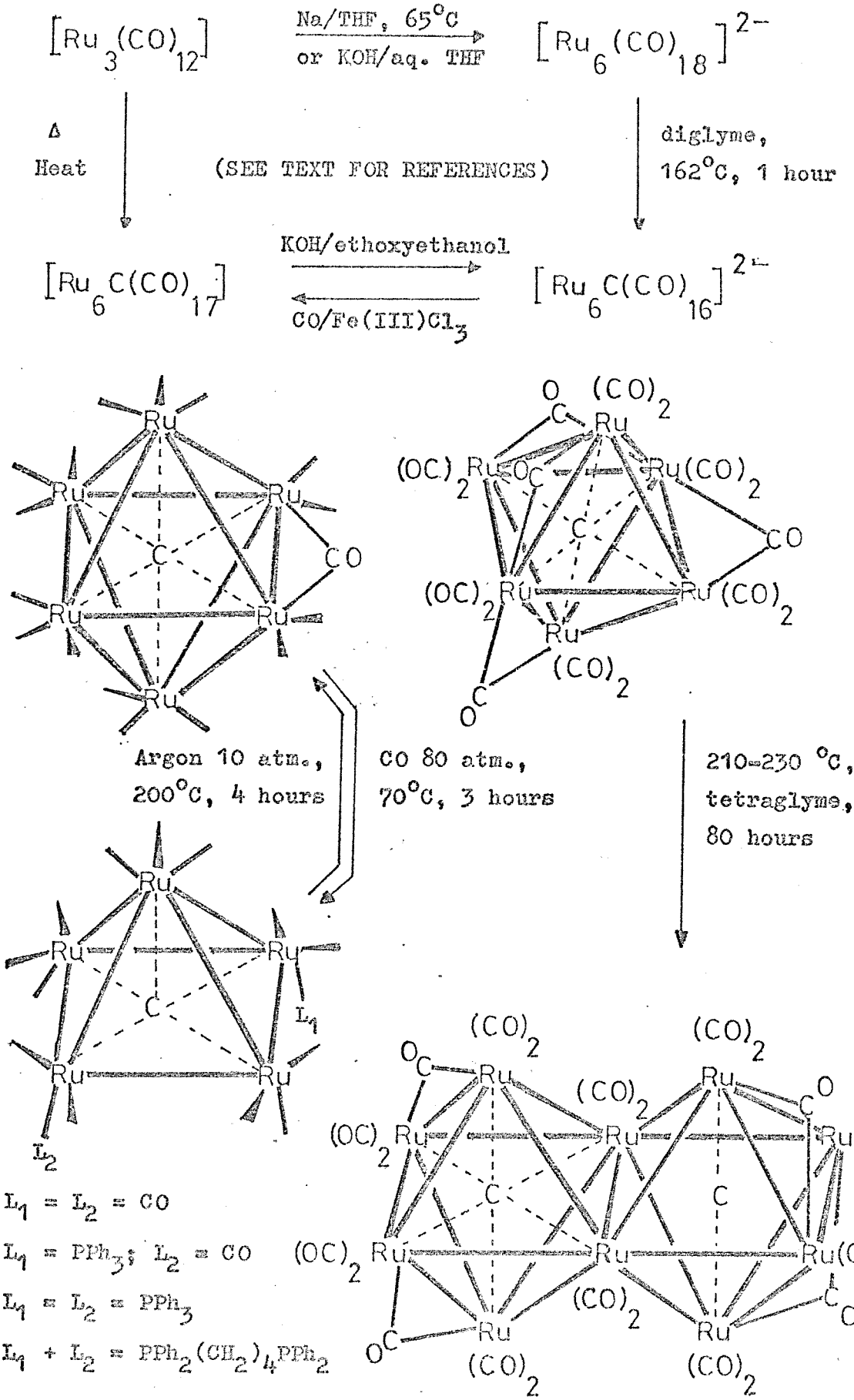
Later, pyrolysis of $[Ru_3(CO)_{12}]$ at 150°C in a sealed tube gave I in low yield (5%) as the only product apart from ruthenium metal(4). The yields increased slightly as the temperature was raised to a maximum of 180°C; above this temperature total conversion to metal occurred. Preparation by this route was taken as conclusive evidence that the carbide results from reduction of a coordinated carbonyl group, since the cluster had been produced in the absence of any other source of carbon. Higher yields were obtained by heating under reflux in n-nonane(2), or even better in di-n-butylether(5). Additional products in these cases, apart from metallic ruthenium, were $[H_2Ru_4(CO)_{13}]$ and $[H_4Ru_4(CO)_{12}]$. These result from reaction of $[Ru_3(CO)_{12}]$ with minute traces of water present under the conditions employed(6). The reaction of $[H_4Ru_4(CO)_{12}]$ with ethylene under pressure is reported to give I in 30% yield(7). Extension of these conditions using $[Ru_3(CO)_{12}]$ instead leads to even higher reproducible yields (ca.70%) if the reaction is carefully controlled(8). This last method does not give decomposition to metal and has been therefore employed as the most convenient route. Until recently the chemistry of I has been very limited. This is presumably due to the difficulty of preparing it in good yields and the inherent problems of identifying any products formed in reactions of larger metal clusters. Access to single-crystal X-ray diffraction techniques is normally required to elucidate the ligand geometry about the metal polyhedra, and then even the latter is not always retained.

As part of a study into the catalytic activity of a series of clusters towards the water-gas shift reaction, it was found that I reacted in alkaline (KOH) ethoxyethanol at 100°C to give a cherry red solution(9). Although this species was not characterised, its reported infrared ν_{CO} spectrum bears a strong resemblance to that of $[Ru_6C(CO)_{16}]^{2-}$, II, as prepared in high yield (60%) from $[Ru_3(CO)_{12}]$ and $[Mn(CO)_5]^-$ under reflux in diglyme(10). Infact I reacts directly with methoxide (Na_2CO_3/MeOH), via attack at a coordinated carbonyl group to yield the isolable anion $[Ru_6C(CO)_{16}(CO_2Me)]^-$, which subsequently reacts with aqueous base to yield II(8). There is a discrepancy between the reported molecular structures of η^6-carbido-hexadecacarbonylhexaruthenate(-2) from X-ray diffraction crystallographic studies on the tetramethylammonium(10) and tetraphenylarsonium(8) salts. The first appears to contain only three asymmetrically edge-bridging carbonyl ligands, whilst the second has four so disposed to give approximate C_{2v} symmetry (Diagram 1). However, in the $[Me_4N]^+$ salt a forth carbonyl is highly disordered and tends towards a semi-bridging position, and the first authors(11) agree that a more precise determination would probably reveal a more recognizable bridging position. The encapsulated carbon has been also verified by ^{13}C NMR on a sample derived from ^{13}CO enriched $[Ru_3(CO)_{12}]$. The spectrum contains two resonances(10) at 213δ (carbonyls) and, a redetermined value(12), at 459δ (carbide) in the appropriate intensities. This conclusively proves that the carbide originates from reduction of a coordinated carbon monoxide. The carbide chemical shift appears to be characteristic of Ru_6C cores with $[(CH_3CNCu)_2Ru_6C(CO)_{16}]$(11) and $[Ru_{10}C_2(CO)_{24}]^{2-}$(12) giving ones at 457 and 458 δ respectively.

Under milder conditions dropwise addition of $[Ru_3(CO)_{12}]$ in THF to aqueous KOH(13) results in the formation of the dianion $[Ru_6(CO)_{18}]^{2-}$ in almost quantitative yields (80%). Treatment with sodium at 65°C produces a similar outcome(14). However, at 162°C (refluxing diglyme) this furnishes a direct route to II in even better yields (80-90%) compared to above. Similarly, pyrolysis of isolated $[Ru_6(CO)_{18}]^{2-}$ under reflux in diglyme gave quantitative conversion to the carbido-anion confirming the intermediate nature of the former. The trapping of evolved carbon dioxide as barium carbonate established the carbide to originate from intramolecular

Diagram 1

Hexaruthenium Cluster Chemistry



reduction of a carbonyl ligand:-

$$[Ru_6(CO)_{18}]^{2-} \xrightarrow{\Delta} [Ru_6C(CO)_{16}]^{2-} + CO_2$$

The formation of an encapsulated carbide cluster from a non-carbido precursor of the same nuclearity raises interesting mechanistic questions. The protonation of $[Ru_6(CO)_{18}]^{2-}$ to $[HRu_6(CO)_{18}]^-$, where neutron diffraction studies(15) have shown the hydride to be interstitual, is an interesting parallel. Extended pyrolysis of $[NEt_4]_2[Ru_6C(CO)_{16}]$ in dry tetraglyme at 210-230°C affords the edge-fused bioctahedral dicarbide cluster $[Ru_{10}(\mu_6\text{-}C)(CO)_{20}(\mu\text{-}CO)_4]^{2-}$ (12) with the structure shown in Diagram 1. Carbonylation of II under mild oxidizing conditions, $Fe(III)Cl_3$, regenerates I in high yield (68%)(14).

$[Ru_6C(CO)_{17}]$ also provides a route into the versatile chemistry of $[Ru_5C(CO)_{15}]$, III, by quantitative carbonylation(16) according to the equation-

$$[Ru_6C(CO)_{17}] \xrightarrow[70°C,\ 3\ hours]{CO,\ 80atm} [Ru_5C(CO)_{15}] + [Ru(CO)_5]$$

-the only other product was confirmed as $[Ru(CO)_5]$ from a high-pressure infrared study(17) and its physical properties. This contrasts with the previously reported yields of ca. 1% as one of the products from reaction of $[H_4Ru_4(CO)_{12}]$ with ethylene(7). An X-ray analysis(16) verified III to be isostructural with the earlier characterised osmium(18) and iron(19) analogues, containing a square-pyramidal Ru_5 arrangement with an exposed carbido-atom. In coordinating solvents, such as acetonitrile or methanol, an immediate reaction occurs giving adducts of the type $[Ru_5C(CO)_{15}(solvent)]$, which is easily reversed in the absence of excess solvent. If III is regarded as an electron deficient nido-octahedra, then its ability to act as an electron-pair acceptor is facilitated by the ease with which the metal framework may undergo rearrangement to produce vacant coordination sites resulting in products which can be regarded as arachno pentagonal bipyramidal structures, as substantiated by the determined molecular structure of $[Ru_5C(CO)_{15}(NCMe)]$(20). With halides the anionic derivatives $[Ru_5C(CO)_{15}X]^-$, X=Cl, Br or I, are obtained which also possess a closely related structure by comparison with the known $[Os_5C(CO)_{15}I]^-$ (21). Protonation of these derivatives, or direct reaction of III with HX, yields the neutral $[HRu_5C(CO)_{15}X]$. Molecular iodine also

forms an addition product, whilst heating to 100°C under 15 atmospheres of hydrogen III reversibly adds hydrogen to give the speculated $[H_2Ru_5C(CO)_{15}]$.

Reaction with phosphines leads to the isolation of substituted products of III. The molecular structures of $[Ru_5C(CO)_{15-n}(PPh_3)_n]$, n=1 or 2, have been established by single-crystal X-ray analysis and as predicted, on electronic and steric grounds, the phosphines adopt axial sites on the basal ruthenium atoms with a trans-disposition about the plane in $[Ru_5C(CO)_{13}(PPh_3)_2]$ (20). With the bidentate phosphines $PPh_2(CH_2)_nPPh_2$, n=1 to 4, the preferred coordination mode varies with different chain lengths and corresponding 'bites'. $[Ru_5C(CO)_{13}\{PPh_2(CH_2)_4PPh_2\}]$(22) is isostructural to $[Ru_5C(CO)_{13}(PPh_3)_2]$, wheras the hydrogenated derivative $[H_2Ru_5C(CO)_{12}\{PPh_2(CH_2)_2PPh_2\}]$ chelates a single basal ruthenium with the phosphorus atoms occupying an axial and equatorial sites(20).

Indirect evidence for a general reaction of $[Ru_6C(CO)_{17}]$ with aromatic rings has been found. Under reflux in the appropriate arene, benzene(4), toluene, xylene, mesitylene(2) or azulene(23), $[Ru_3(CO)_{12}]$ reacts to give, in addition to metallic ruthenium, the parent I and a general species $[Ru_6C(CO)_{14}(arene)]$. Presumably these compounds result from reaction of insitu formed I with the vast excess of arene. An X-ray crystal determination on the mesitylene derivative(24) illustrated that the arene acts as a six-electron donor displacing three carbonyl ligands. It caps an apical ruthenium relative to the square plane containing the single, edge-bridging carbonyl ligand. In addition, this is also one of the metal types coordinated by the organic ligands in $[Ru_6C(CO)_{14}(bitropyl)]$(25), the η^6-μ^3-bitropyl ligand being produced in the redox reaction between II and tropylium bromide(26), and $[Ru_6C(CO)_{15}(hexa\text{-}2,4\text{-}diene)]$(27) as one of the by-products in the preparation of I by the reaction of $[Ru_3(CO)_{12}]$ with ethylene.

Other reported reactions of I include that with the cluster anion $[HOs_3(CO)_{11}]^-$, in the presence of oxygen, to give $[HOs_3(CO)_{10}(\mu_2\text{-}CO_2)Ru_6C(CO)_{16}]^-$(28). Its proposed structure is based on that found by X-ray analysis of a related derivative obtained from reaction of the anion with $[Os_6(CO)_{18}]$(29). No inferences to the number of bridging carbonyls, or their distribution

about the ruthenium core, were made but the same apical metal is probably involved. Reaction of I with $[(PPh_3)_2N][NO_2]$ gives $[Ru_6C(CO)_{15}(NO)]^-$ (85% yield), which reacts with $[NC]^+$ to give $[Ru_6C(CO)_{14}(NO)_2]$ and with Ph_3PAuCl to give $[Ru_6C(CO)_{15}(NO)(AuPPh_3)]$. X-ray analysis of the latter two compounds(30) show two nitrosyl ligands attached to opposite vertices, whilst the $AuPPh_3$ ligand adopts a μ_3-bridging mode. Presumably the hydride in $[HRu_6C(CO)_{15}(NO)]$, obtained by protonation with concentrated H_2SO_4, will be similarly disposed. Reaction of II with $[Cu(CH_3CN)_4][BF_4]$ gave ready synthesis of $[(CH_3CNCu)_2Ru_6C(CO)_{16}]$ which was also shown to have one copper atom capping a trigonal Ru_3 face, with the second juxtaposition on the $CuRu_2$ face(11). This unexpected geometry deviates from that of $[(CH_3CNCu)_2Rh_6C(CO)_{15}]$ where the two copper atoms are on opposite faces of the trigonal prismatic core(31). Although the anticipated fragmentation of the cluster was not realised, direct interaction of I with EtSH, which is capable of acting as a multielectron donor, does occur by opening of the cluster to expose the central carbido-atom. Two products were identified as $[H_2Ru_6C(CO)_{15}(EtS)_2]$ and $[HRu_6C(CO)_{14}(EtS)_3]$; the latter being fully characterised by X-ray diffraction analysis (32). This showed that the carbido-atom has a distorted trigonal by-pyramidal coordination defined by five ruthenium atoms, with the remaining ruthenium swung out from the rest of the cluster and bonded to the edge-bridging thiol ligands. In comparison, I reacts with a number of neutral ligands of potential π-acid character, namely phosphines, arsines(5) and phosphites(32), to give apparently simple substitution products without any opening of the ruthenium octahedron. The precise position of substitution was not established.

$[Ru_6C(CO)_{17}]$ crystallises as a deep red acicular compound. It is slightly soluble in saturated hydrocarbon solvents, but is fairly soluble in chlorinated and aromatic solvents. At room temperature it slowly decomposes, but can be kept almost indefinitely at -25°C. It has been fully characterised by spectroscopic techniques. Its solution (cyclohexane) infrared ν_{CO} spectrum contains five 'terminal' and one weak 'bridging' stretching absorptions. The last one becomes more pronounced when recorded in a solid KBr disc. A parent ion m/e=1096, based on Ru_6=608, is observed in the mass spectrum within an isotopic pattern which

correlates well with a computed isotope distribution for a hexanuclear ruthenium entity. This is followed by seventeen such patterns corresponding to successive losses of carbonyl groups. Apart from the $[Ru_5C]^+$ ion present in comparatively low abundance no other ions corresponding to fragmentation of the Ru_6C core was observed. This illustrates the inherent stability of this unit, probably associated with the presence of the interstitial atom. All this data augments the solid-state structure as determined by a single crystal X-ray diffraction study(3), which confirmed the presence of an interstitial carbide within an hexaruthenium core along with seventeen carbonyl ligands of which one is edge-bridging (Diagram 1).

6.2. Preparation and Full Characterisation of $[Ru_6C(CO)_{16}(PPh_2Et)]$

The preparation of various phosphine and arsine mono-substituted derivatives of I under reasonably mild conditions has been reported(5). Typically, reaction with a two-fold excess of triphenylphosphine under reflux in n-hexane for 3 hours gave $[Ru_6C(CO)_{16}(PPh_3)]$ in high yield (60%). These products were characterised solely on the basis of elemental analysis and infrared spectroscopy. This ability to specifically form mono-substituted derivatives is an attractive feature when considering preparation of anchored variants since it alleviates the need for chromatography. In addition, the central carbon might be expected to give extra stability to the ruthenium cluster core under catalytic conditions; a study into the thermal stability of $[Ru_3(CO)_{12}]$ and I directly adsorbed on silica or alumina attributed the greater resistance of the latter to decomposition to the presence of the interstitial carbide(33). Prior to attempting to isolate a phosphine-tethered adduct a more detailed knowledge of the molecular structure was sort by an indepth study on the homogeneous analogue $[Ru_6C(CO)_{16}(PPh_2Et)]$, IVa, being undertaken. The reaction of I with trimethyl-phosphite was also studied as this ligand acts as a good ^1H NMR probe, and its greater reactivity often leads to further degrees of substitution.

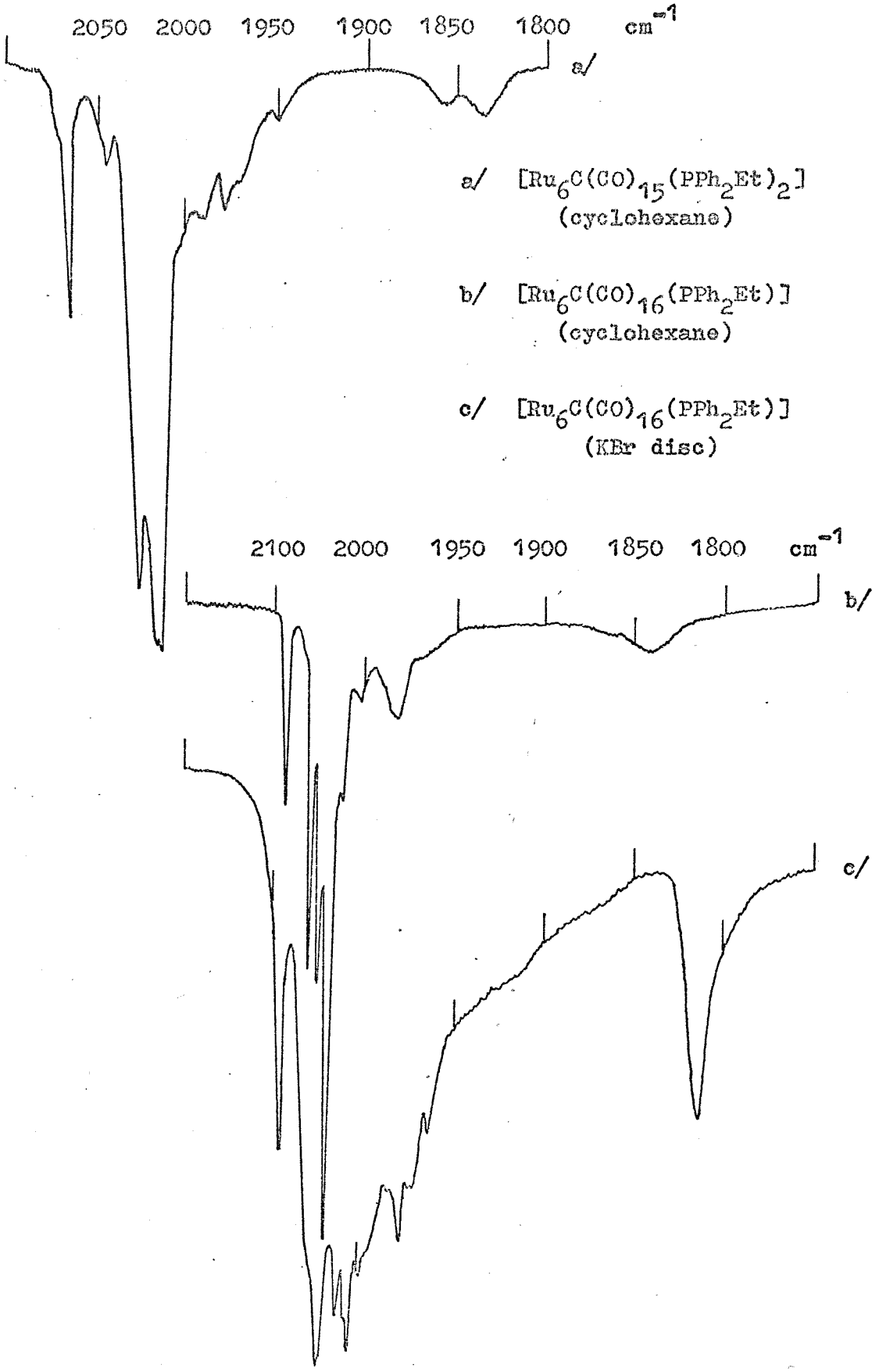
Initially, identical conditions to those described previously were employed. However, with a two-fold excess of PPh_2Et

a second species, later substantiated as $[Ru_6C(CO)_{15}(PPh_2Et)_2]$, Va, was predominantly formed. On addition of the phosphine to the refluxing solution an almost immediate deepening of the colour to a crimson red occurred and infrared ν_{co} monitoring indicated that this corresponded to instantaneous formation of IVa. With reaction time additional bands, at 2065 and 2016 cm^{-1}, due to Va appeared at the expense of those for IVa. Adherence to a stringent stoichiometric quantity of phosphine did lead to isolation of IVa in reproducibly high yields (85%) in the absence of additional products. This implies that Va results from further substitution, and not pyrolysis, of IVa. The rate of reaction indicated that even less exacting conditions were possible, and indeed essentially quantitative conversion was achieved within ½ hour at room temperature. Methylene chloride was used as a suitable solvent for I. These even milder conditions made anchoring an even more attractive proposition. Repetition of the work with PPh_3 proved it to be sound, so yet again subtle changes in the phosphine ligand cause considerable perturbation in the nature and rate of reaction.

The solution (cyclohexane) infrared ν_{co} spectrum confirmed IVa to be analogous with the previously prepared PPh_3 adduct(5). The characteristic broad, bridging-carbonyl, vibration centred at 1845cm^{-1} was observed. Its position showed a definite solvent dependence and in CH_2Cl_2 it appeared at 1833cm^{-1}. This shift to lower frequency is common to all the Ru_6C adducts prepared in this work, but only representative ν_{co}(cyclohexane) data will be given forthwith. Similar, but more pronounced, effects have been also observed for the cluster anion species $[M_3H(CO)_{11}]^-$, M=Ru or Fe (34,35), where they are attributed to interactions between the carbonyl bridge of the cluster anion and the cation in solution, depending upon the polarity of the solvent. Clearly, even in the absence of any coulombic interaction, a weaker process is still present which depends solely on the polarity of both the solvent and solute. The relative intensity of this bridging vibration is greatly enhanced in the infrared ν_{co} spectrum of polycrystalline IVa recorded as a KBr pellet (Diagram 2). Simultaneously it has shifted to an even lower frequency (1815cm^{-1}) and, whilst this may be an extension of the aforementioned process, this probably originates from other interactive forces present in solid-state

Diagram 2

Infrared (ν_{CO}) Spectra for $[Ru_6C(CO)_{17-n}(PPh_2Et)_n]$; n=1 or 2



a/ $[Ru_6C(CO)_{15}(PPh_2Et)_2]$ (cyclohexane)

b/ $[Ru_6C(CO)_{16}(PPh_2Et)]$ (cyclohexane)

c/ $[Ru_6C(CO)_{16}(PPh_2Et)]$ (KBr disc)

spectra. These are amply illustrated by the increased complexity of the terminal carbonyl region which can be largely attributed to correlation field splitting effects(36). These have been used to explain how solid phase frequencies for metal carbonyls are usually lower than those obtained in solution spectra, and progressively more so the lower in the spectrum. In addition, intermolecular vibrational coupling has to be considered whilst, in certain circumstances, site occupancies in the crystal lattice can cause site symmetry splitting of degenerate modes accompanied by unexpected coupling and intensity stealing phenomena(37).

Extensive scanning over a wide range gave only resonances associated with coordinated PPh_2Et in the ^1H NMR ($CDCl_3$, 31°C) spectrum of IVa. This reveals the simplicity of the reaction with the absence of any ligand degradation by contact with the Ru_6C core. Elemental analysis (C and H) was also consistent with the proposed stoichiometry, although within experimental error the possibility of an addition product could not be overruled. Because of this, and in the absence of an observed mass spectrum or any detailed structural information from conventional spectroscopy (including a variable temperature ^{13}C NMR study), a full single crystal X-ray diffraction study was performed to ascertain the precise molecular structure and geometry.

6.2.1. Crystal and Molecular Structure of $[Ru_6C(CO)_{16}(PPh_2Et)]$

Deep red, air stable, crystals of IVa were grown from n-hexane/CH_2Cl_2 solution. Preliminary photographic examination (Weissenberg and Precession) established approximate cell dimensions and revealed the systematic absences h0l for h+l=2n+1; and 0k0 for k=2n+1. These uniquely indicated the centrosymmetric space group $P\,2_1/n$.

Crystal Data for $[Ru_6C(CO)_{16}(PPh_2Et)]$

$C_{31}H_{15}O_{16}PRu_6$ MW=1280.6g.mol^{-1}

Monoclinic	$P\,2_1/n$	x , y , z	$\frac{1}{2}+x$, $\frac{1}{2}-y$, $\frac{1}{2}+z$

	-x ,-y ,-z	$\frac{1}{2}$-x, $\frac{1}{2}$+y, $\frac{1}{2}$-z

Cell dimensions a=18.754(3) b=17.624(3) c=22.841(3)
α=90.0 β=91.94(2) γ=90.0

Z=8

U=7545.9 $Å^3$ F(000)=4863.8 μ(Mo-K$_\alpha$)=23.77cm^{-1}

Density (calc)=2.249g.cm^{-3} Density (flotation)=2.28(1)g.cm^{-3}

R=0.0431 R_W=0.0426 R_G=0.0411 R_M=0.0411

A suitable crystal of computed volume 0.01979mm^3 was used to record three dimensional X-ray intensities of 13,089 unique reflections, with a merging R of 0.0084, with graphite monochromated Mo-K$_\alpha$ radiation (λ=0.71069Å), from two octants of reciprocal space ($3.5 < 2\theta < 60^\circ$) using ω-2θ scan on a Nonius CAD4 diffractometer. All the intensities were corrected for Lorentz and polarisation factors, and the slight crystal deterioration during accumulation compensated for by measuring two standard reflections (6, -1, -9 and 12, 0, -12) every 100 readings. The data was also corrected for absorption (crystal size 0.18_7 x 0.18_7 x 0.67_5 mm, transmission coefficients on the full set ranged from 0.7033 to 0.6097) and excluding all reflections with $F(obs)^2 < 3\sigma(F(obs)^2)$, where the standard deviation was estimated from the counting statistics, gave 10,739 observed structure amplitudes which were used in the structural determination. Accurate cell dimensions were determined and refined by using 25 randomly selected reflections with the CAD4 automatic search, centre, index and least-squares routines.

The structure was solved using the SHELX computer package(38). Initial calculations were performed on an ICL 2970 computer at Southampton University, but in the later stages of refinement they had to be transferred to a larger CDC 7600/194S computer at Manchester University.

The Patterson synthesis gave clear indications from the Ru-Ru vectors around the origin for an Ru_6 octahedron. The unit

Table 1a

Fractional Atomic Coordinates(10^4) and Isotropic Thermal Parameters($Å^2 x 10^4$) for Molecule A

Atom	x/a	y/b	z/c	U
Ru(1A)	4079(1)	4430(1)	2888(1)	
Ru(2A)	4735(1)	5527(1)	2077(1)	
Ru(3A)	4736(1)	3944(1)	1826(1)	
Ru(4A)	3127(1)	3967(1)	1942(1)	
Ru(5A)	3201(1)	5568(1)	2131(1)	
Ru(6A)	3832(1)	4929(1)	1134(1)	
P(1A)	3412(2)	4764(2)	3707(1)	
C(01A)	3971(4)	4727(4)	2024(3)	237(14)
C(02A)	2437(7)	4672(7)	3597(5)	429(32)
C(03A)	1979(7)	4853(7)	4121(5)	504(30)
C(11)	3589(4)	5655(4)	3999(3)	364(25)
C(12)	3388(4)	5910(4)	4598(3)	652(40)
C(13)	3536(4)	6627(4)	4830(3)	739(44)
C(14)	3937(4)	7144(4)	4517(3)	718(41)
C(15)	4191(4)	6944(4)	3971(3)	625(37)
C(16)	4043(4)	6227(4)	3738(3)	487(32)
H(12)	3077	5509	4840	1043(135)
H(13)	3340	6781	5253	1043(135)
H(14)	4052	7699	4697	1043(135)
H(15)	4501	7344	3729	1043(135)
H(16)	4239	6073	3315	1043(135)
C(21)	3589(4)	4103(4)	4298(3)	369(26)
C(22)	3257(4)	3484(4)	4413(3)	645(44)
C(23)	3411(4)	3002(4)	4884(3)	802(48)
C(24)	3950(4)	3189(4)	5294(3)	774(47)
C(25)	4336(4)	3860(4)	5233(3)	832(43)
C(26)	4182(4)	4342(4)	4762(3)	586(33)
H(22)	2839	3339	4096	1043(135)
H(23)	3112	2482	4932	1043(135)
H(24)	4069	2815	5659	1043(135)
H(25)	4753	4005	5550	1043(135)
H(26)	4480	4862	4714	1043(135)
C(1A)	4873(8)	4566(8)	3393(6)	466(36)
O(1A)	5356(7)	4579(7)	3733(5)	737(34)
C(2A)	3995(8)	3431(8)	3116(6)	455(36)

O(2A)	4022(6)	2790(6)	3247(5)	693(33)
C(3A)	5451(9)	5706(9)	2655(7)	583(45)
O(3A)	5910(7)	5858(7)	2994(5)	814(37)
C(4A)	4288(9)	6507(9)	2130(7)	572(43)
O(4A)	4206(7)	7138(7)	2166(5)	746(36)
C(5A)	5419(9)	5775(9)	1515(7)	567(43)
O(5A)	5836(7)	5937(7)	1177(5)	873(39)
C(6A)	5422(10)	3626(10)	2390(8)	694(51)
O(6A)	5885(7)	3478(7)	2709(6)	869(40)
C(7A)	4437(10)	2976(10)	1654(7)	659(49)
O(7A)	4295(8)	2368(9)	1458(6)	1028(49)
C(8A)	5454(9)	3962(9)	1264(7)	582(44)
O(8A)	5922(8)	3973(8)	941(6)	939(44)
C(9A)	2660(9)	3319(9)	2444(7)	529(42)
O(9A)	2355(6)	2930(7)	2768(5)	746(35)
C(10A)	2737(9)	3391(9)	1315(7)	544(44)
O(10A)	2519(7)	3018(7)	941(6)	857(40)
C(11A)	2373(8)	4788(8)	2037(6)	414(35)
O(11A)	1754(6)	4833(6)	2048(4)	640(32)
C(12A)	2774(7)	6135(8)	2721(6)	398(34)
O(12A)	2502(6)	6506(6)	3067(4)	613(29)
C(13A)	2762(8)	6229(8)	1614(6)	470(36)
O(13A)	2463(7)	6631(8)	1280(6)	913(42)
C(14A)	4035(10)	5838(10)	767(7)	681(48)
O(14A)	4143(8)	6418(8)	550(6)	976(44)
C(15A)	2925(10)	4873(10)	756(7)	643(48)
O(15A)	2362(7)	4864(7)	538(5)	885(39)
C(16A)	4236(11)	4360(12)	557(9)	833(61)
O(16A)	4423(8)	3989(8)	157(7)	1149(50)

Table 1b

Fractional Atomic Coordinates(10^4) and Isotropic Thermal Parameters($Å^2 \times 10^4$) for Molecule B

Atom	x/a	y/b	z/c	U
Ru(1B)	9091(1)	5369(1)	2756(1)	
Ru(2B)	9729(1)	5749(1)	1667(1)	

Ru(3B)	9763(1)	4196(1)	2023(1)	
Ru(4B)	8245(1)	4108(1)	2090(1)	
Ru(5B)	8090(1)	5665(1)	1789(1)	
Ru(6B)	8847(1)	4699(1)	1038(1)	
P(1B)	8483(1)	5102(2)	3619(1)	
C(01B)	8969(4)	4983(4)	1922(3)	254(16)
C(02B)	7513(6)	5217(6)	3515(4)	383(28)
C(03B)	7042(7)	5082(7)	4051(5)	580(32)
C(31)	8658(4)	4165(3)	3948(3)	397(25)
C(32)	8421(4)	4040(3)	4537(3)	589(35)
C(33)	8516(4)	3319(3)	4779(3)	853(48)
C(34)	8900(4)	2770(3)	4482(3)	702(31)
C(35)	9188(4)	2942(3)	3943(3)	628(38)
C(36)	9093(4)	3663(3)	3701(3)	496(32)
H(32)	8123	4464	4767	1043(135)
H(33)	8293	3185	5196	1043(135)
H(34)	8973	2212	4670	1043(135)
H(35)	9485	2518	3713	1043(135)
H(36)	9316	3797	3284	1043(135)
C(41)	8687(4)	5740(4)	4163(3)	364(27)
C(42)	8382(4)	6483(4)	4251(3)	547(30)
C(43)	8604(4)	7014(4)	4671(3)	768(43)
C(44)	9180(4)	6852(4)	5054(3)	839(42)
C(45)	9534(4)	6159(4)	5015(3)	831(50)
C(46)	9312(4)	5628(4)	4594(3)	582(36)
H(42)	7937	6608	3955	1043(135)
H(43)	8330	7551	4701	1043(135)
H(44)	9351	7263	5379	1043(135)
H(45)	9980	6033	5311	1043(135)
H(46)	9587	5091	4564	1043(135)
C(1B)	8938(8)	6394(9)	2892(6)	451(39)
O(1B)	8895(6)	7031(6)	2981(5)	679(31)
C(2B)	9922(8)	5378(8)	3242(6)	479(37)
O(2B)	10417(7)	5443(7)	3545(5)	766(35)
C(3B)	10455(9)	6137(9)	2171(7)	609(44)
O(3B)	10921(7)	6349(7)	2458(5)	864(39)
C(4B)	9410(10)	6702(10)	1421(7)	663(49)
O(4B)	9219(7)	7287(8)	1234(6)	940(42)

C(5B)	10396(9)	5659(9)	1070(7)	525(41)
O(5B)	10831(7)	5582(7)	738(5)	764(36)
C(6B)	10419(8)	4052(8)	2661(6)	430(37)
O(6B)	10831(7)	3939(7)	3030(5)	752(35)
C(7B)	9349(9)	3219(9)	2107(7)	562(42)
O(7B)	9286(7)	2561(8)	2152(6)	896(42)
C(8B)	10532(8)	3939(8)	1534(6)	474(37)
O(8B)	10983(6)	3788(6)	1237(5)	641(30)
C(9B)	7819(8)	3646(8)	2739(6)	435(36)
O(9B)	7525(6)	3350(6)	3102(4)	582(29)
C(10B)	7834(8)	3328(8)	1657(6)	436(35)
O(10B)	7615(7)	2810(7)	1387(5)	859(41)
C(11B)	7378(8)	4846(8)	1947(6)	438(37)
O(11B)	6754(6)	4781(6)	1964(4)	577(29)
C(12B)	7579(8)	6379(8)	2222(6)	479(38)
O(12B)	7252(7)	6798(7)	2483(5)	752(37)
C(13B)	7627(9)	6033(9)	1112(7)	599(45)
O(13B)	7343(7)	6276(7)	687(5)	831(37)
C(14B)	8934(9)	5458(9)	458(7)	574(43)
O(14B)	8970(6)	5917(7)	94(5)	740(35)
C(15B)	7990(9)	4337(10)	690(7)	587(48)
O(15B)	7486(7)	4098(7)	465(5)	814(37)
C(16B)	9367(8)	3961(8)	656(6)	494(40)
O(16B)	9663(6)	3507(7)	389(5)	732(34)

Table 1c

Anisotropic Thermal Parameters(10^4)

Atom	U11	U22	U33	U23	U13	U12
Ru(1A)	281(5)	311(5)	278(4)	-7(4)	-6(4)	3(4)
Ru(2A)	262(5)	326(5)	379(5)	5(4)	-8(4)	-40(4)
Ru(3A)	291(5)	348(5)	343(5)	-11(4)	-32(4)	44(4)
Ru(4A)	333(5)	353(5)	336(5)	-45(4)	-8(4)	-80(4)
Ru(5A)	368(6)	362(5)	371(5)	-15(4)	50(4)	74(4)
Ru(6A)	382(6)	402(5)	269(4)	12(4)	-13(4)	-17(4)
P(1A)	315(17)	355(16)	278(14)	-11(12)	0(12)	-18(13)
Ru(1B)	275(5)	295(5)	290(4)	-4(4)	-14(4)	-15(4)

Ru(2B)	282(5)	329(5)	307(4)	11(4)	-6(4)	-72(4)
Ru(3B)	247(5)	325(5)	375(5)	-14(4)	-9(4)	14(4)
Ru(4B)	344(5)	360(5)	363(5)	4(4)	38(4)	-98(4)
Ru(5B)	294(5)	356(5)	345(5)	45(4)	-1(4)	46(4)
Ru(6B)	309(5)	396(5)	278(4)	-5(4)	7(4)	-44(4)
P(1B)	334(17)	319(15)	277(14)	15(12)	-30(12)	41(13)

Table 2

Selected Bond Lengths(Å) and Angles(deg) (with estimated standard deviations in parentheses) for $[Ru_6C(CO)_{16}(PPh_2Et)]$

Molecule A		Molecule B
a) Heavy-atom parameters		
2.972(1)	Ru(1) - Ru(2)	2.875(1)
2.890(1)	Ru(1) - Ru(3)	2.968(1)
2.875(1)	Ru(1) - Ru(4)	3.099(1)
3.088(1)	Ru(1) - Ru(5)	2.897(1)
2.850(1)	Ru(2) - Ru(3)	2.855(1)
2.885(1)	Ru(2) - Ru(5)	3.100(1)
2.894(1)	Ru(2) - Ru(6)	2.839(1)
3.039(1)	Ru(3) - Ru(4)	2.859(1)
2.865(1)	Ru(3) - Ru(6)	2.920(1)
2.856(1)	Ru(4) - Ru(5)	2.841(1)
2.863(1)	Ru(4) - Ru(6)	2.883(1)
2.834(1)	Ru(5) - Ru(6)	2.833(1)
2.359(3)	Ru(1) - P(1)	2.358(3)
125.0(1)	P(1)-Ru(1)-Ru(2)	175.4(1)
173.0(1)	P(1)-Ru(1)-Ru(3)	124.0(1)
109.5(1)	P(1)-Ru(1)-Ru(4)	90.8(1)
89.7(1)	P(1)-Ru(1)-Ru(5)	110.7(1)
b) Metal-carbide parameters		
2.047(6)	Ru(1) - C(01)	2.029(7)
2.010(7)	Ru(2) - C(01)	2.061(8)
2.054(7)	Ru(3) - C(01)	2.042(7)

2.077(7)	Ru(4) - C(01)	2.098(8)
2.089(7)	Ru(5) - C(01)	2.055(8)
2.071(6)	Ru(6) - C(01)	2.084(7)
127.9(5)	C(1)-Ru(1)-C(01)	118.1(5)
120.7(5)	C(2)-Ru(1)-C(01)	128.5(5)
130.7(5)	C(3)-Ru(2)-C(01)	123.9(5)
108.8(5)	C(4)-Ru(2)-C(01)	117.3(6)
128.1(5)	C(5)-Ru(2)-C(01)	129.0(5)
121.2(6)	C(6)-Ru(3)-C(01)	129.1(5)
117.5(6)	C(7)-Ru(3)-C(01)	109.2(5)
131.1(5)	C(8)-Ru(3)-C(01)	131.1(5)
135.6(5)	C(9)-Ru(4)-C(01)	138.8(5)
133.7(5)	C(10)-Ru(4)-C(01)	135.2(5)
93.6(4)	C(11)-Ru(4)-C(01)	91.1(4)
92.1(4)	C(11)-Ru(5)-C(01)	95.0(5)
140.7(4)	C(12)-Ru(5)-C(01)	137.2(5)
132.2(5)	C(13)-Ru(5)-C(01)	132.4(6)
124.9(6)	C(14)-Ru(6)-C(01)	119.9(5)
121.5(6)	C(15)-Ru(6)-C(01)	123.7(6)
124.6(6)	C(16)-Ru(6)-C(01)	125.5(5)

c) Phosphine ligand parameters

1.844(13)	P(1) - C(02)	1.837(11)
1.734(7)	P(1) - C(11/31)	1.840(7)
1.806(7)	P(1) - C(21/41)	1.710(7)
1.530(17)	C(02) - C(03)	1.553(16)
115.6(3)	Ru(1)-P(1)-C(11/31)	115.8(3)
110.0(3)	Ru(1)-P(1)-C(21/41)	111.9(3)
101.6(5)	Ru(1)-P(1)-C(02)	112.0(3)

d) Bridging carbonyl group

2.038(14)	Ru(4) - C(11)	2.099(15)
2.079(14)	Ru(5) - C(11)	2.008(15)
1.165(19)	C(11) - O(11)	1.177(19)
87.8(6)	Ru(4)-C(11)-Ru(5)	87.5(6)
138.3(11)	Ru(4)-C(11)-O(11)	134.4(11)
133.9(11)	Ru(5)-C(11)-O(11)	138.0(11)

e) Terminal carbonyl groups

	Ru-C	
1.924(16)	Maximum	1.908(15)
1.833(18)	Minimum	1.847(14)
1.870(16)	Mean (standard deviation)	1.880(15)
	Ru-C-O	
177.7(14)	Maximum	179.1(12)
162.0(15)	Minimum	161.6(15)
	C-O	
1.162(17)	Mean (standard deviation)	1.149(20)

f) Carbonyl group angles

89.9(4)	C(1)-Ru(1)-C(2)	91.3(6)
84.9(4)	C(1)-Ru(1)-P(1)	88.3(5)
87.8(4)	C(2)-Ru(1)-P(1)	85.5(4)
96.3(7)	C(3)-Ru(2)-C(4)	94.3(7)
87.3(7)	C(3)-Ru(2)-C(5)	89.4(7)
98.1(7)	C(4)-Ru(2)-C(5)	94.1(7)
93.9(8)	C(6)-Ru(3)-C(7)	97.0(5)
89.1(8)	C(6)-Ru(3)-C(8)	86.2(6)
95.2(7)	C(7)-Ru(3)-C(8)	99.4(6)
87.6(7)	C(9)-Ru(4)-C(10)	85.4(6)
91.7(6)	C(9)-Ru(4)-C(11)	92.5(6)
102.2(6)	C(10)-Ru(4)-C(11)	94.1(6)
95.3(6)	C(11)-Ru(5)-C(12)	91.9(6)
92.1(6)	C(11)-Ru(5)-C(13)	96.1(6)
86.0(6)	C(12)-Ru(5)-C(13)	88.4(7)
91.9(8)	C(14)-Ru(6)-C(15)	92.1(7)
92.9(8)	C(14)-Ru(6)-C(16)	96.1(7)
91.7(8)	C(15)-Ru(6)-C(16)	91.1(7)

cell contains two similar but crystallographically non-equivalent molecules and the 12 independent ruthenium atoms were located by multisolution sigma two-sign expansion. The most favourable E-map consisted of the expected two oc tahedra. After refinement of their coordinates all the other non-hydrogen atoms were found from subsequent Fourier maps combined with model building. In both molecules the carbide was the last atom to be located perhaps indicating the low electron density about them.

Full-matrix least-squares refinement of the structure was carried out with anisotropic thermal parameters for Ru and P, and isotropic C and O atoms. The phenyl rings were constrained as rigid groups (C-C=1.395Å) during this process to save computing time, and their hydrogen atoms, given a common refined isotropic temperature factor, placed in geometrically idealised positions and allowed to ride 1.08Å from the relevant carbon atom. A weighting scheme $w=1/\sigma^{-2}(F(obs))$ was applied and gave a satisfactory variation of $w\Delta F^2$ when analysed in terms of sinθ and F(obs). Problems with the amount of data, and the number of refinable parameters, led to the necessity of using a block refinement procedure in which only certain parameters were allowed to refine in each least-squares cycle. Omitting those reflections for which $F(obs)^2 < 4\sigma(F(obs)^2)$ and when $2\theta < 50^\circ$ reduced the number of data points by 2,123 to 8,616 which were used in the refinement. The total number of refined parameters is 456, giving a ratio of reflections/parameters of 18.9. This gave a convergence to a final R value of 0.0431, and the final difference electron-density synthesis showed only weak features (-1.31 < electron density < 1.47 e $Å^{-3}$).

The atomic scattering factors and anomalous dispersion terms for neutral C, O, P and H atoms were taken from the SHELX package and the corresponding values for ruthenium taken from reference 39. In Table 1 are presented the atomic coordinates, anisotropic and isotropic temperature factors, and the hydrogen-atom positions. Some selected bond lengths and angles are tabulated in Table 2.

The molecular structures of the two crystallographically independent molecules (A and B) are shown schematically in Diagram 3. These are reproduced elsewhere(40) as ORTEP(41) drawings

Diagram 3a

Molecular Structure of $[Ru_6C(CO)_{16}(PPh_2Et)]$: Molecule A

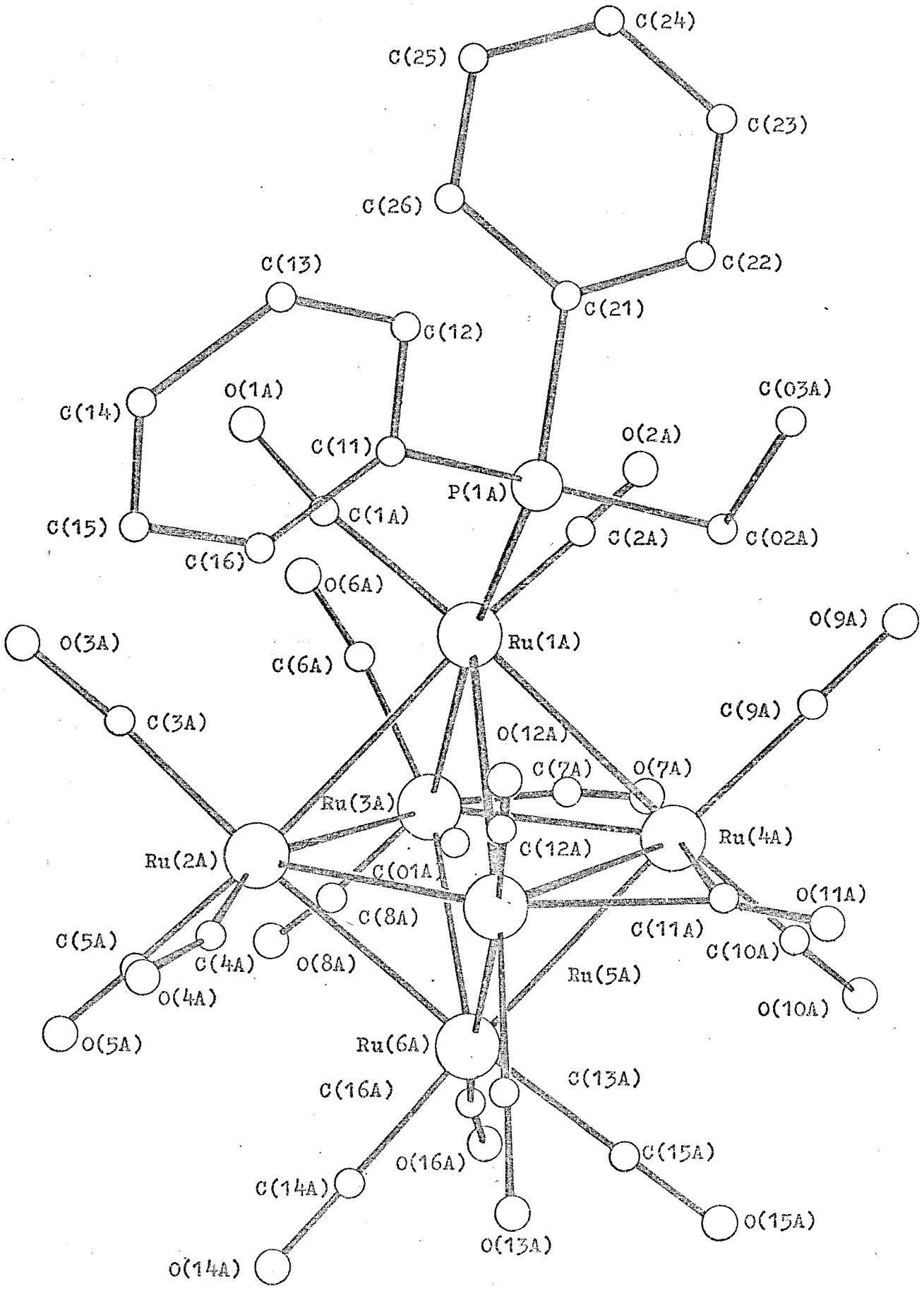
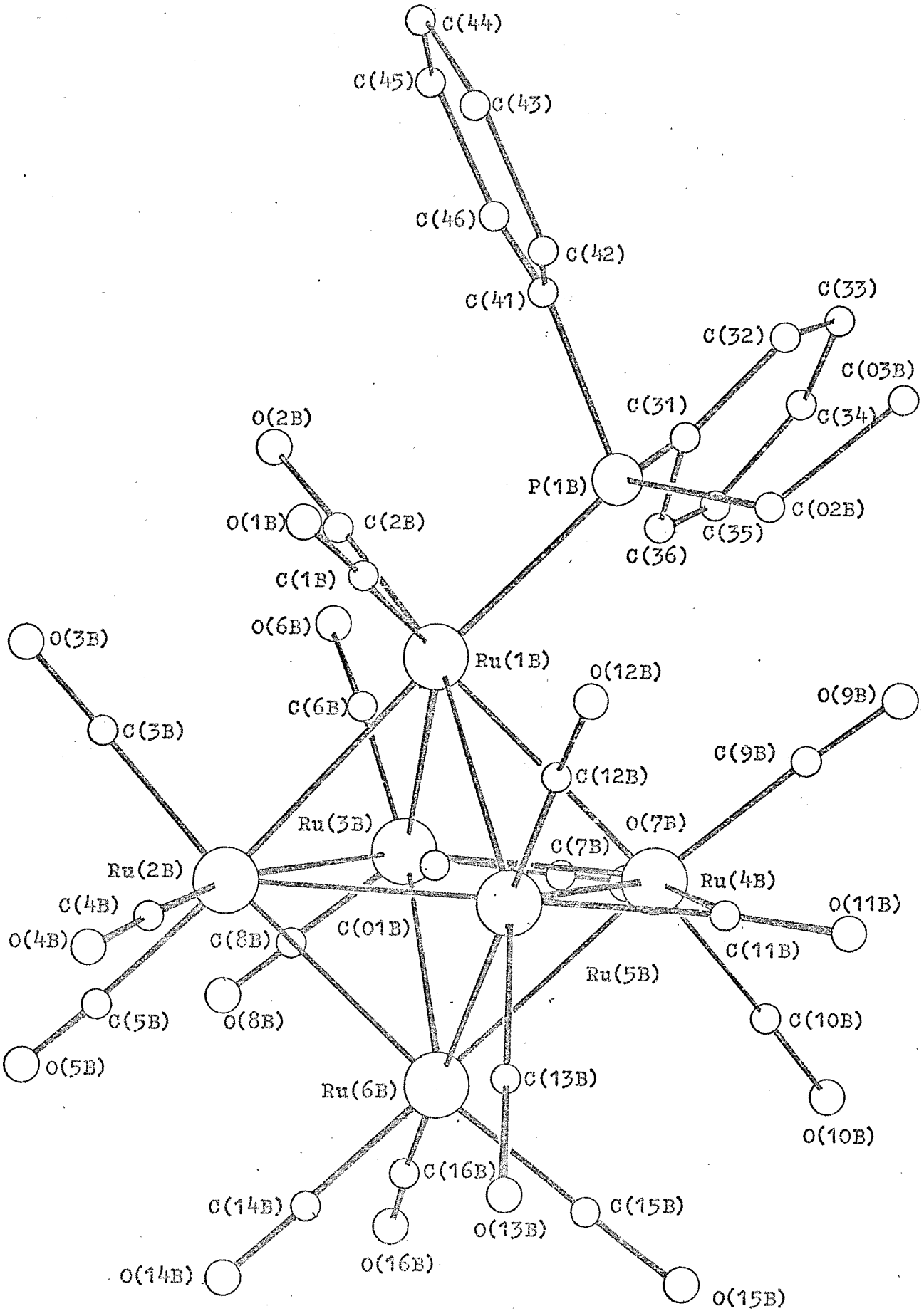


Diagram 3b

Molecular Structure of $[Ru_6C(CO)_{16}(PPh_2Et)]$: Molecule B

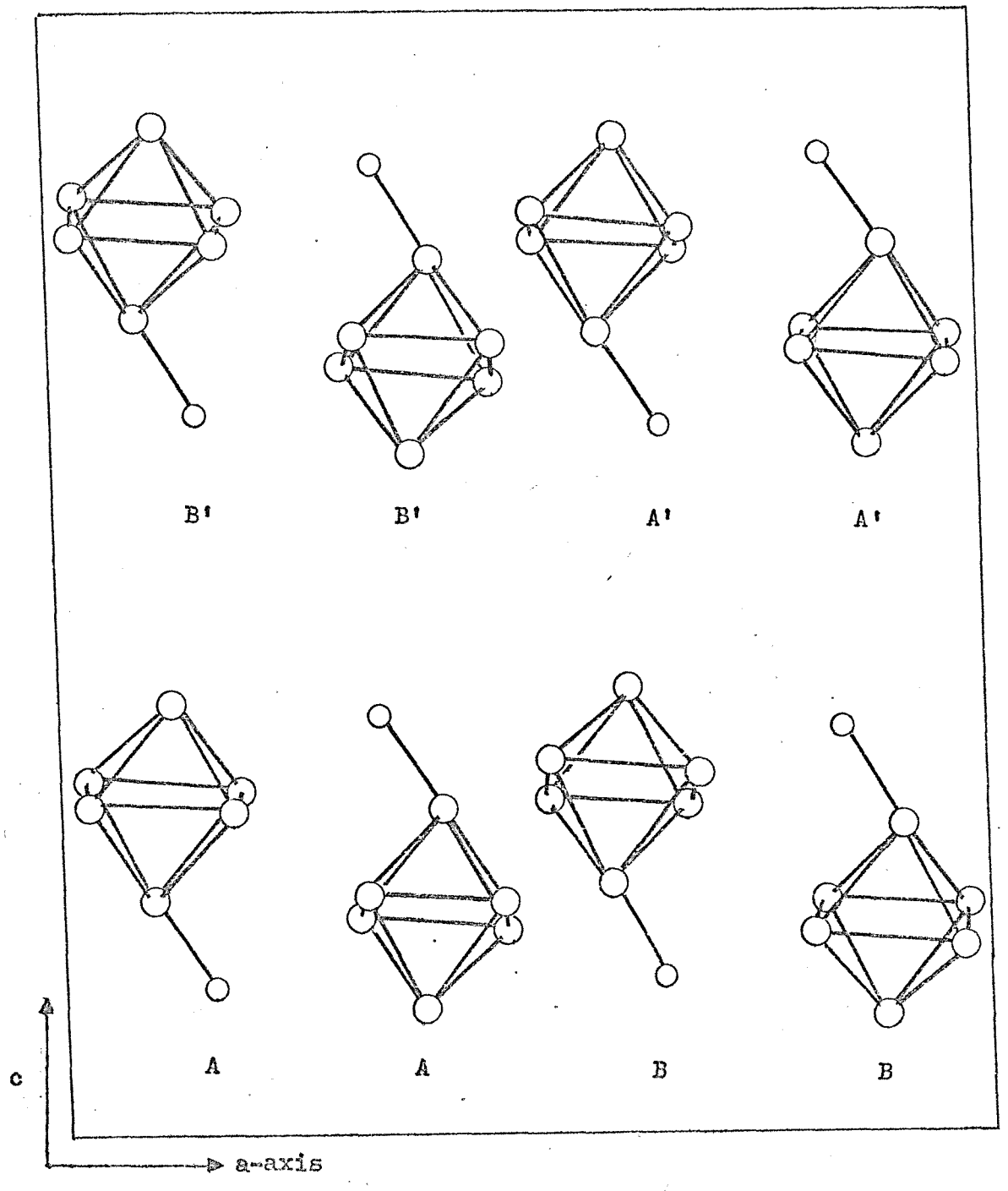


with thermal ellipsoids enclosing 20% probabilities. They possess the basic $[Ru_6C(CO)_{17}]$ structure, but with the phosphine substituting for a terminal carbonyl group on a ruthenium atom sharing a face with the two bridged metal atoms. Interestingly this is the same ruthenium atom bearing the arene ligand in $[Ru_6C(CO)_{14}(C_6H_3Me_3\text{-}1,3,5)]$ (24). The introduced ligand is placed unsymmetrically over the bridging carbonyl rendering each molecule enantiomeric, this appears the most sterically relieved arrangement. The μ_2-ligand is slightly asymmetric being displaced away from the direction of the phosphine but still in the metal plane. One such geometry is shown (Diagram 5a) for an optical isomer of Molecule A, as viewed down the Ru(1A)-C (carbide) bond.

The unit cell, as viewed from infinity in Diagram 4, contains four molecules of both A and B. Each is divided into pairs of the two optical isomers positioned in each corner so that the reflection planes interconvert them. By chance, the presented structures for A and B turn out to be approximately enantiomeric, this is emphasized by the chosen atom numbering scheme. Superimposing the two molecules gives an averaged structure with characteristics similar to that apparent in solution (see later), possessing a pseudo- mirror-plane through the phosphorus, carbide and bridging carbonyl group. The mean Ru-C(carbide) distance of 2.060(26)Å is not significantly different from that reported for I, 2.05A(3); $[Ru_6C(CO)_{14}(C_6H_3Me_3)]$, 2.04Å(24); $[Ru_6C(CO)_{14}$(bitropyl)], 2.06Å(25); and $[Ru_6C(CO)_{15}(C_6H_{10})]$, 2.06Å(27). Although it is scarcely significant, there is a slight lengthening of the mean Ru-Ru bonding distance compared to that in I, 2.912(86) verses 2.903(60) Å. However, a direct comparison of the individual, averaged, Ru-Ru distances (Diagram 5b) for IVa against the corresponding values in I illustrates perhaps more significant variations around the molecule. In particular, there is a noticeable expansion of the upper square-based pyramid capped by the phosphine through increased values for the metal-metal bond lengths to the substituted ruthenium atom. In IVa, this mean is 2.958(92)Å, as compared with a mean of 2.901(49)Å in I. There is a corresponding contraction of the lower polygon. Further, the lengthening is most pronounced for the two distances, Ru(1)-Ru(4) and Ru(1)-Ru(5), on the face encompassing the phosphine and bridging carbonyl group.

Diagram 4

The Crystal Unit Cell for $[Ru_6C(CO)_{16}(PPh_2Et)]$



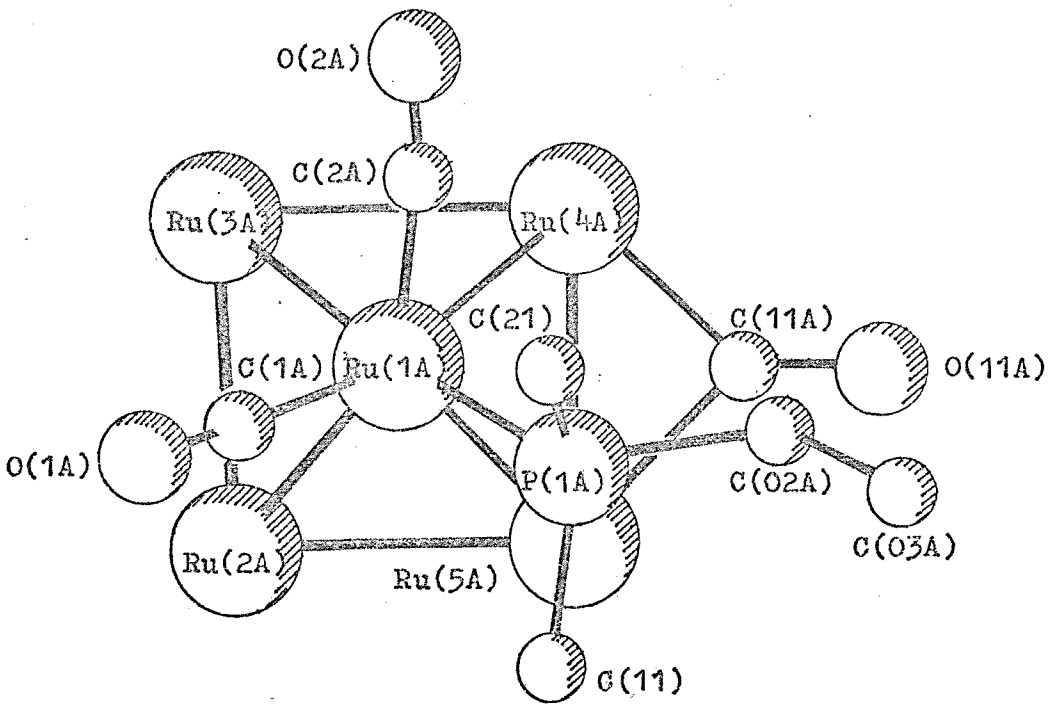
i) The unit cell is viewed from infinity in the positive b direction.

ii) Carbon and oxygen atoms are excluded for clarity.

iii) The molecular packing is shown for the enantiomeric isomers of the two crystallographically distinct molecules.

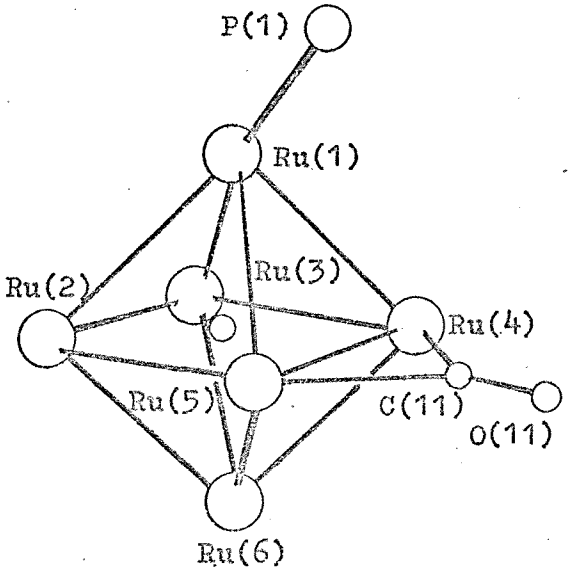
Diagram 5

a) Enantiomeric Nature of Crystalline $[Ru_6C(CO)_{16}(PPh_2Et)]$



View down the Ru(1A)-C(carbide) bond in Molecule A

b) Comparison of Ru-Ru Distances(Å) in $[Ru_6C(CO)_{16}L]$; L=CO or PPh_2Et



$[Ru_6C(CO)_{16}(PPh_2Et)]$		$[Ru_6C(CO)_{17}]$
2.924	Ru(1) - Ru(2)	2.927
2.929	Ru(1) - Ru(3)	2.981
2.987	Ru(1) - Ru(4)	2.885
2.993	Ru(1) - Ru(5)	2.827
2.853	Ru(2) - Ru(3)	2.840
2.993	Ru(2) - Ru(5)	3.034
2.867	Ru(2) - Ru(6)	2.872
2.949	Ru(3) - Ru(4)	2.897
2.893	Ru(3) - Ru(6)	2.917
2.849	Ru(4) - Ru(5)	2.855
2.873	Ru(4) - Ru(6)	2.969
2.834	Ru(5) - Ru(6)	2.858

This probably arises from the steric bulk of the phosphine, but might also represent the first stages of cluster opening caused by increased electron donation from the ligand. In comparison, a contraction of these distances was found in $[Ru_6C(CO)_{14}(C_6H_3Me_3)]$, giving a mean of 2.859(6)Å.

6.2.2. ^{13}C NMR Solution Studies of $[Ru_6C(CO)_{17-n}(PPh_2Et)_n]$; n=0, 1 or 2

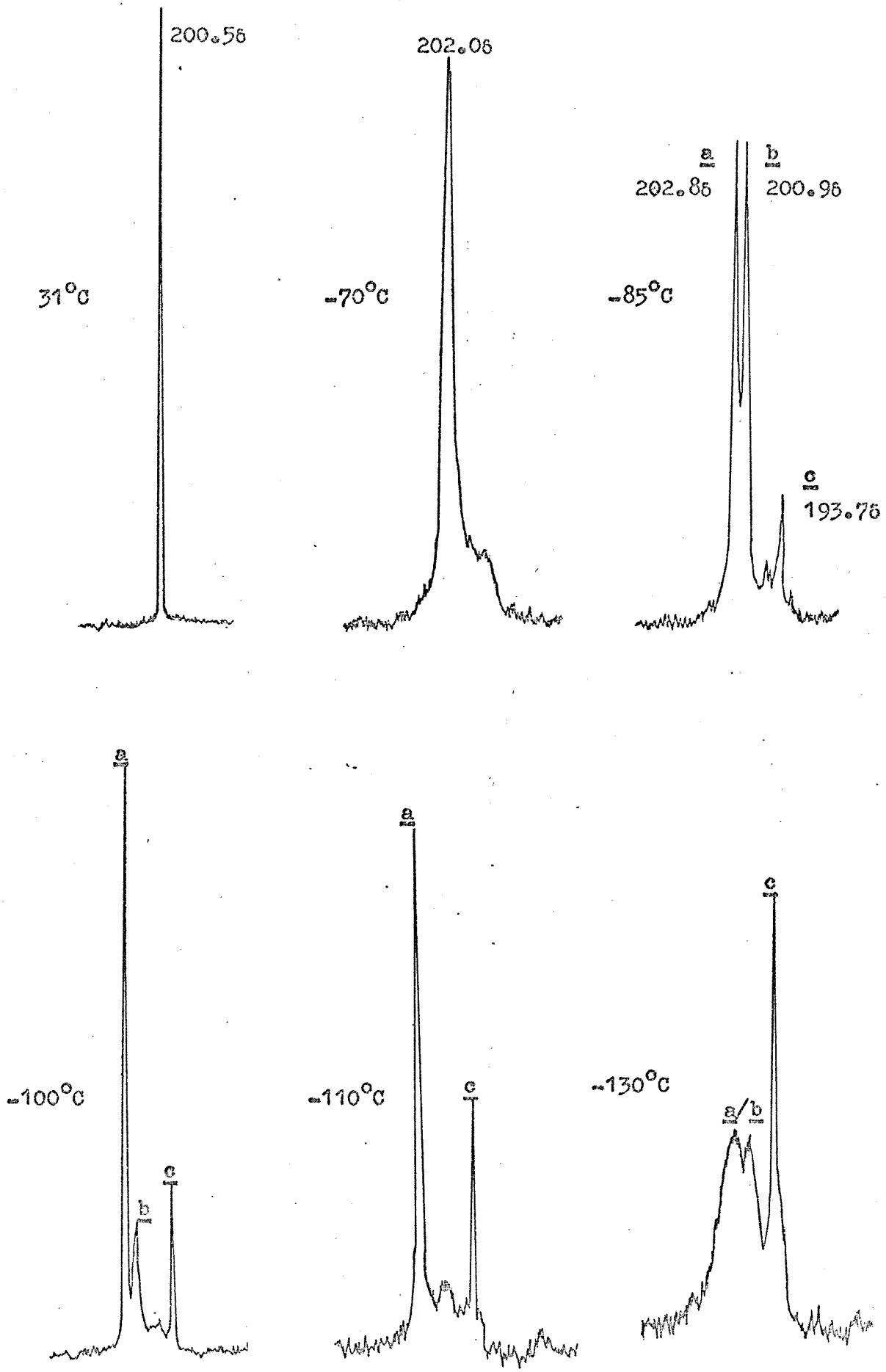
This study was initiated to confirm retention of the solid-state structure of IVa upon solvation, and to possibly reveal some structural information for Va.

Direct substitution was used to prepare ^{13}CO-enriched $[Ru_6C(CO)_{17}]$, by heating a n-hexane solution at 70°C for 90 hours under 90 atom% ^{13}CO in a sealed vessel. No detectable decomposition was observed during this process and the retrieved compound was still a crimson, crystalline, solid. Its infrared ν_{CO} spectrum (CCl_4) indicated that a degree of enrichment had been achieved, as shown by the increased complexity through a larger abundance of ^{13}C-containing vibrations. Unfortunately, this could not substantiate whether enrichment had occurred evenly or in a site preferential manner. The ambient temperature ^{13}C NMR spectrum ($CDCl_3$, 31°C) contained a sharp singlet at 197.146 which remained unchanged at -20°C when sample precipitation precluded further study. This evidently signifies that there is a fast exchange process equivalencing all the carbonyl groups around the metal polyhedron. At room temperature similar temperatures have been also made for other hexa-ruthenium clusters prepared from previously enriched $[Ru_3(CO)_{12}]$ thus excluding any preferential site enrichment. In particular, $[Ru_6C(CO)_{16}]^{2-}$ prepared in this manner shows just a single line plus a broad resonance at much lower field due to the carbide(10), such a signal would not be anticipated in the present investigation because of the different stage of enrichment.

An enriched sample of IVa was then prepared by the method already described. Because of its much higher solubility a variable-temperature ^{13}C NMR study over the much wider range of -130 to +31 °C was possible, using varying mixtures of $CD_2Cl_2/CHCl_2F$ as solvent. The recorded spectra are shown in Diagram 6. Again at ambient conditions a sharp line at 200.56 was observed representing the

Diagram 6

Variable Temperature ^{13}CO NMR Spectra for $[Ru_6C(CO)_{16}(PPh_2Et)]$



averaged resonance. This downward shift relative to that for I is consistent with replacement of a carbonyl by a phosphine ligand. Separate studies(42) have shown that the chemical shift of a coordinated carbon monoxide is sensitive to changes in its stereochemistry and electronic enviroment. Of particular relevance was the observation that replacement of carbon monoxide by a better charge donor increased δ_{CO}; phosphines falling into this category.

On cooling, no significant change was observed in the signal, apart from a small temperature dependence, until below -50°C when it noticeably broadened and eventually collapsed into the baseline at about -65°C. At -70°C a broad signal, 202.0δ, emerged from the coalescence, but by -80°C the highest energy process was completely frozen out and this signal split into two separate signals:- 202.8,a, and 200.9,b, δ. Although their peak heights were approximately equal, weighting to fit their averaged signal indicated actual relative populations of 8:6, as opposed to 7:7, respectively: [((8x202.8)+(6x200.9))/14=202.0]. Simultaneously a third peak also appeared at 193.7δ,c, equivalent to two carbonyl groups. At -100°C, whilst a and c are still very sharp with narrow half-widths, b has broadened considerably as a second process is slowed and by -110°C it has collapsed totally into the baseline. At this temperature a third process begins to slow as a loses intensity relative to c and eventually collapses at -130°C, the lowest temperature studied. Even then, neglecting signal broadening due to loss of resolution as amply illustrated by the $CHCl_2F$ doublet, c remains essentially unchanged. The limitations of the spectrometer cooling system, and the absence of an available solvent, prevented investigation below -130°C; sample solubility itself did not present a problem.

Although in the absence of the low temperature, limiting, spectrum this data remains ambiguous, the observed features can be interpreted on the basis of the 'averaged' crystal structure being retained after solvation. Above ca. -70°C a total scambling of all the carbonyl ligands about the metal-phosphine substrate is observed. Below this temperature two equivalent enviroments are 'frozen out' from this dynamic process as seen by the emergence of c after collapse of the initial signal. Given the relative population of c it is difficult to assign it to any pair except the two carbonyl groups on Ru(1), which are inequivalent by virtue of

the phosphine orientation in the crystal but are averaged very readily in solution and so are equivalenced even at -130°C. Below -80°C the migration between the five remaining ruthenium centres soon ceases and two separate exchange processes are evident, as signified by a and b. If one accepts the 8:6:2 population ratio then the group of six, b, probably represents averaging of the two $Ru(CO)_3$ groups on Ru(2) and Ru(3) cis- to the substituted metal atom. The apparent molecular symmetry precludes discrimination between this occurring via migration between the two rutheniums or by localised rotation at the independent centres. Intuitively the latter is preferred, but with the reservation that this process appears to have a higher activation energy barrier than the one discussed below. This leaves the eight carbonyl groups of the bridge, two $Ru(CO)_2$ moieties, and the last $Ru(CO)_3$ group, trans- to the substituted metal atom, attributed to a. Evidently a localised internuclear exchange process is occurring across the face defined by Ru(4), Ru(5) and Ru(6). This may be promoted by the bridging-ligand, whilst its component chemical shift (ca. 250δ) accounts for the observed downfield position of a. On cooling this motion is slowed preferentially compared to that represented by a, but both signals have collapsed into the baseline at -130°C.

At room temperature the ^{13}C NMR spectrum ($CDCl_3$, 31°C) of a ^{13}CO-enriched sample of Va also exhibited one sharp resonance in the carbonyl region at 204.7δ, again indicating rapid total exchange. This remained unchanged until approximately -70°C whence it collapsed into the baseline. Further cooling resulted in the emergence of several new features from the coalescence but, unfortunately, these were still ill-defined at the lowest temperature studied (-120°C). Obviously from this limited data no structural information can be inferred, however the downfield shift relative to the signals for both I and IVa is again consistent with increased phosphine substitution.

6.3. Reaction of $[Ru_6C(CO)_{17}]$ with Trimethylphosphite

As already described in the presence of excess phosphine $[Ru_6C(CO)_{15}(PPh_2Et)_2]$, Va, is exclusively formed from the reaction of I by heating under reflux in n-hexane. It was identified by

microanalysis, infrared and ^{1}H NMR spectroscopy. Only resonances due to coordinated phosphine were seen in the ^{1}H NMR spectrum ($CDCl_3$, 31°C) despite extensive scanning. No mass spectrum was recorded, no doubt due to decomposition in the probe. Two overlapping vibrations, at 1857vw and 1838vw cm^{-1}, are present in its infrared ν_{co} spectrum (cyclohexane) (Diagram 2, Table 3); in addition to a complex pattern in the terminal carbonyl region. This was interpreted as indicating either an increased proportion of bridging enviroments or structural isomers of Va, with no significant perturbation of the remaining carbonyl distribution. Independent workers(43) also found that at the more forcing conditions of reflux in n-heptane a similar product was obtained with triphenylphosphine. Its reproduced infrared ν_{co} spectrum (Table 3) confirms it to be isostructural with Va, i.e. $[Ru_6C(CO)_{15}(PPh_3)_2]$.

However, this data alone provided only limited structural information for Va and its ^{13}C NMR spectra were equally uninformative. In an attempt to gain a greater insight the reaction of I with $P(OMe)_3$ was investigated. This phosphite tends to be more reactive than phosphines so even further degrees of substitution were anticipated. The sharp doublet in its ^{1}H NMR spectrum also acts as an excellent handle for discriminating isomeric forms. Indeed, by varying the reaction conditions it was possible to isolate each member of the series $[Ru_6C(CO)_{17-n}(P(OMe)_3)_n]$, n=1,2,3 or 4, which were characterised by spectroscopy and microanalysis.

At room temperature stirring a CH_2Cl_2 solution of I with just an equimolar quantity of phosphite results in the isolation of $[Ru_6C(CO)_{16}(P(OMe)_3)]$, IVb, as the only product. This was easily identified by comparison of its infrared ν_{co} spectrum with that of IVa (Table 3). A parent ion m/e=1193, based on Ru_6=608, was observed in the mass spectrum followed by sequential loss of carbon monoxide complicated by phosphite fragmentation. The ^{1}H NMR spectrum ($CDCl_3$, 31°C) gave a sharp doublet centred at 3.77(J_{PH}=12Hz)δ which corresponds to a downfield shift relative to free phosphite, 3.5(J_{PH}=12Hz)δ, as would be expected upon coordination.

Gradually increasing the relative concentration of phosphite results in varying mixtures of the greater substituted products reflecting the approximate molar quantity added. $[Ru_6C(CO)_{15}(P(OMe)_3)_2]$, Vb, was isolated as a red polycrystalline

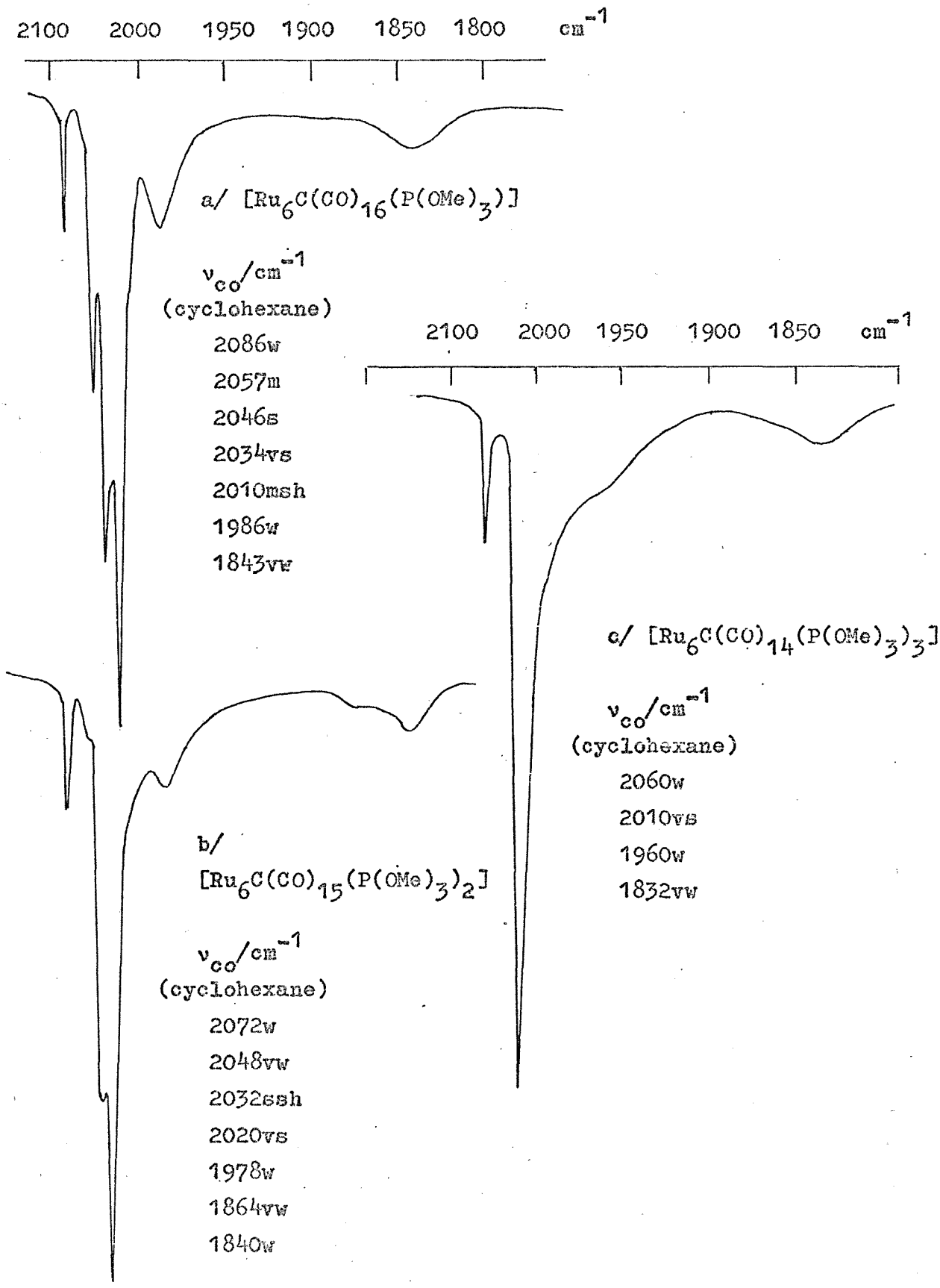
Table 3

Infrared (ν_{CO}) Frequencies of Prepared Hexaruthenium Clusters

Compound	IR ν_{CO}/cm^{-1} (cyclohexane unless stated)			
$[Ru_6C(CO)_{17}]$ (Ref.2)	2064s	2049s	2007w	1993w
	1958w	1854wbr		
(CCl_4)	2067s	2046s	2003w	1850vw
$[Ru_6C(CO)_{16}(PPh_3)]$	2084m	2056vs	2045ms	2029vs
(CCl_4)	2003m	1984m	1844w	
$[Ru_6C(CO)_{16}(PPh_2Et)]$	2084m	2056s	2046s	2032vs
	2020msh	2003w	1985w	1845vw
(KBr disc)	2084m	2053sh	2038vs	2021sh
	2008vs	1997ms	1993sh	1984msh
	1979m	1972m	1962m	1815m
$[Ru_6C(CO)_{16}(P(OMe)_3)]$	2086w	2057m	2046s	2034vs
	2010msh	1986w	1843vw	
$[Ru_6C(CO)_{16}(PPh_2CH_2CH_2SIL)]$	2083w	2055ms	2044s	2030vs
(Nujol mull)	2017sh	1984w	1956vw	1840vw
$[Ru_6C(CO)_{15}(PPh_3)_2]$(Ref.43)	2069wsh	2064w	2046s	2018sbr
	1998w	1987w	1845wbr	
$[Ru_6C(CO)_{15}(PPh_2Et)_2]$	2071wsh	2064m	2045vw	2028s
	2018vs	2014vs	1991w	1979w
	1971wsh	1949vw	1857vw	1838vw
$[Ru_6C(CO)_{15}(P(OMe)_3)_2]$	2072w	2048vw	2032ssh	2020vs
	1978w	1864vw	1840w	
$[Ru_6C(CO)_{15}(PPh_2CH_2CH_2SIL)_2]$	2065m	2045w	2028s	2019vs
(Nujol mull)	1990sh	1974w	1856vw	1835vw
$[Ru_6C(CO)_{14}(P(OMe)_3)_3]$	2060w	2010vs	1960w	1832vw
$[Ru_6C(CO)_{13}(P(OMe)_3)_4]$	2042w	1999vsbr	1965w	1815vw

Diagram 7

Infrared (ν_{CO}) Spectra for $[Ru_6C(CO)_{17-n}(P(OMe)_3)_n]$; n=1-3



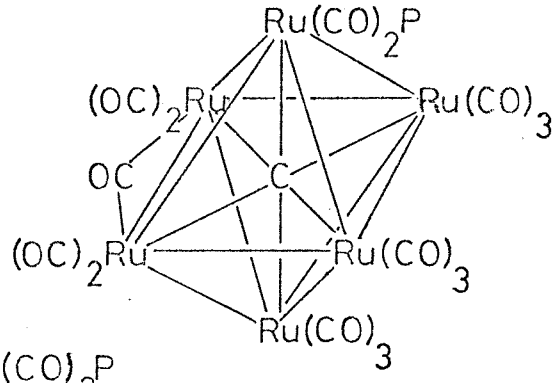
solid. Although no mass spectrum was obtained, within its accepted limitations microanalysis (C and H) was fully consistent with the proposed formulation. The infrared ν_{CO} spectrum of Vb (Diagram 7) is similar to that of Va, again showing an asymmetric bridging feature, whilst its ^{1}H NMR contained two overlapping doublets centred at 3.68(J_{PH}=12Hz) and 3.75(J_{PH}=12Hz) δ, with relative intensities of approximately 1:2 respectively. On first inspection this suggests a trisubstituted product, but careful consideration of the possible spatial arrangements for the molecule allows it to be explained in terms of two separate isomers of Vb. However, to support this hypothesis certain prequisite assumptions are necessary first. Namely, that successive substitution occurs at different metal centres, does not alter the remaining carbonyl distribution, and that the barrier to reaction is significantly higher at the two ruthenium constituting the bridged edge compared to that at the remaining metal atoms. Implicit to the second supposition is that the number of bridging carbonyls does not alter and, whilst this may be true, introducing more electron density at a metal centre is often compensated for by their generation. This is usually rationalised on the basis that bridging carbonyl ligands are capable of delocalizing charge about the cluster.

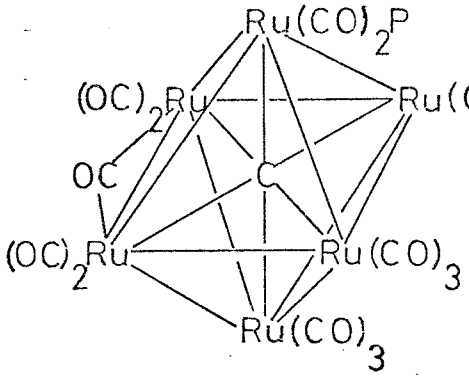
The ^{13}C NMR study on IVa and Va established complete scrambling of the carbonyl groups about the metal polyhedron at ambient temperatures. Then, the carbonyl envelope effectively adopts a spherical distribution on the NMR time-scale, and as such it does not effect any symmetry considerations. Any inequivalence will be conferred by the geometrical disposition of the phosphorus groups at different sites on the octahedron; assuming the barrier to their loss of rigidity is substantially higher. However, the actual time when an incoming PR_3 encounters a cluster with sufficient energy to react will be less than the residence time of a particular ligand permutation, before it 'instantaneously' undergoes some fluxional process. Therefore the position of substitution will be governed by the static structure as defined by X-ray crystallography. Then, within these restraints, only two isomers are possible for Vb with the phosphites either disposed cis-, Vb', or trans-, Vb'', respectively (Diagram 8). Both forms possess a mirror-plane such that their phosphites are symmetry related, and thus will appear as single

Diagram 8

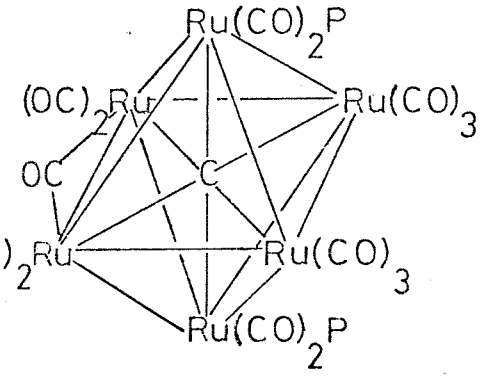
Possible Spatial Arrangements for $[Ru_6C(CO)_{17-n}(P(OMe)_3)_n]$; n=1-4

(IVb)

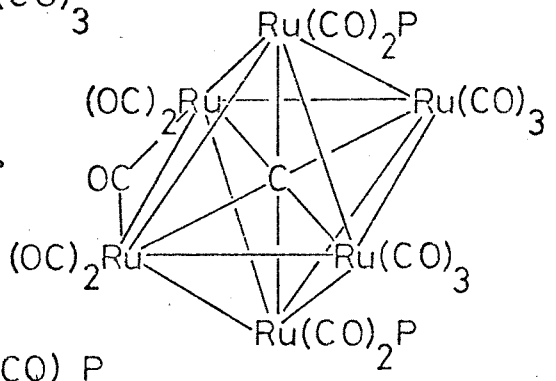


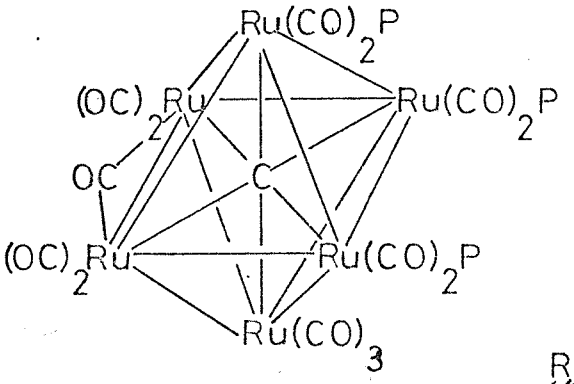


enantiomeric cis-isomers (Vb')

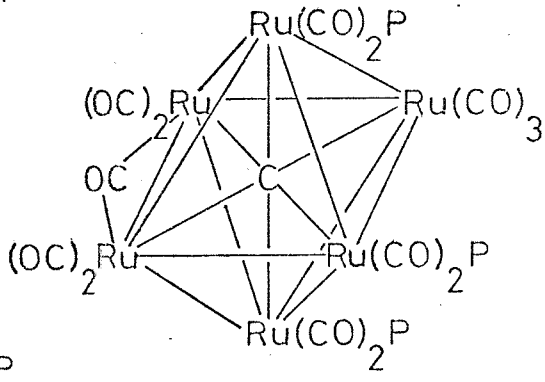


trans-isomer (Vb")



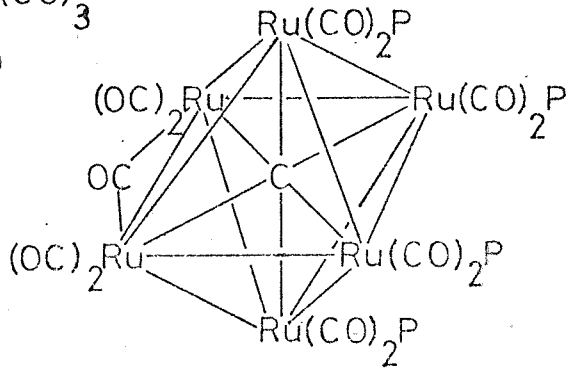


fac-isomer (VI')



mer-isomer (VI")

(VII)



doublets on the ^{1}H NMR spectrum. However, they are sufficiently dissimilar to have different chemical shifts so, provided phosphite attack is non-selective such that site availability is controlling, Vb' will have twice the population of Vb". It is this relative abundance of isomers which is reflected in the observed spectrum, and accounts for the two bridging ν_{CO} absorptions seen in the solution infrared spectra for V derivatives. In the case of Va, or more so with $[Ru_6C(CO)_{15}(PPh_3)_2]$(43), phosphine substitution on their precursors must have a degree of steric (or electronic) control reducing the population of the more hindered cis-isomer.

Further increasing the proportion of $P(OMe)_3$ causes the yields of $[Ru_6C(CO)_{14}(P(OMe)_3)_3]$, VI, to become significant until with slightly more than a three-fold excess it is the major species. It was characterised by microanalysis, in association with ^{1}H NMR and infrared ν_{CO} spectroscopy. The ^{1}H NMR spectrum contains two overlapping doublets at 3.69(J_{PH}=12Hz) and 3.78(J_{PH}=12Hz) δ, with relative intensities of 2:1 respectively. Again within the imposed constraints only two isomeric forms are possible, with the phosphites in either a fac-, VI', or mer-, VI" arrangement. A fac-isomer will possess a C_3-axis on the NMR time-scale so only a single doublet is anticipated. However, the mer- arrangement has only a mirror-plane through the unique phosphite so it will give two doublets in a 2:1 ratio, in agreement with the observed spectrum. Thus, unless the system is complicated by accidental degeneracies for the signals of the two isomers, the mer- isomer is selectively formed. Intuitively this is the expected result from steric considerations, also this mer- form can be derived from either the cis- or trans- isomers of Vb but this is not possible with the fac-arrangement.

Finally, under the more vigorous conditions of heating to reflux in n-hexane with a large excess of phosphite, $[Ru_6C(CO)_{13}(P(OMe)_3)_4]$, VII, is isolated and characterised by ^{1}H NMR, infrared spectroscopy and elemental analysis. Only one spatial arrangement is allowed (Diagram 8), and this is supported by the presence of two pairs of equally intense doublets at 3.69(J_{PH}=12Hz) and 3.75(J_{PH}=12Hz) δ in the ^{1}H NMR spectrum.

All the observed spectral details are adequately explained within the proposed hypothesis. However, without more

precise structural data other possibilities, especially those involving fundamental opening of the metal polyhedron, or rearrangement of the carbonyl distribution, cannot be entirely ruled out. An independent investigation(43) found similar results although some inconsistencies, especially in the case of Vb, exist. However, parent ions were observed in the mass spectra of Vb, VI and VII, and additionally a preliminary X-ray diffraction study on VII confirmed that the phosphites were all bonded to separate ruthenium atoms. Unfortunately the crystal was found to be disordered which, in conjunction with an extremely large unit cell, prevented further refinement.

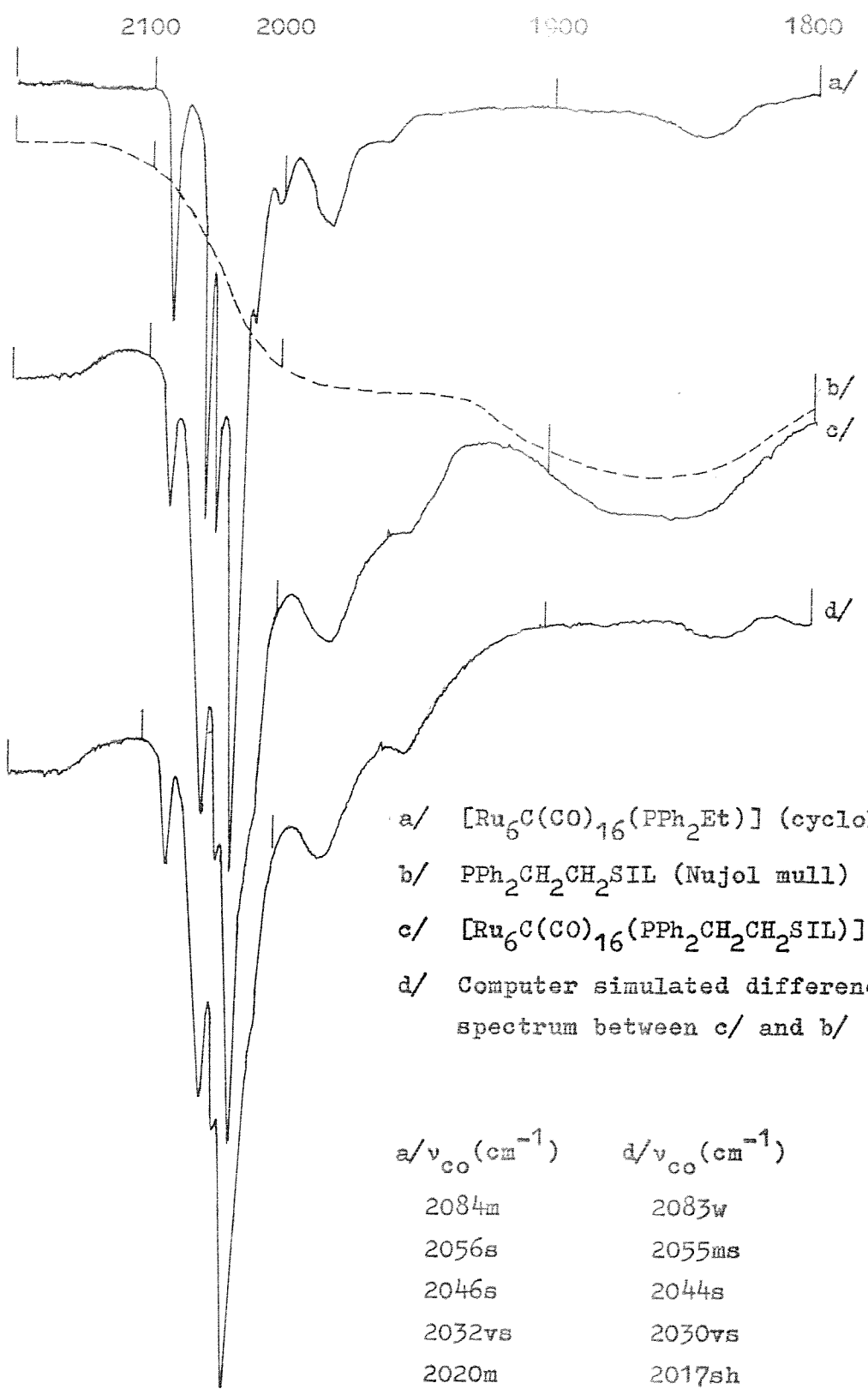
6.4. Preparation and Characterisation of $[Ru_6C(CO)_{17-n}(PPh_2CH_2CH_2SIL)_n]$, n=1 or 2.

A quantity of $PPh_2CH_2CH_2SIL$, from the same batch prepared with Aerosil 200 in Chapter One, was added to a solution of $[Ru_6C(CO)_{17}]$ in dry methylene chloride. The resulting slurry was vigorously stirred for 2 hours at room temperature. Then filtration and repeated washing with fresh solvent yielded a red solid, whilst the filtrate revealed only infrared absorptions synonymous with I. Provided the original solution cotained a large excess of cluster the retrieved silica when mulled gave an infrared ν_{CO} spectrum which showed excellent agreement with that for the isolable model complex IVa (Diagram 9). All the features in the terminal carbonyl region correlated well, but the presence of the broad absorption between 1920-1800 cm^{-1} due to the background silica masked the possible bridging absorption. However, compensating for this by computer subtraction clarified this situation producing a simulated spectrum with a more even baseline over this region and revealing a weak vibration centred at $1840cm^{-1}$. This absorption could be an anomaly of the computation, but it does bear a close resemblance to the bridging frequency for IVa ($1845cm^{-1}$) although the wavenumber shift is greater than preferred. In conclusion, at room temperature the tethered complex $[Ru_6C(CO)_{16}(PPh_2CH_2CH_2SIL)]$, VIII, can be selectively prepared under appropriate conditions, which is essentially isostructural to IVa at the cluster.

An elemental analysis (Ru and P) again highlighted the

Diagram 9

Infrared Spectroscopic Characterisation of $[Ru_6C(CO)_{16}(PPh_2CH_2CH_2SIL)]$



a/ $[Ru_6C(CO)_{16}(PPh_2Et)]$ (cyclohexane)

b/ $PPh_2CH_2CH_2SIL$ (Nujol mull)

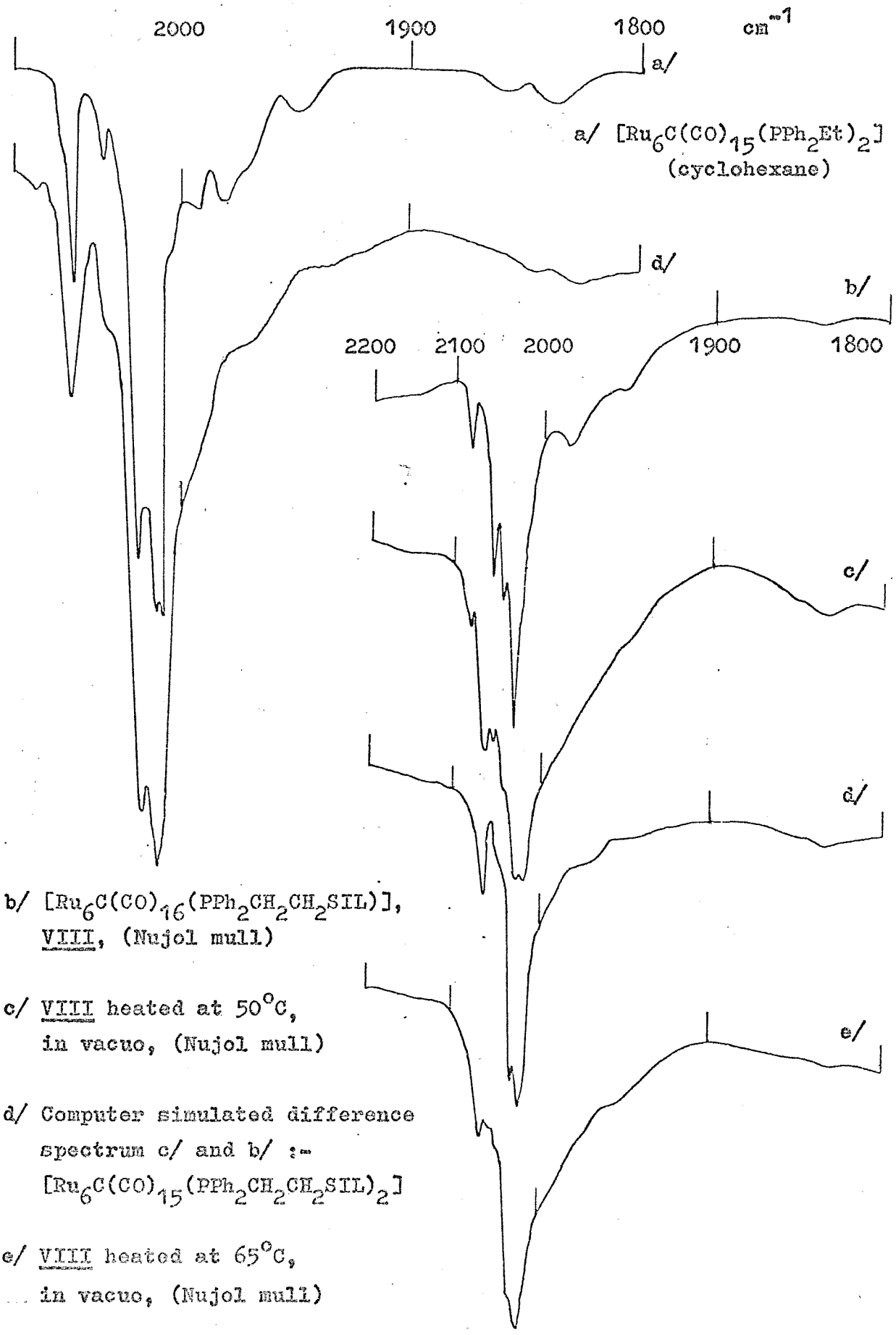
c/ $[Ru_6C(CO)_{16}(PPh_2CH_2CH_2SIL)]$ (Nujol mull)

d/ Computer simulated difference spectrum between c/ and b/

a/ ν_{CO} (cm^{-1})	d/ ν_{CO} (cm^{-1})
2084m	2083w
2056s	2055ms
2046s	2044s
2032vs	2030vs
2020m	2017sh
2003w	-
1985w	1984w
1960vw	1956vw
1845vw	1840vw

Diagram 10

Infrared Spectral Characterisation of $[Ru_6C(CO)_{15}(PPh_2CH_2CH_2SIL)_2]$



b/ $[Ru_6C(CO)_{16}(PPh_2CH_2CH_2SIL)]$, VIII, (Nujol mull)

c/ VIII heated at 50°C, in vacuo, (Nujol mull)

d/ Computer simulated difference spectrum c/ and b/ :- $[Ru_6C(CO)_{15}(PPh_2CH_2CH_2SIL)_2]$

e/ VIII heated at 65°C, in vacuo, (Nujol mull)

major disadvantage of the SCHEME ONE (Chapter One) philosophy with a cluster-to-phosphorus ratio of approximately 1:11.2. This has certain repercussions discussed below. Others(44), by using flash chromatography as a purification stage, used the alternative approach (SCHEME TWO) to prepare VIII by contacting isolated $[Ru_6C(CO)_{16}\{PPh_2CH_2CH_2Si(OEt)_3\}]$ with untreated Aerosil 200 at room temperature for extended periods.

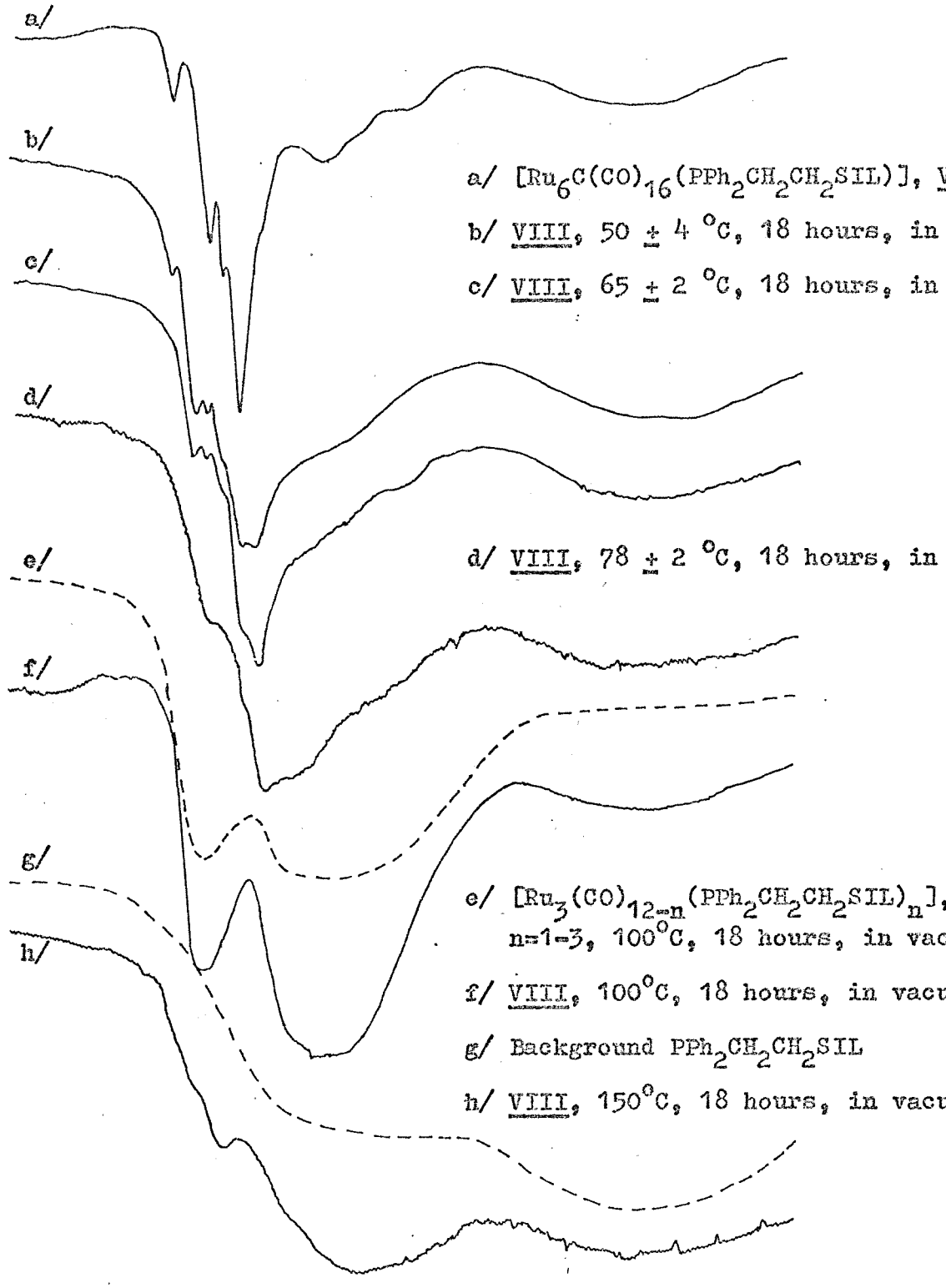
When a more dilute solution of I is contacted with $PPh_2CH_2CH_2SIL$, the recovered silica had a slightly deeper tan appearance and its infrared ν_{CO} spectrum was distorted by additional peaks at 2064 and 2028 cm^{-1}. Storage or mild heating of VIII also gave these additional features and the results of the low temperature (< 65°C) thermolysis study are shown in Diagram 10. At 50°C, bands due to a second complex appear and the computed difference spectrum, scaled on the common band at 2084cm^{-1}, is entirely consistent with the solution spectrum of Va. Hence, this second species is assigned as the disubstituted anchored product $[Ru_6C(CO)_{15}(PPh_2CH_2CH_2SIL)_2]$, IX; again from the bridging ν_{CO} region it appears to exist as two isomers. After heating at 65°C in vacuo, IX is predominant. Clearly, with surface phosphines of varying accessibilities due to their different steric enviroments, anything less than a blanket coverage of I makes disubstitution competitive because of the two-phase nature of initial coordination; so formation of IX becomes significant compared to isolation of VIII. Even in the presence of a high cluster concentration where VIII is selectively formed initially, a sufficient number of sterically hindered phosphines must remain which with thermal activation result in formation of IX.

6.5. Thermal Degradation of $[Ru_6C(CO)_{16}(PPh_2CH_2CH_2SIL)]$

The transformation VIII to IX is the first stage in the sequential pyrolysis of VIII leading eventually to total decarbonylation. This has been studied in detail using self-supported pressed discs by the procedure discribed in Chapter Five. Separate discs of freshly prepared VIII were placed in the evacuable cell and heated to a predetermined temperature in vacuo overnight (ca. 18 hours). After cooling, the recovered pellet was

Diagram 11

Infrared Spectra of recovered Silicas from Pyrolysis of $[Ru_6C(CO)_{16}(PPh_2CH_2CH_2SIL)]$



(All spectra recorded in Nujol mull)

ground and mulled and its infrared ν_{co} spectrum recorded; the initial rate of heating was not found to significantly effect the final outcome. While a well-defined spectrum due to VIII and/or IX was observable up to 65°C, by 80°C the pattern was broader and three ν_{co} absorptions at 2053m, 2011vs and 1997(sh) cm^{-1} were seen. At 100°C, the disc darkened considerably to a deep brown, and now exhibited only two well-defined, broad bands at 2057 and 1984 cm^{-1} of approximately equal intensities. This progression is similar to that experienced for pyrolytic degradation of the phosphine-anchored tri-osmium clusters and can be consequently attributed to breakdown into monomeric units. Continued heating to 150°C brought about considerable deterioration in both the sample and spectral quality. Visually the disc developed a black lustrous appearance, and this was accompanied by almost complete loss of its carbonyl absorptions into the silica background. Weak bands could still be observed at 2068, 2048 and 1972 cm^{-1}. This appears characteristic of aggregated ruthenium metal or a carbide, but the remaining ν_{co} bands apparently do not relate to carbon monoxide adsorbed on silica supported ruthenium(45). This data is presented in Diagram 11.

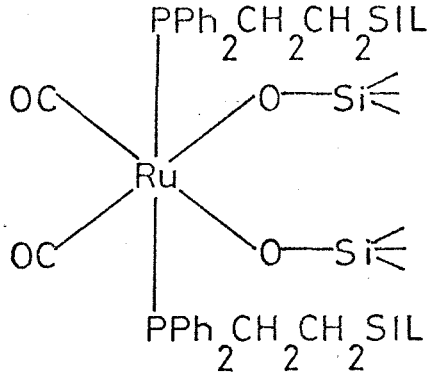
The preparation of $[Ru_3(CO)_{12-n}(PPh_2CH_2CH_2SIL)_n]$, n=1, 2 and (possibly) 3, and its subsequent thermal degradation under vacuum at 100°C to give a surface species characterised by two infrared ν_{co} bands at 2052 and 1981 cm^{-1}, has already been documented in this dissertation. These frequencies were sufficiently different from those reported for pyrolysis of physisorbed $[Ru_3(CO)_{12}]$ on unfunctionalised silica-gel to indicate that the ruthenium atoms were still bonded to phosphorus under these conditions. However, they show a strong enough similarity to the current result from pyrolysed VIII at 100°C to infer that a common material is formed independent of the originally supported cluster and its nuclearity. The same observation was made for $[Ru_3(CO)_{12}]$ and I directly bonded to γ-alumina(33), where tentative assignment to $[Ru(CO)_x(OAl)_y]_n$ species was made by analogy to halogenated/thio- carbonyl compounds. Significantly I was considerably more resilient to this breakdown and this was attributed to the stabilising influence of the carbide. A similar approach can be adopted here by comparison to the reported infrared ν_{co} spectra of various halo-carbonyl-phosphine ruthenium complexes (Table 4). When dealing with the related osmium systems

Table 4

Compound	IR ν_{CO}/cm^{-1}			Reference
VIII breakdown product at 100°C	2057	1984		This work
$[Ru(CO)_4(PPh_3)]$	2060	1980	1940	(46)
	1906			
$[Ru(CO)_3(PPh_3)_2]$	1895			(47)
$[Ru(CO)_3(PPh_3)Cl_2]$	2133	2075	2032	(48)
$[Ru(CO)_2(PPh_2Me)_2Cl_2]$				(49)
cis	2059	1996		
all trans	2014			
all cis	2090	2000		
$[Ru(CO)(PPh_2Me)_3Cl_2]$				(49)
isomer A	1952			
B	1980			
C	1952			
$[Ru(CO)(PPhEt_2)_3HCl]$	1910			(50)
$[Ru(CO)_2(PBu^t_2Ph)Cl_2]_2$	2055	1993		(51)
$[Ru(CO)_2(PPh_3)Cl_2]_2$	2076	2016		(48)
$[Ru(CO)_2(PBu^t_2Ph)Cl]_2$	2024	1988	1949	(51)

in Chapter Five a preference for a surface species of the form $[M(CO)_2(PR_3)(OM)_2]_n$ was expressed based largely on the near unity of the phosphine-to-metal ratio, whereas a better correlation of infrared absorptions was to $[M(CO)_2(PR_3)_2Cl_2]$. Here, with a large excess of potentially available uncoordinated phosphines on the surface, no such limitation exists and, indeed, a good correlation is again seen with the thermally stable, cis- isomer of $[Ru(CO)_2(PPh_2Me)_2Cl_2]$(49). This avoids the need to propose $[Ru(CO)_2(PR_3)(OM)_2]_2$ where the planar bridges offer very improbable surface sites due to steric congestion of the axial ligands at the surface. Another acceptable configuration would be that of $[Ru(CO)_2(PBu^t_2Ph)Cl]_2$(51) because of the bent nature of the halo-bridges. Both possible analogues can be prepared by treating ruthenium trichloride with carbon monoxide, and then adding the

appropriate tertiary phosphine to the resultant solution; the outcoming depending upon its steric bulk. Because the better ν_{co} correlation is to cis-$[Ru(CO)_2(PPh_2Me)_2Cl_2]$ the favoured surface structure of the product from pyrolysis of VIII, at 100°C in vacuo, is that given below. The only reservation is that as the homogeneous analogues tend to be colourless considerable concurrent decomposition must be assumed on the surface to account for its appearance.



An account of a preliminary investigation of VIII as a catalyst for cyclohexene hydrogenation is given in Section 5.10 in the preceding chapter.

6.6. Experimental Section

$[Ru_6C(CO)_{17}]$

a)(5) : A suspension of $[Ru_3(CO)_{12}]$(1.5116g) in di-n-butyl ether(30ml) was heated under reflux for 6 hours. During this time the solution turned a deep purple and deposition of ruthenium metal on the walls of the flask was evident. After allowing to cool the solvent was removed under reduced pressure, and the residue extracted with hot toluene and filtered through Kieselguhr to remove metallic particles. The brick-red solid obtained was then sublimed at 100°C in vacuo(0.1torr) to remove the impurities $[H_4Ru_4(CO)_{12}]$ and $[H_2Ru_4(CO)_{13}]$. The remaining dark purple solid was recrystallised from hot toluene to give $[Ru_6C(CO)_{17}]$(0.2885g); yield=22%.

b)(8,43) : $[Ru_3(CO)_{12}]$(0.2500g) and n-hexane(50ml) were charged into a 100ml Roth autoclave which was then purged and

pressurised with ethylene(50bar). On stirring the pressure dropped, due to ethylene dissolution, and was adjusted to a final value of 20bar. This was then heated for 3 hours at 150°C after which time the stirrer was switched off, the autoclave removed from its heater-housing and allowed to cool. Filtration separated crystalline $[Ru_6C(CO)_{17}]$(0.0926g) from a brown supernatant solution, believed to contain various coordinated ethylene adducts(27), which was discarded; yield=43%.

$[Ru_6C(CO)_{16}(PPh_2Et)]$

An equimolar quantity of PPh_2Et(0.0088g, 0.0408mmol) was added to a solution of $[Ru_6C(CO)_{17}]$(0.0451g, 0.0412mmol) in CH_2Cl_2(35ml). After an immediate darkening in colour the solution was stirred for several hours until total consumption of the starting material, as followed by infrared monitoring, had occurred. Removal of the solvent in vacuo and chromatographing the residue, using ethyl acetate/light petroleum(b.p. 60-80 °C) (1:4v/v) as eluant, gave $[Ru_6C(CO)_{16}(PPh_2Et)]$($R_f$=0.63, 0.0450g) as large acicular crystals; yield=85%.

A similar mixture of reactants heated under reflux in n-hexane(20ml) for ½ hour gave the same result.

Elemental Ananlysis Cald. C 29.05% H 1.17%
Obsd. C 29.40% H 1.22%

$[Ru_6C(CO)_{16}(PPh_3)]$

A suspension of $[Ru_6C(CO)_{17}]$(0.0508g, 0.0464mmol) and PPh_3(0.0247g, 0.0941mmol) was heated under reflux in n-hexane(20ml) for 3 hours. Isolation as above gave $[Ru_6C(CO)_{16}(PPh_3)]$(R_f=0.67, 0.0433g); yield=71%.

$[Ru_6C(CO)_{15}(PPh_2Et)_2]$

$[Ru_6C(CO)_{17}]$(0.0452g, 0.0413mmol) and PPh_2Et(0.0199g, 0.0929mmol) were heated under reflux in n-hexane for 3 hours, during which time the solution changed from a deep red to a dark brown. After removing the solvent on a rotary evaporator, the residue was chromatographed with ethyl acetate/light petroleum (b.p. 60-80 °C) (1:4v/v) to give a single, broad band characterised as $[Ru_6C(CO)_{15}(PPh_2Et)_2]$($R_f$=0.49, 0.0384g); yield=64%.

When a similar mixture was stirred in CH_2Cl_2 for 4 days the same product was obtained.

Elemental Analysis Cald. C 35.99% H 2.04%
Obsd. C 37.24% H 1.90%

$[Ru_6C(CO)_{17-n}(P(OMe)_3)_n]$, n=1,2,3 or 4

a) $[Ru_6C(CO)_{17}]$(0.0280g, 0.0255mmol) was dissolved in CH_2Cl_2(25ml), $P(OMe)_3$(0.0042g, 0.0338mmol) added, and the resulting solution stirred for 2 hours at room temperature. The crimson residue, obtained after removing the solvent under reduced pressure, was chromatographed with CH_2Cl_2/n-hexane (1:1v/v) as eluant to give two distinct bands.

i) $[Ru_6C(CO)_{16}(P(OMe)_3)]$($R_f$=0.37, 0.0133g); yield=44%.
Elemental Analysis Cald. C 20.15% H 0.76%
Obsd. C 19.60% H 1.05%

ii) $[Ru_6C(CO)_{15}(P(OMe)_3)_2]$($R_f$=0.20, 0.0127g); yield=39%.
Elemental Ananlysis Cald. C 20.54% H 1.40%
Obsd. C 20.40% H 1.55%

b) $[Ru_6C(CO)_{17}]$(0.0428g, 0.0391mmol) was dissolved in CH_2Cl_2(25ml), $P(OMe)_3$(0.0149g, 0.12mmol) added, and the solution stirred for 2 hours. The crimson residue obtained was chromatographed, as above, to give two separate bands. The most mobile band was identified as $[Ru_6C(CO)_{15}(P(OMe)_3)_2]$(0.016g); yield=32%. The second, found just above the baseline, was characterised as $[Ru_6C(CO)_{14}(P(OMe)_3)_3]$(0.0285g); yield=53%.
Elemental Analysis Cald. C 20.83% H 1.95%
Obsd. C 21.0% H 1.80%

c) $[Ru_6C(CO)_{17}]$(0.0295g, 0.0269mmol) was heated under reflux in n-hexane(15ml) with $P(OMe)_3$(0.0142g, 0.1142mmol) for 2 hours. After allowing to cool the solvent was removed in vacuo and the brown-purple residue cgromatographed, using n-hexane/ethyl acetate (2:1v/v) as eluant, to give a single product identified as $[Ru_6C(CO)_{13}(P(OMe)_3)_4]$(0.0271g); yield=68%.
Elemental Analysis Cald. C 21.10% H 2.43%
Obsd. C 21.70% H 2.15%

Preparation and Pyrolysis of $[Ru_6C(CO)_{16}(PPh_2CH_2CH_2SIL)]$

A quantity of $PPh_2CH_2CH_2SIL$ was added to a concentrated

solution of $[Ru_6C(CO)_{17}]$ in CH_2Cl_2. The resulting slurry was stirred for 2 hours, after which filtration and atmospheric drying gave a red, particulate solid characterised as $[Ru_6C(CO)_{16}(PPh_2CH_2CH_2SIL)]$. The filtrate was shown to contain only unreacted $[Ru_6C(CO)_{17}]$.

Elemental Ananlysis Ruthenium 0.21 wt/wt%
Phosphorus 0.12

A sample was pressed (10tonnes) into a self-supporting disc which was then held in the evacuable cell and heated to a predetermined temperature under vacuum($2x10^{-2}$torr). After a specified time the disc was allowed to cool to room temperature prior to being removed, mulled and studied by infrared spectroscopy.

6.7. References

1. F.Piacenti, M.Bianchi and E.Benedetti, J.C.S. Chem. Comm., 1967, 775.
2. B.F.G.Johnson, R.D.Johnson and J.Lewis, J. Chem. Soc. (A), 1968, 2865.
3. A.Sirigu, M.Bianchi and E.Benedetti, J.C.S. Chem. Comm., 1969, 596.
4. C.R.Eady, B.F.G.Johnson and J.Lewis, J.C.S. Dalton, 1975, 2606.
5. B.F.G.Johnson, J.Lewis and I.G.Williams, J. Chem. Soc. (A), 1970, 901.
6. C.R.Eady, B.F.G.Johnson and J.Lewis, J. Organometallic Chem., 1973, 57, C84.
7. C.R.Eady, B.F.G.Johnson, J.Lewis and T.Matherson, J. Organometallic Chem., 1973, 57, C82.
8. B.F.G.Johnson, J.Lewis, S.W.Sankey, K.Wong, M.McPartlin and W.J.H.Nelson, J. Organometallic Chem., 1980, 191, C3.
9. C.Ungermann, V.Landis, S.A.Moya, H.Cohen, H.Walker, R.G.Pearson, R.G.Rinker and P.C.Ford, J. Amer. Chem. Soc., 1979, 101, 5922.
10. J.S.Bradley, G.B.Ansell and E.W.Hill, J. Organometallic Chem., 1980, 184, C33.
11. J.S.Bradley, R.L.Pruett, E.W.Hill, G.B.Ansell, M.E.Leonowicz and M.A.Modrick, Organometallics, 1982, 1, 748.
12. C-M.T.Hayward, J.R.Shapley, M.R.Churchill, C.Bueno and A.L.Rheingold, J. Amer. Chem. Soc., 1982, 104, 7347.
13. C.R.Eady, P.F.Jackson, B.F.G.Johnson, J.Lewis, M.C.Malatesta,

M.McPartlin and W.J.H.Nelson, J.C.S. Dalton, 1980, 383.

14. C-M.T.Hayward and J.R.Shapley, Inorg. Chem., 1982, 21, 3816.

15. P.F.Jackson, B.F.G.Johnson, J.Lewis, P.R.Raithby, M.McPartlin, W.J.H.Nelson, K.D.Rouse, J.Allibon and S.A.Mason, J.C.S. Chem. Chem., 1980, 295.

16. D.H.Farrar, P.F.Jackson, B.F.G.Johnson, J.Lewis, J.N.Nicholls and M.McPartlin, J.C.S. Chem. Comm., 1981, 415.

17. J.N.Nicholls, D.H.Farrar, P.F.Jackson, B.F.G.Johnson and J.Lewis, J.C.S. Dalton, 1982, 1395.

18. P.F.Jackson, B.F.G.Johnson, J.Lewis, J.N.Nicholls, M.McPartlin and W.J.H.Nelson, J.C.S. Chem. Comm., 1980, 564.

19. E.H.Braye, L.H.Dahl, W.Hubel and D.L.Wampler, J. Amer. Chem. Soc., 1962, 84, 4633.

20. B.F.G.Johnson, J.Lewis, J.N.Nicholls, J.Puga, P.R.Raithby, M.J.Rosales, M.McPartlin and W.Clegg, J.C.S. Dalton, 1983, 277.

21. P.F.Jackson, B.F.G.Johnson, J.Lewis, J.N.Nicholls, M.McPartlin and W.J.H.Nelson, J.C.S. Chem. Comm., 1980, 564.

22. J.Evans, B.P.Gracey, L.R.Gray and M.Webster, J. Organometallic Chem., 1982, 240, C61.

23. M.R.Churchill and P.H.Bird, J. Amer. Chem. Soc., 1968, 90, 800.

24. R.Mason and W.R.Robinson, J.C.S. Chem. Comm., 1968, 468.

25. G.B.Ansell and J.S.Bradley, Acta Cryst., 1980, B36, 1930.

26. J.S.Bradley and G.B.Ansell, ACS/CSJ Chemical Congress; Honolulu, Hawaii, 1979; Inorganic Abstract 506.

27. P.F.Jackson, B.F.G.Johnson, J.Lewis, P.R.Raithby, G.J.Will, M.McPartlin and W.J.H.Nelson, J.C.S. Chem. Comm., 1980, 1190.

28. G.R.John, B.F.G.Johnson, J.Lewis and K.C.Wong, J. Organometallic Chem., 1979, 169, C23.

29. a) C.R.Eady, B.F.G.Johnson, J.Lewis and M.C.Malatesta, J.C.S. Dalton, 1978, 1358.

b) C.R.Eady, J.J.Guy, B.F.G.Johnson, J.Lewis, M.C.Malatesta and G.M.Sheldrick, J.C.S. Chem. Chem., 1976, 602.

30. B.F.G.Johnson, J.Lewis, W.J.H.Nelson, J.Puga, P.R.Raithby, D.Braga, M.McPartlin and W.Clegg, J. Organometallic Chem., 1983, 243, C13.

31. V.G.Albano, D.Braga, S.Martinengo, P.Chini, M.Sansoni and D.Strumolo, J.C.S. Dalton, 1980, 52.

32. B.F.G.Johnson, J.Lewis, K.Wong and M.McPartlin, J. Organometallic

Chem., 1980, 185, C17.

33. V.L.Kuznetsov, A.T.Bell and Y.I.Yermakov, J. Catal., 1980, 65, 374.

34. B.F.G.Johnson, J.Lewis, P.R.Raithby and G.Suss, J.C.S. Dalton, 1979, 1356.

35. J.R.Wilkinson and L.J.Todd, J. Organometallic Chem., 1976, 118, 119.

36. G.A.Battiston, G.Bor, U.K.Dietler, S.F.A.Kettle, R.Rossetti, G.Sbrignadello and P.L.Stanghellini, Inorg. Chem., 1980, 19, 1961.

37. M.Arif and S.F.A.Kettle, J. Chem. Phys., 1980, 72, 2131.

38. G.M.Sheldrick, 'SHELX, Program for Crystal Structure Determination', University of Cambridge, 1976.

39. 'International Tables for X-ray Crystallography', Kynoch Press, Birmingham, 1974, Vol 4, pp99.

40. S.C.Brown, J.Evans and M.Webster, J.C.S. Dalton, 1981, 2263.

41. C.K.Johnson, 'ORTEP, A Fortran Thermal Ellipsoid Plot Program for Crystal Structure Illustrations', ORNL-5138 (second revision), Oak Ridge National Laboratory, Tennessee, 1965.

42. B.E.Mann, J.C.S. Dalton, 1973, 2012.

43. K.Wong, Ph.D. Thesis, University of Cambridge, 1977.

44. J.Evans and B.P.Gracey, J.C.S. Chem. Comm., 1983, 247.

45. M.F.Brown and R.D.Gonzalez, J. Phys. Chem., 1976, 80, 1731.

46. F.Piacenti, M.Bianchi, E.Benedetti and G.Braca, Inorg. Chem., 1968, 7, 1815.

47. F.Piacenti, M.Bianchi, E.Benedetti and G.Sbrana, J. Inorg. Nucl. Chem., 1967, 29, 1389.

48. B.F.G.Johnson, R.D.Johnson and J.Lewis, J. Chem. Soc. (A), 1969, 792.

49. C.F.Barnard, J.A.Daniels, J.Jeffrey and R.J.Mawby, J.C.S. Dalton, 1976, 953.

50. J.Chatt, B.L.Shaw and A.E.Field, J. Chem. Soc., 1964, 3467.

51. D.F.Gill, B.E.Mann and B.L.Shaw, J.C.S. Dalton, 1973, 311.